NOTE TO USERS

This reproduction is the best copy available.

UMI®

UNIVERSITY OF CALIFORNIA

Los Angeles

Control of Nonlinear and Hybrid Process Systems: Designs for Uncertainty and Constraints

A dissertation submitted in partial satisfaction of the

requirements for the degree of Doctor of Philosophy

in Chemical Engineering

by

Nael H. El-Farra

2004

UMI Number: 3146622

Copyright 2004 by
El-Farra, Nael H.

All rights reserved.

INFORMATION TO USERS

The quality of this reproduction is dependent upon the quality of the copy submitted. Broken or indistinct print, colored or poor quality illustrations and photographs, print bleed-through, substandard margins, and improper alignment can adversely affect reproduction.

In the unlikely event that the author did not send a complete manuscript and there are missing pages, these will be noted. Also, if unauthorized copyright material had to be removed, a note will indicate the deletion.

UMI®

UMI Microform 3146622
Copyright 2004 by ProQuest Information and Learning Company.
All rights reserved. This microform edition is protected against unauthorized copying under Title 17, United States Code.

ProQuest Information and Learning Company
300 North Zeeb Road
P.O. Box 1346
Ann Arbor, MI 48106-1346

© Copyright by

Nael H. El-Farra

2004

The dissertation of Nael H. El-Farra is approved.

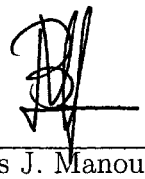

Vasilios J. Manousiouthakis

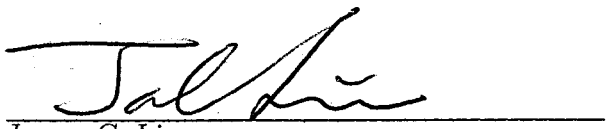

James C. Liao

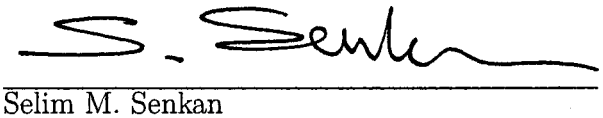

Selim M. Senkan

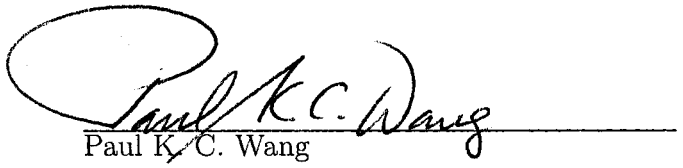

Paul K. C. Wang

Panagiotis D. Christofides, Committee Chair

University of California, Los Angeles

2004

Contents

1 Introduction **1**

1.1 Motivation 1

1.2 Background on analysis and control of nonlinear systems 2

1.3 Examples of nonlinear chemical processes 7

1.3.1 Non-isothermal continuous stirred tank reactors 7

1.3.2 Isothermal continuous crystallizer 8

1.4 Background on analysis control of hybrid systems 9

1.5 Examples of hybrid process systems 12

1.5.1 Fault-tolerant process control systems 12

1.5.2 Switched biological systems 14

1.6 Objectives and organization of the thesis 17

2 Control of Nonlinear Systems with Uncertainty **24**

2.1 Introduction 24

2.2 Preliminaries 25

2.3 Robust inverse optimal state feedback controller design 28

2.3.1 Control problem formulation 28

2.3.2 Controller design under vanishing uncertainties 29
2.3.3 Controller design under non-vanishing uncertainties 37
2.4 Illustrative example 41
2.5 Robust near-optimal output feedback controller design 44
2.5.1 Control problem formulation 47
2.5.2 Near-optimality over the infinite horizon 51
2.5.3 Near-optimality over the finite horizon 56
2.6 Application to a non-isothermal chemical reactor 58
2.6.1 Process description and control problem formulation 58
2.6.2 Controller synthesis and simulation results 62
2.7 Conclusions 73

3 Control of Nonlinear Systems with Uncertainty and Constraints 74

3.1 Introduction 74
3.2 Preliminaries 77
3.2.1 System description 77
3.2.2 Traditional approaches 78
3.2.3 Motivating example 80
3.3 Integrating robustness, optimality, and constraints 90
3.3.1 Control problem formulation 90
3.3.2 Bounded controller synthesis under vanishing uncertainty . . . 92
3.3.3 Bounded controller synthesis under non-vanishing uncertainty 100
3.4 Application to a non-isothermal chemical reactor 103
3.5 Conclusions 109

4 Control of Multivariable Nonlinear Systems **110**

4.1 Introduction 110

4.2 Preliminaries 112

4.3 Bounded robust state feedback control 113

4.3.1 Control problem formulation 113

4.3.2 Controller synthesis 114

4.4 Application to a multivariable chemical reactor 123

4.5 State estimation and output feedback control 132

4.5.1 Control problem formulation 136

4.5.2 Controller synthesis 137

4.6 Robust stabilization of a chemical reactor via output feedback control 142

4.7 Connections with model predictive control 148

4.8 Conclusions 155

5 Hybrid Predictive Control of Constrained Linear Systems **157**

5.1 Introduction 157

5.2 Preliminaries 161

5.2.1 Model predictive control 162

5.2.2 Bounded Lyapunov-based control 164

5.3 Hybrid predictive state feedback control 168

5.3.1 Problem formulation: Uniting MPC and bounded control . . . 169

5.3.2 Stability-based controller switching 171

5.3.3 Performance-driven switching 174

5.3.4 Switching using advanced MPC formulations 178

5.3.5 Simulation example 182
5.4 Hybrid predictive output feedback control 191
5.4.1 Preliminaries 194
5.4.2 Stability properties under output feedback control 196
5.4.3 Hybrid predictive controller design 202
5.4.4 Simulation studies 208
5.5 Conclusions 221

6 Hybrid Predictive Control of Nonlinear and Uncertain Systems 225

6.1 Introduction 225
6.2 Hybrid predictive control of nonlinear systems 229
6.2.1 Preliminaries 229
6.2.2 Controller switching strategies 234
6.2.3 Applications to chemical process examples 246
6.3 Robust hybrid predictive control of nonlinear systems 257
6.3.1 Preliminaries 260
6.3.2 Robust hybrid predictive controller design 264
6.3.3 Application to robust stabilization of a chemical reactor . . . 274
6.4 Conclusions 278

7 Control of Hybrid Systems with Uncertainty and Constraints 285

7.1 Introduction 285
7.2 Switched nonlinear processes with uncertain dynamics 286
7.2.1 State-space description 286

7.2.2 Stability analysis via multiple Lyapunov functions 289
7.2.3 Illustrative example 290
7.3 Coordinating feedback and switching for robust hybrid control 293
7.3.1 Problem formulation and solution overview 293
7.3.2 Hybrid control strategy under vanishing uncertainty 295
7.3.3 Hybrid control strategy under non-vanishing uncertainty . . . 302
7.3.4 Application to input/output linearizable processes 305
7.4 Application to a switched chemical reactor 307
7.5 Conclusions 316

8 Fault-Tolerant Control of Process Systems 317

8.1 Introduction 317
8.2 Preliminaries 322
8.2.1 System description 322
8.2.2 Problem statement and solution overview 323
8.2.3 Motivating example 325
8.3 Fault–tolerant control system design methodology 329
8.3.1 Constrained feedback controller synthesis 330
8.3.2 Characterization of fault–recovery regions 336
8.3.3 Supervisory switching logic design 338
8.3.4 Design of the communication logic 339
8.4 Simulation studies 343
8.4.1 Application to a single chemical reactor 343
8.4.2 Application to two chemical reactors in series 354

8.5 Conclusions 363

9 Analysis and Control of Biological Networks Using Hybrid Systems Theory 364

9.1 Introduction 364

9.2 A Switched system representation of biological networks 369

9.3 Methodology for analysis and control of mode transitions 370

9.4 Application to eukaryotic cell cycle regulation 372

9.5 Application to the bacteriophage λ-switch system 381

9.6 Conclusions 397

10 Analysis and Control of Constrained Parabolic PDE Systems 402

10.1 Introduction 402

10.2 Preliminaries 404

10.2.1 Parabolic PDE systems with input constraints 404

10.2.2 Galerkin's method 407

10.3 Bounded nonlinear control of parabolic PDE systems 409

10.3.1 State feedback control 409

10.3.2 Output feedback control 414

10.4 Application to a diffusion-reaction process 416

10.5 Conclusions 420

11 Analysis and Control of Constrained Particulate Processes 423

11.1 Introduction 423

11.2 Preliminaries 426

11.2.1 Particulate process model with input constraints 426
11.2.2 Motivating example: A continuous crystallizer 428
11.3 Methodological framework for analysis and control 436
11.4 Model reduction 437
11.5 Computation of admissible set-points 440
11.6 Bounded nonlinear control of particulate processes 444
11.6.1 Preliminaries 445
11.6.2 Controller synthesis 447
11.6.3 Application to the crystallizer moment model 454
11.6.4 Controller implementation on the infinite-dimensional system . 460
11.7 Application to a continuous crystallizer with constraints 462
11.8 Conclusions 467

12 Hybrid Control of Spatially Distributed Processes 469

12.1 Introduction 469
12.2 Preliminaries 473
12.2.1 Class of spatially-distributed processes 473
12.2.2 Problem formulation and solution overview 476
12.3 Hybrid control of spatially-distributed processes 478
12.3.1 Galerkin's method 478
12.3.2 Coordinating feedback and switching 480
12.4 Simulation studies 489
12.4.1 Application to a diffusion-reaction process 489
12.4.2 Application to a non-isothermal tubular reactor with recycle . 497

12.5 Conclusions 505

13 Fault-Tolerant Control of Fluid Dynamic Systems **507**

13.1 Introduction 507

13.2 Preliminaries 510

13.2.1 Mathematical description 510

13.2.2 Problem formulation 513

13.3 Fault-tolerant control system design 515

13.3.1 Galerkin's method 515

13.3.2 Coordinating feedback and switching 516

13.4 Simulation results 522

13.5 Conclusions 537

Bibliography **538**

A Proofs of Chapter 2 **570**

B Proofs of Chapter 3 **598**

C Proofs of Chapter 4 **618**

D Proofs of Chapter 5 **629**

E Proofs of Chapter 6 **638**

F Proofs of Chapter 7 **643**

G Proofs of Chapter 11 **651**

H Proofs of Chapter 10 **657**

I Proofs of Chapter 12 664

List of Figures

1.1 Switching between multiple control configurations, each characterized by a different manipulated input, provides a mechanism for fault-tolerant control. 13

2.1 Closed-loop output and manipulated input profiles under the controller of Eq.15 (solid lines), the controller of Eq.15 with $\chi = 0$ (dashed-dotted lines), the controller of Eq.22 (dashed lines), and the high-gain controller (dotted lines). 45

2.2 Control action computed by the controller of Eq.15 (dashed lines) and the controller of Eq.22 (solid lines). 46

2.3 Control actions computed by the static component of the controller of Eq.2.50 (solid lines) and the controller of Eq.2.52 (dashed lines) for $C_A - C_{AS} = -0.4$ (top left), -0.2 (top right), 0.2 (bottom left), 0.4 (bottom right) 63

2.4 Closed-loop output and manipulated input profiles for stabilization under the output feedback controller of Eq.2.50 (dashed lines) and the optimal state feedback controller (solid lines) when no uncertainty is present. 66

2.5 Closed-loop output and manipulated input profiles for reference input tracking under the output feedback controller of Eq.2.50 (dashed lines) and the optimal state feedback controller (solid lines) when no uncertainty is present. 67

2.6 Closed-loop output and manipulated input profiles for stabilization under the robust output feedback controller of Eq.2.55 (dashed lines), the robust optimal state feedback controller (solid lines) and open-loop profile (dotted line). 70

2.7 Closed-loop output and manipulated input profiles for stabilization under the output feedback controller of Eq.2.55 with no uncertainty compensation ($\chi = 0$). 71

2.8 Closed-loop output and manipulated input profiles for reference input tracking under the robust output feedback controller of Eq.2.55 (dashed lines) and the robust optimal state feedback controller (solid lines). . 72

3.1 Startup profiles of the controlled output and manipulated input for the chemical reactor example under the dynamic mixed error-and state-feedback controller with windup compensation given in Eq.3.6 in the absence of uncertainty or constraints (solid line), in the presence of uncertainty with no constraints (dashed line), and in the presence of both uncertainty and constraints (dotted line). 84

3.2 Controlled output and manipulated input profiles in the presence of uncertainty and input constraints under the robust controller of Eq.2.23 (solid line) and the input-output linearizing-based controller of Eq.3.6 (dashed line). 87

3.3 Controlled output and manipulated input profiles under the controller of Eq.2.23 without the robust compensation component ($\chi = 0$). . . . 88

3.4 Closed-loop output and manipulated input profiles under the controller of Eq.2.23 in the presence of uncertainty and input constraints of $|Q| \leq$ 60 KJ/s (solid line), $|Q| \leq 30$ KJ/s (dashed line), and $|Q| \leq 20$ KJ/s (dashed line). 91

3.5 Closed-loop output and manipulated input profiles under the controller of Eqs.30-39 in the presence of process uncertainty and input constraints of $|Q| \leq 60$ KJ/s (solid line) and $|Q| \leq 40$ KJ/s (dashed line). 105

3.6 Closed-loop output and manipulated input profiles for reference input tracking under the controller of Eqs.30-39 in the presence of process uncertainty and input constraints of $|Q| \leq 60$ KJ/s (solid line) and $|Q| \leq 40$ KJ/s (dashed line). 107

3.7 Regions of constraint satisfaction under the bounded controller of Eq.3.10 (top plot) and a robust feedback linearizing controller (bottom plot), $u_{max} = 50$ KJ/s. 108

4.1 Controlled outputs: reactant concentration (top) and reactor temperature (bottom) profiles under the bounded multivariable nonlinear state feedback controller with uncertainty compensation and initial condition inside the stability region (solid), without uncertainty compensation (dashed) and under open-loop conditions (dotted). 127

4.2 Manipulated inputs: inlet reactant concentration (top) and rate of heat input (bottom) profiles under the bounded multivariable nonlinear state feedback controller with uncertainty compensation and initial condition inside the stability region (solid), without uncertainty compensation (dashed) and under open-loop conditions (dotted). 128

4.3 Controlled outputs: reactant concentration (top) and reactor temperature (bottom) profiles under the bounded robust multivariable nonlinear state feedback controller for initial conditions outside the region of guaranteed closed-loop stability. 130

4.4 Manipulated inputs: inlet reactant concentration (top) and rate of heat input (bottom) profiles under the bounded multivariable nonlinear state feedback controller for initial conditions outside the region of guaranteed closed-loop stability. 131

4.5 Controlled outputs: reactant concentration (top) and reactor temperature (bottom) profiles under the bounded robust multivariable nonlinear state feedback controller for a set-point increase of 0.4 mol/L in the reactant concentration and a set-point decrease of 40 K in the reactor temperature. 133

4.6 Manipulated inputs: inlet reactant concentration (top) and rate of heat input (bottom) profiles under the bounded multivariable nonlinear state feedback controller for a set-point increase of 0.4 mol/L in the reactant concentration and a set-point decrease of 40 K in the reactor temperature. 134

4.7 Comparison between the state-space regions where the bounded robust multivariable controller (top) and a multivariable input-output linearizing controller (bottom) satisfy the input constraints. The regions are used to provide estimates of the corresponding stability regions. 135

4.8 Controlled outputs: desired product concentration (top) and reactor temperature (bottom) profiles under the bounded robust multivariable output feedback controller (solid), under the corresponding state feedback controller (dashed), for initial condition within the region of guaranteed stability, and under open-loop conditions (dotted). 149

4.9 Manipulated inputs: inlet reactant concentration (top) and rate of heat input (bottom) profiles under the bounded robust multivariable output feedback controller (solid) and under the corresponding state feedback controller (dashed), for an initial condition within the region of guaranteed stability. 150

5.1 Schematic representation of a hybrid control structure. 159

5.2 A schematic representation of the hierarchical hybrid predictive control structure uniting MPC and bounded control for the stabilization of constrained LTI systems. 170

5.3 A schematic representation of the implementation of the stability-based controller switching proposed in Theorem 5.1. 172

5.4 A schematic representation of the implementation of the controller switching strategy proposed in Theorem 5.2 and how it compares with the scheme proposed in Theorem 5.1. Starting at $x_1(0)$, scheme 2 permits a temporary increase in V under MPC without switching thus allowing MPC to remain in the closed-loop for all times (solid trajectory). Starting at $x_1(0)$, scheme 1 does not allow the increase in V and switches immediately to the bounded controller instead (solid followed by dashed trajectory). Starting at $x_2(0)$, scheme 2 enforces a switch from MPC to the bounded controller when the closed-loop trajectory under MPC is about to leave Ω. 176

5.5 A schematic representation of the implementation of switching when a "stabilizing" MPC formulation is used. Starting at $x(0)$, MPC does not yield a feasible solution and, therefore, the bounded controller is used. When the trajectory crosses the C_2-level set of V, the supervisor checks off-line the feasibility of the MPC and finds that no feasible solution exists. The bounded controller remains in action. Finally, when the trajectory crosses the C_1-level set of V, the supervisor finds that the optimization is feasible and therefore switches to the MPC controller which stays in the closed-loop systems for all future times. . 180

5.6 Closed-loop state trajectory under MPC with $T = 1$ (solid line), under the switching scheme of Theorem 5.1 with $T = 1$ (dashed line), and under MPC with $T = 1.5$ (dotted line). 183

5.7 Input and closed-loop state profiles under MPC with $T = 1$ (solid line), under the switching scheme of Theorem 5.1 with $T = 1$ (dashed line), and under MPC with $T = 1.5$ (dotted line). 184

5.8 Closed-loop state trajectory under the switching scheme of Theorem 5.1 (solid line), and under the switching scheme of Theorem 5.2 (dashed line). 185

5.9 Input and closed-loop state profiles under the switching scheme of Theorem 5.1 (solid line) and under the switching scheme of Theorem 5.2 (dashed line). 186

5.10 Temporal evolution of the Lyapunov function under the switching scheme of Theorem 5.1 (solid line), where the bounded controller is switched in immediately at $t = 0$, and under the switching scheme of Theorem 5.2 (dashed line), where the MPC controller stays in action for all time. 186

5.11 Closed-loop state trajectory starting close to the origin using MPC with $T = 1.2$ (solid line) and from a point farther away in state space using the switching scheme with a horizon length $T = 1.2$ (dashed line) and using only MPC with $T = 1.5$ (dotted line). 188

5.12 Input and closed-loop state profiles starting close to the origin using MPC with $T = 1.2$ (solid line) and from a point farther away in state space using the switching scheme with a horizon length $T = 1.2$ (dashed line) and using only MPC with $T = 1.5$ (dotted line). 189

5.13 Closed-loop state trajectory under MPC (solid line) and under the switching scheme accounting for sampling (dashed line). 192

5.14 Input and closed-loop state profiles under MPC (solid line) and under the switching scheme accounting for sampling (dashed line). 192

5.15 Schematic representation of the evolution of the trajectories of the closed–loop state and state estimate. Starting within Ω_b, the observer gain ensures that, before the state of the closed–loop system reaches the boundary of Ω, the state estimate has converged close enough to the true value of the state, so that the norm of the estimation error is below the allowable error tolerated by the controller within Ω. 199

5.16 Schematic representation of the hierarchical hybrid predictive control structure merging the bounded and model predictive controllers and a state observer. 205

5.17 Schematic representation of the evolution of the closed–loop system under the controller switching strategy proposed in Theorem 5.3. Note that MPC is not activated (even if feasible) before $\hat{x}$ enters Ω_s. 205

5.18 States of the closed–loop system under the proposed hybrid predictive control strategy using two different horizon lengths of $T = 1.5$ (solid) and $T = 3.5$ (dashed) in MPC implementation, and an observer gain parameter of $\beta = 500$. 211

5.19 Manipulated input profiles under the proposed hybrid predictive control strategy using two different horizon lengths of $T = 1.5$ (solid) and $T = 3.5$ (dashed) in MPC implementation, and an observer gain parameter $\beta = 500$. 212

5.20 States of the closed–loop system under the proposed hybrid predictive control strategy using two different gain parameters of $\beta = 500$ (solid) and $\beta = 0.5$ (dashed) in observer implementation, and horizon length of $T = 1.5$ in the predictive controller. 213

5.21 Manipulated input profiles under the proposed hybrid predictive control strategy using two different gain parameters of $\beta = 500$ (solid) and $\beta = 0.5$ (dashed) in observer implementation, and horizon length of $T = 1.5$ in the predictive controller. 214

5.22 Closed–loop states under hybrid predictive control, in the presence of measurement noise and modeling errors, for the case when the observer is initially implemented using $\beta = 500$ and then switched to $\beta = 0.5$ at $t = 1.0$ (solid lines) and the case when the observer is implemented using $\beta = 500$ for all times (dotted lines). The horizon length for the predictive controller is $T = 1.5$. 216

5.23 Manipulated input profiles under the proposed hybrid predictive control strategy in the presence of measurement noise and modeling errors. The solid profiles depict the case when the state observer is initially implemented using $\beta = 500$ and then switched to $\beta = 0.5$ at $t = 1.0$. The dotted profiles depict the case when the state observer is implemented using $\beta = 500$ for all times. The horizon length for the model predictive controller is $T = 1.5$. 217

5.24 Stability region estimate, Ω', based on the linearization of the nonlinear model of Eq.5.33. The solid line depicts the closed–loop state trajectory starting from an initial condition for which MPC (designed based on the linear model with $T = 2$) is feasible and stabilizes the nonlinear closed–loop system, while the dotted line depicts the state trajectory starting from an initial condition for which MPC is infeasible, and the hybrid predictive control strategy is implemented instead to enforce closed–loop stability. 220

5.25 Closed–loop reactant concentration (top) and reactor temperature (bottom) starting from an initial condition for which MPC (designed based on the linear model with $T = 2$) is feasible and stabilizes the nonlinear closed–loop system (solid), and starting from an initial condition for which MPC is infeasible, and the hybrid predictive control strategy is implemented instead to enforce closed–loop stability (dotted). 222

5.26 Rate of heat input (top) and inlet reactant concentration in deviation variable form (bottom) when MPC is implemented (solid) and when the hybrid predictive control strategy is implemented (dotted). . . . 223

6.1 Schematic representation of the hybrid control structure merging MPC and a family of fall–back bounded controllers with their stability regions. 237

6.2 Schematic representation illustrating the main idea of the controller switching scheme proposed in Theorems 6.1 and 6.2. 242

6.3 Implementation of the proposed hybrid control structure: Closed–loop state trajectory under MPC with $T = 0.25$ (solid trajectory), under the switched MPC/bounded controller(3) with $T = 0.25$ (dashed trajectory), under MPC with $T = 0.5$ (dotted trajectory), and under the switched bounded controller(2)/MPC with $T = 0.5$ (dash-dotted line). 249

6.4 Closed-loop reactant concentration profile (a), reactor temperature profile (b) and coolant temperature profile (c) under MPC with $T = 0.25$ (solid trajectory), under the switched MPC/bounded controller(3) with $T = 0.25$ (dashed trajectory), under MPC with $T = 0.5$ (dotted trajectory), and under the switched bounded controller(2)/MPC with $T = 0.5$ (dash-dotted line). 251

6.5 Closed-loop state trajectory under the switching rules of Theorem 6.2 with $T = 0.1$ for MPC. 252

6.6 Closed-loop reactant concentration profile (a), reactor temperature profile (b) and coolant temperature profile (c) under the switching scheme of Theorem 6.2 with $T = 0.1$ for MPC. 254

6.7 Implementation of the proposed hybrid control structure to a continuous crystallizer: two-dimensional projections of the stability region for the 10 distinct combinations of the process states. 256

6.8 Closed-loop profiles of the dimensionless crystallizer moments (a)-(d), the solute concentration in the crystallizer (e) and the manipulated input (f) under MPC with stability constraints (solid line), under MPC without terminal constraints (dashed line), and using the switching scheme of Theorem 6.1 (dotted line). 258

6.9 A schematic representation of the robust hybrid predictive control structure. 265

6.10 Examples of the evolution of the closed–loop state trajectory under the switching scheme of Theorem 6.3. Starting from $x_1(0)$, the trajectory under MPC hits the boundary of the stability region, upon which the bounded controller is switched in. Starting from $x_2(0)$, MPC is able to achieve practical stability. Starting from $x_3(0)$, the trajectory under MPC converges to a limit cycle and, therefore, after a time T_{design} has elapsed, the bounded controller is switched in to enforce convergence close to the origin. 267

6.11 Examples of the evolution of closed–loop state trajectory under the switching scheme of Theorem 6.4: (a) starting from $x(0)$, the closed–loop trajectory under MPC hits the boundary of Ω_1^0 (at T_1), upon which the bounded controller 1 is switched in and implemented until the trajectory enters Ω_1^1, following which MPC is switched back in leading to practical stability, (b) starting from $x(0)$, the closed–loop trajectory under MPC hits the boundary of Ω_1^0 (at T_1), upon which the bounded controller 1 is switched in and implemented until the trajectory enters Ω_1^1, following which MPC is switched back in. The trajectory under MPC hits the boundary of Ω_2^1 ($t = T_2$) at which time the bounded controller 2 is switched in and implemented for all future times. 280

6.12 Closed–loop state trajectories under the bounded controller when initialized within the stability region estimated without taking the uncertainty into account (solid line) and the stability region that accounts for the uncertainty (dashed line). 281

6.13 Closed–loop state (top) and input (bottom) profiles under the bounded controller when initialized within the stability region estimated without taking the uncertainty into account (solid lines) and the stability region that accounts for the uncertainty (dashed lines). 281

6.14 Closed–loop state trajectory: implementation of the robust hybrid predictive controller of Theorem 6.3 using a nominal MPC formulation without stability constraints (solid line) and a nonlinear MPC formulation with stability constraints, from two different initial conditions (dashed and dotted lines). 282

6.15 Closed–loop state (top) and input (bottom) profiles: implementation of the robust hybrid predictive controller of Theorem 6.3 using a nominal MPC formulation without stability constraints (solid lines) and a nonlinear MPC formulation with stability constraints, from two different initial conditions (dashed and dotted lines). 283

6.16 Closed–loop state trajectory: implementation of the robust hybrid predictive controller of Theorem 6.4, with $l = 2$, $N = 1$, using a nominal MPC formulation without stability constraints (solid line). 283

6.17 Closed–loop state (top) and input (bottom) profiles: implementation of the robust hybrid predictive controller of Theorem 6.4, with $l = 2$, $N = 1$, using a nominal MPC formulation without stability constraints (solid line). 284

7.1 A multi-modal representation of a hybrid process, involving a finite family of continuous subsystems and discrete events governing the transitions between them. 287

7.2 Temporal evolution of Multiple Lyapunov Functions for an asymptotically stable switched system consisting of twomodes. 291

7.3 A switched non-isothermal continuous stirred tank reactor. 292

7.4 Implementation of the switching law based on monitoring the evolution of the closed-loop trajectory with respect to stability regions. 300

7.5 Summary of the proposed hybrid control strategy based on coordinating feedback and switching. 302

7.6 Reactor temperature and rate of heat input profiles under the bounded robust controller of the first mode, i.e., control valve closed and $\sigma = 0$ (solid lines) and under open-loop conditions (dashed lines). 310

7.7 Reactor temperature and rate of heat input profiles when the reactor is initially operated in the first mode (control valve closed, $\sigma = 0$) using the corresponding robust controller, then the control valve is opened ($\sigma = 1$) at $t = 12$ min and the robust controller for the second mode is activated in place of the first controller. 311

7.8 Reactor temperature and rate of heat input profiles for the case when mode switching is carried out at $t = 24$ min with no uncertainty present (solid lines) and for the case when uncertainty is present and mode switching (using nominal controllers with $\rho_i = \chi_i = 0$) is carried out at $t = 24$ min (dashed lines). 313

7.9 Reactor temperature and rate of heat input profiles for the cases when uncertainty is present and mode switching (using the bounded robust controllers) is carried out at $t = 24$ min (dashed lines) and at $t = 30$ min (solid lines). 315

8.1 Block diagrams of: (a) a centralized networked control system for a single–unit plant, and (b) a hierarchical distributed networked control architecture for a multi–unit plant. 321

8.2 Process flow diagram of two CSTR units in series. 329

8.3 Summary of the fault–tolerant control strategy, for a two–unit plant, using communication networks. 342

8.4 Switching between multiple control configurations, each characterized by a different manipulated input, provides a mechanism for fault-tolerant control. 346

8.5 Fault–tolerant control structure for a single unit operation, integrating supervisory and feedback control over a communication network. . . . 346

8.6 Stability regions of the three control configurations (I, II, III) considered for the chemical reactor example of Eq.8.13. 349

8.7 Evolution of the closed–loop state profiles under repeated control system failures and subsequent switching by the supervisor from configuration 1 (solid lines) to configuration 2 (dashed lines) to configuration 3 (dotted lines). 350

8.8 Manipulated input profiles for each control configuration as the supervisor switches from configuration 1 to configuration 2 at $t = 2$ hr and from configuration 2 to configuration 3 at $t = 15$ hr. 351

8.9 A phase plot showing the closed–loop state trajectory leaving the intersection zone (I,II & III) during the delay period (dashed–dotted trajectory) rendering configuration 3 destabilizing (dotted trajectory). 352

8.10 Evolution of the closed–loop state profiles when configuration 1 (solid lines) fails at $t = 10$ hr and an overall delay of $\tau_{max} = 8.0$ min elapses before the backup configuration is activated. Activation of configuration 2 preserves closed–loop stability (dashed lines) while activation of configuration 3 leads to instability (dotted lines). 353

8.11 Manipulated input profiles when configuration 1 fails at $t = 10$ hr and an overall delay of $\tau_{max} = 8.0$ min elapses before the backup configuration is activated. 354

8.12 Evolution of the closed–loop state and manipulated input profiles for CSTR 1 under a well–functioning control system (solid) and when the control actuator fail at $t = 5$ min (dashed). 355

8.13 Evolution of the closed–loop state and manipulated input profiles for CSTR 2 under a well–functioning control system. 356

8.14 Evolution of the closed–loop state and manipulated input profiles for CSTR 2 when the controller of the fall–back configuration (Q_2, C_{A03}) is activated immediately after the failure (solid lines), and the open–loop state and input profiles resulting when the fall–back configuration is not activated after the failure (dashed lines). 357

8.15 Fault–recovery region of the fall–back control configuration (Q_2, C_{A03}) for CSTR 2, with constraints $|Q_2| \leq 2.8 \times 10^6\ KJ/hr$ and $|C_{A03} - C^s_{A03}| \leq 0.4\ kmol/m^3$. when failure occurs at $T_f = 5$ min. Activation of the fall–back configuration after a 3 min delay preserves closed–loop stability (top plot), while activation after 4.1 min delay fails to ensure fault–tolerance (bottom plot). 360

8.16 Evolution of the closed–loop state and input profiles when the failure occurs at $T_f = 5$ min and the fall–back configuration (Q_2, C_{A03}), with constraints $|Q_2| \leq 2.8 \times 10^6\ KJ/hr$ and $|C_{A03} - C^s_{A03}| \leq 0.4\ kmol/m^3$ is activated after a total delay of 3 min (solid lines) and after a total delay of 4.1 min. (dashed lines). 361

8.17 Fault–recovery region of the fall–back control configuration (Q_2, C_{A03}) for CSTR 2, with constraints $|Q_2| \leq 1.4 \times 10^7\ KJ/hr$ and $|C_{A03} - C^s_{A03}| \leq 2.0\ kmol/m^3$. when failure occurs at $T_f = 5$ min. Activation of the fall–back configuration after a delay of either 3 min or 4.1 min ensures fault–tolerance. 361

8.18 Evolution of the closed–loop state and manipulated input profiles when the failure occurs at $T_f = 5$ min and the fall–back configuration (Q_2, C_{A03}), with constraints $|Q_2| \leq 1.4 \times 10^7\ KJ/hr$ and $|C_{A03} - C^s_{A03}| \leq 2.0\ kmol/m^3$ is activated after a total delay of 3 min (solid lines) and after a total delay of 4.1 min. (dashed lines). 362

9.1 Phase-plane portraits of the system of Eq.9.4, for different values of k'_2, k''_2, and k_{wee}, showing: (a) Stable steady-state with most MPF inactive, (b) Stable steady-state with most MPF active, (c) Unstable steady-state surrounded by a limit cycle, and (d) Bi-stability: two stable steady-states separated by an unstable saddle point. 374

9.2 (a) A plot showing the overlap of the limit cycle of the oscillatory mode with the domains of attraction for the M-arrested steady-state (entire area above dashed curve) and for the $G2$-arrested steady-state (entire area below the dashed curve), (b) A plot showing that switching from the oscillatory to the bi-stable mode moves the system to different steady-states depending on where switching takes place. In both cases, the oscillatory mode is fixed at $k'_2 = 0.01$, $k''_2 = 10$, $k_{wee} = 2.0$. 376

9.3 The time evolution plots of (a) active MPF, and (b) total cyclin upon switching from the oscillatory to the bi-stable mode at two representative switching times. At $t = 333.5$ min, the state trajectory lies on segment A (see Fig.9.2a) and therefore switching lands the state in the M-arrested steady-state (dash-dotted line), while at $t = 334$ min, switching lands the state in the $G2$-arrested steady-state (dotted line). In both cases, the oscillatory mode is fixed at $k_2' = 0.01$, $k_2'' = 10$, $k_{wee} = 2.0$. 377

9.4 A plot showing that switching from the oscillatory mode (of the following parameter values: $k_2' = 0.01$, $k_2'' = 10$, $k_{wee} = 2.5$) to the bi-stable mode at same time as in Fig.9.2b ($t = 333.5$ min) moves the system to $G2$-arrest steady-state (instead of M-arrest steady-state) because switching does not occur on segment B. Note that the portion of the limit cycle overlapping the stability region of the M-arrested steady-state (segment B) is larger than the one in 9.2a (segment A). 378

9.5 The time evolution plots of (a) active MPF, and (b) total cyclin upon switching from the oscillatory to the bi-stable mode at $t = 333.5$ min. In both cases, the oscillatory mode is fixed at $k_2' = 0.01$, $k_2'' = 10$, $k_{wee} = 2.5$ 379

9.6 A schematic representation of the molecular mechanism responsible for the lysogenic to lytic mode transition in the bacteriophage λ. 382

9.7 A phase plot for the moderate *CI* degradation mode showing that an initial condition within the lysogenic domain of attraction (entire area below the dotted curve) will converge to the lysogenic steady-state (dashed trajectory) and that an initial condition within the lytic domain of attraction (entire area above the dotted curve) will converge to the lytic steady-state (solid trajectory). Here, the *Cro* degradation rate is fixed at $\gamma_y = 0.008$. 386

9.8 A phase plot showing the system of Eq.9.5 being initialized using $\gamma_x = 0.05$ (dashed trajectory) and undergoing: (a) a decrease in the degradation rate of *CI* protein (to $\gamma_x = 0.004$) at $t = 20$, leading the state to converge to the lysogenic steady-state, and (b) an increase in the degradation rate of *CI* protein (to $\gamma_x = 0.1$) at $t = 20$, leading the state to converge to the lytic steady-state. In both cases, the *Cro* degradation rate is fixed at $\gamma_y = 0.008$. 388

9.9 The time evolution plots of the *CI* (left) and *Cro* (right) protein concentrations when the system undergoes a transition from the $\gamma_x = 0.05$ mode (dashed lines) to the $\gamma_x = 0.004$ mode at $t = 20$ and converges (solid lines) to the lysogenic steady-state. The *Cro* degradation rate is fixed at $\gamma_y = 0.008$. 389

9.10 The time evolution plots of the *CI* (left) and *Cro* (right) protein concentrations when the system undergoes a transition from the $\gamma_x = 0.05$ mode (dashed lines) to the $\gamma_x = 0.1$ mode at $t = 20$ and converges (solid lines) to the lytic steady-state. The *Cro* degradation rate is fixed at $\gamma_y = 0.008$. 390

9.11 A phase plot showing the system of Eq.9.5 being initialized using $\gamma_y = 0.008$ (dashed trajectory) and undergoing: (a) a decrease in the degradation rate of *Cro* protein (to $\gamma_y = 0.0005$) at $t = 20$, leading the state to converge to the lytic steady-state, and (b) an increase in the degradation rate of *Cro* protein (to $\gamma_y = 0.06$) at $t = 20$, leading the state to converge to the lysogenic steady-state. In both cases, the *CI* degradation rate is fixed at $\gamma_x = 0.05$. 392

9.12 The time evolution plots of the *CI* (left) and *Cro* (right) protein concentrations when the system initialized at $(x(0), y(0)) = (35, 18)$ undergoes a transition from the $\gamma_y = 0.008$ mode (dashed lines) to the $\gamma_y = 0.0005$ mode at $t = 20$ and converges (solid lines) to the lytic steady-state. The *CI* degradation rate is fixed at $\gamma_x = 0.05$. 393

9.13 The time evolution plots of the *CI* (left) and *Cro* (right) protein concentrations when the system initialized at $(x(0), y(0)) = (35, 18)$ undergoes a transition from the $\gamma_y = 0.008$ mode (dashed lines) to the $\gamma_y = 0.06$ mode at $t = 20$ and converges (solid lines) to the lysogenic steady-state. The *CI* degradation rate is fixed at $\gamma_x = 0.05$. 394

9.14 A phase plot showing the system undergoing a transition from the $\gamma_x = 0.05$ mode (dashed trajectory) to the $\gamma_x = 0.004$ at $t = 70$ and converging (solid trajectory) to the lytic steady-state. The *Cro* degradation rate is fixed at $\gamma_y = 0.008$. 395

9.15 The time evolution plots of the *CI* (left) and *Cro* (right) protein concentrations when the system undergoes a transition from the $\gamma_x = 0.05$ mode (dashed lines) to the $\gamma_x = 0.004$ mode at $t = 70$ and converges (solid lines) to the lytic steady-state. The *Cro* degradation rate is fixed at $\gamma_y = 0.008$. 396

9.16 A phase plot showing the system of Eq.9.5 being initialized using $\gamma_x = 0.05$ (dashed trajectory) and undergoing: (a) a decrease in the degradation rate of *CI* protein (to $\gamma_x = 0.004$) at $t = 40$ and (b) an increase in the degradation rate of *CI* protein (to $\gamma_x = 0.1$) at $t = 40$, both leading the state to converge to the lysogenic steady-state. In both cases, the *Cro* degradation rate is fixed at $\gamma_y = 0.008$. 398

9.17 The time evolution plots of the *CI* (left) and *Cro* (right) protein concentrations when the system initialized at $(x(0), y(0)) = (35, 2)$ undergoes a transition from the $\gamma_x = 0.05$ mode (dashed lines) to the $\gamma_x = 0.004$ mode at $t = 40$ and converges (solid lines) to the lytic steady-state. The *Cro* degradation rate is fixed at $\gamma_y = 0.008$. 399

9.18 The time evolution plots of the *CI* (left) and *Cro* (right) protein concentrations when the system initialized at $(x(0), y(0)) = (35, 2)$ undergoes a transition from the $\gamma_x = 0.05$ mode (dashed lines) to the $\gamma_x = 0.1$ mode at $t = 40$ and converges (solid lines) to the lytic steady-state. The *Cro* degradation rate is fixed at $\gamma_y = 0.008$. 400

10.1 Dependence of the set of feasible initial conditions, for a_1, on actuator location for $u_{max} = 1.4$. 418

10.2 Closed-loop temperature (top) and manipulated input (bottom) profiles for $u_{max} = 1.4$, $z_c = 0.5\pi$, $a_1(0) = 0.7$, under state feedback. . . . 419

10.3 Closed-loop temperature profile for $u_{max} = 1.4$, $z_c = 0.25\pi$, $a_1(0) = 0.7$ under state feedback. 420

10.4 Closed-loop temperature (top) and manipulated input (bottom) profiles for $u_{max} = 1.4$, $z_c = 0.5\pi$, $a_1(0) = 0.7$, under output feedback. . . 421

10.5 Closed-loop temperature profile for $u_{max} = 1.4$, $z_c = 0.25\pi$, $a_1(0) = 0.7$, under output feedback. 422

11.1 Controlled output (crystal concentration) and manipulated input (solute concentration) profiles under PI control in the absence of input constraints. 432

11.2 Controlled output (crystal concentration) and manipulated input (solute concentration) profiles under PI control when $u \in [0, 2]$ (dashed lines) and when $u \in [0, 6]$ (solid lines). 433

11.3 Admissible set-points for crystal concentration for $u \in [0, 6]$. 444

11.4 Controlled output and manipulated input profiles for the crystallizer moment model under the bounded nonlinear controller, for $u \in [0, 6]$ and an initial condition satisfying Eq.11.27. 457

11.5 Controlled output and manipulated input profiles for the crystallizer moment model under the bounded nonlinear controller, for $u \in [0, 6]$ and an initial condition violating Eq.11.27. 458

11.6 Controlled output, manipulated input, and crystal size distribution profiles for the crystallizer process model of Eq.11.4 under the bounded nonlinear controller (solid line) and the PI controller (dashed line) for 0.4 increase in the set-point and $u \in [0, 6]$. 464

11.7 Controlled output, manipulated input, and crystal size distribution evolution profiles for the crystallizer process model of Eq.11.4 under the bounded nonlinear controller, for 0.4 increase in the set-point, in the presence of 5% modeling error in both F and τ, and $u \in [0, 6]$. . . 466

11.8 Controlled output, manipulated input, and crystal size distribution evolution profiles for the crystallizer process model of Eq.11.4 under the bounded nonlinear controller, for 0.4 increase in the set-point, in the presence of actuator and sensor unmodeled dynamics and $u \in [0, 6]$. 468

12.1 Comparison between the control structures arising in (a) the classical control, and (b) the hybrid control paradigms of spatially-distributed systems. 471

12.2 (a) Stability region as a function of actuator location for $u_{max} = 1.4$, (b) Closed-loop dimensionless temperature profile (state feedback) for $a_1(0) = 0.78$ when actuator A is used without switching, (c) Corresponding manipulated input profile. 492

12.3 (a) Closed-loop dimensionless temperature profile (state feedback) for $a_1(0) = 0.78$ when actuator A fails at $t = 1.25$ and actuator B is activated, (b) Closed-loop dimensionless temperature profile (state feedback) for $a_s(0) = 0.78$ when actuator A fails at $t = 1.75$ and actuator B is activated, (c) Corresponding manipulated input profiles for case a (solid) and case b (dashed). 494

12.4 (a) Stability region as a function of actuator location for $u_{max} = 2.5$ (solid) and $u_{max} = 0.5$ (dashed),(b) Closed-loop dimensionless temperature profile (state feedback) for $a_1(0) = 1.3$ when actuator A fails at $t = 1.4$ and actuator C is activated, (c) Closed-loop dimensionless temperature profile (state feedback) for $a_1(0) = 1.3$ when actuator A fails at $t = 1.4$ and actuator B is activated, (d) Corresponding manipulated input profiles for case b (solid) and case c (dashed). 496

12.5 (a) Closed-loop dimensionless temperature profile (output feedback) for $a_1(0) = 1.3$ when actuator A fails at $t = 1.4$ and actuator C is activated, (b) Closed-loop dimensionless temperature profile (output feedback) for $a_1(0) = 1.3$ when actuator A fails at $t = 1.4$ and actuator B is activated, (c) Corresponding manipulated input profiles for case a (solid) and case b (dashed). 498

12.6 Spatiotemporal evolution of the dimensionless tubular reactor temperature profile in the open-loop system. 500

12.7 (a) Controlled output profiles when actuator A ($u_{max} = 0.06$, $z_A = 0$) operates without failure (solid) and when it fails at $t = 0.875$ without activating any of the backup actuators (dashed), (b) Corresponding manipulated input profiles, (c) Closed-loop dimensionless temperature profile when actuator A operates without failure, (d) Closed-loop dimensionless temperature profile when actuator A fails at $t = 0.875$ without activating any of the backup actuators. 503

12.8 (a) Controlled output profiles for the case when actuator A (u_{max} = 0.06, $z_A = 0$) fails at $t = 0.875$ and actuator B ($u_{max} = 0.06$, z_B = 0.2) is activated (solid) and for the case when actuator C (u_{max} = 0.02, $z_C = 0.8$) is activated (dashed) instead of B, (b) Corresponding manipulated input profiles, (c) Closed-loop dimensionless temperature profile when actuator A fails at $t = 0.875$ and actuator B is activated, (d) Closed-loop dimensionless temperature profile when actuator A fails at $t = 0.875$ and actuator C is activated. 504

13.1 Open-loop spatiotemporal profile of $U(z,t)$ for $\nu = 0.2$. 523

13.2 (a) Evolution of the norm of the fast modes, $a_f = [a_3, \cdots, a_{30}]$, and of the two dominant modes, a_1 and a_2, for $\nu = 1.2$. (b) Evolution of the norm of the fast modes (in deviation variable form), $a_f^d = [a_3^d, \cdots, a_{30}^d]$, and of the two dominant modes, a_1^d and a_2^d, for $\nu = 0.2$ (all modes are in deviation variable form). 525

13.3 (a) Stability regions for configuration A (solid ellipse) and for configuration B (dashed ellipse), (b) Closed-loop state profile (state feedback) for $(a_1(0), a_2(0)) = (0.2, 1.5)$ using configuration A without switching, (c) Corresponding manipulated input profiles for u_1 (solid) and u_2 (dashed). 528

13.4 (a) Closed-loop state profile (state feedback) for $(a_1(0), a_2(0)) = (0.2, 1.5)$ when configuration A fails at $t = 3.5$ and configuration B is activated, (b) Corresponding manipulated input profiles for u_1 (solid) and u_2 (dashed). 530

13.5 (a) Closed-loop state profile (state feedback) for $(a_1(0), a_2(0)) = (0.2, 1.5)$ when configuration A fails at $t = 5$ and configuration B is activated, (b) Corresponding manipulated input profiles for u_1 (solid) and u_2 (dashed).531

13.6 (a) Stability regions for configuration A (solid ellipse), configuration B (dashed ellipse), and configuration C, (b) Closed-loop state profile (state feedback) for $(a_1(0), a_2(0)) = (0.2, 1.5)$ when configuration A fails at $t = 3.5$ and configuration C is activated, (b) Corresponding manipulated input profiles for u_1 (solid) and u_2 (dashed). 533

13.7 (a) Closed-loop state profile (state feedback) for $(a_1(0), a_2(0)) = (0.2, 1.5)$ when configuration A fails at $t = 3.5$ and configuration B is activated, (b) Corresponding manipulated input profiles for u_1 (solid) and u_2 (dashed). 534

13.8 (a) Closed-loop state profile (output feedback) for $(a_1(0), a_2(0)) = (0.2, 1.5)$ when configuration A fails at $t = 3.5$ and configuration B is activated, (b) Corresponding manipulated input profiles for u_1 (solid) and u_2 (dashed). 535

13.9 (a) Closed-loop state profile (output feedback) for $(a_1(0), a_2(0)) = (0.2, 1.5)$ when configuration A fails at $t = 5$ and configuration B is activated, (b) Corresponding manipulated input profiles for u_1 (solid) and u_2 (dashed). 536

List of Tables

2.1 Process parameters and steady-state values for the reactor of Eq.2.47. 60

3.1 Process parameters and steady-state values for the reactor of Eq.3.4. 81

4.1 Process parameters and steady-state values for the reactor of Eq.4.15. 124

4.2 Process parameters and steady-state values for the reactor of Eq.4.22. 144

5.1 Process parameters and steady–state values for the reactor of Eq.5.33. 218

6.1 Process parameters and steady–state values for the reactor of Eq.6.18. 247

6.2 Process parameters and steady–state values for the reactor of Eq.6.41. 276

7.1 Process parameters and steady-state values for the reactor of Eq.7.5. 293

8.1 Process parameters and steady–state values for the reactors of Eq.8.2. 327

8.2 Process parameters and steady–state values for the reactor of Eq.8.13. 345

9.1 Parameter values for the cell cycle model in Eq.9.4. 373

9.2 Steady-state values (u_s, v_s) for the cell cycle model for different values of k_2', k_2'', k_{wee}. 373

9.3 Parameter values for the bacteriophage λ model in Eq.9.5. 384

9.4 Steady-state values (x_s,y_s) for the lysogenic, lytic and unstable states for different values of γ_x and γ_y. 385

11.1 Process parameters and dimensionless variables for the crystallizer model of Eq.11.4. 430

11.2 Initial conditions and controller parameters for the implementation on the crystallizer moment model. 456

11.3 Controller parameters for the implementation on the infinite-dimensional crystallizer model. 463

ACKNOWLEDGMENTS

I am grateful to my advisor, Professor Panagiotis Christofides, for his guidance and support in the course of my doctoral work.

I would like to thank Professor Vasilios Manousiouthakis, Professor James Liao, Professor Selim Senkan, and Professor Paul Wang for agreeing to participate in my examination committee.

Special acknowledgments to my family for their constant support, encouragement, and dedication.

VITA

October 21, 1972	Born, Kuwait City, Kuwait
1998	B.Sc., Chemical Engineering University of California, Los Angeles Los Angeles, CA
1997-1998	Outstanding Bachelor of Science Award School of Engineering and Applied Science University of California, Los Angeles
1997-1998	Outstanding Bachelor of Science Award Department of Chemical Engineering University of California, Los Angeles
1998-2002	Chancellor's Fellowship University of California, Los Angeles
1998-2004	Teaching and Research Assistant Department of Chemical Engineering University of California, Los Angeles
1999-2000	Teaching Assistant of the year Award American Institute of Chemical Engineers UCLA Student Chapter
2000	Best Presentation Session Award, session FP10 American Control Conference, Chicago, IL
2001-2002	Doctoral Dissertation Fellowship University of California, Los Angeles
2003	Best Presentation Session Award, session FM18 American Control Conference, Denver, CO
2003-2004	Outstanding Ph.D Student Award Department of Chemical Engineering University of California, Los Angeles
2003-2004	The Edward K. Rice Outstanding Doctoral Student Award UCLA Engineering Alumni Association
2004	Best Presentation Session Award American Control Conference, Boston, MA

PUBLICATIONS AND PRESENTATIONS

El-Farra, N. H., Armaou, A., and Christofides, P. D. (November 1999). Analysis and Control of Parabolic PDEs with Input Constraints. *American Institute of Chemical Engineers Annual Meeting*, paper 208ag, Dallas, TX.

El-Farra, N. H., and Christofides, P. D. (November 1999). Integrating Robustness, Optimality and Constraints in Control of Nonlinear Processes. *American Institute of Chemical Engineers Annual Meeting*, paper 228g, Dallas, TX.

El-Farra, N. H., Christofides P. D. (2000). Robust Optimal Control and Estimation of Constrained Nonlinear Processes. *Computers & Chemical Engineering*, 24:801-807.

El-Farra, N. H., and Christofides, P. D. (November 2000). Bounded Robust Control of Constrained Multivariable Nonlinear Processes. *American Institute of Chemical Engineers Annual Meeting*, paper 250a, Los Angeles, CA.

El-Farra, N. H., and Christofides, P. D. (November 2000). Nonlinear Control of Combined Discrete-Continuous Processes Using Multiple Lyapunov Functions. *American Institute of Chemical Engineers Annual Meeting*, paper 253b, Los Angeles, CA.

El-Farra, N. H., and Christofides, P. D. (2001). Robust Near-Optimal Output Feedback Control of Nonlinear Systems. *International Journal of Control*, 74:133-157.

El-Farra, N. H., and Christofides, P. D. (2001). Integrating Robustness, Optimality and Constraints in Control of Nonlinear Processes. *Chemical Engineering Science*, 56:1841-1868.

El-Farra, N. H., Chiu, T., and Christofides, P. D. (2001). Analysis and Control of Particulate Processes with Input Constraints. *AIChE Journal*, 47:1849-1865.

El-Farra, N. H., and Christofides, P. D. (May 2001). Constrained Control of Size Distribution in Particulate Processes Using Population Balances. *1st Southern California Applied Mathematics Workshop*, California Institute of Technology.

El-Farra, N. H., and Christofides, P. D. (June 2001). Some New Results on Lyapunov-based Control of Nonlinear Systems. *2nd Southern California Nonlinear Control*

Workshop, University of California, San Diego.

El-Farra, N. H., and Christofides, P. D. (November 2001). A Practical Approach for Nonlinear Controller Design and Estimation under Uncertainty and Constraints. *American Institute of Chemical Engineers Annual Meeting*, paper 286a, Reno, NV.

El-Farra, N. H., and Christofides, P. D. (November 2001). Integrating Feedback and Switching for Control of Spatially Distributed Systems. *American Institute of Chemical Engineers Annual Meeting*, paper 287h, Reno, NV.

El-Farra, N. H., and Christofides, P. D. (November 2001). Integrating Feedback and Switching for Control of Spatially Distributed Systems. *American Institute of Chemical Engineers Annual Meeting*, paper 287h, Reno, NV.

El-Farra, N. H., and Christofides, P. D. (2002). Switching and Feedback Laws for Control of Constrained Switched Nonlinear Systems. *Lecture Notes in Computer Science Series*, C. J. Tomlin and M. R. Greenstreet (Eds.), 2289:164-178, Springer-Verlag, Berlin.

El-Farra, N. H., and Christofides, P. D. (2002). Nonlinear Process Control: Novel Controller Designs for Chemical Processes with Uncertainty and Constraints. *Chemical Process Control-6*, AIChE Symposium Series, J. B. Rawlings, B. A. Ogunnaike and J. W. Eaton (Eds.), 98:369-373.

El-Farra, N. H., and Christofides, P. D. (May 2002). Integrating Feedback and Switching for Control of Parabolic PDE Systems. *2nd Southern California Applied Mathematics Workshop*, University of California, Los Angeles.

El-Farra, N. H., and Christofides, P. D. (July 2002). Coordinated Feedback and Switching for Robust Control of Nonlinear Switched Systems. *Society of Industrial and Applied Mathematics 50th Annual Meeting*, Philadelphia, Pennsylvania.

El-Farra, N. H., and Christofides, P. D. (November 2002). Coordinating Supervisory Control and Feedback in Hybrid Process Systems. *American Institute of Chemical Engineers Annual Meeting*, paper 260f, Indianapolis, IN.

El-Farra, N. H., and Christofides, P. D. (November 2002). Uniting Bounded Control

and MPC for Stabilization of Constrained Linear Systems: Output Feedback. *American Institute of Chemical Engineers Annual Meeting*, paper 252e, Indianapolis, IN.

El-Farra, N. H., and Christofides, P. D. (November 2002). Hybrid Control of Spatially-Distributed Processes. *American Institute of Chemical Engineers Annual Meeting*, paper 257b, Indianapolis, IN.

Ray, P., El-Farra, N. H., and Christofides, P. D. (November 2002). Fault-Tolerant Control of Flows: Coordinating Feedback and Switching. *American Institute of Chemical Engineers Annual Meeting*, paper 256c, Indianapolis, IN.

El-Farra, N. H., Armaou, A., and Christofides, P. D. (2003). Analysis and Control of Parabolic PDE Systems with Input Constraints. *Automatica*, 39:715-725.

El-Farra, N. H., Christofides, P. D., and Liao J. C. (2003). Analysis of Nitric Oxide Consumption by Erythrocytes in Blood Vessels Using a Distributed Multi-cellular Model. *Annals of Biomedical Engineering*, 31:294-309.

El-Farra, N. H., and Christofides, P. D. (2003). Bounded Robust Control of Constrained Multivariable Nonlinear Processes. *Chemical Engineering Science*, 58:3025-3047.

El-Farra, N. H., and Christofides, P. D. (2003). Hybrid Control of Parabolic PDEs: Handling Faults of Constrained Control Actuators. *Lecture Notes in Computer Science Series*, O. Maler and A. Pneuli (Eds.), 2623:172-187, Springer-Verlag, Berlin.

El-Farra, N. H., and Christofides, P. D. (2003). Coordinating Feedback and Switching for Control of Hybrid Nonlinear Processes. *AIChE Journal*, 49:2079-2098.

El-Farra, N. H., Lou, Y., and Christofides, P. D. (2003). Fault-Tolerant Control of Fluid Dynamic Systems via Coordinated Feedback and Switching. *Computers & Chemical Engineering*, 27:1913-1924.

El-Farra, N. H., and Christofides, P. D. (2003). Robust Inverse Optimal Control Laws for Nonlinear Systems. *International Journal of Robust & Nonlinear Control*, 13:1371-1388.

El-Farra, N. H., Mhaskar, P., and Christofides, P. D. (October 2003). Hybrid Predictive Control of Nonlinear Systems. *6th Southern California Nonlinear Control Workshop*, University of California, San Diego.

Mhaskar, P., El-Farra, N. H., and Christofides, P. D. (October 2003). Predictive Control of Switched Nonlinear Systems. *7th Southern California Nonlinear Control Workshop*, University of Southern California, Los Angeles.

El-Farra, N. H., Christofides, P. D., and Liao, J. C. (November 2003). Computational Modeling and Simulation of Nitric Oxide Transport and Consumption in Blood Vessels. *American Institute of Chemical Engineers Annual Meeting*, paper 127b, San Francisco, CA.

El-Farra, N. H., and Christofides, P. D. (November 2003). Analysis of Biological Regulatory Networks using Hybrid Systems Theory. *American Institute of Chemical Engineers Annual Meeting*, paper 463h, San Francisco, CA.

El-Farra, N. H., Gani, A., and Christofides, P. D. (November 2003). Fault-Tolerant Control of Nonlinear Process Systems: Integrating Optimal Actuator/Sensor Placement, Feedback and Supervisory Control. *American Institute of Chemical Engineers Annual Meeting*, paper 440b, San Francisco, CA.

El-Farra, N. H., Mhaskar, P., and Christofides, P. D. (November 2003). Predictive Control of Hybrid Process Systems. *American Institute of Chemical Engineers Annual Meeting*, paper 439ad, San Francisco, CA.

El-Farra, N. H., Mhaskar, P., and Christofides, P. D. (2004). Uniting Bounded Control and MPC for Stabilization of Constrained Linear Systems. *Automatica*, 40:101-110.

El-Farra, N. H., and Christofides, P. D. (2004). Coordinating Feedback and Switching for Control of Spatially-Distributed Processes. *Computers & Chemical Engineering*, 28:111-128, 2004.

El-Farra, N. H., Mhaskar, P., and Christofides, P. D. (2004). Hybrid Predictive Control of Nonlinear Systems: Method and Applications to Chemical Processes. *International Journal of Robust & Nonlinear Control*, 14:199-225.

Mhaskar, P., El-Farra, N. H., and Christofides, P. D. (2004). Hybrid Predictive Control of Process Systems. *AIChE Journal*, 50:1242-1259.

Mhaskar, P., El-Farra, N. H., and Christofides, P. D. (2004). Robust Hybrid Predictive Control of Nonlinear Systems. *Automatica*, accepted for publication.

Shi, D., El-Farra, N. H., Li, M., Mhaskar, P., and Christofides, P. D. (2004). Predictive Control of Particle Size Distribution in Particulate Processes. *Proceedings of 2nd International Conference on Population Balance Modeling*, 17 pages, Valencia, Spain.

El-Farra, N. H., Gani, A., and Christofides, P. D. (2004). Fault-Tolerant Control of Multi-unit Process Systems Using Communication Networks. *Proceedings of 7th IFAC Symposium on Dynamics and Control of Process Systems*, 6 pages, Cambridge, MA.

Mhaskar, P., El-Farra, N. H., and Christofides, P. D. (2004). Predictive Control of Switched Nonlinear Processes with Scheduled Mode Transitions. *Proceedings of 7th IFAC Symposium on Dynamics and Control of Process Systems*, 6 pages, Cambridge, MA.

El-Farra, N. H., Mhaskar, P., and Christofides, P. D. (2004). A Hybrid Predictive Control Approach for Output Feedback Stabilization of Constrained Linear Systems. *Proceedings of American Control Conference*, pp. 578-583, Boston, MA.

Mhaskar, P., El-Farra, N. H., and Christofides, P. D. (2004). A Method For PID Controller Tuning Using Nonlinear Control Techniques. *Proceedings of American Control Conference*, pp. 2925-2930, Boston, MA.

Mhaskar, P., El-Farra, N. H., and Christofides, P. D. (2004). Stabilization of Switched Nonlinear Systems Using Predictive Control. *Proceedings of American Control Conference*, pp. 560-565, Boston, MA.

Dubljevic, S., El-Farra, N. H., Mhaskar, P., and Christofides, P. D. (2004). Predictive Control of Parabolic PDEs with State and Control Constraints. *Proceedings of American Control Conference*, pp. 254-260, Boston, MA.

ABSTRACT OF THE DISSERTATION

Control of Nonlinear and Hybrid Process Systems:
Designs for Uncertainty and Constraints

by

Nael H. El-Farra
Doctor of Philosophy in Chemical Engineering
University of California, Los Angeles, 2004

Professor Panagiotis D. Christofides, Chair

The increased emphasis placed on safe and efficient plant operation dictates the need for advanced process control and monitoring systems that account for a host of fundamental and practical problems arising in chemical processes. Central to these problems are the issues of strong nonlinear behavior, model uncertainty, control actuator constraints and coupled discrete-continuous (hybrid) dynamics. While the co-presence of uncertainty and constraints is known to create a conflict in the control design objectives, at this stage, there is no rigorous, yet practical, approach for nonlinear controller design that accounts explicitly and simultaneously for the effects of uncertainty and constraints. Furthermore, process control research has focused predominantly on continuous dynamic processes modeled by ordinary differential equations, while there are many instances when the overall process response depends on a rather intricate interaction between discrete and continuous variables. Examples of discrete events in chemical processes include inherent physico-chemical discontinuities

such as phase changes and flow reversals, instrumentation with discrete settings such as binary sensors and on/off valves, logic-based switching for supervisory and safety control tasks, and actuator/sensor faults. Processes with strong discrete-continuous interactions cannot be effectively controlled with existing control techniques that do not account for the presence of discrete events.

Motivated by the above considerations, this doctoral thesis develops a general and practical framework for the analysis and control of nonlinear and hybrid process systems with uncertainty and constraints. For continuous dynamic nonlinear systems, the proposed framework yields novel Lyapunov-based nonlinear controller designs with well-characterized robustness, optimality and constraint-handling capabilities. For hybrid systems with switched dynamics, the control approach is based on the integrated synthesis, via Lyapunov techniques, of nonlinear feedback controllers with well-characterized stability regions and supervisory switching laws that orchestrate, on the basis of these regions, the transitions between the constituent modes in a way that enforces the desired control objectives in the overall closed-loop system. The proposed controller designs are applied to chemical processes of industrial interest and their effectiveness and advantages over existing control methods is documented through simulations.

Chapter 1

Introduction

1.1 Motivation

The last few decades have witnessed a dramatic change in the chemical process industries. Modern industrial processes have become now highly integrated with respect to material and energy flows, constrained ever more tightly by high quality product specifications, and subject to increasingly strict safety and environmental regulations. These more stringent operating conditions have placed new constraints on the operating flexibility of the process and made the performance requirements for process plants increasingly difficult to satisfy. The increased emphasis placed on safe and efficient plant operation dictates the need for continuous monitoring of the operation of a chemical plant and effective external intervention (control) to guarantee satisfaction of the operational objectives. In this light, it is only natural that the subject of process control has become increasingly important in both the academic and industrial communities. In fact, without process control it would not be possible to operate most modern processes safely and profitably, while satisfying plant quality standards.

The design of effective/advanced process control and monitoring systems that can meet these demands, however, can be quite a challenging undertaking given the host/multitude of fundamental and practical problems that arise in process control systems and transcend the boundaries of specific applications. Although they may vary from one application to another and have different levels of significance, these issues remain generic in their relationship to the control design objectives. Central to these issues is the requirement that the control system provide satisfactory performance in the presence of strong process nonlinearities, model uncertainty, control actuator constraints and combined discrete-continuous (hybrid) dynamics. Process nonlinearities, plant-model mismatch, actuator constraints and hybrid dynamics represent some of the more salient features whose frequently-encountered co-presence in many chemical processes can lead to severe performance deterioration and even closed-loop instability, if not appropriately accounted for in the controller design. In the remainder of this chapter, we highlight the origin and implications of these problems in the context of chemical process control applications and review some of the relevant results in the literature.

1.2 Background on analysis and control of nonlinear systems

The objective of this section is to provide a review of results on nonlinear process control with special emphasis on nonlinear control of chemical processes with uncertainty and constraints. This review is not intended to be exhaustive; its objective is to provide the necessary background for the results of this thesis. For smoothness of the flow of the chapter, review of results on the analysis and control of continuous-time process systems with discrete events is deferred to Section 1.4 below.

Many chemical processes, including high purity distillation columns, highly exother-

mic chemical reactors, and batch systems, are inherently nonlinear and cannot be effectively controlled and monitored with controllers and estimators designed on the basis of approximate linear or linearized process models. Typical sources of nonlinear behavior arising in chemical processes include complex reaction mechanisms, the Arrhenius temperature dependence of reaction rates, and radiative heat transfer phenomena, to name a few. The limitations of traditional linear control and estimation methods in dealing with nonlinear chemical processes have become increasingly apparent as chemical processes may be required to operate over a wide range of conditions due to large process upsets or set point changes. Motivated by this, the area of nonlinear process control has been one of the most active research areas within the chemical engineering community over the last two decades. The main bulk of the research has focused on nonlinear lumped parameter processes (i.e., processes described by systems of nonlinear ordinary differential equations (ODEs)), where important contributions have been made including the synthesis of state feedback controllers [141, 180, 182, 136, 163]; the design of state estimators [162, 280, 275, 274, 164] and output feedback controllers [74, 73, 279, 190, 60]; the synthesis of well-conditioned controllers for nonlinear multiple-time-scale systems [65, 66, 59, 60]; the synthesis of controllers for time-delay systems [184, 135, 13, 14, 15, 286]; the analysis and control of nonlinear systems using functional expansions [35, 129, 130]; control design using concepts from thermodynamics [7, 321, 320, 105, 127]; and the design of nonlinear model predictive controllers [322, 252, 121, 231, 305, 215, 144, 176, 109, 264, 242, 265, 246, 268, 323]. Successful experimental applications of the above nonlinear control methods to lumped parameter chemical processes have been also reported including control of distillation columns [201], polymerization reactors [272, 281, 282], pH neutralization processes [312, 313, 230] and anaerobic digestion processes [256]. Excellent reviews of results in the area of nonlinear process control can be found in

[181, 182, 179, 39, 3, 250, 195, 136].

In addition to nonlinear behavior, many industrial process models are characterized by the presence of time-varying uncertainties such as unknown process parameters and external disturbances which, if not accounted for in the controller design, may cause performance deterioration and even closed-loop instability. Motivated by the problems caused by model uncertainty on the closed-loop behavior, the problem of designing controllers for nonlinear systems with uncertain variables, that enforce stability and output tracking in the closed-loop system, has received significant attention in the past. For feedback linearizable nonlinear systems with constant uncertain variables, adaptive techniques have been employed to design controllers that enforce asymptotic stability and output tracking (see, for example, [262, 292, 156, 211, 186, 34, 86, 318]). On the other hand, for feedback linearizable nonlinear systems with time-varying uncertain variables that satisfy the so-called matching condition, Lyapunov's direct method has been used to design robust state feedback controllers that enforce boundedness and arbitrary degree of asymptotic attenuation of the effect of uncertainty on the output (e.g., [183, 20, 199, 243, 4, 68, 64]; a review of results on controller design via Lyapunov's direct method can be found in [70, 199]). More recently, robust output feedback controllers have been also designed through combination of robust state feedback controllers with high-gain observers [168, 210, 60].

While the above works provide systematic methods for adaptive and robust control design, they do not lead in general to controllers that are optimal with respect to a meaningful cost (i.e., these controllers do not guarantee achievement of the control objectives with the smallest possible control action). This is an important limitation especially in light of the fact that the capacity of control actuators used to regulate

chemical processes is almost always limited. Such limitations arise typically due to the finite capacity of control actuators (e.g., bounds on the magnitude of the opening of valves). Input constraints restrict our ability to freely modify the dynamic behavior of a chemical process and compensate for the effect of model uncertainty through high-gain feedback control. The ill-effects due to actuator constraints manifest themselves, for example, in the form of sluggishness of response and loss of stability. Additional problems that arise in the case of dynamic controllers include undesired oscillations and overshoots, a phenomenon usually referred to as "windup". The problems caused by input constraints have consequently motivated many studies on the dynamics and control of chemical processes subject to input constraints. Notable contributions in this regard include controller design and stability analysis within the model predictive control framework [192, 71, 302, 246, 268, 263], constrained linear [56] and nonlinear [57] quadratic-optimal control, the design of anti-windup schemes in order to prevent excessive performance deterioration of an already designed controller when the input saturates [174, 161, 166, 232, 48, 300, 158], the study of the nonlinear bounded control problem for a class of two and three state chemical reactors [12, 11], the characterization of regions of closed-loop stability under static state feedback linearizing controllers [157], and some general results on the dynamics of constrained nonlinear systems [159]. However, these control methods do not explicitly account for robust uncertainty attenuation.

An approach to address the design of robust optimal controllers is within the nonlinear H_∞ control framework (e.g., [303, 234]). However, the practical applicability of this approach is still questionable because the explicit construction of the controllers requires the analytic solution of the steady-state Hamilton-Jacobi-Isaacs (HJI) equation which is not a feasible task except for simple problems. An alternative approach

to robust optimal controller design which does not require solving the HJI equation is the inverse optimal approach proposed originally by Kalman [155] and introduced recently in the context of robust stabilization in [112]. Inverse problems have a long history in control theory (e.g., see [155, 296, 226]). The central idea of the inverse optimal approach is to compute a robust stabilizing control law together with the appropriate penalties that render the cost functional well-defined and meaningful in some sense. This approach provides a convenient route for robust optimal controller design and is well-motivated by the fact that the closed-loop robustness achieved as a result of controller optimality is largely independent of the specific choice of the cost functional [271] so long as this cost functional is a meaningful one. The appealing features of the inverse optimal approach have motivated its use for the design of robust optimal controllers in [111, 112, 185]. These controllers, however, do not lead to an arbitrary degree of attenuation of the effect of uncertainty on the closed-loop output. This is a particularly desirable feature in the case of non-vanishing uncertainty that changes the nominal equilibrium point of the system. Results on robust optimal control of chemical processes have been also derived within a model predictive control framework [25, 26, 323, 263].

Summarizing, a close look at the available literature reveals that the existing process control methods lead to the synthesis of controllers that can deal with either model uncertainty or input constraints, but not simultaneously and effectively with both. This inability clearly limits the achievable control quality and closed-loop performance, especially in light of the frequently-encountered simultaneous presence of uncertainty and constraints in chemical processes. Therefore, the development of a unified framework for control of nonlinear systems that explicitly accounts for the presence of model uncertainty and input constraints is expected to have a significant

impact on process control.

1.3 Examples of nonlinear chemical processes

1.3.1 Non-isothermal continuous stirred tank reactors

Consider two well–mixed, non–isothermal continuous stirred tank reactors (CSTRs) in series, where three parallel irreversible elementary exothermic reactions of the form $A \xrightarrow{k_1} B$, $A \xrightarrow{k_2} U$ and $A \xrightarrow{k_3} R$ take place, where A is the reactant species, B is the desired product and U, R are undesired byproducts. The feed to CSTR 1 consists of pure A at flow rate F_0, molar concentration C_{A0} and temperature T_0, and the feed to CSTR 2 consists of the output of CSTR 1 and an additional fresh stream feeding pure A at flow rate F_3, molar concentration C_{A03} and temperature T_{03}. Due to the non–isothermal nature of the reactions, a jacket is used to remove/provide heat to both reactors. Under standard modeling assumptions, a mathematical model of the plant can be derived from material and energy balances and takes the following form:

$$\begin{aligned}
\frac{dT_1}{dt} &= \frac{F_0}{V_1}(T_0 - T_1) + \sum_{i=1}^{3}\frac{(-\Delta H_i)}{\rho c_p}R_i(C_{A1}, T_1) + \frac{Q_1}{\rho c_p V_1} \\
\frac{dC_{A1}}{dt} &= \frac{F_0}{V_1}(C_{A0} - C_{A1}) - \sum_{i=1}^{3}R_i(C_{A1}, T_1) \\
\frac{dT_2}{dt} &= \frac{F_1}{V_2}(T_1 - T_2) + \frac{F_3}{V_2}(T_{03} - T_2) + \sum_{i=1}^{3}\frac{(-\Delta H_i)}{\rho c_p}R_i(C_{A2}, T_2) + \frac{Q_2}{\rho c_p V_2} \\
\frac{dC_{A2}}{dt} &= \frac{F_1}{V_2}(C_{A1} - C_{A2}) + \frac{F_3}{V_2}(C_{A03} - C_{A2}) - \sum_{i=1}^{3}R_i(C_{A2}, T_2)
\end{aligned} \tag{1.1}$$

where $R_i(C_{Aj}, T_j) = k_{i0}\exp\left(\frac{-E_i}{RT_j}\right)C_{Aj}$, for $j = 1, 2$. T, C_A, Q, and V denote the temperature of the reactor, the concentration of species A, the rate of heat input/removal from the reactor, and the volume of reactor, respectively, with subscript 1 denoting CSTR 1 and subscript 2 denoting CSTR 2. ΔH_i, k_i, E_i, $i = 1, 2, 3$,

denote the enthalpies, pre–exponential constants and activation energies of the three reactions, respectively, c_p and ρ denote the heat capacity and density of the reactor. The above model consists of a set of continuous-time nonlinear differential equations; note in particular the nonlinear dependence of the reaction rates, $R_i(C_{Aj}, T_j)$, on reactor temperature. The above system typically exhibits steady-state multiplicity. For example, using typical values for the process parameters (see Chapter 8), the system describing the first CSTR, with $Q_1 = 0$, has three steady–states: two locally asymptotically stable and one unstable. The unstable steady–state of the first CSTR also corresponds to three steady–states for the second CSTR (with $Q_2 = 0$), one of which is unstable.

A typical control problem for this process is to regulate the reactor temperature and/or reactant concentration by manipulating the rate of heat input subject to constraints. Typical sources of uncertainty include external time-varying disturbance in the feed temperature and/or inlet reactant concentration as well as parametric uncertainty in the heat of reaction.

1.3.2 Isothermal continuous crystallizer

Consider the following fifth-order nonlinear model describing the evolution of the first four moments of the crystal size distribution, and the solute concentration, in an isothermal continuous crystallizer:

$$\begin{aligned} \dot{x}_0 &= -x_0 + (1 - x_3) Da \exp\left(\frac{-F}{y^2}\right) \\ \dot{x}_1 &= -x_1 + y x_0 \\ \dot{x}_2 &= -x_2 + y x_1 \\ \dot{x}_3 &= -x_3 + y x_2 \\ \dot{y} &= \frac{1 - y - (\alpha - y) y x_2}{1 - x_3} + \frac{u}{1 - x_3} \end{aligned} \tag{1.2}$$

where x_i, $i = 0, 1, 2, 3$, are dimensionless moments of the crystal size distribution, y is a dimensionless concentration of the solute in the crystallizer, and u is a dimensionless concentration of the solute in the feed (the reader may refer to [54, 89] for a detailed process description, population balance modeling of the crystal size distribution and derivation of the moments model, and to [62] for further results and references in this area). In the above process model, a primary source of nonlinearity comes from the Arrhenius-like type dependence of the nucleation rate on the solute concentration. Using typical values of the dimensionless process parameters: $F = 3.0$, $\alpha = 40.0$ and $Da = 200.0$, it can be shown that, at the nominal operating condition of $u^{nom} = 0$, the above system has an unstable equilibrium point surrounded by a stable limit cycle. The open-loop behavior of the crystallizer is therefore characterized by sustained oscillations. A typical control objective is to suppress the oscillations and stabilize the system at the unstable equilibrium point (corresponding to a desired crystal size distribution) by manipulating the solute feed concentration, u, subject to constraints.

1.4 Background on analysis control of hybrid systems

Traditionally, most of the research work in process control has been concerned predominantly with the control of continuous dynamic processes described by ordinary differential equations. Yet, there are many examples of chemical and biological processes where the dynamical properties of the system depend on a rather intricate interaction between discrete and continuous variables. These are referred to as hybrid processes because they involve coupled continuous dynamics and discrete events that together drive the overall system response in time and space. In many of these applications, the continuous behavior often arises as a manifestation of the underlying physical laws governing the process, such as momentum, mass, and energy conser-

vation, and is modeled by continuous-time differential equations. Discrete behavior, on the other hand, is ubiquitously multi-faceted and can originate from a variety of sources, including: (1) inherent physico-chemical discontinuities in the continuous process dynamics, such as phase changes, flow reversals, shocks and transitions, (2) the use of measurement sensors and control actuators with discrete settings/positions (e.g., binary sensors, on/off valves, pumps, heatings with constant current, motors with speed control), and (3) the use of logic-based switching for supervisory and safety control tasks.

Another common source of hybrid behavior in chemical processes comes from the interaction of the process with its operating environment. Changes in raw materials, energy sources, and product specifications, together with fluctuations in market demands, forecasts and the concomitant adjustments in management decisions, lead invariably to the superposition of discrete events on the basically continuous process dynamics, in the form of controlled transitions between different operational regimes. Regardless of whether the hybrid (combined discrete-continuous) behavior arises as an inherent feature of the process itself, its operation, or its control system, the overall process behavior in all of these instances is characterized by structurally different dynamics in different situations (regimes), and is, therefore, more appropriately viewed as intervals of piecewise continuous behavior (corresponding to material and energy flows) interspersed by discrete transitions governed by a higher-level decision-making entity.

The traditional approach of dealing with these systems in many areas of industrial control has been to separate the continuous control from the discrete control. In recent years, however, it has become increasingly evident that the interaction of discrete events with even simple continuous dynamics can lead to complex unpredictable dy-

namics and, consequently, to very undesirable outcomes (particularly in safety-critical applications) if not explicitly accounted for in the control system design. As efficient and profitable process operation becomes more dependent on the control system, the need to design flexible, reliable and effective control systems that can explicitly handle the intermixture of continuous and discrete dynamics, is increasingly apparent. Such flexibility and responsiveness play a critical role in achieving optimum production rates, high-quality products, minimizing waste to the environment and operating as efficiently as possible. These considerations, together with the abundance of hybrid phenomena in chemical processes, provide a strong motivation for the development of analytical tools and systematic methods for the analysis and control of these systems in a way that explicitly captures the combined discrete-continuous interactions and their effects.

Even though tools for the analysis and control of purely continuous-time processes exist and, to a large extent, are well-developed, similar techniques for combined discrete-continuous systems are limited at present primarily due to the difficulty of extending the available concepts and tools to account for the hybrid nature of these systems and their changing dynamics, which makes them more difficult to describe, analyze, or control. These challenges, coupled with the abundance of hybrid phenomena in many engineering systems in general, have fostered a large and growing body of research work on a diverse array of problems, including the modeling (e.g., [315, 33]), simulation (e.g., [33]), optimization (e.g., [126]), stability analysis (e..g, [138, 81]), and control (e.g., [37, 145, 177, 104]) of several classes of hybrid systems. Continued progress notwithstanding, important theoretical and practical problems remain to be addressed in this area, including the development of a unified and practical approach for control that deals effectively with the co-presence of strong nonlinearities

in the continuous dynamics, model uncertainty, actuator constraints, and combined discrete-continuous interactions.

1.5 Examples of hybrid process systems

1.5.1 Fault-tolerant process control systems

The ability of the control system to deal with failure situations typically requires consideration of multiple control configurations and switching between them to preserve closed-loop stability in the event that the active control configuration fails. The occurrence of actuator faults, and the concomitant switching between different control configurations, give rise to hybrid closed-loop dynamics. As an example, consider a well–mixed, non–isothermal continuous stirred tank reactor where three parallel irreversible elementary exothermic reactions of the form $A \xrightarrow{k_1} B$, $A \xrightarrow{k_2} U$ and $A \xrightarrow{k_3} R$ take place, where A is the reactant species, B is the desired product and U, R are undesired byproducts. The feed to the reactor consists of pure A at flow rate F, molar concentration C_{A0} and temperature T_{A0}. Due to the non–isothermal nature of the reactions, a jacket is used to remove/provide heat to the reactor. Under standard modeling assumptions, a mathematical model of the process can be derived from material and energy balances and takes the following form:

$$\begin{aligned}
\frac{dT}{dt} &= \frac{F}{V}(T_{A0} - T) + \sum_{i=1}^{3} \frac{(-\Delta H_i)}{\rho c_p} k_{i0} \exp\left(\frac{-E_i}{RT}\right) C_A + \frac{Q}{\rho c_p V} \\
\frac{dC_A}{dt} &= \frac{F}{V}(C_{A0} - C_A) - \sum_{i=1}^{3} k_{i0} \exp\left(\frac{-E_i}{RT}\right) C_A \qquad (1.3) \\
\frac{dC_B}{dt} &= -\frac{F}{V} C_B + k_{10} \exp\left(\frac{-E_1}{RT}\right) C_A
\end{aligned}$$

where C_A and C_B denote the concentrations of the species A and B, respectively, T denotes the temperature of the reactor, Q denotes the rate of heat input to the reactor,

V denotes the volume of the reactor, ΔH_i, k_i, E_i, $i = 1, 2, 3$, denote the enthalpies, pre–exponential constants and activation energies of the three reactions, respectively, c_p and ρ denote the heat capacity and density of the reactor. For typical values of the process parameters (see Chapter 8), the process model has three steady–states: two locally asymptotically stable and one unstable.

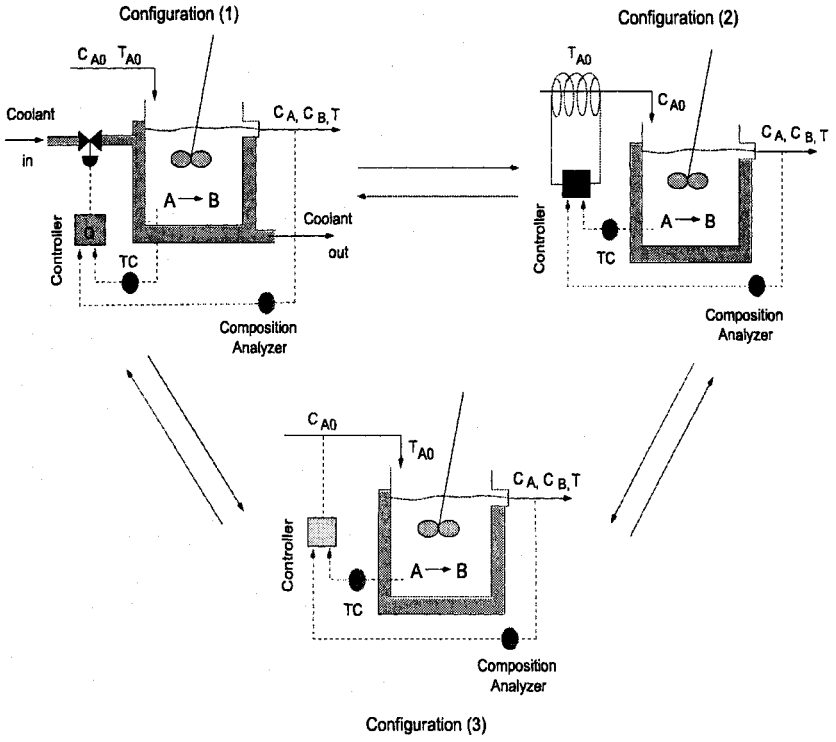

Figure 1.1: Switching between multiple control configurations, each characterized by a different manipulated input, provides a mechanism for fault-tolerant control.

The control objective is to stabilize the reactor at the open–loop unstable steady–state. Operation at this point is typically sought to avoid high temperatures while, simultaneously, achieving reasonable reactant conversion. To accomplish this objective in the presence of control system failures, we consider the following manipulated input candidates (see Figure 1.1):

1. Rate of heat input, $u_1 = Q$, subject to the constraint $|Q| \leq u_{max}^1 = 748\ KJ/s$.

2. Inlet stream temperature, $u_2 = T_{A0} - T_{A0}^s$, subject to the constraint $|u_2| \leq u_{max}^2 = 100\ K$.

3. Inlet reactant concentration, $u_3 = C_{A0} - C_{A0}^s$, subject to the constraint $|u_3| \leq u_{max}^3 = 4\ kmol/m^3$.

Each of the above manipulated inputs represents a continuous control configuration (or control–loop) that, by itself, can stabilize the reactor using available measurements of the reactor temperature, reactant and product concentrations. The first loop involving the heat input, Q, as the manipulated variable is considered as the primary control configuration. In the event of a total failure in this configuration, however, a higher-level supervisor will have to activate one of the other two fall–back configurations in order to maintain closed–loop stability. The main question in this case is typically how to design the supervisory switching logic in order to orchestrate safe transitions between the constituent configurations and guarantee stability of the overall switched closed-loop system.

1.5.2 Switched biological systems

The dynamics of many biological systems often involve switching between many qualitatively different modes of behavior. At the molecular level, for example, the fundamental process of inhibitor proteins turning off the transcription of genes by RNA polymerase reflects a switch between two continuous processes. An example of this is the classic genetic switch observed in the bacteriophage λ, where two distinct behaviors, lysis and lysogeny, each with different mathematical models, are seen. Also, at the cellular level, the cell growth and division in a eukaryotic cell is usually described as a sequence of four processes, each being a continuous process that is triggered by a set of conditions or events. As an example, consider a network of biochemical

reactions, based on cyclin-dependent kinases and their associated proteins, which are involved in cell cycle control in frog egg development. A detailed description of this network is given in [229] where the authors used standard principles of biochemical kinetics and rate equations to construct a nonlinear dynamic model of the network that describes the time evolution of the key species including free cyclin, the M-phase promoting factor (MPF), and other regulatory enzymes. For illustration purposes, we will consider below the simplified network model derived by the authors (focusing only on the positive-feedback loops in the network) which captures the basic stages of frog egg development. The model is given by:

$$\begin{aligned} \frac{du}{dt} &= \frac{k_1'}{G} - \left(k_2' + k_2'' u^2 + k_{wee}\right) u + \left(k_{25}' + k_{25}'' u^2\right)\left(\frac{v}{G} - u\right) \\ \frac{dv}{dt} &= k_1' - (k_2' + k_2'' u^2) v \end{aligned} \tag{1.4}$$

where u is a dimensionless concentration of active MPF and v is a dimensionless concentration of total cyclin, k_2' and k_2'' are rate constants for the low-activity and high activity forms, respectively, of cyclin degradation; k_{25}' and k_{25}'' are rate constants for the low-activity and high activity forms, respectively, of tyrosine dephosphorylation of MPF; k_1' is a rate constant for cyclin synthesis, k_{wee} is the rate constant for inhibition of Wee1, an enzyme responsible for the tyrosine phosphorylation of MPF (which inhibits MPF activity). Bifurcation and phase-plane analysis of the above model [229] shows that, by changing the values of k_2', k_2'' and k_{wee}, the following four modes of behavior are predicted:

- A G2-arrested state (blocked before the G2-M transition) characterized by high cyclin concentration and little MPF activity. This corresponds to a unique, asymptotically stable steady-state ($k_2' = 0.01$, $k_2'' = 10$, $k_{wee} = 3.5$).
- An M-arrested state (blocked before the meta- to anaphase transition) state

with lots of active MPF. This corresponds to a unique, asymptotically stable steady-state ($k_2' = 0.01$, $k_2'' = 0.5$, $k_{wee} = 2.0$).

- An oscillatory state (alternating phases of DNA synthesis and mitosis) exhibiting sustained, periodic fluctuation of MPF activity and total cyclin protein. This corresponds to a stable limit cycle surrounding an unstable equilibrium point ($k_2' = 0.01$, $k_2'' = 10$, $k_{wee} = 2.0$).

- Co-existing stable steady-states of G2 arrest and M arrest. This corresponds to three steady-states; one unstable and two locally asymptotically stable ($k_2' = 0.015$, $k_2'' = 0.1$, $k_{wee} = 3.5$).

The above analysis predicts that the network can be switched between different modes by changes in parameter values. For example, slight increases in k_2', k_{wee}, accompanied by a significant drop in k_2'' (which could be driven, for example, by down-regulation of cyclin degradation) can induce a transition from the oscillatory mode of MPF activity (early embryo stage) to the bi-stable mode. These parameter typically include rate constants and total enzyme concentrations that are under genetic control. Changing the expression of certain genes will change the parameter values of the model and move the network across bifurcation boundaries into regions of qualitatively different behavior. An important question that hybrid systems theory can be used to answer for the above system is how to determine when switching between two modes needs to take place in order to achieve a certain desired steady-state (e.g.,, whether the cell cycle will get arrested in the G2 or the M phase state upon switching from the oscillatory to the bistable mode).

1.6 Objectives and organization of the thesis

Motivated by the fact that many industrially-important processes are characterized by strong nonlinearities, model uncertainty, constraints and combined discrete-continuous dynamics, and the lack of general nonlinear and hybrid control methods for such systems, the broad objectives of the present thesis are:

- To develop a rigorous, yet practical, unified framework for the design of nonlinear feedback control laws for processes modeled by nonlinear systems with uncertain variables and manipulated input constraints, that integrates robustness, optimality, and explicit constraint-handling capabilities in the controller designs and provide an explicit characterization of the stability and performance properties of the designed controllers.

- To develop a general hybrid nonlinear control methodology, for hybrid nonlinear processes with switched, constrained and uncertain dynamics, that integrates the synthesis of lower-level nonlinear feedback controllers with the design of the upper-level supervisor switching logic.

- To provide fundamental understanding and insight into the nature of the control problem for nonlinear and hybrid processes as well as the limitations imposed by nonlinearities, uncertainty, constraints and the coupling of continuous dynamics with discrete events on our ability to steer the dynamics of such systems.

- To illustrate the application of the proposed controller design and analysis methods to chemical and biological systems of practical interest and document their effectiveness and advantages with respect to traditional control methods.

The rest of the thesis is organized as follows. Chapter 2 presents robust inverse optimal controller designs for input/output linearizable nonlinear systems with time-varying bounded uncertain variables. Under full state feedback, the controller designs are obtained by re-shaping the scalar nonlinear gain of Sontag's formula in a way that meets different robustness and optimality objectives under vanishing and non-vanishing uncertainty. Combination of the state feedback controllers with high-gain observers and appropriate saturation filters that eliminate observer peaking is then employed to design dynamic robust output feedback controllers that enforce semi-global closed-loop stability and achieve near-optimal performance, provided that the observer gain is sufficiently large. The implementation of the controllers is illustrated using models of chemical reactors with uncertainty.

Chapter 3 focuses on nonlinear systems of the type considered in Chapter 2, that include both time-varying uncertain variables and manipulated input constraints, and presents a unified framework that integrates robustness, optimality, and explicit constraint-handling capabilities in the controller synthesis. Using a general state-space Lyapunov-based approach, the proposed framework leads to the derivation of explicit analytical formulas for bounded robust nonlinear state feedback controllers with well-characterized stability and performance properties. The proposed controllers are shown to guarantee closed-loop stability and robust asymptotic set-point tracking with an arbitrary degree of attenuation of the effect of uncertainty on the output of the closed-loop system, and provide an explicit characterization of the region of closed-loop stability in terms of the size of the uncertainty and constraints. The proposed control method is illustrated through a chemical reactor example and compared with more traditional process control strategies.

Chapter 4 extends the control method presented in Chapter 3 to multi-input multi-output (MIMO) nonlinear processes with uncertainty and input constraints, under both state and output feedback. The output feedback controller design enforces the same closed-loop stability and performance properties under state feedback and practically preserves the state feedback region of constrained closed-loop stability. The developed controllers are applied to non-isothermal multivariable chemical reactor examples with uncertainty, input constraints, and incomplete state measurements. The chapter concludes with a discussion that attempts to put in perspective the proposed control approach with respect to the nonlinear model predictive control (MPC) approach.

Having laid the foundation for bounded Lyapunov-based control techniques in Chapters 3 and 4, we turn in Chapters 5 and 6 to take advantage of the well-characterized stability properties of these designs, through hybrid control techniques, to aid the implementation of model predictive controllers. We start in Chapter 5 with linear time-invariant systems with input constraints and develop a hybrid predictive control structure that unites MPC and bounded control in a way that reconciles the tradeoffs between their respective stability and performance properties. The basic idea is to embed the implementation of MPC within the stability region of the bounded controller and use this controller as a fall–back mechanism. In the event that the predictive controller is unable to stabilize the closed–loop system, supervisory switching from MPC to the bounded controller guarantees closed–loop stability. Extensions of the hybrid predictive control strategy to address the output feedback stabilization problem are also presented. The hybrid predictive control strategy is shown to provide, irrespective of the MPC formulation, a safety net for the practical implementation of MPC. Chapter 6 generalizes the hybrid predictive control struc-

ture to address the stabilization problem for nonlinear and uncertain systems, and demonstrates the efficacy of the proposed strategies through applications to chemical process examples.

Chapter 7 focuses on developing a hybrid nonlinear control methodology for hybrid nonlinear processes with model uncertainty and input constraints. These are systems that consist of a finite family of continuous uncertain nonlinear dynamical subsystems, subject to hard constraints on their manipulated inputs, together with a higher-level supervisor that governs the transitions between the constituent modes. The key feature of the proposed control methodology is the integrated synthesis, via multiple Lyapunov functions (MLFs), of: (1) a family of lower-level robust bounded nonlinear feedback controllers that enforce robust stability in the constituent uncertain modes, and provide an explicit characterization of the stability region for each mode under uncertainty and constraints, and (2) upper-level robust switching laws that orchestrate safe transitions between the modes in a way that guarantees robust stability in the overall switched closed-loop system. The proposed hybrid control method is applied to robustly stabilize an exothermic chemical reactor with switched dynamics, model uncertainty and actuator constraints, at an unstable steady-state.

Chapter 8 presents an application of the hybrid control methodology developed in Chapter 7 to the problem of designing fault–tolerant control systems for plants with multiple, distributed interconnected processing units. The approach brings together tools from Lyapunov–based control and hybrid systems theory and is based on a hierarchical distributed architecture that integrates lower–level feedback control of the individual units with upper–level logic–based supervisory control over communication networks. The proposed approach provides explicit guidelines for managing the interplays between the coupled tasks of feedback control, fault–tolerance and com-

munication. The efficacy of the proposed approach is demonstrated through chemical process examples.

Chapter 9 develops a methodology for the dynamic analysis and control of mode transitions in switched biological networks. The proposed approach is based on the notion of coupling the switching logic to the stability regions of the constituent modes of the switched system, introduced in Chapter 7. The results shed light on why certain naturally-occurring mode transitions seem to always favor a certain steady-state behavior, and also provide insight into how and when the network designer should enforce the transition in order to bring about a desired steady-state behavior. The proposed methodology is demonstrated using models of biological networks that arise in cell cycle regulation and the bacteriophage λ-switch system.

In the last four chapters of the thesis, we shift our focus to distributed process systems, modeled by systems of partial differential equations (PDEs), and develop constrained and hybrid nonlinear control methodologies for various classes of these systems, that build in part on the tools developed in the preceding chapters. We begin in Chapter 10 by developing a general framework for the analysis and control of quasi-linear parabolic PDE systems with input constraints, which arise frequently in the modeling of transport-reaction processes. Initially, a finite-dimensional ordinary differential equation (ODE) system that captures the dominant dynamics of the PDE system is derived using Galerkin's method. This ODE system is then used as the basis for the synthesis, via Lyapunov techniques, of bounded nonlinear feedback controllers that enforce closed-loop stability and provide, simultaneously, an explicit characterization of the limitations imposed by input constraints on both the admissible initial states and admissible control actuator locations that can be used to guarantee closed-loop stability. The proposed analysis and controller synthesis results

are used to stabilize an unstable steady-state of a diffusion-reaction process.

Chapter 11 develops a general methodology for the analysis and control of spatially-homogeneous particulate processes with input constraints. Initially, a model reduction procedure based on the method of weighted residuals is presented for the construction of finite-dimensional ODE systems that accurately reproduce the dynamics of the particulate process. These ODE systems are then used to identify the set of feasible control objectives (set-points) that can be achieved in the presence of constraints. This information, together with the derived ODE systems, is then used as the basis for the synthesis of practically-implementable nonlinear bounded output feedback controllers that enforce exponential stability in the closed-loop system and achieve particle size distributions with desired characteristics, in the presence of input constraints. Precise closed-loop stability conditions are given and controller implementation issues are addressed. The proposed methodology is applied to a continuous crystallizer, which exhibits open-loop unstable (oscillatory) behavior, and shown to cope effectively with the problem of constraints.

Chapter 12 addresses the problem of coordinating feedback and switching in control of spatially-distributed processes described by highly dissipative, constrained PDE systems. Under the assumption that the eigenspectrum of the spatial differential operator can be partitioned into a finite slow set and an infinite stable fast complement, Galerkin's method is initially used to derive a finite-dimensional ODE system that captures the dominant dynamics of the PDE system. The ODE system is then used as the basis for the integrated synthesis, via Lyapunov techniques, of a stabilizing nonlinear feedback controller, together with a switching law that orchestrates the switching between the admissible control actuator configurations, in a way that respects actuator constraints, accommodates conflicting control objectives,

and guarantees closed-loop stability. Precise conditions that guarantee stability of the constrained closed-loop PDE system under switching are provided. Finally, the proposed methodology is applied to stabilize an unstable steady-state of a diffusion-reaction process and a non-isothermal tubular reactor with recycle, under constraints and control actuator failure.

Chapter 13 focuses on the problem of coupling feedback and switching between actuator configurations for fault-tolerant control of fluid dynamic systems modeled by highly-dissipative PDEs with constrained control actuators. The results constitute a generalization of the results in Chapter 12 to higher-order dissipative PDEs that can model fluid flows. The problem is addressed on the basis of finite-dimensional Galerkin approximations of the PDE system and entails the integrated synthesis, via Lyapunov techniques, of stabilizing nonlinear feedback controllers together with stabilizing switching laws that orchestrate the switching between the admissible control actuator configurations, in a way that respects actuator constraints, accommodates inherently conflicting control objectives, and guarantees closed-loop stability. Precise conditions that guarantee stability of the constrained closed-loop system under switching are provided. The proposed control methodology is demonstrated through an application to the problem of suppression of wave formation, achieved via the stabilization of the zero solution of the Kuramoto-Sivashinsky equation (KSE) with periodic boundary conditions, in the presence of control actuator constraints and faults.

Finally, the proofs of all the results are given in the appendix.

Chapter 2

Control of Nonlinear Systems with Uncertainty

2.1 Introduction

In this chapter, we consider nonlinear systems with time-varying uncertain variables and present robust inverse optimal controller designs that enforce an arbitrary degree of attenuation of the effect of uncertainty on the output of the closed-loop system. The controller designs are obtained by re-shaping the scalar nonlinear gain of Sontag's formula in a way that guarantees the desired uncertainty attenuation properties in the closed-loop system. The proposed re-shaping is made different for vanishing and non-vanishing uncertainties so as to meet different robustness and optimality objectives.

The rest of the chapter is organized as follows. In Section 2.2 we introduce the class of uncertain nonlinear systems considered and review some preliminaries on inverse optimal controller design. Then in Section 2.3 we formulate the robust inverse optimal state feedback control problem, for both vanishing and non-vanishing uncertainties, and present the proposed gain re-shaping procedure, and the resulting

control laws, for each case. We discuss some of the advantages of the proposed gains relative to others that have been introduced in the literature. In contrast to previous works, the uncertain variables considered do not obey state-dependent bounds and, in the non-vanishing case, are not only persistent over time but can also change the nominal equilibrium point of the system. In Section 2.4 we present a simulation example to illustrate the performance of the state feedback controllers and compare it with other possible controller designs. In Section 2.5, we address the output feedback control problem by combining the state feedback controllers with appropriate high gain observers. We show that the output feedback controllers enforce closed-loop stability and robust asymptotic output tracking for initial conditions and uncertainty in arbitrarily large compact sets, as long as the observer gain is sufficiently large. Utilizing the inverse optimal control approach and singular perturbation techniques, this approach is shown to yield a near-optimal output feedback design in the sense that the performance of the resulting output feedback controllers can be made arbitrarily close to that of the robust inverse optimal state feedback controllers, when the observer gain is sufficiently large. The developed controllers are successfully applied in Section 2.6 to a chemical reactor example. The state feedback control results in this chapter were first presented in [97], while the output feedback control results were first presented in [92]

2.2 Preliminaries

We consider single-input single-output (SISO), uncertain continuous-time nonlinear systems with the following state-space description:

$$\begin{aligned} \dot{x} &= f(x) + g(x)u + \sum_{k=1}^{q} w_k(x)\theta_k(t) \\ y &= h(x) \end{aligned} \tag{2.1}$$

where $x \in \mathbb{R}^n$ denotes the vector of state variables, $u \in \mathbb{R}$ denotes the manipulated input, $\theta_k(t) \in \mathcal{W}_k \subset \mathbb{R}$ denotes the k-th uncertain (possibly time-varying) but bounded variable taking values in a nonempty compact convex subset $\mathcal{W}_k$ of $\mathbb{R}$, and $y \in \mathbb{R}$ denotes the output to be controlled. Without loss of generality, we assume that the origin is an equilibrium point of the nominal system ($u(t) = \theta_k(t) \equiv 0$) of Eq.2.1. This can always be achieved by working with deviation variables. The uncertain variable $\theta_k(t)$ may describe time-varying parametric uncertainty and/or exogenous disturbances. The vector functions $f(x)$, $w_k(x)$ and $g(x)$, and the scalar function $h(x)$ are assumed to be sufficiently smooth. Throughout the chapter, the notation $\|\theta\|$ is used to denote ess.sup.$|\theta(t)|$, $t \geq 0$ where the function θ is measurable (with respect to the Lebesgue measure). Given a measurable function $f : \mathcal{T} \rightarrow \mathbb{R}$, where $\mathcal{T}$ is a measure space with measure μ, the essential supremum is defined as ess.sup.$f(t) = \inf\{M : \mu\{t : f(t) > M\} = 0\}$, i.e. it is the smallest positive integer M such that $|f|$ is bounded by M almost everywhere. For simplicity, we will suppress the time-dependence in the notation of the uncertain variable $\theta_k(t)$.

Preparatory for its use as a tool for robust optimal controller design, we begin by reviewing the concept of inverse optimality introduced in the context of robust stabilization in [112]. To this end, consider the system of Eq.2.1 with $q = 1$ and $w(0) = 0$. Also, let $l(x)$ and $R(x)$ be two continuous scalar functions such that $l(x) \geq 0$ and $R(x) > 0 \; \forall \, x \in \mathbb{R}^n$ and consider the problem of finding a feedback control law $u(x)$ for the system of Eq.2.1 that achieves asymptotic stability of the origin and minimizes the infinite time cost functional:

$$J = \int_0^\infty (l(x) + uR(x)u)\, dt \tag{2.2}$$

The steady-state Hamilton-Jacobi-Isaacs (HJI) equation associated with the system

of Eq.2.1 and the cost of Eq.2.2 is:

$$0 \equiv \inf_{u \in \mathbb{R}} \sup_{\theta \in \mathcal{W}} (l(x) + uR(x)u + L_f V + L_g V u + L_w V \theta) \tag{2.3}$$

where the value function V is the unknown. A smooth positive-definite solution V to this equation will lead to a continuous state feedback $u(x)$ of the form:

$$u = -p(x) = -\frac{1}{2} R^{-1}(x) L_g V \tag{2.4}$$

which provides stability, optimality, and robustness with respect to the disturbance θ. However, such a smooth solution may not exist or may be extremely difficult to compute. Suppose, instead, that we were able to find a positive-definite radially unbounded C^1 scalar function V such that:

$$\inf_{u \in \mathbb{R}} \sup_{\theta \in \mathcal{W}} (L_f V + L_g V u + L_w V \theta) < 0 \quad \forall x \neq 0 \tag{2.5}$$

Now, if we can find a meaningful cost functional (i.e., $l(x) \geq 0$, $R(x) > 0$) such that the given V is the corresponding value function, then we will have indirectly obtained a solution to the HJI equation and can therefore compute the optimal control law of Eq.2.4. Such reasoning motivates following the inverse path. In the inverse approach, a stabilizing feedback control law is designed first and then shown to be optimal with respect to a well-defined and meaningful cost functional of the form of Eq.2.2. The problem is inverse because the weights $l(x)$ and $R(x)$ in the cost functional are a posteriori computed from the chosen stabilizing feedback control law, rather than a priori specified by the designer.

A stabilizing control law $u(x)$ is said to be inverse optimal for the system of Eq.2.1 if it can be expressed in the form of Eq.2.4 where the negative-definiteness of $\dot{V}$ is

achieved with the control $u^* = -\frac{1}{2}p(x)$, that is:

$$\begin{aligned} \sup_{\theta \in \mathcal{W}} \dot{V} &= \sup_{\theta \in \mathcal{W}} \left(L_f V + L_g V u^* + L_w V \theta \right) \\ &= L_f V - \frac{1}{2} L_g V p(x) + |L_w V| \theta_b \; < \; 0 \quad \forall \, x \neq 0 \end{aligned} \tag{2.6}$$

where the worst-case uncertainty (i.e., the one that maximizes $\dot{V}$) is given by $\theta = sgn[L_w V(x)]\theta_b$ where $\theta_b = \|\theta\|$ (which is clearly an admissible uncertainty since it is both measurable and bounded). When the function $l(x)$ is set equal to $l(x) = -\sup_{\theta \in \mathcal{W}} \dot{V}$, then V is a solution to the following steady-state HJI equation:

$$0 \;\equiv\; l(x) + L_f V - \frac{1}{4} L_g V R^{-1}(x) L_g V + |L_w V| \theta_b \tag{2.7}$$

and the optimal (minimal) value of the cost J is $V(x(0))$. Finally, we recall the definition of input-to-state stability (ISS) for a system of the form of Eq.2.1.

Definition 2.1 *[277] The system in Eq.2.1 (with $u \equiv 0$) is said to be ISS with respect to θ if there exist a function β of class KL and a function γ of class K such that for each $x_\circ \in \mathbb{R}^n$ and for each measurable, essentially bounded input $\theta(\cdot)$ on $[0, \infty)$ the solution of Eq.2.1 with $x(0) = x_\circ$ exists for each $t \geq 0$ and satisfies:*

$$|x(t)| \;\leq\; \beta(|x(0)|, t) + \gamma(\|\theta\|), \;\; \forall \, t \geq 0 \tag{2.8}$$

2.3 Robust inverse optimal state feedback controller design

2.3.1 Control problem formulation

Referring to the uncertain nonlinear system of Eq.2.1, we consider the following two control problems. In the first problem, we assume that the uncertain variables are vanishing (i.e., $w_k(0)\theta_k = 0$) which means that the origin is an equilibrium point of the uncertain system of Eq.2.1. We focus on the synthesis of robust nonlinear state

feedback controllers of the general form:

$$u = \mathcal{P}(x, \bar{v}) \tag{2.9}$$

where $\mathcal{P}(x, \bar{v})$ is a scalar function and $\bar{v} = [v\ v^{(1)}\ \cdots\ v^{(r)}]^T$ is a generalized reference input ($v^{(k)}$ denotes the k-th time-derivative of the reference input v which is assumed to be a sufficiently smooth function of time), that enforce global asymptotic stability and asymptotic output tracking with attenuation of the effect of the uncertainty on the output in the closed-loop system, and are optimal with respect to a meaningful, infinite time cost functional that imposes penalty on the control action. In the second control problem, we assume that the uncertain variables are non-vanishing (i.e., $w_k(0)\theta_k \neq 0$). With this assumption, the origin is no longer an equilibrium point for the uncertain system. The objective here is to synthesize robust nonlinear state feedback controllers of the form of Eq.2.9 that guarantee global boundedness of the trajectories, enforce the discrepancy between the output and the reference input to be asymptotically arbitrarily small, and minimize a meaningful cost functional defined over a finite time interval. In both control problems, the controller is designed using combination of geometric and Lyapunov techniques. In particular, the design is carried out by combining a Sontag-like control law with a robust control design proposed in [68]. The analysis of the closed-loop system is performed by utilizing the concept of input-to-state stability and nonlinear small gain theorem-type arguments, and optimality is established using the inverse optimal control approach.

2.3.2 Controller design under vanishing uncertainties

In order to proceed with the synthesis of the controllers, we will impose the following assumptions on the system of Eq.2.1. The first assumption allows transforming the system of Eq.2.1 into a partially linear form and is motivated by the requirement of

output tracking.

Assumption 2.1 *There exists an integer r and a set of coordinates:*

$$\begin{bmatrix} \zeta \\ \eta \end{bmatrix} = \begin{bmatrix} \zeta_1 \\ \zeta_2 \\ \vdots \\ \zeta_r \\ \eta_1 \\ \vdots \\ \eta_{n-r} \end{bmatrix} = T(x) = \begin{bmatrix} h(x) \\ L_f h(x) \\ \vdots \\ L_f^{r-1} h(x) \\ T_1(x) \\ \vdots \\ T_{n-r}(x) \end{bmatrix} \tag{2.10}$$

where $T_1(x), \cdots, T_{n-r}(x)$ are scalar functions such that the system of Eq.2.1 takes the form:

$$\begin{aligned} \dot{\zeta} &= A\zeta + bL_f^r h(T^{-1}(\zeta,\eta)) + bL_g L_f^{r-1} h(T^{-1}(\zeta,\eta))u + b\sum_{k=1}^{q} L_{wk} L_f^{r-1} h(T^{-1}(\zeta,\eta))\theta_k \\ \dot{\eta} &= \Psi(\zeta,\eta,\theta) \end{aligned} \tag{2.11}$$

where Ψ is an $(n-r) \times 1$ nonlinear vector function,

$$A = \begin{bmatrix} 0 & 1 & 0 & \cdots & 0 \\ 0 & 0 & 1 & \cdots & 0 \\ \vdots & & & & \vdots \\ 0 & 0 & 0 & \cdots & 1 \\ 0 & 0 & 0 & \cdots & 0 \end{bmatrix}, \quad b = \begin{bmatrix} 0 \\ 0 \\ \vdots \\ 1 \end{bmatrix} \tag{2.12}$$

A is an $r \times r$ matrix, b is an $r \times 1$ vector, and $L_g L_f^{r-1} h(x) \neq 0$ for all $x \in \mathbb{R}^n$. Moreover, for each $\theta \in \mathbb{R}^q$, the states ζ, η are bounded if and only if the state x is bounded; and $(\zeta,\eta) \to (0,0)$ if and only if $x \to 0$.

Assumption 2.1 includes the matching condition of the proposed robust control method; loosely speaking, it states that the uncertain variables cannot have a stronger

effect on the controlled output than the manipulated input. We note that the change of variables of Eq.2.10 is independent of θ (this is because the vector field, $g(x)$, that multiplies the input u is independent of θ) , and is invertible, since, for every x, the variables ζ, η are uniquely determined by Eq.2.10. Introducing the notation $e = [e_1\ e_2\ \cdots\ e_r]^T$ where $e_i = \zeta_i - v^{(i-1)}$, $i = 1, \cdots, r$, the system of Eq.2.11 can be re-written as:

$$\begin{aligned} \dot{e} &= \bar{f}(e, \eta, \bar{v}) + \bar{g}(e, \eta, \bar{v})u + \sum_{k=1}^{q} \bar{w}_k(e, \eta, \bar{v})\theta_k \\ \dot{\eta} &= \Psi(e, \eta, \theta, \bar{v}) \end{aligned} \tag{2.13}$$

where $\bar{f}(\cdot) = Ae + b\left(L_f^r h(T^{-1}(e, \eta, \bar{v})) - v^{(r)}\right)$, $\bar{g}(\cdot) = bL_g L_f^{r-1} h(T^{-1}(e, \eta, \bar{v}))$, $\bar{w}_k(\cdot) = bL_{wk} L_f^{r-1} h(T^{-1}(e, \eta, \bar{v}))$.

Following [68],the requirement of input-to-state stability of the η subsystem of Eq.2.13 is imposed to allow the synthesis of a robust state feedback controller that enforces the requested properties in the closed-loop system for any initial condition. Assumption 2.2 that follows states this requirement.

Assumption 2.2 *The dynamical system:*

$$\dot{\eta} = \Psi(e, \eta, \theta, \bar{v}) \tag{2.14}$$

is ISS with respect to e uniformly in θ, $\bar{v}$.

In most practical applications, there exists partial information about the uncertain terms of the process model. Information of this kind may result from physical considerations, preliminary simulations, experimental data, etc. In order to achieve attenuation of the effect of the uncertain variables on the output, we will quantify the possible knowledge about the uncertain variables by assuming the existence of known bounds that capture the size of the uncertain variables for all times.

Assumption 2.3 *There exist known positive constants θ_{bk} such that $\|\theta_k(t)\| \leq \theta_{bk}$.*

Theorem 2.1 below provides a formula of the robust state feedback controller and states precise conditions under which the proposed controller enforces the desired properties in the closed-loop system. The proof of this theorem is given in the appendix.

Theorem 2.1 *Consider the uncertain nonlinear system of Eq.2.1, for which Assumptions 2.1-2.3 hold, under the feedback control law:*

$$u = -\left[c_0 + r_s(x) + r_d(x, \rho, \chi, \phi, \theta_b)\right] L_{\bar{g}} V \tag{2.15}$$

where

$$r_s(x) = \left(\frac{L_{\bar{f}} V + \sqrt{(L_{\bar{f}} V)^2 + (L_{\bar{g}} V)^4}}{(L_{\bar{g}} V)^2} \right) \tag{2.16}$$

$$r_d(x, \rho, \chi, \phi, \theta_b) = \left(\frac{\rho + \chi \sum_{k=1}^{q} \theta_{bk} |L_{wk} L_f^{r-1} h(x)|}{(L_g L_f^{r-1} h(x))^2 (\frac{|L_{\bar{g}} V|}{|L_g L_f^{r-1} h(x)|} + \phi)} \right) \tag{2.17}$$

where $V = e^T P e$, P *is a positive-definite matrix that satisfies* $A^T P + PA - Pbb^T P < 0$, *and* c_0, ρ, χ, *and* ϕ *are adjustable parameters that satisfy* $c_0 > 0$, $\rho > 0$, $\chi > 2$, *and* $\phi > 0$. *Furthermore, assume that the uncertain variables in Eq.2.1 are vanishing in the sense that there exists positive real numbers* δ_k *such that* $|\bar{w}_k(e, \eta, \bar{v})| \leq \delta_k |2b^T P e|$ $\forall\ e \in D$, *where* $D = \{e \in \mathbb{R}^r : |2b^T P e| \leq \phi(\frac{1}{2}\chi - 1)^{-1}\}$. *Then for any initial condition, there exists* $\phi^* > 0$ *such that if* $\phi \leq \phi^*$, *the following holds:*

(1) The origin of the closed-loop system is asymptotically stable.

(2) The output of the closed-loop system satisfies a relation of the form:

$$\limsup_{t \to \infty} |y(t) - v(t)| = 0 \tag{2.18}$$

(3) The control law of Eqs.2.15-2.17 minimizes the cost functional:

$$J_v = \int_0^\infty (l(e) + uR(x)u)dt \tag{2.19}$$

where $R(x) = \frac{1}{2}[c_0 + r_s(x) + r_d(x, \rho, \chi, \phi, \theta_b)]^{-1} > 0 \quad \forall\ x \in \mathbb{R}^n$, $l(e) = -L_{\bar{f}} V + \frac{1}{4} L_{\bar{g}} V R^{-1}(x) L_{\bar{g}} V - \sum_{k=1}^{q} |L_{wk} V| \theta_{bk} \geq k |2b^T P e|^2$ *for some real number,* $k > 0$, *and the minimum cost is* $J_v^* = V(e(0))$.

Remark 2.1 Referring to the controller of Eqs.2.15-2.17, one can easily observe that it is comprised of two components. The first component:

$$u_s = -[c_0 + r_s(x)]L_{\bar{g}}V \tag{2.20}$$

is responsible for achieving stabilization and reference-input tracking in the nominal closed-loop system (i.e., with $\theta(t) \equiv 0$). This component, with $c_0 = 0$, is the so-called Sontag's formula proposed in [278] and is continuous everywhere in the state-space (and smooth away from the origin) since V satisfies the small control property (see [278, 271] for further details on this issue). The second component of the controller:

$$u_r = -r_d(x, \rho, \chi, \phi, \theta_b)L_{\bar{g}}V \tag{2.21}$$

enforces, on the other hand, output tracking with an arbitrary degree of asymptotic attenuation of the effect of θ on y. This component is also continuous everywhere since $L_g L_f^{r-1} h(x) \neq 0$ for all x (from Assumption 2.1) and $\phi > 0$. A key feature of the uncertainty compensator of Eq.2.21 is the presence of a scaling term of the form $\frac{|x|}{|x| + \phi}$ which allows us, not only to tune the degree of uncertainty attenuation (by adjusting ϕ), but also to use smaller and smaller control effort to cancel the uncertainties as the state gets closer and closer to the equilibrium point. The full weight (gain) of the compensator is used only when the state is far from the equilibrium point (since ϕ is small).

Remark 2.2 The re-shaping of the scalar gain of the nominal L_gV controller of Eq.2.20, via the addition of the uncertainty compensator of Eq.2.21, allows us to achieve attenuation of the effect of θ on y without using unreasonably large (high-gain) control action. The use of a high-gain controller of the form $u = \frac{1}{\epsilon} u_s$ where ϵ is a small positive parameter could also lead to uncertainty attenuation at the expense of employing unnecessarily large control action (see the example in Section 2.4 for a numerical verification of this fact).

Remark 2.3 The control law of Eqs.2.15-2.17 possesses four adjustable parameters that directly influence the performance of the output of the closed-loop system and

the achievable level of uncertainty attenuation. The positive parameter c_0 allows a certain degree of flexibility in shaping the dynamic behavior of the closed-loop output response as desired. To see this, we note that by computing the time-derivative of V along the trajectories of the closed-loop system, the following estimate can be obtained (see Part 1 of the Proof of Theorem 2.1):

$$\dot{V} \leq -c_0(L_{\bar{g}}V)^2 - \sqrt{(L_{\bar{f}}V)^2 + (L_{\bar{g}}V)^4} \tag{2.22}$$

From the above equation, it is transparent that the choice of c_0 affects how negative the time-derivative of V is along the closed-loop trajectories and can therefore be made so as to make this derivative more or less negative as requested. For example, a large value for c_0 will make $\dot{V}$ more negative and therefore generate a faster transient response. Note that a positive value of c_0 is not necessary for stabilization (since $\dot{V}$ is negative-definite even when $c_0 = 0$ as can be seen from Eq.2.22); however, a positive value of c_0 helps both in shaping $\dot{V}$ and in ensuring the positivity of the penalty weights in the cost functional of Eq.2.19 (see Part 2 of the Proof of Theorem 2.1 for the detailed calculations). The positive parameter ρ also helps in ensuring the positivity of the penalty weights; however, its central role is to provide an additional robustness margin that increases the negativity of $\dot{V}$ and, thus, provides a sufficient counterbalance to the undesirable effect of the uncertainty on $\dot{V}$ to guarantee global asymptotic stability. As can be seen from the calculations in Part 1 of the Proof of Theorem 2.1, a zero value of ρ guarantees only boundedness of the closed-loop state (but not asymptotic stability). The remaining two parameters, χ and ϕ, are primarily responsible for achieving the desired degree of attenuation of the effect of uncertainty on the closed-loop output. A significant degree of attenuation can be achieved by selecting ϕ to be sufficiently small and/or χ to be sufficiently large. While robust stability can be achieved using any value of χ satisfying $\chi > 1$, a value satisfying $\chi > 2$ is necessary to ensure the positive-definiteness of the weight function, $l(e)$, in the cost functional of Eq.2.19, and thus to ensure meaningful optimality.

Remark 2.4 Regarding the properties of the cost functional of Eq.2.19, we observe

that J_v is well-defined according to the formulation of the optimal control problem for nonlinear systems [271] because of the following properties of $l(e)$ and $R(x)$. The function $l(e)$ is continuous, positive-definite, and bounded from below by a class $\mathcal{K}$ function of the norm of e (see Part 2 of the Proof of Theorem 2.1). The function $R(x)$ is continuous, strictly positive, and the term $uR(x)u$ has a unique global minimum at $u = 0$ implying a larger control penalty for u farther away from zero. Moreover, owing to the vanishing nature of the uncertain variables and the global asymptotic stability of the origin of the closed-loop system, J_v is defined on the infinite-time interval and is finite.

Remark 2.5 Note that since $l(e) \geq k|2b^T Pe|^2$, where k is a positive constant (details of this calculation are given in the Part 2 of the Proof of Theorem 2.1 in the Appendix), the cost functional of Eq.2.19 includes penalty on the tracking error $e = v - y$ and its time-derivatives up to order r, and not on the full state of the closed-loop system. This is consistent with the requirement of output tracking. The term $-\sum_{k=1}^{q}|L_{wk}V|\theta_{bk}$ in Eq.2.19 is a direct consequence of the worst-case uncertainty formulation of the HJI equation (see Eq.2.3).

Remark 2.6 The linear growth bound on the functions $\bar{w}_k(e, \eta, \bar{v})$ is imposed to ensure that the results of Theorem 2.1 hold globally. Note, however, that this condition is required to hold only over the set D (containing the origin) whose size can be made arbitrarily small by appropriate selection of the tuning parameters, ϕ and χ. This bound is consistent with the vanishing nature of the uncertain variables considered in this section, since it implies that the functions $\bar{w}_k(e, \eta, \bar{v})$ vanish when $e = 0$. We observe that locally (i.e., in a sufficiently small compact neighborhood of the origin), this growth condition is automatically satisfied due to the local Lipschitz properties of the functions $\bar{w}_k$. Finally, we note that the imposed growth assumption can be readily relaxed via a slight modification of the controller synthesis formula. One such modification, for example, is to replace the term $|L_{wk}L_f^{r-1}h(x)|$ in Eq.2.15 by the term $|L_{wk}L_f^{r-1}h(x)|^2$. Using a standard Lyapunov argument, one can show that the

resulting controller globally asymptotically stabilizes the system without imposing the linear growth condition on the functions $\bar{w}_k$ over D. However, we choose not to modify the original controller design because such modification will possibly increase the gain of the controller, prompting the expenditure of unnecessarily large control action.

Remark 2.7 In contrast to feedback linearizing controllers, the controller of Eqs.2.15-2.17 has two desirable properties not present in the feedback linearizing design. The first property is the fact that the controller of Eqs.2.15-2.17 recognizes the beneficial effect of the term $L_{\bar{f}}V$ when $L_{\bar{f}}V < 0$ and prevents its unnecessary cancellation. In this case, the term $L_{\bar{f}}V$ is a stabilizing term whose cancellation may generate positive feedback and destabilize the process. Such a situation can arise whenever the process under consideration is open-loop stable or contains beneficial nonlinearities that help drive the process towards the desired steady-state. Under such circumstances, the term $(L_{\bar{f}}V)^2$ in Eqs.2.15-2.17 guards against the wasteful cancellation of such nonlinearities (by essentially deactivating the cancelling term $L_{\bar{f}}V$) and helps the controller avoid the expenditure of large control effort. This is particularly important when the process operating conditions start relatively far away from the equilibrium point in which case the feedback linearizing designs may generate a huge control effort to cancel process nonlinearities. The second property that the controller of Eqs.2.15-2.17 possesses is the fact that it dominates the term $L_{\bar{f}}V$, instead of cancelling it, when $L_{\bar{f}}V > 0$. This situation arises, for example, when the process is open-loop unstable. In this case, the term L_fV is a destabilizing one that must be eliminated. The controller of Eqs.2.15-2.17, however, eliminates the term by domination rather than by cancellation. This property guards against the non-robustness of cancellation designs which increases the risk of instability due to the presence of other uncertainty not taken into account in the controller design. This means that input perturbations (or, equivalently, an error in implementing the control law) will be tolerated by the design presented in Theorem 2.1 in the sense that the trajectories will remain bounded.

Remark 2.8 Referring to the practical implementation of the controller of Eqs.2.15-2.17, we note that even though the controller is continuous at the origin, it is not smooth at that point and, therefore, when implemented in simulations, the numerical integration could result in a chattering-like behavior for the control input near the origin (this problem arises because of the piecewise, or "non-smooth," form of the Sontag's formula). In practice, this problem can be circumvented/alleviated via a slight modification of the control law, whereby a sufficiently small positive real number, ϵ, is added to the $(L_{\bar{g}}V)^2$ term in the denominator of Sontag's formula in order to smoothen out the control action. The addition of this parameter obviously destroys the asymptotic stability capability of the controller and leads to some offset in the closed-loop response. However, this offset can be made arbitrarily small by choosing ϵ sufficiently small (practical stability). Clearly, a tradeoff exists between the smoothness of the control action (which favors a relatively large ϵ) and the size of the offset (a small offset favors a relatively small ϵ). Therefore, in tuning the controller, ϵ should be chosen in a way that balances this tradeoff.

2.3.3 Controller design under non-vanishing uncertainties

To proceed with the main results for the case of non-vanishing uncertain variables, we let Assumptions 2.1 and 2.3 hold and modify Assumption 2.2 to the following one.

Assumption 2.4 *The dynamical system of Eq.2.14 is ISS with respect to e, θ, uniformly in $\bar{v}$.*

Theorem 2.2 *Let Assumptions 2.1, 2.3, and 2.4 hold and assume that the uncertain variables in Eq.2.1 are non-vanishing in the sense that there exist positive real numbers $\bar{\delta}_k$, μ_k such that $|\bar{w}_k(e,\eta)| \leq \bar{\delta}_k|2b^TPe|+\mu_k \; \forall \; e \in D$. Consider the uncertain nonlinear system of Eq.2.1 under the control law:*

$$u = -\left[c_0 + r_s(x) + r_d(x,\rho,\chi,\phi,\theta_b)\right] L_{\bar{g}}V \tag{2.23}$$

where c_0, r_s, r_d, χ, ϕ *and* V *were defined in Theorem 2.1. Then for any initial condition and for every positive real number* d, *there exists* $\phi^*(d) > 0$ *such that if* $\phi \in (0, \phi^*(d)]$, *the following holds:*

(1) The trajectories of the closed-loop system are bounded.

(2) The output of the closed-loop system satisfies a relation of the form:

$$\limsup_{t\to\infty} |y(t) - v(t)| \leq d \tag{2.24}$$

(3) The control law of Eq.2.15 minimizes the cost functional:

$$J_n = \lim_{t\to T_f} V(e(t)) + \int_0^{T_f} (\bar{l}(e) + u\bar{R}(x)u)dt \tag{2.25}$$

with a minimum cost, $J_n^* = V(e(0))$, *where* $\bar{l}(e(t)) = -L_{\bar{f}}V + \frac{1}{4}L_{\bar{g}}V\bar{R}^{-1}(x)L_{\bar{g}}V - \sum_{k=1}^{q}|L_{wk}V|\theta_{bk} > 0 \;\; \forall\, t \in [0, T_f]$, $T_f = \inf\{T \geq 0 : e(t) \in \Gamma \;\forall\, t \geq T\}$, $\Gamma = \{e \in \mathbb{R}^r : e^T P e \leq \lambda_{max}(P)\epsilon^2\}$, $\epsilon = \max\{\alpha_1^{-1}(2\bar{\phi}^*), \alpha_2^{-1}(2\bar{\phi}^*)\}$, $\bar{\phi}^* = \sum_{k=1}^{q}\mu_k\theta_{bk}\phi^*$, $\alpha_1(\cdot)$, $\alpha_2(\cdot)$ *are class* $\mathcal{K}$ *functions that satisfy, respectively,* $\alpha_1(|e|) \leq \sqrt{(L_{\bar{f}}V)^2 + (L_{\bar{g}}V)^4}$ *and* $\alpha_2(|e|) \leq \frac{1}{2}\left[-L_{\bar{f}}V + \sqrt{(L_{\bar{f}}V)^2 + (L_{\bar{g}}V)^4}\right]$, *and* $\bar{R}(x) = -\frac{1}{2}\left[c_0 + r_s(x) + r_d(x, \rho, \chi, \phi, \theta_b)\right]^{-1} > 0$.

Remark 2.9 Note that the cost functional of Eq.2.25 differs from that of Eq.2.19 in two ways. First, owing to the persistent nature of the uncertainty in this case ($\bar{w}_k(0, \eta, \bar{v}) \neq 0$) and the fact that asymptotic convergence to the equilibrium point of the nominal system is no longer possible, J_n cannot achieve a finite value over the infinite time interval. Therefore, the cost functional of Eq.2.19 is defined only over a finite time interval $[0, T_f]$. The size of this interval is given by the time required for the tracking error trajectory to reach and enter a compact ball Γ, centered around the origin, without ever leaving again. In the Proof of Theorem 2.2, we show that $\dot{V} < 0$ outside this ball, which implies that – once inside – the closed-loop trajectory cannot escape. The size of Γ scales with $\phi(\chi - 1)^{-1}$ and, depending on the desired degree of attenuation of the effect of the uncertainty on the output, can be made arbitrarily small by adjusting the controller tuning parameters ϕ and χ. Therefore

one can practically get as close as desired to the nominal equilibrium point. In addition to the terminal time, T_f, the cost functional of Eq.2.25 imposes a terminal penalty given by the term $\lim_{t \to T_f} V(e)$ to penalize the tracking error trajectory for its inability to converge to the origin for $t > T_f$. Note that since the error trajectory of the closed-loop system converges to the ball Γ as time tends to T_f, the cost functional of Eq.2.25 is meaningful in the sense that $\bar{l}(e) \geq \bar{k}|2b^T Pe|^2$ and $\bar{R}(x) > 0 \ \forall \, t \in [0, T_f]$.

Remark 2.10 It is important to compare the controller design proposed in Theorem 2.2 with the following robust nonlinear controller based on the design proposed in [68]:

$$u = \frac{1}{L_g L_f^{r-1} h(x)} \sum_{i=0}^{r} \frac{\beta_i}{\beta_r} (v^{(i)} - L_f^i h(x)) + u_r \tag{2.26}$$

where u_r was defined in Eq.2.21, which is continuous (since $L_g L_f^{r-1} h(x) \neq 0$ and $\phi > 0$) and guarantees boundedness of the trajectories of the closed-loop system and output tracking with an arbitrary degree of asymptotic attenuation of the effect of θ on y. The controller of Eq.2.26 consists of a term that cancels the nonlinearities of the system of Eq.2.11 with $\theta(t) \equiv 0$ that can be cancelled by feedback, and a term that compensates for the effect of θ on y. While the control law of Eq.2.26 can be shown to be optimal with respect to some performance index, it remains to be seen whether the index is meaningful or not. In particular, we note that the feedback linearizing component of the controller of Eq.2.26 may generate unnecessarily large control action to cancel beneficial nonlinearities and, therefore, may not in general be optimal with respect to a meaningful performance index. Consequently, we use the normal form of Eq.2.37 not for the design of the controller but only for the construction of V. The choice of $V = e^T Pe$ is made to simplify the explicit formula of the controller in the context of a specific application. Of course, this choice for V is not unique and many other positive-definite functions whose time-derivative along the trajectories of the closed-loop system can be rendered negative-definite via feedback could be used.

Remark 2.11 An alternative to the gain-reshaping procedure underlying the controller designs in Theorems 2.1 and 2.2 is the one proposed in [185] which involves

incorporating the uncertainty compensator within (rather than adding it to) the "nominal" gain of Sontag's formula. The resulting L_gV controller in this case has a scalar gain that is structurally-similar to that of Sontag's formula, except that the term L_fV appears with the uncertainty compensator added to it. In particular, when the compensator of Eq.2.21 is used, this gain-reshaping approach yields the following control law:

$$u = -\left(\frac{L_{\bar{f}}^*V + \sqrt{(L_{\bar{f}}^*V)^2 + (L_{\bar{g}}V)^4}}{(L_{\bar{g}}V)^2}\right) L_{\bar{g}}V \tag{2.27}$$

where

$$L_{\bar{f}}^*V = L_{\bar{f}}V + \chi\sum_{k=1}^{q}\theta_{bk}|L_{\bar{w}k}V|\left(\frac{|2Pe|}{|2Pe|+\phi}\right) \tag{2.28}$$

Using calculations similar to those in the appendix, one can show that the above control law is also globally robustly stabilizing and inverse optimal with respect to a meaningful cost. However, a potential drawback of this design is the fact that it can limit the ability of the controller to fully "cancel out" the uncertainty, especially when $L_{\bar{f}}^*V$ is negative. This in turn can lead either to a level of asymptotic uncertainty attenuation smaller than that achieved by the controllers of Eq.2.15 and Eq.2.23, or to larger control action in order to enforce the same attenuation level. To illustrate this point, consider the following system:

$$\dot{x} = u + \theta \tag{2.29}$$

Since the system is scalar, we take $V = \frac{1}{2}x^2$ and get $L_gV = L_wV = x$ and . For this choice, the control law based on Eq.2.23 is:

$$u = -\left(1 + \frac{\chi\theta_b}{|x|+\phi}\right)x \tag{2.30}$$

while the control law based on Eqs.2.27-2.28 is:

$$u = -\left(\frac{\chi\theta_b}{|x|+\phi} + \sqrt{1+\left(\frac{\chi\theta_b}{|x|+\phi}\right)^2}\right)x \tag{2.31}$$

It is straightforward to verify that, for the same choice of tuning parameters ϕ and χ, both controllers enforce the same level of asymptotic uncertainty attenuation, with

an ultimate bound on the state of $|x| \leq d$ where $d = \phi(\chi - 1)^{-1}$. However, it is also clear that the controller gain in Eq.2.31 is higher, point-wise, than that of the control law in Eq.2.30. The discrepancy between the two gains reflects the cost of incorporating the uncertainty compensator within a Sontag-type gain in Eq.2.31 as opposed to adding it to the nominal gain of Sontag's formula as done in Eq.2.30. Note that to reduce the controller gain in Eq.2.31 requires an increase in ϕ and/or reduction in χ which, in either case, implies a lesser level of uncertainty attenuation (larger residual set).

Remark 2.12 Referring to the practical applications of the result of Theorem 2.2, one has to initially verify whether Assumptions 2.1 and 2.4 hold for the process under consideration. Then, given the bounds θ_{bk}, Eq.2.23 can be used to compute the explicit formula for the controller. Finally, given the asymptotic tracking error desired, d, which can be chosen arbitrarily close to zero, the value of ϕ^* should be computed (usually through simulations) to achieve $\limsup_{t\to\infty}|y(t) - v(t)| \leq d$.

2.4 Illustrative example

In order to illustrate the performance of the developed control law, we consider a continuous stirred tank reactor where an irreversible first-order exothermic reaction of the form $A \xrightarrow{k} B$ takes place. The inlet stream consists of pure A at flow rate $F = 100\ L/min$, concentration $C_{A0} = 1.0\ mol/L$ and temperature $T_{A0} = 300\ K$. Under standard modeling assumptions, the mathematical model for the process takes the form:

$$\begin{aligned} \frac{dC_A}{dt} &= \frac{F}{V}(C_{A0} - C_A) - k_0 \exp\left(\frac{-E}{RT}\right) C_A \\ \frac{dT}{dt} &= \frac{F}{V}(T_{A0} - T) + \frac{(-\Delta H_{nom})}{\rho_m c_p} k_0 \exp\left(\frac{-E}{RT}\right) C_A + \frac{Q}{\rho_m c_p V} \end{aligned} \tag{2.32}$$

where C_A denotes the reactant concentration, T denotes the reactor temperature, Q denotes the rate of heat input to the reactor, $V = 100\ L$ is the volume of the

reactor, $k_0 = 7.0\ min^{-1}$, $E = 27.4\ KJ/mol$, $\Delta H_{nom} = 718\ KJ/mol$ are the pre-exponential constant, the activation energy, and the enthalpy of the reaction, $c_p = 0.239\ J/g \cdot K$ and $\rho_m = 1000\ g/L$, are the heat capacity and fluid density in the reactor. For these values of process parameters, the process (with $Q = 0$) has an unstable equilibrium point at $(C_{As}, T_s) = (0.731\ mol/L, 1098.5\ K)$. The control objective is the regulation of the reactant concentration at the (open-loop) unstable equilibrium point, in the presence of time-varying, persistent disturbances in the feed temperature and uncertainty in the heat of reaction, by manipulating the rate of heat input Q.

Defining the variables $x_1 = (C_A - C_{As})/C_{As}$, $x_2 = (T - T_s)/T_s$, $u = Q/(\rho_m c_p V T_s)$, $\theta_1(t) = T_{A0} - T_{A0s}$, $\theta_2(t) = \Delta H - \Delta H_{nom}$, $y = x_1$, where the subscript s denotes the steady-state values, it is straightforward to verify that the process model of Eq.2.32 can be cast in the form of Eq.2.1 with:

$$\begin{aligned} f(x) &= \begin{bmatrix} 0.368 - x_1 - \delta(x_1, x_2) \\ -0.736 - x2 + 2\delta(x_1, x_2) \end{bmatrix}, \quad g(x) = \begin{bmatrix} 0 \\ 1 \end{bmatrix}, \\ w_1(x) &= \begin{bmatrix} 0 \\ \dfrac{1}{T_s} \end{bmatrix}, \quad w_2(x) = \begin{bmatrix} 0 \\ \dfrac{C_{As}}{\rho_m c_p T_s}\delta(x_1, x_2) \end{bmatrix} \end{aligned} \tag{2.33}$$

where $\delta(x_1, x_2) = (1 + x_1)\exp\left(2 - \dfrac{3}{x_2 + 1}\right)$, and has a relative degree $r = 2$. To simulate the effect of the uncertainty, we consider the time-varying functions $\theta_k(t) = \theta_{bk} sin(t)$, $k = 1, 2$ with upper bounds $\theta_{b1} = 30\ K$ and $\theta_{b2} = 28.7\ KJ/mol$, respectively. To proceed with the design of the controller, we initially use the coordinate transformation $e_1 = x_1$, $e_2 = 0.368 - x_1 - \delta(x_1, x_2)$ to cast the input/output dynamics of the system of Eq.2.32 in the following form:

$$\dot{e} = \bar{f}(e) + \bar{g}(e)u + \bar{w}_1(e)\theta_1 + \bar{w}_2(e)\theta_2 \tag{2.34}$$

where the functions $\bar{f}$, $\bar{g}$, $\bar{w}_1$, $\bar{w}_2$ can be computed directly from Eq.2.13. Note that

the uncertainties considered are non-vanishing and, therefore, we use the result of Theorem 2.2 to design the necessary controller which takes the form of Eq.2.15 with $\rho = 0$, $q = 2$, $r = 2$, and $P = \begin{bmatrix} 1 & 0.45 \\ 0.45 & 1 \end{bmatrix}$. Moreover, the following values are used for the tuning parameters of the controller: $\phi = 0.0001$, $\chi = 1.6$, and $c_0 = 0.0001$ to guarantee that the output of the closed-loop system satisfies a relation of the form $\limsup_{t\to\infty} |y - v| \leq 0.005$.

Closed-loop simulations were performed to evaluate the robustness and optimality properties of the controller. The results are shown by the solid lines in Figure 2.1, which depict the controlled output (top) and manipulated input (bottom) profiles. One can immediately see that the robust optimal controller drives the closed-loop output close to the desired steady-state, while attenuating the effect of the uncertainty on the output. Included also in Figure 2.1 is the closed-loop output profile (top plot, dashed-dotted line) and corresponding input profile (bottom plot, dashed-dotted line) when the controller of Eq.2.15 is implemented without the uncertainty compensation component ($\chi = 0$). It is clear from the result that the effect of uncertainty is significant and leads to poor transient performance and offset.

For the sake of comparison, we also considered the robust nonlinear controller of Eq.2.26 (see Remark 2.2 above) as well as the nonlinear high-gain controller of the form $u = \frac{1}{\epsilon}[c_0 + r_s(x)]L_{\bar{g}}V$ where no uncertainty compensation is included and ϵ is a small positive number. The results for these two cases (starting from the same initial condition) are shown in Figure 2.1 by the dashed and dotted lines, respectively, for a choice of the tuning parameters: $\beta_0 = 4$, $\beta_1 = 9$, $\beta_2 = 1$, $\epsilon = 0.05$. It is clear from the input profiles that, compared with these two controllers, the controller of Eq.2.15 starts by requesting significantly smaller control action to achieve a relatively faster closed-loop response and enforce, asymptotically, the same level of attenuation of the

effect of uncertainty on x_1. Finally, in order to establish the fact that the robust optimal controller of Eq.2.15 does not use unnecessary control action compared with the controller of Eq.2.26, we compared the control actions generated by the two controllers for a broad range of x_1 and x_2. The results are shown in Figure 2.2 and clearly indicate that the controller of Eq.2.15 (dashed lines) uses smaller control action, point-wise, than the controller of Eq.2.26 (solid lines).

2.5 Robust near-optimal output feedback controller design

In section 2.3, we addressed the problem of synthesizing robust optimal *state* feedback control laws for a large class of nonlinear systems. The practical applicability of these control laws, however, rests on the assumption of accessibility of all process states for measurement. In chemical process control – more so than in most other control areas – however, the complete state cannot be measured in general (e.g., concentrations of certain species are not accessible on-line) and therefore the state feedback controllers proposed in chapter 2.3 may not be directly suited for practical applications. In the past few years, significant advances have been made in the direction of output feedback controller design for the purpose of robustly stabilizing nonlinear systems. Important contributions in this area include general results on robust output feedback stabilization using the controller-observer combination approach (e.g., [293, 294]), adaptive output feedback control (e.g., [211, 212]), and robust output feedback controller design for various classes of nonlinear systems (e.g., [168, 210, 60]). In addition to these approaches, other methods for constructing robust stabilizers via output feedback, which do not necessarily appeal to the principle of "composing a state feedback with estimates of the states" have been explored, including output feedback control within the H_∞ control framework (e.g., [149, 151, 152]) and the

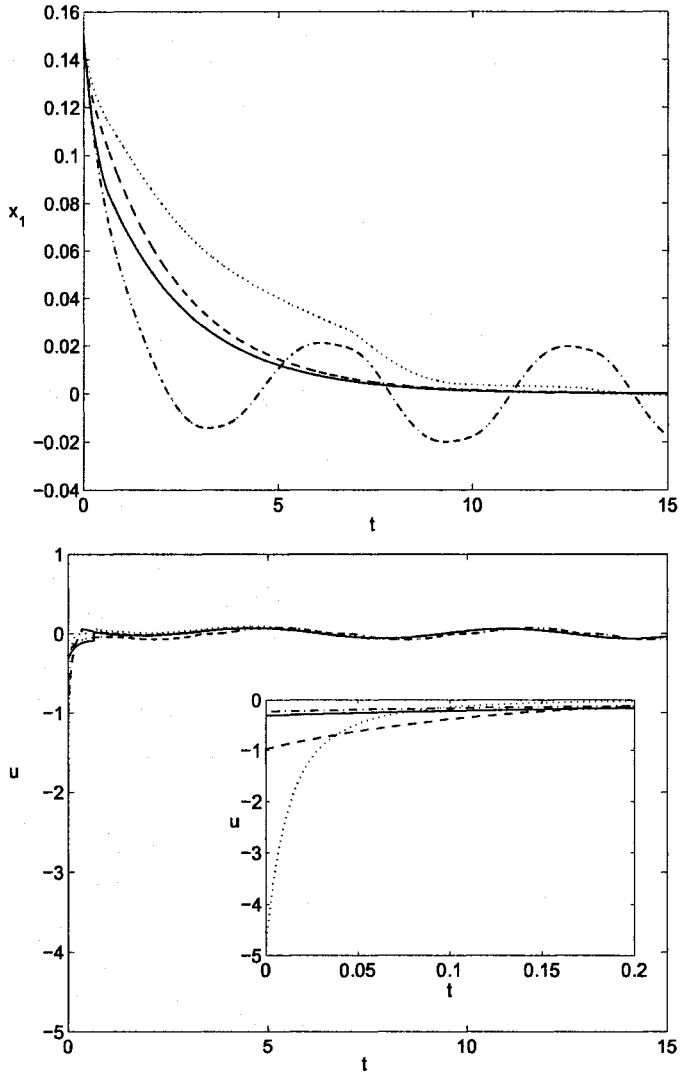

Figure 2.1: Closed-loop output and manipulated input profiles under the controller of Eq.15 (solid lines), the controller of Eq.15 with $\chi = 0$ (dashed-dotted lines), the controller of Eq.22 (dashed lines), and the high-gain controller (dotted lines).

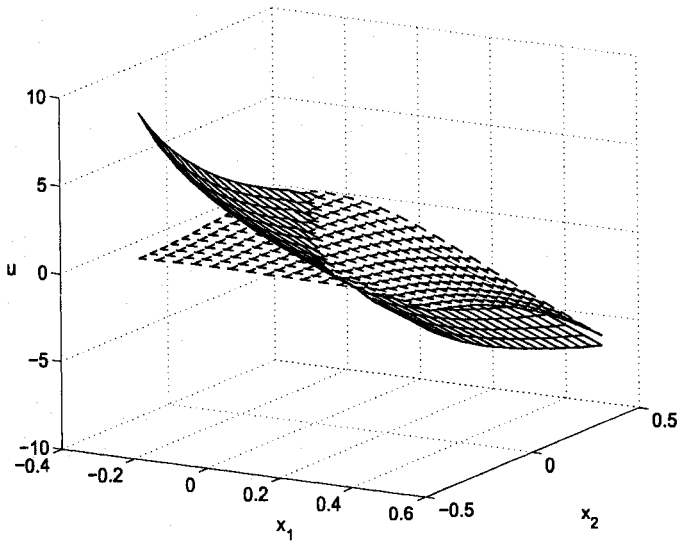

Figure 2.2: Control action computed by the controller of Eq.15 (dashed lines) and the controller of Eq.22 (solid lines).

recursive stabilization scheme proposed in [150].

In this section, we address the problem of synthesizing robust near-optimal *output* feedback controllers for a broad class of nonlinear systems with time-varying bounded uncertain variables. Under the assumptions of input-to-state stable (ISS) inverse dynamics and vanishing uncertainty, a dynamic controller is synthesized through combination of a high-gain observer with a robust optimal state feedback controller designed via Lyapunov's direct method and shown through the inverse optimal approach to be optimal with respect to a meaningful cost defined on the infinite time-interval. The dynamic output feedback controller enforces exponential stability and asymptotic output tracking with attenuation of the effect of the uncertain variables on the output of the closed-loop system for initial conditions and uncertainty in arbitrarily large compact sets, as long as the observer gain is sufficiently large. Utilizing the inverse optimal control approach and standard singular perturbation techniques, this approach is shown to yield a near-optimal output feedback design in the sense that

the performance of the resulting output feedback controller can be made arbitrarily close to that of the robust optimal state feedback controller on the infinite time-interval, when the observer gain is sufficiently large. For systems with non-vanishing uncertainty, the same controllers are shown to ensure boundedness of the states, robust asymptotic output tracking, and near-optimality over a finite time-interval. The developed controllers are successfully applied to a chemical reactor example.

2.5.1 Control problem formulation

Referring to the system of Eq.2.1, we consider two control problems with different control objectives. In the first problem, we consider the class of systems described by Eq.2.1 where the uncertain variable terms are assumed to be vanishing (i.e., $w_k(0)\theta_k = 0$ for any $\theta_k \in \mathcal{W}_k$ where the origin is the equilibrium point of the system $\dot{x} = f(x)$). In this case, the origin is also an equilibrium point for the uncertain system of Eq.2.1. The objective in this problem is to synthesize robust nonlinear dynamic output feedback controllers of the form:

$$\begin{aligned} \dot{\omega} &= \mathcal{F}(\omega, y, \bar{v}) \\ u &= \mathcal{P}(\omega, y, \bar{v}, t) \end{aligned} \tag{2.35}$$

where $\omega \in \mathbb{R}^s$ is a state, $\mathcal{F}(\omega, y, \bar{v})$ is a vector function, $\mathcal{P}(\omega, y, \bar{v}, t)$ is a scalar function, $\bar{v} = [v\ v^{(1)}\ \cdots\ v^{(r)}]^T$ is a generalized reference input ($v^{(k)}$ denotes the k-th time derivative of the reference input v, which is assumed to be a sufficiently smooth function of time), that: (a) enforce exponential stability in the closed-loop system, (b) guarantee asymptotic robust output tracking with an arbitrary degree of attenuation of the effect of the uncertainty on the output, and (c) are near-optimal with respect to a meaningful cost functional, defined over the infinite time-interval, that imposes penalty on the control action and the worst-case uncertainty. The near-optimality property, to be made more precise mathematically in Theorem 2.3 below, is sought

in the sense that the performance of the dynamic output feedback controller can be made arbitrarily close to the optimal performance of the corresponding robust optimal state feedback controller over the infinite time-interval.

In the second control problem, we again consider the system of Eq.2.1. In this case, however, we assume that the uncertain variable terms are non-vanishing (i.e., $w_k(0)\theta_k \neq 0$). Under this assumption, the origin is no longer an equilibrium point of the system of Eq.2.1. The objective in this problem is to synthesize robust nonlinear dynamic output feedback controllers of the form of Eq.2.35 that: (a) guarantee boundedness of the closed-loop trajectories, (b) enforce the discrepancy between the output and reference input to be asymptotically arbitrarily small, and (c) are near-optimal with respect to a meaningful cost defined over a finite time-interval, in the sense that their performance can be made arbitrarily close to the optimal performance of the corresponding robust optimal state feedback controllers over the same time-interval.

In both control problems, the design of the dynamic controllers is carried out using combination of a high-gain observer and the robust optimal state feedback controllers proposed in Section 2.3. In particular, referring to Eq.2.35, the system $\dot{\omega} = \mathcal{F}(\omega, y, \bar{v})$ is synthesized to provide estimates of the system state variables, while the static component, $\mathcal{P}(\omega, y, \bar{v}, t)$, is synthesized to enforce the requested properties in the closed-loop system. The analysis of the closed-loop system employs standard singular perturbation techniques (due to the high-gain nature of the observer) and utilizes the concept of input-to-state stability (see Definition 2.1) and nonlinear small gain theorem-type arguments. Near-optimality is established through the inverse optimal approach (see Section 2.2) and using standard singular perturbation results. The requested closed-loop properties in both control problems are enforced for arbitrarily large initial conditions and uncertainty provided that the gain of the observer is

sufficiently large (semi-global type result).

In order to proceed with the design of the desired output feedback controllers, we need to impose the following three assumptions on the system of Eq.2.1. The first assumption is motivated by the requirement of output tracking and allows transforming the system of Eq.2.1 into a partially linear form.

Assumption 2.5 *There exists an integer r and a set of coordinates:*

$$\begin{bmatrix} \zeta \\ \eta \end{bmatrix} = \begin{bmatrix} \zeta_1 \\ \zeta_2 \\ \vdots \\ \zeta_r \\ \eta_1 \\ \vdots \\ \eta_{n-r} \end{bmatrix} = \mathcal{X}(x) = \begin{bmatrix} h(x) \\ L_f h(x) \\ \vdots \\ L_f^{r-1} h(x) \\ \chi_1(x) \\ \vdots \\ \chi_{n-r}(x) \end{bmatrix} \tag{2.36}$$

where $\chi_1(x), \cdots, \chi_{n-r}(x)$ are nonlinear scalar functions of x, such that the system of Eq.2.1 takes the form:

$$\begin{aligned}
\dot{\zeta}_1 &= \zeta_2 \\
&\vdots \\
\dot{\zeta}_{r-1} &= \zeta_r \\
\dot{\zeta}_r &= L_f^r h(\mathcal{X}^{-1}(\zeta,\eta)) + L_g L_f^{r-1} h(\mathcal{X}^{-1}(\zeta,\eta))u + \sum_{k=1}^{q} L_{wk} L_f^{r-1} h(\mathcal{X}^{-1}(\zeta,\eta))\theta_k \\
\dot{\eta}_1 &= \Psi_1(\zeta,\eta) \\
&\vdots \\
\dot{\eta}_{n-r} &= \Psi_{n-r}(\zeta,\eta) \\
y &= \zeta_1
\end{aligned} \tag{2.37}$$

where $L_g L_f^{r-1} h(x) \neq 0$ for all $x \in \mathbb{R}^n$, $\theta \in \mathbb{R}^q$. Moreover, for each $\theta \in \mathbb{R}^q$, the states ζ, η are bounded if and only if the state x is bounded; and $(\zeta,\eta) \to (0,0)$ if and only if $x \to 0$.

Remark 2.13 We note that the change of variables of Eq.2.36 is independent of θ and invertible, since, for every x, the variables ζ, η are uniquely determined by Eq.2.36. This implies that if we can estimate the values of ζ, η for all times, using appropriate state observers, then we automatically obtain estimates of x for all times. This property will be exploited later to synthesize a state estimator for the system of Eq.2.1 on the basis of the system of Eq.2.37. We also note that Assumption 2.5 includes the matching condition of our robust control method. In particular, we consider systems of the form Eq.2.1 for which the uncertain variables enter the system in the same equation with the manipulated input. This assumption is more restrictive than Assumption 2.1 used in Section 2.3.2 to solve the same robust control problem via state feedback and is motivated by our requirement to eliminate the presence of θ in the η-subsystem of the system of Eq.2.37. This requirement and the stability requirement of Assumption 2.6 below will allow including in the controller a replica of the η-subsystem of Eq.2.37 which provides estimates of the η states (see Theorem 2.3 below).

Introducing the notation $e = [e_1 \; e_2 \; \cdots \; e_r]^T$ where $e_i = \zeta_i - v^{(i-1)}$, $i = 1, \cdots, r$, the system of Eq.2.37 can be re-written as:

$$\begin{aligned} \dot{e} &= \bar{f}(e, \eta, \bar{v}) + \bar{g}(e, \eta, \bar{v})u + \sum_{k=1}^{q} \bar{w}_k(e, \eta, \bar{v})\theta_k \\ \dot{\eta} &= \Psi(e, \eta, \bar{v}) \end{aligned} \tag{2.38}$$

where $\bar{f}(\cdot) = Ae + b\left(L_f^r h(\mathcal{X}^{-1}(e, \eta, \bar{v})) - v^{(r)}\right)$, $\bar{g}(\cdot) = bL_g L_f^{r-1} h(\mathcal{X}^{-1}(e, \eta, \bar{v}))$, $\bar{w}_k(\cdot) = bL_{wk} L_f^{r-1} h(\mathcal{X}^{-1}(e, \eta, \bar{v}))$, the matrix A and column vector b are defined in Eq.2.12. Following the same development presented in Section 2.3, we use the above normal form of Eq.2.38 to construct a quadratic Lyapunov function, $V = e^T P e$, for our controller design, where the positive-definite matrix P is chosen to satisfy the following Riccati inequality:

$$A^T P + PA - Pbb^T P \; < \; 0 \tag{2.39}$$

Assumption 2.6 *The system:*

$$\begin{aligned} \dot{\eta}_1 &= \Psi_1(e, \eta, \bar{v}) \\ &\vdots \\ \dot{\eta}_{n-r} &= \Psi_{n-r}(e, \eta, \bar{v}) \end{aligned} \tag{2.40}$$

is ISS with respect to e, uniformly in $\bar{v}$*, with* $\beta_\eta(|\eta(0)|, t) = K_\eta|\eta(0)|e^{-at}$ *where* $K_\eta \geq 1$*,* $a > 0$ *are real numbers, and exponentially stable when* $e = 0$*.*

Remark 2.14 Following [68], the requirement of input-to-state stability of the system of Eq.2.40 with respect to ζ is imposed to allow the synthesis of a robust state feedback controller that enforces the requested properties in the closed-loop system for arbitrarily large initial conditions and uncertain variables. On the other hand, the requirement that $\beta_\eta(|\eta(0)|, t) = K_\eta e^{-at}$ allows incorporating in the robust output feedback controller a dynamical system identical to the one of Eq.2.40 that provides estimates of the variables η. Assumption 2.6 is satisfied by many chemical processes (see, for example, [65] and the chemical reactor example of Section 2.6).

We are now in a position to state the main results of this chapter. In what follows we present the results for the case of vanishing uncertainty first, and then provide the parallel treatment for case of non-vanishing uncertainty.

2.5.2 Near-optimality over the infinite horizon

Theorem 2.3 below provides an explicit formula for the robust near-optimal output feedback controller and states precise conditions under which the proposed controller enforces the desired properties in the closed-loop system. The proof of this theorem is given in Appendix A.

Theorem 2.3 *Consider the uncertain nonlinear system of Eq.2.1, for which Assump-*

tions 2.3, 2.5 and 2.6 hold, under the robust output feedback controller:

$$\begin{aligned}
\dot{\tilde{y}} &= \begin{bmatrix} -La_1 & 1 & 0 & \cdots & 0 \\ -L^2a_2 & 0 & 1 & \cdots & 0 \\ \vdots & \vdots & \vdots & \ddots & \vdots \\ -L^{r-1}a_{r-1} & 0 & 0 & \cdots & 1 \\ -L^r a_r & 0 & 0 & \cdots & 0 \end{bmatrix} \tilde{y} + \begin{bmatrix} La_1 \\ L^2a_2 \\ \vdots \\ L^{r-1}a_{r-1} \\ L^r a_r \end{bmatrix} y \\
\dot{\omega}_1 &= \Psi_1(sat(\tilde{y}), \omega) \\
&\vdots \\
\dot{\omega}_{n-r} &= \Psi_{n-r}(sat(\tilde{y}), \omega) \\
u &= p(\hat{x}, c_0, \rho, \chi, \phi, \theta_b)
\end{aligned} \tag{2.41}$$

where $p(\cdot) = -[c_0 + r_s(\hat{x}) + r_d(\hat{x}, \rho, \chi, \phi, \theta_b)]\widehat{L_{\bar{g}}V}$, *the functions* r_s, r_d *were defined in Eqs.2.16-2.17,* $\hat{x} = \mathcal{X}^{-1}(sat(\tilde{y}), \omega))$, $V = e^T P e$, P *is a positive-definite matrix that satisfies Eq.2.39, and* c_0, ρ, χ, *and* ϕ *are adjustable parameters that satisfy* $c_0 > 0$, $\rho > 0$, $\chi > 2$, *and* $\phi > 0$. *Furthermore, assume that the uncertain variables are vanishing in the sense defined in Theorem 2.1 and let* $\epsilon = \frac{1}{L}$. *Then, for each set of positive real numbers* $\delta_x, \delta_\theta, \delta_{\bar{v}}$, *there exists* $\phi^* > 0$ *and for each* $\phi \in (0, \phi^*]$, *there exists an* $\epsilon^*(\phi) > 0$, *such that if* $\phi \in (0, \phi^*]$, $\epsilon \in (0, \epsilon^*(\phi)]$, $sat(\cdot) = \min\{1, \frac{\zeta_{max}}{|\cdot|}\}(\cdot)$ *with* ζ_{max} *being the maximum value of the vector* $[\zeta_1 \ \zeta_2 \ \cdots \ \zeta_r]$ *for* $|\zeta| \leq \beta_\zeta(\delta_\zeta, 0)$ *where* β_ζ *is a class* $\mathcal{KL}$ *function and* δ_ζ *is the maximum value of the vector* $[h(x) \ L_f h(x) \ \cdots L_f^{r-1}h(x)]$ *for* $|x| \leq \delta_x$, $|x(0)| \leq \delta_x$, $\|\theta\| \leq \delta_\theta$, $\|\bar{v}\| \leq \delta_{\bar{v}}$, $|\tilde{y}(0)| \leq \delta_\zeta$, $\omega(0) = \eta(0) + O(\epsilon)$, *the following holds:*

(1) The origin of the closed-loop system is exponentially stable.

(2) The output of the closed-loop system satisfies a relation of the form:

$$\limsup_{t \to \infty} |y(t) - v(t)| = 0 \tag{2.42}$$

(3) The output feedback controller of Eq.2.41 is near-optimal with respect to the cost functional of Eq.2.19 in the sense that $J_v^* \longrightarrow V(e(0))$ *as* $\epsilon \longrightarrow 0$, *where* $J_v^* = J_v(u = p(\hat{x}))$.

Remark 2.15 The robust output feedback controller of Eq.2.41 consists of a high-gain observer which provides estimates of the derivatives of the output y up to order $r-1$, denoted as $\tilde{y}_0, \tilde{y}_1, \cdots, \tilde{y}_{r-1}$, and thus estimates of the variables $\zeta_1, \ldots, \zeta_r$ (note that from Assumption 2.5 it follows directly that $\zeta_k = \frac{d^{k-1}y}{dt^{k-1}}, k = 1, \cdots, r$), an observer that simulates the inverse dynamics of the system of Eq.2.37, and a static state feedback controller (see discussion in remark 3.2 below) that attenuates the effect of the uncertain variables on the output and enforces reference input tracking. To eliminate the peaking phenomenon associated with the high-gain observer, we use a standard saturation function, *sat*, to eliminate wrong estimates of the output derivatives for short times. We choose to saturate $\tilde{y}_0, \tilde{y}_1, \ldots, \tilde{y}_{r-1}$ instead of the control action as was proposed in [171], because in most practical applications, it is possible to use knowledge of process operating conditions to derive nonconservative bounds on the actual values of the output derivatives.

Remark 2.16 The static component of the controller of Eq.2.41 is the same as that given in Theorem 2.1, except that it is now a function of the state estimate and not the actual state. The first component is a generalization of Sontag's formula proposed in [278] where the parameter c_0 was introduced to ensure the strict positivity of $R(x)$. Recall from Theorem 2.1 that the static component of the feedback controller of Eq.2.15 (with $\hat{x} = x$) is optimal with respect to a meaningful cost of the form of Eq.2.19 and that the minimum cost achieved under the state feedback controller is $V(e(0))$.

Remark 2.17 The near-optimality property established in Theorem 2.3 for the output feedback controller of Eq.2.41 is defined in the sense that the infinite-horizon cost incurred by implementing this controller on the system of Eq.2.1 tends to the minimum cost achieved by implementing the robust optimal state feedback controller (i.e., u of Eq.2.41 with $\hat{x} = x$) when the gain of the observer is chosen to be sufficiently large. It is important therefore to realize that near-optimality of the controller of Eq.2.41 is a consequence of two integral factors. The first is the optimality of the

static component of the controller (state feedback problem), and the second is the high-gain nature of the observer which can be exploited to make the performance of the output feedback controller arbitrarily close to that of the state feedback controller over the infinite time-interval. Instrumental in this regard is the use of the saturation function (see Remark 2.15) which allows the use of arbitrarily large values of the observer gain to achieve the desired degree of near-optimality without the detrimental effects of observer peaking. Combining other types of observers that do not possess these properties with the static component of Eq.2.41, therefore, will not lead to a near-optimal feedback controller design in the sense of Theorem 2.3.

Remark 2.18 A stronger near-optimality result than the one established in Theorem 2.3 can be obtained in a sufficiently small neighborhood of the origin of the system of Eq.2.1, where the functions $l(e)$ and $R(x)$ satisfy the Lipschitz property. Over such a neighborhood, it can be shown, using the local Lipschitz properties, that the cost computed using the output feedback controller of Eq.2.41 is, in fact, $O(\epsilon)$ close to the optimal cost attained under the optimal state feedback controller (i.e. $J_v^* = V(e(0)) + O(\epsilon)$).

Remark 2.19 Owing to the presence of the fast (high-gain) observer in the dynamical system of Eq.2.41, the closed-loop system can be cast as a two time-scale system and, therefore, represented in the following singularly perturbed form, where $\epsilon = \frac{1}{L}$ is the singular perturbation parameter:

$$\begin{aligned}
\epsilon \dot{e}_o &= A e_o + \epsilon b \Omega(x, \hat{x}, \theta, \phi, \bar{v}) \\
\dot{\omega}_1 &= \Psi_1(sat(\tilde{y}), \omega) \\
&\vdots \\
\dot{\omega}_{n-r} &= \Psi_{n-r}(sat(\tilde{y}), \omega) \\
\dot{x} &= f(x) + g(x)\mathcal{A}(\hat{x}, \bar{v}, \phi) + \sum_{k=1}^{q} w_k(x)\theta_k(t)
\end{aligned} \tag{2.43}$$

where e_o is a vector of the auxiliary error variables $\hat{e}_i = L^{r-i}(y^{(i-1)} - \tilde{y}_i)$ (see part 1 of the proof of Theorem 2.3 in the appendix for the details of the notation used). It is clear from the above representation that, within the singular perturbation formulation, the observer states, e_o, which are directly related to the estimates of the output and its derivatives up to order $r-1$, constitute the fast states of the singularly perturbed system of Eq.2.43, while the ω states of the observer and the states of the original system of Eq.2.1 represent the slow states. Owing to the dependence of the controller of Eq.2.41 on both the slow and fast states, the control action computed by the static component in Eq.2.41 is not $O(\epsilon)$ close to that computed by the state feedback controller for all times. After the decay of the boundary layer term e_o, however, the static component in Eq.2.41 approximates the state feedback controller to within $O(\epsilon)$.

Remark 2.20 Although the results of theorem 3.1 were developed for the class of systems described by Eq.2.1, these results can be easily extended to the more general two time-scale systems with the following state-space description:

$$\begin{aligned} \dot{x} &= f_1(x,\theta(t)) + Q_1(x,\theta(t))z + g_1(x)u \\ \bar{\epsilon}\dot{z} &= f_2(x,\theta(t)) + Q_2(x,\theta(t))z + g_2(x)u \\ y &= h(x) \end{aligned} \tag{2.44}$$

where the parameter ϵ introduced in Theorem 2.3 can now be re-defined as $\epsilon = max\{\frac{1}{L}, \bar{\epsilon}\}$. In fact, the fast nature of the observer used in Eq.2.41, which allows treatment of the closed-loop system within the singular perturbations framework, makes such an extension quite natural without the need to impose any additional restrictive assumptions. For some related results on near-optimal control of singularly perturbed systems, the reader is referred to [114, 58, 113].

It is important to point out that the result of Theorem 2.3 is novel even in the case of no plant-model mismatch, where $\theta(t) \equiv 0$. The following corollary states the result for this case:

Corollary 2.1 *Suppose the assumptions of Theorem 2.3 are satisfied for the nonlinear system of Eq.2.1 with* $\theta_k(t) \equiv 0$, *then the closed-loop system properties (1)-(3) given in Theorem 2.3 hold under the output feedback controller of Eq.2.41 with* $\rho = \chi = 0$.

2.5.3 Near-optimality over the finite horizon

We now turn to the second control problem posed earlier where the uncertain variable terms in Eq.2.1 are non-vanishing. To this end, we modify Assumption 2.6 to the following one.

Assumption 2.7 *The system of Eq.2.40 is ISS with respect to* e, *uniformly in* $\bar{v}$, *with* $\beta_\eta(|\eta(0)|, t) = K_\eta |\eta(0)| e^{-at}$ *where* $K_\eta \geq 1$, $a > 0$ *are real numbers.*

Theorem 2.4 below provides an explicit formula for the construction of the necessary robust near-optimal output feedback controller and states precise conditions under which the proposed controller enforces the desired properties in the closed-loop system. The proof of this theorem is given in Appendix A.

Theorem 2.4 *Consider the uncertain nonlinear system of Eq.2.1, for which Assumptions 2.3, 2.5 and 2.7 hold, under the robust output feedback controller:*

$$
\begin{aligned}
\dot{\tilde{y}} &= \begin{bmatrix} -La_1 & 1 & 0 & \cdots & 0 \\ -L^2a_2 & 0 & 1 & \cdots & 0 \\ \vdots & \vdots & \vdots & \ddots & \vdots \\ -L^{r-1}a_{r-1} & 0 & 0 & \cdots & 1 \\ -L^r a_r & 0 & 0 & \cdots & 0 \end{bmatrix} \tilde{y} + \begin{bmatrix} La_1 \\ L^2a_2 \\ \vdots \\ L^{r-1}a_{r-1} \\ L^r a_r \end{bmatrix} y \\
\dot{\omega}_1 &= \Psi_1(sat(\tilde{y}), \omega) \\
&\vdots \\
\dot{\omega}_{n-r} &= \Psi_{n-r}(sat(\tilde{y}), \omega) \\
u &= p(\hat{x}, c_0, \rho, \chi, \phi, \theta_b)
\end{aligned}
\tag{2.45}
$$

where $p(\cdot) = -[c_0 + r_s(\hat{x}) + r_d(\hat{x}, \rho, \chi, \phi, \theta_b)]\widehat{L_{\bar{g}}V}$, *Furthermore, assume that the functions* $\bar{w}_k(\zeta, \eta)$ *are non-vanishing in the sense defined in Theorem 2.2 and let* $\epsilon = \frac{1}{L}$. *Then, for each set of positive real numbers* δ_x, δ_θ, $\delta_{\bar{v}}$, d, *there exists* $\phi^* > 0$ *and for each* $\phi \in (0, \phi^*]$, *there exists an* $\epsilon^*(\phi) > 0$, *such that if* $\phi \in (0, \phi^*]$, $\epsilon \in (0, \epsilon^*(\phi)]$, $sat(\cdot) = \min\{1, \frac{\zeta_{max}}{|\cdot|}\}(\cdot)$ *with* ζ_{max} *being the maximum value of the vector* $[\zeta_1 \ \zeta_2 \ \cdots \ \zeta_r]$ *for* $|\zeta| \leq \beta_\zeta(\delta_\zeta, 0) + d$ *where* β_ζ *is a class* $\mathcal{KL}$ *function and* δ_ζ *is the maximum value of the vector* $[h(x) \ L_f h(x) \ \cdots L_f^{r-1}h(x)]$ *for* $|x| \leq \delta_x$, $|x(0)| \leq \delta_x$, $\|\theta\| \leq \delta_\theta$, $\|\bar{v}\| \leq \delta_{\bar{v}}$, $|\tilde{y}(0)| \leq \delta_\zeta$, $\omega(0) = \eta(0) + O(\epsilon)$, *the following holds:*

(1) The trajectories of the closed-loop system are bounded.

(2) The output of the closed-loop system satisfies a relation of the form:

$$\limsup_{t\to\infty} |y(t) - v(t)| \leq d \tag{2.46}$$

(3) The output feedback controller of Eq.2.45 is near-optimal with respect to the cost functional of Eq.2.25 in the sense that $J_n^* \longrightarrow V(e(0))$ *as* $\epsilon \longrightarrow 0$, *where* $J_n^* = J_n(u = \tilde{p}(\hat{x}))$.

Remark 2.21 Note that owing to the persistent nature of the uncertainty in this case, asymptotic convergence of the closed-loop system to the equilibrium point of the nominal system (i.e. $\theta(t) \equiv 0$) is no longer possible. Therefore, the cost functional J cannot achieve a finite value over the infinite time-interval. Instead, J is defined over a finite time-interval $[0, T_f]$ whose size is determined by the time required for the tracking error trajectory to reach and enter the ball Γ without ever leaving again. Depending on the desired degree of uncertainty attenuation, the size of this ball can be tuned by adjusting the parameters ϕ and χ. An additional consequence of the non-vanishing uncertainty is the appearance of the terminal penalty term $\lim_{t\to T_f} V(e(t))$ in the cost functional of Eq.2.25 which accounts for the fact that the closed-loop trajectories do not converge asymptotically to the origin for $t > T_f$.

Remark 2.22 In contrast to the output feedback controller design of Theorem 2.3, the controller design of Theorem 2.4 is near-optimal in the sense that the cost incurred

by implementing this controller to the system of Eq.2.1 can be made arbitrarily close to the optimal cost achieved by the corresponding robust optimal state feedback controller, for times in the finite interval $[0, T_f]$, by choosing the gain of the observer to be sufficiently large. As a consequence of the non-vanishing uncertainty, near-optimality can be established on the finite time-interval only and not for all times.

Remark 2.23 Referring to the practical applications of the result of Theorem 2.4, one has to initially verify whether Assumptions 2.5 and 2.7 hold for the process under consideration and compute the bounds θ_{bk}. Then, Eq.2.41 can be used to compute the explicit formula of the controller. Finally, given the ultimate uncertainty attenuation level desired, d, the values of ϕ^* and the observer gain L should be computed (usually through simulations) to achieve $\limsup_{t\to\infty}|y(t) - v(t)| \leq d$ and guarantee the near-optimal performance of the controller.

2.6 Application to a non-isothermal chemical reactor

2.6.1 Process description and control problem formulation

To illustrate the implementation and performance of the output feedback controller design presented in the previous chapter theoretical results presented in this chapter, we consider a well-mixed continuous stirred tank reactor where three parallel irreversible elementary endothermic reactions of the form $A \xrightarrow{k_1} D$, $A \xrightarrow{k_2} U$ and $A \xrightarrow{k_3} R$ take place, where A is the reactant species, D is the desired product and U, R are undesired byproducts. The feed to the reactor consists of pure A at flow rate F, molar concentration C_{A0} and temperature T_{A0}. Due to the endothermic nature of the reactions, a heating jacket is used to provide heat to the reactor. Under standard modeling assumptions, a mathematical model of the process can be derived from

material and energy balances and takes the following form:

$$\begin{aligned} V\frac{dC_A}{dt} &= F(C_{A0} - C_A) - \sum_{i=1}^{3} k_{i0} \exp\left(\frac{-E_i}{RT}\right) C_A V \\ V\frac{dC_D}{dt} &= -FC_D + k_{10} \exp\left(\frac{-E_1}{RT}\right) C_A V \\ V\frac{dT}{dt} &= F(T_{A0} - T) + \sum_{i=1}^{3} \frac{(-\Delta H_i)}{\rho c_p} k_{i0} \exp\left(\frac{-E_i}{RT}\right) C_A V + \frac{UA}{\rho c_p}(T_c - T) \end{aligned} \tag{2.47}$$

where C_A and C_D denote the concentrations of the species A and D, T denotes the temperature of the reactor, T_c denotes the temperature of the heating jacket, V denotes the volume of the reactor, ΔH_i, k_{i0}, E_i, $i = 1, 2, 3$, denote the enthalpies, pre-exponential constants and activation energies of the three reactions, respectively, c_p and ρ denote the heat capacity and density of the reactor, and U denotes the heat transfer coefficient between the reactor and the heating jacket. The values of the process parameters and the corresponding steady-state values are given in Table 2.1. It was verified that these conditions correspond to a stable equilibrium point of the system of Eq.2.47. The control problem is formulated as the one of regulating the concentration of the desired product C_D by manipulating the temperature of the fluid in the heating jacket T_c. Within the posed control problem we distinguish and address the following two scenarios. In the first scenario, the control objective is achieved in the absence of any model uncertainty or exogenous disturbances in the process. By contrast, the control objective in the second scenario is accomplished in the presence of uncertainty. In the latter scenario, the enthalpies of the three reactions $\Delta H_i, i = 1, 2, 3$ and the feed temperature T_{A0} are assumed to be the main uncertain variables present. Defining $x_1 = C_A - C_{As}$, $x_2 = C_D - C_{Ds}$, $x_3 = T - T_s$, $u = T_c - T_{cs}$, $\theta_1 = \Delta H_1 - \Delta H_{10}$, $\theta_2 = \Delta H_2 - \Delta H_{20}$, $\theta_3 = \Delta H_3 - \Delta H_{30}$, $\theta_4 = T_{A0} - T_{A0s}$, $y = C_D - C_{Ds}$, where the subscript s denotes the steady-state values and ΔH_{D0}, ΔH_{U0}, ΔH_{R0} are the nominal values for the enthalpies, the process model of Eq.2.47

Table 2.1: Process parameters and steady-state values for the reactor of Eq.2.47.

V	=	1.00	m^3
A	=	6.0	m^2
U	=	1000.0	$kcal\ hr^{-1}\ m^{-2}\ K^{-1}$
R	=	1.987	$kcal\ kmol^{-1}\ K^{-1}$
C_{A0s}	=	3.75	$kmol\ m^{-3}$
T_{A0s}	=	310.0	K
T_{cs}	=	320.0	K
ΔH_{10}	=	5.4×10^3	$kcal\ kmol^{-1}$
ΔH_{20}	=	5.1×10^3	$kcal\ kmol^{-1}$
ΔH_{30}	=	5.0×10^4	$kcal\ kmol^{-1}$
k_{10}	=	3.36×10^6	hr^{-1}
k_{20}	=	7.21×10^6	hr^{-1}
k_{30}	=	1.25×10^7	hr^{-1}
E_1	=	8.0×10^3	$kcal\ kmol^{-1}$
E_2	=	9.0×10^3	$kcal\ kmol^{-1}$
E_3	=	9.5×10^3	$kcal\ kmol^{-1}$
c_p	=	0.231	$kcal\ kg^{-1}\ K^{-1}$
ρ	=	900.0	$kg\ m^{-3}$
F	=	3.0	$m^3\ hr^{-1}$
C_{AS}	=	0.913	$kmol\ m^{-3}$
C_{DS}	=	1.66	$kmol\ m^{-3}$
T_s	=	302.0	K

can be written in the form of Eq.2.1 where:

$$f(x) = \begin{bmatrix} \frac{F}{V}(C_{A0} - C_{As} - x_1) - \sum_{i=1}^{3} k_{i0} \exp\left(\frac{-E_i}{R(x_3 + T_s)}\right)(x_1 + C_{As}) \\ -\frac{F}{V}(C_{Ds} + x_2) + k_{10} \exp\left(\frac{-E_1}{R(x_3 + T_s)}\right)(x_1 + C_{As}) \\ \frac{F}{V}(T_{A0s} - T_s - x_3) + \sum_{i=1}^{3} \frac{(-\Delta H_i)}{\rho c_p} k_{i0} \exp\left(\frac{-E_i}{R(x_3 + T_s)}\right)(x_1 + C_{As}) \\ + \frac{UA}{\rho c_p}(T_{cs} - T_s - x_3) \end{bmatrix}$$

$$g(x) = \begin{bmatrix} 0 \\ 0 \\ \frac{UA}{\rho c_p} \end{bmatrix}, \quad w_i(x) = \begin{bmatrix} 0 \\ 0 \\ k_{i0} \exp\left(\frac{-E_i}{R(x_3 + T_s)}\right)(x_1 + C_{As}) \end{bmatrix}, \quad i = 1, 2, 3$$

$$w_4(x) = \begin{bmatrix} 0 \\ 0 \\ \frac{F}{V} \end{bmatrix}, \quad h(x) = \begin{bmatrix} x_2 \end{bmatrix}$$

Using the following coordinate transformation:

$$\begin{bmatrix} \zeta_1 \\ \zeta_2 \\ \eta_1 \end{bmatrix} = \begin{bmatrix} h(x) \\ L_f h(x) \\ t(x) \end{bmatrix} = \begin{bmatrix} x_2 \\ -\frac{F}{V}(C_{Ds} + x_2) + k_{10} \exp\left(\frac{-E_1}{R(x_3 + T_s)}\right)(x_1 + C_{As}) \\ x_1 \end{bmatrix} \tag{2.48}$$

and the notation $\bar{f}(e, \eta, \bar{v}) = [e_2 \quad L_f^2 h(x) - v^{(2)}]^T$, $\bar{g}(e, \eta, \bar{v}) = [0 \quad L_g L_f h(x)]^T$, $\bar{w}_k(e, \eta, \bar{v}) = [0 \quad L_{wk} L_f h(x)]^T$, $k = 1, 2, 3, 4$, the process model can be cast in the

following form:

$$\begin{aligned} \dot{e} &= \bar{f}(e,\eta,\bar{v}) + \bar{g}(e,\eta,\bar{v})u + \sum_{k=1}^{4}\bar{w}_k(e,\eta,\bar{v})\theta_k \\ \dot{\eta} &= \Psi(e,\eta,\bar{v}) \\ y &= e_1 + v \end{aligned} \tag{2.49}$$

2.6.2 Controller synthesis and simulation results

We now proceed with the design of the controller and begin with the first scenario where no uncertainty is assumed to be present in the process model (i.e. $\theta_k \equiv 0$). Owing to the absence of uncertainty in this case, we use the result of Corollary 2.1 to design the controller. It can be easily verified that the system of Eq.2.49 satisfies the Assumptions of the corollary and therefore the necessary output feedback controller (whose practical implementation requires measurements of C_D only) takes the form:

$$\begin{aligned} \dot{\tilde{y}}_1 &= \tilde{y}_2 + La_1(y - \tilde{y}_1) \\ \dot{\tilde{y}}_2 &= L^2 a_2(y - \tilde{y}_1) \\ \dot{\omega}_1 &= \frac{F}{V}(C_{A0} - C_{As} - \hat{x}_1) - \sum_{i=1}^{3} k_{i0}\exp\left(\frac{-E_i}{R(\hat{x}_3 + T_s)}\right)(\hat{x}_1 + C_{As}) \\ u &= -\left(c_0 + \frac{L_{\hat{f}}\hat{V} + \sqrt{(L_{\hat{f}}\hat{V})^2 + (L_{\hat{g}}\hat{V})^4}}{(L_{\hat{g}}\hat{V})^2}\right) L_{\hat{g}}\hat{V} \end{aligned} \tag{2.50}$$

where

$$\begin{aligned} V &= e^T P e, \quad P = \begin{bmatrix} 1 & c \\ c & 1 \end{bmatrix}, \quad c \in (0,1) \\ L_{\hat{f}}\hat{V} &= 2\left((\hat{x}_2 - v) + c\left(L_f h(\hat{x}) - v^{(1)}\right)\right)\left(L_f h(\hat{x}) - v^{(1)}\right) \\ &+ 2\left(c\,(\hat{x}_2 - v) + \left(L_f h(\hat{x}) - v^{(1)}\right)\right)\left(L_f^2 h(\hat{x}) - v^{(2)}\right) \\ L_{\hat{g}}\hat{V} &= 2\left(c\,(\hat{x}_2 - v) + \left(L_f h(\hat{x}) - v^{(1)}\right)\right) L_g L_f h(\hat{x}) \end{aligned} \tag{2.51}$$

For the sake of comparison, we consider also the nonlinear output feedback controller synthesized based on the concepts of feedback linearization and proposed in [60] with the static component:

$$u = -\frac{1}{L_g L_f h(\hat{x})} \left\{ \frac{\beta_0}{\beta_2}(\hat{x}_2 - v) + \frac{\beta_1}{\beta_2}(L_f h(\hat{x}) - v^{(1)}) + (L_f^2 h(\hat{x}) - v^{(2)}) \right\} \quad (2.52)$$

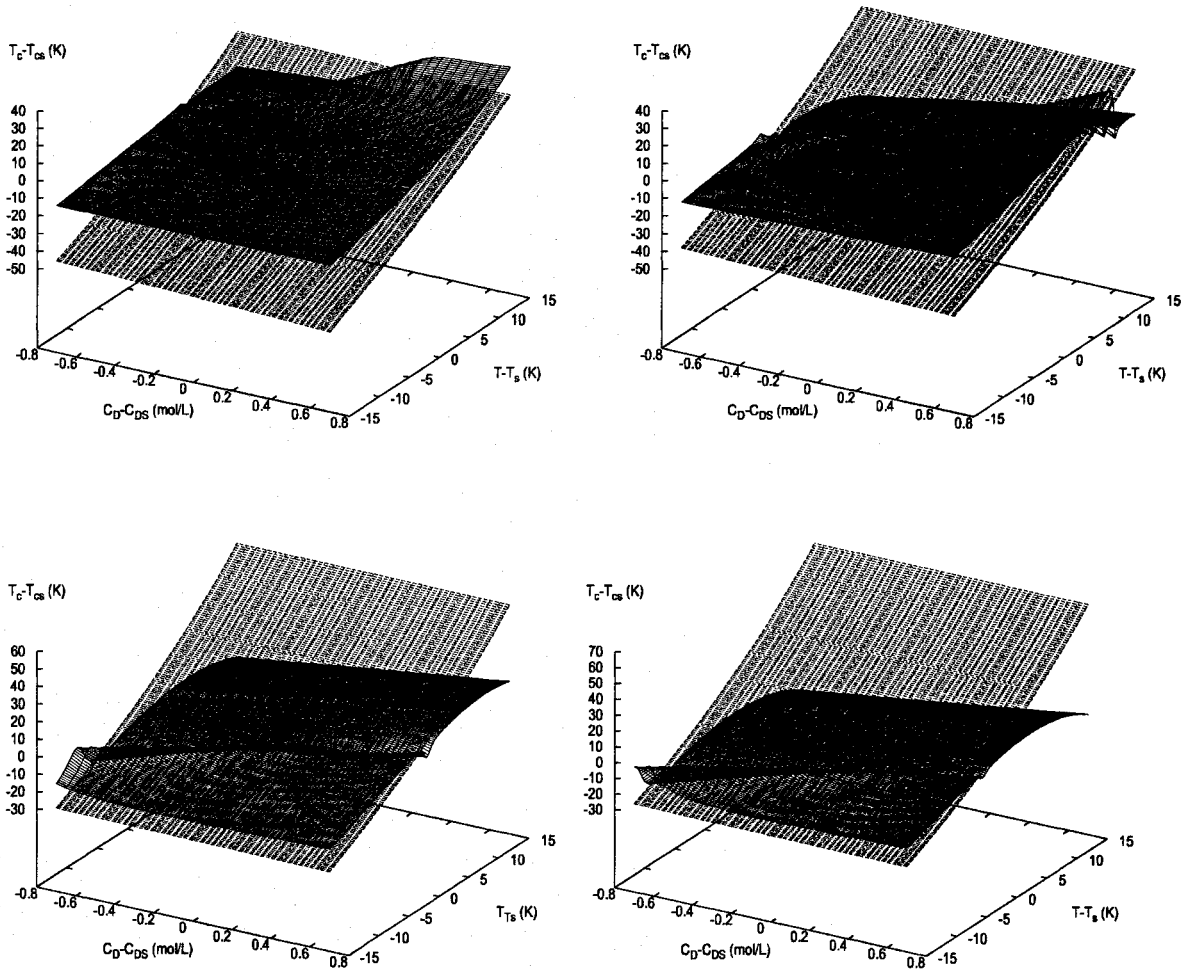

Figure 2.3: Control actions computed by the static component of the controller of Eq.2.50 (solid lines) and the controller of Eq.2.52 (dashed lines) for $C_A - C_{AS} = -0.4$ (top left), -0.2 (top right), 0.2 (bottom left), 0.4 (bottom right)

Before we present the simulation results for the first scenario, we first establish the fact that the static *state* feedback component of the controller of Eq.2.50 does not expend unnecessary control effort in comparison with the static controller of Eq.2.52. To this end, we compared the control actions generated by the two controllers for a broad range of T and C_D. The results are shown in Figure 2.6.2 for several values of C_A. Clearly, the controller of Eq.2.50 utilizes smaller control action than that of Eq.2.52.

Two sets of simulation runs were performed to evaluate the performance and near-optimality properties of the dynamic output feedback controller of Eq.2.50. The following values were used for the controller and observer parameters: $c_0 = 0.1$, $\alpha = 1.0$, $c = 0.99$, $L = 3000$, $a_1 = 10$, $a_2 = 20$, $a_m = 1.0$.

In the first set of simulation runs, we evaluated the capability of the controller to steer the process to the steady-state given in Table 2.1 starting from arbitrary initial conditions. Figure 2.4 shows the controlled output profile and the corresponding manipulated input profile. Clearly, the controller successfully steers the process to the desired steady-state. Also shown in the figure is a comparison between the output feedback controller of Eq.2.50 and the corresponding state feedback controller (i.e., the static component of Eq.2.50 with $\hat{x} = x$) synthesized under the assumption that all process states are available for measurement. It was shown in Section 2.3.2 that the state feedback controller is optimal with respect to a meaningful cost of the form of Eq.2.19. From Figure 2.4, one can immediately observe that the controlled output and manipulated input profiles obtained under the output feedback controller are very close to the profiles obtained under the state feedback controller. This comparison then makes clear the fact that the controller of Eq.2.50 is near-optimal in the sense that its performance approaches the optimal performance of the state

feedback controller when the observer gain is sufficiently high. To further illustrate the near-optimality result, we compared the costs associated with both the state feedback and output feedback controllers. The costs were computed and found to be 0.250 and 0.257, respectively, further confirming the near-optimality of the controller of Eq.2.50.

In the second set of simulation runs, we tested the output tracking capabilities of the output feedback controller of Eq.2.50. The process was initially assumed to be at the steady-state given in Table 2.1 and then a 0.5 mol/L decrease in the value of the reference input was imposed ($v = -0.5$). Figure 2.5 shows the profiles of the controlled output of the process and of the corresponding manipulated input. One can immediately observe that the controller successfully drives the output to the desired new reference input value. The figure also shows the closeness of the controlled output and manipulated input profiles obtained under the output feedback and state feedback controllers. It is clear that the tracking capabilities of the output feedback controller approach those of the optimal state feedback controller and therefore the controller of Eq.2.50 is near-optimal.

We now consider the second scenario where we account for the presence of uncertainty in the process. The following time-varying uncertain variables were considered in the simulation runs:

$$\begin{aligned} \theta_i(t) &= 0.4\,(-\Delta H_{i0})\,[1 + sin(2t)]\,, \quad i = 1, 2, 3 \\ \theta_4(t) &= 0.07 T_{A0s}\,[1 + sin(2t)] \end{aligned} \tag{2.53}$$

The upper bounds on the uncertain variables were taken to be $\theta_{bi} = 0.4\,|(-\Delta H_{i0})|$, for $i = 1, 2, 3$, $\theta_{b4} = 0.07 T_{A0s}$. Moreover, the following values were used for the tuning parameters of the controller and the observer: $c_0 = 0.1$, $c = 0.99$, $\phi = 0.005$, $\chi = 1.1$, $L = 30000$, $a_1 = 10$, $a_2 = 20$, $a_m = 1.0$ to guarantee that the output of the closed-loop

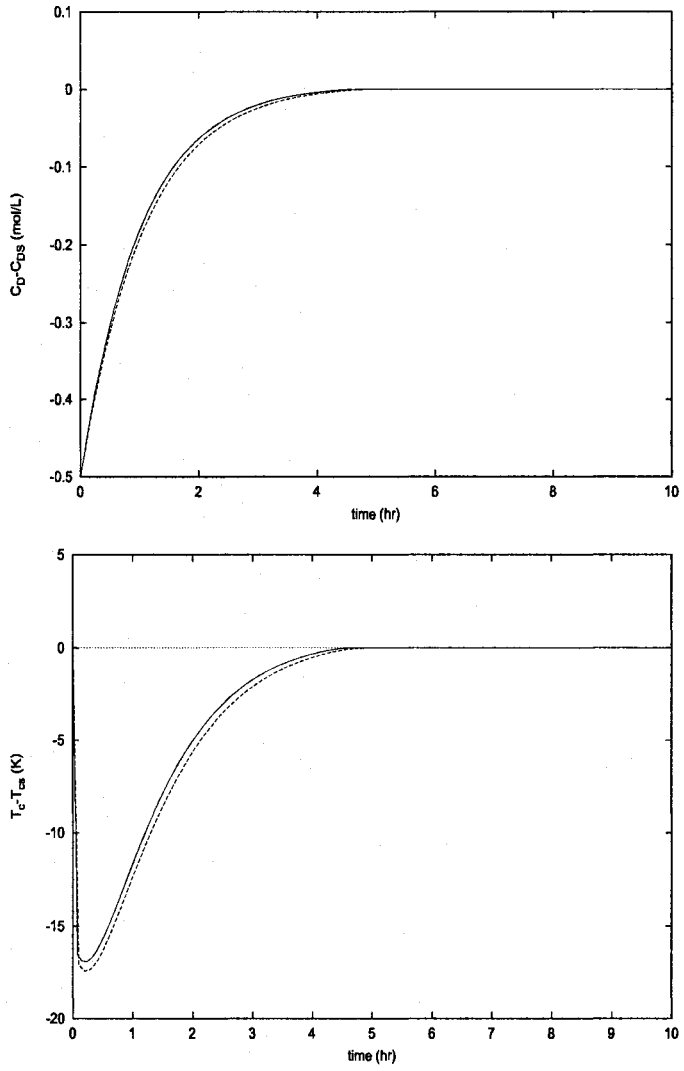

Figure 2.4: Closed-loop output and manipulated input profiles for stabilization under the output feedback controller of Eq.2.50 (dashed lines) and the optimal state feedback controller (solid lines) when no uncertainty is present.

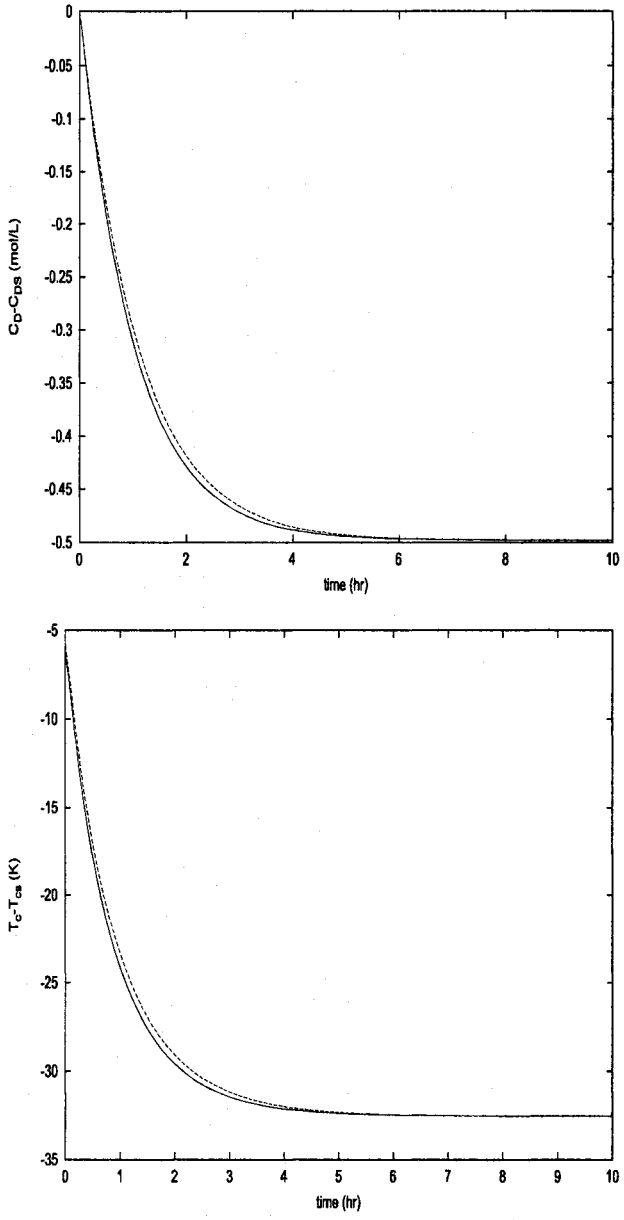

Figure 2.5: Closed-loop output and manipulated input profiles for reference input tracking under the output feedback controller of Eq.2.50 (dashed lines) and the optimal state feedback controller (solid lines) when no uncertainty is present.

system satisfies a relation of the following form:

$$\limsup_{t\to\infty} |y - v| \leq 0.005 \tag{2.54}$$

To design the necessary controller in this case, we note that since the $\bar{w}_k$ functions defined in Eq.2.49 do not vanish at the origin, the uncertain variables considered here are non-vanishing. Therefore, we use the result of Theorem 2.4 to construct the necessary robust output feedback controller which takes the following form:

$$\begin{aligned}
\dot{\tilde{y}}_1 &= \tilde{y}_2 + La_1(y - \tilde{y}_1) \\
\dot{\tilde{y}}_2 &= L^2 a_2(y - \tilde{y}_1) \\
\dot{\omega}_1 &= \frac{F}{V}(C_{A0} - C_{As} - \hat{x}_1) - \sum_{i=1}^{3} k_{i0} \exp\left(\frac{-E_i}{R(\hat{x}_3 + T_s)}\right)(\hat{x}_1 + C_{As}) \\
u &= -\left(c_0 + \frac{L_{\hat{f}}\hat{V} + \sqrt{(L_{\hat{f}}\hat{V})^2 + (L_{\hat{g}}\hat{V})^4}}{(L_{\hat{g}}\hat{V})^2} + \chi \frac{\sum_{k=1}^{4} \theta_{bk} |L_{wk} L_f h(\hat{x})|}{L_g L_f h(\hat{x})^2 (\frac{|L_{\hat{g}}\hat{V}|}{|L_g L_f h(x)|} + \phi)}\right) L_{\hat{g}}\hat{V}
\end{aligned} \tag{2.55}$$

where V, $L_{\hat{f}}\hat{V}$, $L_{\hat{g}}\hat{V}$ were defined in Eq.2.51.

Several sets of simulation studies were performed to assess the performance, robustness, and near-optimality properties of the dynamic robust output feedback controller of Eq.2.55. In the first set of simulations, we tested the ability of the controller to drive the output of the process close to the desired steady-state starting from arbitrary initial conditions despite the presence of uncertainty. Figure 2.6 shows the controlled output profile and the manipulated input profile. One can immediately see that the effect of the uncertainty has been significantly reduced (compare with the output of the open-loop system) and the output of the process remains very close to the desired steady-state satisfying the requirement of Eq.2.54. Included in the figure also are the controlled output and manipulated input profiles for the process under the

optimal state feedback controller (i.e., the static component of Eq.2.55 with $\hat{x} = x$) which was shown in Theorem 2.2 to be optimal with respect to the cost functional of Eq.2.25 with $\hat{x} = x$. It is clear from the figure that the profiles obtained under the output feedback controller follow closely those obtained under the optimal state feedback controller and, therefore, the robust output feedback controller of Eq.2.55 is near-optimal.

In the second set of simulations, we investigated the significance of the term responsible for uncertainty compensation in the controller of Eq.2.55. To this end, we implemented the controller of Eq.2.55 on the process without the uncertainty compensation component. The closed-loop output and manipulated input profiles for this simulation run are given in Figure 2.7. It is clear that the effect of the uncertain variables is appreciable, leading to poor transient performance and offset and that uncertainty compensation is required to achieve the control objective.

In the last set of simulations performed, we tested the output tracking capabilities of the controller of Eq.2.55 for a 0.5 mol/L decrease in the value of the reference input. The resulting closed-loop output and manipulated input profiles, shown in Figure 2.8, clearly establish the capability of the output feedback controller of Eq.2.55 to enforce the requirement of Eq.2.54, despite the presence of uncertainty. Furthermore, Figure 2.8 establishes the near-optimality of the output feedback controller within the context of robust output tracking. This is evident from the closeness of the performance of the robust output feedback controller of Eq.2.55 to that of the corresponding robust optimal state feedback controller.

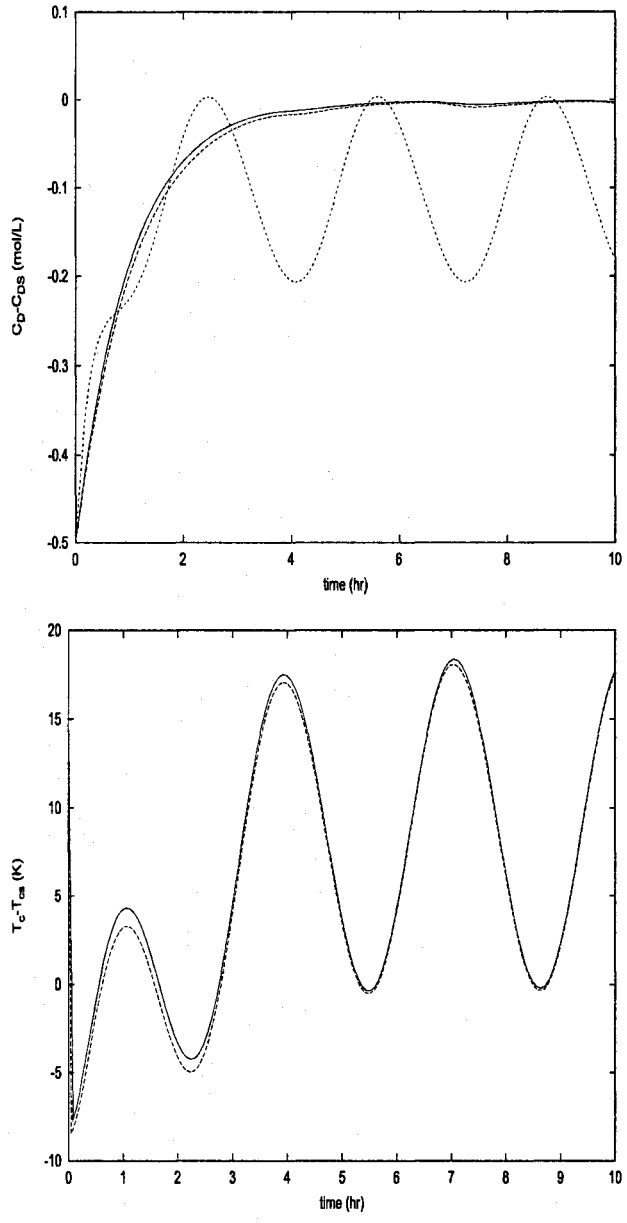

Figure 2.6: Closed-loop output and manipulated input profiles for stabilization under the robust output feedback controller of Eq.2.55 (dashed lines), the robust optimal state feedback controller (solid lines) and open-loop profile (dotted line).

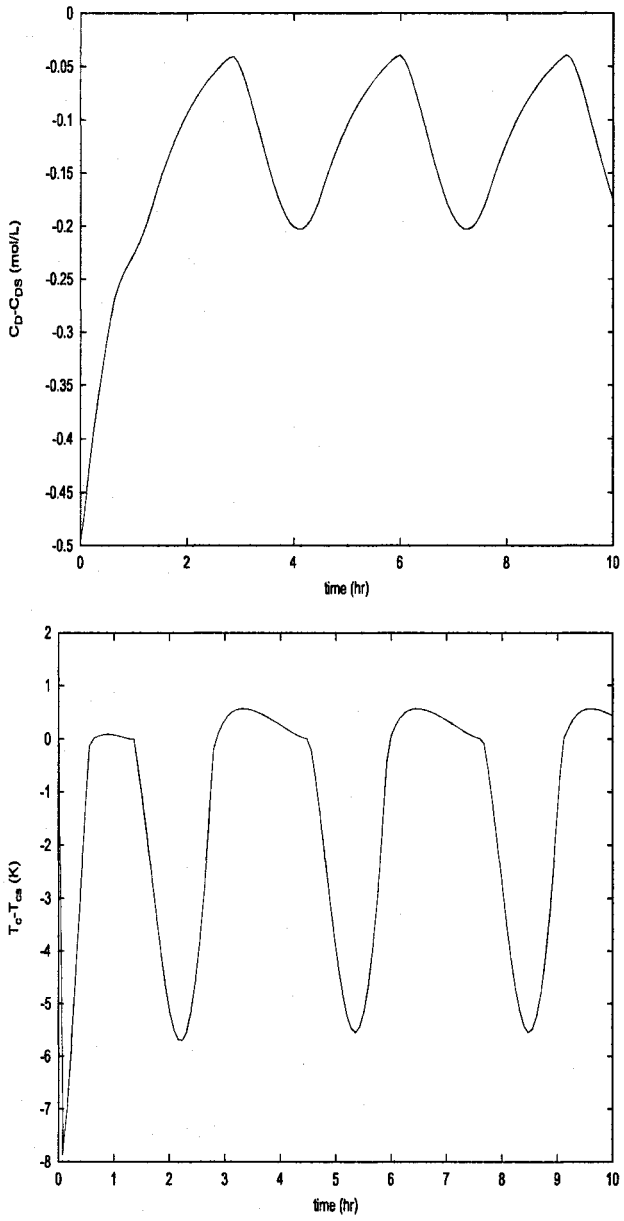

Figure 2.7: Closed-loop output and manipulated input profiles for stabilization under the output feedback controller of Eq.2.55 with no uncertainty compensation ($\chi = 0$).

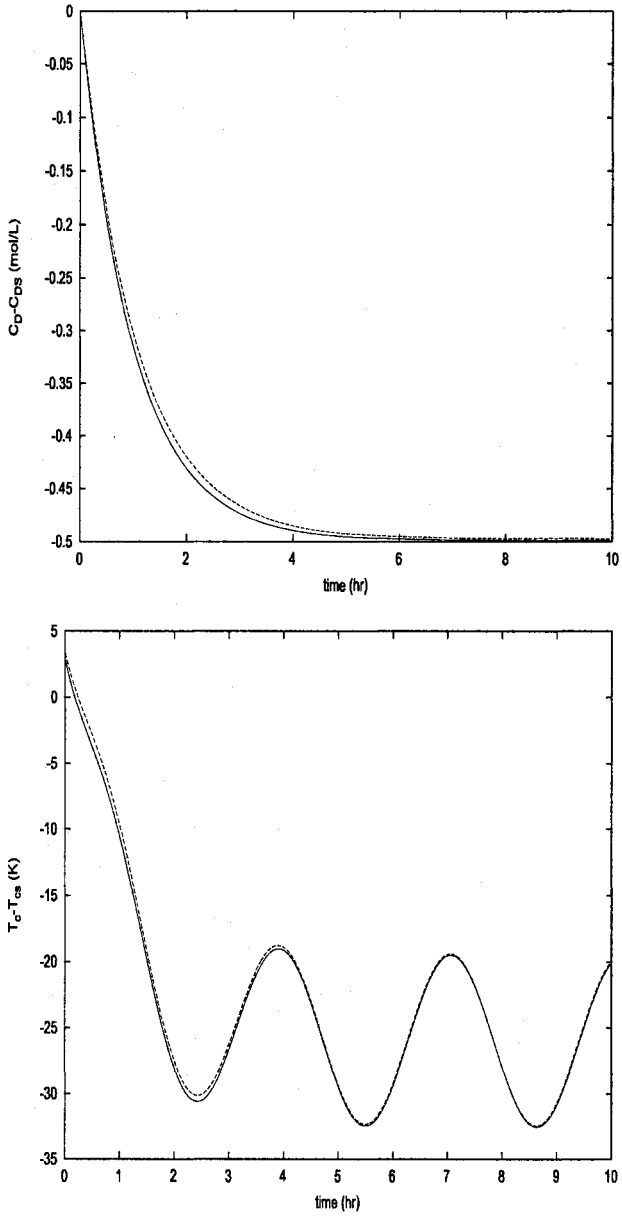

Figure 2.8: Closed-loop output and manipulated input profiles for reference input tracking under the robust output feedback controller of Eq.2.55 (dashed lines) and the robust optimal state feedback controller (solid lines).

2.7 Conclusions

In this chapter, we presented robust inverse optimal controller designs for input/output linearizable nonlinear systems with time-varying bounded uncertain variables. Under full state feedback, the controller designs were obtained by re-shaping the scalar nonlinear gain of Sontag's formula in a way that guarantees the desired uncertainty attenuation properties in the closed-loop system. The proposed re-shaping was made different for vanishing and non-vanishing uncertainties so as to meet different robustness and optimality objectives. For systems with vanishing uncertainty, the proposed controller design was shown to enforce global asymptotic stability, robust asymptotic output tracking and inverse optimality with respect to an infinite-time cost functional that includes penalty on the control effort. For systems with non-vanishing uncertainty, the designed controllers were shown to ensure boundedness of the states, robust asymptotic output tracking with an arbitrary degree of attenuation of the effect of uncertainty, and optimality with respect to a meaningful cost defined on a finite time-interval. In the absence of full state measurements, combination of the state feedback controllers with high-gain observers and appropriate saturation filters (to eliminate observer peaking) was employed to design dynamic robust output feedback controllers. Under vanishing uncertainty, the output feedback controllers were shown to enforce asymptotic stability stability, robust asymptotic output tracking with uncertainty attenuation, and near-optimal performance over the infinite time-interval for arbitrarily large initial conditions and uncertainty, provided that the observer gain is sufficiently large. Under persistent uncertainty, the same controllers were shown to guarantee boundedness of the states, robust output tracking with uncertainty attenuation, and near-optimality over a finite time-interval. The developed controllers were successfully tested on non-isothermal stirred tank reactors with uncertainty.

Chapter 3

Control of Nonlinear Systems with Uncertainty and Constraints

3.1 Introduction

In addition to nonlinear behavior and model uncertainty, one of the ubiquitous characteristics of process control systems is the presence of hard constraints on the manipulated input. At this stage, most existing process control methods lead to the synthesis of controllers that can deal with either model uncertainty or input constraints, but not simultaneously or effectively with both. This clearly limits the achievable control quality and closed-loop performance, especially in view of the commonly-encountered co-presence of uncertainty and constraints in chemical processes. Therefore, the development of a unified framework for control of nonlinear systems that explicitly accounts for the presence of model uncertainty and input constraints is expected to have a significant impact on process control.

While the individual presence of either model uncertainty or input constraints poses its own unique set of problems that must be dealt with at the stage of con-

troller design, the combined presence of both uncertainty and constraints is far more problematic for process stability and performance. The difficulty here emanates not only from the cumulative effect of the co-presence of the two phenomena but also from the additional issues that arise from the interaction of the two. At the core of these issues are the following two problems:

- The co-presence of model uncertainty and input constraints creates an inherent conflict in the controller design objectives of the control policy to be implemented. On the one hand, suppressing the influence of significant external disturbances typically requires large (high-gain) control action. On the other hand, the availability of such action is often limited by the presence of input constraints. Failure to resolve this conflict will render any potential control strategy essentially ineffective.

- The set of feasible process operating conditions under which the process can be operated safely and reliably is significantly restricted by the co-presence of uncertainty and constraints. While input constraints by themselves place fundamental limitations on the size of this set (and consequently on our ability to achieve certain control objectives), these limitations are even stronger when uncertainty is present. Intuitively, many of the feasible operating conditions permitted by constraints under nominal conditions (i.e., predicted using a nominal model of the process) cannot be expected to continue to be feasible in the presence of significant plant-model mismatch. The success of a control strategy, therefore, hinges not only on the design of effective controllers, but also on the ability to predict a priori the feasible conditions under which the designed controllers are guaranteed to work in the presence of both uncertainty and constraints.

A natural approach to resolve the apparent conflict between the need to compensate for model uncertainty through high-gain control action and the presence of input constraints that limit the availability of such action is the design of robust controllers which expend reasonable control effort to achieve stabilization and uncertainty attenuation. This problem was addressed in Chapter 2 where we synthesized, through Lyapunov's direct method, robust inverse optimal nonlinear controllers that use reasonable control effort to enforce stability and asymptotic output tracking with attenuation of the effect of the uncertain variables on the output of the closed-loop system. The resulting controllers, although better equipped to handle input constraints than feedback linearizing controllers, do not explicitly account for input constraints and, therefore, offer no a priori guarantees regarding the desired closed-loop stability and performance in the presence of arbitrary input constraints.

In this chapter, we develop a unified framework for control of constrained uncertain nonlinear processes that integrates robustness, optimality, and explicit constraint-handling capabilities in the controller synthesis and provides, simultaneously, an explicit and intuitive characterization of the regions of guaranteed closed-loop stability. Using a general state-space Lyapunov-based approach, the developed framework yields a direct nonlinear controller design method that accounts explicitly for closed-loop stability and performance in the presence of uncertainty and input constraints. The basic idea is the development of a scaling procedure, inspired by the results in [204] for systems without uncertainty, that bounds the robust optimal controllers synthesized in Chapter 2. This leads to the derivation of explicit analytical formulas for bounded robust controllers with well-characterized stability and performance properties. The rest of this chapter is organized as follows. In Section 3.2, we present the class of systems we consider in this chapter and highlight some of the shortcomings of

conventional process control strategies in dealing with constrained nonlinear processes subject to uncertainty. In Section 3.3, we present the controller design methodology for systems with both vanishing an non-vanishing time-varying uncertain variables. We show that, for processes with vanishing uncertainty, the developed controllers guarantee asymptotic closed-loop stability and robust asymptotic set-point tracking with an arbitrary degree of attenuation of the effect of uncertainty on the output of the closed-loop system in the presence of input constraints. For processes with non-vanishing uncertainty, the controllers are shown to ensure boundedness of the states and robust asymptotic output tracking in the presence of input constraints. Finally, in Section 3.4, the proposed control method is illustrated through a chemical reactor example and compared with existing process control strategies. The results of this chapter were first presented in [91].

3.2 Preliminaries

3.2.1 System description

We consider the class of continuous-time, single-input single-output (SISO) nonlinear processes with uncertain variables and manipulated input constraints, with the following state-space description:

$$\begin{aligned} \dot{x} &= f(x) + g(x)u + \sum_{k=1}^{q} w_k(x)\theta_k(t) \\ u(t) &\in \mathcal{U} \\ y &= h(x) \end{aligned} \tag{3.1}$$

where $x \in \mathbb{R}^n$ denotes the vector of process state variables, $u \in \mathcal{U} \subset \mathbb{R}$ denotes the constrained manipulated input taking values in the set, $\mathcal{U} := \{u \in \mathbb{R} : |u| \leq u_{max}\}$, where u_{max} is a positive real number that captures the size of the constraints, $\theta_k(t) \in$

$\mathcal{W}_k \subset \mathbb{R}$ denotes the k-th uncertain (possibly time-varying) but bounded variable taking values in a nonempty compact convex subset $\mathcal{W}_k$ of $\mathbb{R}$, $y \in \mathbb{R}$ denotes the output to be controlled. The uncertain variable, $\theta_k(t)$, may describe time-varying parametric uncertainty and/or exogenous disturbances. To simplify the presentation of our results, we assume without loss of generality that the origin is the equilibrium point of the nominal system of Eq.3.1 (i.e., with $u(t) = \theta_k(t) \equiv 0$). The vector functions, $f(x)$, $w_k(x)$ and $g(x)$, and the scalar function, $h(x)$, are assumed to be sufficiently smooth. In the remainder of this chapter, for simplicity, we will suppress the time-dependence in the notation of the uncertain variable, $\theta_k(t)$. The class of systems described by Eq.3.1 is general enough to be of practical interest (see the application studies throughout the chapter), yet specific enough to allow the meaningful synthesis of controllers.

3.2.2 Traditional approaches

Most of nonlinear analytical controllers emanating from the area of geometric process control are input-output linearizing and induce a linear input-output response in the absence of constraints [182, 148]. For the class of processes modeled by equations of the form of Eq.3.1 with $\theta_k \equiv 0$ and relative order r and under the minimum phase assumption, the appropriate linearizing state feedback controller is given by:

$$u = \frac{1}{L_g L_f^{r-1} h(x)} \left(v - L_f^r h(x) - \beta_1 L_f^{r-1} h(x) - \cdots - \beta_{r-1} L_f h(x) - \beta_r h(x) \right) \tag{3.2}$$

and induces the linear input-output dynamics given by:

$$\frac{d^r y}{dt} + \beta_1 \frac{d^{r-1} y}{dt} + \cdots + \beta_{r-1} \frac{dy}{dt} + \beta_r y = v \tag{3.3}$$

where the tunable parameters, $\beta_1 \cdots \beta_r$, are essentially closed-loop time constants that influence and shape the output response. The nominal stability of the process is

guaranteed by placing the roots of the polynomial $s^r + \beta_1 s^{r-1} + \cdots + \beta_{r-1} s + \beta_r$ in the open left-half of the complex plane. Since the control law of Eq.3.2 does not possess the ability to reject unmeasured disturbances or track exogenous signals, an external linear controller with "integral" action is typically employed around the static state feedback linearizing controller to ensure an offsetless response in the presence of constant disturbances and model errors. In the event of input saturation, however, the controller dynamics will result in the problem of windup, causing deterioration in the closed-loop performance and stability properties of the controller due to the wrong update of the states of the linear controller around the linearizing controller. Motivated by these problems, recent research efforts on the analytical control of constrained nonlinear processes have focused on devising various compensatory schemes and modifications of the above approach to offer greater flexibility in obtaining a desirable closed-loop output response in the presence of constraints and compensate for windup [300, 158].

Despite the improvement that may be achieved in the closed-loop performance using the above approaches, these schemes continue to face two fundamental limitations in their ability to effectively handle the co-presence of model uncertainty and input constraints. The first such limitation is the use of input-output linearizing control techniques to synthesize the necessary control laws. Despite being an effective control strategy in the absence of constraints, a major drawback of input-output linearizing control techniques, in general, is their inherent lack of direct constraint handling capabilities. One reason for this is the fact that these techniques rely on cancelling out process nonlinearities using feedback and may therefore generate unnecessarily large control effort to cancel beneficial process nonlinearities. The cost of cancelling the nonlinearities can be large enough to unnecessarily saturate the control input, poten-

tially leading to closed-loop instability or performance deterioration. Modifying such controllers a posteriori to account for the presence of input constraints may result in an unnecessary restriction of operation in a relatively small region around the desired set-point and makes the stability analysis of the closed-loop system a difficult task. The second limitation of existing process control techniques relates to the continued use of integral or integral-like action to compensate for the effect of disturbances. These techniques, while suited for constant disturbances, may yield unsatisfactory robustness in the presence of time-varying disturbances.

Realizing the above limitations clearly motivates the need for an alternative, direct controller design strategy for nonlinear processes with time-varying uncertainty and input constraints, that avoids the above mentioned shortcomings and guarantees, *a priori*, the desirable performance and stability properties of the closed-loop system in the presence of arbitrary disturbances and input constraints. Before presenting the details of this strategy, let us first demonstrate, by means of a benchmark chemical process example, some of the limitations of existing process control strategies.

3.2.3 Motivating example

To illustrate some of the detrimental effects of time-varying uncertainty and input constraints on the closed-loop stability and performance under input-output linearizing controllers, we simulate in this subsection the startup performance of a nonisothermal chemical reactor under the generalized mixed error- and state-feedback controller proposed in Theorem 1 in [300], which employs input-output linearizing control techniques and inherently compensates for windup. Consider a continuous stirred tank reactor where an irreversible, exothermic first-order reaction of the form $A \xrightarrow{k} B$ takes place. The inlet stream consists of pure A at flow rate F, concentration C_{A0} and tem-

perature T_{A0}. Under standard modeling assumptions, the mathematical model for the process takes the form:

$$\begin{aligned} V\frac{dC_A}{dt} &= F(C_{A0} - C_A) - k_0 \exp\left(\frac{-E}{RT}\right) C_A V \\ V\frac{dT}{dt} &= F(T_{A0} - T) + \frac{(-\Delta H)}{\rho c_p} k_0 \exp\left(\frac{-E}{RT}\right) C_A V + \frac{Q}{\rho c_p} \end{aligned} \tag{3.4}$$

where C_A denotes the concentration of species A, T denotes the temperature of the reactor, V denotes the volume of the reactor, k_0, E and ΔH denote the pre-exponential constant, the activation energy, and the enthalpy of the reaction, respectively, c_p and ρ denote the heat capacity and density of the fluid in the reactor, and Q denotes the rate of heat input to the reactor. The steady-state values and process parameters are given in Table 3.1.

Table 3.1: Process parameters and steady-state values for the reactor of Eq.3.4.

V	=	100.0	L
R	=	8.314	$J/mol.K$
C_{A0}	=	1.0	mol/L
T_{A0s}	=	310.0	K
ΔH	=	-4.78×10^4	J/mol
k_0	=	7.20×10^{10}	min^{-1}
E	=	8.31×10^4	J/mol
c_p	=	0.239	$J/g.K$
ρ	=	1000.0	g/L
F	=	100.0	L/min
C_{As}	=	0.577	mol/L
T_s	=	395.3	K

The control objective is to stabilize and maintain the temperature of the reactor at the open-loop unstable steady-state value given in Table 3.1, in the presence of time-varying disturbances in the feed temperature and uncertainty in the enthalpy of the reaction, by manipulating the rate of heat input. Defining $x_1 = C_A$, $x_2 = T$, $u = Q$, $\theta_1 = T_{A0} - T_{A0s}$, $\theta_2 = \Delta H - \Delta H_{nom}$, $y = x_2$, where the subscript

s denotes the steady-state values, the process model of Eq.3.4 can be recast in the form of Eq.3.1 with:

$$f(x) = \begin{bmatrix} \frac{F}{V}(C_{A0} - C_A) - k_0 \exp\left(\frac{-E}{RT}\right) C_A \\ \frac{F}{V}(T_{A0s} - T) + \frac{-\Delta H_{nom}}{\rho c_p} k_0 \exp\left(\frac{-E}{RT}\right) C_A \end{bmatrix}, \quad g(x) = \begin{bmatrix} 0 \\ \frac{1}{\rho c_p V} \end{bmatrix}$$

$$w_1(x) = \begin{bmatrix} 0 \\ \frac{F}{V} \end{bmatrix}, \quad w_2(x) = \begin{bmatrix} 0 \\ k_0 \exp\left(\frac{-E}{RT}\right) C_A \end{bmatrix} \tag{3.5}$$

and $h(x) = x_2$. For this process, the relative degree is well-defined and $r = 1$ since $\left(L_g h = \frac{1}{\rho c_p V} \neq 0\right)$. The system is also minimum phase due to the asymptotic stability of its zero-dynamics. Therefore, the controller proposed in [300] takes the following form:

$$\begin{aligned} \dot{\eta}_1 &= -\frac{1}{\beta_1}\eta_1 + \frac{1}{\beta_1}\left[T + \beta_1\left(\frac{F}{V}(T_{A0} - T) + \frac{-\Delta H_{nom}}{\rho c_p} k_0 \exp\left(\frac{-E}{RT}\right) C_A + \frac{u}{\rho c_p V}\right)\right] \\ \dot{\zeta}_1 &= -\frac{1}{\gamma_1}\zeta_1 + \frac{1}{\gamma_1}(\eta_1 + e), \\ u &= sat\left\{\frac{\rho c_p V}{\gamma_1}\left[\eta_1 + e + \left(\frac{\gamma_1}{\beta_1} - 1\right)\zeta_1 - \frac{\gamma_1}{\beta_1}T - \gamma_1 R(C_A, T)\right]\right\} \end{aligned} \tag{3.6}$$

where $e = T_s - T$, $\eta_1(0) = T(0)$, $\zeta_1(0) = T(0)$ and

$$R(C_A, T) = \left[\frac{F}{V}(T_{A0} - T) + \frac{-\Delta H_{nom}}{\rho c_p} k_0 \exp\left(\frac{-E}{RT}\right) C_A\right]$$

The following time-varying uncertain variables are considered:

$$\theta_1(t) = 0.1 T_{A0s} sin(3t), \quad \theta_2(t) = 0.5\,(-\Delta H_{nom})\, sin(3t) \tag{3.7}$$

The physical motivation for considering sinusoidal variations in the heat of reaction is the fact that heat of reaction is a function of temperature. Therefore, in the

presence of sinusoidal variations (disturbances) in the feed temperature, the reactor temperature and heat of reaction will vary sinusoidally in time.

Figure 3.1 depicts the reactor temperature and heat input profiles under the generalized mixed error- and state-feedback controller of Eq.3.6 with $\beta_1 = 0.5\ min, \gamma_1 = 0.35\ min$. The solid line represents the response when there is no limit on the heat input to the reactor (i.e., $|Q| < \infty$) and no disturbances or model errors are present. In this case, the controller successfully stabilizes the process at the desired steady-state. The dashed line in Figure 3.1 corresponds to the startup performance of the reactor in the presence of the time-varying uncertain variables considered in Eq.3.7 but no limits on the rate of heat input are imposed. It is clear from the oscillatory behavior of the response that the controller fails to stabilize the process at the desired steady-state or attenuate the effect of uncertainty on the closed-loop output. Note that the controller generates a huge control effort to try to compensate for the effect of uncertainty on the output of the closed-loop system. The controller starts by requesting excessive heat which together with the higher rate of heat production by the reaction at the higher temperatures later prompts the controller to demand excessive cooling. The closed-loop instability is even more profound when limits are imposed on the rate of heat input to the reactor rendering the excessive heating or cooling requirements infeasible. This is indicated by the dotted line in Figure 3.1 which corresponds to the response of the reactor in the presence of uncertainty and constraints on the rate of heat input to the reactor ($|Q| \leq 80$ KJ/s).

The above example highlights an important feature of the class of nonlinear controllers given by Eq.3.2 – as well as other existing feedback linearizing controllers with windup compensation schemes in general – which is their lack of optimality. Since such controllers employ cancellations to achieve their objective, they cannot be

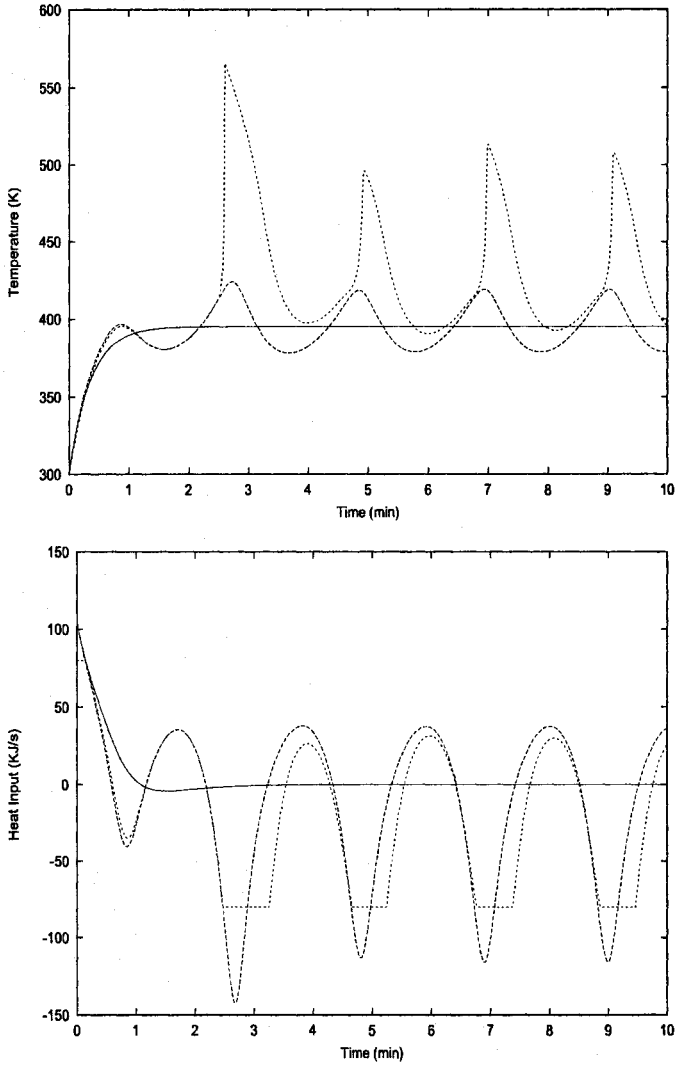

Figure 3.1: Startup profiles of the controlled output and manipulated input for the chemical reactor example under the dynamic mixed error-and state-feedback controller with windup compensation given in Eq.3.6 in the absence of uncertainty or constraints (solid line), in the presence of uncertainty with no constraints (dashed line), and in the presence of both uncertainty and constraints (dotted line).

expected to be optimal with respect to any reasonable criteria [112]. A direct consequence of this lack of optimality is the wasteful expenditure of control action leading to the unnecessary saturation of control actuators. In the presence of time-varying uncertainty, the inability of the controller to compensate properly for the disturbances further confounds the loss of stability and performance deterioration problems.

Let us now apply the robust inverse optimal control laws proposed Chapter 2 to the non-isothermal chemical reactor considered above. The aim of this application is to evaluate the capabilities of this class of controllers in handling the co-presence of uncertainty and constraints, and compare them with those of feedback linearizing-based designs. To this end, consider the same control objective and uncertain variables described earlier in this section. Note that the uncertain variables considered are non-vanishing. Therefore, we use the result of Theorem 2.2 to construct the appropriate controller. Using the control Lyapunov function, $V = \frac{1}{2}c\,(T - T_s)^2$, where $c > 0$, the controller takes the form of Eq.2.23 where:

$$\begin{aligned} L_{\bar{f}}V &= c\,(T - T_s)\left[\frac{F}{V}(T_{A0} - T) + \frac{-\Delta H_{nom}}{\rho c_p}k_0 \exp\left(\frac{-E}{RT}\right)C_A\right] \\ L_{\bar{g}}V &= c\,(T - T_s)\frac{1}{\rho c_p V},\ L_{w1}h(x) = \frac{F}{V},\ L_{w2}h(x) = k_0 \exp\left(\frac{-E}{RT}\right)C_A \end{aligned} \tag{3.8}$$

The following values were used for the controller tuning parameters, $c_0 = 0.1$, $\rho = 0$, $c = 1.0$, $\phi = 0.01$, $\chi = 2.1$, to guarantee that the output of the closed-loop system satisfies a relation of the form:

$$\limsup_{t\to\infty} |T(t) - T_s| \leq 0.01 \tag{3.9}$$

Figure 3.2 depicts the temperature and rate of heat input profiles for the reactor under the robust optimal controller of Eq.2.23 (solid-line) in the presence of both the time-varying uncertainty of Eq.3.7 and constraints on the rate of heat input to the reactor ($|Q| \leq 80$ KJ/s). For the sake of comparison, the corresponding plots under

the input-output linearizing-based controller of Eq.3.6 (dashed-line) are included. It is clear that while the controller of Eq.3.6 fails to stabilize the process at the desired steady-state or compensate for the disturbances, the robust inverse optimal controller of Eq.2.23 successfully drives the process close to the desired steady-state and at the same time attenuates the effect of uncertainty on the reactor temperature. The different outcomes can be understood by inspecting the rate of heat input profiles in Figure 3.2. Due to its optimality and explicit handling of uncertainty, the controller of Eq.2.23 does not expend unnecessary control effort or demand infeasible excessive heating or cooling of the reactor to robustly stabilize the reactor temperature from the given initial condition. By contrast, the controller of Eq.3.6 employs integral action and generates unnecessarily large control action causing the control actuators to saturate. The combination of integral action dynamics and input saturation is responsible for the unstable behavior exhibited under this controller in Figure 3.2.

To investigate the significance of the term responsible for uncertainty attenuation in the controller of Eq.2.23, the controller was implemented on the process without the uncertainty compensation component (i.e., setting $\chi = 0$). The closed-loop output and manipulated input profiles for this case are given in Figure 3.2.3. It is clear that the effect of process uncertainty is significant, leading to poor transient performance and offset and that uncertainty compensation is required to achieve the control objective.

Note that the robust controller of Eq.2.23 successfully achieved the control objective in the presence of input constraints despite the fact that the controller was not designed to explicitly deal with the problem of constraints. The inherent capability of the controller to use reasonable control effort to robustly stabilize the process assisted the controller in naturally avoiding the limitations imposed on the rate of heat input.

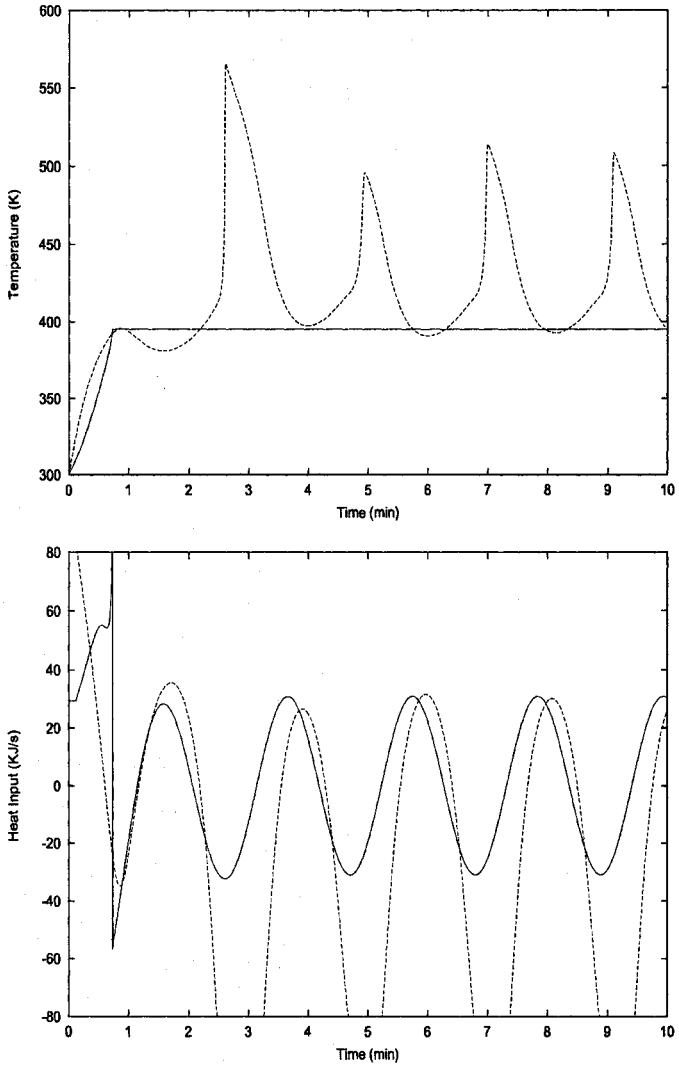

Figure 3.2: Controlled output and manipulated input profiles in the presence of uncertainty and input constraints under the robust controller of Eq.2.23 (solid line) and the input-output linearizing-based controller of Eq.3.6 (dashed line).

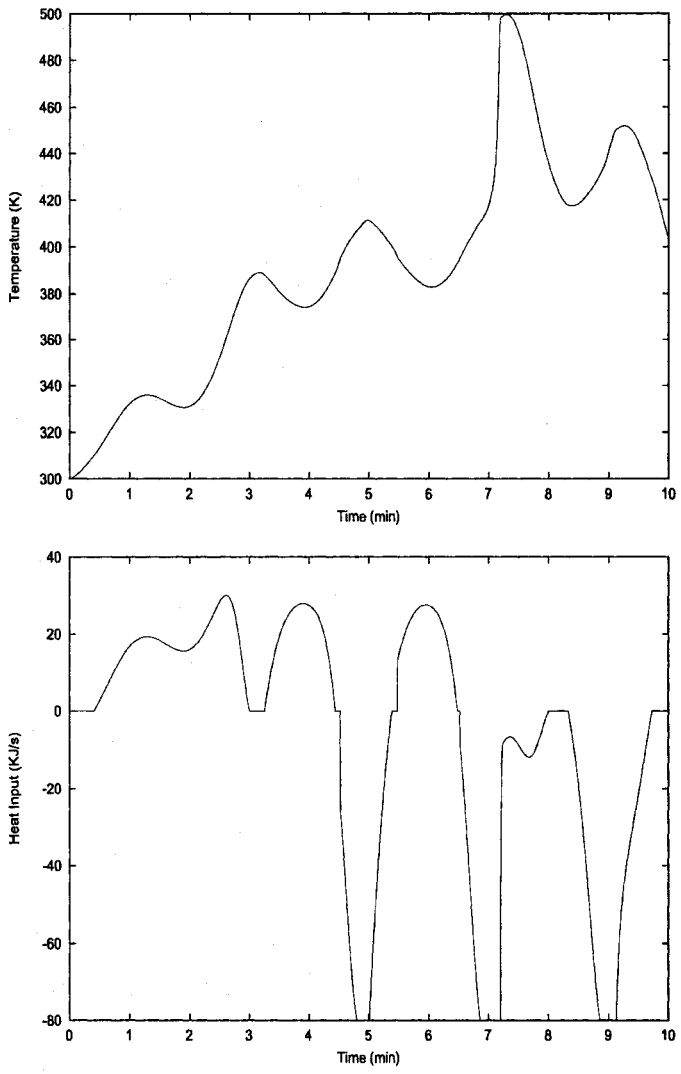

Figure 3.3: Controlled output and manipulated input profiles under the controller of Eq.2.23 without the robust compensation component ($\chi = 0$).

While optimal expenditure of the control action is clearly a necessary tool that the controller must possess to handle input constraints, it might not be sufficient. For example, one can envision situations where the input constraints are tight enough such that the control objectives cannot be met, irrespective of the particular choice of control law, owing to the fundamental limitations imposed by the constraints on the process dynamics. Under such circumstances, it is natural to ask how and whether the robust inverse optimal controller will continue to enforce the requested stability and performance specifications in the presence of increasingly tight input constraints.

Figure 3.4 provides an answer to this question and shows the temperature and rate of heat input profiles for the cases when $|Q| \leq 60$ KJ/s (solid line), $|Q| \leq 30$ KJ/s (dashed line) and $|Q| \leq 20$ KJ/s (dotted line). It is clear from the figure that although the controller continues to successfully stabilize the process and achieve asymptotic uncertainty attenuation when $|Q| \leq 60$ KJ/s, the transient performance of the process begins to deteriorate when $|Q| \leq 30$ KJ/s (note the overshoot) and, eventually, the controller is unable to stabilize the process when $|Q| \leq 20$ KJ/s. In this case, the available control energy is apparently insufficient to robustly stabilize the reactor temperature at the desired set-point starting from the given initial condition. It is important to note here that this conclusion could not be reached before implementing the controller. The simulation results of Figure 3.4 therefore point out the fact that while the robust inverse optimal controller may be better equipped to handle the co-presence of uncertainty and constraints in some cases, it provides no explicit or a priori guarantees regarding stability in the presence of arbitrary input constraints. More specifically, the controller design does not provide the necessary knowledge of the set of admissible initial states that guarantee achievement of the desired control objectives in the presence of input constraints. To address this issue, we present in the

next section a direct robust inverse optimal controller design method that accounts simultaneously for closed-loop performance and stability in the presence of input constraints. The proposed controllers are conceptually aligned with those given in Chapter 2 but have the additional benefits of: (a) integrating robustness, optimality, and explicit constraint-handling in the controller design and (b) providing an explicit and a priori characterization of the regions of guaranteed closed-loop stability.

3.3 Integrating robustness, optimality, and constraints

3.3.1 Control problem formulation

Having illustrated some the possible advantages of the robust inverse optimal controller designs presented in Chapter 2 for controlling constrained uncertain nonlinear processes, we proceed in this section to extend those controller designs to incorporate the additional capability of explicitly handling constraints. In particular, we seek robust inverse optimal controllers of the general form of Eq.2.9 that satisfy the constraints, $|u| \leq u_{max}$, and enforce the desired closed-loop stability, robust asymptotic output tracking, and inverse optimality properties within well-defined regions of the state-space. The key idea behind the new design is that of bounding the robust inverse optimal controllers and is inspired by the results on bounded control presented in [204] for systems without uncertainty.

Using the same state-space Lyapunov-based framework developed in Chapter 2, we derive bounded robust nonlinear control laws that explicitly depend on the magnitude of manipulated input constraints, and generate the necessary control action accordingly. In addition to the explicit incorporation of input constraints, the bounding procedure of yields an explicit characterization of the set of admissible initial conditions starting from where the desired control objectives are guaranteed in the

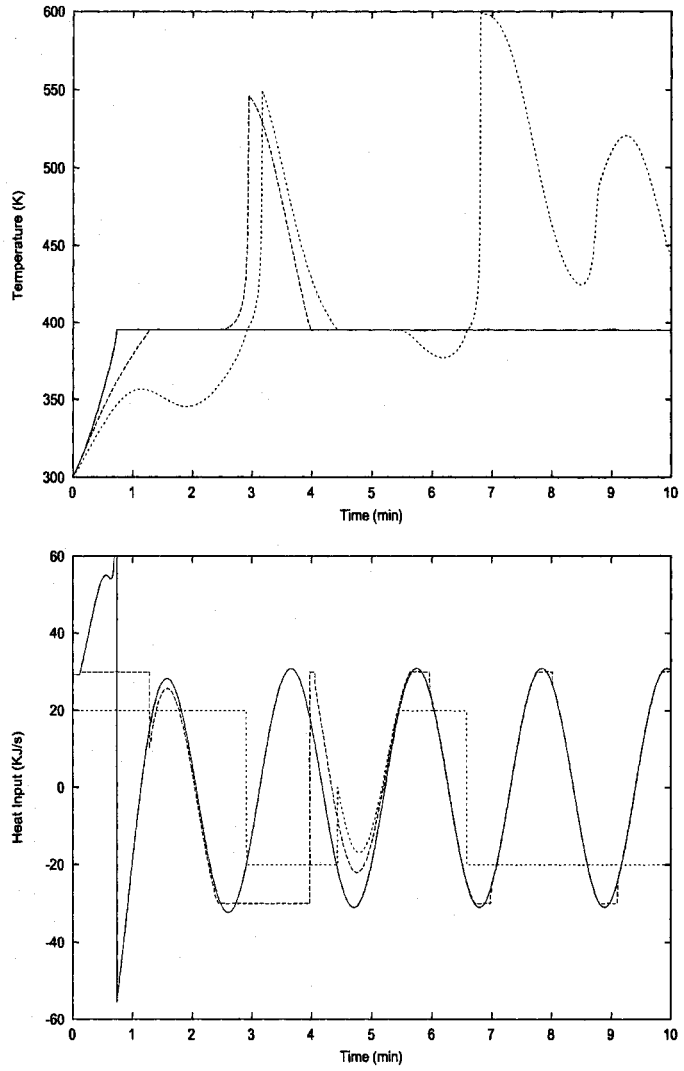

Figure 3.4: Closed-loop output and manipulated input profiles under the controller of Eq.2.23 in the presence of uncertainty and input constraints of $|Q| \leq 60$ KJ/s (solid line), $|Q| \leq 30$ KJ/s (dashed line), and $|Q| \leq 20$ KJ/s (dashed line).

presence of uncertainty and constraints (region of closed-loop stability). Therefore, given the constraints on the the manipulated input, one can directly ascertain how large the resulting region of closed-loop stability is and check, a priori, whether a certain initial condition belongs to this region. Alternatively, given a desired size of the region of closed-loop stability for a process, one can determine the necessary bounds on the manipulated input.

3.3.2 Bounded controller synthesis under vanishing uncertainty

In this subsection, we consider nonlinear processes of the form of Eq.3.1 with vanishing uncertainty and focus on the design of bounded robust inverse optimal nonlinear state feedback control laws that: (a) enforce asymptotic stability and asymptotic robust output tracking in the constrained uncertain closed-loop system, (b) minimize a meaningful performance index defined on the infinite time-interval, and (c) possess a well-defined and explicit characterization of their regions of closed-loop stability. Theorem 3.1 below provides the desired control laws and states precise conditions under which the desired properties hold. The proof of this theorem is given in Appendix B.

Theorem 3.1 *Consider the constrained uncertain nonlinear process of Eq.3.1, for which Assumptions 2.1-2.3 hold, under the static state feedback law:*

$$\begin{aligned} u &= -p(x, u_{max}, \theta_b, \rho, \chi, \phi)\beta(x) \\ &= -\left(\frac{\alpha_1(x) + \omega(x, \theta_b, \rho, \chi)\Lambda(e, \phi) + \sqrt{\alpha_2^2(x, \theta_b, \rho, \chi) + (u_{max}\beta(x))^4}}{\beta^2(x)\left[1 + \sqrt{1 + (u_{max}\beta(x))^2}\right]} \right) \beta(x) \end{aligned} \tag{3.10}$$

where $\alpha_1 = L_{\bar{f}}V$, $\omega = \rho|2b^TPe| + \chi\sum_{k=1}^{q}\theta_{bk}|L_{\bar{w}k}V|$, $\Lambda = |2b^TPe|/(|2b^TPe| + \phi)$, $\alpha_2 = \alpha_1 + \omega$, $\beta = L_{\bar{g}}V$, $V = e^TPe$, *P is a positive-definite matrix that satisfies Eq.2.39, and* ρ, χ *and* ϕ *are adjustable parameters that satisfy* $\rho > 0$, $\chi > 1$ *and* $\phi > 0$. *Assume*

further that the uncertain variables in Eq.3.1 are vanishing in the sense defined in Theorem 2.1. Then for any initial condition starting from where the evolution of the closed-loop system satisfies:

$$L_{\bar{f}}^{*}V + \chi\sum_{k=1}^{q}\theta_{bk}|L_{\bar{w}k}V| \;\leq\; u_{max}|L_{\bar{g}}V| \tag{3.11}$$

where $L_{\bar{f}}^{*}V = L_{\bar{f}}V + \rho|2b^{T}Pe|$, *there exists* $\phi^{*} > 0$ *such that if* $\phi \in (0, \phi^{*}]$, *the following holds:*

(1) The origin of the closed-loop system is asymptotically stable.

(2) The output of the closed-loop system satisfies a relation of the form:

$$\limsup_{t\to\infty}|y(t) - v(t)| = 0 \tag{3.12}$$

Furthermore, if the trajectories of the closed-loop system evolve such that $\forall\ t \geq 0$*:*

$$L_{\bar{f}}^{**}V\left[2 + 4\sqrt{1 + (u_{max}L_{\bar{g}}V)^{2}}\right] \;\leq\; \sqrt{(L_{\bar{f}}^{**}V)^{2} + (u_{max}L_{\bar{g}}V)^{4}} \tag{3.13}$$

where $L_{\bar{f}}^{**}V = L_{\bar{f}}^{*}V + \chi\sum_{k=1}^{q}\theta_{bk}|L_{\bar{w}k}V|$, *and* χ *is chosen to satisfy* $\chi > 2$, *then:*

(3) The static state feedback control law of Eq.3.10 is optimal with respect to the cost functional:

$$J \;=\; \int_{0}^{\infty}(l(e) + uR(x)u)dt \tag{3.14}$$

where $R(x) = \frac{1}{2}p^{-1}(x) > 0$ *and* $l(e) = -L_{\bar{f}}V + \frac{1}{4}L_{\bar{g}}VR^{-1}(x)L_{\bar{g}}V - \sum_{k=1}^{q}|L_{wk}V|\theta_{bk} \geq \sigma|2b^{T}Pe|^{2} \geq 0$, *for some* $\sigma > 0$.

Remark 3.1 Theorem 3.1 proposes a direct robust nonlinear controller design method that accounts explicitly and simultaneously for closed-loop performance and stability in the presence of model uncertainty and input constraints. Note that the bounded control law of Eq.3.10 uses explicitly the available knowledge of both the bounds on the uncertain variables (i.e., θ_{bk}) and the manipulated input constraints (i.e., u_{max}) to generate the necessary control action. This is in contrast to the two-step approach typically employed in process control strategies which first involves the design of a

controller for the unconstrained process and then accounts for the input constraints through a suitable anti-windup modification to attenuate the adverse effects of improperly handled input constraints.

Remark 3.2 In addition to proposing a direct controller design strategy, Theorem 3.1 provides an explicit characterization of the region in the state-space where the desired closed-loop stability and set-point tracking properties outlined in the theorem are guaranteed. This characterization is obtained from the inequality of Eq.3.11, which describes explicitly a region in the state-space where the time-derivative of the Lyapunov function is guaranteed to be negative-definite along the trajectories of the closed-loop system under uncertainty and constraints. Any closed-loop trajectory that evolves (i.e., starts and remains) within this region is guaranteed to converge to the origin. As will be detailed in the next remark, the inequality of Eq.3.11 provides a useful guide for identifying a priori (before implementing the controller) the set of admissible initial conditions starting from where closed-loop stability is guaranteed. This aspect of the proposed design has important practical implications for efficient process operation since it provides plant operators with a systematic and easy-to-implement guide to identify feasible initial conditions for process operation. Considering the fact that the presence of disturbances and constraints limits the conditions under which the process can be operated safely and reliably, the task of identifying these conditions becomes a central one. This is particularly significant in the case of unstable plants where lack of such a priori knowledge can lead to undesirable consequences.

Remark 3.3 Referring to the region described by the inequality of Eq.3.11 – which we will denote by $\mathcal{S}$ in what follows – it is important to note that even though a trajectory starting in $\mathcal{S}$ will move from one Lyapunov surface to an inner Lyapunov surface with lower energy (because $\dot{V} < 0$), there is no guarantee that the trajectory will remain forever in $\mathcal{S}$, since it is not necessarily a region of invariance. Once the trajectory leaves $\mathcal{S}$, however, there is no guarantee that $\dot{V} < 0$. Therefore, in order to

use the inequality of Eq.3.11 to identify the admissible initial conditions starting from where closed-loop stability is guaranteed, we need to find (or estimate) the largest invariant set within $\mathcal{S}$ to guarantee that a trajectory starting in $\mathcal{S}$ remains in the region for all future times. A reasonable estimate is provided by the set:

$$\Omega_c = \{x \in \mathbb{R}^n : \bar{V}(x) \leq c\}$$

when Ω_c is bounded and contained in $\mathcal{S}$ and $\dot{\bar{V}}(x) < 0$ over $\mathcal{S}$. This estimate can be made less conservative by selecting the value of c sufficiently large. Referring to the above definition of the invariant set, Ω_c, it is important to note that the Lyapunov function, $\bar{V}$, is in general not the same as the Lyapunov function, V, given in the statement of Theorem 3.1. The function $\bar{V}$ is based on the full system (i.e., the $\zeta - \eta$ interconnected system of Eq.2.11 while V is based only on the $\zeta-$subsystem. The reason for the difference is the fact that owing to the ISS property of the η-subsystem (see Assumption 2.2), only a Lyapunov function based on the ζ-subsystem, namely $V = e^T P e$, is needed and used to design a control law that stabilizes the full closed-loop system. However, in constructing Ω_c, we need to guarantee that the evolution of x (and, hence, both the ζ and η subsystems) is confined within $\mathcal{S}$. Therefore, the Lyapunov function in this case must account for the evolution of the η states as well. One possible choice for $\bar{V}$ is a composite Lyapunov function, $\bar{V} = V_e + V_\eta$ whose time-derivative is negative-definite at all points satisfying Eq.3.11, where V_e is taken to be the same as the Lyapunov function V given in Theorem 3.1 and V_η is another Lyapunov function for the η-subsystem. The existence of V_η is guaranteed from converse Lyapunov theorems owing to the ISS and asymptotic stability properties of the η-subsystem, and can be computed given the particular structure for this system. For nonlinear systems with relative degree $r = n$, the choice $\bar{V} = V = e^T P e$ is sufficient.

Remark 3.4 The inequality of Eq.3.11 captures the dependence of the size of the region of closed-loop stability on both uncertainty and input constraints. The tighter the input constraints are (i.e., smaller u_{max}), for example, the smaller the resulting

closed-loop stability region. Similarly, the larger the plant-model mismatch (i.e., larger θ_{bk}), the smaller the closed-loop stability region. This is quite intuitive since under such conditions (tighter constraints and larger uncertainty), fewer and fewer initial conditions will satisfy the inequality of Eq.3.11 resulting in a smaller closed-loop stability region. Finally, note that according to the inequality of Eq.3.11, the largest region of closed-loop stability under the control law of Eq.3.10 is obtained in the absence of constraints (i.e., as $u_{max} \rightarrow \infty$).

Remark 3.5 The inequality of Eq.3.11 reveals an interesting interplay between the controller design parameters and the uncertainty in influencing the size of the resulting region of guaranteed closed-loop stability. To this end, note the multiplicative appearance of the parameter, χ, and the bound on the uncertainty, θ_{bk}, in Eq.3.11. In the presence of significant process disturbances, one typically selects a large value for χ to achieve an acceptable level of robust performance of the controller. According to the inequality of Eq.3.11, this comes at the expense of obtaining a smaller region of closed-loop stability. Alternatively, if one desires to expand the region of closed-loop stability by selecting a small value for χ, this may be achieved at the expense of obtaining an unsatisfactory degree of uncertainty attenuation or will be limited to cases where the uncertainty is not too large (i.e., small θ_{bk}) where a large value for χ is not needed. Therefore, while the presence of the design parameter χ in Eq.3.11 offers the possibility of enlarging the region of guaranteed closed-loop stability, a balance must always be maintained between the desired degree of uncertainty attenuation and the desired size of the region of closed-loop stability.

Remark 3.6 Theorem 3.1 explains some of the main advantages of using a Lyapunov framework for our development and why it is a natural framework to address the problem within an analytical setting. Owing to the versatility of the Lyapunov approach in serving both as a useful robust inverse optimal design tool (see Chapter 2) and an efficient analysis tool, the proposed controller design method of Theorem 3.1 integrates explicitly the two seemingly separate tasks of controller design and

closed-loop stability analysis into one task. This is in contrast to other controller design approaches where a suitable control law is designed first to meet certain design specifications and then a Lyapunov function is found to analyze the closed-loop stability characteristics. Using a Lyapunov function to examine the closed-loop stability under a predetermined non-Lyapunov based control law (e.g., a feedback linearizing controller) usually results in a rather conservative stability analysis and yields conservative estimates of the region of closed-loop stability. In the approach proposed by Theorem 3.1, however, the Lyapunov function used to characterize the region of guaranteed closed-loop stability under the control law of Eq.3.10 is itself the same Lyapunov function used to design the controller and is therefore a natural choice to analyze the closed-loop system.

Remark 3.7 In the special case when the term $L_f V$ is negative and no process disturbances are present (i.e., $\theta_{bk} = 0$), the closed-loop stability and performance properties outlined in Theorem 3.1 can be made to hold globally by setting $\rho = 0$. This follows from the fact that when $L_f V < 0$, $\theta_{bk} = 0$ and $\rho = 0$, the inequality of Eq.3.11 is automatically satisfied everywhere in the state-space. Consequently, the closed-loop stability and set-point tracking properties are satisfied for any initial condition; hence the global nature of the result. The significance of this result is that it establishes the fact that, for open-loop stable nonlinear systems of the form of Eq.3.1 (where $L_f V < 0$), asymptotic stability and output tracking can always be achieved globally in the presence of arbitrary input constraints using the class of bounded control laws of Eq.3.10, both in the case when no uncertainty is present and in the case when the uncertainty is mild enough that Eq.3.11 continues to be satisfied.

Remark 3.8 Despite the conceptual similarities between the controller of Eq.3.10 and that of Eq.2.15, the two control laws differ in several fundamental respects. First, the control law of Eq.3.10 is inherently bounded by u_{max} and generates control action that satisfies the input constraints within the region described by the inequality of Eq.3.11. By contrast, the control law of Eq.2.15 is unbounded and may compute

larger control action that violates the constraints within the same region. Second, the control law of Eq.3.10 possesses a well-defined region of guaranteed stability and performance properties in the state-space. One can, therefore, determine a priori whether a particular initial condition is feasible. No explicit characterization of this region is available for the control law of Eq.2.15. Finally, while the tasks of nominal stabilization and uncertainty attenuation could be conceptually distinguished and assigned separately to the two components of the control law of Eq.2.15, this is no longer possible for the controller of Eq.3.10 due to the presence of the term $\chi\theta_{bk}\,|L_{\bar{w}k}V|$ in the radicand, which is a direct consequence of the bounding procedure of the controller.

Remark 3.9 As part of its optimal character and in a somewhat similar fashion to the control law of Eq.2.15, the control law of Eq.3.10 recognizes the beneficial effects of process nonlinearities and does not expend unnecessary control effort to cancel them. However, unlike the controller of Eq.2.15, the control law of Eq.3.10 has the additional ability to recognize the extent of the effect of uncertainty on the process and prevent its cancellation if this effect is not significant. To understand this point, recall that the controller of Eq.2.15 prevents the unnecessary cancellation of the term L_fV – which does not include the uncertainty – when it is negative. This controller, therefore, compensates for the presence of any model uncertainty it detects and does not discriminate between small or large uncertainty. In contrast, the controller of Eq.3.10 now recognizes the beneficial effect of the entire term $L_fV + \chi\theta_{bk}|L_{\bar{w}k}V|$ (rather than just the term L_fV) when it is negative and prevents its unnecessary and wasteful cancellation. Note that this term now includes the uncertainty. Therefore, if the plant-model mismatch is not too significant, such that the term, $L_fV+\chi\theta_{bk}|L_{\bar{w}k}V|$, remains negative in the presence of such uncertainty, the controller will prevent the expenditure of unnecessary control effort to cancel such uncertainty. Essentially the controller realizes, through the negative sign of this term, that the uncertainty present in the process does not have a strong enough adverse effect to warrant its cancellation. Therefore the control law of Eq.3.10 has the ability to discriminate between small and

large model uncertainty and assess the need for reasonable control effort expenditure accordingly.

Remark 3.10 Although the controller of Eq.3.10 uses small control action to achieve robust stabilization in the presence of constraints, the rigorous proof of inverse optimality of this controller with respect to a cost functional of the form of Eq.3.14 requires careful consideration. In contrast to the stability and set-point tracking properties which are guaranteed provided that the closed-loop trajectory remains within the region of Eq.3.11, optimality is guaranteed provided that the evolution of the closed-loop trajectory is confined within a smaller region characterized by Eq.3.13. In the Proof of Theorem 3.1 (see Appendix B), we establish through the inverse optimal approach that the evolution of the trajectories of the closed-loop system within this sub-region renders the cost functional of Eq.3.14 meaningful and guarantees that the controller of Eq.3.10 minimizes this cost. The fact that the optimality region is, in general, a subset of the stability region can be understood in light of the bounded nature of the controller of Eq.3.10. In contrast to their unbounded counterparts, bounded controllers tend to experience a reduction in their stability margins near the boundary of the stability region (note in particular that the negativity of $\dot{V}$ decreases as we approach the boundary of the region of Eq.3.11). These margins, however, are needed in the inverse optimal approach to establish meaningful optimality. Therefore, to guarantee optimality, one must step back from the boundary of the region of Eq.3.11 and restrict the evolution of the trajectories in a smaller region where stability margins are sufficient to render the cost functional meaningful.

Remark 3.11 Similar to the cost functional of Eq.2.19, the one given in Eq.3.14 places meaningful penalties on the tracking error, $e = v - y$, and its time-derivatives up to order r and on the control action. Furthermore, J is well-defined according to the formulation of the optimal control problem for nonlinear systems [271] because of the following properties of $l(e)$ and $R(x)$. The function $l(e)$ is continuous, positive-definite, and bounded from below by a class $\mathcal{K}$ function of the norm of e. The

function $R(x)$ is continuous, strictly positive, and the term $uR(x)u$ has a unique global minimum at $u = 0$, implying a larger control penalty for u farther away from zero. These properties are the only requirements needed to guarantee that the optimality of the controller of Eq.3.10 is meaningful and ensure that the controller enjoys the desired robustness and optimality benefits, regardless of the specific interpretation of what the weights, $l(e)$ and $R(x)$, represent. This is one of the basic tenets of the inverse optimal approach. Finally, owing to the vanishing nature of the uncertain variables and the asymptotic stability of the closed-loop system, J is defined on the infinite time-interval and is finite.

3.3.3 Bounded controller synthesis under non-vanishing uncertainty

In this subsection, we consider nonlinear processes of the form of Eq.3.1 with non-vanishing uncertainty and focus on the design of continuous bounded robust optimal nonlinear state feedback control laws that, in the presence of input constraints: (a) enforce boundedness of the closed-loop trajectories and robust output tracking, (b) minimize a meaningful performance index defined on a finite time-interval, and (c) possess a well-defined and explicit characterization of their regions of closed-loop stability. Theorem 3.2 below provides the desired control laws and states precise conditions under which the desired properties hold. The proof of this theorem is given in Appendix B.

Theorem 3.2 *Let Assumptions 2.1, 2.3, and 2.4 hold and assume that the uncertain variables in Eq.3.1 are non-vanishing in the sense defined in Theorem 2.2. Consider the uncertain nonlinear system of Eq.3.1 under the static state feedback law of Eq.3.10 with $\rho = 0$. Then for any initial condition starting from where the evolution of the closed-loop system satisfies:*

$$L_{\bar{f}}V + \chi\sum_{k=1}^{q}\theta_{bk}|L_{\bar{w}k}V| \;\leq\; u_{max}|L_{\bar{g}}V| \tag{3.15}$$

and for every positive real number d, there exists $\phi^*(d) > 0$ such that if $\phi \in (0, \phi^*(d)]$, the following holds:

(1) The trajectories of the closed-loop system are bounded.

(2) The output of the closed-loop system satisfies a relation of the form:

$$\limsup_{t\to\infty} |y(t) - v(t)| \leq d \tag{3.16}$$

Furthermore, if the trajectories of the closed-loop system evolve such that $\forall\ 0 \leq t \leq T_f$:

$$L'_{\bar{f}}V \left[2 + 4\sqrt{1 + (u_{max}L_{\bar{g}}V)^2}\right] \ \leq \ \sqrt{(L'_{\bar{f}}V)^2 + (u_{max}L_{\bar{g}}V)^4} \tag{3.17}$$

where $L'_{\bar{f}}V = L_{\bar{f}}V + \chi\sum_{k=1}^{q}\theta_{bk}|L_{\bar{w}k}V|$, and χ is chosen to satisfy $\chi > 2$, then:

(3) The static state feedback control law of Eq.3.10 minimizes the cost functional:

$$J \ = \ \lim_{t\to T_f} V(e(t)) + \int_0^{T_f} (l(e) + uR(x)u)dt \tag{3.18}$$

where $R(x) > 0$, $l(e) = -L_{\bar{f}}V + \frac{1}{4}L_{\bar{g}}V\bar{R}^{-1}(x)L_{\bar{g}}V - \sum_{k=1}^{q}|L_{wk}V|\theta_{bk} > 0\ \forall\ t \in [0, T_f]$, $T_f = \inf\{T \geq 0 : e(t) \in \Gamma\ \forall\ t \geq T\}$, $\Gamma = \{e \in \mathbb{R}^r : e^TPe \leq \lambda_{max}(P)\bar{\epsilon}^2\}$, $\bar{\epsilon} = \max\{\alpha_2^{-1}(2\epsilon(\phi^*)), \alpha_3^{-1}(2\epsilon(\phi^*))\}$, $\epsilon(\phi^*) = \sum_{k=1}^{q}\theta_{bk}\bar{\delta}_k(\phi^*)^2(\chi/2-1)^{-2} + \sum_{k=1}^{q}\theta_{bk}\mu_k\phi^*(\chi/2-1)^{-1}$, $\alpha_2(\cdot)$, $\alpha_3(\cdot)$ are class $\mathcal{K}$ functions and $\bar{\delta}_k$, μ_k are given in Theorem 2.2.

Remark 3.12 Note that the cost functional of Eq.3.18 resembles that of Eq.2.25 presented in Theorem 2.2. It is defined only on a finite time-interval due to the presence of persistent uncertainty that makes asymptotic convergence to the nominal equilibrium point impossible. In addition, it contains a terminal penalty term to penalize the inability of the tracking error trajectories to converge to the origin. The only difference between the two cost functionals lies in the specific forms of the weights $R(x)$ and $l(e)$. Nonetheless, these weights are well-defined and meaningful in both cases rendering the respective control laws optimal with respect to meaningful performance indices.

Remark 3.13 Referring to the practical applications of the result of Theorem 3.2, one has to initially verify whether Assumptions 2.1 and 2.4 hold for the process under consideration and determine the available bounds on the uncertain variables, θ_{bk}. Next, given the available constraints on the manipulated input, the inequality of Eq.3.15 should be used to check whether the particular initial condition to start the process is admissible and whether the desirable closed-loop properties in Theorem 3.2 are guaranteed to hold. Then, Eq.3.10 can be used to compute the explicit formula for the controller. Finally, given the desired asymptotic tracking error, d, (which can be chosen arbitrarily close to zero), the value of ϕ^* should be computed (usually through simulations) to achieve $\limsup_{t\to\infty}|y(t) - v(t)| \leq d$. The basic guideline for tuning the parameter ϕ is to select a sufficiently small value in order to achieve a small d. Therefore, one initially selects a small value for ϕ and carries out simulations to check if the desired d is achieved. If not, then ϕ must be reduced further until the desired asymptotic tracking error is achieved.

Remark 3.14 It is important to note that the results of Theorems 3.1 and 3.2 can be extended to nonlinear systems with multiple equilibria. In this case, however, caution must be exercised when using the inequalities of Eq.3.11 and Eq.3.15 to compute the stability region of a certain equilibrium point in the presence of input constraints. Recall that, in the case of a single equilibrium point, these inequalities provide an estimate of the domain of attraction starting from where the trajectories are *guaranteed* to converge to the equilibrium point. Owing to the presence of multiple equilibrium points, however, it is possible for this region to enclose other equilibria and, therefore, portions of the region may be shared by the domains of attraction of these other equilibria. In this case, the inequalities of Eqs.3.11-3.15 describe regions in the state-space starting from where it is just *possible* to steer the process to the corresponding equilibrium point with the available control energy. To guarantee, a priori, convergence to the desired equilibrium point, one can identify, using the techniques reviewed in [170], regions of invariance (within the regions described by Eqs.3.11 and 3.15) around the desired equilibrium point, to exclude the possibility

of the system stabilizing at other undesired equilibrium points (see also [159] for a discussion on this issue).

3.4 Application to a non-isothermal chemical reactor

In this section, we revisit the exothermic continuous stirred tank chemical reactor example considered in Section 3.2.3 to illustrate the ability of the bounded robust controllers proposed in Section 3.3 to effectively handle the co-presence of model uncertainty and manipulated input constraints. To this end, consider the same control problem of regulating the reactor temperature by manipulating the rate of heat input to the reactor. Also consider the same time-varying disturbances and uncertainty in the feed temperature and heat of reaction given in Eq.3.7. To proceed with the design of the bounded controller, we note that the uncertain variables under consideration are non-vanishing and therefore we use the result of Theorem 3.2 to construct the controller. Using the quadratic Lyapunov function, $V = \frac{1}{2}c(T - T_s)^2$, the desired control law takes the form of Eq.3.10, with $\rho = 0$, where:

$$\begin{aligned} L_{\bar{f}}V + \chi\sum_{k=1}^{q}\theta_{bk}|L_{\bar{w}k}V| &= c\,(T - T_s)\left[\frac{F}{V}(T_{A0} - T) + \frac{-\Delta H_{nom}}{\rho c_p}k_0 \exp\left(\frac{-E}{RT}\right)C_A\right] \\ &+ \chi\left[\theta_{b1}\frac{F}{V} + \theta_{b2}k_0 \exp\left(\frac{-E}{RT}\right)C_A\right]c|T - T_s| \\ L_{\bar{g}}V &= c\,(T - T_s)\frac{1}{\rho c_p V} \end{aligned} \tag{3.19}$$

The following values were used for the controller tuning parameters: $c = 1.0$, $\phi = 0.01$ and $\chi = 2.1$, to guarantee that the output satisfies a relation of the form of Eq.3.9. Several sets of simulations were performed to evaluate the performance, robustness, and constraint-handling abilities of the controller of Eq.3.10. In the first set of simulations, we examined the startup performance of the reactor and tested the ability of

the controller to drive and maintain the reactor temperature at the desired (unstable) steady-state in the presence of uncertainty and manipulated input constraints. Figure 3.5 shows the temperature and rate of heat input profiles for the cases when $|Q| \leq 60$ KJ/s (solid line) and $|Q| \leq 40$ KJ/s (dashed line). In both cases, one can immediately see that the controller achieves the desired stability and performance properties successfully despite the presence of uncertainty and hard limitations on the rate of heat input. The bounded robust optimal controller uses the information available on the maximum or minimum rate of heat input allowable to compute the necessary rate of heating or cooling to be provided to the reactor resulting in no discrepancy between the controller output and the actual input to the reactor. Therefore, not only is the control effort generated by the controller of Eq.3.10 minimal (due to optimality), but in addition, the controller confines its action within the limits imposed by the input constraints. This feature allows the controller to satisfy the imposed constraints without sacrifice in performance, in contrast to other controllers designed in the absence of constraints and then de-tuned to satisfy the constraints at the expense of yielding poor performance. Note also that robustness against the presence of time-varying uncertainty is achieved by explicitly incorporating information about the uncertainty in the controller design. This robustness could not be achieved using integral action which confounded the closed-loop instability and performance problems in the presence of relatively less tight constraints (see Figure 3.1).

In the second set of simulation runs, we tested the robust output tracking capabilities of the controller of Eq.3.10. Starting from the steady-state given in Table 3.1, we considered a 50° K decrease in the value of the temperature set-point. The resulting temperature and rate of heat input profiles are given in Figure 3.6 for the case when $|Q| \leq 60$ KJ/s (solid line) and $|Q| \leq 40$ KJ/s (dashed line). The figure

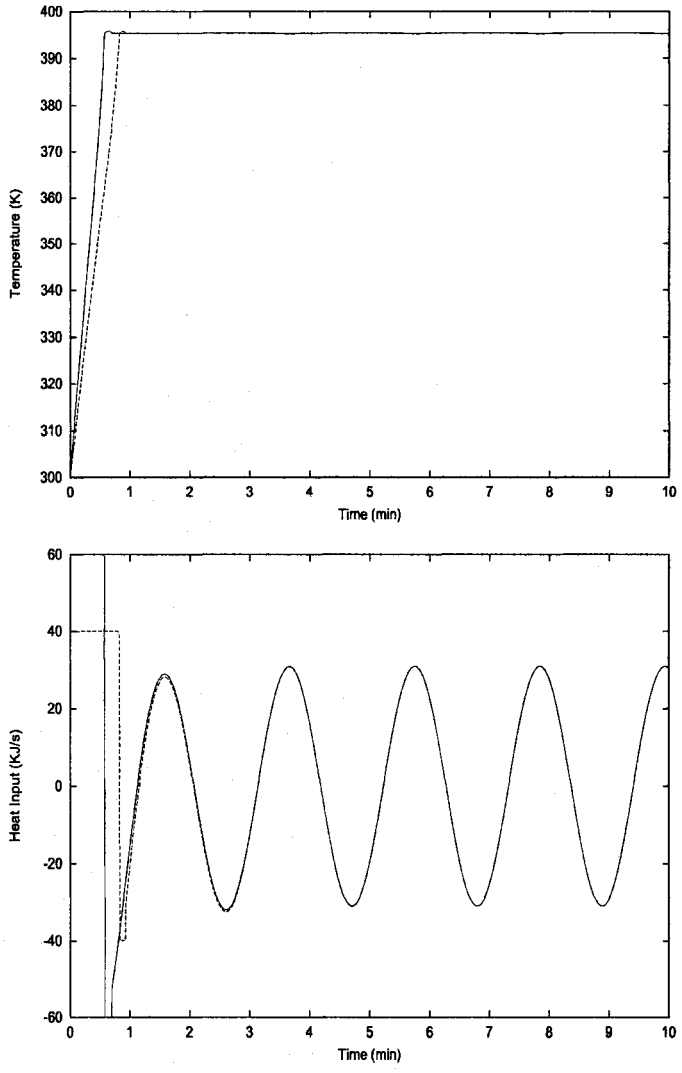

Figure 3.5: Closed-loop output and manipulated input profiles under the controller of Eqs.30-39 in the presence of process uncertainty and input constraints of $|Q| \leq 60$ KJ/s (solid line) and $|Q| \leq 40$ KJ/s (dashed line).

clearly establishes the ability of the controller to achieve robust output tracking in the presence of input constraints.

Finally, using the inequality of Eq.3.15, we computed the region where the bounded controller satisfies the constraints, for the case when $u_{max} = 50$ KJ/s and $\chi = 1.1$. The resulting region is depicted Figure 3.7 (top plot). For the sake of comparison, we included in the same figure the estimate associated with a robust input/output linearizing controller designed using the results in [68] (bottom plot). The latter estimate was obtained using the procedure proposed in [157]. Both regions basically depict the points in the concentration-temperature space where the input constraints are satisfied. From this comparison, it is clear that the region of guaranteed closed-loop stability associated with the bounded controller is larger. This means that one can safely operate the process and guarantee stability starting from a wider range of initial conditions than that where the feedback linearizing controller is guaranteed to work. The larger region of guaranteed closed-loop stability for the controller of Eq.3.10 is a consequence of the fact that the bounded controller is designed to account explicitly for input constraints while the input/output linearizing controller is not. Furthermore, the fact that the input/output linearizing controller may generate unnecessarily large control action to cancel beneficial process nonlinearities renders many of the initial conditions that lie far from the equilibrium point inadmissible, since the control energy required to stabilize the process starting from these conditions is often larger than the control action available from the input constraints. In the case of the bounded controller, however, many of these initial conditions are admissible since the controller avoids the use of unnecessarily large control action to stabilize the process and, consequently, the required control action is more likely to satisfy the imposed constraints. The end result then is a larger region of guaranteed

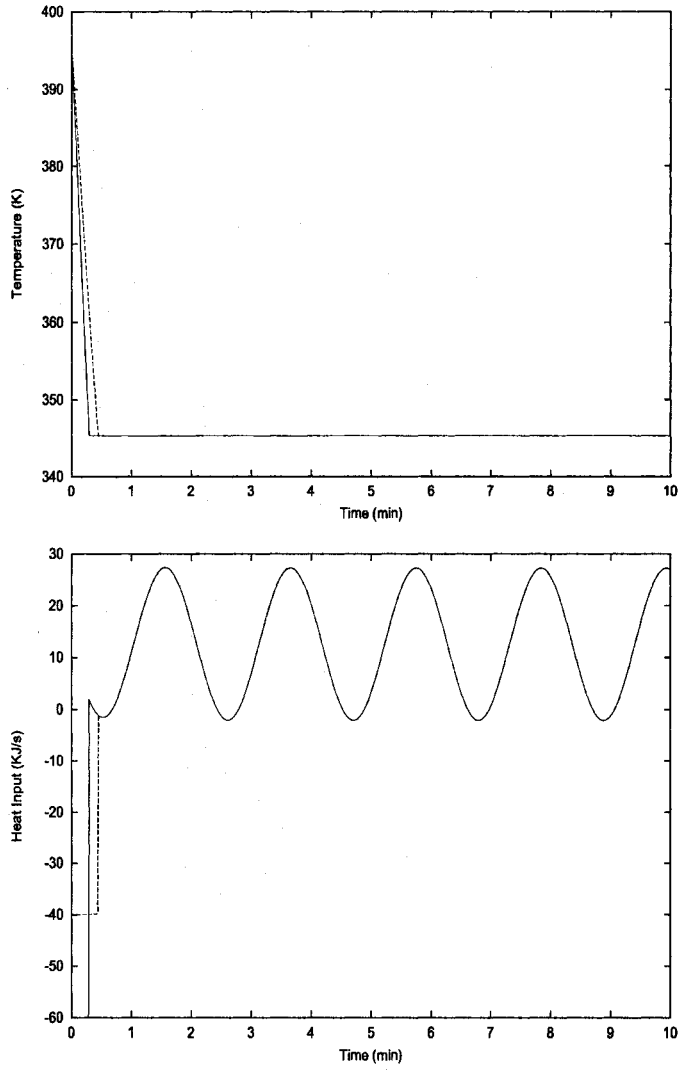

Figure 3.6: Closed-loop output and manipulated input profiles for reference input tracking under the controller of Eqs.30-39 in the presence of process uncertainty and input constraints of $|Q| \leq 60$ KJ/s (solid line) and $|Q| \leq 40$ KJ/s (dashed line).

closed-loop stability. Note that the region depicted in Figure 3.7 is presented only for illustration purposes and is not needed for the stability analysis which is performed directly using Eq.3.11 (which can be used for both the two-dimensional system of Eq.3.4 as well as any other higher-order system.)

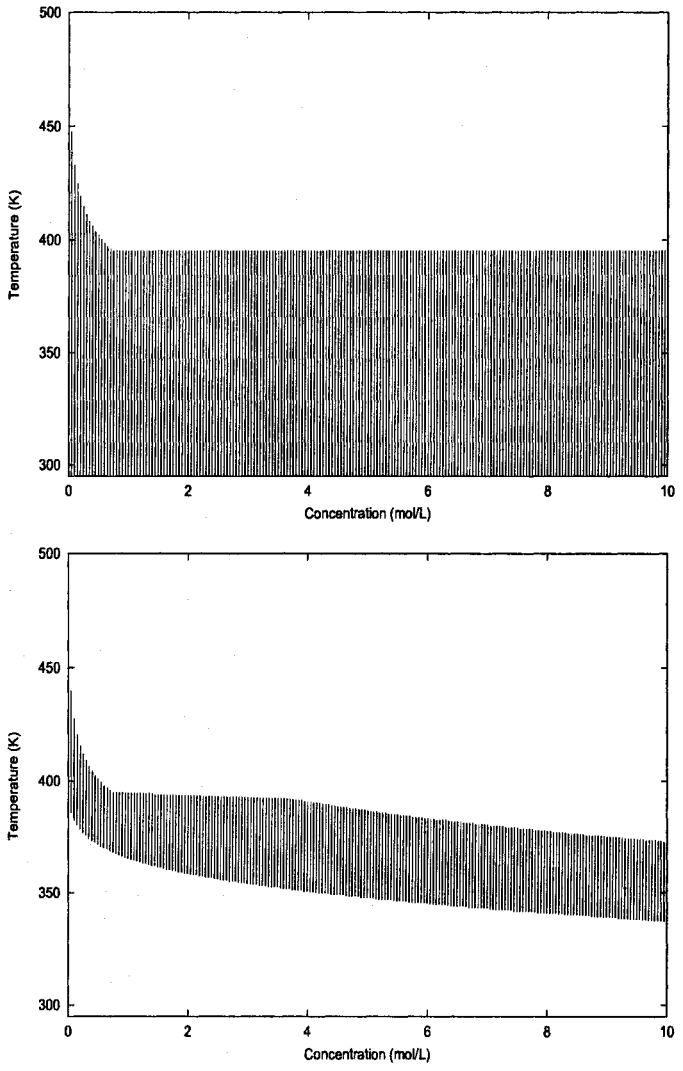

Figure 3.7: Regions of constraint satisfaction under the bounded controller of Eq.3.10 (top plot) and a robust feedback linearizing controller (bottom plot), $u_{max} = 50$ KJ/s.

3.5 Conclusions

A unified framework for control of single-input single-output constrained uncertain nonlinear processes that integrates robustness, optimality, and explicit constraint-handling capabilities in the controller synthesis was presented. The developed Lyapunov-based framework led to the synthesis of bounded robust optimal state feedback control laws with well-characterized stability and performance properties and provided, at the same time, an explicit and intuitive characterization of the state-space regions of guaranteed closed-loop stability in terms of the input constraints and model uncertainty. For processes with vanishing uncertainty, the developed controllers were shown to guarantee asymptotic stability and asymptotic robust output tracking with attenuation of the effect of uncertainty on the output of the closed-loop system in the presence of input constraints. For processes with non-vanishing uncertainty, the same controllers were shown to ensure boundedness of the states and robust asymptotic output tracking in the presence of input constraints. The performance of the control laws was illustrated through the use of a chemical reactor example and compared with other process control strategies.

Chapter 4

Control of Multivariable Nonlinear Systems

4.1 Introduction

The Lyapunov-based controller design method presented in Chapter 3 was developed for single-input single-output (SISO) nonlinear processes with model uncertainty and input constraints, under the assumption of full state feedback. Virtually all practical process control systems are characterized by multivariable interactions where the control problem involves the regulation of more than one output by manipulating more than one input. When input constraints are not dealt with explicitly in the controller design, multivariable interactions can cause further deterioration in the process performance due to problems such as process directionality. In addition, the lack of complete state measurements renders state feedback controller designs not directly suitable for practical implementation and necessitates the design of appropriate state estimators.

Motivated by these considerations, we focus in this chapter on state and out-

put feedback control of multi-input multi-output (MIMO) nonlinear processes with model uncertainty and input constraints. A Lyapunov-based nonlinear controller design approach that accounts explicitly and simultaneously for process nonlinearities, model uncertainty, input constraints, multivariable interactions, and the lack of full state measurements is proposed. When measurements of the full state are available, the approach leads to the explicit synthesis of bounded robust multivariable nonlinear state feedback controllers that enforce stability and robust asymptotic set-point tracking in the constrained uncertain closed-loop system and provide, at the same time, an explicit characterization of the region of guaranteed closed-loop stability. When complete state measurements are not available, a combination of the state feedback controllers with high-gain state observes and appropriate saturation filters, is employed to synthesize bounded robust multivariable output feedback controllers that require only measurements of the outputs for practical implementation. The resulting output feedback design enforces the same closed-loop stability and performance properties of the state feedback controllers and, in addition, practically preserves the region of guaranteed closed-loop stability obtained under state feedback, provided that the observer gain is sufficiently large. The developed state and output feedback controllers are applied successfully to non-isothermal multivariable chemical reactor examples with uncertainty, input constraints, and incomplete state measurements. Finally, we conclude the chapter with a discussion that attempts to put in perspective the proposed Lyapunov-based control approach with respect to the nonlinear model predictive control (MPC) approach, and discuss the implications of our results for the practical implementation of MPC in control of uncertain nonlinear processes with input constraints. The results of this chapter were first presented in [94].

4.2 Preliminaries

We consider multi-input multi-output (MIMO) nonlinear processes with uncertain variables and input constraints, with the following state-space description:

$$\begin{aligned} \dot{x} &= f(x) + \sum_{i=1}^{m} g_i(x)u_i + \sum_{k=1}^{q} w_k(x)\theta_k(t) \\ y_i &= h_i(x), \quad i = 1, \cdots, m \end{aligned} \tag{4.1}$$

where $x \in \mathbb{R}^n$ denotes the vector of process state variables, $u = [u_1 \ u_2 \ \cdots \ u_m]^T$ denotes the vector of constrained manipulated inputs taking values in a nonempty convex subset, $U = \{u \in \mathbb{R}^m : |u| \leq u_{max}\}$, $|\cdot|$ is the Euclidean norm of a vector, u_{max} is a positive real number that captures the maximum magnitude of the Euclidean norm of the vector of manipulated inputs allowed by the constraints, $\theta_k(t) \in \mathcal{W} \subset \mathbb{R}$ denotes the k-th uncertain (possibly time-varying) but bounded variable taking values in a nonempty compact convex subset of $\mathbb{R}$, $y_i \in \mathbb{R}$ denotes the i-th output to be controlled. The uncertain variable, $\theta_k(t)$, may describe time-varying parametric uncertainty and/or exogenous disturbances. It is assumed that the origin is the equilibrium point of the nominal (i.e., with $u(t) = \theta_k(t) \equiv 0$) system of Eq.4.1. The vector functions, $f(x)$, $g_i(x)$, $w_k(x)$, and the scalar functions $h_i(x)$ are assumed to be sufficiently smooth on their domains of definition. Throughout the chapter, the Lie derivative notation will used. In particular, $L_f\bar{h}$ denotes the standard Lie derivative of a scalar function $\bar{h}(x)$ with respect to the vector function $f(x)$, $L_f^k\bar{h}$ denotes the k-th order Lie derivative and $L_{g_i}L_f^{k-1}\bar{h}$ denotes the mixed Lie derivative where $g_i(x)$ is a vector function. We will also need the definition of a class $\mathcal{KL}$ function. A function $\beta(s,t)$ is said to be of class $\mathcal{KL}$ if, for each fixed t, the function $\beta(s,\cdot)$ is continuous, increasing, and zero at zero and, for each fixed s, the function $\beta(\cdot,t)$ is nonincreasing and tends to zero at infinity.

Referring to the system of Eq.4.1, we define the relative order of the output, y_i, with respect to the vector of manipulated inputs, u, as the smallest integer r_i for which:

$$\left[L_{g_1}L_f^{r_i-1}h_i(x) \ \cdots \ L_{g_m}L_f^{r_i-1}h_i(x)\right] \not\equiv [0 \ \cdots \ 0] \tag{4.2}$$

or $r_i = \infty$ if such an integer does not exist. We also define the characteristic matrix [148]:

$$C(x) = \begin{bmatrix} L_{g_1}L_f^{r_1-1}h_1(x) & \cdots & L_{g_m}L_f^{r_1-1}h_1(x) \\ \vdots & \cdots & \vdots \\ L_{g_1}L_f^{r_m-1}h_m(x) & \cdots & L_{g_m}L_f^{r_m-1}h_m(x) \end{bmatrix} \tag{4.3}$$

4.3 Bounded robust state feedback control

In this section, we focus on the state feedback control problem where the full process state is assumed to be available for measurement. The output feedback control problem will be discussed in Section 4.5. We begin in Section 4.3.1 with the control problem formulation and then present the controller synthesis results in Section 4.3.2.

4.3.1 Control problem formulation

In order to formulate our control problem, we consider the MIMO nonlinear process of Eq.4.1 and assume initially that the uncertain variable terms are vanishing in the sense that $w_k(0) = 0$ (note that this does not require the variable θ_k itself to vanish over time). Under this assumption, the origin – which is an a nominal equilibrium point – continues to be an equilibrium point for the uncertain process. The results for the case when the uncertain variables are non-vanishing (i.e., perturb the nominal equilibrium point) are discussed later on (see Remark 4.7 below). For the control problem at hand, our objective is two fold. The first is to synthesize, via Lyapunov-based control

methods, a bounded robust multivariable nonlinear state feedback control law of the general form:

$$u = \mathcal{P}(x, u_{max}, \bar{v}) \tag{4.4}$$

that enforces the following closed-loop properties in the presence of uncertainty and input constraints, including: (a) asymptotic stability, and (b) robust asymptotic reference-input tracking with an arbitrary degree of attenuation of the effect of the uncertainty on the outputs of the closed-loop system. In Eq.4.4, $\mathcal{P}(x, \bar{v})$ is an m-dimensional bounded vector function (i.e., $|u| \leq u_{max}$), $\bar{v}$ is a generalized reference input which is assumed to be a sufficiently smooth function of time. Our second objective is to explicitly characterize the region of guaranteed closed-loop stability associated with the controller, namely the set of admissible initial states starting from where, stability and robust output tracking can be guaranteed in the constrained uncertain closed-loop system.

4.3.2 Controller synthesis

To proceed with the controller synthesis task, we will impose the following three assumptions on the process of Eq.4.1. We initially assume that there exists a coordinate transformation that renders the system of Eq.4.1 partially linear. This assumption is motivated by the requirement of robust output tracking and is formulated precisely below.

Assumption 4.1 *There exist a set of integers,* $\{r_1, r_2, \ldots, r_m\}$, *and a coordinate transformation* $(\zeta, \eta) = T(x)$ *such that the representation of the system of Eq.4.1, in*

the (ζ, η) *coordinates, takes the form:*

$$\begin{aligned}
\dot{\zeta}_1^{(i)} &= \zeta_2^{(i)} \\
&\vdots \\
\dot{\zeta}_{r_i-1}^{(i)} &= \zeta_{r_i}^{(i)} \\
\dot{\zeta}_{r_i}^{(i)} &= L_f^{r_i} h_i(x) + \sum_{j=1}^{m} L_{g_j} L_f^{r_i-1} h_i(x) u_j + \sum_{k=1}^{q} L_{w_k} L_f^{r_i-1} h_i(x) \theta_k \\
\dot{\eta}_1 &= \Psi_1(\zeta, \eta, \theta) \\
&\vdots \\
\dot{\eta}_{n-\sum_i r_i} &= \Psi_{n-\sum_i r_i}(\zeta, \eta, \theta) \\
y_i &= \zeta_1^{(i)}, \quad i = 1, \ldots, m
\end{aligned} \tag{4.5}$$

where $x = T^{-1}(\zeta, \eta)$, $\zeta = [\zeta^{(1)^T} \cdots \zeta^{(m)^T}]^T$, $\eta = [\eta_1 \cdots \eta_{n-\sum_i r_i}]^T$, $\theta = [\theta_1 \cdots \theta_q]^T$.

Assumption 4.1 includes the matching condition of our robust control methodology. In particular, we consider systems of the form Eq.4.1 for which the time-derivatives of the outputs, y_i, up to order $r_i - 1$, are independent of the uncertain variables, θ_k. Notice that this condition is different from the standard one which restricts the uncertainty to enter the system of Eq.4.1 in the same equation with the manipulated inputs, u_i. Defining the tracking error variables, $e_k^{(i)} = \zeta_k^{(i)} - v_i^{(k-1)}$, and introducing the vector notation, $e^{(i)} = [e_1^{(i)}\ e_2^{(i)}\ \cdots\ e_{r_i}^{(i)}]^T$, $e = [e^{(1)^T}\ e^{(2)^T}\ \cdots\ e^{(m)^T}]^T$, where $i = 1, \cdots, m$, $k = 1, \cdots, r_i$, the ζ-subsystem of Eq.4.5 can be re-written in the following more compact form:

$$\dot{e} = Ae + r(e, \eta, \bar{v}) + B\left[C_1(x)u + C_2(x)\theta\right] \tag{4.6}$$

where A, B are constant matrices of dimensions $(\sum_{i=1}^m r_i) \times (\sum_{i=1}^m r_i)$ and $(\sum_{i=1}^m r_i) \times m$, respectively, $r(e, \eta, \bar{v})$ is a $(\sum_{i=1}^m r_i) \times 1$ continuous nonlinear vector function, and $\bar{v} = [\bar{v}_1^T\ \bar{v}_2^T\ \cdots\ \bar{v}_m^T]^T$ where $\bar{v}_i = [v_i\ v_i^{(1)}\ \cdots\ v_i^{(r_i)}]^T$ is a smooth vector function, and $v_i^{(k)}$ is

the k-th time derivative of the external reference input v_i (which is assumed to be a smooth function of time.) The specific forms of these functions are omitted for brevity. The $m \times m$ matrix, $C_1(x)$, is the characteristic matrix of the system of Eq.4.1 defined in Eq.4.3 while $C_2(x)$ is an $m \times q$ matrix that is structurally-similar to $C_1(x)$, except that the vector fields, g_i, are replaced by w_k. In order to simplify the presentation of the main results, the matrix $C_1(x)$ will be assumed nonsingular uniformly in x. This assumption can be readily relaxed if robust dynamic state feedback, instead of robust static state feedback, is used to solve the control problem (see [148] for details). Finally, we define the function $\bar{f}(e, \eta, \bar{v}) = Ae + r(e, \eta, \bar{v})$, denote by $\bar{g}_i(e, \eta, \bar{v})$ the i-th column of the matrix function $g(x) = BC_1(x),\ i = 1, \cdots m$, and denote by $\bar{w}_k(e, \eta, \bar{v})$ the k-th column of the matrix function $W(x) = BC_2(x),\ k = 1, \cdots q$.

Following [91], the requirement of input-to-state stability is imposed on the η-subsystem of Eq.4.5 to ensure bounded stability of the internal dynamics and allow the synthesis of the desired controller on the basis of the e-subsystem. This assumption, stated below, is standard in the process control literature concerned with enforcing output tracking and is satisfied by many practical systems, including the chemical reactor models studied in this chapter which do not exhibit non-minimum phase behavior (see also [68, 91] for additional examples).

Assumption 4.2 *The dynamical system:*

$$\begin{aligned} \dot{\eta}_1 &= \Psi_1(e, \eta, \theta, \bar{v}) \\ &\vdots \\ \dot{\eta}_{n-\sum_i r_i} &= \Psi_{n-r}(e, \eta, \theta, \bar{v}) \end{aligned} \tag{4.7}$$

is ISS with respect to e uniformly in θ, $\bar{v}$.

In order to achieve attenuation of the effect of the uncertain variables on the outputs, we assume the existence of known (but not necessarily small) bounds that

capture the size of the uncertain variables for all times.

Assumption 4.3 *There exist known constants θ_{bk} such that $\|\theta_k\| \leq \theta_{bk}$ where $\|\theta_k\|$ denotes ess.sup.$|\theta(t)|$, $t \geq 0$.*

Theorem 4.1 that follows provides the explicit synthesis formula for the desired bounded robust multivariable state feedback control law and states precise conditions that guarantee closed-loop stability and robust asymptotic output tracking in the presence of uncertainty and input constraints. The key idea in the proposed controller design is that of bounding a robust Lyapunov-based controller, and is inspired by the results on bounded control in [204] for systems without uncertainty. Analysis of the closed-loop system utilizes combination of standard Lyapunov techniques together with the concept of input-to-state stability and nonlinear small-gain type arguments. The proof of the theorem can be found in Appendix C.

Theorem 4.1 *Consider the constrained uncertain nonlinear process of Eq.4.1, for which Assumptions 4.1-4.3 hold, under the static state feedback law:*

$$u = -\frac{1}{2}R^{-1}(x)\left(L_{\bar{g}}V\right)^T \tag{4.8}$$

where

$$\frac{1}{2}R^{-1}(x) = \frac{L_{\bar{f}}^{*}V + \sqrt{\left(L_{\bar{f}}^{**}V\right)^2 + \left(u_{max}|(L_{\bar{g}}V)^T|\right)^4}}{|(L_{\bar{g}}V)^T|^2\left[1+\sqrt{1+\left(u_{max}|(L_{\bar{g}}V)^T|\right)^2}\right]} \tag{4.9}$$

and

$$\begin{aligned} L_{\bar{f}}^{*}V &= L_{\bar{f}}V + \left(\rho|2Pe| + \chi\sum_{k=1}^{q}\theta_{bk}|L_{\bar{w}k}V|\right)\left(\frac{|2Pe|}{|2Pe|+\phi}\right) \\ L_{\bar{f}}^{**}V &= L_{\bar{f}}V + \rho|2Pe| + \chi\sum_{k=1}^{q}\theta_{bk}|L_{\bar{w}k}V| \end{aligned} \tag{4.10}$$

$V = e^TPe$, P is a positive-definite matrix that satisfies the Riccati matrix inequality, $A^TP + PA - PBB^TP < 0$, $L_{\bar{g}}V = [L_{\bar{g}_1}V \cdots L_{\bar{g}_m}V]$ is a row vector, and ρ, χ and

ϕ are adjustable parameters that satisfy $\rho > 0$, $\chi > 1$ and $\phi > 0$. Let Π be the set defined by:

$$\Pi(\theta_b, u_{max}) \;=\; \{x \in \mathbb{R}^n : L_{\bar{f}}^{**}V \;\leq\; u_{max}|(L_{\bar{g}}V)^T|\} \tag{4.11}$$

Then, if the origin is contained in the interior of Π, given any initial condition, $x_0 \in \Omega$, where $\Omega = \{x \in \mathbb{R}^n : |x| \leq \delta_s\}$ is an invariant subset of Π, there exists $\phi^* > 0$ such that if $\phi \in (0, \phi^*]$:

(1) The origin of the constrained closed-loop system is asymptotically stable (i.e., there exists a function β of class $\mathcal{KL}$ such that $|x(t)| \leq \beta(|x_0|, t), \forall\, t \geq 0$).
(2) The outputs of the closed-loop system satisfy a relation of the form:

$$\limsup_{t\to\infty} |y_i(t) - v_i(t)| = 0,\; i = 1, \cdots, m \tag{4.12}$$

Remark 4.1 In addition to the explicit controller synthesis formula, Theorem 4.1 provides an explicit characterization of the region in the state-space where the desired closed-loop stability and set-point tracking properties are guaranteed under the proposed control law. This characterization is obtained from the inequality of Eq.4.11 which describes a closed state-space region where the time-derivative of the Lyapunov function is guaranteed to be negative-definite, along the trajectories of the constrained uncertain closed-loop system, and the control action satisfies the input constraints. Provided that the origin is contained in the interior of the region described by the set Π, any closed-loop trajectory that evolves within this region is guaranteed to converge to the origin with the available control action. In fact, it is not difficult to see how this inequality is closely linked to the classical Lyapunov stability condition:

$$\dot{V} \;=\; L_{\bar{f}}V + L_{\bar{g}}Vu + \sum_{k=1}^{q} L_{\bar{w}_k}V\theta_k \;\leq\; 0 \tag{4.13}$$

when the additional requirements that $|u| \leq u_{max}$ and $|\theta_k| \leq \theta_{bk}$ are imposed on Eq.4.13. The key idea here is that by taking the constraints directly into account (i.e., bounding the controller), we automatically obtain information about the region where both stability is guaranteed and the input constraints are respected. The inequality of Eq.4.11 can therefore be used to identify the set of admissible initial

states starting from where closed-loop stability is guaranteed under uncertainty and constraints (region of closed-loop stability). A reasonable estimate of the stability region can be obtained by computing an invariant subset, Ω, (preferably the largest) within the set Π (see [91] for further details). This invariant subset can then be used to check a priori (i.e., before controller implementation) whether closed-loop stability is guaranteed starting from a given initial condition. It is important to note here that the representation of the invariant subset by a Euclidean ball of size δ_s in Theorem 4.1 is done only for notational convenience; the stability results of the theorem hold for any invariant subset (which can be of arbitrary shape) that can be constructed within Π and contains the origin in its interior. Note that, since the set Π is closed, this requires that the origin lie in the interior of Π. This assumption assures the existence of an invariant subset and can be checked prior to the practical implementation of the results of the theorem. However, it can be shown by means of local Lipschitz arguments that, if the vector fields are sufficiently smooth on their domains of definition and the adjustable parameters in Eq.4.11 chosen properly, this assumption is automatically satisfied.

Remark 4.2 By inspection of the inequality in Eq.4.11, it is clear that the size of the set, Π, is dependent on the size of the constraints and the size of the uncertainty. Therefore, under extremely tight constraints (u_{max} close to zero) and/or large plant-model mismatch, this set may contain only the origin (particularly for open-loop unstable processes where $L_{\tilde{f}}V > 0$). In this case, the origin would be the only admissible initial condition for which closed-loop stability can be guaranteed. In most applications of practical interest, however, the stability region contains the origin in its interior and is not empty (see the chemical reactor examples studied in Sections 4.4 and 4.6 for a demonstration of this fact). As discussed in Section 4.7, another feature of the inequality of Eq.4.11 is that it suggests a general way for estimating the stability region, which can be used in conjunction with other approaches (such as optimization-based control approaches) to provide the necessary a priori closed-loop stability guarantees. Although the inequality of Eq.4.11 pertains specifically to

the bounded robust controller of Eq.4.8-4.9, similar ideas can be used to identify the feasible initial conditions for other control approaches.

Remark 4.3 Regarding the continuity properties of the controller of Eq.4.8-4.9, it is important to note that this controller is smooth, away from the origin, because the functions $L_{\tilde{f}}^{*}V$, $L_{\tilde{f}}^{**}V$, $L_{\tilde{g}}V$ are smooth on their domains of definition. In addition, the controller is continuous at the origin because the Lyapunov function, $V = e^{T}Pe$, satisfies the small control property for the system of Eq.4.6 (see [278] as well as Chapter 4 in [112] for further details and illustrations of this point). These continuity properties can be proven by following the same arguments used in the Proof of Theorem 1 in [278] to prove continuity of the nominal (i.e., with $\theta \equiv 0$) unbounded version of the controller (see also the Proof of Proposition 3.43 in [271] for a similar proof). The same arguments can be extended to the bounded robust controller of Eqs.4.8-4.10.

Remark 4.4 An important problem, frequently encountered in the control of multivariable processes with input constraints, is the problem of directionality. This is a performance deterioration problem that arises when a multivariable controller, designed on the basis of the unconstrained MIMO process, is "clipped" to achieve a feasible plant input. Unlike the SISO case, clipping an unconstrained controller output to achieve a feasible plant input may not lead in MIMO systems to a plant output that is closest to the unconstrained plant output, thus steering the plant in the wrong directions and leading to performance deterioration. Controllers that do not account explicitly for input constraints suffer from this problem and often require the design of directionality compensators to prevent the resulting excessive performance deterioration (see, for example, [283]). It is important to note that the Lyapunov-based control approach proposed in Theorem 4.1 avoids the directionality problem by taking input constraints directly into account in the controller design. In particular, note that the controller of Eqs.4.8-4.10 inherently respects the constraints within the region described by Eq.4.11 and, therefore, starting from any initial condition in Ω, there is never a mismatch between the controller output and actual plant input at

any time.

Remark 4.5 The bounded nonlinear controller of Eqs.4.8-4.10 possesses certain optimality properties characteristic of its ability to use reasonable control action to accomplish the desired closed-loop objectives. Using techniques from the inverse optimal control approach (see, for example, [112, 271, 91]), one can rigorously prove that, within a well-defined subset of the set Π, this controller is optimal with respect to a meaningful, infinite-time cost functional of the form:

$$J = \int_0^\infty (l(e) + u^T R(x) u) dt \tag{4.14}$$

where $l(e)$ is a positive-definite penalty on the tracking error and its time-derivatives, up to order r_{i-1},that is bounded below by a quadratic function of the norm of the tracking error, and $R(x) > 0$ is a positive-definite penalty weight on the control action, and thus the above cost functional imposes sensible penalties on both the tracking error and control action. The inverse optimal approach provides a rigorous framework for associating meaningful optimality (i.e., meaningful performance criteria) with certain stabilizing controllers (such as those of Eq.4.8) and therefore helps explain the basis for their optimality properties. An advantage of this approach is that it allows the design of optimal feedback controllers without recourse to the unwieldy task of solving the Hamilton-Jacobi-Isaacs equation which is the optimality condition for the robust stabilization problem. Inverse optimal control design is motivated by the fact that both the optimality benefits (e.g., avoiding wasteful cancellation of beneficial nonlinearities) and the robustness properties that the controller possesses as a consequence of optimality (e.g., stability margins) are largely independent of the specific choice of the cost functional as long as it is a meaningful one. Finally, one can easily show that the minimum cost achieved by the state feedback controller is $V(e(0))$.

Remark 4.6 The inequality of Eq.4.11 captures the classical tradeoff between stability and performance. To see this, note that the size of the region of guaranteed closed-loop stability (obtained from Eq.4.11) can be enlarged by using small values for

the controller tuning parameters χ and ρ. This enlargement of the stability region, however, comes at the expense of the controller's robust performance, since large values for the tuning parameters χ and ρ are typically required to achieve a significant degree of attenuation of the effect of disturbances and plant-model mismatch on the outputs of the closed-loop system. Therefore, in selecting the controller tuning parameters, one must strike a balance between the need to stabilize the process from a given initial condition and the requirement of achieving a satisfactory level of uncertainty attenuation.

Remark 4.7 The result of Theorem 4.1 can be extended to the case when the uncertain variables in Eq.4.1 are non-vanishing. In this case, starting from any initial state within the invariant set Ω, the bounded robust controller of Eqs.4.8-4.10 enforces boundedness of the process states and robust asymptotic output tracking with an arbitrary degree of attenuation of the effect of uncertainty on the outputs of the closed-loop system. Owing to the persistent nature of the uncertainty, asymptotic convergence to the origin in this case is not possible under continuous feedback. Instead, the controller sends, in finite-time, the closed-loop trajectory into a small neighborhood of the origin. The size of this neighborhood (i.e., the asymptotic tracking error) can be made arbitrarily small by selecting the tuning parameters ϕ to be sufficiently small and/or selecting the tuning parameter χ to be sufficiently large. The problem of non-vanishing uncertainty was addressed in detail in Chapter 2 for SISO nonlinear processes. It is worth noting that the use of a Lyapunov-based control approach allows the synthesis of a robust controller that can effectively attenuate the effect of both constant and time-varying persistent uncertainty on the closed-loop outputs, which cannot be achieved using classical uncertainty compensation techniques, including integral action and parameter adaptation in the controller. For nonlinear controller design, Lyapunov methods provide useful and systematic synthesis tools (see, for example, [163]).

Remark 4.8 Referring to the practical implementation of the proposed control ap-

proach, we initially verify whether Assumptions 4.1-4.2 hold for the nonlinear process under consideration, and determine the available bounds on the uncertain variables. Next, given the constraints on the manipulated inputs, the inequality of Eq.4.11 is used to compute the estimate of the region of guaranteed closed-loop stability, Ω, and check whether a given initial condition is admissible. Then, the synthesis formula of Eq.4.8-4.10 is used to design the controller which is then implemented on the process. Note that the actual controller synthesis requires only off-line computations, including differentiation and algebraic calculations to compute the various terms in the analytical controller formula of Eq.4.8-4.9. This task can be easily coded into a computer using available software for symbolic manipulations (e.g., MATHEMATICA). Furthermore, the approach provides explicit guidelines for the selection of the tuning parameters that guarantee closed-loop stability and the desired robust performance. For example, the tuning parameters χ and ϕ are responsible for achieving the desired degree of uncertainty attenuation. A large value for χ (greater than one) and a small value for ϕ (close to zero) lead to significant attenuation of the effect of uncertainty on the closed-loop outputs.

4.4 Application to a multivariable chemical reactor

Consider a well-mixed continuous stirred tank reactor where an irreversible elementary exothermic reaction of the form $A \xrightarrow{k} B$ takes place. The feed to the reactor consists of pure A at flow rate F, molar concentration C_{A0} and temperature T_{A0}. Under standard modeling assumptions, the process model takes the following form:

$$\begin{aligned} V\frac{dC_A}{dt} &= F(C_{A0} - C_A) - k_0 \exp\left(\frac{-E}{RT}\right) C_A V \\ V\frac{dT}{dt} &= F(T_{A0} - T) + \frac{(-\Delta H)}{\rho c_p} k_0 \exp\left(\frac{-E}{RT}\right) C_A V + \frac{Q}{\rho c_p} \end{aligned} \tag{4.15}$$

where C_A denotes the concentration of species A, T denotes the temperature of the reactor, Q denotes the rate of heat input to the reactor, V denotes the volume of

the reactor, k_0, E, ΔH denote the pre-exponential constant, the activation energy, and the enthalpy of the reaction, c_p and ρ, denote the heat capacity and density of the fluid in the reactor. The steady-state values and process parameters are given in Table 4.1. For these parameters, it was verified that the given equilibrium point is an unstable one (the system also possesses two locally asymptotically stable equilibrium points).

Table 4.1: Process parameters and steady-state values for the reactor of Eq.4.15.

V	=	100.0	L
R	=	8.314	$J/mol.K$
C_{A0}	=	1.0	mol/L
T_{A0s}	=	310.0	K
ΔH	=	-4.78×10^4	J/mol
k_0	=	7.20×10^{10}	min^{-1}
E	=	8.31×10^4	J/mol
c_p	=	0.239	$J/g.K$
ρ	=	1000.0	g/L
F	=	100.0	L/min
C_{As}	=	0.577	mol/L
T_s	=	395.3	K

The control objective is to regulate both the reactor temperature and reactant concentration at the (open-loop) unstable equilibrium point by manipulating both the rate of heat input/removal and the inlet reactant concentration. The control objective is to be accomplished in the presence of: (1) time-varying persistent disturbances in the feed stream temperature, (2) parametric uncertainty in the value of the heat of reaction, and (3) hard constraints on the manipulated inputs. Defining $x_1 = C_A$, $x_2 = T$, $u_1 = C_{A0} - C_{A0s}$, $u_2 = Q$, $\theta_1(t) = T_{A0} - T_{A0s}$, $\theta_2(t) = \Delta H - \Delta H_{nom}$, $y_1 = C_A$, $y_2 = T$, where the subscript s denotes the steady-state value and ΔH_{nom} denotes the nominal value of the heat of reaction, the process model of Eq.4.15 can be cast in the

form of Eq.4.1 with:

$$f(x) = \begin{bmatrix} \frac{F}{V}(C_{A0s} - C_A) - k_0 \exp\left(\frac{-E}{RT}\right) C_A \\ \frac{F}{V}(T_{A0s} - T) + \frac{(-\Delta H_{nom})}{\rho c_p} k_0 \exp\left(\frac{-E}{RT}\right) C_A \end{bmatrix}, \; g_1(x) = \begin{bmatrix} \frac{F}{V} \\ 0 \end{bmatrix}$$

$$g_2(x) = \begin{bmatrix} 0 \\ \frac{1}{\rho c_p V} \end{bmatrix}, \; w_1(x) = \begin{bmatrix} 0 \\ \frac{F}{V} \end{bmatrix}, w_2(x) = \begin{bmatrix} 0 \\ k_0 \exp\left(\frac{-E}{RT}\right) C_A \end{bmatrix} \quad (4.16)$$

$h_1(x) = x_1$, $h_2(x) = x_2$. In all simulation runs, the following time-varying function was considered to simulate the effect of exogenous disturbances in the feed temperature:

$$\theta_1(t) = \theta_0 sin(3t) \quad (4.17)$$

where $\theta_0 = 0.08 T_{A0s}$. In addition, a parametric uncertainty of 50% in the heat of reaction was considered, i.e., $\theta_2(t) = 0.5\,(-\Delta H_{nom})$. The upper bounds on the uncertain variables were therefore taken to be $\theta_{b1} = 0.08 T_{A0s}$, $\theta_{b2} = 0.5\,|(-\Delta H_{nom})|$. Also, the following constraints were imposed on the manipulated inputs: $|u_1| \leq 1.0\ mol/L$ and $|u_2| \leq 92\ KJ/s$.

A quadratic Lyapunov function of the form $V = (C_A - C_{As})^2 + (T - T_s)^2$ was used to design the multivariable bounded robust controller of Eqs.4.8-4.10 and to compute the associated region of guaranteed closed-loop stability with the aid of Eq.4.11. Since the uncertainty considered is non-vanishing (see Remark 4.7), the following values were used for the tuning parameters: $\chi = 8.0$, $\phi = 0.0001$, $\rho = 0.01$ to guarantee that the outputs of the closed-loop system satisfy a relation of the form $\limsup_{t \to \infty} |y_i - v_i| \leq 0.0005$, $i = 1, 2$.

Several closed-loop simulation runs were performed to evaluate the robustness and constraint-handling capabilities of the multi-variable controller. Figure 4.1 depicts the startup reactor temperature and reactant concentration profiles for an initial

condition that lies within the stability region computed from Eq.4.11. The solid lines represent the process response when the bounded robust controller is tuned properly and implemented on the process. The dashed lines correspond to the response when the controller is designed and implemented without the robust uncertainty compensation component (i.e., $\chi = 0$). Finally, the dotted lines represent the open-loop response. When compared with the open-loop profiles, it is clear that, starting from the given admissible initial condition, the properly tuned bounded robust controller successfully drives both outputs to the desired steady-state, in the presence of input constraints, while simultaneously attenuating the effect of the uncertain variables on the outputs. It should be noted that this conclusion was reached a priori (before controller implementation) based on the characterization of the stability region given in Theorem 4.1. From the dashed profiles we see that the uncertain variables have a significant effect on the process outputs and that failure to explicitly account for them in the controller design leads to instability and poor transient performance. Figure 4.2 shows the corresponding profiles for the manipulated inputs. Note that since the initial condition is chosen within the region of guaranteed stability, the well-tuned multivariable controller generates, as expected, control action (solid lines) that respects the constraints imposed.

In Figure 4.3, we tested the ability of the controller to robustly stabilize the process at the desired steady-state, starting from initial conditions that lie outside the region of guaranteed closed-loop stability. In this case, no a priori guarantees can be made regarding closed-loop stability. In fact, from the process response denoted by the dashed lines in Figure 4.3, we see that, starting from the given initial condition, the controller is unable to successfully stabilize the process or attenuate the effect of uncertainty on the process outputs. The reason for this can be seen from the

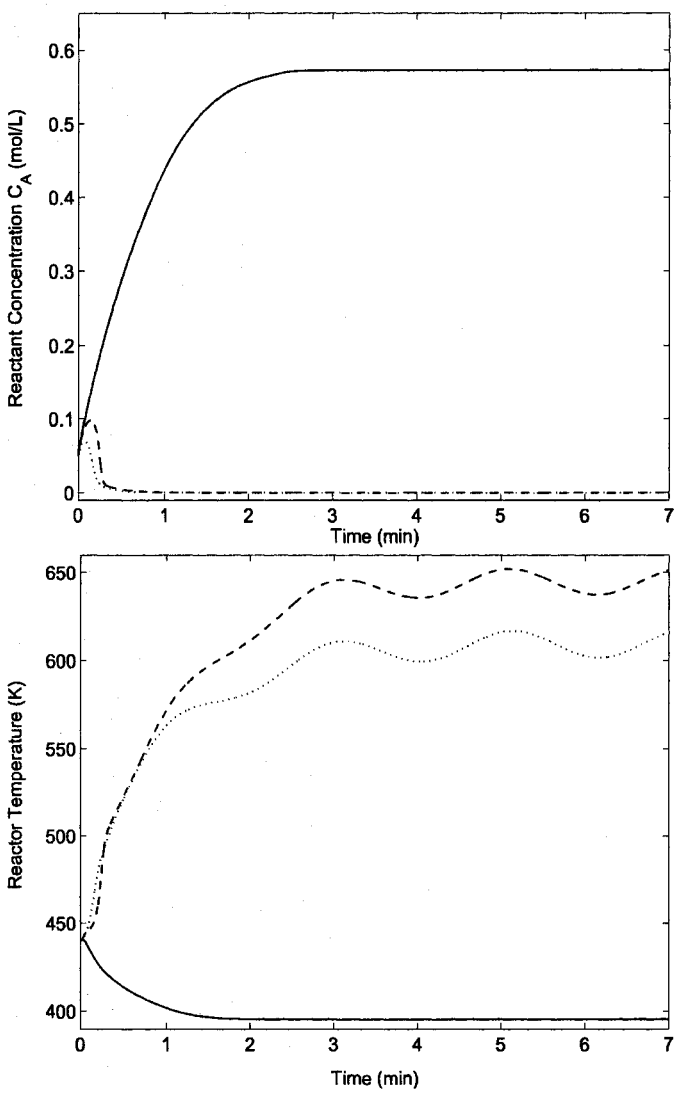

Figure 4.1: Controlled outputs: reactant concentration (top) and reactor temperature (bottom) profiles under the bounded multivariable nonlinear state feedback controller with uncertainty compensation and initial condition inside the stability region (solid), without uncertainty compensation (dashed) and under open-loop conditions (dotted).

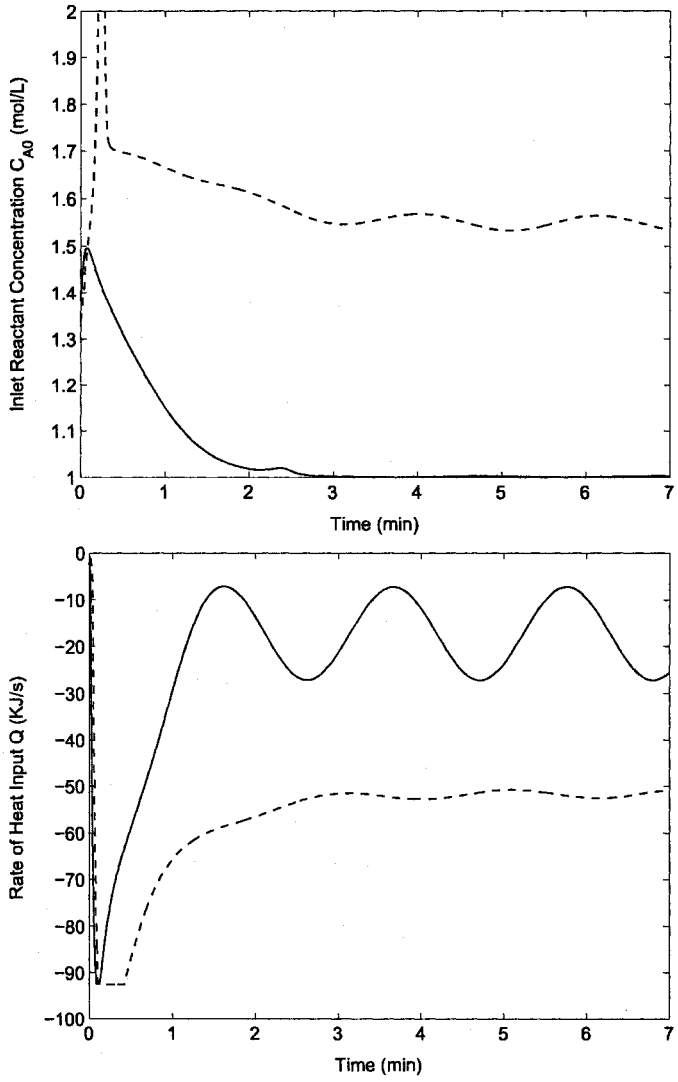

Figure 4.2: Manipulated inputs: inlet reactant concentration (top) and rate of heat input (bottom) profiles under the bounded multivariable nonlinear state feedback controller with uncertainty compensation and initial condition inside the stability region (solid), without uncertainty compensation (dashed) and under open-loop conditions (dotted).

corresponding manipulated inputs' profiles in Figure 4.4 (dashed lines) which show that both the inlet reactant concentration and rate of heat input stay saturated for all times, indicating that stabilizing the process from the given initial condition requires significantly larger control action, which the controller is unable to provide due to the constraints. The combination of insufficient reactant material in the incoming feed stream and insufficient cooling of the reactor prompt an increase in the reaction rate and, subsequently, an increase in the reactor temperature and depletion of the reactant material in the reactor. Note that since the region of guaranteed closed-loop stability given in Theorem 4.1 does not necessarily capture all the admissible initial conditions (this remains an resolved problem in control), it is possible for the controller to robustly stabilize the process starting from some initial conditions outside this region. An example of this is shown by the controlled outputs and manipulated inputs' profiles denoted by solid lines in Figures 4.3-4.4, respectively.

In addition to robust stabilization, we also tested the robust set-point tracking capabilities of the controller under uncertainty and constraints. The results for this case are shown in Figures 4.5-4.6 which depict the profiles of the controlled outputs and manipulated inputs, respectively, in response to a 0.4 mol/L increase in the reactant concentration set-point and 40 K decrease in the reactor temperature set-point. It is clear from the figures that the controller successfully achieves the requested tracking while simultaneously attenuating the effect of uncertainty and generating control action that respects the constraints imposed. Finally, the state-space region where the bounded robust multivariable controller satisfies the input constraints was computed using Eq.4.11 and is depicted in Figure 4.7 (top plot). For the sake of comparison, we included in Figure 4.7 (bottom plot) the corresponding region for a multivariable input-output linearizing controller that cancels process nonlinearities

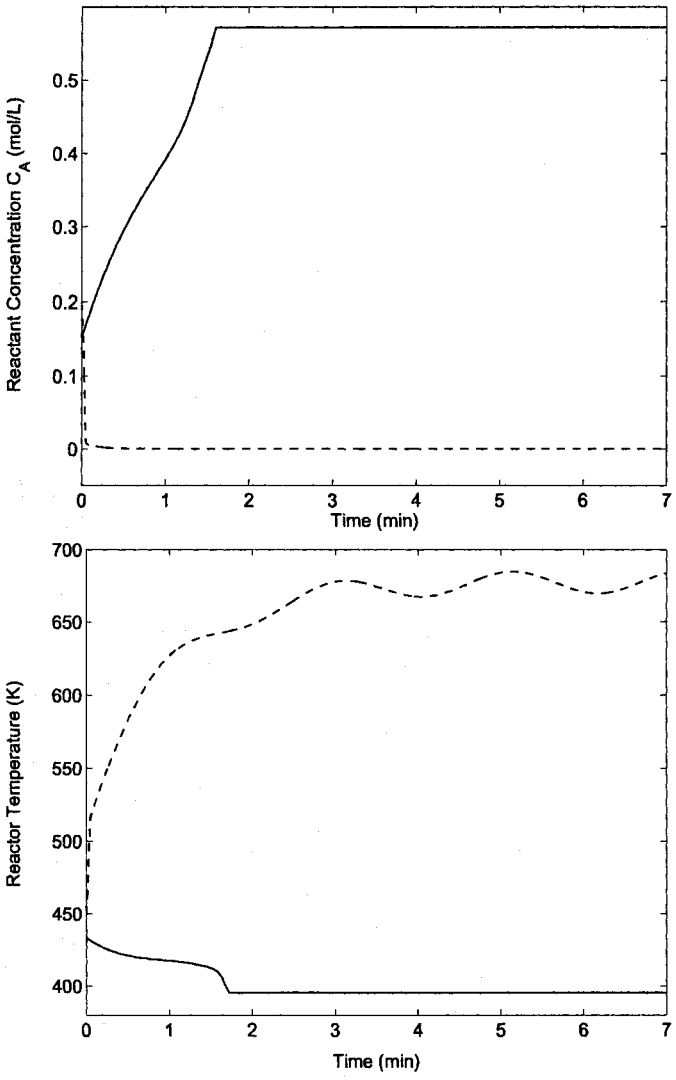

Figure 4.3: Controlled outputs: reactant concentration (top) and reactor temperature (bottom) profiles under the bounded robust multivariable nonlinear state feedback controller for initial conditions outside the region of guaranteed closed-loop stability.

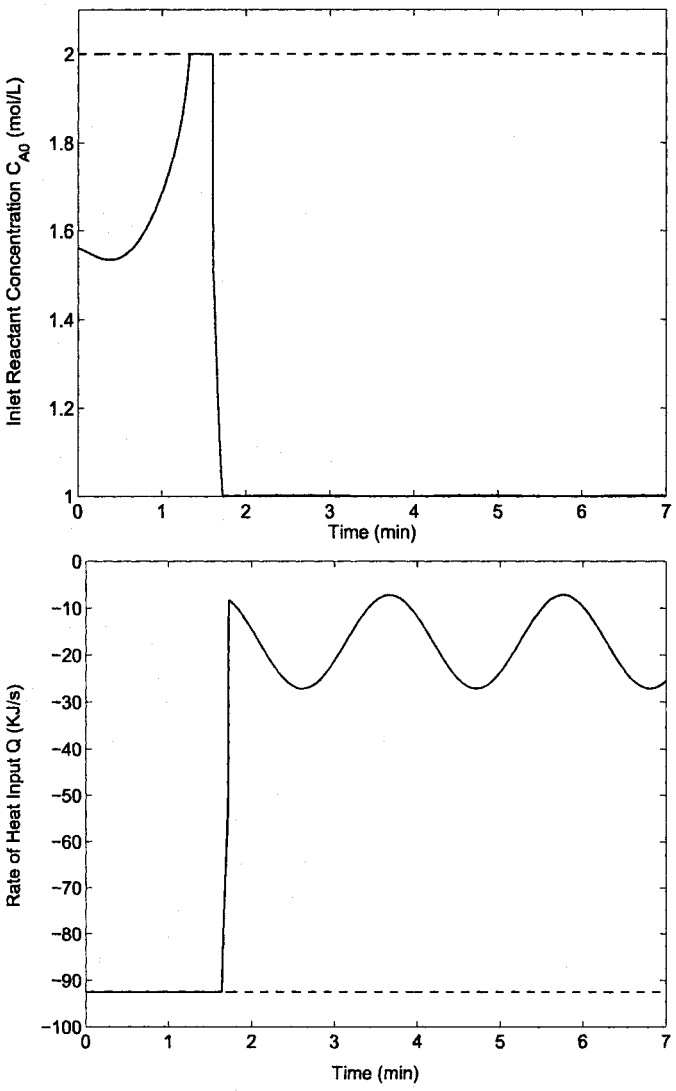

Figure 4.4: Manipulated inputs: inlet reactant concentration (top) and rate of heat input (bottom) profiles under the bounded multivariable nonlinear state feedback controller for initial conditions outside the region of guaranteed closed-loop stability.

(the stabilizing linear terms were not included since the associated stabilization cost of these terms would yield an even smaller region). Evolution of the closed-loop trajectories within either region (which is insured by constructing the largest invariant subregion within) guarantees closed-loop stability. It is clear from the comparison that the bounded robust multivariable controller satisfies the constraints for a wider range of process operating conditions. This is a consequence of the fact that, unlike the input-output linearizing controller, the bounded multivariable controller accounts explicitly for constraints. Furthermore, the cost of cancelling process nonlinearities by the linearizing controller renders many initial conditions that are far from the equilibrium point infeasible. In contrast, the bounded controller avoids the unnecessary cancellation of nonlinearities and employs reasonably smaller control action to stabilize the process. This, in turn, results in a larger set of operating conditions that satisfy the constraints.

4.5 State estimation and output feedback control

The feedback controller of Eqs.4.8-4.10 was designed under the assumption of accessibility of all process states for measurement. In chemical process control, however, more so than in other control areas, the complete state often cannot be measured. For example, the concentration of certain intermediates in chemical reactors may not be accessible for online measurements and therefore cannot be used directly for feedback purposes. In the past few years, significant advances have been made in the direction of output feedback controller design for the purpose of robustly stabilizing nonlinear systems. In this section, we address the problem of synthesizing bounded robust *output* feedback controllers for the class of constrained uncertain multivariable nonlinear processes in Eq.4.1. Owing to the explicit presence of time-varying

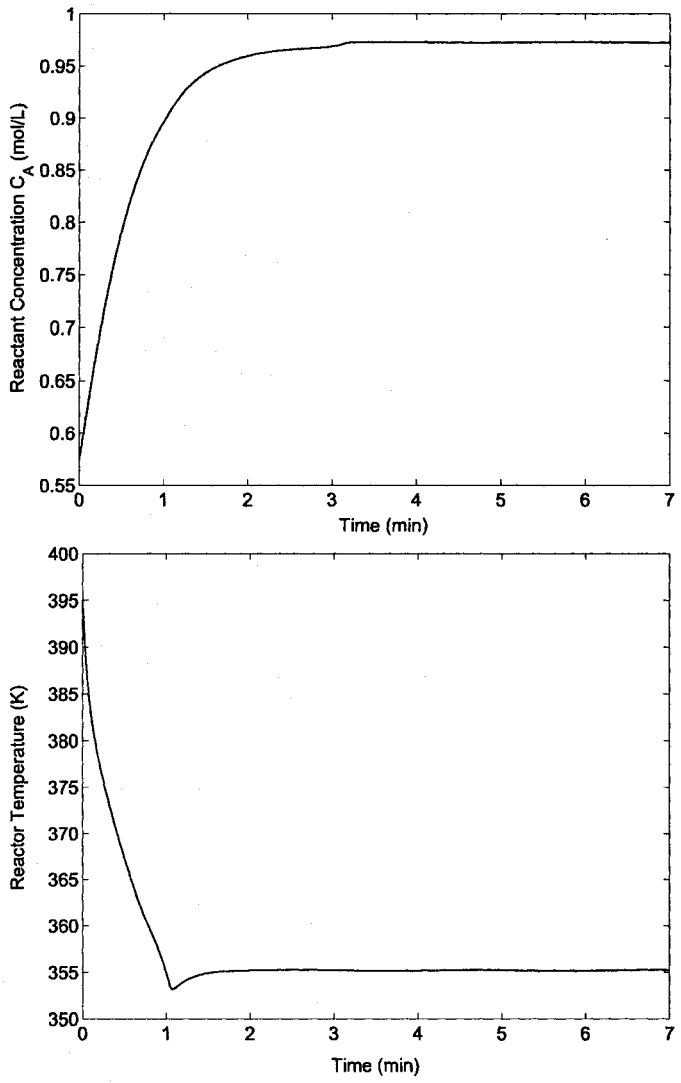

Figure 4.5: Controlled outputs: reactant concentration (top) and reactor temperature (bottom) profiles under the bounded robust multivariable nonlinear state feedback controller for a set-point increase of 0.4 mol/L in the reactant concentration and a set-point decrease of 40 K in the reactor temperature.

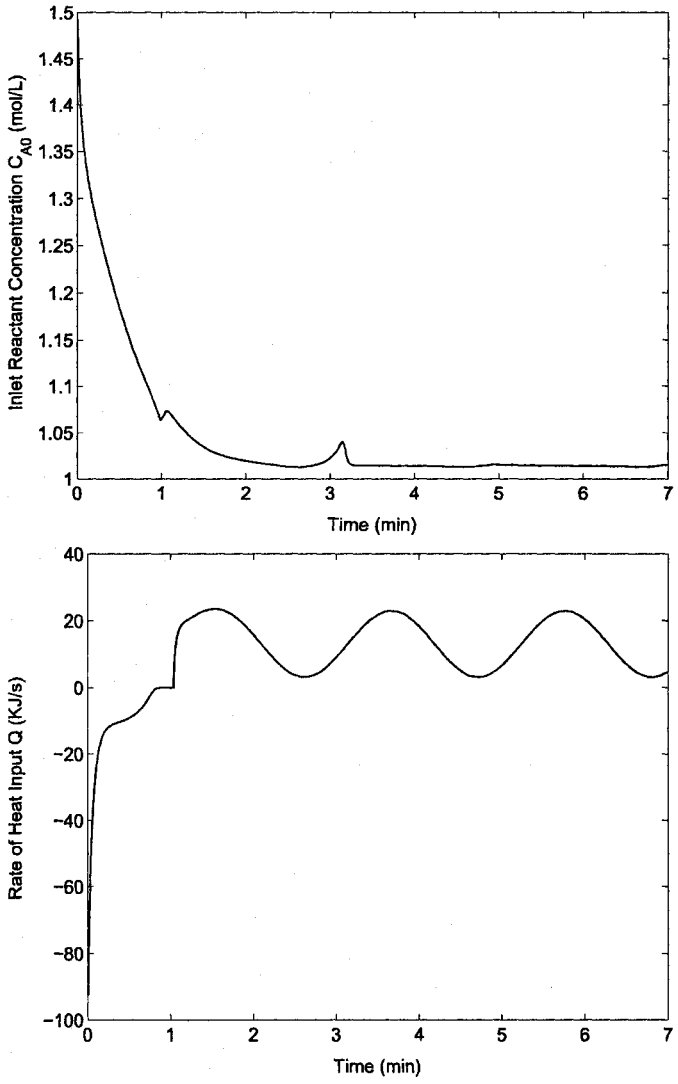

Figure 4.6: Manipulated inputs: inlet reactant concentration (top) and rate of heat input (bottom) profiles under the bounded multivariable nonlinear state feedback controller for a set-point increase of 0.4 mol/L in the reactant concentration and a set-point decrease of 40 K in the reactor temperature.

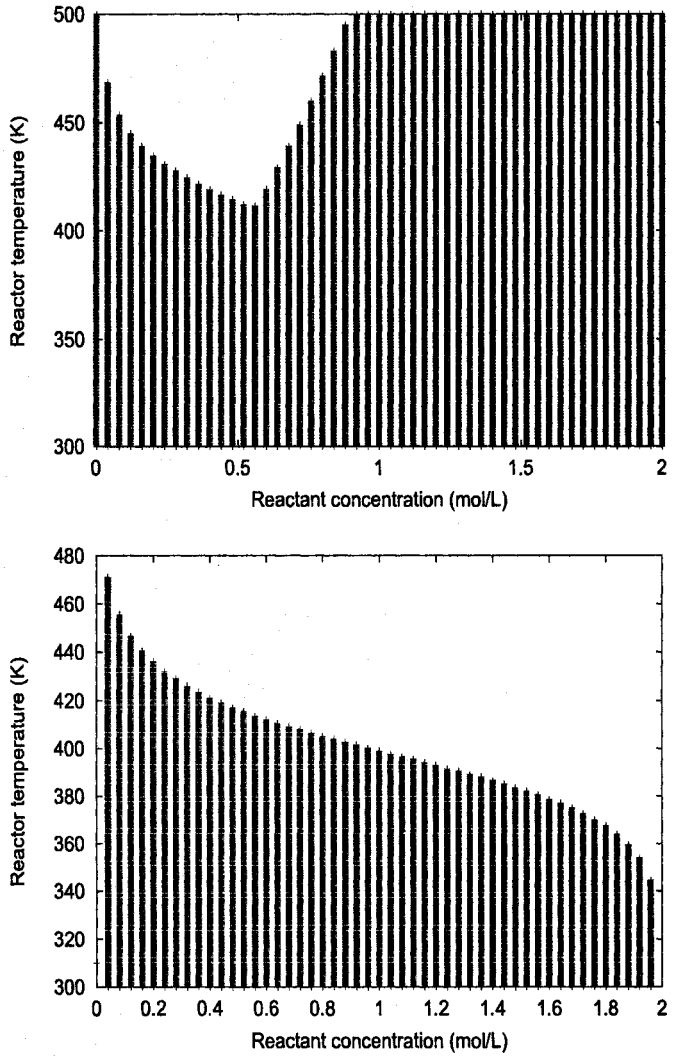

Figure 4.7: Comparison between the state-space regions where the bounded robust multivariable controller (top) and a multivariable input-output linearizing controller (bottom) satisfy the input constraints. The regions are used to provide estimates of the corresponding stability regions.

uncertain variables in the process of Eq.4.1, the approach that is followed for output feedback controller design is based on combination of high-gain observers and state feedback controllers (see also [293, 168, 210, 60] for results on output feedback control for unconstrained nonlinear systems). To this end, we initially formulate the control problem in Section 4.5.1 and then present it solution in Section 4.5.2.

4.5.1 Control problem formulation

Referring to the system of Eq.4.1, our objective is to synthesize a bounded robust nonlinear dynamic output feedback controller of the form:

$$\begin{aligned} \dot{\omega} &= \mathcal{F}(\omega, y, \bar{v}) \\ u &= \mathcal{P}(\omega, y, \bar{v}) \end{aligned} \tag{4.18}$$

where $\omega \in \mathbb{R}^s$ is an observer state, $\mathcal{F}(\omega, y, \bar{v})$ is a vector function, $\mathcal{P}(\omega, y, \bar{v})$ is a *bounded* vector function, $\bar{v}$ is a generalized reference input, that: (a) enforces, in the presence of actuator constraints, exponential stability and asymptotic robust output tracking with arbitrary degree of attenuation of the effect of the uncertainty on the output, and (b) provides an explicit characterization of the region where the aforementioned properties are guaranteed.

The design of the dynamic controller is carried out using combination of a high-gain state observer and the bounded robust state feedback controller proposed in Section 4.3. In particular, the system $\dot{\omega} = \mathcal{F}(\omega, y, \bar{v})$ in Eq.4.18 is constructed to provide estimates of the process state variables from the measured outputs, while the bounded static component, $\mathcal{P}(\omega, y, \bar{v})$, is synthesized to enforce the requested properties in the closed-loop system and at the same time provide the necessary explicit characterization of the region of guaranteed closed-loop stability. The stability analysis of the closed-loop system employs singular perturbation techniques (due to the high-gain nature of the observer) and utilizes the concept of input-to-state

stability and nonlinear small gain theorem-type arguments.

4.5.2 Controller synthesis

In order to proceed with the controller synthesis task, we need to slightly modify Assumption 4.1 to the following one.

Assumption 4.4 *There exist a set of integers,* $\{r_1, r_2, \ldots, r_m\}$, *and a coordinate transformation,* $(\zeta, \eta) = T(x)$, *such that the representation of the system of Eq.4.1, in the* (ζ, η) *coordinates, takes the form of Eq.4.5 with:*

$$\begin{aligned} \dot{\eta}_1 &= \Psi_1(\zeta, \eta) \\ &\vdots \\ \dot{\eta}_{n-\sum_i r_i} &= \Psi_{n-\sum_i r_i}(\zeta, \eta) \end{aligned} \tag{4.19}$$

We note that the change of variables of Eq.4.5 and Eq.4.19 is independent of θ and invertible since, for every x, the variables, ζ and η, are uniquely determined by Eq.4.5 and Eq.4.19. This implies that if we can estimate the values of ζ, η for all times, using appropriate state observers, then we automatically obtain estimates of x for all times. This property will be exploited later to synthesize a state estimator for the system of Eq.4.1 on the basis of the system of Eq.4.5. We also note that Assumption 4.4 includes the matching condition of our robust control method. In particular, we consider systems of the form Eq.4.1 for which the uncertain variables enter the system in the same equation with the manipulated inputs. This assumption is motivated by our requirement to eliminate the presence of θ in the η-subsystem. This requirement and the stability requirement of Assumption 4.5 below will allow including in the controller a replica of the η-subsystem of Eq.4.19 which provides estimates of the η states.

Assumption 4.5 *The system of Eq.4.19 is ISS with respect to ζ with $\beta_\eta(|\eta(0)|,t) = K_\eta|\eta(0)|e^{-at}$ where K_η, a are positive real numbers and $K_\eta \geq 1$.*

We are now ready to state the main result of this section. Theorem 4.2 that follows provides the explicit synthesis formula for the desired bounded robust output feedback controller and states precise conditions that guarantee closed-loop stability and robust asymptotic output tracking in the presence of uncertainty and input constraints. The proof of the theorem can be found in the Appendix C.

Theorem 4.2 *Consider the constrained uncertain nonlinear process of Eq.4.1, for which Assumptions 4.3-4.5 hold, under the output feedback controller:*

$$\begin{aligned}
\dot{\tilde{y}}^{(i)} &= A\tilde{y}^{(i)} + F_i(y_i - y_0^{(i)}) \\
\dot{\omega}_1 &= \Psi_1(sat(\tilde{y}),\omega) \\
&\vdots \\
\dot{\omega}_{n-\sum r_i} &= \Psi_{n-\sum r_i}(sat(\tilde{y}),\omega) \\
u &= -\frac{1}{2}R^{-1}(\hat{x})\left(\widehat{L_{\bar{g}}V}\right)^T
\end{aligned} \tag{4.20}$$

where $\hat{x} = T^{-1}(sat(\tilde{y}),\omega)$, $\tilde{y} = [\tilde{y}^{(1)^T} \cdots \tilde{y}^{(m)^T}]^T$, $\omega = [\omega_1 \cdots \omega_{n-\sum_i r_i}]^T$, $F_i = [L_i a_1^{(i)} \; L_i^2 a_2^{(i)} \cdots L_i^{r_i} a_{r_i}^{(i)}]^T, i = 1,\cdots,m$. Let $\bar{\epsilon} = max\{1/L_i\}$. Then for each pair of positive real numbers (δ_b, d) such that $\beta(\delta_b,0) + d \leq \delta_s$, where $\beta(\cdot,\cdot)$ and δ_s were defined in Theorem 4.1, and for each pair of positive real numbers $(\delta_\theta, \delta_{\bar{v}})$, there exists $\phi^* > 0$, and for each $\phi \in (0,\phi^*]$, there exists $\bar{\epsilon}^*(\phi) > 0$, such that if $\phi \in (0,\phi^*]$, $\bar{\epsilon} \in (0,\bar{\epsilon}^*(\phi)]$, $sat(\cdot) = min\{1, \zeta_{max}/|\cdot|\}(\cdot)$ with ζ_{max} being the maximum value of the vector ζ for $|\zeta| \leq \beta_\zeta(\delta_\zeta,0)$ where β_ζ is a class $\mathcal{KL}$ function and δ_ζ is the maximum value of the vector $[l_1^T(x) \; l_2^T(x) \cdots l_m^T(x)]^T$ for $|x| \leq \delta_b$, where $l_i(x) = [h_i(x) \; L_f h_i(x) \cdots L_f^{r_i-1}h_i(x)]^T$, $|x(0)| \leq \delta_b$, $\|\theta\| \leq \delta_\theta$, $\|\bar{v}\| \leq \delta_{\bar{v}}$, $|\tilde{y}(0)| \leq \delta_\zeta$, $\omega(0) = \eta(0) + O(\epsilon)$, the following holds in the presence of constraints:

(1) The origin of the closed-loop system is asymptotically (and locally exponentially)

stable.

(2) The outputs of the closed-loop system satisfy a relation of the form:

$$\limsup_{t\to\infty} |y_i(t) - v_i(t)| = 0,\ i = 1, \cdots, m \tag{4.21}$$

Remark 4.9 The robust output feedback controller of Eq.4.20 consists of: (1) m high-gain observers, each of which provides estimates of the derivatives of one of the m controlled outputs, y_i, up to order $r_i - 1$, and thus estimates of the variables $\zeta_1^{(i)}, \ldots, \zeta_{r_i}^{(i)}$, (2) an observer that simulates the inverse dynamics of the system of Eq.4.19, and (3) a bounded robust static feedback controller (see Theorem 4.1) that uses measurements of the outputs and estimates of the states to attenuate the effect of the uncertain variables on the process outputs and enforce reference input tracking. The use of high-gain observers allows us to achieve a certain degree of separation in the output feedback controller design, where the observer design is carried out independently of the state feedback design. This is possible because of the disturbance rejection properties of high-gain observers that allow asymptotic recovery of the performance achieved under state feedback, where "asymptotic" here refers to the behavior of the system as the poles of the observer approach infinity. It is important to note here that while such "separation principle" holds for the class of feedback linearizable nonlinear systems considered in this chapter, one should not expect the task of observer design to be independent from the state feedback design for more general nonlinear systems. In fact, even in linear control design, when model uncertainties are taken into consideration, the design of the observer cannot be separated from the design of the state feedback control.

Remark 4.10 In designing the output feedback controller of Eq.4.20, we use a standard saturation function, *sat*, to eliminate the peaking phenomenon typically exhibited by high-gain observers in their transient behavior. The origin of this phenomenon owes to the fact that as the observer poles approach infinity, its exponential modes will decay to zero arbitrarily fast, but the amplitude of these modes will approach infinity, thus producing impulsive-like behavior. To eliminate observer peaking, we

use the saturation filter in conjunction with the high-gain observers to eliminate (or filter out) wrong estimates of the process output derivatives provided by the observer for short times. The idea here is to exploit our knowledge of an estimate of the stability region obtained under state feedback (Ω) – where the process states evolve – to derive bounds on the actual values of the outputs' derivatives, and then use these bounds to design the saturation filter. Therefore, during the short transient period when the estimates of the high-gain observers exhibit peaking, the saturation filter eliminates those estimates which exceed the state feedback bounds, thus preventing peaking from being transmitted to the plant. Over the same period, the estimation error decays to small values, while the state of the plant remains close to its initial value. The validity of this idea is justified via asymptotic analysis from singular perturbation theory (see Proof of Theorem 4.2 in Appendix C).

Remark 4.11 An important consequence of the combined use of high-gain observers and saturation filters is that the region of closed-loop stability obtained under state feedback remains practically preserved under output feedback. Specifically, starting from any compact subset of initial conditions (whose size is fixed by δ_b) within the state feedback region, there always exist observer gains such that the dynamic *output* feedback controller of Eq.4.8 continues to enforce asymptotic stability and reference-input tracking in the constrained uncertain closed-loop system, when the observer gains are selected to be sufficiently large. Instrumental in deriving this result is the use of the saturation filter, which allows us to use arbitrarily large observer gains, in order to recover the state feedback region, without suffering the detrimental effects of observer peaking. Note that the size of the output feedback region (δ_b) can be made close to that of the state feedback region (δ_s) by selecting d to be sufficiently small which, in turn, can be done by making $\bar{\epsilon}$ sufficiently small. Therefore, although combination of the bounded state feedback controller with the observer results in some loss (given by d) in the size of the region of guaranteed closed-loop stability, this loss can be made small by selecting $\bar{\epsilon}$ to be sufficiently small. As expected, the nature of this semi-regional result is consistent with the semi-global result obtained

in Chapter 2 for the unconstrained case.

Remark 4.12 In addition to preserving the stability region, the controller-observer combination of Eq.4.20 practically preserves the optimality properties of the state feedback controller explained in Remark 4.5. The output feedback controller design is near-optimal in the sense that the cost incurred by implementing this controller tends to the optimal cost achieved by implementing the bounded state feedback controller when the observer gains are taken to be sufficiently large. Using standard singular perturbation arguments, one can show that cost associated with the output feedback controller is $O(\bar{\epsilon})$ close to the optimal cost associated with the state feedback controller (i.e., $J_{min} = V(e(0)) + O(\bar{\epsilon})$). The basic reason for near-optimality is the fact that by choosing $\bar{\epsilon}$ to be sufficiently small, the observer states can be made to converge quickly to the process states. This fact can be exploited to make the performance of the output feedback controller arbitrarily close to that of the optimal state feedback controller (see Chapter 2 for an analogous result for the unconstrained case).

Remark 4.13 Owing to the presence of the fast (high-gain) observer in the dynamical system of Eq.4.20, the closed-loop system can be cast as a singularly perturbed system, where $\bar{\epsilon} = \max\{1/L_i\}$ is the singular perturbation parameter. Within this system, the states of the high-gain observers, which provide estimates of the outputs and their derivatives, constitute the fast states, while the ω states of the observer and the states of the original system of Eq.4.1 under state feedback represent the slow states. Owing to the dependence of the controller of Eq.4.20 on both the slow and fast states, the control action computed by the static component in Eq.4.20 is not $O(\bar{\epsilon})$ close to that computed by the state feedback controller for all times. After the decay of the boundary layer term (fast transients of the high-gain observers), however, the static component in Eq.4.20 approximates the state feedback controller to within $O(\bar{\epsilon})$.

Remark 4.14 It is important to note that the asymptotic stability results of Theorem 4.1 (Theorem 4.2) are regional (semi-regional) and nonlocal. By definition, a

local result is one that is valid provided that the initial conditions are sufficiently small. In this regard, neither the result of Theorem 4.1 nor that of Theorem 4.2 requires the initial conditions to be sufficiently small in order for stability to be guaranteed. The apparent limitations imposed on the size of the initial conditions that guarantee closed-loop stability follow from the fundamental limitations imposed by the input constraints and uncertainty, as can be seen from Eq.4.11. In the absence of constraints, for example, one can establish asymptotic stability globally for the state feedback problem and semi-globally for the output feedback case. In fact, one of the valuable features of the results in Theorems 4.1 and 4.2 is that they provide an explicit procedure for constructing reasonably large estimates of the stability region that depend only on the magnitude of the constraints and the size of the uncertainty, which therefore allows one to start from initial conditions farther away (from the equilibrium point) than would be possible using approaches where no explicit characterization of the stability region is available and consequently one often has to restrict the initial conditions to be sufficiently close to the origin.

4.6 Robust stabilization of a chemical reactor via output feedback control

To illustrate an application of the output feedback controller design presented in the previous section, we consider in this section a well-mixed continuous stirred tank reactor where three parallel irreversible elementary exothermic reactions of the form $A \xrightarrow{k_1} D$, $A \xrightarrow{k_2} U$ and $A \xrightarrow{k_3} R$ take place, where A is the reactant species, D is the desired product and U, R are undesired byproducts. The feed to the reactor consists of pure A at flow rate F, molar concentration C_{A0} and temperature T_{A0}. Due to the non-isothermal nature of the reactions, a jacket is used to remove/provide heat to the reactor. Under standard modeling assumptions, a mathematical model of the process

can be derived from material and energy balances and takes the following form:

$$\begin{aligned} V\frac{dT}{dt} &= F(T_{A0}-T)+\sum_{i=1}^{3}\frac{(-\Delta H_i)}{\rho c_p}k_{i0}\exp\left(\frac{-E_i}{RT}\right)C_A V+\frac{Q}{\rho c_p} \\ V\frac{dC_A}{dt} &= F(C_{A0}-C_A)-\sum_{i=1}^{3}k_{i0}\exp\left(\frac{-E_i}{RT}\right)C_A V \\ V\frac{dC_D}{dt} &= -FC_D+k_{10}\exp\left(\frac{-E_1}{RT}\right)C_A V \end{aligned} \tag{4.22}$$

where C_A and C_D denote the concentrations of the species A and D, T denotes the temperature of the reactor, Q denotes rate of heat input/removal from the reactor, V denotes the volume of the reactor, ΔH_i, k_i, E_i, $i = 1, 2, 3$, denote the enthalpies, pre-exponential constants and activation energies of the three reactions, respectively, c_p and ρ denote the heat capacity and density of the reactor. The values of the process parameters and the corresponding steady-state values are given in Table 4.2. It was verified that these conditions correspond to an unstable equilibrium point of the process of Eq.4.22.

The control problem is formulated as the one of regulating both the concentration of the desired product, C_D, and the reactor temperature, T, at the unstable steady-state by manipulating the inlet reactant concentration, C_{A0}, and the rate of heat input, Q, provided by the jacket. The control objective is to be accomplished in the presence of: (1) exogenous time-varying disturbances in the feed stream temperature, (2) parametric uncertainty in the enthalpy of the three reaction, and (3) hard constraints on the manipulated inputs. Defining $x_1 = T$, $x_2 = C_A$, $x_3 = C_D$, $u_1 = Q$, $u_2 = C_{A0} - C_{A0s}$, $\theta_i = \Delta H_i - \Delta H_{i0}$, $i = 1, 2, 3$, $\theta_4 = T_{A0} - T_{A0s}$, $y_1 = x_1$, $y_2 = x_3$, where the subscript s denotes the steady-state values and ΔH_{i0} are the nominal values for the enthalpies, the process model of Eq.4.22 can be written in the

Table 4.2: Process parameters and steady-state values for the reactor of Eq.4.22.

V	$=$	1000.0	L
R	$=$	8.314	$J/mol.K$
C_{A0s}	$=$	4.0	mol/L
T_{A0s}	$=$	300.0	K
ΔH_1	$=$	-5.0×10^4	J/mol
ΔH_2	$=$	-5.2×10^4	J/mol
ΔH_3	$=$	-5.4×10^4	J/mol
k_{10}	$=$	5.0×10^4	min^{-1}
k_{20}	$=$	5.0×10^3	min^{-1}
k_{30}	$=$	5.0×10^3	min^{-1}
E_1	$=$	5.0×10^4	J/mol
E_2	$=$	7.53×10^4	J/mol
E_2	$=$	7.53×10^4	J/mol
c_p	$=$	0.231	$J/g.K$
ρ	$=$	1000.0	g/L
F	$=$	83.3	L/min
T_s	$=$	390.97	K
C_{As}	$=$	3.58	mol/L
C_{Ds}	$=$	0.42	mol/L

form of Eq.4.1 with:

$$f(x) = \begin{bmatrix} \frac{F}{V}(T_{A0s} - T) + \sum_{i=1}^{3} \frac{(-\Delta H_{i0})}{\rho c_p} k_{i0} \exp\left(\frac{-E_i}{RT}\right) C_A \\ \frac{F}{V}(C_{A0s} - C_A) - \sum_{i=1}^{3} k_{i0} \exp\left(\frac{-E_i}{RT}\right) C_A \\ -\frac{F}{V} C_D + k_{10} \exp\left(\frac{-E_1}{RT}\right) C_A \end{bmatrix}, \quad g_1(x) = \begin{bmatrix} \frac{1}{\rho c_p V} \\ 0 \\ 0 \end{bmatrix}$$

$$g_2(x) = \begin{bmatrix} 0 \\ \frac{F}{V} \\ 0 \end{bmatrix}, \quad w_i(x) = \begin{bmatrix} k_{i0} \exp\left(\frac{-E_i}{RT}\right) C_A \\ 0 \\ 0 \end{bmatrix}, \quad i = 1, 2, 3, \quad w_4(x) = \begin{bmatrix} \frac{F}{V} \\ 0 \\ 0 \end{bmatrix}$$

$h_1(x) = x_1$, $h_2(x) = x_3$. To simulate the effect of uncertainty on the process outputs, we consider a time-varying function of the form of Eq.4.17, with $\theta_0 = 0.03 T_{A0}$, to simulate the effect of external disturbances in the feed temperature. We also consider a parametric uncertainty of 50% in the values of the enthalpies. Therefore, the bounds on the uncertain variables are taken to be $\theta_{bk} = 0.5\,|(-\Delta H_{k0})|$, $k = 1, 2, 3$, $\theta_{b4} = 0.03 T_{A0s}$. Also, the following constraints are imposed on the manipulated inputs: $|u_1| \leq 25\ KJ/s$ and $|u_2| \leq 4.0\ mol/L$.

For this process, the relative degrees of the process outputs, with respect to the vector of manipulated inputs, are $r_1 = 1$, $r_2 = 2$, respectively. Using Eq.4.3, it can be verified that the decoupling matrix $C(x)$ is nonsingular and that the assumptions of Theorem 4.2 are satisfied. In order to proceed with controller synthesis, we initially use the following coordinate transformation (in error variables form):

$$\begin{bmatrix} e_1 \\ e_2 \\ e_3 \end{bmatrix} = \begin{bmatrix} \zeta_1^{(1)} - v_1 \\ \zeta_1^{(2)} - v_2 \\ \zeta_2^{(2)} - v_2^{(1)} \end{bmatrix} = \begin{bmatrix} h_1(x) - v_1 \\ h_2(x) - v_2 \\ L_f h_2(x) \end{bmatrix} = \begin{bmatrix} x_1 - v_1 \\ x_3 - v_2 \\ -\frac{F}{V} C_D + k_{30} \exp\left(\frac{-E_3}{RT}\right) C_A \end{bmatrix}$$

to cast the process model in its input-output form of Eq.4.6, which is used directly for output feedback controller design. The necessary controller, whose practical implementation requires measurements of T and C_D only, consists of a combination of two high-gain observers (equipped with appropriate saturation filters) that provide estimates of the process states and a bounded robust static feedback component. The static component is designed, with the aid of the explicit synthesis formula in Eqs.4.8-4.10, using a quadratic Lyapunov function of the form $V = e^T P e$, where:

$$P = \begin{bmatrix} 1 & 0 & 0 \\ 0 & \sqrt{3} & 1 \\ 0 & 1 & \sqrt{3} \end{bmatrix} \tag{4.23}$$

which is also used to compute an estimate of the region of guaranteed closed-loop stability using Eq.4.11. The high-gain observers are designed using Eq.4.20 and consist of a replica of the linear part of the system of Eq.4.6 plus a linear gain multiplying the discrepancy between the actual and the estimated values of the outputs. The output feedback controller takes the following form:

$$\begin{aligned} \dot{\tilde{y}}_1^{(1)} &= L_1 a_1^{(1)} (y_1 - \tilde{y}_1^{(1)}) \\ \dot{\tilde{y}}_1^{(2)} &= \tilde{y}_2^{(2)} + L_2 a_1^{(2)} (y_2 - \tilde{y}_1^{(2)}) \\ \dot{\tilde{y}}_2^{(2)} &= L_2^2 a_2^{(2)} (y_2 - \tilde{y}_1^{(2)}) \\ u &= -\frac{1}{2} R^{-1}(sat(\tilde{y})) \left(\widehat{L_{\tilde{g}} V}\right)^T \end{aligned} \tag{4.24}$$

where $\tilde{y}_1^{(1)}$, $\tilde{y}_1^{(2)}$, $\tilde{y}_2^{(2)}$ are the estimates of the reactor temperature, reactant concentration, and desired product concentration, respectively, and the saturation filter is defined as:

$$sat(\tilde{y}_i^{(j)}) = \left\{ \begin{array}{ll} a_{m,i}^{(j)}, & \tilde{y}_i^{(j)} \geq a_m^{(j)} \\ \tilde{y}_i^{(j)}, & -a_{m,i}^{(j)} \leq \tilde{y}_i^{(j)} \leq a_{m,i}^{(j)} \\ -a_{m,i}^{(j)}, & \tilde{y}_i^{(j)} \leq -a_{m,i}^{(j)} \end{array} \right\} \tag{4.25}$$

The following values were used for the controller and observer parameters: $\chi = 3.5$, $\phi = 0.0001$, $\rho = 0.001$, $L_1 = 100$, $a_1^{(1)} = 10$, $L_2 = 400$, $a_1^{(2)} = 40$, $a_2^{(2)} = 400$, $a_{m,1}^{(1)} = 395$, $a_{m,1}^{(2)} = 4$, $a_{m,2}^{(2)} = 0.5$ to ensure that the process outputs satisfy a relation of the form $\limsup_{t\to\infty} |y_i - v_i| \leq 0.0005$, $i = 1, 2$.

Closed-loop simulations were performed to evaluate the robust stabilization capabilities of the output feedback controller, starting from an initial condition inside the stability region, and compare its performance with that of the state feedback controller and the open-loop response. Figures 4.8-4.9 depict the controlled outputs (desired product concentration and reactor temperature) and manipulated inputs (inlet reactant concentration and rate of heat input) profiles, respectively, under output feedback control (solid lines), under state feedback control (dashed lines) assuming all process states are available for measurement, and under no control (dotted lines). It is clear from the comparison with the open-loop profiles that the output feedback controller successfully drives both controlled outputs close to the desired steady-state while simultaneously attenuating the effect of disturbances and model uncertainty on the process outputs and generating control action that respects the constraints imposed. Note that the controlled outputs and manipulated inputs' profiles obtained under the output feedback controller (solid lines) are very close to the profiles obtained under the state feedback controller (dashed lines). This closeness, starting from the same initial condition, illustrates two important features of the output feedback design. The first is the fact that, by selecting the observer gains to be sufficiently large, the performance of the output feedback controller approaches (or recovers) that of the state feedback controller. Since the process response under state feedback control can be shown to be optimal (in the inverse sense) with respect to a meaningful cost (see Remark 4.5), the performance of the output feedback controller then is near-optimal

with respect to the same cost. The second feature is that the set of admissible initial conditions, starting from where stability of the constrained closed-loop system is guaranteed under state feedback, remains practically preserved when the observer gain is chosen sufficiently large.

4.7 Connections with model predictive control

The purpose of this section is to put the bounded robust Lyapunov-based control approach proposed in this chapter in perspective with respect to the nonlinear model predictive control approach, for control of uncertain nonlinear processes with input constraints. Currently, in the chemical process industry, Model-based Predictive Control (MPC) is an established advanced control technique whose success in several commercial applications is well-documented in the literature. The popularity of this approach stems largely from its ability to handle, among other issues, multivariable interactions, constraints, and optimization requirements, all in a consistent, systematic manner. This success notwithstanding, a number of important theoretical and practical problems – particularly within the nonlinear context – continue to be active areas of research. Our objective in this section is to highlight some of the implications of the proposed Lyapunov-based control approach for dealing with some of these problems and assisting the capabilities of the MPC approach. In particular, we illustrate how some of the conceptual tools put forth by the Lyapunov-based approach can be used to address the issue of providing a priori closed-loop stability guarantees for the MPC algorithm. Towards this end, we will initially review how the control problem is formulated within the MPC framework and what are the main tools required to solve it for constrained uncertain nonlinear processes. For a more in-depth discussion of the theoretical and practical issues within model predictive control, the reader is referred

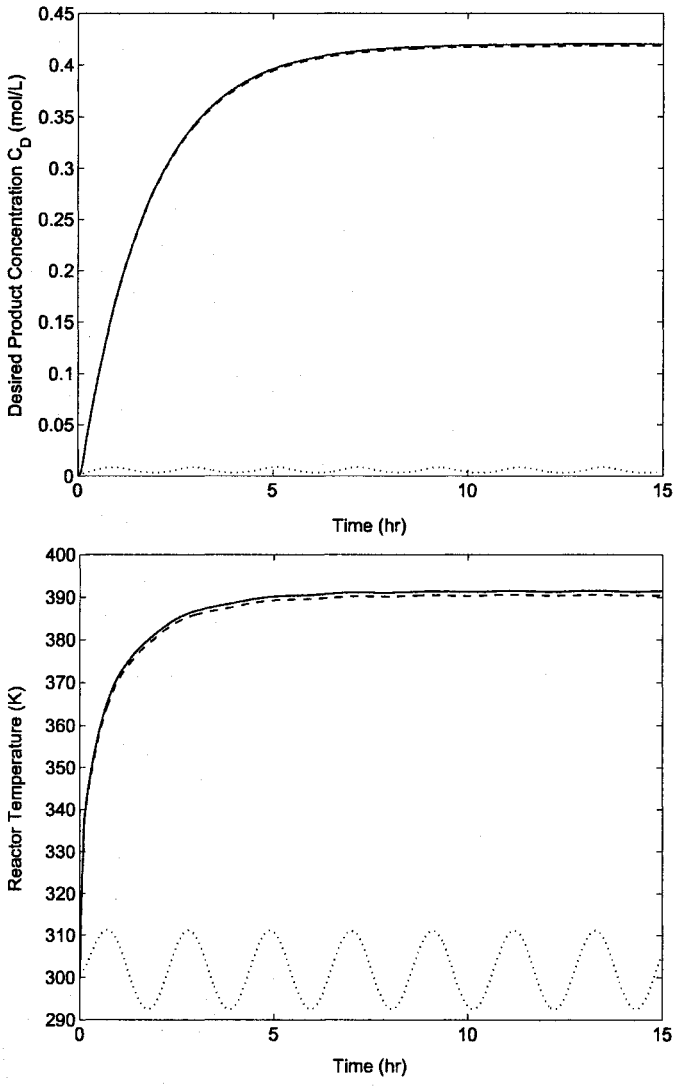

Figure 4.8: Controlled outputs: desired product concentration (top) and reactor temperature (bottom) profiles under the bounded robust multivariable output feedback controller (solid), under the corresponding state feedback controller (dashed), for initial condition within the region of guaranteed stability, and under open-loop conditions (dotted).

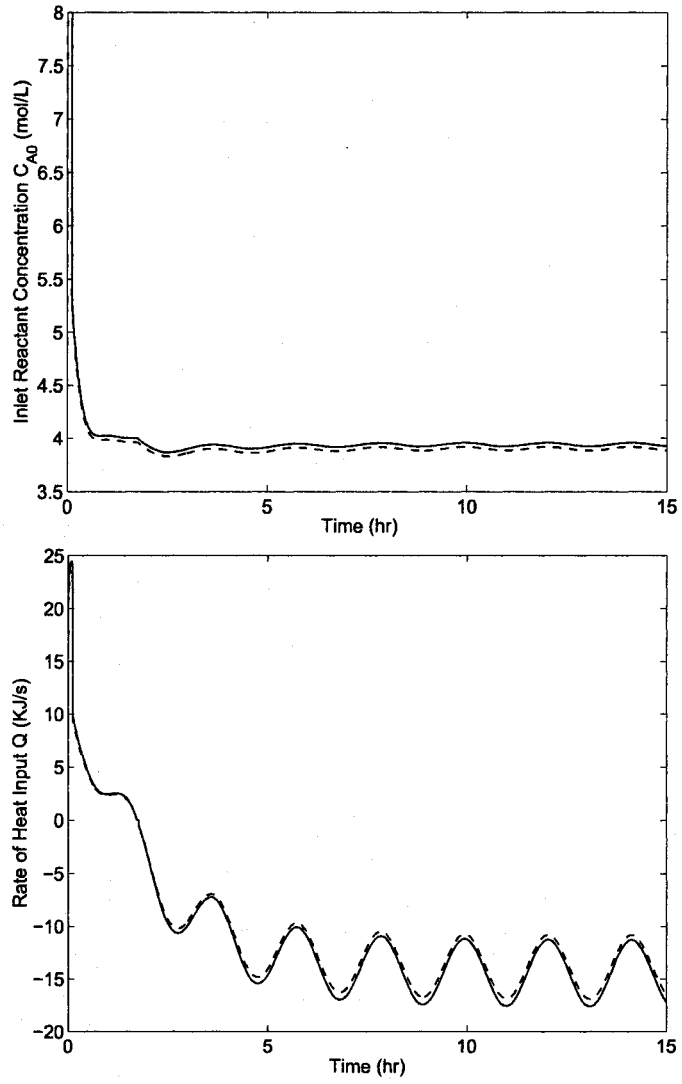

Figure 4.9: Manipulated inputs: inlet reactant concentration (top) and rate of heat input (bottom) profiles under the bounded robust multivariable output feedback controller (solid) and under the corresponding state feedback controller (dashed), for an initial condition within the region of guaranteed stability.

to the following extensive reviews [225, 215, 195, 248] and the references therein.

To simplify our discussion, let us consider first the nominal case where no modeling errors or disturbances are present ($\theta_k \equiv 0$ in Eq.4.1). Also since the MPC algorithm is typically implemented with digital computers, we will use the discrete version of Eq.4.1:

$$x_{k+1} = f(x_k) + g(x_k)u_k \tag{4.26}$$

For this case, MPC is conventionally formulated as solving on-line a finite-horizon optimal control problem of the form:

$$\min_{\mathcal{U}_k} \quad \sum_{i=1}^{p} x_{k+i|k}^T Q x_{k+i|k} + \sum_{i=0}^{m-1} u_{k+i|k}^T R u_{k+i|k} \tag{4.27}$$

$$x_{k+i|k} \in \mathcal{X}, i = 1, \cdots, p \tag{4.28}$$

$$u_{k+i|k} \in \mathcal{V}, i = 0, \cdots, m-1 \tag{4.29}$$

where $x_{k+i|k}$ stands for the prediction of x_{k+i} based on $x_{k|k}$, and the vector $\mathcal{U}_k = [u_{k|k}^T, \cdots, u_{k+m-1|k}^T]^T$ represents the input trajectory to be computed. Q and R are positive-definite matrices, p is the prediction horizon, m is the number of control moves, and Eqs.4.28-4.29 represent the hard constraints on the future states and manipulated inputs. At each k-th sample time, information is received about the current state of the process and based on this information together with the process model, the dependence of future states on the future manipulated inputs can be predicted. The future input trajectory is then determined according to the given optimality criterion and implemented until the next sample time, when the entire process is repeated based on new information. What results therefore is a discrete feedback control law, $u_k = \phi(x_{k|k})$, that is given *implicitly* through the optimization problem, which must be solved at each time step. Note that since the future input trajectory is computed solely on the basis of the current information, MPC is an

open-loop optimal control policy. The open-loop formulation allows for significant reduction in the complexity of the problem, by avoiding the intractable dynamic programming problem arising from optimal feedback control, but can also lead to worse performance than what is achievable with feedback control [195]. A conceptual parallel to be noted here is that the Lyapunov-based control approach proposed in this chapter also avoids the intractable Hamilton-Jacobi-Bellman equation (HJB) (or the HJI equation in the case with uncertainty) which is the optimality condition for the stabilization problem, though through inverse, rather than open-loop, optimal control. What results in this case therefore is an explicit feedback law (see Theorem 4.1) that is optimal with respect to a meaningful (though not specified a priori) cost functional. Note also that in both approaches performance deterioration problems, such as process directionality in constrained multivariable processes, do not arise since the constraints are explicitly accounted for in the controller design.

When the process of Eq.4.26 is linear, the cost quadratic, the sets $\mathcal{X}$ and $\mathcal{V}$ convex, the MPC optimization problem reduces to a quadratic program for which efficient software exists and, consequently, a number of control-relevant issues have been explored, including issues of closed-loop stability, performance, implementation, and constraint satisfaction. However, when the system is nonlinear, the optimization problem will in general be non-convex even if the cost functional and constraints are convex, and therefore a host of difficulties impacting on the implementability of the model predictive controller ensue (see [215] for a detailed discussion of these issues). In addition to the computational difficulties of solving a nonlinear optimization problem at each time step, the implementation of MPC in this case comes without any well-established closed-loop properties, even nominal ones [248]. Unless a nonlinear MPC controller is exhaustively tested by simulation over the whole range of potential

initial states, doubt will always remain as to whether or not a state will be encountered for which an acceptable solution to the finite-horizon problem can be found. Note that, in contrast, the bounded nonlinear feedback controller of Eqs.4.8-4.10, comes with well-characterized closed-loop stability and performance properties (both nominal and in the presence of uncertainty) through the inequality of Eq.4.11, which is suited for the practical computation of the set of feasible initial states starting from where the constrained closed-loop system is guaranteed to be stable (see also Remark 4.1). We will return to this point shortly in our discussion to illustrate how similar ideas for characterizing the stability region can be used to provide a priori stability guarantees for the MPC approach.

Let us now turn our attention to the problem of controlling nonlinear systems with both model uncertainty and input constraints. Addressing the problem within an MPC framework in this case usually leads to a min-max formulation. For example, consider the case of time-varying uncertainty and let us assume that θ_k is a time sequence and $\theta_k \in \Theta \ \forall k$ where Θ is a compact set. The following min-max MPC formulation can be derived from game theory [195]:

$$\min_{\mathcal{U}_k} \max_{\theta_{k|k},\cdots,\theta_{k+p-1|k}} \quad \sum_{i=1}^{p} x_{k+i|k}^T Q x_{k+i|k} + \sum_{i=0}^{m-1} u_{k+i|k}^T R u_{k+i|k} \tag{4.30}$$

$$x_{k+i|k} \in \mathcal{X}, i = 1, \cdots, p \tag{4.31}$$

$$u_{k+i|k} \in \mathcal{V}, i = 0, \cdots, m-1 \tag{4.32}$$

$$\theta_{k+i|k} \in \Theta, i = 0, \cdots, p-1 \tag{4.33}$$

Solution to the above program computes an open-loop input trajectory that minimizes the "worst-case" cost for the chosen prediction horizon. It should be noted that the state constraint of Eq.4.31 must be satisfied for all possible sequences of $\theta_{k+i|k}$. The above optimization, which is non-convex in general (even for linear systems), must

be solved on-line at each time step. In addition to the concomitant computational difficulties associated with this optimization, the above approach does not provide any explicit guarantees for closed-loop stability. Note that although the Lyapunov-based control approach proposed in Theorem 4.1 accounts explicitly for nonlinearities, uncertainty and input constraints, it does not account explicitly for state constraints. To deal with this problem, one may formulate the constrained states as additional outputs to be controlled. Obviously, this may require the use of more control inputs and is therefore restricted to cases where the number of state constraints is not too large. It is to be noted also that the MPC formulation allows for incorporating state constraints directly as part of the constrained optimization problem (see Eq.4.31) even though an actual solution to the nonlinear min-max optimization problem is difficult to obtain in general.

In addition to providing a solution to the control problem for uncertain nonlinear systems with input constraints, the Lyapunov-based approach also suggests a systematic way of obtaining closed-loop stability guarantees for the MPC algorithm. The idea here is to incorporate the Lyapunov stability condition of Eq.4.13 (using a pre-determined control Lyapunov function as is done, for example, in contractive MPC [317] and CLF-based Receding Horizon Control [254, 239]) as an additional inequality constraint on the optimization problem. This condition represents a constraint on the control input and applies only to the initial control action, and not the entire manipulated input trajectory computed, since it is only the first control move in that sequence that is actually implemented. Satisfaction of this constraint guarantees closed-loop stability. Then, using techniques similar to those used in deriving Eq.4.11, one can obtain an estimate of the closed-loop stability region associated with the MPC controller. For example, when $\theta_k \equiv 0$, it is not difficult to see that a

condition of the form:

$$L_f V \leq -u_{max}|(L_g V)^T| \tag{4.34}$$

is sufficient to guarantee that the Lyapunov function decreases monotonically along the trajectories of the closed-loop system (i.e., $\dot{V} < 0$) regardless of the control input, so long as it satisfies the constraints (i.e., for any $|u| \leq u_{max}$). Therefore, if the set described by Eq.4.34 contains the origin in its interior, one can obtain a set of feasible initial conditions (by computing the largest invariant subset within) starting from where the constrained finite-horizon optimization problem is guaranteed to have a solution for every point in the set. Note that the condition derived in Eq.4.34 is more conservative than the one in Eq.4.11. This owes to the fact that the estimate of Eq.4.11 applies specifically to the bounded robust controller of Eqs.4.8-4.10 while the estimate of Eq.4.34 is independent of the control law. A similar expression to that of Eq.4.34 can be derived to estimate the stability region and provide stability guarantees when uncertainty is present. More research work is needed in this direction to establish rigorously these possible links with model predictive control (see Chapters 5 and 6 for some results in this direction) and address computational issues that arise in the practical implementation of nonlinear MPC.

4.8 Conclusions

A Lyapunov-based nonlinear controller design methodology, for MIMO nonlinear processes with uncertain dynamics, actuator constraints, and incomplete state measurements, was developed. Under the assumption that all process states are accessible for measurement, the approach led to the explicit synthesis of bounded robust multivariable nonlinear feedback controllers that enforce stability and robust asymptotic reference-input tracking in the constrained uncertain closed-loop system and provide,

at the same time, an explicit characterization of the region of guaranteed closed-loop stability. When complete state measurements are not available, a combination of the bounded robust state feedback controllers with high-gain state observes and appropriate saturation filters, was employed to synthesize bounded robust multivariable output feedback controllers that require only measurements of the outputs for practical implementation. The resulting output feedback design was shown to inherit the same closed-loop stability and performance properties of the state feedback controller and, in addition, practically preserve the region of guaranteed closed-loop stability obtained under state feedback. The developed state and output feedback controllers were applied successfully to non-isothermal chemical reactor examples with uncertainty, input constraints, and incomplete state measurements. Finally, a discussion was provided to put the proposed Lyapunov-based approach in perspective with respect to the nonlinear model predictive control approach, and the implications of our results in the practical implementation of MPC were highlighted.

Chapter 5

Hybrid Predictive Control of Constrained Linear Systems

5.1 Introduction

Model Predictive Control (MPC), also known as receding horizon control (RHC), is a popular control method for handling constraints (both on manipulated inputs and state variables) within an optimal control setting [257]. In MPC, the control action is obtained by solving repeatedly, on–line, a finite–horizon constrained open–loop optimal control problem. The popularity of this approach stems largely from its ability to handle, among other issues, multi–variable interactions, constraints on controls and states, and optimization requirements, all in a consistent, systematic manner. Its success in many commercial applications is also well–documented in the literature (see, for example, [117, 241]). These considerations have motivated numerous research investigations into the stability properties of model predictive controllers and led to a plethora of MPC formulations that focus on closed-loop stability (see, for example, [165, 120, 252, 79] and the review paper [214]).

The significant progress in understanding and improving the stability properties of MPC notwithstanding, the issue of obtaining, *a priori* (i.e., before controller implementation), an explicit characterization of the region of constrained closed–loop stability for model predictive controllers remains to be adequately addressed. The difficulty in this direction owes in part to the fact that the stability of MPC feedback loops depends on a complex interplay between several factors such as the choice of the horizon length, the penalties in the performance index, the initial condition and the constraints on the state variables and manipulated inputs. *A priori* knowledge of the stability region requires an explicit characterization of these interplays which is a very difficult task. This difficulty can impact on the practical implementation of MPC by imposing the need for extensive closed–loop simulations over the whole set of possible initial conditions to check for closed–loop stability, or by potentially limiting operation within an unnecessarily small neighborhood of the nominal equilibrium point.

The desire to implement control approaches that allow for an explicit characterization of their stability properties has motivated significant work on the design of stabilizing control laws, using Lyapunov techniques, that provide explicitly–defined, large regions of attraction for the closed–loop system; the reader may refer to [173] for a survey of results in this area. In Chapters 3 and 4, a class of Lyapunov–based bounded robust nonlinear controllers, inspired by the results on bounded control originally presented in [204], was developed. The controllers enforce robust stability in the closed–loop system and provide, at the same time, an explicit characterization of the region of guaranteed closed–loop stability. Despite their well–characterized stability and constraint–handling properties, those Lyapunov–based controllers are not guaranteed to be optimal with respect to an arbitrary performance criterion (in

Chapter 3 we show that the proposed controllers are inverse optimal with respect to meaningful cost functionals).

However, the fact that Lyapunov–based control methods provide an easily implementable controller with an explicitly characterized stability region for the closed–loop system motivates developing control techniques that use the *a priori* guarantees of stability provided by the bounded controller as a safety net for the implementation of the high performance model predictive controller. Reconciliation of different controllers (designed to satisfy different control objectives) calls for invoking the hybrid control paradigm, where the control structure consists of a blend of continuous (i.e., classical) controllers and discrete components (for example, a logic–based supervisor that orchestrates switching between the various continuous controllers; see Figure 5.1).

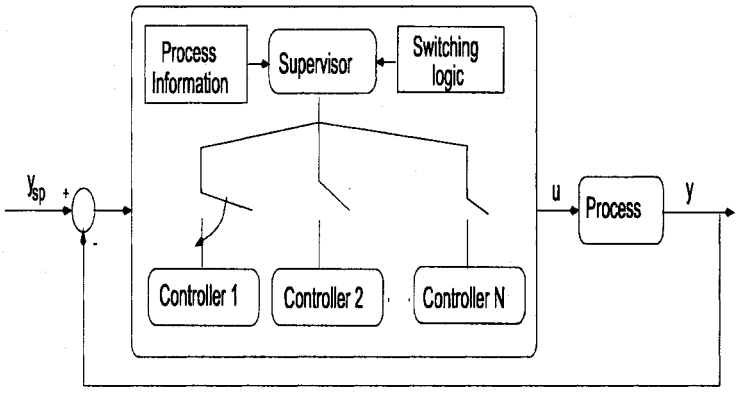

Figure 5.1: Schematic representation of a hybrid control structure.

Motivated by the above considerations, we develop in this chapter a hybrid predictive control structure that seamlessly unites MPC and bounded control, for the stabilization of linear systems with input constraints, in a way that allows both approaches to complement the stability and performance properties of each other. The guiding principle in developing the hybrid predictive control structure is the idea of decoupling

performance requirements from the task of characterizing the region of constrained closed-loop stability. Specifically, by relaxing the optimality requirement, an explicit bounded feedback control law is designed and an explicit large estimate of the region of constrained closed-loop stability – which is not unnecessarily conservative – is computed. The predictive controller – which minimizes a given cost functional subject to the same constraints – is then designed and implemented within the stability region of the bounded controller, which is used a "fall–back" in the event that MPC is unable to achieve closed–loop stability (due, for example, to improper tuning of MPC parameters). Switching laws, that place appropriate restrictions on the evolution of the closed–loop trajectory under MPC, are then constructed to orchestrate the transition between the two controllers in a way that reconciles the tradeoffs between their respective stability and performance properties and guarantees closed–loop stability for all initial conditions within the stability region of the bounded controller. The switching scheme is shown to provide a safety net for the practical implementation of MPC by providing, through off–line computations, a priori knowledge of a large set of initial conditions for which closed-loop stability is guaranteed.

The general idea of switching, between different controllers or models, for the purpose of achieving some objective that either cannot be achieved or is more difficult to achieve using a single controller (or model) has been widely used in the literature, and in a variety of contexts. Examples include controller switching in gain scheduled control (e.g., [259]), logic-based switching in adaptive control (e.g., [137]), hybrid control of mixed logical dynamical (MLD) systems [37], the use of multiple linear models for transition control (e.g., [31, 285]) and scheduled predictive control (e.g., [24]) of nonlinear processes. The developed hybrid predictive control structure developed here differs from other hybrid control structures found in the literature,

in the sense that it employs *structurally different* controllers as a tool for reconciling the objectives of optimal stabilization of the constrained closed-loop system (through MPC) and the a priori (off-line) determination of set of initial conditions for which closed-loop stability is guaranteed (through bounded control).

The rest of the chapter is organized as follows. In Section 5.2, we present some preliminaries that describe the class of systems considered and review briefly how the constrained control problem is addressed in both the bounded control and model predictive control approaches. We then proceed in Section 5.3 to formulate the hybrid control problem within the framework of switched systems and present the hybrid predictive control structure under the assumption of full state feedback. The theoretical underpinnings and practical implications of the proposed hybrid predictive control structure are highlighted, and possible extensions of the supervisory switching logic, that address a variety of practical implementation issues, are discussed. The implementation of the various switching schemes proposed is demonstrated through numerical simulations. In Section 5.4, we extend the hybrid predictive control structure to address the problem of output feedback stabilization. The state feedback control results of this chapter were first presented in [102] while the output feedback control results were presented in [219].

5.2 Preliminaries

In this chapter, we consider the problem of asymptotic stabilization of continuous-time linear time-invariant (LTI) systems with input constraints, with the following state-space description:

$$\dot{x}(t) = Ax(t) + Bu(t) \tag{5.1}$$

$$u(t) \in \mathcal{U} \subset \mathbb{R}^m \tag{5.2}$$

where $x = [x_1 \cdots x_n]^T \in \mathbb{R}^n$ denotes the vector of state variables, $u = [u_1 \cdots u_m]^T$ is the vector of manipulated inputs, taking values in a compact and convex subset of $\mathbb{R}^m$, $\mathcal{U} := \{u \in \mathbb{R}^m : \|u\| \leq u_{max}\}$, that contains the origin in its interior. The matrices A and B are constant $n \times n$ and $n \times m$ matrices, respectively. The pair (A, B) is assumed to be controllable. Throughout the chapter, the notation $\|\cdot\|$ is used to denote the standard Euclidean norm of a vector, while the notation $\|\cdot\|_Q$ refers to the weighted norm, defined by $\|x\|_Q^2 = x'Qx$ for all $x \in \mathbb{R}^n$, where Q is a positive-definite symmetric matrix and x' denotes the transpose of x. Furthermore, the notation $x(T^-)$ is used to denote the limit of the trajectory, $x(t)$, as T is approached from the left, i.e., $x(T^-) = \lim_{t \to T^-} x(t)$.

In order to provide the necessary background for the main results of this chapter, we will briefly review in the remainder of this section the design procedure for, and the stability properties of, both the model predictive and bounded controllers which constitute the two components of the hybrid control structure.

5.2.1 Model predictive control

We consider model predictive control of the system described by Eq.5.1, subject to the control constraints of Eq.5.2. The control action at time t is conventionally obtained by solving, on–line, a finite horizon optimal control problem [215] of the form:

$$P(x,t) \quad : \quad \min\{J(x,t,u(\cdot))|u(\cdot) \in S\} \tag{5.3}$$

where $S = S(t,T)$ is the family of piecewise continuous functions (functions continuous from the right), with period Δ, mapping $[t, t+T]$ into $\mathcal{U}$ and T is the specified horizon. A control $u(\cdot)$ in S is characterized by the sequence $\{u[k]\}$ where $u[k] := u(k\Delta)$. A control $u(\cdot)$ in S satisfies $u(t) = u[k]$ for all $t \in [k\Delta, (k+1)\Delta)$. The performance

index is given by:

$$J(x,t,u(\cdot)) \;=\; \int_t^{t+T} \left[\|x^u(s;x,t)\|_Q^2 + \|u(s)\|_R^2\right] ds + F(x(t+T)) \tag{5.4}$$

where R and Q are strictly positive–definite symmetric matrices, $x^u(s;x,t)$ denotes the solution of Eq.5.1, due to control u, with initial state x at time t, and $F(\cdot)$ denotes the terminal penalty. In addition to penalties on the state and control action, the objective function may also include penalties on the rate of change of the input, reflecting limitations on actuator speed (for example, a large valve requiring few seconds to change position). The minimizing control. $u^0(\cdot) \in S$, is then applied to the process over the interval $[k\Delta, (k+1)\Delta)$ and the procedure is repeated indefinitely. This defines an implicit model predictive control law:

$$M(x) \;:=\; u^0(t;x,t) \tag{5.5}$$

It is well known that the control law defined by Eqs.5.3–5.5 is not necessarily stabilizing. To achieve closed-loop stability, early versions of MPC focused on tuning the horizon length, T, and/or increasing the terminal penalty (see [40] for a survey of these approaches), while more recent formulations focused on imposing stability constraints on the optimization (see [2, 37, 214] for surveys of different constraints proposed in the literature and the concomitant theoretical issues) or using off–line computations to come up with explicit model predictive control laws (see, for example, [237]). The additional stability constraints serve either to enforce convergence of the states of the closed–loop system to the equilibrium point, or to force the states to reach some invariant terminal set at the end of the horizon.

Remark 5.1 By incorporating stability conditions directly as part of the optimization problem, asymptotic stability under state feedback MPC is guaranteed provided that the initial condition is chosen so that the optimization yields a feasible solution.

However, the implicit nature of the MPC control law, obtained through repeated on–line optimization, limits our ability to obtain, *a priori*, an explicit characterization of the admissible initial conditions starting from where the given model predictive controller (with fixed horizon length) is guaranteed to be feasible and enforce asymptotic stability. This set is a complex function of the constraints and the horizon length. Estimates of sufficiently large horizon lengths that ensure stability (see, for example, [56]) are typically conservative and, if used, may lead to a significant computational burden due to the increased size of the optimization problem. Therefore, in practice, the initial conditions and/or horizon lengths are usually chosen using ad hoc criteria and tested through closed–loop simulations which can add to the computational burden in implementing the model predictive controller. This motivates implementing MPC within a hybrid control structure that provides a "fall–back" controller for which a region of constrained closed–loop stability can be obtained off–line. Lyapunov–based controller design techniques provide a natural framework for the design of a stabilizing "fall–back" controller for which an explicit characterization of the region of closed–loop stability can be obtained.

5.2.2 Bounded Lyapunov-based control

Consider the Lyapunov function candidate, $V = x'Px$, where P is a positive–definite symmetric matrix that satisfies the Riccati equation:

$$A'P + PA - PBB'P = -\bar{Q} \tag{5.6}$$

for some positive–definite matrix $\bar{Q}$. Using this Lyapunov function, we can construct, using a modification of Sontag's formula for bounded controls proposed in [204] (see also Chapter 4), the following bounded nonlinear controller:

$$u(x) \;=\; -2k(x)B'Px \;:=\; b(x) \tag{5.7}$$

where

$$k(x) = \left(\frac{L_f^* V + \sqrt{\left(L_f^* V\right)^2 + \left(u_{max} \|(L_g V)'\|\right)^4}}{\|(L_g V)'\|^2 \left[1 + \sqrt{1 + \left(u_{max} \|(L_g V)'\|\right)^2}\right]} \right) \tag{5.8}$$

with $L_f^* V = x'(A'P + PA)x + \rho x'Px$, $(L_g V)' = 2B'Px$ and $\rho > 0$. This controller is continuous everywhere in the state–space and smooth away from the origin. Using a Lyapunov argument, one can show that whenever the closed–loop state trajectory evolves within the state–space region described by the set:

$$\Phi(u_{max}) \;=\; \{x \in \mathbb{R}^n : L_f^* V < u_{max} \|(L_g V)'\|\} \tag{5.9}$$

the resulting control action respects the constraints (i.e., $\|u\| \leq u_{max}$) and enforces, simultaneously, the negative–definiteness of the time–derivative of V along the trajectories of the closed–loop system (see Appendix D). Note that the size of the set, $\Phi(u_{max})$, depends on the magnitude of the constraints in a way such that the tighter the constraints, the smaller the region described by this set. Starting from any initial state within $\Phi(u_{max})$, asymptotic stability of the constrained closed–loop system can be guaranteed, provided that the closed–loop trajectory remains within the region described by $\Phi(u_{max})$. To ensure this, we consider initial conditions that belong to an invariant subset – preferably the largest – which we denote by $\Omega(u_{max})$. A similar idea was used in Chapters 3 and 4 in the context of bounded robust control of constrained nonlinear systems. One way of constructing such a subset is using the level sets of V (see Chapter 4 in [170] for details), i.e.:

$$\Omega(u_{max}) \;=\; \{x \in \mathbb{R}^n : x'Px \leq c_{max}\} \tag{5.10}$$

where $c_{max} > 0$ is the largest number for which all nonzero elements of $\Omega(u_{max})$ are contained within $\Phi(u_{max})$. The invariant region described by the set $\Omega(u_{max})$ provides an estimate of the stability region, starting from where the origin of the

constrained closed–loop system under the control law of Eqs.5.7–5.8 is guaranteed to be asymptotically stable.

Remark 5.2 The bounded control law of Eqs.5.7-5.8 will be used in Section 5.3 to illustrate the basic idea of the proposed hybrid control scheme. Our choice of using this particular design is motivated by its explicit structure and well-defined region of stability. However, the hybrid predictive control structure is not restricted to this choice of bounded controllers; and any other analytical bounded control law, with an explicit structure and well-defined region of closed–loop stability, can also be used in implementing the proposed control strategy including, for example, the bounded controls developed in [291] for certain classes of constrained linear systems.

Remark 5.3 It is worth noting that the bounded nonlinear control law of Eqs.5.7-5.8 can be viewed as a "linear" controller with a variable (state-dependent) nonlinear gain. The fact that the nonlinear gain is shaped to account explicitly for the presence of input constraints allows one to obtain a larger region, in the state space, where the controller respects the constraints, than would be obtained, for example, by bounding (clipping) a constant-gain linear controller that has already been designed without taking the constraints into account. To illustrate this point, consider, for example, the scalar system $\dot{x} = x + u$ for which the LQR controller $u = -2x$, which minimizes the cost functional $J = \int_0^\infty u^2(t)dt$, has already been designed in the absence of constraints. When input constraints with magnitude $\|u\| \leq u_{max}$ are imposed, it is clear that this controller respects these constraints for all $\|x\| \leq \frac{u_{max}}{2}$. In contrast, we see from Eq.5.9 that the bounded control law of Eqs.5.7-5.8 respects the same constraints for all $\|x\| \leq u_{max}$.

Remark 5.4 The stability region under a given stabilizing control law is typically only a subset of the null controllable region (the exact computation of which remains an open research problem). Furthermore, while the level sets of V provide only an estimate of the stability region under the bounded controller, less conservative

estimates that capture larger portions of the null controllable region can be obtained using, for example, a combination of several Lyapunov functions (see, for example, [147] and Chapter 6 for some examples). In general, well–tuned bounded control laws provide larger estimates of the stability region than controllers designed without taking the constraints into account (see Remark 5.3 and Chapter 3 for further details on this issue).

Remark 5.5 Referring to the optimality properties of the bounded controller, it should be noted that, within a well–defined subset of Ω, this class of controllers can be shown to be inverse optimal with respect to some meaningful, yet unspecified *a priori*, cost functional that imposes meaningful penalties on the state and control action (see the Proof of Theorem 3.1 in Appendix B for an analogous proof and further details). However, unless this cost functional (which is determined only after controller design) coincides with the actual cost functional considered by the control system designer (this conclusion cannot be ascertained *a priori*), the performance of the bounded controller will not be optimal with respect to the actual cost functional. An explicit quantitative characterization of the cost incurred by implementing the bounded controller in this case is difficult to obtain. Furthermore, given an arbitrary cost functional, there is no transparent way of "tuning" the bounded controller to achieve optimality since, by design, the goal of the bounded controller is to achieve stabilization for an explicitly–defined set of initial conditions.

Remark 5.6 When comparing the optimality properties of the bounded and predictive controllers, it is important to realize that, in general, it is possible that the total cost of steering the system from the initial state to the origin under the bounded controller could be less than the total cost incurred under MPC. Keep in mind that MPC formulations typically consider minimizing a given cost over some finite horizon. Therefore, for a given objective function of the form of Eq.5.4 for example, by solving the optimization problem once and implementing the resulting input trajectory in its entirety, the cost of taking the system from the initial state to the state at the end

of the horizon under MPC is guaranteed to be smaller than the corresponding cost for the bounded controller. However, since MPC implementation involves repeated optimizations (i.e., only the first control move of the input trajectory is implemented each time), one could in some cases end up with a higher total cost for MPC. This possibility, however, cannot be ascertained *a priori* (i.e., before implementing both controllers and computing the total cost).

5.3 Hybrid predictive state feedback control

By comparing the bounded and MPC controller designs reviewed in the previous section, some tradeoffs with respect to their stability and optimality properties are observed. For example, while the bounded controller possesses a well-defined region of admissible initial conditions that guarantee closed-loop stability in the presence of constraints, the performance of this controller is not guaranteed to be optimal with respect to an arbitrary performance criterion. On the other hand, MPC is well-suited for handling constraints within an optimal control setting; however, the analytical characterization of its set of admissible initial conditions is a more difficult task than it is through bounded control. In this section, we show how to reconcile the two approaches by means of a hybrid switching scheme that combines the desirable properties of both approaches.

To clearly present our approach, we will focus in this section only on the state feedback problem where measurements of the entire state, $x(t)$, are assumed to be available for all t. The case when state measurements are available only at discrete sampling instants is discussed in Section 5.3.5, while the case of output feedback is treated in Section 5.4.

5.3.1 Problem formulation: Uniting MPC and bounded control

Consider the linear time-invariant system of Eq.5.1, subject to input constraints, $\|u\| \leq u_{max}$, for which the bounded controller of Eqs.5.7-5.8 and the predictive controller of Eqs.5.3-5.5 have been designed. We formulate the controller switching problem as the one of designing a set of switching laws that orchestrate the transition between MPC and the bounded controller in a way that: (1) respects input constraints, (2) guarantees asymptotic stability of the origin of the closed-loop system starting from any initial condition in the set $\Omega(u_{max})$ defined in Eq.5.10, and (3) guarantees recovery of the MPC performance whenever the pertinent stability criteria are met. For a precise statement of the problem, we first cast the system of Eq.5.1 as a switched system of the form:

$$\begin{aligned} \dot{x} &= Ax + Bu_{i(t)} \\ \|u_i\| &\leq u_{max} \\ i(t) &\in \{1, 2\} \end{aligned} \tag{5.11}$$

where $i : [0, \infty) \rightarrow \{1, 2\}$ is the switching signal which is assumed to be a piecewise continuous (from the right) function of time, implying that only a finite number of switches between the two controllers is allowed on any finite interval of time. The index, $i(t)$, which takes values in the finite set, $\{1, 2\}$, represents a discrete state that indexes the control input, u, with the understanding that $i(t) = 1$ if and only if $u_i(x(t)) = M(x(t))$ (i.e., MPC is used) and $i(t) = 2$ if and only if $u_i(x(t)) = b(x(t))$ (i.e., bounded control is used). The value of $i(t)$ is determined by a higher-level supervisor responsible for executing the transition between the two controllers. Our goal is to construct a switching law:

$$i(t) = \psi(x(t), t) \tag{5.12}$$

that provides the supervisor with the switching times that ensure stabilizing transitions between the two controllers. This, in turn, determines the time-course of the discrete state, $i(t)$. A schematic representation of the proposed hybrid predictive control structure is depicted in Figure 5.2.

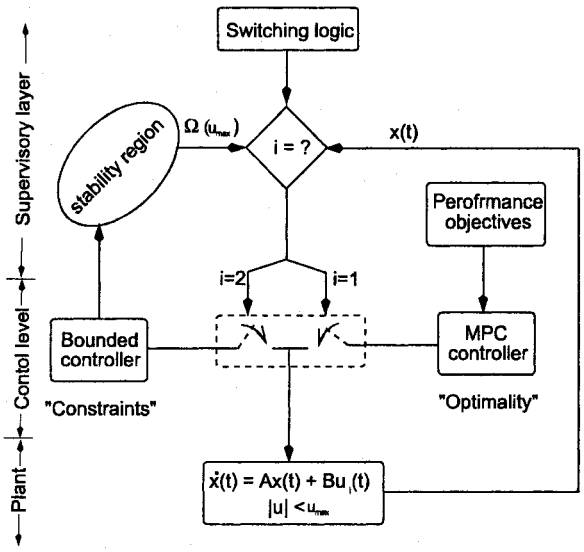

Figure 5.2: A schematic representation of the hierarchical hybrid predictive control structure uniting MPC and bounded control for the stabilization of constrained LTI systems.

In the remainder of this section, we present three switching schemes that address this problem. The first scheme is formalized in Theorem 5.1 (Section 5.3.2) and focuses primarily on closed-loop stability, while the second scheme, given in Theorem 5.2 (Section 5.3.3), extends the first one to accommodate closed-loop performance considerations as well. For illustration purposes, both the stability-based and performance-based schemes use a classical MPC formulation. Finally, in Section 5.3.4, we present the third switching scheme (feasibility-based switching) which shows how more advanced MPC formulations can also be accommodated by appropriate choice of the switching logic. The proofs of Theorems 5.1 and 5.2 are given in Appendix D.

5.3.2 Stability-based controller switching

Theorem 5.1 *Consider the constrained LTI system of Eq.5.11, with an initial condition $x(0) := x_0 \in \Omega(u_{max})$, where $\Omega(u_{max})$ was defined in Eq.5.10, under the model predictive controller of Eqs.5.3-5.5. Also let $T_s > 0$ be the earliest time for which the closed-loop state satisfies:*

$$- \parallel x(T_s^-) \parallel_{\bar{Q}}^2 + \parallel B'Px(T_s^-) \parallel^2 + 2x'(T_s^-)PBu(T_s^-) \geq 0 \tag{5.13}$$

and suppose that:

$$i(t) = \left\{ \begin{array}{ll} 1, & 0 \leq t < T_s \\ & \\ 2, & t \geq T_s \end{array} \right\} \tag{5.14}$$

where $i(t) = 1 \Leftrightarrow u_i(x(t)) = M(x(t))$ and $i(t) = 2 \Leftrightarrow u_i(x(t)) = b(x(t))$. Then the origin of the closed-loop system is asymptotically stable in the presence of input constraints.

Remark 5.7 Theorem 5.1 describes a stability-based switching strategy for control of linear systems with input constraints. The three main components of this strategy include the bounded controller, the model predictive controller, and a higher-level supervisor that orchestrates the switching between the two controllers. The implementation of this hybrid control strategy is best understood through the following stepwise procedure (see also Figure 5.3):

- Given the system model of Eq.5.1 and the constraints on the input, design the bounded controller using Eqs.5.7-5.8. Given the performance objective and a choice of the horizon length, design the MPC controller.
- Compute the stability region estimate for the bounded controller, $\Omega(u_{max})$, using Eqs.5.9-5.10.
- Initialize the closed-loop system, using MPC, at an initial condition, x_0, within $\Omega(u_{max})$.

- Monitor the evolution of the closed-loop trajectory (by checking Eq.5.13 at each time) until the earliest time, T_s, that Eq.5.13 is met.
- At the earliest time that Eq.5.13 is met, discontinue MPC implementation, switch to the bounded controller and implement it for all future times.

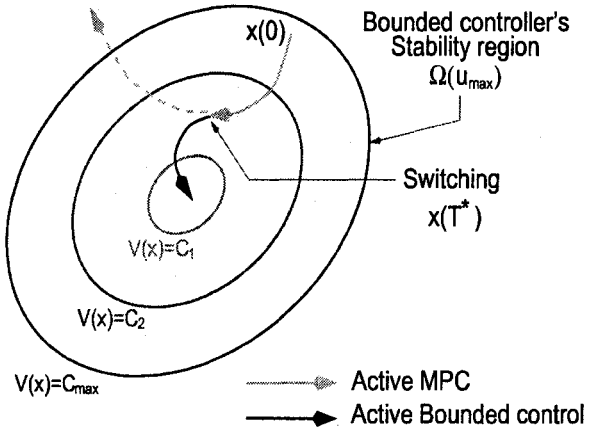

Figure 5.3: A schematic representation of the implementation of the stability-based controller switching proposed in Theorem 5.1.

Remark 5.8 The relations of Eqs.5.13-5.14 represent the switching rule that the supervisor observes when deciding if a switch between the two controllers is needed. The implementation of this rule requires only the evaluation of the algebraic expression on the left hand-side in Eq.5.13, which is the rate at which the Lyapunov function (used in designing the bounded controller and characterizing its stability region) grows or decays along the trajectories of the closed-loop system. By observing this rule, the supervisor is essentially tracking the temporal evolution of V under MPC, so that whenever an increase in V is detected after its initial implementation, MPC is disengaged from the closed-loop and the bounded controller is switched in, thus steering the closed-loop trajectory to the origin asymptotically. This logic guarantees that, under MPC, the closed-loop trajectory never escapes $\Omega(u_{max})$ before the bounded controller can be switched in.

Remark 5.9 Note that in the case when the condition in Eq.5.13 is never fulfilled – i.e.. the Lyapunov function continues to decay monotonically along the closed-loop trajectories under MPC – the switching rule of Eq.5.14 ensures that only MPC is implemented for all times (no switching occurs) since it is asymptotically stabilizing. In this case, the MPC performance is fully recovered.

Remark 5.10 Note that the proposed approach does not turn $\Omega(u_{max})$ into a stability region for MPC. What the approach does, however, is turn $\Omega(u_{max})$ into a stability region for the switched closed-loop system. The value of this can be understood in light of the difficulty in obtaining, a priori, an analytical characterization of the set of admissible initial conditions that the MPC controller can steer to the origin in the presence of input constraints. By using the bounded controller as a fall-back controller, the switching scheme allows us to safely initialize the closed-loop system anywhere within $\Omega(u_{max})$ using MPC, with the guarantee that the bounded controller can always intervene (through switching) to "rescue" closed-loop stability in case the closed-loop starts to become unstable under MPC (due, for example, to a poor choice of the initial condition or improper tuning of MPC). This safety feature distinguishes the bounded controller from other fall-back controllers that could be used, such as PID controllers, which do not provide a priori knowledge of the constrained stability region and, therefore, do not guarantee a safe transition in the case of unstable plants. For these controllers, a safe transition is critically dependent on issues such as whether or not the operator is able to properly tune the controller online, which, if not achieved, can possibly result in instability and/or performance degradation. The transition from the MPC to the bounded controller, on the other hand, is not fraught with such uncertainty and is always safe because of the a priori knowledge of the stability region. This aspect helps make plant operation safer and smoother.

Remark 5.11 When compared with Lyapunov-based MPC approaches (e.g., contractive MPC [238], CLF-based RHC [239]), we find that the proposed hybrid scheme also employs a Lyapunov stability condition to guarantee closed-loop asymptotic sta-

bility. However, the Lyapunov stability condition is enforced at the supervisory level, via continuous monitoring of the temporal evolution of V, rather than being incorporated as an inequality constraint on the optimization problem, as is customarily done in Lyapunov-based MPC approaches. This fact may help reduce the complexity of the optimization problem in some cases, without loss of stability, by reducing the number of constraints on the optimization. The underlying idea here is that of decoupling the stability requirement from optimality. In the proposed hybrid scheme, it is switching to the bounded controller, with its well-defined stability region, that safeguards against potential closed-loop instability arising as a consequence of implementing the MPC controller, for which the stability region is not known a priori. On the other hand, the MPC controller provides, by design, the desired high performance under constraints. The switching logic then ensures that any such "optimal" solution is implemented only when it is asymptotically stabilizing.

Remark 5.12 Note that no assumption is made regarding how fast the optimization needs to be solved for the MPC controller to be implemented because even if this time is relatively significant and the plant dynamics are unstable, implementation of the switching rule in Theorem 5.1 guarantees an "instantaneous" switch to the stabilizing bounded controller.

5.3.3 Performance-driven switching

While the switching scheme proposed in Theorem 5.1 guarantees closed-loop stability for all initial conditions within $\Omega(u_{max})$, the implementation of this scheme can, in some cases, place limitations on the achievable closed-loop performance by (unnecessarily) restricting the implementation of MPC and using the bounded controller in its place. In particular, note that the switching rule of Eqs.5.13-5.14 does not permit any transient increase in V under MPC and requires that, at the first instance such an increase is detected, the supervisor immediately terminate the implementation of

MPC and switch to the bounded controller instead. Given, however, that a temporary, finite increase in V does not necessarily translate into closed-loop instability, this particular switching rule is restrictive in the sense that it does not give MPC any further chance to stay in the closed-loop despite the fact that the observed initial increase in V might actually be followed by monotonic decay (in which case MPC would be stabilizing, yet not implemented because of the particular switching rule used). Clearly in such a scenario, and since MPC provides the high performance controller, it would be desirable to keep MPC in the closed-loop instead of switching to the bounded controller as Theorem 5.1 would require. To allow for greater flexibility in recovering the performance of MPC, without concern for loss of stability, we propose in this section an extension of the switching strategy of Theorem 5.1 by relaxing the switching rule. This is described in the Theorem 5.2 below and shown schematically in Figure 5.4. The proof of the theorem can be found in Appendix D

Theorem 5.2 *Consider the constrained LTI system of Eq.5.11, under the model predictive controller of Eqs.5.3-5.4, with an initial condition* $x(0) := x_0 \in \Omega(u_{max})$, *as defined in Theorem 5.1, and let* $T_b > 0$ *be the earliest time for which the closed-loop state satisfies:*

$$x^T(T_b^-)Px(T_b^-) \;=\; c_{max} \tag{5.15}$$

Also let $\{T_i, i = 1, \cdots, N,\ N < \infty\}$ *be a set of times such that, if exist:*

$$-\parallel x(T_i^-) \parallel_Q^2 + \parallel B'Px(T_i^-) \parallel^2 + 2x'(T_i^-)PBu(T_i^-) \;=\; 0 \tag{5.16}$$

Then the switching rule:

$$i(t) \;=\; \left\{ \begin{array}{ll} 1, & 0 \leq t < \min\{T_b, T_N\} \\ & \\ 2, & t \geq \min\{T_b, T_N\} \end{array} \right\} \tag{5.17}$$

where $i(t) = 1 \Leftrightarrow u_i(x(t)) = M(x(t))$ *and* $i(t) = 2 \Leftrightarrow u_i(x(t)) = b(x(t))$, *guarantees that the origin of the closed-loop system is asymptotically stable in the presence of input constraints.*

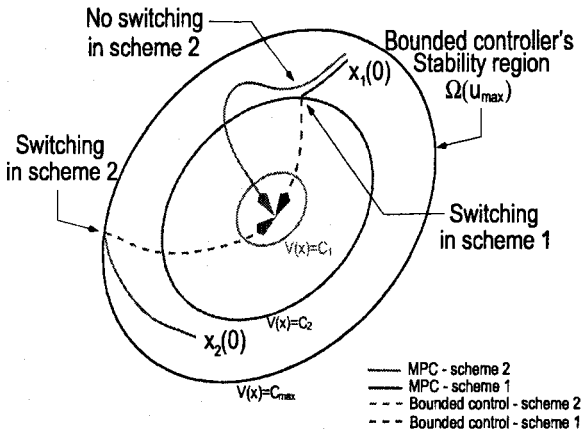

Figure 5.4: A schematic representation of the implementation of the controller switching strategy proposed in Theorem 5.2 and how it compares with the scheme proposed in Theorem 5.1. Starting at $x_1(0)$, scheme 2 permits a temporary increase in V under MPC without switching thus allowing MPC to remain in the closed-loop for all times (solid trajectory). Starting at $x_1(0)$, scheme 1 does not allow the increase in V and switches immediately to the bounded controller instead (solid followed by dashed trajectory). Starting at $x_2(0)$, scheme 2 enforces a switch from MPC to the bounded controller when the closed-loop trajectory under MPC is about to leave Ω.

Remark 5.13 The basic idea of the switching scheme of Theorem 5.2 is to allow MPC to remain in the closed-loop system even if V increases for some time, provided that the closed-loop trajectory does not leave $\Omega(u_{max})$ during this time. This requirement is necessary because this region is not invariant under MPC and, therefore, once the trajectory leaves, there are no guarantees that it can ever be steered back to the origin, whether using MPC or even the bounded controller. Note, however, that this requirement by itself guarantees only boundedness of the closed-loop trajectory. To ensure asymptotic convergence to the origin, V must be made to decrease after some time. To accomplish this, a choice needs to be made as to how long the increases in V can be tolerated before switching to the bounded controller is deemed necessary. In the statement of Theorem 5.2, this user-specified choice is quantified by N which represents the maximum number of times that $\dot{V}$ is allowed by the designer to

change sign. This requirement is intended to avoid scenarios where V neither keeps monotonically increasing nor decreasing for all times.

Remark 5.14 Note that the times T_b and T_i are not known a priori. They are implicity defined by the relations of Eqs.5.15-5.16, respectively, which are continuously checked on-line by the supervisor. The switching scheme proposed in Theorem 5.2 then is best understood as follows. For illustration purposes we choose $N = 2$. The closed-loop system is initialized within $\Omega(u_{max})$ using MPC, and the temporal evolution of V is monitored on-line. Suppose that V keeps increasing monotonically until, at some time t, Eq.5.15 is satisfied (trajectory hits boundary of $\Omega(u_{max})$). In this case, we have that $T_b = t$ and that T_1, T_2, if exist, must be greater than t. Therefore $\min\{T_b, T_2\} = t$ and, according to the switching law of Eq.5.17, MPC implementation should be terminated and the bounded controller switched in at T_b. Now suppose, instead, that at some time $\bar{t} < t$, Eq.5.16 is satisfied, then in this case we would have $T_1 = \bar{t}$, $T_b = t$. Since T_2 in this case, if exists, is greater than t, we set $\min\{T_b, T_2\} = t$ which implies that MPC should be switched off again at T_b. Finally, consider the case when Eq.5.16 is satisfied at two consecutive times, $t^* < \bar{t}$, prior to which Eq.5.15 is not fulfilled. Then in this case, we have $T_1 = t^*$, $T_2 = \bar{t}$, and T_b, if exists, must be greater than $\bar{t}$. Therefore, we set $\min\{T_b, T_2\} = \bar{t}$ and conclude that MPC should be switched off at $\bar{t}$. To summarize, in all the cases, switching is done either when the trajectory gets "close" to the boundary of the stability region or after $\dot{V}$ has changed sign N times, whichever occurs first.

Remark 5.15 The switching schemes proposed in Theorems 5.1 and 5.2 can be further generalized to allow for multiple switchings between MPC and the bounded controller. In this case, when switched in, the bounded controller need not stay in the closed-loop for all future times. Instead, it is employed only until it brings the closed-loop state trajectory sufficiently closer to the origin (for example, to a predetermined inner level set of V) at which point MPC is activated once again. This scheme offers the possibility of further enhancement in closed-loop performance (over

that obtained from the bounded controller) by implementing MPC for longer periods of time (as permitted by stability considerations). It also allows for the possibility of stabilizing the closed-loop system starting from initial conditions for which a given (fixed-horizon) MPC controller is not stabilizing. This can occur, for example, when the stability region for such a controller is contained within $\Omega(u_{max})$. In this case, only a finite number of switches between the two controllers is needed to steer the closed-loop trajectory to that point, beyond which the MPC controller can stay in the closed-loop for all times (with no further switching).

5.3.4 Switching using advanced MPC formulations

In Theorems 5.1 and 5.2, a classical MPC formulation (with no stability constraints) was used as an example to illustrate the basic idea of controller switching and how it can be used to aid MPC implementation. The value of the hybrid predictive control structure (see Figure 5.3), however, is not restricted to classical MPC formulations, and extends to any MPC formulation for which a priori knowledge of the set of admissible initial conditions is lacking (or computationally expensive to obtain). The structure can be adapted to more advanced versions of MPC by appropriate design of the switching logic. To illustrate this point, consider the case when advanced MPC algorithms, that employ stability constraints in the optimization formulation, are used to compute the control action. An example of such formulations is the following one:

$$\begin{array}{rrcl} \min\limits_{u(\cdot)} & \int_t^{t+T} & (x'(s)Qx(s)+u'(s)Ru(s))ds & \\ s.t. & \dot{x}(t) & = & Ax(t)+Bu(t),\ \ x(0)=x_0 \\ & u(\cdot) & \in & S \\ & x(t+T) & = & 0 \end{array} \tag{5.18}$$

which uses a terminal equality constraint (note that other types of stability constraints, such as control Lyapunov function (CLF)-based inequality constraints of the form $V(x(t+T)) < V(x(t))$ can be treated similarly). When the above formula-

tion is used to compute the MPC control law in our switching scheme, it is clear that monitoring the evolution of the closed-loop trajectory (which was the basis for the implementation of the switching rules in Theorems 5.1 and 5.2) is no longer appropriate as a switching criterion, since, by definition, a closed-loop trajectory that solves the above optimization will not "evolve" unless it stabilizes at the origin. By incorporating stability conditions as part of the constrained optimization problem, asymptotic stability under MPC can be guaranteed provided that the initial optimization yields a feasible solution. However, inclusion of the stability constraints does not, by itself, provide any a priori explicit knowledge of the feasible initial conditions, which must then be identified through simulations. This observation suggests that the hybrid control structure can be used here to safeguard closed-loop stability in the event of MPC infeasibility. Specifically, in lieu of monitoring the growth of V, a different switching logic, based on the feasibility of the optimization in Eq.5.18, needs to be implemented. The switching algorithm in this case can be summarized as follows (see also Figure 5.5 for a schematic representation):

- Given any initial condition, x_0, within $\Omega(u_{max})$, check, off-line, whether the constrained optimization in Eq.5.18 yields a feasible solution. If a solution exists, no switching is needed and MPC can be implemented for all time.
- If an initial feasible solution is not found, implement the bounded controller instead, i.e., set $u(0) = b(x_0)$.
- While the bounded controller is in the closed-loop, continue to check, off-line, and as frequently as is desired, the feasibility of the optimization in Eq.5.18.
- At the earliest time that a feasible solution is found, switch to the MPC controller, else the bounded controller remains active.

The above discussion underscores an important attribute of the proposed hybrid control structure, and that is the fact that it is not proposed as a substitute for stability constraints (even though it guarantees stability when the MPC formulation is not stabilizing), but as a reliable fall-back mechanism from which any MPC formulation can benefit.

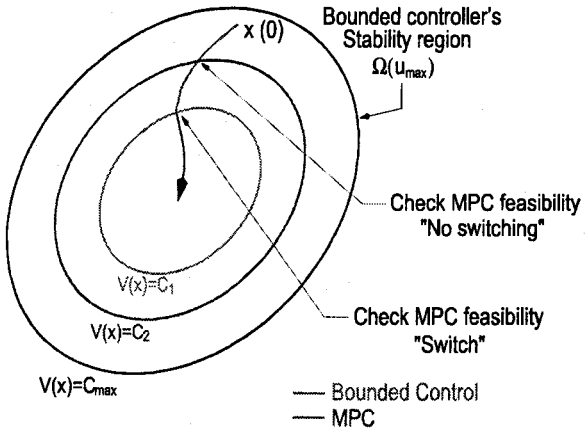

Figure 5.5: A schematic representation of the implementation of switching when a "stabilizing" MPC formulation is used. Starting at $x(0)$, MPC does not yield a feasible solution and, therefore, the bounded controller is used. When the trajectory crosses the C_2-level set of V, the supervisor checks off-line the feasibility of the MPC and finds that no feasible solution exists. The bounded controller remains in action. Finally, when the trajectory crosses the C_1-level set of V, the supervisor finds that the optimization is feasible and therefore switches to the MPC controller which stays in the closed-loop systems for all future times.

Remark 5.16 An important issue in the practical implementation of MPC is the selection of the horizon length. It is well known that this selection can have a profound effect on nominal closed-loop stability, and results are available in the literature that establish, under certain assumptions, the existence of "sufficiently large" finite horizons that ensure stability (see, for example, [252, 56]). However, a priori knowledge (without closed-loop simulations) of the critical horizon length that guarantees closed-loop stability, from an arbitrary initial condition, is currently not available. Therefore, in practice the horizon length is typically chosen based on available selection criteria,

tested through closed-loop simulations, and varied, if necessary, to achieve stability. Note that in all the switching schemes proposed in Section 5.2.2, closed-loop stability is maintained independent of the horizon length, and therefore selection of the horizon length can be made solely on the basis of what is computationally practical for the size of the optimization problem, without increasing, unnecessarily, the horizon length (and consequently the computational load) out of concern for stability.

Remark 5.17 The supervisory checks required in the implementation of all the switching schemes developed in this chapter do not incur any additional computational costs beyond that involved in MPC implementation alone. In the event that MPC is infeasible from a given initial condition (due, for example, to insufficient number of control moves), the supervisor checks as frequently as desired the initial feasibility of the MPC by actually solving the optimization problem at each time step and implementing the resulting solution (if found). If a solution is not found at a given time step, the supervisor implements the bounded controller (an inexpensive algebraic computation) and continues, in the mean time, to solve the optimization until it finds a feasible solution to implement.

Remark 5.18 The switching schemes proposed in this chapter differ, both in their objective and implementation, from other MPC formulations involving switching which have appeared earlier in the literature. For example, in dual mode MPC [222] the strategy includes switching from MPC to a locally stabilizing controller once the state is brought near the origin by MPC. The purpose of switching in this approach is to relax the terminal equality constraint whose implementation is computationally burdensome for nonlinear systems. However, the set of initial conditions for which MPC is guaranteed to steer the state close to the origin is not explicitly known a priori. In contrast, switching from MPC to the bounded controller is used in our work only to prevent any potential closed-loop instability arising from implementing MPC without the a priori knowledge of the admissible initial conditions. So depending on the stability properties of the chosen MPC, switching may or may not occur, and if it

occurs, it can take place near or far from the origin. Finally, we note that the notion of "switching" from a predictive to an unconstrained LQR controller, for times beyond a finite control horizon, has been used in [289, 56, 267] in the context of determining a finite horizon that solves the infinite horizon constrained LQR problem.

5.3.5 Simulation example

Consider the following linear system:

$$\dot{x} = \begin{bmatrix} 0.5 & 0.25 \\ 0.5 & 1 \end{bmatrix} x + \begin{bmatrix} 1 & 0 \\ 0 & 1 \end{bmatrix} u \tag{5.19}$$

where both inputs u_1, u_2 are constrained in the interval $[-5, 5]$. It is straightforward to verify that the open-loop system has an unstable equilibrium point at the origin (A has two positive eigenvalues). We initially use Eqs.5.7-5.8 to design the bounded controller and construct its stability region via Eqs.5.9-5.10. The matrix P is chosen to be:

$$P = \begin{bmatrix} 1.13 & 0.82 \\ 0.82 & 1.87 \end{bmatrix} \tag{5.20}$$

For the MPC controller, the parameters in the objective function of Eq.5.4 are chosen as penalty on the states, $Q = qI$, with $q = 1$ and penalty on the control inputs, $R = rI$, with $r = 3$. A higher penalty on u is indicative of the requirement of driving the state to the origin with less control action. We also choose a horizon length of $T = 1$ in implementing the MPC controller. The resulting quadratic program is solved using the MATLAB subroutine QP, and the set of ODEs are integrated using the MATLAB solver ODE45.

As shown by the solid curve in Figure 5.6, applying the MPC controller from the initial condition $x_0 = [6 \ -2]^T$ (which belongs to the stability region of the bounded controller, Ω, represented by the ellipse in Figure 5.6) leads to closed-loop instability. The corresponding input and output profiles are shown by the solid lines in Figure

5.7. Using the switching scheme of Theorem 5.1, however, we find that the supervisor detects an increase in V at $t = 1.7$ and therefore immediately switches at this time from the MPC controller to the bounded controller in order to preserve closed-loop stability. As expected, the bounded controller asymptotically stabilizes the plant (see dashed lines in Figures 5.6 and 5.7). It is important to note that one could try to tune the horizon length further in order to achieve stability using the MPC controller. For example, we see from the dotted lines in Figures 5.6 and 5.7 that stability can be achieved by increasing the horizon length to $T = 1.5$. However, this conclusion could not be reached a priori, i.e., before running the closed-loop simulation in its entirety to check whether the choice $T = 1.5$ is appropriate. In contrast, closed-loop stability starting from the given initial condition, is guaranteed, a priori, under the switching scheme of Theorem 5.1.

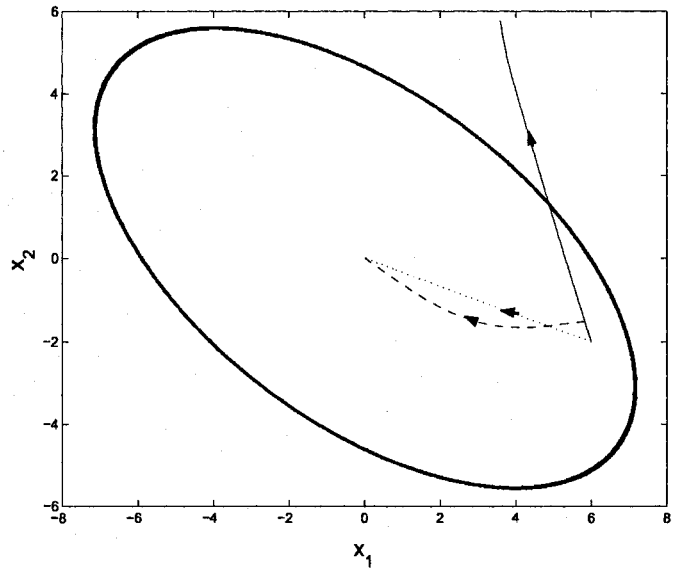

Figure 5.6: Closed-loop state trajectory under MPC with $T = 1$ (solid line), under the switching scheme of Theorem 5.1 with $T = 1$ (dashed line), and under MPC with $T = 1.5$ (dotted line).

In the next simulation run, we demonstrate how the switching scheme of Theorem

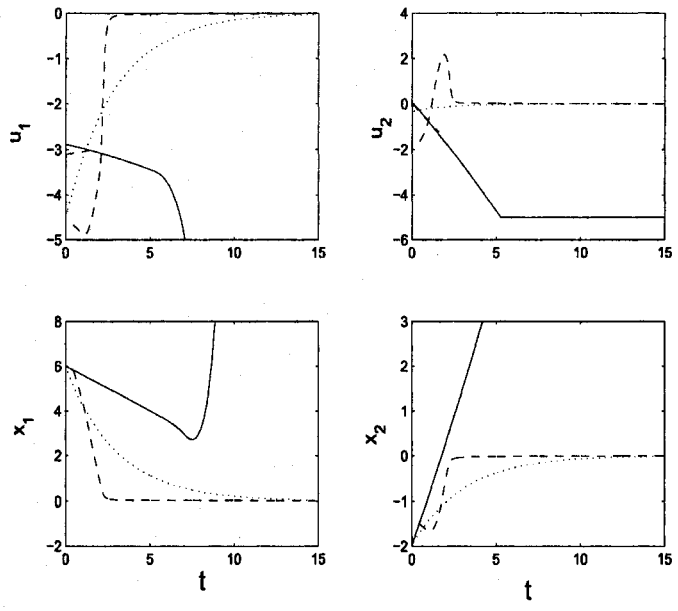

Figure 5.7: Input and closed-loop state profiles under MPC with $T = 1$ (solid line), under the switching scheme of Theorem 5.1 with $T = 1$ (dashed line), and under MPC with $T = 1.5$ (dotted line).

5.2 can be used to enhance closed-loop performance by allowing greater flexibility in implementing the MPC controller. To this end, we again consider the initial condition $x_0 = [6 \ -2]^T \in \Omega$. For the MPC controller, the objective function includes penalty on the state with $q = .5$ and penalty on the inputs with $r = 1$. We also include a quadratic penalty on the rate of input change weighted by the matrix $S = sI$ with $s = 40$. The horizon length is chosen to be $T = 1.5$. Initially, we implement the MPC controller and use the switching scheme of Theorem 5.1 to stabilize the closed-loop system. In this case, an increase in V is detected immediately (at $t = 0$) by the supervisor which, consequently, switches automatically to the bounded controller. The results for this case are depicted by the solid curves in Figures 5.8 and 5.9, which reflect the closed-loop performance under the bounded controller. However, when the switching scheme of Theorem 5.2 is used, we find that the MPC controller stays

in action, for all times, thus providing the desired optimal performance and, at the same time, asymptotically stabilizing the closed-loop system without the need for switching. The results are shown by the dashed curves in Figures 5.8 and 5.9. So, while the first switching scheme selects the bounded controller, the second one selects the MPC controller. The reason for the difference between the two scenarios is the fact that the switching law in the second scheme tolerates the initial increase in V (see Figure 5.10) since this increase does not land the state outside the stability region and is shortly followed by continuous decrease, and thus keeps the MPC controller in the closed-loop.

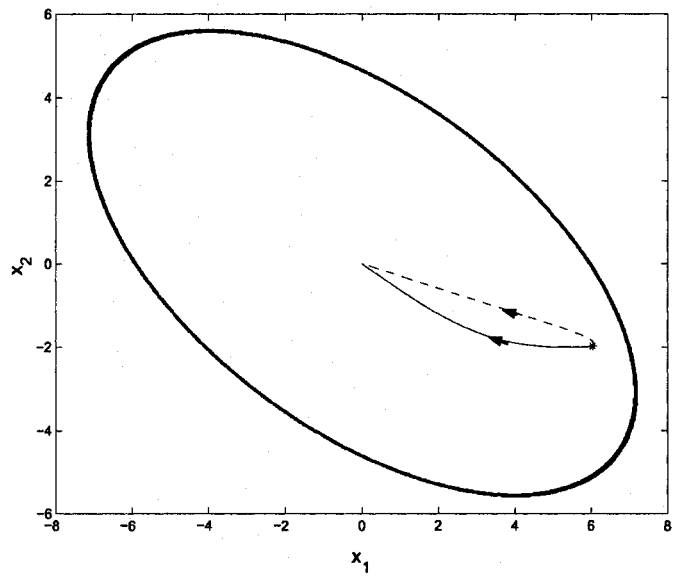

Figure 5.8: Closed-loop state trajectory under the switching scheme of Theorem 5.1 (solid line), and under the switching scheme of Theorem 5.2 (dashed line).

In the following set of simulation runs, we demonstrate an application of the feasibility-based switching scheme, proposed in Section 5.3.4, which uses a stable version of MPC, specifically, one employing a terminal equality constraint. For the MPC controller, the parameters in the objective function (Eq.5.18) are chosen as $q = 1$ and $r = 1$. The horizon length is chosen to be $T = 1.2$. As shown by the solid

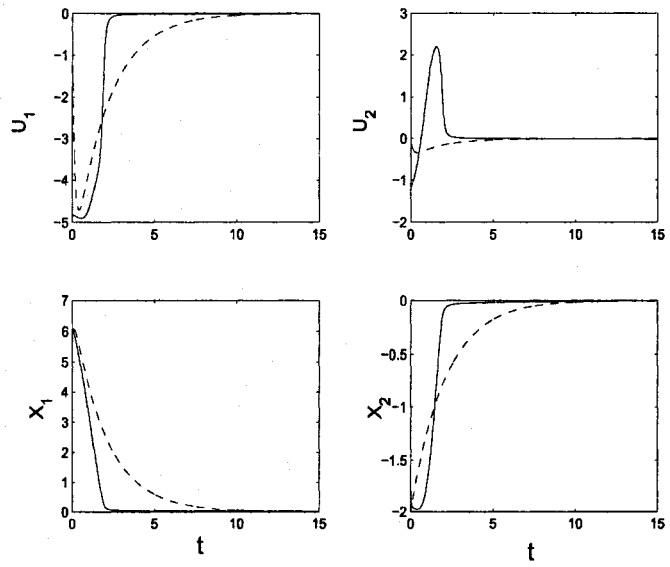

Figure 5.9: Input and closed-loop state profiles under the switching scheme of Theorem 5.1 (solid line) and under the switching scheme of Theorem 5.2 (dashed line).

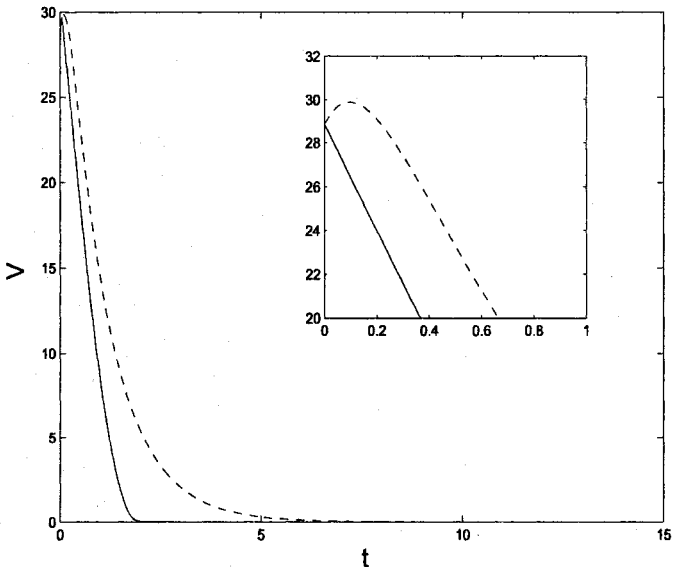

Figure 5.10: Temporal evolution of the Lyapunov function under the switching scheme of Theorem 5.1 (solid line), where the bounded controller is switched in immediately at $t = 0$, and under the switching scheme of Theorem 5.2 (dashed line), where the MPC controller stays in action for all time.

lines in Figure 5.11, starting from an initial condition, $x_0 = [2 \ -2]^T$, MPC is found to be feasible and is therefore implemented and kept in the closed-loop for all times driving the trajectory asymptotically to the origin. The corresponding input and output profiles are shown by the solid lines in Figure 5.12. The scenario, therefore, represents a reasonably well-tuned MPC for initial conditions around the origin. Now suppose that, after settling at the origin, a temporary disturbance drives the closed-loop trajectory to the point $x_i = [5 \ -5]^T$ (which is still within the stability region of the bounded controller). After the disturbance disappears, MPC starting from this initial condition is found to be infeasible and, therefore, the bounded controller is employed instead. Implementation of the bounded controller proceeds until the closed-loop trajectory crosses the level set denoted by Ω_2 in Figure 5.11, which occurs at $t = 0.6$. At this point, feasibility of MPC is checked again and the MPC controller is found to be feasible. Consequently, the bounded controller is terminated immediately and the MPC controller is employed in the closed-loop for the remaining time (inside Ω_2). This scenario is shown by the dashed lines in Figures 5.11 and 5.12. Once again, note that using a higher value of the horizon length, $T = 1.5$ can lead to MPC being feasible from the initial condition $x_i = [5 \ -5]^T$ (dotted lines in Figures 5.11 and 5.12). This implies that, once the closed-loop state is driven by the disturbance to x_i, a re-tuning of the horizon length can make MPC feasible. However, a priori knowledge of the value of the horizon length that is guaranteed to work could not be obtained short of testing feasibility at that condition. The prospect of disturbances throwing the system around would therefore necessitate running extensive closed loop simulations to determine such a value. The feasibility-based switching scheme on the other hand clearly guarantees closed-loop stability for any value of the horizon length. Following the disturbance, it drives the closed-loop trajectory to a point at which the original MPC controller (with $T = 1.2$) becomes feasible again and can therefore be

implemented. In this particular example, feasibility was checked only at one level set. The frequency of feasibility checking could be made larger by introducing more level sets, or by checking feasibility at predetermined times.

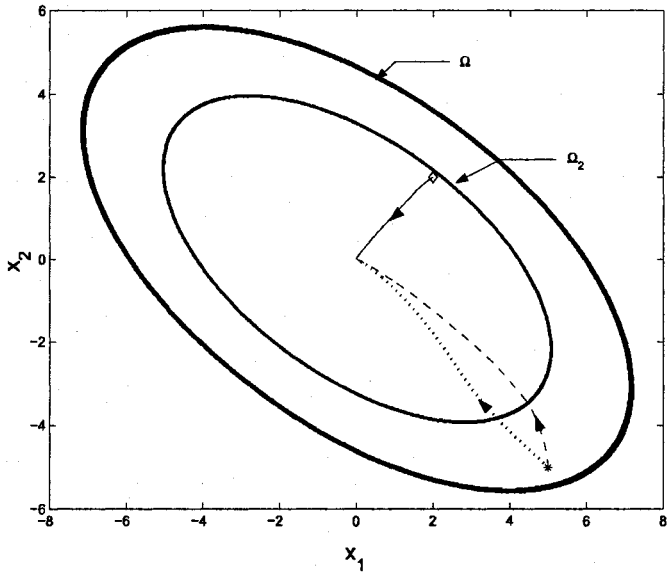

Figure 5.11: Closed-loop state trajectory starting close to the origin using MPC with $T = 1.2$ (solid line) and from a point farther away in state space using the switching scheme with a horizon length $T = 1.2$ (dashed line) and using only MPC with $T = 1.5$ (dotted line).

In the last set of simulation runs, we demonstrate an example of how the switching schemes can be used (or modified) in the case when state measurements are not available continuously, but are rather available only at discrete sampling instants. For simplicity and clarity of presentation, we focus our discussion only on the switching scheme of Theorem 5.2. Recall that the implementation of the switching rule in Theorem 5.2 requires continuous monitoring of the state trajectory to prevent its potential escape under MPC from the set $\Omega(u_{max})$. The restricted access to state information during the time periods between the sampling instants, however, implies the possibility that, during the first such period after the MPC controller of Eq.5.3-5.4 is implemented, the closed-loop state trajectory could leave the stability region Ω

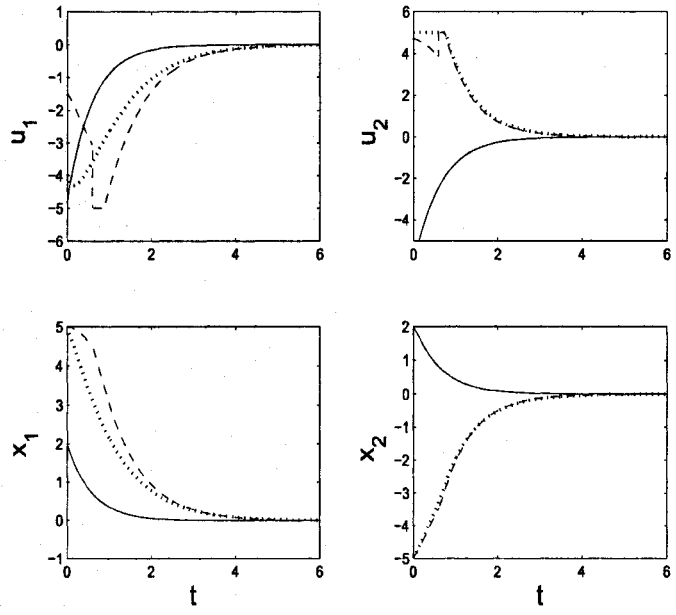

Figure 5.12: Input and closed-loop state profiles starting close to the origin using MPC with $T = 1.2$ (solid line) and from a point farther away in state space using the switching scheme with a horizon length $T = 1.2$ (dashed line) and using only MPC with $T = 1.5$ (dotted line).

before such an escape is detected, especially if the initial condition is chosen close to the boundary of Ω and/or the sampling period is too large. In this case, closed-loop stability cannot be guaranteed, and any switching to the bounded controller will be too late to recover from the instability of MPC. To guard against this possibility, we slightly modify the switching rule by restricting the implementation of MPC within a subset of Ω. This subset, henceforth denoted by Ω_2 and referred to as the safety zone, is defined as the set of all states starting from where the closed-loop trajectory is guaranteed to remain within Ω after a single sampling period. An estimate of this set can be obtained from:

$$\Omega_2 = \left\{ x \in \mathbb{R}^n : \sqrt{V(x)} \geq \sqrt{c_{max}} \exp\left(-\frac{\alpha\Delta}{2}\right) - \frac{\beta}{\alpha}\left(1 - \exp\left(-\frac{\alpha\Delta}{2}\right)\right) \right\} \tag{5.21}$$

where Δ is the sampling period, $\alpha = \dfrac{\lambda_{max}(PBB'P)}{\lambda_{min}(P)} > 0$, $\beta = 2u_{max}\sqrt{\alpha} > 0$, $\lambda_{max}(\cdot)$ and $\lambda_{min}(\cdot)$ are, respectively, the maximum and minimum eigenvalues of the given matrix. The above estimate is obtained by writing the appropriate Lyapunov dissipation inequality for the system, majorizing the right hand side using appropriate bounds and, finally, integrating both sides of the inequality from $t = 0$ ($V = V(x)$) to $t = \Delta$ ($V = c_{max}$). Since the implementation of MPC is restricted to Ω_2, only the bounded controller is used in the annular region between Ω and Ω_2.

To illustrate the implementation of the resulting switching scheme in the case of measurement sampling, we consider the case when the state measurements arrive every 0.1 time units ($\Delta = 0.1$). This sampling period is found to be sufficiently small for the bounded controller to be stabilizing. For the MPC controller, the parameters in the objective function (Eq.5.4) are chosen as $q = 0.5$, $r = 2$ and $s = 40$. The horizon length is chosen to be $T = 1.5$. The safety zone, Ω_2, is constructed using Eq.5.21 to ensure that starting from Ω_2, the state cannot escape Ω in one sampling

period. As stated earlier, this ensures that an increase in V under MPC can be detected by the supervisor before the trajectory goes outside the stability region of the bounded controller. Starting from the initial condition, $x_0 = [-3 \ -2.5]$, as shown by the solid lines in Figure 5.13, the closed-loop state trajectory is clearly unstable under MPC. The corresponding input and state profiles are shown by the solid lines in Figure 5.14. Note that since the closed-loop is initialized outside Ω_2, the closed-loop trajectory under MPC was able to escape Ω before being detected. To remedy this problem, the bounded controller is employed, starting from $x_0 = [-3 \ -2.5]$, until the closed-loop state is driven inside Ω_2. Once inside the safety zone, the MPC controller is switched in which, as can be seen from the dashed lines in Figures 5.13 and 5.14, asymptotically stabilizes the closed-loop system. It is important to keep in mind that Ω_2 is not necessarily a stability region for MPC. Therefore, even when the MPC controller is activated only inside Ω_2, it is possible for the closed-loop trajectory to leave the set at some future time. However, if this happens the supervisor will be able, at the next sampling instance, to detect this behavior and switch back to the bounded controller, before the trajectory can escape the stability region of the bounded controller, Ω.

5.4 Hybrid predictive output feedback control

The hybrid predictive control structure presented in Section 5.3 was developed under the assumption of full state feedback. In this section, we address the hybrid predictive control problem under output feedback. Due to the absence of complete state measurements, a state observer is constructed to provide the controllers, as well as the supervisor, with appropriate state estimates. The observer is tuned in a way so as to guarantee closed–loop stability for all initial conditions within the bounded con-

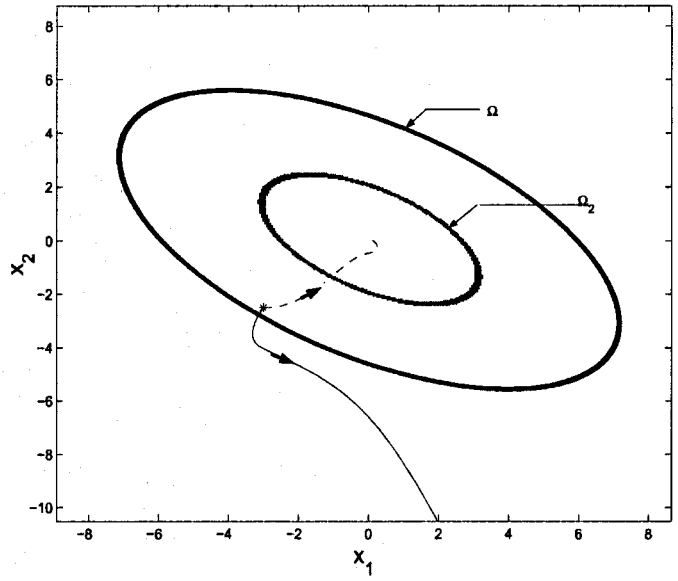

Figure 5.13: Closed-loop state trajectory under MPC (solid line) and under the switching scheme accounting for sampling (dashed line).

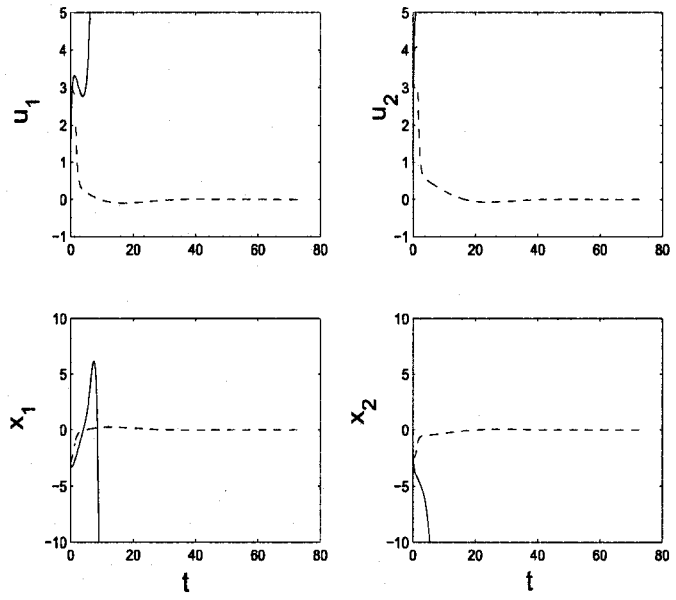

Figure 5.14: Input and closed-loop state profiles under MPC (solid line) and under the switching scheme accounting for sampling (dashed line).

troller's output feedback stability region (which can be chosen arbitrarily close in size to its state feedback counterpart, provided that the observer gain is sufficiently large). Switching laws, that monitor the evolution of the state estimates, are then derived to orchestrate the transition between the two controllers in a way that reconciles their respective stability and performance properties and safeguards closed–loop stability in the event of MPC infeasibility or instability.

In addition to the set of switching rules being different from the ones proposed in Section 5.3 under state feedback, an important characteristic of the hybrid predictive control strategy under output feedback is the inherent coupling, brought about by the lack of full state measurements, between the tasks of controller design, characterization of the stability region and supervisory switching logic design, on one hand, and the task of observer design, on the other. The rest of this section is organized as follows. In Section 5.4.1, we present some preliminaries that describe the class of systems considered and review the design of a Luenberger state observer. Next, in Section 5.4.2 we discuss the stability properties, of both MPC and Lyapunov–based bounded control, under output feedback. Then, in Section 5.4.3, we present the hybrid predictive output feedback control structure. The theoretical underpinnings and practical implications of the proposed hybrid predictive control structure are highlighted, and possible extensions of the supervisory switching logic, that address a variety of practical implementation issues, are discussed. Finally, in Section 5.4.4, two simulation studies are presented to demonstrate the implementation and evaluate the effectiveness of the proposed control strategy, as well as test its robustness with respect to modeling errors and measurement noise.

5.4.1 Preliminaries

We consider the problem of output feedback stabilization of continuous–time linear time–invariant (LTI) systems with input constraints, with the following state–space description:

$$\dot{x} = Ax + Bu \tag{5.22}$$

$$y = Cx \tag{5.23}$$

$$u \in \mathcal{U} \subset \mathbb{R}^m \tag{5.24}$$

where C is a constant $k \times n$ matrix. The pair (A, B) is assumed to be controllable and the pair (C, A) observable.

We will now briefly review the design of a Luenberger state observer for the system of Eqs.5.22–5.23 which will be used later in the development of the hybrid predictive control structure (see Remark 5.19 below for a discussion on the use of other possible estimation schemes). Specifically, we consider a standard Luenberger state observer described by:

$$\dot{\hat{x}} = A\hat{x} + Bu + L(y - C\hat{x}) \tag{5.25}$$

where $\hat{x} = [\hat{x}_1 \cdots \hat{x}_n]' \in \mathbb{R}^n$ denotes the vector of estimates of the state variables and L is a constant $n \times k$ matrix that multiplies the discrepancy between the actual and estimated outputs. Under the state observer of Eq.5.25, the estimation error in the closed–loop system, defined as $e = x - \hat{x}$, evolves, independently of the controller, according to the following equation:

$$\dot{e} = (A - LC)e \tag{5.26}$$

The pair $(C,\ A)$ is assumed to be observable in the sense that the observer gain matrix, L, can be chosen such that the norm of the estimation error in Eq.5.26 evolves

according to $\|e(t)\| \leq \kappa(\beta)\|e(0)\|\exp(-\beta t)$, where $-\beta < 0$ is the largest eigenvalue of $A - LC$ and $\kappa(\beta)$ is a polynomial function of β.

Remark 5.19 Referring to the state observer of Eq.5.25, it should be noted that the results presented in this section are not restricted to this particular class of observers. Any other observer that allows us to control the rate of decay of the estimation error at will, can be used. Our choice of using this particular observer design is motivated by the fact that it provides a transparent relationship between the temporal evolution of the estimation error bound and the observer parameters. For example, this design guarantees convergence of the state estimates in a way such that for larger values of β, the error decreases faster. As we discuss later (see the hybrid predictive control section), the ability to ensure a sufficiently fast decay of the estimation error is necessary in order to guarantee closed–loop stability under output feedback control. This requirement or constraint on the error dynamics is present even when other estimation schemes, such as moving horizon observers, are used (for example, see [223, 247]) to ensure closed–loop stability. For such observers, however, it is difficult in general to obtain a transparent relationship between the tunable observer parameters and the error decay rate.

Remark 5.20 For large values of β, the estimation error could possibly increase to large values before eventually decaying to zero (a phenomenon known as "peaking"; see [287]). However, this does not pose a problem in our design because the physical constraints on the manipulated inputs prevent transmission of the incorrect estimates to the process (see also Remark 5.24 for a detailed discussion of this issue). In the special case when C is a square matrix of rank n, the observer gain matrix, L, can be chosen as $L = AC^{-1} - RC^{-1}$, where R is a diagonal matrix whose diagonal elements are of the form $R_{ii} = -\beta a_i$, where $a_i \neq a_j \geq 1$. For this choice of L, the evolution of each error state is completely decoupled from the rest of the error states, i.e., each error state evolves according to $\dot{e}_i = -\beta a_i e_i$. In this case, no peaking occurs since each error term decreases monotonically.

5.4.2 Stability properties under output feedback control

Model predictive control

For the sake of a concrete illustration of the hybrid predictive control strategy, we will consider the following stabilizing MPC formulation [165, 221], which includes a terminal equality constraint in the optimization problem (see Remark 5.21 below for more advanced MPC formulations that can also be used). This model predictive controller is mathematically described by:

$$J_s(x,t,u(\cdot)) = \int_t^{t+T} (x'(s)Qx(s) + u'(s)Ru(s))ds \tag{5.27}$$

$$\begin{aligned} u(\cdot) &= argmin\{J_s(x,t,u(\cdot))|u(\cdot) \in S\} := M_s(x) \\ s.t. \quad \dot{x} &= Ax + Bu, \quad x(0) = x_0 \\ u(\cdot) &\in S \\ x(t+T) &= 0 \end{aligned} \tag{5.28}$$

Remark 5.21 Recall from the discussion in Section 5.3.4 that the hybrid predictive control strategy (whether under state or output feedback) is not restricted to any particular MPC formulation. The results apply to any MPC formulation for which *a priori* knowledge of the set of admissible initial conditions is lacking (or computationally expensive to obtain). In this sense, the above formulation is really intended as a symbolic example of stabilizing MPC formulations, with the understanding that other advanced MPC formulations that employ less restrictive constraints and/or penalties on the state at the end of the horizon can be used. Examples include formulations with terminal inequality constraints, such as contractive MPC (see, for example, [238, 175]) and CLF–based receding horizon control (see, for example, [239]), as well as formulations that employ a combination of terminal penalties and inequality constraints (see. for example, [50, 207, 290]). The reader is referred to [214] for a more exhaustive list.

Remark 5.22 By incorporating stability conditions directly as part of the optimization problem in Eq.5.28, asymptotic stability under state feedback MPC is guaranteed provided that the initial condition is chosen so that the optimization yields a feasible solution. However, the implicit nature of the MPC control law, obtained through repeated on–line optimization, limits our ability to obtain, *a priori*, an explicit characterization of the admissible initial conditions starting from where the given model predictive controller (with fixed horizon length) is guaranteed to be feasible and enforce asymptotic stability. This set is a complex function of the constraints and the horizon length. Estimates of sufficiently large horizon lengths that ensure stability (for example, see [56]) are typically conservative and, if used, may lead to a significant computational burden due to the increased size of the optimization problem. Therefore, in practice, the initial conditions and/or horizon lengths are usually chosen using ad hoc criteria and tested through closed–loop simulations which can add to the computational burden in implementing the model predictive controller. The difficulties encountered in characterizing the stability region under state feedback control carry over to the case of output feedback control, where the lack of state measurements requires that the control action be computed using the state estimates. Feasibility of the MPC optimization problem based on the state estimates, however, does not guarantee closed–loop stability or even the continued feasibility of the ensuing state estimates. This motivates implementing MPC within a hybrid control structure that provides a "fall–back" controller for which a region of constrained closed–loop stability can be obtained off–line. Lyapunov–based controller design techniques provide a natural framework for the design of a stabilizing "fall–back" controller for which an explicit characterization of the region of closed–loop stability can be obtained.

Lyapunov–based bounded control

In this section, we couple the bounded state feedback controller of Eqs.5.7-5.8 with the state observer of Eq.5.25 to design an output feedback controller and characterize

the stability properties of the resulting closed–loop system including the set of initial conditions for which closed–loop stability is guaranteed. When a state estimator of the form of Eq.5.25 is used, the resulting closed–loop system is composed of a cascade, between the error system and the plant, of the form:

$$\begin{aligned} \dot{x} &= Ax + Bu(x - e) \\ \dot{e} &= (A - LC)e \end{aligned} \tag{5.29}$$

Note that the values of the states used in the controller contain errors. The state feedback stability region, therefore, is not exactly preserved under output feedback. However, by exploiting the error dynamics of Eq.5.26, it is possible to recover arbitrarily large compact subsets of the state feedback stability region, provided that the poles of the observer are placed sufficiently far in the left half of the complex plane (which can be accomplished by choosing the observer gain parameter β sufficiently large). This idea is consistent with earlier results on semi–global output feedback stabilization of unconstrained systems using high–gain observers (for example, see [293, 210, 60]).

By viewing the estimation error as a dynamic perturbation to the state feedback problem, the basic idea, in constructing the output feedback controller and characterizing its stability region, is to design the observer in a way that exploits the robustness of the state feedback controller with respect to bounded estimation errors. To this end, given the state feedback stability region, Ω, we initially quantify the robustness margin by deriving a bound on the estimation error, $e_m > 0$, that can be tolerated by the state feedback controller, in the sense that the closed–loop state trajectory does not escape Ω for all $\|e\| \leq e_m$. Once this bound is computed, the idea is to initialize the states and the state estimates within any subset $\Omega_b \in \Omega$ and choose a consistent observer gain matrix L (parameterized by β) to ensure that, before the states reach the boundary of Ω, the norm of the estimation error has decayed to a value less than

e_m (see Figure 5.15 for a pictorial representation of this idea). These arguments are formalized in Propositions 5.1 and 5.2 below (the proofs are given in Appendix D).

Proposition 5.1 *Consider the constrained LTI system of Eqs.5.22–5.24 under the bounded control law of Eqs.5.7–5.8 with $u = u(x-e)$, where e is the state measurement error. Then, there exists a positive real number, e_m, such that if $x(0) \in \Omega$ and $\|e(t)\| \leq e_m \; \forall \, t \geq 0$, then $x(t) \in \Omega \; \forall \, t \geq 0$.*

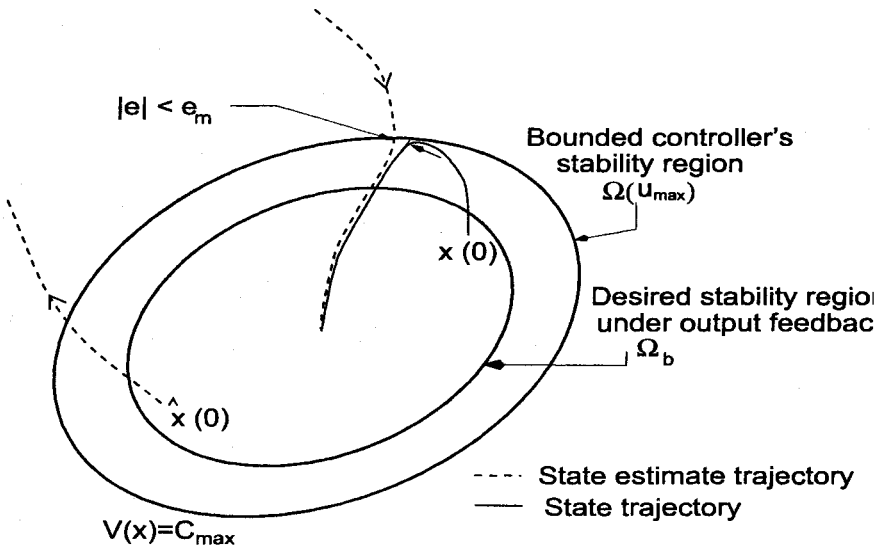

Figure 5.15: Schematic representation of the evolution of the trajectories of the closed–loop state and state estimate. Starting within Ω_b, the observer gain ensures that, before the state of the closed–loop system reaches the boundary of Ω, the state estimate has converged close enough to the true value of the state, so that the norm of the estimation error is below the allowable error tolerated by the controller within Ω.

Remark 5.23 The bounded control law of Eqs.5.7–5.8 will be used in the next section to illustrate the basic idea of the proposed hybrid control scheme. Our choice of using this particular design is motivated by its explicit structure and well–defined region of stability, which allows for an estimation of the robustness margin of the state feedback controller with respect to bounded measurement errors. However, the results of this work are not restricted to this particular choice of bounded controllers.

Any other analytical bounded control law, with an explicit structure and well–defined region of robust stability with respect to bounded measurement errors, can also be used in implementing the proposed control strategy.

Proposition 5.2 *Consider the constrained LTI system of Eqs.5.22–5.24, the state observer of Eq.5.25 and the bounded control law of Eqs.5.7–5.8. Then, given any positive real number, δ_b, such that $\Omega_b = \{x \in \mathbb{R}^n : \|x\|_P^2 \leq \delta_b\} \subset \Omega$, there exists a positive real number β^* such that if $\|x(0)\|_P^2 \leq \delta_b$, $\|\hat{x}(0)\|_P^2 \leq \delta_b$ and $\beta \geq \beta^*$, the origin of the constrained closed–loop system is asymptotically stable.*

Remark 5.24 Since the only assumption on C is that the pair (C, A) is observable, the observer states may "peak" before they converge to the true state values. This, however, does not pose a problem in our design because: (a) the physical constraints on the manipulated input eliminate the occurrence of instability due to peaking of the state estimates (i.e., they prevent transmission of peaking to the process), and (b) by "stepping back" from the boundary of the state feedback stability region and choosing an appropriate value for β, the design ensures that the system states cannot leave the stability region of the bounded controller before the estimation errors have gone below the permissible value.

Remark 5.25 In principle, the stability region under output feedback, Ω_b, can be chosen as close as desired to Ω by increasing the observer gain parameter β. However, it is well–known that large observer gains can amplify measurement noise and induce poor performance (see the simulation studies section for how this issue is addressed in observer implementation). This points to a fundamental tradeoff that cannot be resolved by simply changing the estimation scheme. For example, while one could replace the high–gain observer design with other observer designs (for example, a moving horizon estimator) to get a better handle on measurement noise, it is difficult in such schemes to obtain an explicit relationship between the observer tuning parameters and the output feedback stability region.

Remark 5.26 Note that, for the bounded controller, initializing x and $\hat{x}$ within Ω_b guarantees that x cannot escape Ω because of the inherent robustness of the bounded controller design with respect to bounded estimation errors (see the proof of Proposition 5.2 in the appendix). For MPC, however, there is no guarantee that x will stay in Ω, even if both x and $\hat{x}$ are initialized within Ω_b, and, therefore, whenever MPC is used, it will be necessary to rely on the evolution of the estimate, $\hat{x}(t)$, to deduce whether $x(t)$ is or is not within Ω. As we discuss in greater detail in the next section, the ability to reliably deduce the position of the true state at any given time is essential to the ability of the bounded controller to "step in" to preserve closed–loop stability in the event of failure of MPC (see Remark 5.29). One way of ascertaining bounds on the position of the true states, by looking only at the values of the estimates, is described in Proposition 5.3 below. The proof of this proposition is given in the appendix.

Proposition 5.3 *Consider the constrained system of Eqs.5.22–5.24, the state observer of Eq.5.25 and the bounded control law of Eqs.5.7–5.8. Let*

$$T_d^* := \frac{1}{\beta} \ln \left(\frac{\kappa(\beta) e_{max}(0)}{\epsilon \sqrt{c_{max}/\lambda_{max}(P)}} \right)$$

for some $0 < \epsilon < 1$ *where* $e_{max}(0) = \max_{\hat{x}(0),x(0)\in\Omega_b} \|\hat{x}(0) - x(0)\|$. *Then, there exists a positive real number* $\delta_s^* < c_{max}$ *such that for all* $\delta_s \leq \delta_s^*$, *and for all* $t \geq T_d^*$, $\hat{x}'(t)P\hat{x}(t) \leq \delta_s \Longrightarrow x'(t)Px(t) \leq c_{max}$.

Remark 5.27 The above proposition establishes the existence of a set, $\Omega_s := \{x \in \mathbb{R}^m : x'Px \leq \delta_s\}$, that allows us to ascertain bounds on the position of the true state, by looking only at whether the estimate is within this set. Specifically, for a given bound on the norm of the estimation error, at any given time, if the state estimate is within Ω_s, then we can conclude with certainty that the true state cannot be outside of Ω, irrespective of the controller being used (see the proof in the appendix for the mathematical details of this argument). Note also that the size of Ω_s depends on

the size of the error, and, therefore, as time evolves and the estimation error keeps decreasing, the size of Ω_s approaches that of Ω.

5.4.3 Hybrid predictive controller design

Consider the LTI system of Eqs.5.22–5.24, for which the bounded controller of Eqs.5.7–5.8, the state estimator of Eq.5.25 and the model predictive controller of Eqs.5.27–5.28 have been designed. The control problem is formulated as the one of designing a set of switching laws that orchestrate the transition between the predictive controller and the bounded controller under output feedback in a way that: (1) respects input constraints, (2) guarantees asymptotic stability of the origin of the closed–loop system starting from any initial condition within arbitrarily large compact subsets of the state feedback stability region of the bounded controller, and (3) accommodates the optimality requirements of MPC whenever possible (i.e., when closed–loop stability is guaranteed). For a precise statement of the problem, we first cast the system of Eqs.5.22–5.24 as a switched linear system of the form:

$$\begin{aligned} \dot{x} &= Ax + Bu_{i(t)} \\ y &= Cx \\ \|u_i\| &\leq u_{max} \\ i(t) &\in \{1,2\} \end{aligned} \tag{5.30}$$

where $i : [0,\infty) \rightarrow \{1,2\}$ is the switching signal which is assumed to be a piecewise continuous (from the right) function of time, implying that only a finite number of switches is allowed on any finite interval of time. The index $i(t)$, which takes values in the finite set $\{1,2\}$, represents a discrete state that indexes the control input, $u(\cdot)$, with the understanding that $i(t) = 1$ if and only if $u_i(\hat{x}(t)) = b(\hat{x}(t))$ (i.e., the bounded controller is implemented in the closed–loop system), and $i(t) = 2$ if and only if $u_i(\hat{x}(t)) = M_s(\hat{x}(t))$ (i.e., MPC is implemented in the closed–loop system).

Our goal, is to construct a switching law, based on the available state estimates:

$$i(t) \;=\; \psi(\hat{x}(t), t) \tag{5.31}$$

that provides the set of switching times that ensure asymptotically stabilizing transitions between the predictive and bounded controllers, in the event that the predictive controller is unable to enforce closed–loop stability for a given initial condition within Ω. In the remainder of this section, we present a switching scheme that addresses this problem. Theorem 5.3 below summarizes the main result (the proof is given in Appendix D).

Theorem 5.3 *Consider the constrained system of Eq.5.30, the bounded controller of Eqs.5.7–5.8, the state estimator of Eq.5.25, and the MPC law of Eqs.5.27–5.28. Let* $x(0) \in \Omega_b$, $\hat{x}(0) \in \Omega_b$, $\beta \geq \beta^*$, $\delta_s \leq \delta_s^*$, $\Omega_s(T_d^*) = \{x \in \mathbb{R}^n : x'Px \leq \delta_s(T_d^*)\}$, *and* $0 < T_d < T_{min} := \min\{t \geq 0 : V(x(0)) = \delta_b, V(x(t)) = c_{max}, u(t) \in \mathcal{U}\}$, *where* Ω_b, β^* *were defined in Proposition 5.2, and* δ_s^*, T_d^* *were defined in Proposition 5.3. Let* $T_m \geq \max\{T_d, T_d^*\}$ *be the earliest time for which* $\hat{x}(T_m) \in \Omega_s$ *and the MPC law prescribes a feasible solution,* $M_s(\hat{x}(T_m))$. *Also, let* $T_f > T_m$ *be the earliest time for which* $\dot{V}(\hat{x}(T_f)) \geq 0$. *Then, the following switching rule:*

$$i(t) \;=\; \left\{ \begin{array}{ll} 1, & 0 \leq t < T_m \\ 2, & T_m \leq t < T_f \\ 1, & t \geq T_f \end{array} \right\} \tag{5.32}$$

where $i(t) = 1$ *if and only if* $u_i(\hat{x}(t)) = b(\hat{x}(t))$ *and* $i(t) = 2$ *if and only if* $u_i(\hat{x}(t)) = M_s(\hat{x}(t))$, *asymptotically stabilizes the origin of the closed–loop system.*

Remark 5.28 Figure 5.16 depicts a schematic representation of the hybrid predictive control structure proposed in Theorem 5.3. The four main components of this structure include the state estimator, the bounded controller, the predictive controller, and

a high–level supervisor that orchestrates the switching between the two controllers. The implementation of the control strategy is best understood through the following stepwise procedure (see Figure 5.17):

1. Given the system of Eq.5.22 and the constraints of Eq.5.24, design the bounded controller using Eqs.5.7–5.8. Given the performance objective, design the predictive controller.

2. Compute the stability region estimate for the bounded controller under state feedback, Ω, using Eqs.5.9–5.10 and, for a choice of the output feedback stability region, $\Omega_b \subset \Omega$, compute e_m, β and T_d defined in Propositions 5.1 and 5.2.

3. Compute the region Ω_s and T_d^* (see Proposition 5.3) which ensure that $\hat{x} \in \Omega_s \Rightarrow x \in \Omega$ for all times greater than T_d^*.

4. Initialize the closed–loop system at any initial condition, $x(0)$, within Ω_b, under the bounded controller using an initial guess for the state, $\hat{x}(0)$, within Ω_b. Keep the bounded controller active for a period of time, $[0, T_m)$.

5. At $t = T_m$ (by which time $\hat{x} \in \Omega_s$), test the feasibility of MPC using values of the estimates generated by the state observer. If MPC yields no feasible solution, keep implementing the bounded controller.

6. If MPC is feasible, disengage the bounded controller from the closed–loop system and implement the predictive controller instead. Keep MPC active for as long as $\hat{x} \in \Omega_s$ and $V(\hat{x})$ keeps decaying.

7. At the first instance that either $V(\hat{x})$ begins to increase under MPC, or MPC runs into infeasibilities, switch back to the bounded controller and implement it for all future times; else keep the predictive controller active.

Remark 5.29 An important feature that distinguishes the switching logic of Theorem 5.3 from the state feedback logic in Section 5.3 is the fact that, in the output

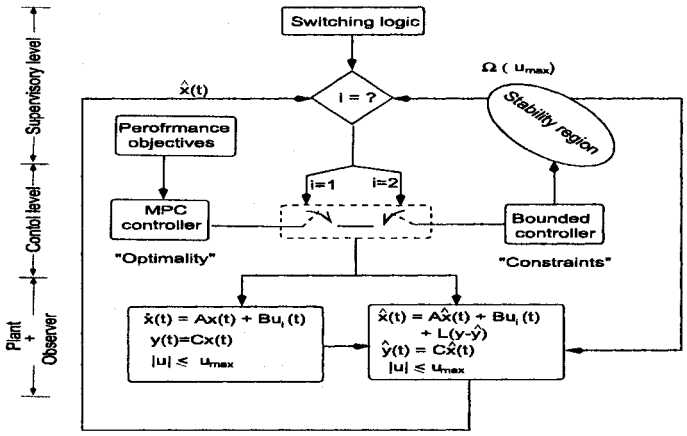

Figure 5.16: Schematic representation of the hierarchical hybrid predictive control structure merging the bounded and model predictive controllers and a state observer.

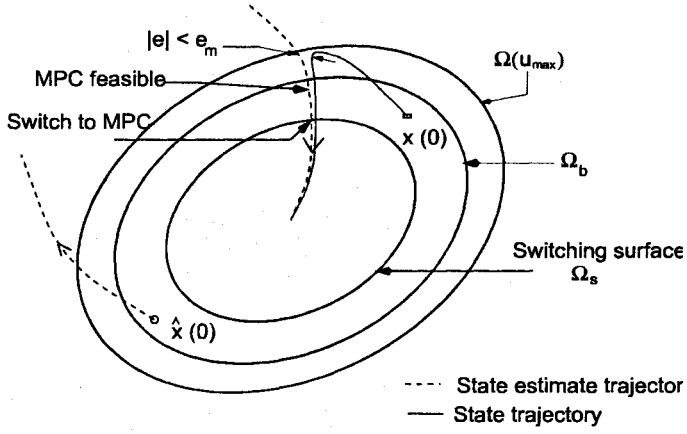

Figure 5.17: Schematic representation of the evolution of the closed–loop system under the controller switching strategy proposed in Theorem 5.3. Note that MPC is not activated (even if feasible) before $\hat{x}$ enters Ω_s.

feedback case, MPC implementation does not commence until some period of time, $[0, T_m)$, has elapsed, even if MPC is initially feasible. The rationale for this delay (during which only bounded control is implemented) is the need to ensure that, by the time MPC is implemented, the norm of the estimation error has already decayed to sufficiently low values that would allow the bounded controller to preserve closed–loop stability in the event that MPC needs to be switched out after its implementation. More specifically, before MPC can be safely activated, the supervisor needs to make sure that: (1) the estimation error has decayed to levels below e_m, and (2) the state, x, will be contained within Ω at any time that MPC could be switched out after its implementation. The first requirement ensures that the bounded controller, when (and if) reactivated, is able to tolerate the estimation error and still be stabilizing within Ω (see Proposition 5.1). This requirement also implies that T_m must be greater than T_d, which is the time beyond which the observer design guarantees $\|e\| \leq e_m$ (see Part 1 of the Proof of Proposition 5.2). The second requirement, on the other hand, implies that MPC cannot be safely switched in before the estimate enters Ω_s and the norm of the error is such that $\hat{x} \in \Omega_s \Longrightarrow x \in \Omega$ (see Remarks 5.26-5.27). Recall from Proposition 5.3 that this property holds for all $t \geq T_d^*$; hence T_m must also be greater than T_d^*, i.e., $T_m \geq \max\{T_d, T_d^*\}$. For times greater than T_m, the implementation of MPC can be safely tested without fear of closed–loop instability, since even if $\hat{x}$ tries to escape Ω_s (possibly indicating that x under MPC is about to escape Ω), the switching rule allows the supervisor to switch back immediately to the bounded controller (before $\hat{x}$ leaves Ω_s), thus guaranteeing that at the switching time $\hat{x} \in \Omega_s$, $x \in \Omega$ and $\|e\| \leq e_m$, which altogether imply that the bounded controller, once switched in, will be asymptotically stabilizing (see the Proof of Theorem 5.3 for the mathematical details of this argument).

Remark 5.30 The proposed approach does not require or provide any information as to whether the model predictive controller itself is asymptotically stabilizing or not, starting from any initial condition within Ω_b. In other words, the approach does not turn Ω_b into a stability region for MPC. What the approach does, however, is turn

Ω_b into a stability region for the switched closed–loop system. The value of this can be understood in light of the difficulty in obtaining, *a priori*, an analytical characterization of the set of admissible initial conditions that the model predictive controller can steer to the origin in the presence of input constraints. Given this difficulty, by embedding MPC implementation within Ω_b and using the bounded controller as a fall–back controller, the switching scheme of Theorem 5.3 allows us to safely initialize the closed–loop system anywhere within Ω_b with the guarantee that the bounded controller can always intervene to preserve closed–loop stability in case the MPC is infeasible or destabilizing (due, for example, to a poor choice of the initial condition and/or improper tuning of the horizon length).

Remark 5.31 Note that, once MPC is switched in, if $V(\hat{x})$ continues to decrease monotonically, then the predictive controller will be implemented for all $t \geq T_m$. In this case, the optimal performance of the predictive controller is practically recovered. Note also, that in this approach, the state–feedback predictive controller design is not required to be robust with respect to state measurement errors (see [125] for examples when MPC is not robust) because even if it is not robust, closed–loop stability can always be guaranteed by switching back to the bounded controller (within its associated stability region) which provides the desired robustness with respect to the measurement errors.

Remark 5.32 Even though the result of Theorem 5.3 was derived using the MPC formulation of Eqs.5.27–5.28, it is important to point out that the same result applies to MPC formulations that employ different types of stability constraints (see Remark 5.21). The basic commonality between the formulation of Eqs.5.27–5.28 and other stability–handling formulations is the fact that, in all of these formulations, the implementation of MPC depends on whether the optimization problem, subject to the stability constraints, is feasible or not. This issue of feasibility is therefore accommodated in the switching logic by requiring the supervisor to check the feasibility of MPC in addition to monitoring the evolution of V. On the other hand, when a con-

ventional MPC formulation (i.e., one with no stability constraints) is used, potential infeasibility of the optimization problem is no longer a concern, and, therefore, in this case the supervisory switching logic rests only on monitoring the evolution of V.

Remark 5.33 In conventional MPC formulations (with no stability constraints), the objective function is typically a tuning parameter that can be manipulated, by arbitrarily changing the weighting matrices, to ensure stability. In the hybrid predictive control framework, on the other hand, since closed–loop stability is guaranteed by the bounded controller, the objective function and the weights, instead of being arbitrarily tuned to guarantee stability, can be chosen to reflect actual physical costs and satisfy desirable performance objectives (for example, fast closed–loop response).

5.4.4 Simulation studies

In this section, two simulation studies are presented to demonstrate the implementation, and evaluate the effectiveness, of the proposed hybrid predictive control strategy as well as test its robustness with respect to modeling errors and measurement noise.

Illustrative example

In this section, we demonstrate an application of the proposed hybrid predictive control strategy to a three dimensional linear system where only two of the states are measured. Specifically, we consider an exponentially unstable linear system of the form of Eqs.5.22–5.23 with

$$A = \begin{bmatrix} 0.55 & 0.15 & 0.05 \\ 0.15 & 0.40 & 0.20 \\ 0.10 & 0.15 & 0.45 \end{bmatrix}, \; B = \begin{bmatrix} 1 & 0 \\ 0 & 1 \\ 1 & 1 \end{bmatrix}, \; C = \begin{bmatrix} 1 & 0 & 0 \\ 0 & 0 & 1 \end{bmatrix},$$

where both inputs u_1, u_2 are constrained in the interval $[-1, 1]$. Using Eqs.5.7–5.8, we initially designed the bounded controller and constructed its stability region, Ω,

via Eqs.5.9–5.10. The matrix P was chosen as:

$$P = \begin{bmatrix} 6.5843 & 4.2398 & -3.830 \\ 4.2398 & 3.6091 & -2.667 \\ -3.830 & -2.667 & 2.8033 \end{bmatrix}$$

and the observer gain parameter was chosen to be $\beta = 500$ to ensure closed–loop stability for all initial conditions within a set $\Omega_b \subset \Omega$. For the model predictive controller, the parameters in the objective function of Eq.5.27 were chosen as $Q = qI$, with $q = 1$ and $R = rI$, with $r = 0.1$. We also chose a horizon length of $T = 1.5$ in implementing the predictive controller of Eqs.5.27–5.28. The resulting quadratic program was solved using the MATLAB subroutine QuadProg, and the set of ODEs integrated using the MATLAB solver ODE45.

In the first simulation run (solid lines in Figures 5.18–5.19), the states were initialized at $x_0 = [0.75 \ -0.5 \ 1.0]'$, while the observer states were initialized at $\hat{x}_0 = [0 \ 0 \ 0]'$ (which belong to the stability region of the bounded controller, Ω_b). The supervisor employs the bounded controller, while continuously checking the feasibility of MPC. At $t = 5.45$, MPC (based on the state estimates) becomes feasible and is implemented in the closed–loop system to achieve asymptotic stability. The total cost of stabilization achieved by the switching strategy (as measured by Eq.5.27) is $J = 80.12$. The switching scheme leads to better performance when compared with the scenario where the bounded controller is implemented for all times (the cost in this case is $J = 121.07$), and also better than the model predictive controller, because, starting from this initial condition, the predictive controller prescribes no feasible control move (equivalent to an infinite value for the objective function). Note that even though feasibility of MPC could have been achieved earlier by increasing the horizon length to $T = 3.5$ (dashed lines in Figures 5.18–5.19), this conclusion could not be reached *a priori*, i.e., before running the closed–loop simulation in its entirety to check whether the choice $T = 3.5$ is appropriate. In the absence of any *a priori* knowledge of the

necessary horizon length, for a given initial condition, the proposed hybrid predictive control can be used to guarantee closed–loop stability regardless of the choice of the horizon length.

In the second set of simulation results, we demonstrate the need for a choice of an observer gain consistent with the choice of Ω_b. To this end, we consider an observer design with a low gain ($\beta = 0.5$) placing the observer poles at $-0.5, -1.0, -1.5$. With the low observer gain, the estimates take a long time to converge to the true state values, resulting in the implementation of "incorrect" control action for a large period of time, by the end of which the states have already escaped out of Ω (even though the states and state estimates were initiated within Ω_b), thus resulting in closed–loop instability (dashed lines in Figures 5.20–5.21). Recall that stability was achieved when the observer gain was chosen to be $\beta = 500$ in the first set of simulation runs (the state and input profiles for this case are reproduced by the solid lines in Figures 5.20–5.21 for convenience of comparison).

To recover, as closely as possible, the state feedback stability region, large values of the observer gain are needed. However, it is well–known that high observer gains can amplify measurement noise and induce poor performance. These observations point to a fundamental tradeoff that cannot be resolved by simply changing the estimation scheme (see Remark 5.25). For example, if the observer gain consistent with the choice of the output feedback stability region is abandoned, the noise problem may disappear, but then stability cannot be guaranteed. One approach to avoid this problem in practice is to initially use a large observer gain that ensures quick decay of the initial estimation error, and then switch to a low observer gain. In the following simulation, we demonstrate how this idea, in conjunction with switching between the controllers, can be used to mitigate the undesirable effects of measurement noise. To

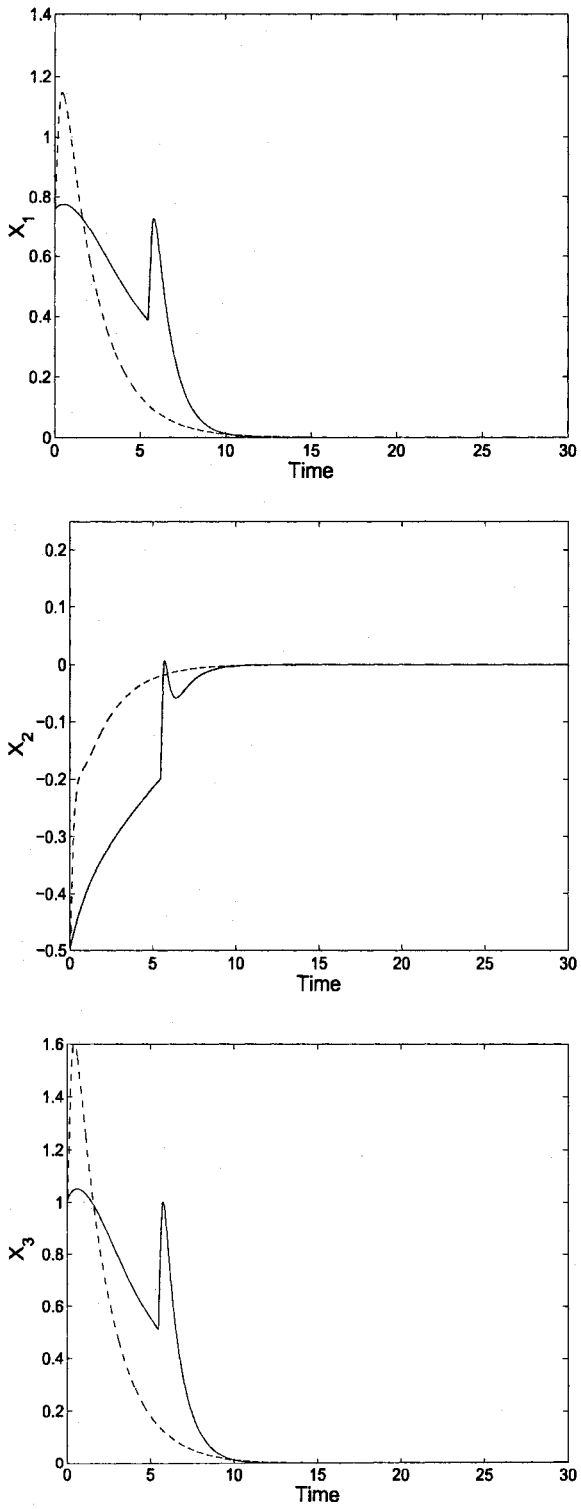

Figure 5.18: States of the closed–loop system under the proposed hybrid predictive control strategy using two different horizon lengths of $T = 1.5$ (solid) and $T = 3.5$ (dashed) in MPC implementation, and an observer gain parameter of $\beta = 500$.

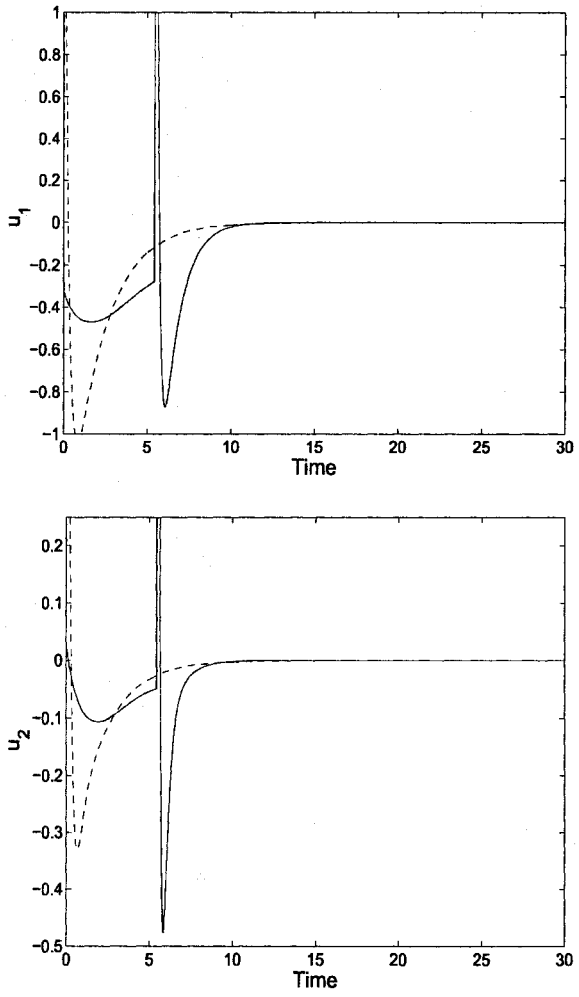

Figure 5.19: Manipulated input profiles under the proposed hybrid predictive control strategy using two different horizon lengths of $T = 1.5$ (solid) and $T = 3.5$ (dashed) in MPC implementation, and an observer gain parameter $\beta = 500$.

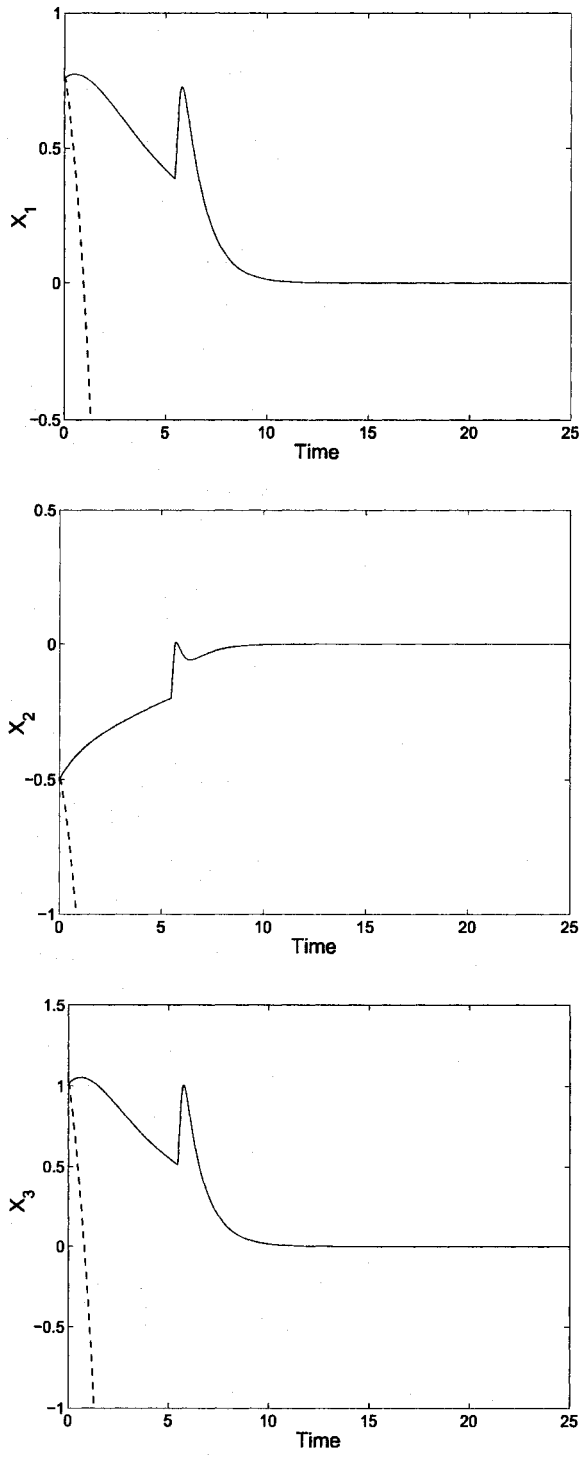

Figure 5.20: States of the closed–loop system under the proposed hybrid predictive control strategy using two different gain parameters of $\beta = 500$ (solid) and $\beta = 0.5$ (dashed) in observer implementation, and horizon length of $T = 1.5$ in the predictive controller.

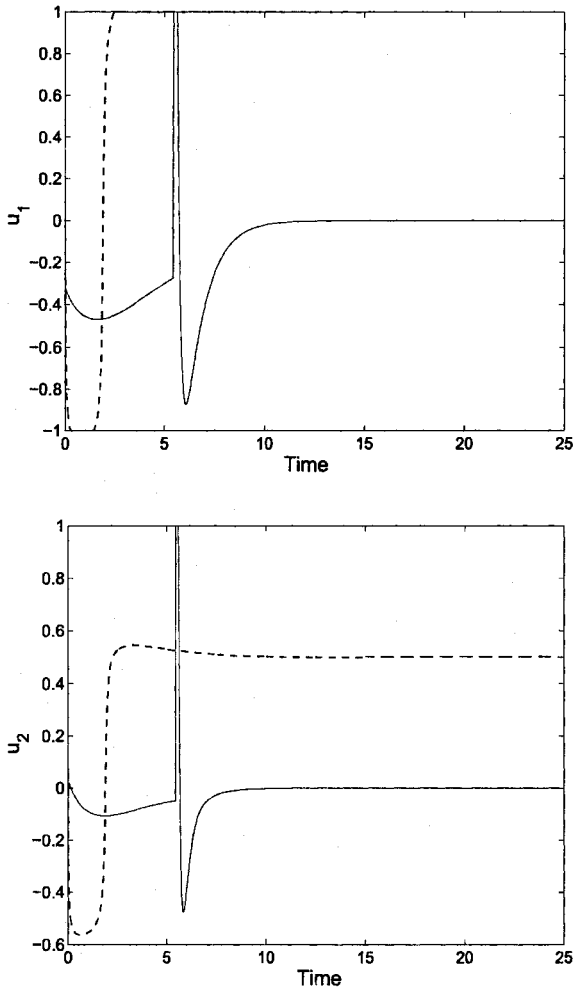

Figure 5.21: Manipulated input profiles under the proposed hybrid predictive control strategy using two different gain parameters of $\beta = 500$ (solid) and $\beta = 0.5$ (dashed) in observer implementation, and horizon length of $T = 1.5$ in the predictive controller.

illustrate this point, we switch between the high and low observer gains used in the first two simulation runs and demonstrate the attenuation of noise. Specifically, we consider the nominal system described by Eqs.5.22–5.23 (see the first paragraph of this subsection for the values of A, B and C), together with model uncertainty and measurement noise. The model matrix A_m (used for controller and observer design) is assumed to be within five percent error of the system matrix A and the sensors are assumed to introduce noise in the measured outputs as $y(t) = Cx(t) + \delta(t)$ where $\delta(t)$ is a random gaussian noise with zero mean and a variance of 0.01. As seen by the solid lines in Figure 5.22, starting from the initial condition, $x_0 = [0.75 \ -0.5 \ 1.0]'$, using a high observer gain followed by a switch to a low observer gain at $t = 1.0$, and a switch from bounded control to MPC at $t = 3.5$, the supervisor is still able to preserve closed–loop stability, while at the same time resulting in a smoother control action (solid lines in Figure 5.23) when compared to the case where a high observer gain is used for the entire duration of the simulation (dotted lines in Figures 5.22–5.23).

Application to a chemical reactor example

In this subsection, we consider a nonlinear chemical reactor example to test the robustness of the proposed hybrid predictive control structure (designed on the basis of the linearization of the nonlinear model around the operating steady–state) with respect to modeling errors arising due to the presence of nonlinear terms. Specifically, we consider a well–mixed continuous stirred tank reactor where an irreversible elementary exothermic reaction of the form $A \xrightarrow{k} B$, takes place, where A is the reactant species and B is the product. The feed to the reactor consists of pure A at flow rate F, molar concentration C_{A0} and temperature T_{A0}. A jacket is used to remove/provide heat to the reactor. Under standard modelling assumptions, a mathematical model of the process can be derived from material and energy balances and takes the following

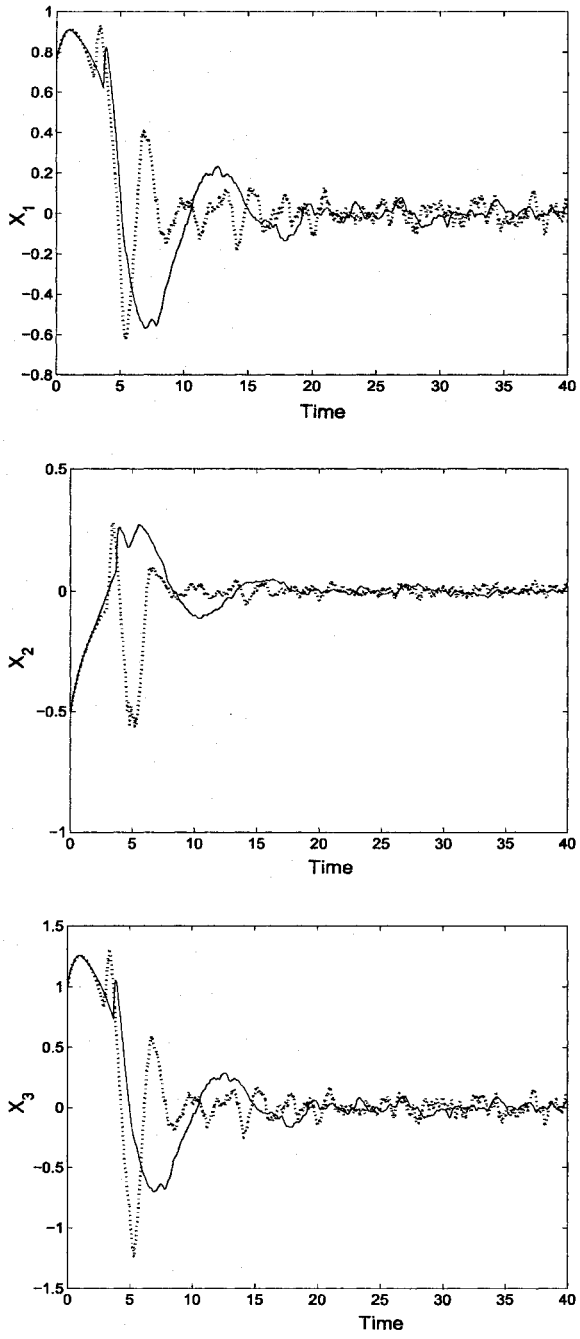

Figure 5.22: Closed–loop states under hybrid predictive control, in the presence of measurement noise and modeling errors, for the case when the observer is initially implemented using $\beta = 500$ and then switched to $\beta = 0.5$ at $t = 1.0$ (solid lines) and the case when the observer is implemented using $\beta = 500$ for all times (dotted lines). The horizon length for the predictive controller is $T = 1.5$.

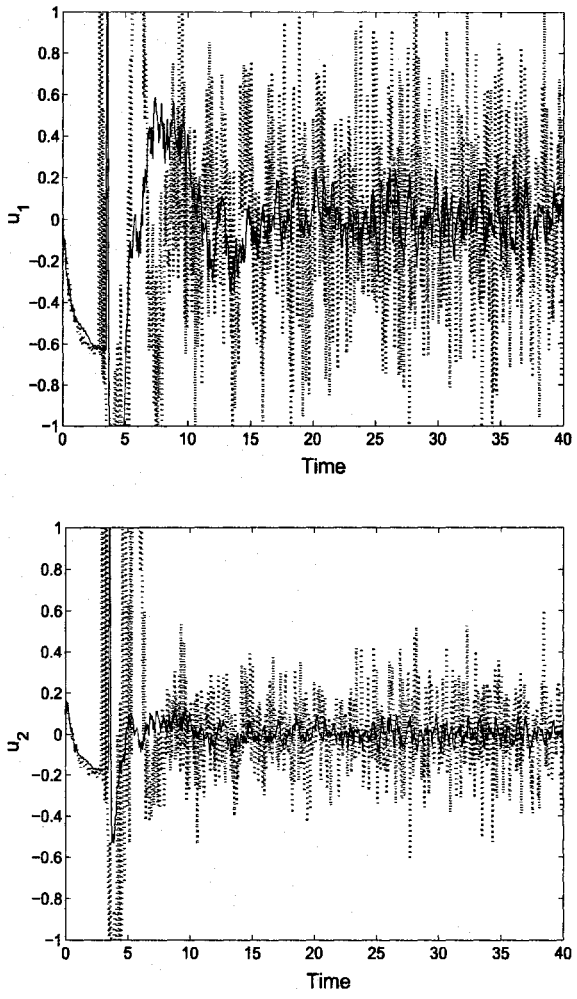

Figure 5.23: Manipulated input profiles under the proposed hybrid predictive control strategy in the presence of measurement noise and modeling errors. The solid profiles depict the case when the state observer is initially implemented using $\beta = 500$ and then switched to $\beta = 0.5$ at $t = 1.0$. The dotted profiles depict the case when the state observer is implemented using $\beta = 500$ for all times. The horizon length for the model predictive controller is $T = 1.5$.

form:

$$\begin{aligned} V\frac{dT_R}{dt} &= F(T_{A0} - T_R) + \frac{(-\Delta H)}{\rho c_p} k_0 \exp\left(\frac{-E}{RT_R}\right) C_A V + \frac{Q}{\rho c_p} \\ V\frac{dC_A}{dt} &= F(C_{A0} - C_A) - k_0 \exp\left(\frac{-E}{RT_R}\right) C_A V \end{aligned} \tag{5.33}$$

where C_A denotes the concentrations of the species A, T_R denotes the temperature of the reactor, Q denotes rate of heat input/removal from the reactor, V denotes the volume of the reactor, ΔH, k, E denote the enthalpy, pre–exponential constant and activation energy of the reaction, c_p and ρ denote the heat capacity and density of the reactor, respectively. The values of the process parameters are given in Table 5.1. It was verified that these conditions correspond to three steady–states, one unstable (given in Table 1) and two locally asymptotically stable.

Table 5.1: Process parameters and steady–state values for the reactor of Eq.5.33.

V	=	0.1	m^3
R	=	8.314	$kJ/kmol \cdot K$
C_{A0s}	=	1.0	$kmol/m^3$
T_{A0s}	=	310.0	K
ΔH	=	-4.78×10^4	$kJ/kmol$
k_0	=	1.2×10^9	s^{-1}
E	=	8.314×10^4	$kJ/kmol$
c_p	=	0.239	$kJ/kg \cdot K$
ρ	=	1000.0	kg/m^3
F	=	1.67×10^{-3}	m^3/s
T_{Rs}	=	395.33	K
C_{As}	=	0.57	$kmol/m^3$

The control problem is to regulate both the outlet concentration of the reactant, C_A, and the reactor temperature, T_R, at the unstable steady–state by manipulating the inlet reactant concentration, C_{A0}, and the rate of heat input, Q, provided by the jacket. The control objective is to be accomplished in the presence of constraints on the manipulated inputs ($|Q| \leq 1$ KJ/min, $|\Delta C_{A0}| = |C_{A0} - C_{A0s}| \leq 1$ mol/L) using

only measurements of the reactor temperature. For the purpose of implementing the control scheme, the process model of Eq.5.33 was linearized around the unstable steady–state, and the resulting linear model was used for the design of the hybrid predictive control structure. Using Eqs.5.7–5.8, we initially designed the bounded controller and constructed its stability region via Eqs.5.9–5.10. The matrix P was chosen as:

$$P = \begin{bmatrix} 0.027 & 0.47 \\ 0.47 & 15.13 \end{bmatrix}$$

and the observer gain parameter was chosen to be $\beta = 5$. It should be noted here that, because of the linearization effect, the largest invariant region, Ω, computed using Eqs.5.9–5.10 applied to the linear model, includes physically meaningless initial conditions ($C_A < 0$) and, therefore, a smaller level set, $\Omega' \subset \Omega$, that includes only physically meaningful initial conditions, was chosen and used as the stability region estimate for the bounded controller (see Figure 5.24). For the predictive controller, the parameters in the objective function of Eq.5.27 were chosen as $Q = qI$, with $q = 1$ and $R = rI$, with $r = 1$. We also chose a horizon length of $T = 2$ in implementing the predictive controller of Eqs.5.27–5.28. The resulting quadratic program was solved using the MATLAB subroutine QuadProg, and the set of ODEs integrated using the MATLAB solver ODE45. In all simulations, the controllers, designed on the basis of the linearization around the unstable steady–state, were implemented on the nonlinear system of Eq.5.33.

As seen by the solid lines in Figures 5.25–5.26, starting from the point (T_R, C_A) = (395.53 K, 0.47 $kmol/m^3$), the model predictive controller is able to stabilize the process at the desired steady–state, (T_{RS}, C_{AS}) = (395.33 K, 0.57 $kmol/m^3$). From the initial condition, (T_R, C_A) = (397.33 K, 0.67 $kmol/m^3$), however, the model predictive controller yields an infeasible solution. Therefore, using the proposed

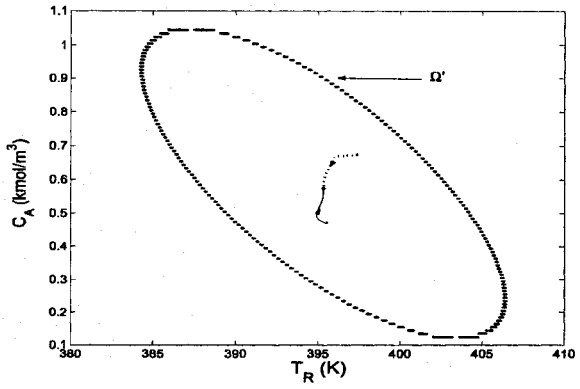

Figure 5.24: Stability region estimate, Ω', based on the linearization of the nonlinear model of Eq.5.33. The solid line depicts the closed–loop state trajectory starting from an initial condition for which MPC (designed based on the linear model with $T = 2$) is feasible and stabilizes the nonlinear closed–loop system, while the dotted line depicts the state trajectory starting from an initial condition for which MPC is infeasible, and the hybrid predictive control strategy is implemented instead to enforce closed–loop stability.

hybrid control strategy (dotted lines in Figures 5.25–5.26), the supervisor implements the bounded controller in the closed–loop system, while continuously checking the feasibility of MPC. At $t = 0.9$ seconds, MPC is found to be feasible and the supervisor switches to the model predictive controller, which in turn stabilizes the nonlinear closed–loop system at the desired steady–state. These results clearly demonstrate a certain degree of robustness that the proposed hybrid predictive control structure possesses with respect to modeling errors (arising in this case due to neglecting the nonlinearities).

Remark 5.34 In both simulation studies presented above, we have treated robustness as a practical implementation issue and performed simulations that test the performance of the control strategy in the event of some plant–model mismatch to show that the hybrid predictive controller does posses some robustness margins that make it suited for practical implementation. We note that our objective here is not to incorporate robustness explicitly into the controller design, but rather to investigate

the robustness margins of the controllers. The issue of incorporating robustness explicitly into the hybrid predictive control strategy is beyond the scope of the current work and is the subject of other research work (see [100]). Furthermore, within predictive control, a common approach to the robust controller design problem is through the min–max type formulations. However, these formulations are well–known to be computationally demanding and, more importantly, suffer from similar difficulties in identifying the set of initial conditions from which robust closed–loop stability can be guaranteed *a priori*.

5.5 Conclusions

In this chapter, a hybrid predictive control structure, uniting MPC and bounded control, was developed for the stabilization of linear time-invariant systems with input constraints. Both the state and output feedback control problems were considered. Under full state feedback, the hybrid predictive control structure consists of three components: a bounded controller with a well-defined stability region, a high-performance model predictive controller, and a higher-level supervisor that orchestrates the switching between the two controllers in a way that: (1) guarantees closed-loop stability for all initial conditions within the stability region of the bounded controller, and (2) reconciles the stability and performance properties of the two controllers. The proposed hybrid control structure was used to construct a number of switching schemes that address a variety of control objectives, such as closed-loop stability (stability-based switching) and closed-loop performance (performance-driven switching). A switching scheme was also developed for more advanced formulations of MPC (feasibility-based switching). In each case, the switching logic was tailored to deal with the specific MPC formulation used and the specific objectives sought.

The hybrid predictive control structure was then extended to address the output

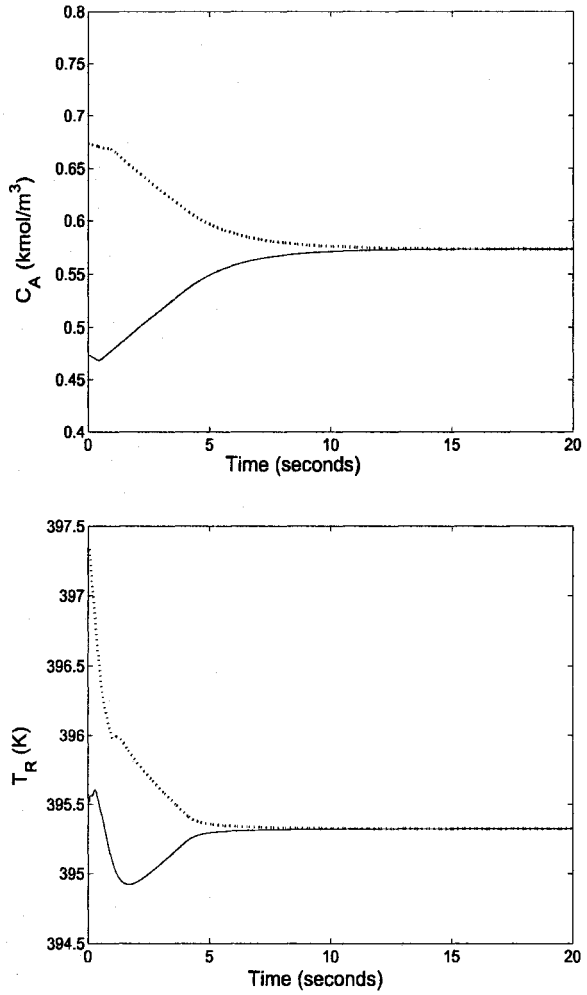

Figure 5.25: Closed–loop reactant concentration (top) and reactor temperature (bottom) starting from an initial condition for which MPC (designed based on the linear model with $T = 2$) is feasible and stabilizes the nonlinear closed–loop system (solid), and starting from an initial condition for which MPC is infeasible, and the hybrid predictive control strategy is implemented instead to enforce closed–loop stability (dotted).

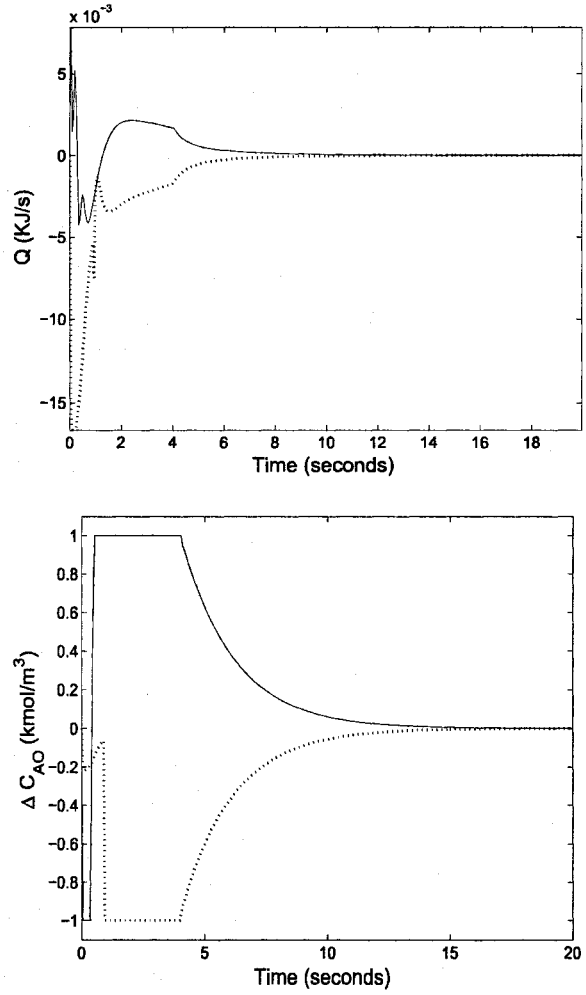

Figure 5.26: Rate of heat input (top) and inlet reactant concentration in deviation variable form (bottom) when MPC is implemented (solid) and when the hybrid predictive control strategy is implemented (dotted).

feedback stabilization problem, via the addition of an appropriate state observer to provide the controllers, as well as the supervisor, with appropriate state estimates. The observer was tuned in a way so as to guarantee closed–loop stability for all initial conditions within the bounded controller's output feedback stability region (which can be chosen arbitrarily close in size to its state feedback counterpart, provided that the observer gain is sufficiently large). Switching laws, that monitor the evolution of the state estimates, were derived to orchestrate the transition between the two controllers in the event of MPC infeasibility or instability.

The hybrid predictive control structure was shown to provide, irrespective of the specific MPC formulation used, a safety net for the practical implementation of state and output feedback MPC by providing, through off–line computations, *a priori* knowledge of a large set of initial conditions for which stability of the switched closed–loop system is guaranteed. Finally, simulation studies were presented throughout the chapter to demonstrate the implementation and evaluate the effectiveness of the proposed hybrid predictive control strategy, as well as test its robustness with respect to modeling errors and measurement noise.

Chapter 6

Hybrid Predictive Control of Nonlinear and Uncertain Systems

6.1 Introduction

In Chapter 5, we developed a hybrid predictive control strategy for the stabilization of constrained linear systems and demonstrated some of its benefits in terms of providing a safety net for the practical implementation of MPC. In this chapter, we focus on nonlinear systems, with and without uncertainty, and show how the hybrid predictive control strategy can be extended in several directions to address the constrained stabilization problem for these systems and aid MPC implementation. To motivate the hybrid predictive control structure for nonlinear and uncertain systems, we note that the practical implementation difficulties of MPC are in general more pronounced for nonlinear and uncertain systems than in the linear case.

For example, when the system is linear, the cost quadratic, and the constraints convex, the MPC optimization problem reduces to a quadratic program for which efficient software exists and, consequently, a number of control-relevant issues have

been explored, including issues of closed–loop stability, performance, implementation and constraint satisfaction (see, for example, the tutorial paper [249]). For nonlinear systems, several nonlinear model predictive control (NMPC) schemes have been developed in the literature (see, for example, [213, 222, 50, 175, 288, 207, 290]) that focus on the issues of stability, constraint satisfaction and performance optimization for nonlinear systems. A common idea of these approaches is to enforce stability by means of suitable penalties and constraints on the state at the end of the finite optimization horizon. Because of the system nonlinearities, however, the resulting optimization problem is non-convex and, therefore, much harder to solve, even if the cost functional and constraints are convex. The computational burden is more pronounced for NMPC algorithms that employ terminal stability constraints (e.g., equality constraints) whose enforcement requires intensive computations that typically cannot be performed within a limited time–window.

In addition to the computational difficulties of solving a nonlinear optimization problem at each time step, one of the key challenges that impact on the practical implementation of NMPC is the inherent difficulty of characterizing, *a priori*, the set of initial conditions starting from where a given NMPC controller is guaranteed to stabilize the closed–loop system. For finite–horizon MPC, an adequate characterization of the stability region requires an explicit characterization of the complex interplay between several factors, such as the initial condition, the size of the constraints, the horizon length, the penalty weights, etc. Use of conservatively large horizon lengths to address stability only increases the size and complexity of the nonlinear optimization problem and could make it intractable. Furthermore, since feasibility of NMPC is determined through on-line optimization, unless a NMPC controller is exhaustively tested by simulation over the whole range of potential initial states, doubt will al-

ways remain as to whether or not a state will be encountered for which an acceptable solution to the finite horizon problem can be found.

The above host of theoretical and computational issues continue to motivate research efforts in this area. Most available predictive control formulations for nonlinear systems, however, either do not explicitly characterize the stability region, or provide estimates of this region based on linearized models, used as part of some scheduling scheme between a set of local predictive controllers. The idea of scheduling of a set of local controllers to enlarge the operating region was proposed earlier in the context of analytic control of nonlinear systems (e.g., see [217, 200]) and requires an estimate of the region of stability for the local controller designed at each scheduling point. Then by designing a set of local controllers with their estimated regions of stability overlapping each other, supervisory scheduling of the local controllers can move the state through the intersections of the estimated regions of stability of different controllers to the desired operating point. Similar ideas were used in [53, 307] for scheduled predictive control of nonlinear systems. All of these approaches require the existence of an equilibrium surface that connects the scheduling points, and the resulting stability region estimate is the union of the local stability regions, which typically forms an envelope around the equilibrium surface. Stability region estimates based on linearization, however, are inherently conservative.

For systems with uncertainty, the MPC problem has been approached either as an analysis problem, where the robustness properties of nominal MPC formulations are analyzed (see, for example, [120, 78, 208]), or as a synthesis problem, where the goal is to develop MPC formulations that explicitly account for uncertainty (see [37, 214] for surveys of results in this area). The problem of designing robust predictive controllers for uncertain linear systems has been extensively investigated (see, for

example, [49, 196, 266, 72, 197, 36, 308]) and is typically addressed within a min–max optimization framework, where the optimization problem is solved in a way such that the constraints are satisfied for all possible realizations of the bounded uncertainty.

For uncertain nonlinear systems, the problem of robust MPC design continues to be an area of ongoing research (see, for example, [222, 107, 206, 1, 260, 194]). While min-max formulations provide a natural setting within which to address this problem, computational complexity remains a very serious issue. The computational burden stems in part from the nonlinearity of the model which makes the optimization problem non–convex and, therefore, generally hard to solve. Performing the min–max optimization over the non-convex problem further increases the computational complexity of the optimization problem and makes it unsuitable for the purpose of on–line implementation. These implementation difficulties are further compounded by the inherent difficulty of obtaining, *a priori* (i.e., before controller implementation), an explicit characterization of the set of initial conditions for which closed–loop stability, under any nonlinear MPC formulation (with or without stability conditions, and with or without robustness considerations), can be guaranteed in the presence of uncertainty and constraints. Faced with these difficulties, in current industrial implementation, the robust stability of MPC controllers is usually tested through extensive simulations.

The rest of this chapter is organized as follows. In Section 6.2, we develop a hybrid predictive control structure for the stabilization of nonlinear systems with input constraints. The central idea is to use a family of bounded nonlinear controllers, each with an explicitly characterized stability region, as fall–back controllers, and embed the operation of MPC within the union of these regions. In the event that the given predictive controller (which can be linear, nonlinear, or even scheduled) is unable to sta-

bilize the closed–loop system (e.g., due to failure of the optimization algorithm, poor choice of the initial condition, insufficient horizon length, etc.), supervisory switching from MPC to any of the bounded controllers, whose stability region contains the trajectory, guarantees closed–loop stability. Two representative switching schemes that address (with varying degrees of flexibility) stability and performance considerations are described, and possible extensions of the supervisory switching logic, to address a variety of practical implementation issues, are discussed. The efficacy of the proposed approach is demonstrated through applications to chemical reactor and crystallization process examples. In Section 6.3, we extend the hybrid predictive control structure to nonlinear systems with input constraints and uncertain variables, and show that the resulting robust hybrid predictive control structure provides a safety net for the implementation of any available MPC formulation, designed with or without taking uncertainty into account. Two representative switching schemes that address robust stability and performance objectives are described to highlight the effect of uncertainty on the design of the switching logic. Finally, the implementation and efficacy of the robust hybrid predictive control strategy are demonstrated through simulations using a chemical reactor example. The results of this chapter were first presented in [101] and [220].

6.2 Hybrid predictive control of nonlinear systems

6.2.1 Preliminaries

In this section, we consider the problem of asymptotic stabilization of continuous-time nonlinear systems with input constraints, with the following state-space description:

$$\dot{x}(t) = f(x(t)) + g(x(t))u(t) \tag{6.1}$$

$$\|u\| \leq u_{max} \tag{6.2}$$

where $x = [x_1 \cdots x_n]' \in \mathbb{R}^n$ denotes the vector of state variables, $u = [u_1 \cdots u_m]'$ is the vector of manipulated inputs, $u_{max} \geq 0$ denotes the bound on the manipulated inputs, $f(\cdot)$ is a sufficiently smooth $n \times 1$ nonlinear vector function, and $g(\cdot)$ is a sufficiently smooth $n \times m$ nonlinear matrix functions. Without loss of generality, it is assumed that the origin is the equilibrium point of the unforced system (i.e., $f(0) = 0$). Throughout the chapter, the notation, $\|\cdot\|$, will be used to denote the standard Euclidean norm of a vector, while the notation $\|\cdot\|_Q$ refers to the weighted norm, defined by $\|x\|_Q^2 = x'Qx$ for all $x \in \mathbb{R}^n$, where Q is a positive–definite symmetric matrix and x' denotes the transpose of x. In order to provide the necessary background for the main results in Section 6.2.2, we will briefly review in the remainder of this section the design procedure for, and the stability properties of, both the bounded and model predictive controllers, which constitute the basic components of our hybrid control scheme. For clarity of presentation, we will focus only on the state feedback problem where measurements of $x(t)$ are assumed to be available for all t (see Remark 6.14 below for a discussion on the issue of measurement sampling and how it can be handled).

Bounded Lyapunov-based control

Consider the system of Eqs.6.1-6.2, for which a family of control Lyapunov functions (CLFs), $V_k(x)$, $k \in \mathcal{K} \equiv \{1, \cdots, p\}$ has been found (see Remark 6.1 below for a discussion on the construction of CLFs). Using each control Lyapunov function, we construct, using the results in [204] (see also [91, 94]), the following continuous bounded control law:

$$u_k(x) = -k_k(x)(L_g V_k)'(x) := b_k(x) \tag{6.3}$$

where

$$k_k(x) = \frac{L_f V_k(x) + \sqrt{\left(L_f V_k(x)\right)^2 + \left(u_{max}\|(L_g V_k)'(x)\|\right)^4}}{\|(L_g V_k)'(x)\|^2 \left[1 + \sqrt{1 + \left(u_{max}\|(L_g V_k)'(x)\|\right)^2}\right]} \tag{6.4}$$

$L_f V_k(x) = \dfrac{\partial V_k(x)}{\partial x} f(x)$, $L_g V_k(x) = [L_{g_1} V_k(x) \cdots L_{g_m} V_k(x)]'$ and $g_i(x)$ is the i-th column of the matrix $g(x)$. For the above controller, it can be shown (see, for example, the Proof of Theorem 5.1 in Appendix D), using standard Lyapunov arguments, that whenever the closed–loop state trajectory, x, evolves within the state–space region described by the set:

$$\Phi_k(u_{max}) = \{x \in \mathbb{R}^n : L_f V_k(x) < u_{max}\|(L_g V_k)'(x)\|\} \tag{6.5}$$

then the controller satisfies the constraints, and the time-derivative of the Lyapunov function is negative–definite. Therefore, starting from any initial state within the set, $\Phi_k(u_{max})$, asymptotic stability of the origin of the constrained closed–loop system can be guaranteed, provided that the state trajectory remains within region described by $\Phi_k(u_{max})$ whenever $x \neq 0$. To ensure this, we consider initial conditions that belong to an invariant subset (preferably the largest), $\Omega_k(u_{max})$. One way to construct such a subset is using the level sets of V_k, i.e.,

$$\Omega_k(u_{max}) = \{x \in \mathbb{R}^n : V_k(x) \leq c_k^{max}\} \tag{6.6}$$

where $c_k^{max} > 0$ is the largest number for which $\Phi_k(u_{max}) \supset \Omega_k(u_{max}) \backslash \{0\}$. The union of the invariant regions described by the set:

$$\Omega(u_{max}) = \bigcup_{k=1}^{p} \Omega_k(u_{max}) \tag{6.7}$$

then provides an estimate of the stability region, starting from where the origin of the constrained closed–loop system, under the appropriate control law from the family of Eqs.6.3-6.4, is guaranteed to be asymptotically stable.

Remark 6.1 CLF-based stabilization of nonlinear systems has been studied extensively in the nonlinear control literature (see, for example, [22, 204, 112, 271]). The construction of constrained CLFs (i.e., CLFs that take the constraints into account) remains a difficult problem (especially for nonlinear systems) that is the subject of ongoing research. For several classes of nonlinear systems that arise commonly in the modeling of practical systems, systematic and computationally feasible methods are available for constructing unconstrained CLFs (CLFs for the unconstrained system) by exploiting the system structure. Examples include the use of quadratic functions for feedback linearizable systems and the use of back-stepping techniques to construct CLFs for systems in strict feedback form. In this chapter, the bounded controllers in Eqs.6.3-6.4 are designed using unconstrained CLFs, which are also used to explicitly characterize the associated regions of stability via Eqs.6.5-6.6. While the resulting estimates do not necessarily capture the entire domain of attraction, we will use them throughout the chapter only for a concrete illustration of the basic ideas of the results. It is possible to obtain substantially improved (i.e., less conservative) estimates by using, for example, a combination of several CLFs (see Section 6.2.3 for examples).

Model predictive control

In this section, we consider model predictive control of the system described by Eq.6.1, subject to the control constraints of Eq.6.2. In the literature, several MPC formulations are currently available, each with its own merits and limitations. While the hybrid predictive control structure is not restricted to any particular MPC formulation (see Remark 6.6 and Chapter 5 for further details on this issue), we will briefly describe here the "traditional" formulation for the purpose of highlighting some of the theoretical and computational issues involved in the nonlinear setting. For this case, MPC at state x and time t is conventionally obtained by solving, on-line, a finite

horizon optimal control problem [215] of the form:

$$P(x,t) \quad : \quad \min\{J(x,t,u(\cdot))|u(\cdot) \in S\} \tag{6.8}$$

$$s.t. \ \dot{x} \quad = \quad f(x) + g(x)u \tag{6.9}$$

where $S = S(t,T)$ is the family of piecewise continuous functions (functions continuous from the right), with period Δ, mapping $[t, t+T]$ into $\mathcal{U} := \{u \in \mathbb{R}^m : \|u\| \leq u_{max}\}$ and T is the specified horizon. Eq.6.9 is a nonlinear model describing the time evolution of the states x. A control $u(\cdot)$ in S is characterized by the sequence $\{u[k]\}$ where $u[k] := u(k\Delta)$. A control $u(\cdot)$ in S satisfies $u(t) = u[k]$ for all $t \in [k\Delta, (k+1)\Delta)$. The performance index is given by:

$$J(x,t,u(\cdot)) \quad = \quad \int_t^{t+T} \left[\|x^u(s;x,t)\|_Q^2 + \|u(s)\|_R^2\right] ds + F(x(t+T)) \tag{6.10}$$

where R and Q are strictly positive–definite, symmetric matrices and $x^u(s;x,t)$ denotes the solution of Eq.6.1, due to control u, with initial state x at time t and $F(\cdot)$ denotes the terminal penalty. The minimizing control $u^0(\cdot) \in S$ is then applied to the plant over the interval $[k\Delta, (k+1)\Delta)$ and the procedure is repeated indefinitely. This defines an implicit model predictive control law:

$$M(x) \quad = \quad argmin(J(x,t,u(\cdot))) \quad = u^0(t;x,t) \tag{6.11}$$

While the use of a nonlinear model as part of the optimization problem is desirable to account for the system's nonlinear behavior, it also raises a number of well-known theoretical and computational issues [215] that impact on the practical implementation of MPC. For example, in the nonlinear setting, the optimization problem is non-convex and, in general, harder to solve than in the linear case. Furthermore, the issue of closed–loop stability is typically addressed by introducing penalties and constraints on the state at the end of the finite optimization horizon (see [214] for a

survey of different constraints proposed in the literature). Imposing constraints adds to the computational complexity of the nonlinear optimization problem which must be solved at each time instance.

Even if the optimization problem could be solved in a reasonable time, any guarantee of closed–loop stability remains critically dependent upon making the appropriate choice of the initial condition, which must belong to the predictive controller's region of stability (or feasibility), which, in turn, is a complex function of the constraints, the performance objective, and the horizon length. However, the implicit nature of the nonlinear MPC law, obtained through repeated on-line optimization, limits our ability to obtain, *a priori* (i.e., before controller implementation), an explicit characterization of the admissible initial conditions starting from where a given MPC controller (with a fixed performance index and horizon length) is guaranteed to asymptotically stabilize the nonlinear closed–loop system. Therefore, the initial conditions and the horizon lengths are usually tested through closed–loop simulations, which can add to the computational burden prior to the implementation of MPC.

6.2.2 Controller switching strategies

In this section, we show how to reconcile the bounded nonlinear control and model predictive control approaches by means of switching schemes that provides a safety net for the implementation of MPC to nonlinear systems with input constraints. To this end, consider the constrained nonlinear system of Eqs.6.1-6.2, for which the bounded controllers of Eqs.6.3-6.4 and the predictive controller of Eqs.6.8-6.11 have been designed. The hybrid predictive control problem is formulated as the one of designing a set of switching laws that orchestrate the transition between MPC and the bounded controllers in a way that guarantees asymptotic stability of the origin

of the closed–loop system starting from any initial condition in the set, $\Omega(u_{max})$, defined in Eq.6.7, respects input constraints, and accommodates the performance requirements whenever possible. For a precise statement of the problem, the system of Eq.6.1 is first cast as a switched nonlinear system of the form:

$$\begin{aligned} \dot{x} &= f(x) + g(x)u_{i(t)} \\ \|u_i\| &\leq u_{max} \\ i(t) &\in \{1,2\} \end{aligned} \tag{6.12}$$

where $i : [0,\infty) \rightarrow \{1,2\}$ is the switching signal, which is assumed to be a piecewise continuous (from the right) function of time, implying that only a finite number of switches, between the predictive and bounded controllers, is allowed on any finite interval of time. The index, $i(t)$, which takes values in the set $\{1,2\}$, represents a discrete state that indexes the control input $u(\cdot)$, with the understanding that $i(t) = 1$ if and only if $u_i(x(t)) = M(x(t))$ and $i(t) = 2$ if and only if $u_i(x(t)) = b_k(x(t))$ for some $k \in \mathcal{K}$. Our goal is to construct a switching law, $i(t) = \psi(x(t), t)$, that provides the set of switching times that ensure stabilizing transitions between the predictive and bounded controllers, in the event that the predictive controller is unable to enforce closed–loop stability. This in turn determines the time-course of the discrete state, $i(t)$.

In the remainder of this section, two switching schemes that address the above problem are presented. The first scheme is given in Theorem 6.1 and focuses primarily on the issue of closed–loop stability, while the second scheme, given in Theorem 6.2, provides more flexible switching rules that guarantee closed–loop stability and, simultaneously, enhance the overall closed–loop performance beyond that obtained from the first scheme. The proofs of both theorems are given in Appendix E.

Stability-based controller switching

Theorem 6.1 *Consider the constrained nonlinear system of Eq.6.12, with any initial condition* $x(0) := x_0 \in \Omega_k(u_{max})$, *for some* $k \in \mathcal{K} \equiv \{1, \cdots, p\}$, *where* Ω_k *was defined in Eq.6.6, under the model predictive controller of Eqs.6.8-6.11. Also, let* $\bar{T} \geq 0$ *be the earliest time for which either the closed–loop state, under MPC, satisfies:*

$$L_f V_k(x(\bar{T})) + L_g V_k(x(\bar{T}))M(x(\bar{T})) \;\; \geq \;\; 0 \tag{6.13}$$

or the MPC algorithm fails to prescribe any control move. Then, the switching rule given by:

$$i(t) \;\; = \;\; \left\{ \begin{array}{ll} 1, & 0 \leq t < \bar{T} \\ & \\ 2, & t \geq \bar{T} \end{array} \right\} \tag{6.14}$$

where $i(t) = 1 \Leftrightarrow u_i(x(t)) = M(x(t))$ *and* $i(t) = 2 \Leftrightarrow u_i(x(t)) = b_k(x(t))$, *guarantees that the origin of the switched closed–loop system is asymptotically stable.*

Remark 6.2 Theorem 6.1 describes a stability-based switching strategy for control of nonlinear systems with input constraints. The main components of this strategy include the predictive controller, a family of bounded nonlinear controllers, with their estimated regions of constrained stability, and a high–level supervisor that orchestrates the switching between the controllers. A schematic representation of the hybrid control structure is shown in Figure 6.1. The implementation procedure of this hybrid control strategy is outlined below:

- Given the system model of Eq.6.1, the constraints on the input and the family of CLFs, design the bounded controllers using Eqs.6.3-6.4. Given the performance objective, set up the MPC optimization problem.

- Compute the stability region estimate for each of the bounded controllers, $\Omega_k(u_{max})$, using Eqs.6.5-6.6, for $k = 1, \ldots, p$, and $\Omega(u_{max}) = \bigcup_{k=1}^{p} \Omega_k(u_{max})$.

- Initialize the closed–loop system under MPC at any initial condition, x_0, within

Ω, and identify a CLF, $V_k(x)$, for which the initial condition is within the corresponding stability region estimate, Ω_k.

- Monitor the temporal evolution of the closed–loop trajectory (by checking Eq.6.13 at each time) until the earliest time that either Eq.6.13 holds or the MPC algorithm prescribes no solution, $\bar{T}$.
- If such a $\bar{T}$ exists, discontinue MPC implementation, switch to the k-th bounded controller (whose stability region contains x_0) and implement it for all future times.

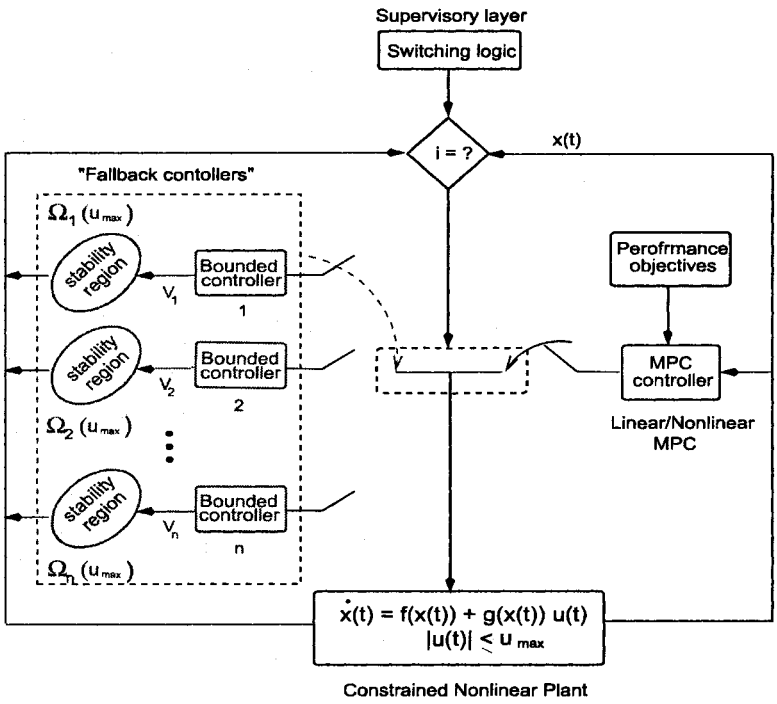

Figure 6.1: Schematic representation of the hybrid control structure merging MPC and a family of fall–back bounded controllers with their stability regions.

Remark 6.3 The use of multiple CLFs to design a family of bounded controllers, with their estimated regions of stability, allows us to initialize the closed–loop system from a larger set of initial conditions than in the case when a single CLF is used. Note, however, that once the initial condition is fixed, this determines both the region where

MPC operation will be confined (and monitored) and the corresponding fall–back bounded controller to be used in the event of MPC failure. If the initial condition falls within the intersection of several stability regions, then any of the corresponding bounded controllers can be used as the fall–back controller.

Remark 6.4 The relation of Eqs.6.13-6.14 represents the switching rule that the supervisor observes when contemplating whether a switch, between MPC and any of the bounded controllers at a given time, is needed. The left hand-side of Eq.6.13 is the rate at which the Lyapunov function grows or decays along the trajectories of the closed–loop system, under MPC, at time $\bar{T}$. By observing this rule, the supervisor tracks the temporal evolution of V_k under MPC such that whenever an increase in V_k is detected after the initial implementation of MPC (or if the MPC algorithm fails to prescribe any control move due, for example, to failure of the optimization algorithm), the predictive controller is disengaged from the closed–loop system, and the appropriate bounded controller is switched in, thus steering the closed–loop trajectory to the origin asymptotically. This switching rule, together with the choice of the initial condition, guarantee that the closed–loop trajectory, under MPC, never escapes $\Omega_k(u_{max})$ before the corresponding bounded controller can be activated.

Remark 6.5 In the case when the condition of Eq.6.13 is never fulfilled (i.e., MPC continues to be feasible for all times and the Lyapunov function continues to decay monotonically for all times ($\bar{T} = \infty$)), the switching rule of Eq.6.14 ensures that only MPC is implemented for all times and that no switching to the fall–back controllers takes place. In this case, MPC is stabilizing and its performance is fully recovered by the hybrid control structure. This particular feature underscores the central objective of the hybrid control structure, which is not to replace or subsume MPC but, instead, to provide a safe environment for the implementation of any optimal predictive control policy for which *a priori* guarantees of stability are not available. Note also that, to the extent that stability under MPC is captured by the given Lyapunov function, the notion of switching, as described in Theorem 6.1, does not result in

loss of performance, since the transition to the bounded controller takes place only if MPC is infeasible or destabilizing. Clearly, under these circumstances the issue of performance is not very meaningful for the predictive controller.

Remark 6.6 The fact that closed–loop stability is guaranteed, for all $x_0 \in \Omega$ (through supervisory switching), independently of whether MPC itself is stabilizing or not, allows us to use any desired MPC formulation within the switching scheme (and not just the one mentioned in Theorem 6.1), whether linear or nonlinear, and with or without terminal stability constraints or terminal penalties, without concern for loss of stability. This flexibility of using any desired MPC formulation has important practical implications for reducing the computational complexities that arise in implementing predictive control algorithms to nonlinear systems by allowing, for example, the use of less-computationally demanding NMPC formulations, or even the use of linear MPC algorithms instead (based on linearized models of the plant), with guaranteed stability (see Section 6.2.3 for examples). In all cases, by embedding the operation of the chosen MPC algorithm within the large and well-defined stability regions of the bounded controllers, the switching scheme provides a safe fall–back mechanism that can be called upon at any moment to preserve closed–loop stability should MPC become unable to achieve closed–loop stability. Finally, we note that the Lyapunov functions used by the bounded controllers can also be used as a guide to design and tune the MPC in case a Lyapunov-based constraint is used at the end of the prediction horizon.

Remark 6.7 Note that no assumption is made regarding how fast the MPC optimization needs to be solved since, even if this time is relatively significant and the plant dynamics are unstable, the implementation of the switching rule in Theorem 6.1 guarantees an "instantaneous" switch to the appropriate stabilizing bounded controller before such delays can adversely affect closed–loop stability (the times needed to check Eqs.6.13-6.14 and compute the control action of the bounded controller are insignificant as they involve only algebraic computations). This feature is valuable

when computationally-intensive NMPC formulations fail, in the course of the online optimization, to provide an acceptable solution in a reasonable time. In this case, switching to the bounded controller allows us to safely abort the optimization without loss of stability.

Remark 6.8 One of the important issues in the practical implementation of finite–horizon MPC is the selection of the horizon length. It is well known that this selection can have a profound effect on nominal closed–loop stability as well as the size and complexity of the optimization problem. For NMPC, however, *a priori* knowledge of the shortest horizon length that guarantees closed–loop stability, from a given set of initial conditions (alternatively, the set of feasible initial conditions for a given horizon length) is not available. Therefore, in practice the horizon length is typically chosen using *ad hoc* selection criteria, tested through extensive closed–loop simulations, and varied, if necessary, to achieve stability. In the switching scheme of Theorem 6.1, closed–loop stability is maintained independently of the horizon length. This allows the predictive control designer to choose the horizon length solely on the basis of what is computationally practical for the size of the optimization problem, and without increasing, unnecessarily, the horizon length (and consequently the computational load) out of concern for stability. Furthermore, even if a conservative estimate of the necessary horizon length were to be ascertained for a small set of initial conditions before MPC implementation (say through extensive closed–loop simulations and testing), then if some disturbance were to drive the state outside of this set during the on-line implementation of MPC, this estimate may not be sufficient to stabilize the closed–loop system from the new state. Clearly, in this case, running extensive closed–loop simulations on-line to try to find the new horizon length needed is not a feasible option, considering the computational difficulties of NMPC as well as the significant delays that would be introduced until (and if) the new horizon could be determined. In contrast to the on-line re-tuning of MPC, stability can be preserved by switching to the fall–back controllers (provided that the disturbed state still lies within Ω).

Remark 6.9 When compared with other MPC-based approaches, the proposed hybrid control scheme is conceptually aligned with Lyapunov-based approaches in the sense that it, too, employs a Lyapunov stability condition to guarantee asymptotic closed–loop stability. However, this condition is enforced at the supervisory level, via continuous monitoring of the temporal evolution of V_k and explicitly switching between two controllers, rather than being incorporated in the optimization problem, as is customarily done in Lyapunov-based MPC approaches, whether as a terminal inequality constraint (e.g., contractive MPC [238, 175], CLF-based RHC for unconstrained nonlinear systems [239]) or through a CLF-based terminal penalty (e.g., [288, 290]). The methods proposed in these works do not provide an explicit characterization of the set of states starting from where feasibility and/or stability is guaranteed *a priori*. Furthermore, the idea of switching to a fall–back controller with a well-characterized stability region, in the event that the MPC controller does not yield a feasible solution, is not considered in these approaches.

Enhancing closed–loop performance

The switching rule in Theorem 6.1 requires monitoring only one of the CLFs (any one for which $x_0 \in \Omega_k$) and does not permit any transient increase in this CLF under MPC (by switching immediately to the appropriate bounded controller). While this condition is sufficient to guarantee closed–loop stability, it does not take full advantage of the behavior of other CLFs at the switching time. For example, even though a given CLF, say V_1, may start increasing at time $\bar{T}$ under MPC, another CLF, say V_2, (for which $x(\bar{T})$ lies inside the corresponding stability region) may still be decreasing (see Figure 6.2). In this case, it would be desirable to keep MPC in the closed–loop (rather than switch to the bounded controller) and start monitoring the growth of V_2 instead of V_1, because if V_2 continues to decay, then MPC can be kept active for all times and its performance fully recovered. To allow for such flexibility, we extend in

the remainder of this section the switching strategy of Theorem 6.1 by relaxing the switching rule. This is formalized in the following theorem whose proof is given in the Appendix E.

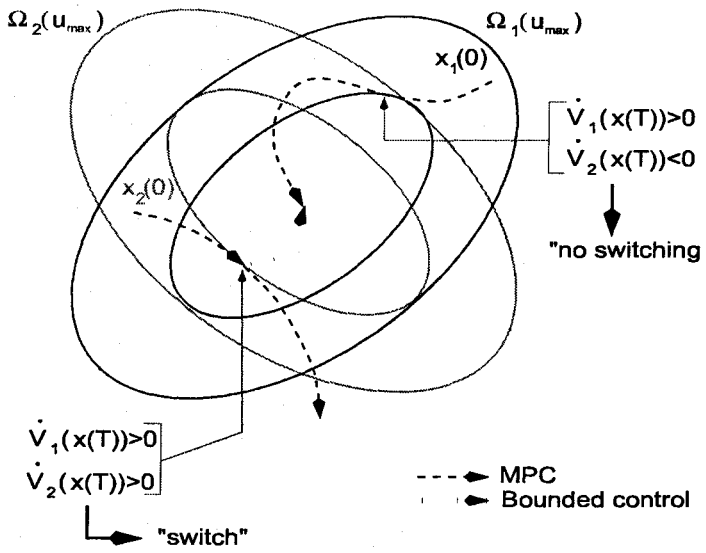

Figure 6.2: Schematic representation illustrating the main idea of the controller switching scheme proposed in Theorems 6.1 and 6.2.

Theorem 6.2 *Consider the constrained nonlinear system of Eq.6.12, with any initial condition* $x(0) := x_0 \in \Omega(u_{max})$, *where* $\Omega(u_{max})$ *was defined in Eq.6.7, under the model predictive controller of Eqs.6.8-6.11. Let* $T_k \geq 0$ *be the earliest time for which:*

$$\begin{aligned} V_k(x(T_k))) &\leq c_k^{max} \\ L_f V_k(x(T_k)) + L_g V_k(x(T_k)) M(x(T_k)) &\geq 0, \quad k \in \mathcal{K} \end{aligned} \tag{6.15}$$

and define:

$$T_k^*(t) = \left\{ \begin{array}{ll} T_k, & 0 \leq t \leq T_k \\ 0, & t > T_k \end{array} \right\} \tag{6.16}$$

Then, the switching rule given by:

$$i(t) = \left\{ \begin{array}{ll} 1, & 0 \leq t < T^* \\ 2, & t \geq T^* \end{array} \right\} \tag{6.17}$$

where $T^* = \min\{T^i, T^f\}$, $T^i \geq 0$ *is the earliest time for which the MPC algorithm fails to prescribe any control move, and* $T^f = \max_j\{T_j^*\}$ *for all* j *such that* $x(t) \in \Omega_j(u_{max})$, *guarantees that the origin of the switched closed–loop system is asymptotically stable.*

Remark 6.10 The implementation of the switching scheme proposed in Theorem 6.2 can be understood as follows:

- Initialize the closed–loop system using MPC at any initial condition, x_0, within Ω, and start monitoring the growth of all the Lyapunov functions whose corresponding stability regions contain the state.
- The supervisor disregards (i.e., permanently stops monitoring) any CLF whose value ceases to decay (i.e., any CLF for which the condition of Eq.6.15 holds) by setting the corresponding $T_k^*(t)$ to zero for all future times.
- As the closed–loop trajectory continues to evolve, the supervisor includes in the pool of Lyapunov functions it monitors any CLF for which the state enters the corresponding stability region, provided that this CLF has not been discarded at some earlier time.
- Continue implementing MPC as long as at least one of the CLFs being monitored is decreasing and the MPC algorithm yields a solution.
- If at any time, there is no active CLF (this corresponds to T^f), or if the MPC algorithm fails to prescribe any control move (this corresponds to T^i), switch to the bounded controller whose stability region contains the state at this time, else the MPC controller stays in the closed–loop system.

Remark 6.11 The purpose of permanently disregarding a given CLF, once its value begins to increase, is to avoid (or "break") a potential perpetual cycle in which the value of such a CLF increases (at times when other CLFs are decreasing) and then decreases (at times when other CLFs are increasing) and keeps repeating this pattern without decaying to zero. The inclusion of such a CLF among the pool of active CLFs

used to decide whether MPC should be kept active, would result in MPC staying in the closed–loop indefinitely, but without actually converging to the origin (i.e., only boundedness of the closed–loop state can be established but not asymptotic stability). Instead of disregarding, for all future times, a CLF that begins to increase at some point, however, an alternative strategy is to consider such a CLF in the supervisory decision-making only if its value, at the current state, falls below the value from which it began to increase. This idea is similar to the one used in the stability analysis of switched systems using multiple Lyapunov functions (MLFs) (see Chapter 7 for further details on this issue). The greater CLF-monitoring flexibility resulting from this policy can increase the likelihood of MPC implementation and enhanced closed–loop performance, while still guaranteeing asymptotic stability.

Remark 6.12 The switching schemes proposed in Theorems 6.1 and 6.2 can be further generalized to allow for multiple switchings between MPC and the bounded controllers. For example, if a given MPC is initially found infeasible (due, for example, to some terminal equality constraints), the bounded controller can be activated initially, but need not stay in the closed–loop system for all future times. Instead, it could be employed only until it brings the closed–loop trajectory to a point where MPC becomes feasible, at which time MPC can take over (see Section 6.2.3 for illustrations of this scenario). This scheme offers the possibility of further enhancement in the closed–loop performance by implementing MPC for all the times that it is feasible (instead of using the bounded controller). If MPC runs into any feasibility or stability problems, then the bounded controller can be re-activated. Chattering problems, due to back and forth switching, are avoided by allowing only a finite number of switches over any finite time-interval.

Remark 6.13 Note that the implementation of the switching schemes proposed in Theorems 6.1 and 6.2 can be easily adapted to the case when actuator dynamics are not negligible and, consequently, a sudden change in the control action (resulting from switching between controllers) may not be achieved instantaneously. A new estimate

of the stability region under the bounded controllers can be generated by sufficiently "stepping back" from the boundary of the original stability region estimate, in order to prevent the escape of the closed–loop trajectory as a result of the implementation of possibly incorrect control action for some time (due to the delay introduced by the actuator dynamics). The switching schemes can then be applied as described in Theorems 6.1 and 6.2, using the revised estimate of the stability region for the family of bounded controllers.

Remark 6.14 When the proposed hybrid control schemes are applied to a process on-line, state measurements are typically available only at discrete sampling instants (and not continuously). In this case, the restricted access that the supervisor has to the state evolution between sampling times can lead to the possibility that the closed–loop state trajectory under MPC may leave the stability region without being detected, particularly if the initial condition is close to the boundary of the stability region and/or the sampling period is too large. In such an event, switching to the bounded controller at the next sampling time may be too late to recover from the instability of MPC. To guard against this possibility, the switching rules in Theorems 6.1 and 6.2 can be modified by restricting the implementation of MPC within a subset of the stability region, computed such that, starting from this subset, the system trajectory is guaranteed to remain within the stability region after one sampling period. Explicit estimates of this subset, which is parameterized by the sampling period, can be readily obtained off-line by computing (or estimating) the time-derivative of the Lyapunov function under the maximum allowable control action and then integrating both sides of the resulting inequality over one sampling period. Note that this computation of a "worst-case" estimate does not require knowledge of the solution of the closed–loop system.

Remark 6.15 The hybrid predictive control schemes proposed in this chapter can be extended to deal with the case when both input and state constraints are present. In one possible extension, state constraints would be incorporated directly as part of

the constrained optimization problem that yields the model predictive control law. In addition, estimates of the stability regions for the bounded controllers would be obtained by intersecting the region described by Eq.6.5 with the region described by the state constraints, and computing the largest invariant subset within the intersection. Using these estimates (which now account for both input and state constraints), implementation of the switching schemes can proceed following the same logic outlined for each case.

6.2.3 Applications to chemical process examples

In this section, we present two simulation studies of chemical process examples to demonstrate the implementation of the proposed hybrid predictive control structure and evaluate its effectiveness.

Application to a chemical reactor example

We consider a continuous stirred tank reactor where an irreversible, first-order exothermic reaction of the form $A \xrightarrow{k} B$ takes place. The inlet stream consists of pure A at flow rate F, concentration C_{A0} and temperature T_{A0}. Under standard modeling assumptions, the mathematical model for the process takes the form:

$$\begin{aligned} \dot{C_A} &= \frac{F}{V}(C_{A0} - C_A) - k_0 \exp\left(\frac{-E}{RT_R}\right) C_A \\ \dot{T_R} &= \frac{F}{V}(T_{A0} - T_R) + \frac{(-\Delta H)}{\rho c_p} k_0 \exp\left(\frac{-E}{RT_R}\right) C_A + \frac{UA}{\rho c_p V}(T_c - T) \end{aligned} \tag{6.18}$$

where C_A denotes the concentration of the species A, T_R denotes the temperature of the reactor, T_c is the temperature of the coolant in the surrounding jacket, U is the heat–transfer coefficient, A is the jacket area, V is the volume of the reactor, k_0, E, ΔH are the pre-exponential constant, the activation energy, and the enthalpy of the reaction, c_p and ρ, are the heat capacity and fluid density in the reactor. The

values of all process parameters can be found in Table 6.1. At the nominal operating condition of $T_c^{nom} = 302\ K$, the system has three equilibrium points, one of which is unstable. The control objective is to stabilize the reactor at the unstable equilibrium point $(C_A^s,\ T_R^s) = (0.52, 398.9)$ using the coolant temperature, T_c, as the manipulated input with constraints: $275\ K \leq T_c \leq 370\ K$.

Table 6.1: Process parameters and steady-state values for the reactor of Eq.6.18.

V	$=$	100.0	L
E/R	$=$	8000	K
C_{A0}	$=$	1.0	mol/L
T_{A0}	$=$	400.0	K
ΔH	$=$	-2.0×10^5	J/mol
k_0	$=$	4.71×10^8	min^{-1}
c_p	$=$	1.0	$J/g.K$
ρ	$=$	1000.0	g/L
UA	$=$	1.0×10^5	$J/min.K$
F	$=$	100.0	L/min
C_A^s	$=$	0.52	mol/L
T_R^s	$=$	398.97	K
T_c^{nom}	$=$	302	K

Defining $x = [x_1\ \ x_2]' = [(C_A - C_A^s)\ \ (T_R - T_R^s)]'$ and $u = T_c - T_c^{nom}$, the process model of Eq.6.18 can be written in the form of Eq.6.1. Defining an auxiliary output, $y = h(x) = x_1$ (for the purpose of designing the controller), and using the invertible coordinate transformation: $\xi = [\xi_1\ \xi_2]' = T(x) = [x_1\ f_1(x)]'$, where $f_1(x) = \dot{x}_1$, the system of Eq.6.18 can be transformed into the following partially linear form:

$$\dot{\xi} = A\xi + bl(\xi) + b\alpha(\xi)u \tag{6.19}$$

where $A = \begin{bmatrix} 0 & 1 \\ 0 & 0 \end{bmatrix}$, $b = [0\ 1]'$, $l(\xi) = L_f^2 h(T^{-1}(\xi))$ is the second-order Lie derivative of $h(\cdot)$ along the vector field $f(\cdot)$, $\alpha(\xi) = L_g L_f h(T^{-1}(\xi))$ is the mixed order Lie derivative. The system of Eq.6.19 will be used to design the bounded controllers and compute their estimated regions of stability. A common choice of CLFs for this

system is quadratic functions of the form, $V_k = \xi' P_k \xi$, where the positive–definite matrix P_k is chosen to satisfy the Riccati matrix inequality: $A'P_k + P_k A - P_k bb' P_k < 0$. The following matrices

$$P_1 = \begin{bmatrix} 1.45 & 1.0 \\ 1.0 & 1.45 \end{bmatrix}, \; P_2 = \begin{bmatrix} 0.55 & 0.1 \\ 0.1 & 0.55 \end{bmatrix}, \; P_3 = \begin{bmatrix} 8.02 & 3.16 \\ 3.16 & 2.53 \end{bmatrix} \tag{6.20}$$

were used to construct a family of three CLFs and three bounded controllers, and compute their stability region estimates, Ω_k, $k = 1, 2, 3$, in the ξ-coordinate system. The corresponding stability regions in the (C_A, T_R) coordinate system are then computed using the transformation $\xi = T(x)$ defined earlier. The union of these regions, Ω', is shown in Figure 6.3.

For the design of the predictive controller, a linear MPC formulation (based on the linearization of the process model around the unstable equilibrium point) with terminal equality constraints, $x(t + T) = 0$, is chosen for the sake of illustration (other MPC formulations that use terminal penalties, instead of terminal equality constraints, could also be used). The parameters in the objective function of Eq.6.10 are chosen as $Q = qI$, with $q = 1$, $R = rI$, with $r = 1.0$, and $F = 0$. We also choose a horizon length of $T = 0.25$ in implementing the MPC controller. The resulting quadratic program is solved using the MATLAB subroutine QuadProg, and the set of nonlinear ODEs is integrated using the MATLAB solver ODE45.

As shown by the solid trajectory in Figure 6.3, starting from the initial condition $[C_A(0) \;\; T_R(0)]' = [0.46 \;\; 407.0]'$, MPC using a horizon length of $T = 0.25$ yields a feasible solution, and when implemented in the closed–loop, stabilizes the nonlinear closed–loop system. The corresponding state and input profiles are shown in Figures 6.4(a)-(c). Starting from the initial condition $[C_A(0) \;\; T_R(0)]' = [0.45 \;\; 385.0]'$ (dashed lines in Figures 6.3-6.4), however, the linear MPC controller is infeasible. Recognizing that the initial condition is within the stability region estimate, Ω'_3, the supervisor

implements the third bounded controller, while continuously checking feasibility of MPC. At $t = 0.4$, the predictive controller becomes feasible and, therefore, the supervisor switches to MPC and keeps monitoring the evolution of V_3. In this case, the value of V_3 keeps decreasing and MPC stays in the closed–loop for all future times, thus asymptotically stabilizing the nonlinear plant. Note that, from the same initial condition, if the horizon length in the MPC is increased to $T = 0.5$, MPC yields a feasible solution and, when implemented, asymptotically stabilizes the closed–loop system (dotted lines in Figures 6.3-6.4). However, the initial feasibility, based on the linearized model, does not necessarily imply that the predictive controller will be stabilizing, or for that matter even feasible at future times. Furthermore, this value of the horizon length (which yields a feasible solution) could not be determined *a priori* (without actually solving the optimization problem with the given initial condition), and stability of the closed–loop could not be ascertained, *a priori*, without running the closed–loop simulation in its entirety.

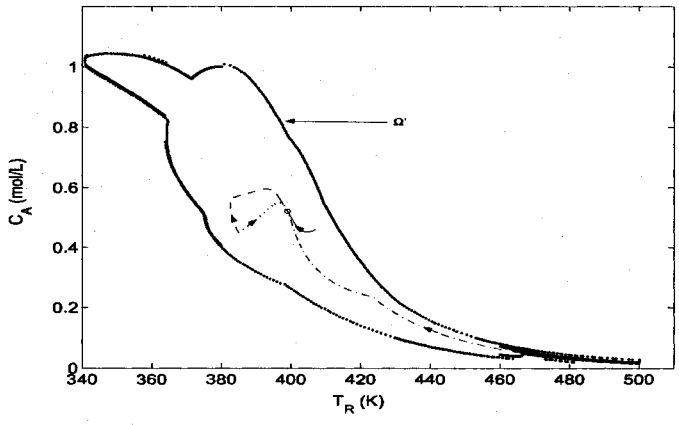

Figure 6.3: Implementation of the proposed hybrid control structure: Closed–loop state trajectory under MPC with $T = 0.25$ (solid trajectory), under the switched MPC/bounded controller(3) with $T = 0.25$ (dashed trajectory), under MPC with $T = 0.5$ (dotted trajectory), and under the switched bounded controller(2)/MPC with $T = 0.5$ (dash-dotted line).

While our particular choice of implementing linear MPC (using the linearized model) facilitates implementation by making the optimization problem more easily solvable, the stabilizability of a given initial condition is limited, not only by the possibility of insufficient horizon length, but also by the linearization procedure itself. To demonstrate this, we consider an initial condition, $[C_A(0) \;\; T_R(0)]' = [0.028 \;\; 484.0]'$, belonging to the stability region Ω', (dash-dotted lines in Figures 6.3-6.4). For this initial condition, linear MPC is found infeasible, no matter how large T is chosen to be, suggesting that this initial condition is outside the feasibility region based on the linear model. Therefore, using the Lyapunov function, V_2, (since the initial condition belongs to Ω_2'), the supervisor activates the second bounded controller which brings the state trajectory closer to the desired equilibrium point, while continuously checking feasibility of linear MPC. At $t = 1.925$, the predictive controller with $T = 0.5$ is found to be feasible and is, therefore, employed in the closed–loop system to asymptotically stabilize the closed–loop system.

To demonstrate some of the performance benefits of using the more flexible switching rules in Theorem 6.2, we consider the same control problem, described above, with relaxed constraints on the manipulated input: $250\ K \leq T_c \leq 500\ K$. Using these constraints, a new set of four bounded controllers are designed using a family of four CLFs of the form $V_k = \xi' P_k \xi$, $k = 1, 2, 3, 4$, where:

$$P_1 = \begin{bmatrix} 1.03 & 0.32 \\ 0.32 & 3.26 \end{bmatrix}, P_2 = \begin{bmatrix} 0.4 & 0.32 \\ 0.32 & 1.28 \end{bmatrix}, P_3 = \begin{bmatrix} 1.45 & 1.0 \\ 1.0 & 1.45 \end{bmatrix}, P_4 = \begin{bmatrix} 4.78 & 2.24 \\ 2.24 & 2.14 \end{bmatrix} \tag{6.21}$$

The stability region estimates of the controllers, Ω_k, $k = 1, 2, 3, 4$, are depicted in Figure 6.5. The relaxed input constraints are also incorporated in the design of the predictive controller, using the same MPC formulation employed in the preceding simulations. Starting from the initial condition $[C_A(0) \;\; T_R(0)]' = [0.75 \;\; 361.0]'$

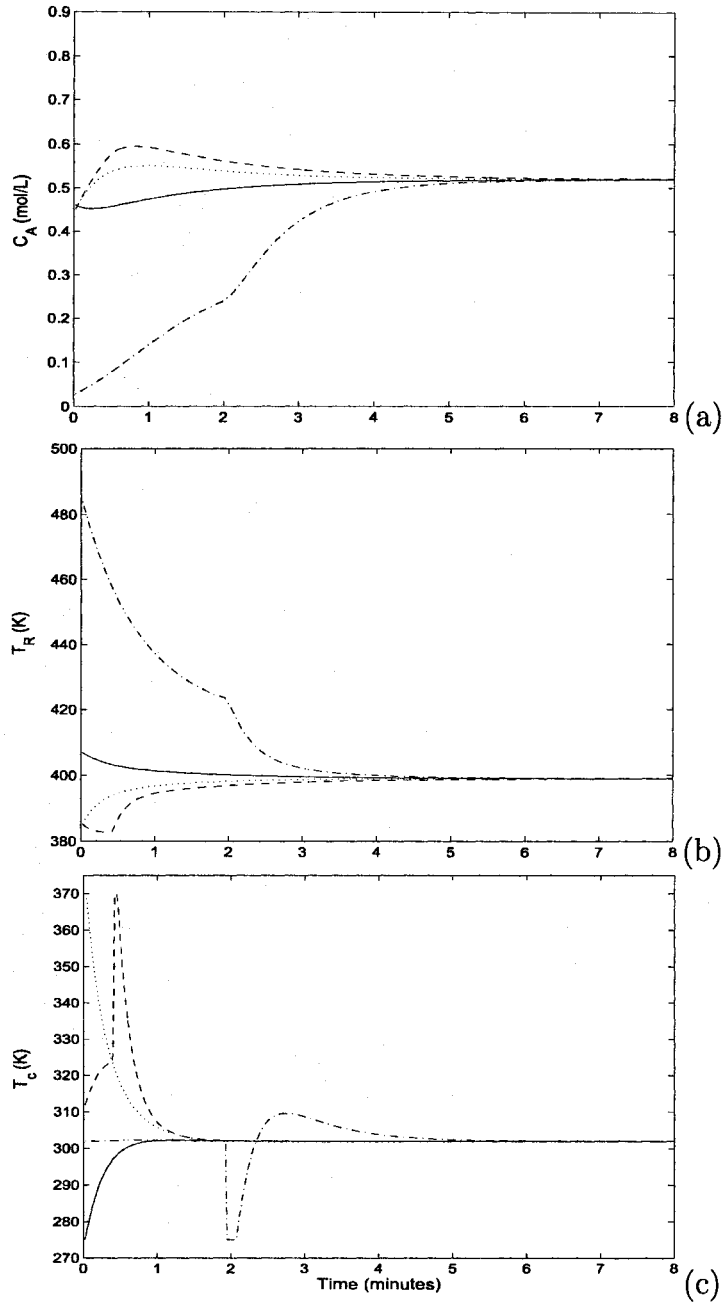

Figure 6.4: Closed-loop reactant concentration profile (a), reactor temperature profile (b) and coolant temperature profile (c) under MPC with $T = 0.25$ (solid trajectory), under the switched MPC/bounded controller(3) with $T = 0.25$ (dashed trajectory), under MPC with $T = 0.5$ (dotted trajectory), and under the switched bounded controller(2)/MPC with $T = 0.5$ (dash-dotted line).

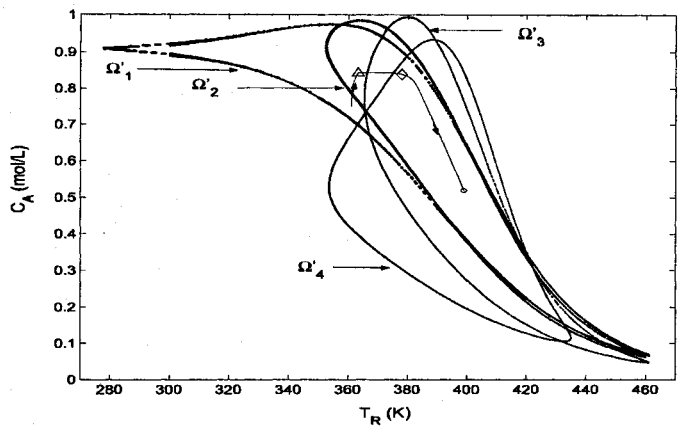

Figure 6.5: Closed-loop state trajectory under the switching rules of Theorem 6.2 with $T = 0.1$ for MPC.

(Figures 6.6(a)-(c)), the predictive controller, with $T = 0.1$, does not yield a feasible solution and, therefore, the supervisor implements the first bounded controller, using V_1, instead. At $t = 0.95$, however, MPC yields a feasible solution and, therefore, the supervisor switches to MPC. Even though $\dot{V}_1 > 0$ at this time, recognizing the fact that the state at this time ($[0.84 \;\; 363.3]'$, denoted by $\triangle$ in Figure 6.5) belongs to Ω'_2 and that $\dot{V}_2 < 0$, the supervisor continues to implement MPC while monitoring $\dot{V}_2$ (instead of V_1). At $t = 1.1$, the supervisor detects that $\dot{V}_2 > 0$. However, the state at this time ($[0.84 \;\; 378.0]'$, denoted by $\diamondsuit$ in Figure 6.5) is within Ω'_3 where $\dot{V}_3 < 0$. Therefore, the supervisor continues the implementation of MPC while monitoring V_3. From this point onwards, V_3 continues to decay monotonically and MPC is implemented in the closed–loop system for all future times to achieve asymptotic stability. Note that the switching scheme of Theorem 6.1 would have dictated a switch back to the first bounded controller at $t = 0.95$ and would not have allowed for MPC to be implemented in closed–loop, leading to a total cost of $J = 1.81 \times 10^6$ for the objective function of Eq.6.10. The switching rules in Theorem 6.2, on the other hand, allow the implementation of MPC for all the times that it is feasible,

leading to a lower total cost of $J = 1.64 \times 10^5$, while guaranteeing, at the same time, closed–loop stability.

Application to a continuous crystallizer example

We consider a continuous crystallizer described by a fifth-order moment model of the following form:

$$\begin{aligned} \dot{x}_0 &= -x_0 + (1 - x_3) Da \exp\left(\frac{-F}{y^2}\right) \\ \dot{x}_1 &= -x_1 + y x_0 \\ \dot{x}_2 &= -x_2 + y x_1 \\ \dot{x}_3 &= -x_3 + y x_2 \\ \dot{y} &= \frac{1 - y - (\alpha - y) y x_2}{1 - x_3} + \frac{u}{1 - x_3} \end{aligned} \tag{6.22}$$

where x_i, $i = 0, 1, 2, 3$, are dimensionless moments of the crystal size distribution, y is a dimensionless concentration of the solute in the crystallizer, and u is a dimensionless concentration of the solute in the feed (the reader may refer to [54, 89] for a detailed process description, population balance modeling of the crystal size distribution and derivation of the moments model, and to [62] for further results and references in this area). The values of the dimensionless process parameters are chosen to be: $F = 3.0$, $\alpha = 40.0$ and $Da = 200.0$. For these values, and at the nominal operating condition of $u^{nom} = 0$, the above system has an unstable equilibrium point, surrounded by a stable limit cycle. The control objective is to stabilize the system at the unstable equilibrium point, $x^s = [x_o^s \; x_1^s \; x_2^s \; x_3^s \; y^s]' = [0.0471, \; 0.0283, \; 0.0169, \; 0.0102, \; 0.5996]'$, where the superscript s denotes the desired steady–state, by manipulating the dimensionless solute feed concentration, u, subject to the constraints: $-1 \leq u \leq 1$.

To facilitate the design of the bounded controller, we initially transform the system of Eq.6.22 into the normal form. To this end, we define the auxiliary output variable,

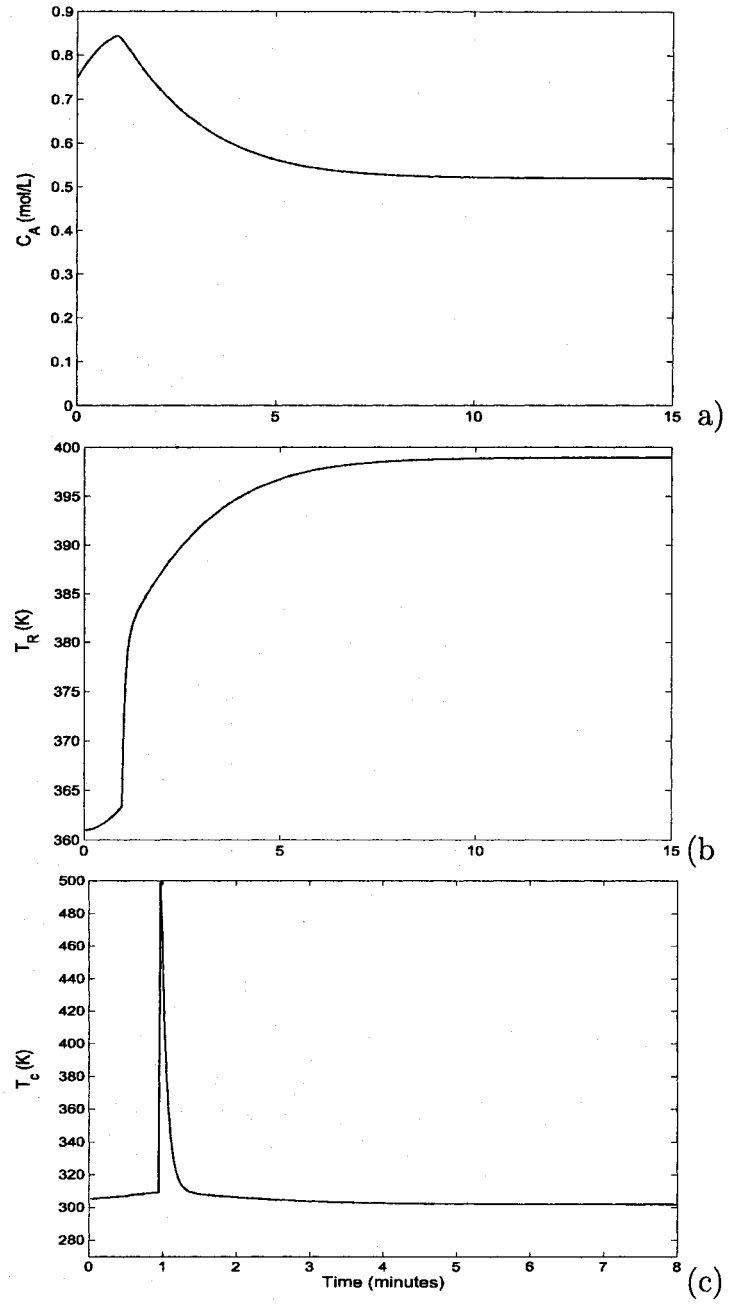

Figure 6.6: Closed-loop reactant concentration profile (a), reactor temperature profile (b) and coolant temperature profile (c) under the switching scheme of Theorem 6.2 with $T = 0.1$ for MPC.

$\bar{y} = h(x) = x_0$, and introduce the invertible coordinate transformation: $[\xi' \ \eta']' = T(x) = [x_0 \ f_1(x) \ x_1 \ x_2 \ x_3]'$, where $\xi = [\xi_1 \ \xi_2]' = [x_0 \ f_1(x)]'$, $\bar{y} = \xi_1$, $f_1(x) = -x_0 + (1 - x_3)Da\exp(-F/y^2)$, and $\eta = [\eta_1 \ \eta_2 \ \eta_3]' = [x_1 \ x_2 \ x_3]'$. The state-space description of the system in the transformed coordinates takes the form:

$$\begin{aligned} \dot{\xi} &= A\xi + bl(\xi,\eta) + b\alpha(\xi,\eta)u \\ \dot{\eta} &= \Psi(\eta,\xi) \end{aligned} \tag{6.23}$$

where $A = \begin{bmatrix} 0 & 1 \\ 0 & 0 \end{bmatrix}$, $b = [0 \ 1]'$, $l(\xi,\eta) = L_f^2 h(T^{-1}(\xi,\eta))$ is the second-order Lie derivative of the scalar function, $h(\cdot)$, along the vector field $f(\cdot)$, and $\alpha(\xi,\eta) = L_g L_f h(T^{-1}(\xi,\eta))$ is the mixed Lie derivative. The forms of $f(\cdot)$ and $g(\cdot)$ can be obtained by re-writing the system of Eq.6.22 in the form of Eq.6.1, and are omitted for brevity.

The partially-linear ξ-subsystem in Eq.6.23 is used to design a bounded controller that stabilizes the full interconnected system of Eq.6.23 and, consequently, the original system of Eq.6.22. For this purpose, a quadratic function of the form, $V_\xi = \xi' P \xi$, is used as a CLF in the controller synthesis formula of Eq.6.3, where the positive–definite matrix, P, is chosen to satisfy the Riccati matrix equality: $A'P + PA - Pbb'P = -Q$ where Q is a positive–definite matrix. An estimate of the region of constrained closed–loop stability for the full system is obtained by defining a composite Lyapunov function of the form $V_c = V_\xi + V_\eta$, where $V_\eta = \eta' P_\eta \eta$ and P_η is a positive–definite matrix, and choosing a level set of V_c, Ω_c, for which $\dot{V}_c < 0$ for all x in Ω_c. The two-dimensional projections of the stability region are shown in Figure 6.7 for all possible combinations of the system states.

In designing the predictive controller, a linear MPC formulation, with a terminal equality constraint of the form $x(t+T) = 0$, is chosen (based on the linearization of the process model of Eq.6.22 around the unstable equilibrium point). The parameters

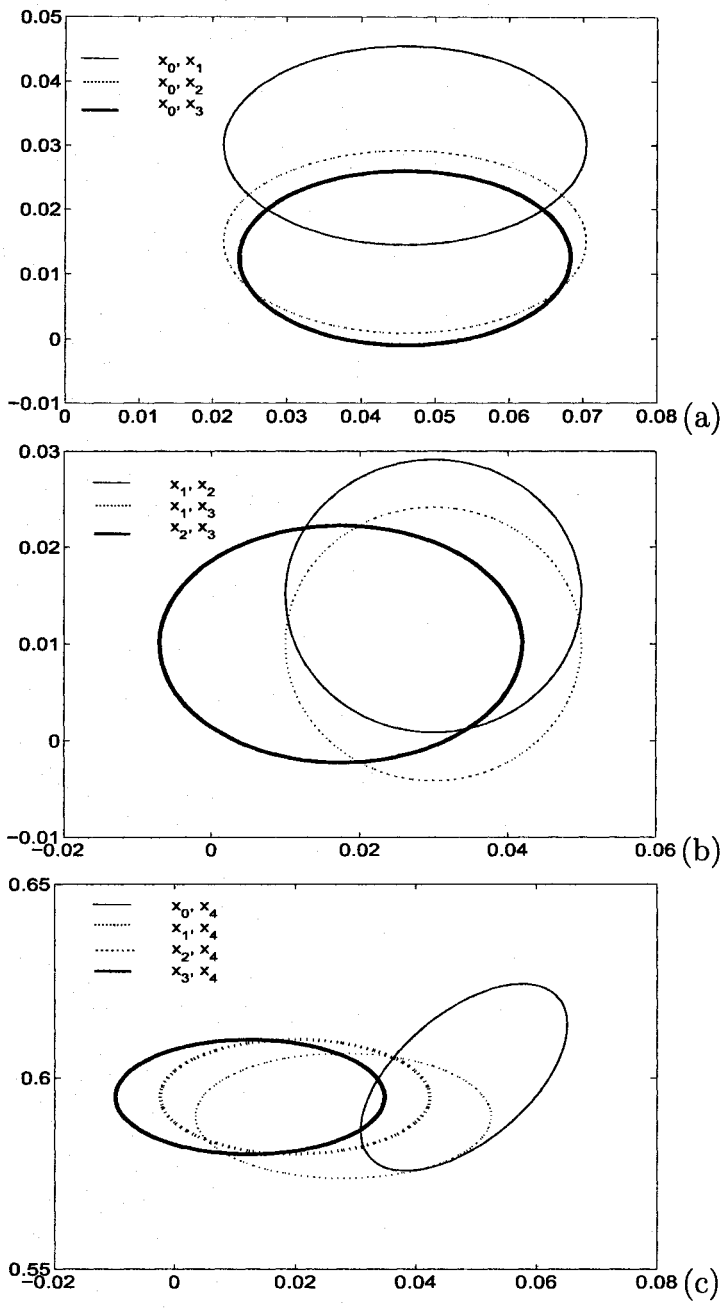

Figure 6.7: Implementation of the proposed hybrid control structure to a continuous crystallizer: two-dimensional projections of the stability region for the 10 distinct combinations of the process states.

in the objective function of Eq.6.10 are taken to be: $Q = qI$, with $q = 1$, $R = rI$, with $r = 1.0$, and $F = 0$. We also choose a horizon length of $T = 0.5$ in implementing the predictive controller. The resulting quadratic program is solved using the MATLAB subroutine QuadProg, and the nonlinear closed–loop system is integrated using the MATLAB solver ODE45.

In the first set of simulation runs, we test the ability of the predictive controller to stabilize the closed–loop system starting from the initial condition, $x(0) = [0.046 \;\; 0.0277 \;\; 0.0166 \;\; 0.01 \;\; 0.58]'$. The result is shown by the solid lines in Figure 6.8(a)–(e) where it is seen that the predictive controller, with a horizon length of $T = 0.5$, is able to stabilize the closed–loop system at the desired equilibrium point. Starting from the initial condition $x(0) = [0.032 \;\; 0.035 \;\; 0.010 \;\; 0.009 \;\; 0.58]'$, however, the predictive controller yields no feasible solution. If the terminal equality constraint is removed, to make MPC yield a feasible solution, we see from the dashed lines in Figure 6.8(a)–(e) that the resulting control action cannot stabilize the closed–loop system and sends the system states into a limit cycle. On the other hand, when the switching scheme of Theorem 6.1 is employed, the supervisor immediately switches to the bounded controller which in turn stabilizes the closed–loop system at the desired equilibrium point. This is depicted by the dotted lines in Figure 6.8(a)–(e)). The manipulated input profiles for the three scenarios are shown in Figure 6.8(f).

6.3 Robust hybrid predictive control of nonlinear systems

In the previous section, a hybrid predictive control strategy was developed for nonlinear systems with no uncertainty. In the presence of uncertainty, however, the nominal controllers (designed without taking the uncertainty into account) may not be stabilizing as the uncertainty fundamentally alters the nominal stability region of the

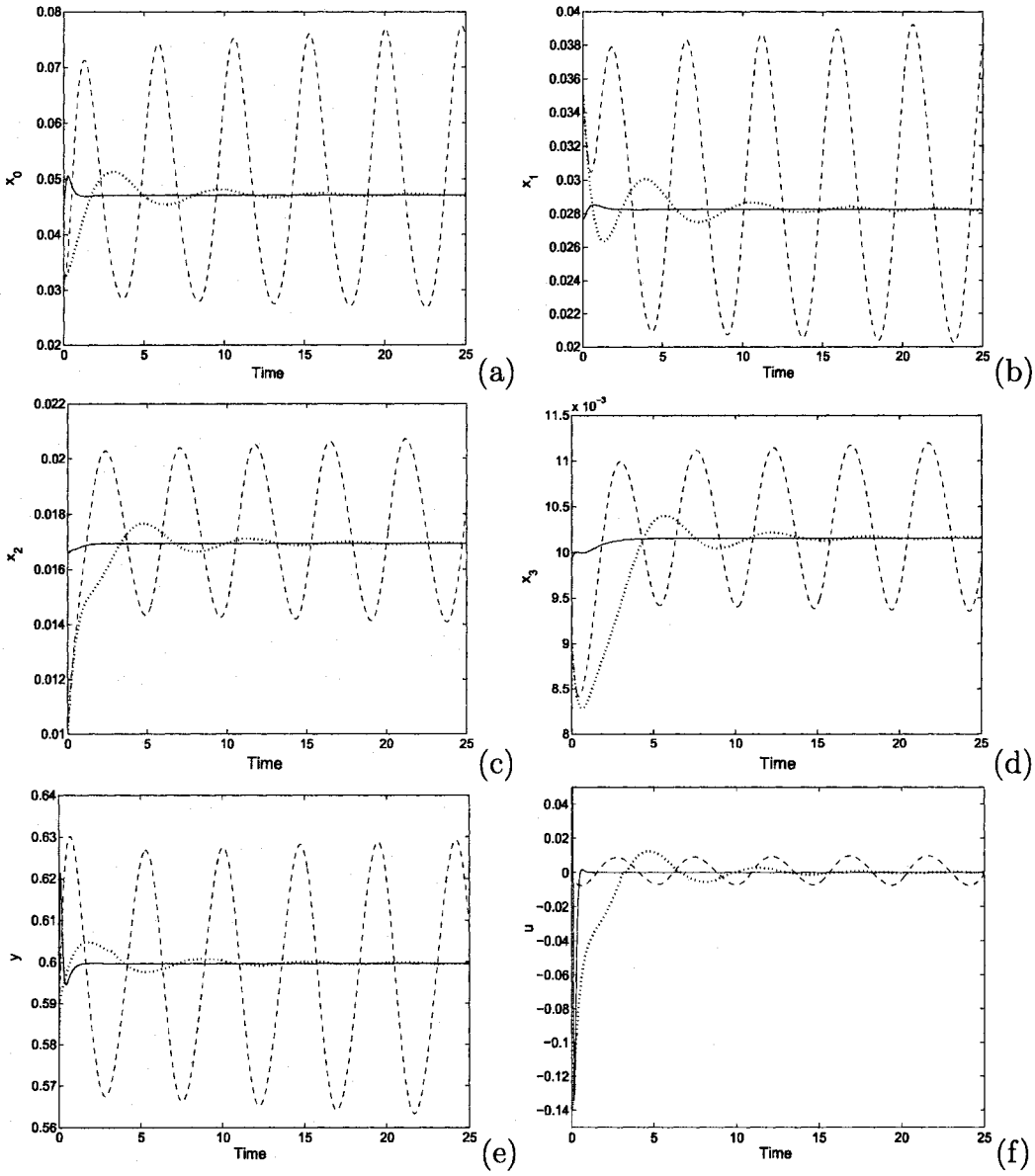

Figure 6.8: Closed-loop profiles of the dimensionless crystallizer moments (a)-(d), the solute concentration in the crystallizer (e) and the manipulated input (f) under MPC with stability constraints (solid line), under MPC without terminal constraints (dashed line), and using the switching scheme of Theorem 6.1 (dotted line).

closed-loop system. Furthermore, simply replacing the fall–back controller by an appropriate robust controller and implementing the same switching logics proposed in the previous section may lead to a switching scheme that is too conservative, resulting in the implementation of the fall–back controller for almost all times and severely restricting the chances of MPC implementation. Motivated by these considerations, we consider in this section nonlinear systems with input constraints and uncertain variables, and develop a robust hybrid predictive control structure that provides a safety net for the implementation of any available MPC formulation, designed with or without taking uncertainty into account. The key idea is to use a Lyapunov–based robust controller, for which an explicit characterization of the closed–loop robust stability region can be obtained, to provide a stability region within which MPC can be implemented. This is achieved by devising a set of switching laws that orchestrate switching between MPC and the bounded robust controller in a way that exploits the performance of MPC whenever possible, while using the bounded robust controller as a fall–back mechanism that can be switched in to preserve robust closed–loop stability in the event that MPC fails to prescribe a control move (due, for example, to computational problems or infeasibility) or leads to instability (due, for example, to inappropriate penalties and/or horizon length in the objective function).

The rest of this section is organized as follows. In Section 6.3.1, some mathematical preliminaries are presented to describe the class of uncertain nonlinear systems under consideration and briefly review how the robust constrained control problem is addressed within the bounded control and MPC frameworks. In Section 6.3.2, the controller switching problem is formulated, and two representative switching schemes, that address robust stability and performance objectives, are described. Finally in Section 6.3.3, the implementation and efficacy of the robust hybrid predictive control

structure are demonstrated through simulations using a chemical reactor example.

6.3.1 Preliminaries

We consider nonlinear systems with uncertain variables and input constraints, with the following state–space description:

$$\begin{aligned} \dot{x} &= f(x) + G(x)u(t) + W(x)\theta(t) \\ & u(t) \in \mathcal{U} \end{aligned} \tag{6.24}$$

where $x \in \mathbb{R}^n$ denotes the vector of state variables, $u(t) = [u^1(t) \cdots u^m(t)]'$ denotes the vector of constrained manipulated inputs, taking values in a nonempty convex subset $\mathcal{U}$ of $\mathbb{R}^m$, where $\mathcal{U} = \{u \in \mathbb{R}^m : \|u\| \leq u_{max}\}$, $\|\cdot\|$ is the Euclidean norm of a vector, $u_{max} \geq 0$ is the magnitude of input constraints, and $\theta(t) = [\theta^1(t) \cdots \theta^q(t)]' \in \Theta \subset \mathbb{R}^q$ denotes the vector of uncertain (possibly time–varying) but bounded variables taking values in a nonempty compact convex subset of $\mathbb{R}^q$. The vector of uncertain variables, $\theta(t)$, may describe time–varying parametric uncertainty and/or exogenous disturbances. It is assumed that the origin is the equilibrium point of the nominal (i.e., $u(t) = \theta(t) \equiv 0$) system of Eq.6.24. The vector function, $f(x)$, the matrices, $G(x) = [g^1(x) \cdots g^m(x)]$ and $W(x) = [w^1(x) \cdots w^q(x)]$, where $g^i(x) \in \mathbb{R}^n$, $i = 1 \cdots m$, and $w^i(x) \in \mathbb{R}^n$, $i = 1 \cdots q$, are assumed to be sufficiently smooth on their domains of definition.

In order to provide the necessary background for the main results in Section 6.3.2, we will briefly review in the remainder of this section the design procedure and the stability properties of a Lyapunov–based bounded robust controller and a model predictive controller, which together constitute the two components of the robusy hybrid predictive control structure. For simplicity, we will focus only on the state feedback problem where measurements of the entire state, $x(t)$, are assumed to be available for all t.

Bounded robust Lyapunov–based control

Consider the nonlinear system of Eq.6.24, where the uncertain variables, $W(x)\theta$, are assumed to be non–vanishing (in the sense that the uncertainty changes the nominal equilibrium point) and a robust control Lyapunov function (RCLF) [112], V, exists. Due to the non–vanishing nature of the uncertainty, asymptotic convergence to the origin cannot be achieved via continuous feedback. However, the states of the closed–loop system can be steered, in finite time, to an arbitrarily small (invariant) neighborhood of the origin by appropriate choice of the controller (practical stability). In order to enforce boundedness of the closed–loop trajectories and achieve an arbitrary degree of attenuation of the effect of the uncertain variables on the states, the existence of known (not necessarily small) bounds that capture the size of the uncertain variables for all times is assumed.

Using the RCLF, V, the following bounded robust state feedback control law can be designed (see Chapters 3 and 4 for details on similar controller designs):

$$u = -k(x, \theta_b, u_{max}) \left(L_G V\right)' \tag{6.25}$$

$$k(x, \theta_b, u_{max}) = \left\{ \begin{array}{ll} \dfrac{L_f^* V + \sqrt{\left(L_f^{**} V\right)^2 + \left(u_{max} \|(L_G V)'\|\right)^4}}{\|(L_G V)'\|^2 \left[1 + \sqrt{1 + \left(u_{max}\|(L_G V)'\|\right)^2}\right]} & , \ \|(L_G V)'\| \neq 0 \\ 0 & , \ \|(L_G V)'\| = 0 \end{array} \right\} \tag{6.26}$$

$$\begin{aligned} L_f^* V &= L_f V + (\rho \|x\| + \chi \theta_b \|L_W V\|) \left(\frac{\|x\|}{\|x\| + \phi}\right) \\ L_f^{**} V &= L_f V + \rho \|x\| + \chi \theta_b \|L_W V\| \end{aligned} \tag{6.27}$$

where $L_G V = [L_{g^1} V \ \cdots \ L_{g^m} V]$ is a row vector, θ_b is a positive real number such that $\|\theta(t)\| \leq \theta_b$, for all $t \geq 0$, and ρ, χ and ϕ are adjustable parameters that satisfy

$\rho > 0$, $\chi > 1$ and $\phi > 0$. Let Π be the set defined by:

$$\Pi(\theta_b, u_{max}) \;=\; \{x \in \mathbb{R}^n : L_f^{**}V \;\leq\; u_{max}\|(L_G V)'\|\} \tag{6.28}$$

and assume that the origin is contained in the interior of Π. Also, let Ω be a subset of Π, defined by:

$$\Omega \;=\; \{x \in \mathbb{R}^n : V(x) \leq c^{max}\} \tag{6.29}$$

Then, given any positive real number, d, such that:

$$\mathbb{D} \;:=\; \{x \in \mathbb{R}^n : \|x\| \leq d\} \;\subset\; \Omega \tag{6.30}$$

and for any initial condition, $x_0 \in \Omega$, it can be shown that there exists a positive real number, ϵ^*, such that if $\phi/(\chi - 1) < \epsilon^*$, the states of the closed–loop system satisfy $x(t) \in \Omega \; \forall \; t \geq 0$ and $\limsup_{t \to \infty} \|x(t)\| \leq d$ (see Appendix C for an analogous proof).

Remark 6.16 The critical features that makes a given controller a suitable fall–back component in the robust hybrid predictive control structure (to be proposed in Section 6.3.2) include: (1) it should guarantee stability in the presence of uncertainty and constraints, and (2) it should allow for an explicit characterization of the closed–loop stability region (the set of initial conditions starting from where robust closed–loop stability under input constraints and bounded uncertain variables is guaranteed). The bounded robust controller given in Eqs.6.25-6.27 (inspired in part by the results on bounded control in [204] for systems without uncertainty) is an example of such a controller design, chosen to illustrate the robust hybrid predictive control structure. The results however are not limited to this particular choice of controllers and any other robust controller that provides, *a priori* (i.e., before controller implementation), an explicit characterization of the robust stability region can be used. Finally, note that when the uncertain variables in Eq.6.24 are vanishing (in the sense that the uncertainty does not change the nominal equilibrium point), then starting from any initial state within Ω, the bounded robust controller of Eqs.6.25–6.27 enforces asymptotic closed–loop stability.

Model Predictive Control

For the purpose of illustrating the main results, we describe here a symbolic MPC formulation that incorporates most existing MPC formulations as special cases. This is not a new formulation of MPC; the general description is only intended for the purpose of highlighting the fact that the robust hybrid predictive control structure (to be proposed in the next section) can incorporate any available MPC formulation. In MPC, the control action at time t is conventionally obtained by solving, on–line, a finite horizon optimal control problem. The generic form of the optimization problem can be described as:

$$J_s(x,t,u(\cdot)) = \int_t^{t+T} (x'(s)Qx(s) + u'(s)Ru(s))ds + F(x(t+T)) \tag{6.31}$$

$$\begin{aligned} u(\cdot) &= argmin\{max\{J_s(x,t,u(\cdot))|\theta(\cdot) \in \Theta\}|u(\cdot) \in S\} := M_s(x) \\ s.t. \quad \dot{x}(t) &= f(x(t)) + G(x(t))u(t) + W(x(t))\theta(t), \quad x(0) = x_0 \\ x(t+T) &\in \Omega_{MPC}(x,t,\theta) \end{aligned} \tag{6.32}$$

where $S = S(t,T)$ is the family of piecewise continuous functions, with period Δ, mapping $[t, t+T]$ into the set of admissible controls, T is the horizon length and θ is the bounded uncertainty assumed to belong to a set Θ. A control $u(\cdot)$ in S is characterized by the sequence $\{u[k]\}$ where $u[k] := u(k\Delta)$ and satisfies $u(t) = u[k]$ for all $t \in [k\Delta, (k+1)\Delta)$. J_s is the performance index, R and Q are strictly positive-definite, symmetric matrices and the function $F(x(t+T))$ represents a penalty on the states at the end of the horizon. The maximization over θ may not be carried out if the MPC version used is not a min-max type formulation. The set $\Omega_{MPC}(x,t,\theta)$ could be a fixed, terminal set or may represent inequality constraints (as in the case of MPC formulations that require some norm of the state, or a Lyapunov function for the system, to decrease at the end of the horizon). This stability constraint may or may not account for uncertainty. The stability guarantees in MPC formulations (with or

without explicit stability conditions, and with or without robustness considerations, and whether or not it is a min-max type formulation) are dependent on the assumption of initial feasibility. Obtaining an explicit characterization of the closed–loop stability region of the predictive controller under uncertainty and constraints remains a difficult task.

6.3.2 Robust hybrid predictive controller design

Consider the nonlinear system of Eq.6.24 with input constraints, $\|u\| \leq u_{max}$, and bounded non–vanishing uncertainty, $\|\theta\| \leq \theta_b$, for which: (1) a predictive controller of the form of Eqs.6.31–6.32 and the bounded robust controller of Eqs.6.25–6.27 have been designed, and (2) the set, Ω, starting from where the convergence of the closed–loop states to an arbitrarily small (invariant) neighborhood of the origin, $\mathbb{D}$, under the bounded robust controller, is ensured, has been computed using Eqs.6.28–6.29. We formulate the controller switching problem as the one of designing a set of switching laws that orchestrate the transition between the predictive controller and the bounded controller in a way that: (1) enforces boundedness of the closed–loop trajectories with an arbitrary degree of uncertainty attenuation, (2) guarantees convergence of the closed–loop states, in finite time, to the set $\mathbb{D}$ (practical stability), starting from any initial condition within Ω, and (3) allows recovering the MPC performance whenever the pertinent stability criteria are met. For a precise statement of the problem, we first cast the system of Eq.6.24 as a switched system of the form:

$$\begin{aligned} \dot{x} &= f(x) + G(x)u_{i(t)} + W(x)\theta(t) \\ \|u_{i(t)}\| &\leq u_{max},\ i(t) \in \{1,2\} \end{aligned} \tag{6.33}$$

where $i : [0,\infty) \rightarrow \{1,2\}$ is the switching signal which is assumed to be a piecewise continuous (from the right) function of time, implying that only a finite number of switches between the two controllers is allowed on any finite–time interval. The

index, $i(t)$, represents a discrete state that indexes the control input, u, with the understanding that $i(t) = 1$ if and only if $u_i(x(t)) = M_s(x(t))$ (i.e., MPC is used) and $i(t) = 2$ if and only if $u_i(x(t)) = b(x(t))$ (i.e., bounded control is used). The value of $i(t)$ is determined by a higher–level supervisor responsible for executing the transition between the two controllers. Our goal is to construct a switching law, $i(t) = \psi(x(t), t)$, that provides the supervisor with the switching times that ensure stabilizing transitions between the two controllers. A schematic representation of the proposed hybrid control structure is depicted in Figure 6.9.

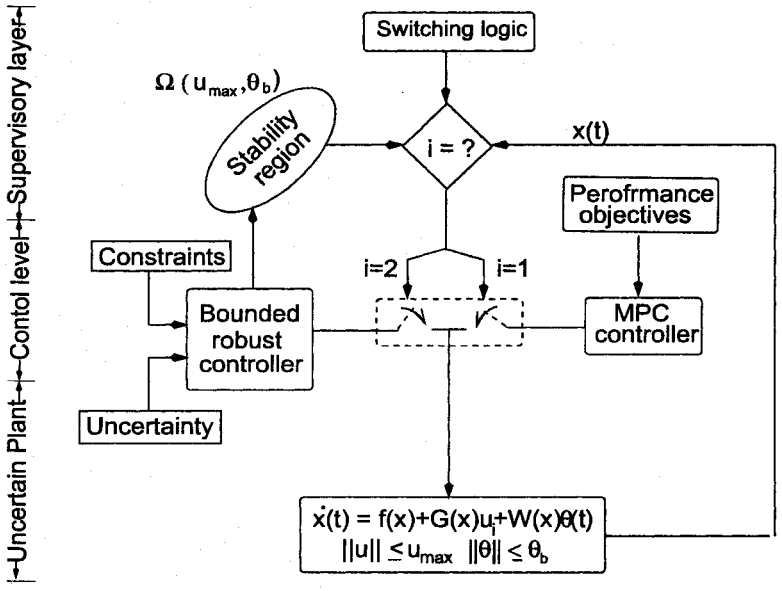

Figure 6.9: A schematic representation of the robust hybrid predictive control structure.

In the remainder of this section, two switching schemes are presented. The first scheme is given in Theorem 6.3 and focuses primarily on the issue of robust closed–loop stability, while the second scheme, given in Theorem 6.4, provides more flexible switching rules that guarantee robust closed–loop stability and, in addition, enhance the overall closed–loop performance. The proofs of both theorems are given in the Appendix E.

Robust stability-based controller switching

Theorem 6.3 *Consider the switched nonlinear system of Eq.6.33, the model predictive controller of Eqs.6.31–6.32 and the bounded controller design of Eqs.6.25–6.27. Let* $x(0) := x_0 \in \Omega$, *and initially set* $T_s = T_D = T_{inf} = \infty$. *At the earliest time,* $t \geq 0$, *for which the closed–loop state under MPC satisfies*

$$V(x(t^-)) \;=\; c^{max} \tag{6.34}$$

set $T_s = t$. *At the earliest time for which the closed–loop state under MPC satisfies:*

$$\|x(t)\| \;\leq\; d \tag{6.35}$$

where d *was defined in Eq.6.30, set* $T_D = t$. *Finally, at the earliest time,* t, *that MPC is infeasible, set* $T_{inf} = t$. *Define* $T_{switch} = \min\{T_s, T_D, T_{design}, T_{inf}\}$, *where* $0 \leq T_{design} < \infty$ *is arbitrary. Then the switching rule:*

$$i(t) \;=\; \left\{ \begin{array}{ll} 1, & 0 \leq t < T_{switch} \\ & \\ 2, & t \geq T_{switch} \end{array} \right\} \tag{6.36}$$

guarantees that the state of the switched closed–loop system is bounded and that $\limsup_{t\to\infty} \|x(t)\| \leq d$.

Remark 6.17 The design and implementation of the robust hybrid predictive control scheme can be understood algorithmically as follows:

- Given the nonlinear system of Eq.6.24, the bounds on the uncertain variables and the constraints on the manipulated inputs, design the bounded robust controller of Eqs.6.25–6.27, and calculate an estimate of its stability region, Ω.
- Design/pick an MPC formulation (the MPC formulation could be min–max optimization-based, linear or nonlinear, and with or without stability constraints). For convenience, we refer to the MPC formulation of Eqs.6.31–6.32.
- Given any $x_0 \in \Omega$, check the feasibility of the optimization in Eqs.6.31–6.32 (for a given horizon length, T) at $t = 0$.

- If feasible, start implementing MPC (i.e., set $u(0) = M_s(x_0)$).
- If at any time, MPC becomes infeasible ($t = T_{inf}$), or the states of the closed–loop system approach the boundary of Ω ($t = T_s$; see the scenario starting form $x_1(0)$ in Figure 6.10), or the closed–loop states enter the set $\mathbb{D}$ ($t = T_D$; see the scenario starting form $x_2(0)$ in Figure 6.10), then switch to the bounded controller, else keep MPC active in the closed–loop system until a time T_{design} (see the scenario starting form $x_3(0)$ in Figure 6.10).
- Switch to the bounded robust controller at T_s, T_D, T_{design}, or T_{inf}, whichever comes earliest, and implement it in the closed–loop system to achieve practical closed–loop stability.

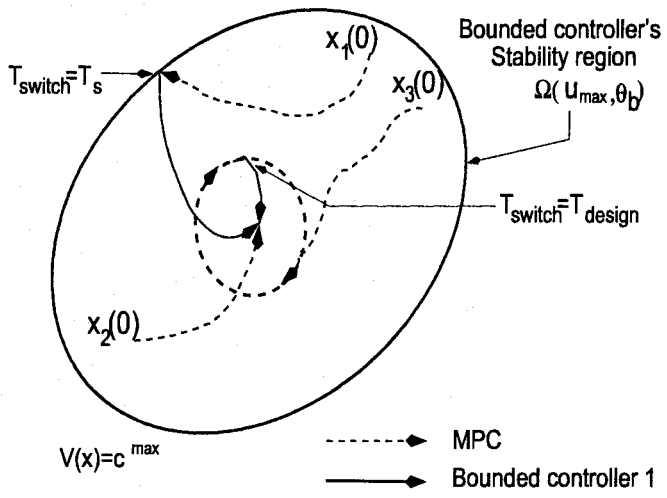

Figure 6.10: Examples of the evolution of the closed–loop state trajectory under the switching scheme of Theorem 6.3. Starting from $x_1(0)$, the trajectory under MPC hits the boundary of the stability region, upon which the bounded controller is switched in. Starting from $x_2(0)$, MPC is able to achieve practical stability. Starting from $x_3(0)$, the trajectory under MPC converges to a limit cycle and, therefore, after a time T_{design} has elapsed, the bounded controller is switched in to enforce convergence close to the origin.

Remark 6.18 The stability guarantees in various MPC formulations is contingent upon the assumption of initial feasibility of the optimization problem, and the set

of initial conditions for which the optimization problem is feasible is not explicitly characterized. By using the bounded robust controller as a fall–back controller, the switching scheme allows us to safely initialize the closed–loop system anywhere within Ω using MPC. The use of the fall-back controller turns Ω into a stability region for the switched closed–loop system because the bounded controller can always intervene (through switching) to maintain closed–loop stability in case the closed–loop system is infeasible under MPC or starts to become unstable under MPC (due, for example, to using a computationally simple, nominal MPC that does not take uncertainty into account).

Remark 6.19 The purpose of introducing the design parameter, T_{design}, (which is the time beyond which only the bounded robust controller is implemented) is to ensure convergence to $\mathbb{D}$ and avoid possible cases where the closed–loop states, under MPC, could wander forever inside Ω without actually converging to, and staying within, $\mathbb{D}$ (see, for example, the scenario starting form $x_3(0)$ in Figure 6.10). Other possible means of ensuring convergence to $\mathbb{D}$ include switching to the bounded controller when $\dot{V} \geq 0$ under MPC (see, for example, the switching rules in Chapter 5 and Section 6.2.2). However, in the presence of uncertainty, if a nominal MPC design is being used, such a condition might be very restrictive in the sense that it may terminate MPC implementation too early. For example, it could be that the nominal MPC is able to practically stabilize the closed–loop system when implemented in the closed–loop system for all times, yet is unable to maintain negative-definiteness of V for all times due to the disturbances (see Section 6.3.3 for a demonstration of this point in the context of a chemical process example). If the switching schemes in Section 6.2.2 (designed for systems without uncertainty) were to be used, it would dictate an immediate switch to the bounded controller, thus failing to exploit the high performance of MPC. The parameter T_{design}, on the other hand, if chosen large enough, provides ample time for the predictive controller to be implemented and possibly achieve practical stabilization.

Remark 6.20 Note that, while the result of Theorem 6.3 holds for any arbitrary value of the design parameter, T_{design}, the choice of this parameter provides a handle for extracting better performance out of the robust hybrid predictive control structure (through the possibility of the extended use of MPC). To achieve this, the value of T_{design} can be suitably altered, depending on the specific MPC formulation being used. For example, if a robust MPC design that guarantees stability for the uncertain nonlinear system is used, T_{design} can be chosen to be practically infinity. In this case, if MPC is feasible, it could be implemented for practically most of the time to stabilize the closed–loop system (the stability safeguards provided by the bounded controller are still required because the stability of any MPC formulation, robust or otherwise, are based on the assumption of initial feasibility, which cannot be verified short of running closed-loop simulations to test a given initial condition). On the other hand, if a "nominal," computationally inexpensive formulation of MPC is used, it is possible that it drives the states close to the origin, but is unable to enforce convergence to the set $\mathbb{D}$. In this case, T_{design} could be chosen in a way such that after MPC has driven the states close to the origin, the bounded controller is switched in (and MPC switched out) to enforce convergence to $\mathbb{D}$ and achieve the desired degree of uncertainty attenuation.

Remark 6.21 When the uncertainty is vanishing, the same switching scheme proposed in Theorem 6.3 can be applied by simply setting $d = 0$. Recall that, under vanishing uncertainty, the bounded controller guarantees asymptotic closed–loop stability for all $x(0) \in \Omega$ and therefore the set, $\mathbb{D}$, becomes the origin (see [100] for how the switching scheme is designed in the case of linear systems with vanishing disturbances).

Remark 6.22 The fact that closed–loop stability is guaranteed, for all $x_0 \in \Omega$ (through supervisory switching), independently of whether MPC itself is stabilizing or not, allows us to use any desired MPC formulation within the switching scheme (whether linear or nonlinear, with or without stability constraints, and with or with-

out uncertainty considerations) without concern for loss of stability. This flexibility has important practical implications for reducing the computational complexities that arise in implementing predictive control algorithms to nonlinear systems with uncertainty by allowing, for example, the use of less computationally–demanding formulations. In all cases, by embedding the operation of the chosen MPC algorithm within the well–defined stability region of the bounded robust controller, the switching scheme provides a safe fall–back mechanism that can be called upon at any moment to preserve closed–loop stability should MPC become unable to achieve closed–loop stability. Note also that no assumption is made regarding how fast the MPC optimization needs to be solved since, even if this time is significant and the plant dynamics are unstable, the implementation of the switching rule in Theorem 6.3 guarantees an immediate switch to the stabilizing bounded robust controller before such delays can adversely affect closed–loop stability (the times needed to check Eqs.6.34–6.36 and compute the control action of the bounded controller are insignificant as they involve only algebraic computations).

Enhancing closed–loop performance

The switching rule in Theorem 6.3 relies on a single bounded controller as back up, and uses the stability region estimate generated from a single Lyapunov function within which it restricts the evolution of the closed–loop state trajectory under MPC. While this is sufficient to guarantee robust closed–loop stability, the switching logic may limit the chances of MPC implementation (and thus limit the resulting closed-loop performance) in cases when the closed–loop state under MPC might temporarily leave the stability region of the bounded controller, but eventually converge to $\mathbb{D}$. Furthermore, the switching scheme in Theorem 6.3 prescribes only a single switch from MPC to the bounded controller which is then implemented in the closed–loop for all future times. By not allowing for multiple switches, the switching scheme might not be

able to take advantage of MPC implementation in cases where MPC is not stabilizing from one initial condition but is stabilizing from another initial condition. In this section we present a switching scheme that relaxes the switching rules of Theorem 6.3 in two directions, in order to take better advantage of the optimal performance of MPC. In one direction, to expand the region within which MPC implementation is allowed, we use a combination of several Lyapunov functions ($V_k, k = 1, \cdots, l$, where l is the number of bounded controllers), and MPC is allowed to remain in the closed–loop system as long as the closed–loop state trajectory does not escape the union of the stability regions ($\Omega_L = \bigcup_{k=1}^{l} \Omega_k$). In the second direction, to allow for the possibility of multiple switches between the predictive and bounded controllers, at any time the closed–loop state trajectory hits the boundary of the union of the stability regions, the appropriate bounded controller is switched in and implemented only until it brings the state within a (pre–determined) smaller subregion where MPC is re–activated once again and confined.

With the availability of $l + 1$ controllers (l bounded controllers and the MPC controller) that can be used, we recast the system of Eq.6.24 as a switched system of the form:

$$\begin{aligned} \dot{x} &= f(x) + G(x)u_{i(t)} + W(x)\theta(t) \\ \|u_{i(t)}\| &\leq u_{max},\ i(t) \in \{1, 2, \cdots, l+1\} \end{aligned} \tag{6.37}$$

where $i(t) = k$ if and only if $u_i(x(t)) = b_k(x(t))$ (i.e., the k-th bounded controller is used) and $i(t) = l + 1$ if and only if $u_i(x(t)) = M_s(x(t))$ (i.e., MPC is used). We also define, for the l bounded controllers, and the robust control Lyapunov functions, $V_k,\ k = 1, \cdots, l,\ 0 < \alpha < 1,\ c_{k,j}^{max} = \alpha^j c_k^{max},\ \Omega_k^j = \{x \in \mathbb{R}^n : V_k(x) \leq c_{k,j}^{max}\}$ and $\Omega_L^j = \bigcup_{k=1}^{l} \Omega_k^j$, for $j = 0, \cdots, N-1$ where $N < \infty$ is an integer, and $d^{max} = \max_{k=1,\cdots,l}\{d_k\}$, where d_k are arbitrarily small positive numbers such that $\mathbb{D}_k = \{x \in \mathbb{R}^n : \|x\| \leq$

$d_k\} \subset \Omega_k^{N-1}$. The notation, $\partial\Omega$, will also be used to denote the boundary of a closed set, Ω.

We are now in a position to present the relaxed switching scheme which is formalized in Theorem 6.4. The proof of this theorem is given in Appendix E.

Theorem 6.4 *Consider the constrained switched nonlinear system of Eq.6.37, the model predictive controller of Eqs.6.31–6.32 and the l bounded controllers of the form of Eqs.6.25–6.27, designed using the Lyapunov functions V_k, $k = 1, \cdots, l$. Consider any initial condition, $x(0) := x_0 \in \Omega_L^0$, and initially set $T_0 = 0$, $T_1 = T_2 = \cdots = T_N = T_D = \infty$. At the earliest time, $t \geq 0$, for which the closed–loop state under MPC satisfies:*

$$\|x(t)\| \leq d^{max} \tag{6.38}$$

set $T_D = t$. At the earliest time, $t \geq 0$, under MPC such that:

$$x(t) \in \partial\Omega_L^{j-1},\ x(t^-) \in \Omega_L^{j-1} \text{ and } T_{j-1} < \infty \tag{6.39}$$

for some $j \in \{1, \cdots, N\}$, or MPC is infeasible, set $T_j = t$. Define $T_{switch} = \min\{T_D, T_N, T_{design}\}$, where $0 \leq T_{design} < \infty$ is arbitrary. Then the switching rule:

$$i(t) = \left\{ \begin{array}{ll} l+1, & 0 \leq T_j \leq t \leq T_{j+1} \leq T_{switch},\ j = 0, \cdots, N-1 \text{ and } x \in \Omega_L^j \\ a, & 0 \leq T_j \leq t \leq T_{j+1} \leq T_{switch},\ j = 0, \cdots, N-1 \text{ and } x \notin \Omega_L^j \\ f, & t \geq T_{switch} \end{array} \right\} \tag{6.40}$$

for some $a \in \{1, \cdots, l\}$ for which $x(T_j) \in \Omega_a^{j-1}$, and for some $f \in \{1, \cdots, l\}$ for which $x(T_{switch}) \in \Omega_f^0$, guarantees that the state of the switched closed–loop system is bounded and $\limsup_{t \to \infty} \|x(t)\| \leq d^{max}$.

Remark 6.23 The implementation of the switching scheme proposed in Theorem 6.4 can be understood as follows (see also the schematic representation in Figure 6.11 for an example when $l = N = 2$):

- For each Lyapunov function, V_k, $k = 1, \cdots, l$: construct a bounded controller using Eqs.6.25-6.27, a set of N concentric level sets, Ω_k^j, $j = 0, \cdots, N-1$, with $\Omega_k^{N-1} \subset \Omega_k^{N-2} \subset \cdots \subset \Omega_k^1 \subset \Omega_k^0$, and a terminal set, $\mathbb{D}_k$, fully contained in Ω_k^{N-1}.

- Initialize the closed–loop system using MPC at any initial condition, x_0, within Ω_L^0 (the union of the level sets Ω_k^0) and start monitoring the position of the state of the closed–loop system.

- At the earliest time that the closed-loop state approaches the boundary of Ω_L^0, or MPC is infeasible, switch to bounded control (this corresponds to encountering T_1; see Figure 6.11).

- Implement any of the bounded controllers whose stability region contains the state at T_1 until the state enters Ω_L^1 (the union of the level sets Ω_k^1) after which switch back to MPC and implement it in the closed–loop system (in Figure 6.11 this happens when the state enters Ω_1^1).

- If the closed–loop state under MPC does not escape the boundary of Ω_L^1 and MPC continues to be feasible, keep MPC in the closed–loop system (this happens in Figure 6.11(a) where the state continues to stay within Ω_L^1). If the closed–loop state, however, tries to escape the boundary of Ω_L^1 (this happens in Figure 6.11(b) when the state hits the boundary of Ω_2^1 at $t = T_2$) or MPC is infeasible again, switch to bounded control and implement it until the states are driven inside the next safety zone where MPC is re–activated and confined (note that each time MPC is switched back in, its implementation is confined within a smaller safety zone since $\Omega_L^1 \supset \Omega_L^2 \supset \cdots \supset \Omega_L^{N-1}$). Repeat this process until either the state under MPC is about to escape the N-th safety zone, Ω_L^{N-1}, or the state enters the largest terminal set, $\mathbb{D}_{max}$, or a time greater than the design parameter, T_{design}, has elapsed. At the earliest time that any of these events takes place, switch permanently to any of the bounded controllers whose stability region contains the state at the time to ensure practical stability of the

closed–loop system.

Remark 6.24 Even though the switching scheme of Theorem 6.4 allows back and forth switching between MPC and the bounded controllers, chattering is avoided by virtue of the fact that the switching scheme limits the maximum number of switches to N and requires a finite–time interval to elapse in between consecutive switchings of MPC, which is the time it takes the appropriate bounded controller to drive the state from an outer level set to an inner one (note that the level sets of a given V_k are finitely–spaced since α is strictly less than one; see Figure 6.11 for an illustration). The bounded controller is invoked to bring the state of the closed–loop system closer to the terminal set. Switching back to MPC and trying to implement it in the closed–loop system is valuable because in some cases MPC may be feasible/stabilizing from this new initial condition, which is closer to the terminal set.

Remark 6.25 Both N, the maximum allowable number of switches between MPC and the bounded controllers, and T_{design} serve as design parameters that help take advantage of MPC performance, while still guaranteeing robust stability. Note that while the theorem allows for the possibility of N switches between MPC and the bounded controllers, it does not necessarily dictate that N switches take place (see Figure 6.11(a) for example). If the predictive controller itself is able to achieve practical stability, then back and forth switching between the predictive and bounded controllers is not required and, therefore, not executed.

6.3.3 Application to robust stabilization of a chemical reactor

Consider a well–mixed continuous stirred tank reactor where an irreversible elementary exothermic reaction of the form $A \xrightarrow{k} B$ takes place. The feed to the reactor consists of pure A at flow rate F, molar concentration C_{A0} and temperature T_{A0}.

Under standard modeling assumptions, the process model takes the following form:

$$\begin{aligned} V\frac{dC_A}{dt} &= F(C_{A0} - C_A) - k_0 \exp\left(\frac{-E}{RT}\right) C_A V \\ V\frac{dT}{dt} &= F(T_{A0} - T) + \frac{(-\Delta H)}{\rho c_p} k_0 \exp\left(\frac{-E}{RT}\right) C_A V + \frac{Q}{\rho c_p} \end{aligned} \tag{6.41}$$

where C_A denotes the concentration of species A, T denotes the temperature of the reactor, Q denotes the rate of heat input to the reactor, V denotes the volume of the reactor, k_0, E, ΔH denote the pre–exponential constant, the activation energy, and the enthalpy of the reaction, c_p and ρ denote the heat capacity and density of the fluid in the reactor. The steady–state values and process parameters are given in Table 6.2. For these parameters, it was verified that the given equilibrium point is an unstable one (the system also possesses two other locally asymptotically stable equilibrium points). The control objective is to regulate both the reactor temperature and reactant concentration at the (open–loop) unstable equilibrium point by manipulating both the rate of heat input/removal and the inlet reactant concentration. Defining $x_1 = C_A - C_{As}$, $x_2 = T - T_s$, $u_1 = C_{A0} - C_{A0s}$, $u_2 = Q$, $\theta_1(t) = T_{A0} - T_{A0s}$, $\theta_2(t) = \Delta H - \Delta H_{nom}$, where the subscript s denotes the steady–state value and ΔH_{nom} denotes the nominal value of the heat of reaction, the process model of Eq.6.41 can be cast in the form of Eq.6.24. In all simulation runs, the following time–varying function was considered to simulate the effect of exogenous disturbances in the feed temperature: $\theta_1(t) = \theta_0 sin(3t)$, where $\theta_0 = 0.08 T_{A0s}$. In addition, a parametric uncertainty of 50% in the heat of reaction was considered, i.e., $\theta_2(t) = 0.5\,(-\Delta H_{nom})$. The upper bounds on the uncertain variables were therefore taken to be $\theta_{b1} = 0.08 T_{A0s}$, $\theta_{b2} = 0.5\,|(-\Delta H_{nom})|$. Also, the following constraints were imposed on the manipulated inputs: $|u_1| \leq 1.0\ mol/L$ and $|u_2| \leq 92\ KJ/s$.

A quadratic Lyapunov function of the form $V = (C_A - C_{As})^2 + \left(\frac{1}{T_{Aos}}(T - T_s)\right)^2$ was used to design the bounded robust controller of Eqs.6.25–6.27 and compute the as-

Table 6.2: Process parameters and steady–state values for the reactor of Eq.6.41.

V	=	0.1	m^3
R	=	8.314	$kJ/kmol \cdot K$
C_{A0s}	=	1.0	$kmol/m^3$
T_{A0s}	=	310.0	K
ΔH	=	-4.78×10^4	$kJ/kmol$
k_0	=	1.2×10^9	s^{-1}
E	=	8.314×10^4	$kJ/kmol$
c_p	=	0.239	$kJ/kg \cdot K$
ρ	=	1000.0	kg/m^3
F	=	1.67×10^{-3}	m^3/s
T_{Rs}	=	395.33	K
C_{As}	=	0.57	$kmol/m^3$

sociated region of guaranteed closed–loop stability, using Eqs.6.28–6.29. The following values were used for the tuning parameters: $\chi = 1.01$, $\phi = 0.0001$, $\rho = 0.01$ to guarantee that the closed–loop states satisfy a relation of the form $\limsup_{t\to\infty} \|x(t)\| \leq 0.0005$. The set of nonlinear ODEs was integrated using the MATLAB solver, ODE45, and the optimization problem in MPC was solved using the MATLAB nonlinear constrained optimization solver, *fmincon*.

Figure 6.12 shows the stability region for the nominal bounded controller (Ω), and the bounded robust controller ($\Omega(u_{max}, \theta_b)$), which, as expected, is smaller in size since it accounts for the presence of uncertainty. As can be seen from the solid lines in Figures 6.12–6.13, when the nominal bounded controller (Eqs.6.25–6.27 with $\chi = 0$) is implemented, the desired uncertainty attenuation is not achieved. In contrast, from the dashed lines in Figures 6.12–6.13, it is clear that, starting from the same initial condition, the properly tuned bounded robust controller successfully drives both states to the desired steady–state, in the presence of input constraints, while simultaneously attenuating the effect of the uncertain variables on the states. We see from this comparison that the uncertain variables have a significant effect on the

states and that failure to explicitly account for them in the controller design leads to poor transient performance and the inability to enforce convergence close to the origin.

The next set of simulation runs demonstrate the use of the robust hybrid predictive control strategy of Theorem 6.3. In the first scenario, a nominal nonlinear MPC formulation, without stability constraints, is used as part of the robust predictive control structure (setting $\Omega_{MPC} = \mathbb{R}^n$, $F(x(t+T)) = 0$, $T = 0.02$ minutes in Eqs.6.31–6.32) and with the design parameter $T_{design} = 10$ minutes. The solid lines in Figures 6.14–6.15 represent the states of the closed–loop system initialized from a point within the stability region $\Omega(u_{max}, \theta_b)$. After the initial implementation of MPC, the supervisor detects, at $t = 0.6$ seconds, that the closed–loop states are close to the boundary of $\Omega(u_{max}, \theta_b)$ and therefore switches to the bounded robust controller to stabilize the closed–loop system. In the next scenario, a stabilizing formulation of MPC is used (requiring the states to go to a small invariant set at the end of the horizon), with a horizon length of $T = 0.02$ and a $T_{design} = 20$ minutes. For the initial condition of the trajectory shown by the dashed lines in Figures 6.14–6.15, the MPC controller yields a feasible solution and drives the states close to the origin. In this case, since the MPC is able to achieve the desired degree of uncertainty attenuation, it is implemented for all future times. For the initial condition depicted by the dotted lines in Figures 6.14–6.15, however, the MPC controller does not yield a feasible solution, and therefore the supervisor initially implements the bounded robust controller. At $t = 0.465$ minutes, the supervisor detects that MPC becomes feasible and, therefore, switches it in (and switches the bounded controller out) leading to closed–loop stability.

Finally, we demonstrate the implementation of the relaxed switching scheme of

Theorem 6.4 using two Lyapunov functions. Figure 6.16 shows the stability region for the two bounded controllers used as part of the robust hybrid predictive controller. We use a nominal nonlinear MPC formulation, without stability constraints, as part of the robust predictive control structure (setting $\Omega_{MPC} = \mathbb{R}^n$, $F(x(t+T)) = 0$, $T =$ 0.02 minutes in Eqs.6.31–6.32) and with the design parameter $T_{design} = 3$ minutes. The solid lines in Figures 6.16–6.17 represent the states of the closed–loop system initialized, under MPC, from a point within the stability region Ω_2. As seen in Figure 6.16, the switching logic allow MPC to be implemented in the closed–loop even though the states escape out of Ω_2, since they are still within Ω_1. Note also that in this case the nominal MPC does not enforce the desired degree of uncertainty attenuation (note the oscillations) and, therefore, after the time T_{design} has elapsed, the supervisor implements the bounded controller (associated with Ω_2) in the closed–loop system to achieve practical stabilization.

6.4 Conclusions

In this chapter, we presented hybrid predictive control strategies for the stabilization of input-constrained nonlinear systems with and without uncertainty. In the absence of uncertainty, the strategy involved using a family of bounded nonlinear controllers, each with an explicitly characterized stability region, as fall–back controllers and embedding the operation of MPC within the union of these regions. In the event that the predictive controller was unable to stabilize the closed–loop system, supervisory switching from MPC to any of the bounded controllers, whose stability region contained the trajectory at the switching time, guaranteed closed–loop stability. The strategy was subsequently extended to nonlinear systems with time-varying, bounded uncertain variables. The resulting robust hybrid predictive control strategy involved

using a bounded robust controller, with a well-characterized region of robust stability, as a fall–back mechanism and devising a set of switching rules that take the uncertainty into account and orchestrate, accordingly, the transition from MPC to bounded control to maintain robust closed–loop stability in the event that the predictive controller was unable to maintain it. The proposed strategies were shown to provide, through appropriate construction of the switching logic and irrespective of the MPC formulation used, a safety net for the implementation of predictive control algorithms to nonlinear and uncertain systems. The efficacy of the proposed strategies was demonstrated through applications to chemical process examples.

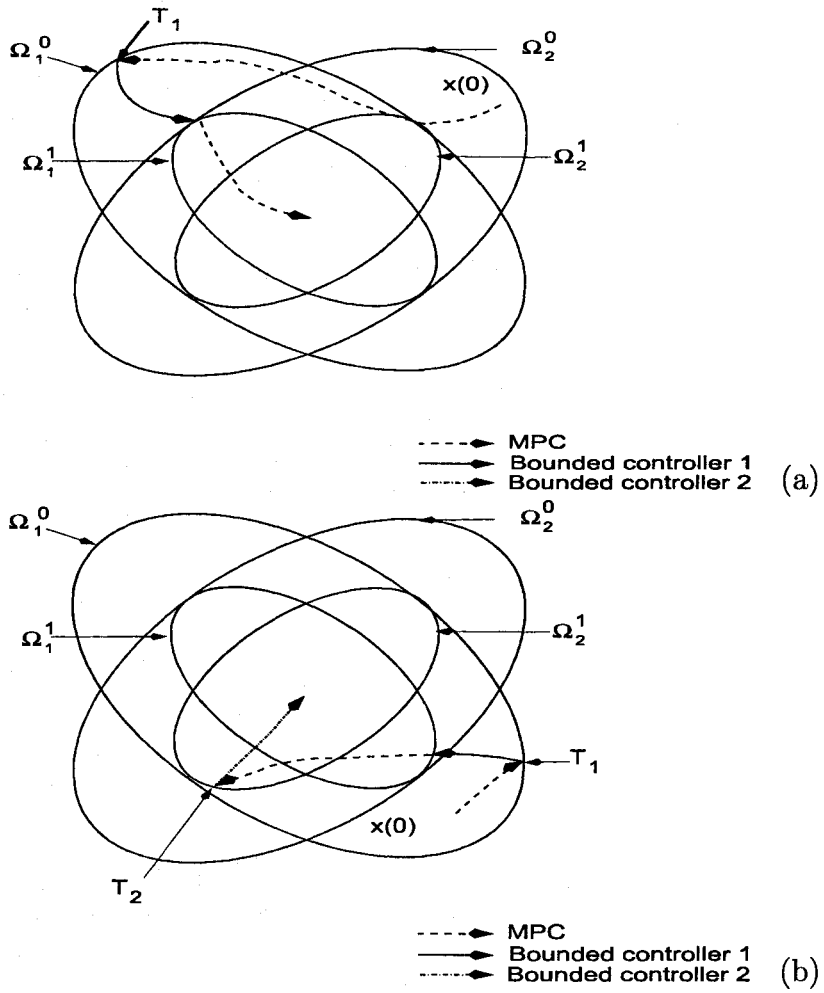

Figure 6.11: Examples of the evolution of closed–loop state trajectory under the switching scheme of Theorem 6.4: (a) starting from $x(0)$, the closed–loop trajectory under MPC hits the boundary of Ω_1^0 (at T_1), upon which the bounded controller 1 is switched in and implemented until the trajectory enters Ω_1^1, following which MPC is switched back in leading to practical stability, (b) starting from $x(0)$, the closed–loop trajectory under MPC hits the boundary of Ω_1^0 (at T_1), upon which the bounded controller 1 is switched in and implemented until the trajectory enters Ω_1^1, following which MPC is switched back in. The trajectory under MPC hits the boundary of Ω_2^1 ($t = T_2$) at which time the bounded controller 2 is switched in and implemented for all future times.

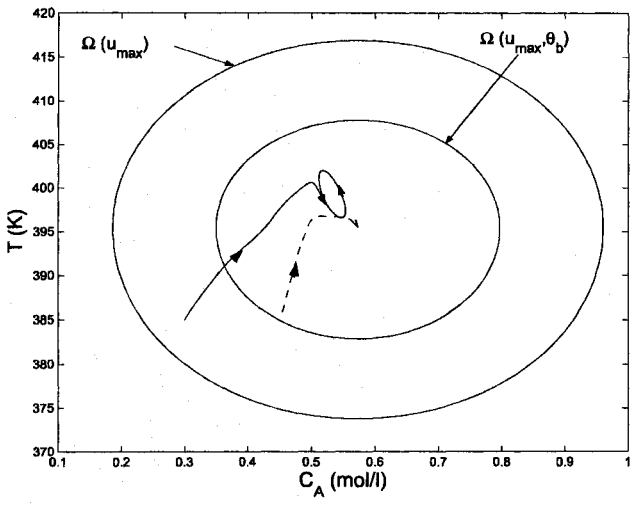

Figure 6.12: Closed–loop state trajectories under the bounded controller when initialized within the stability region estimated without taking the uncertainty into account (solid line) and the stability region that accounts for the uncertainty (dashed line).

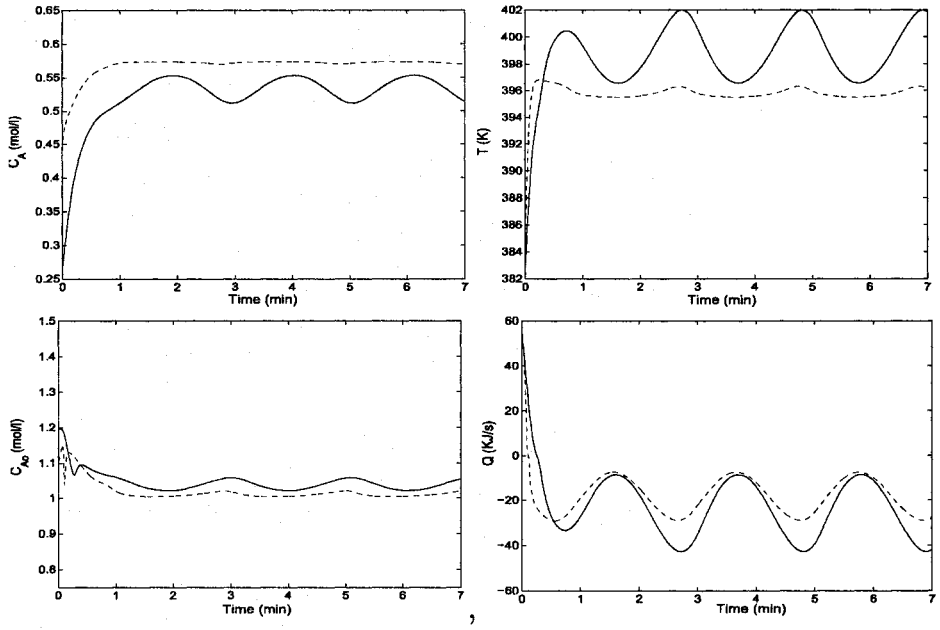

Figure 6.13: Closed–loop state (top) and input (bottom) profiles under the bounded controller when initialized within the stability region estimated without taking the uncertainty into account (solid lines) and the stability region that accounts for the uncertainty (dashed lines).

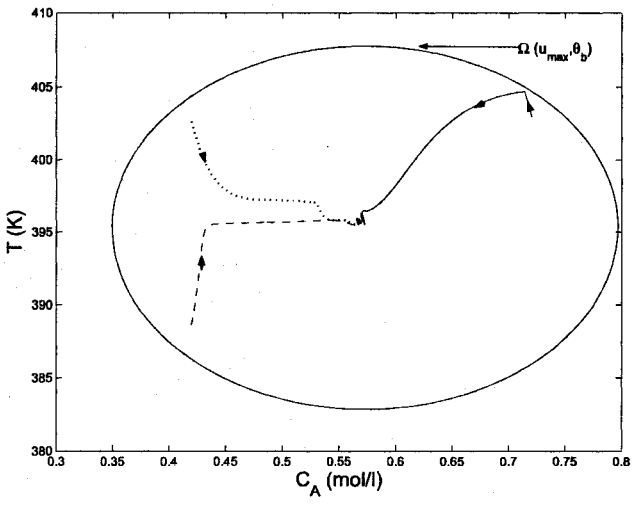

Figure 6.14: Closed–loop state trajectory: implementation of the robust hybrid predictive controller of Theorem 6.3 using a nominal MPC formulation without stability constraints (solid line) and a nonlinear MPC formulation with stability constraints, from two different initial conditions (dashed and dotted lines).

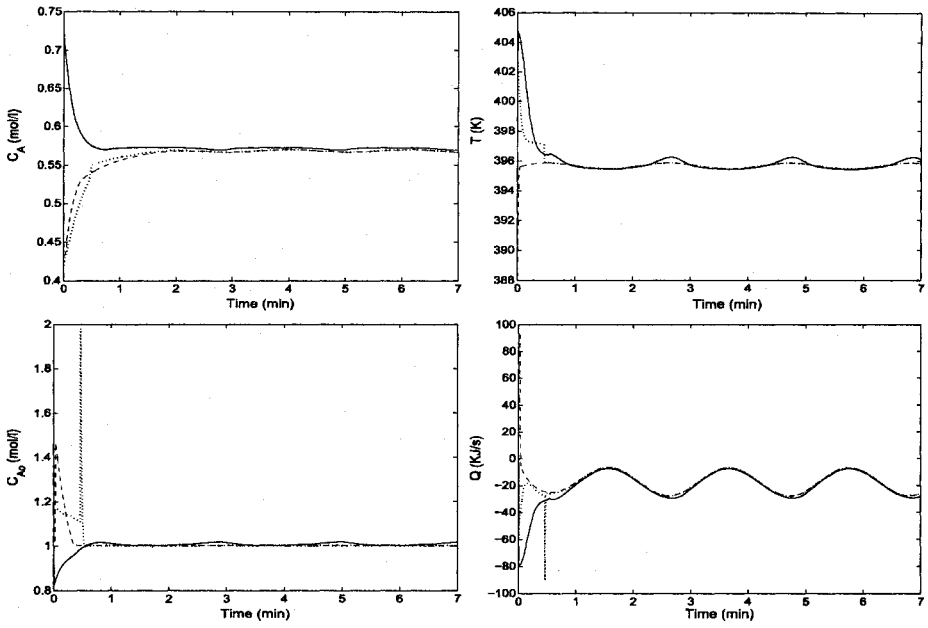

Figure 6.15: Closed–loop state (top) and input (bottom) profiles: implementation of the robust hybrid predictive controller of Theorem 6.3 using a nominal MPC formulation without stability constraints (solid lines) and a nonlinear MPC formulation with stability constraints, from two different initial conditions (dashed and dotted lines).

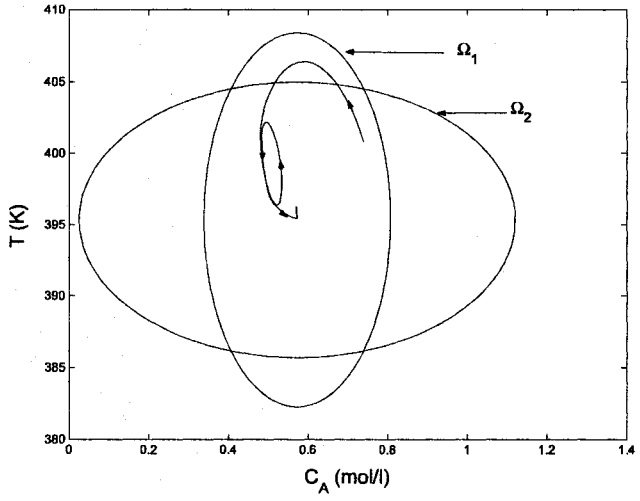

Figure 6.16: Closed–loop state trajectory: implementation of the robust hybrid predictive controller of Theorem 6.4, with $l = 2$, $N = 1$, using a nominal MPC formulation without stability constraints (solid line).

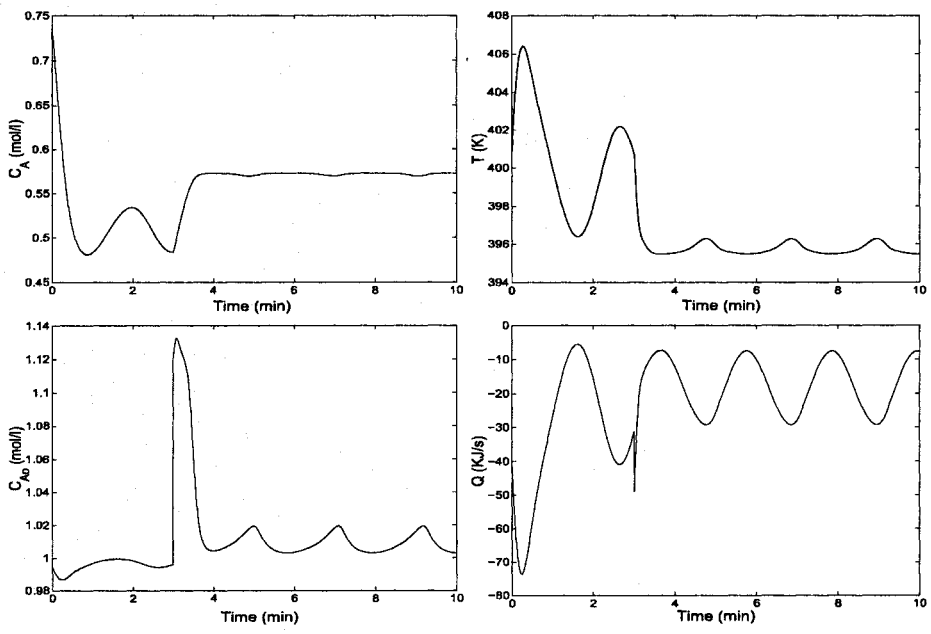

Figure 6.17: Closed–loop state (top) and input (bottom) profiles: implementation of the robust hybrid predictive controller of Theorem 6.4, with $l = 2$, $N = 1$, using a nominal MPC formulation without stability constraints (solid line).

Chapter 7

Control of Hybrid Systems with Uncertainty and Constraints

7.1 Introduction

In this chapter, we develop a hybrid nonlinear control methodology for a broad class of switched nonlinear processes whose dynamics are both constrained and uncertain. These are systems that consist of a finite family of continuous uncertain nonlinear dynamical subsystems, subject to hard constraints on their manipulated inputs, together with a higher-level supervisor that governs the transitions between the constituent modes. The key feature of the proposed control methodology is the integrated synthesis, via multiple Lyapunov functions (MLFs), of: (1) a family of lower-level robust bounded nonlinear feedback controllers that enforce robust stability in the constituent uncertain modes, and provide an explicit characterization of the stability region for each mode under uncertainty and constraints, and (2) upper-level robust switching laws that orchestrate safe transitions between the modes in a way that guarantees robust stability in the overall switched closed-loop system. The proposed hybrid control method is applied, through computer simulations, to robustly stabilize an

exothermic chemical reactor with switched dynamics, model uncertainty and actuator constraints, at an unstable steady-state. The results in this chapter were first presented in [95].

7.2 Switched nonlinear processes with uncertain dynamics

7.2.1 State-space description

We consider the class of switched uncertain nonlinear processes described by the following state-space representation:

$$\begin{aligned} \dot{x}(t) &= f_{\sigma(t)}(x(t)) + G_{\sigma(t)}(x(t))u_{\sigma(t)} + W_{\sigma(t)}(x(t))\theta_{\sigma(t)}(t) \\ \sigma(t) &\in \mathcal{I} = \{1, \cdots, N\} \end{aligned} \tag{7.1}$$

where $x(t) \in \mathbb{R}^n$ denotes the vector of continuous process state variables, $u(t) = [u^1(t) \cdots u^m(t)]^T \in \mathcal{U} \subset \mathbb{R}^m$ denotes the vector of control inputs taking values in a nonempty compact convex subset of $\mathbb{R}^m$ that contains the origin in its interior, $\theta(t) = [\theta^1(t) \cdots \theta^q(t)]^T \in \Theta \subset \mathbb{R}^q$ denotes the vector of uncertain (possibly time-varying) – but bounded – variables taking values in a nonempty compact convex subset of $\mathbb{R}^q$. The uncertain variables, $\theta(t)$, may describe time-varying parametric uncertainty and/or exogenous disturbances. $\sigma : [0, \infty) \rightarrow \mathcal{I}$ is the switching signal which is assumed to be a piecewise continuous (from the right) function of time, implying that only a finite number of switches is allowed on any finite interval of time. $\sigma(t)$, which takes values in the finite index set $\mathcal{I}$, represents a discrete state that indexes the vector field $f(\cdot)$, the matrices $G(\cdot)$ and $W(\cdot)$, the control input $u(\cdot)$, and the uncertain variable $\theta(\cdot)$, which altogether determine $\dot{x}$. For each value that the discrete state, σ, assumes in $\mathcal{I}$, the temporal evolution of the continuous state, x, is governed by a different set of differential equations. Processes of the form of Eq.7.1 are therefore of variable structure; they consist of a finite family of N continuous-

time uncertain nonlinear subsystems (or modes) and some rules for switching between them (see Figure 7.1 for a graphical representation). These rules define a switching sequence that describes the temporal evolution of the discrete state. Note that, by indexing the vector of uncertain variables, $\theta(t)$, and the matrix $W(x)$ in Eq.7.1 by σ, it is implied that the constituent modes do not necessarily share the same uncertain variables nor are they equally affected by them. The uncertainty is therefore allowed to influence the dynamics of different modes differently.

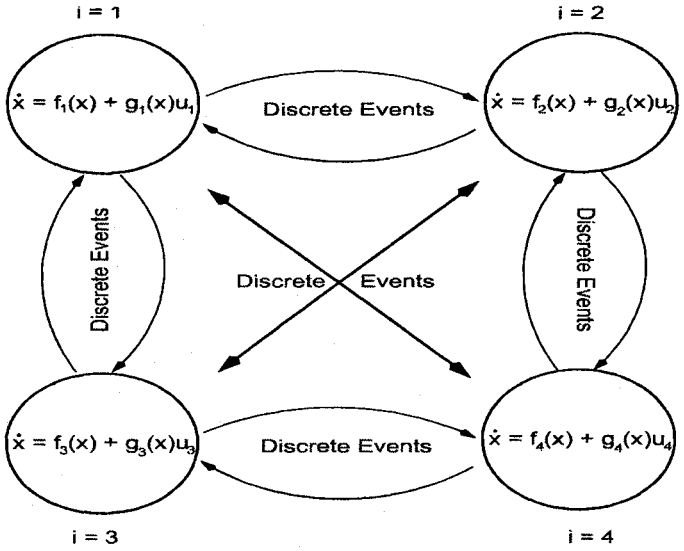

Figure 7.1: A multi-modal representation of a hybrid process, involving a finite family of continuous subsystems and discrete events governing the transitions between them.

Throughout the chapter, the notation t_{i_k} and $t_{i'_k}$ is used to denote the k-th times that the i-th subsystem is switched in and out, respectively, i.e. $\sigma(t^+_{i_k}) = \sigma(t^-_{i'_k}) = i$, for all $k \in Z_+$. With this notation, it is understood that, when the i-th mode is active, the continuous state evolves according to $\dot{x} = f_i(x) + G_i(x)u_i + W_i(x)\theta_i$ for $t_{i_k} \leq t < t_{i'_k}$. It is assumed that all entries of the vector functions $f_i(x)$, the $n \times m$ matrices $G_i(x)$, the $n \times q$ matrices $W_i(x)$ are sufficiently smooth on $\mathbb{R}^n$ and, without loss of generality, that the origin is the nominal equilibrium point of each mode, i.e. $f_i(0) = 0$ for all

$i \in \mathcal{I}$. We also assume that the state, x, does not jump at the switching instants, i.e. the solution, $x(\cdot)$, is everywhere continuous. Note that changes in the discrete state $\sigma(t)$ (i.e., transitions between the continuous dynamical modes) may, in general, be a function of time, state, or both. When changes in $\sigma(t)$ depend only on inherent process characteristics, the switching is referred to as autonomous. However, when $\sigma(t)$ is chosen by some higher process such as a controller or human operator, the switching is referred to as controlled. In this chapter, we focus on controlled switching where mode transitions are decided and executed by some higher-level supervisor. This class of systems arises naturally in the context of coordinated supervisory and feedback control of chemical process systems (see the illustrative example below and the simulation study in Section 7.4).

Finally, we recall the definition of a robust control Lyapunov function which will be used in the development of the main results of this chapter.

Definition 7.1 *[112] A smooth, proper, and positive-definite function $V : \mathbb{R}^n \to \mathbb{R}_+$ is called a robust control Lyapunov function for a system of the form $\dot{x} = f(x) + G(x)u + W(x)\theta$ when there exist a function, $\alpha_v(\cdot)$, of class $\mathcal{K}$, and $c_v > 0$ such that:*

$$\inf_{u \in \mathcal{U}} \sup_{\theta \in \mathcal{W}} \left[L_f V(x) + L_G V(x) u + L_W V(x) \theta + \alpha_v(x) \right] \; < \; 0 \tag{7.2}$$

whenever $V(x) > c_v$, where $L_f V(x) = \frac{\partial V}{\partial x} f(x)$, $L_G V(x)$ and $L_W V(x)$ are row vectors of the form $[L_{g_1} V(x) \cdots L_{g_m} V(x)]$ and $[L_{w_1} V(x) \cdots L_{w_q} V(x)]$, respectively, with g_k and w_k referring to the k-th columns of the matrices G and W, respectively.

For several classes of nonlinear systems of practical interest, systematic methods are available for the construction of Lyapunov functions that can be used as control Lyapunov functions (see the discussion on feedback linearizable processes in Section 7.3.4 and the example in Section 7.4).

7.2.2 Stability analysis via multiple Lyapunov functions

For purely continuous-time nonlinear processes, Lyapunov techniques provide useful tools for stability analysis as well as nonlinear and robust controller design (e.g., see [91]). The basic conceptual idea behind any Lyapunov design is that of "energy shaping", where an appropriate "energy" function (called a Lyapunov function) is chosen for the system, and the controller is designed in a way that enforces the monotonic decay of this function along the trajectories of the closed-loop system (energy dissipation). Given the view of hybrid processes as a finite collection of continuous-time nonlinear processes with discrete events that govern the transition between them, it is quite intuitive to exploit Lyapunov tools to analyze stability of hybrid processes. In this direction, one of the main tools for analyzing stability is multiple Lyapunov functions (MLFs) (e.g., see [81]). The MLF framework extends, in many respects, the classical energy shaping idea of Lyapunov analysis for continuous-time systems to switched systems, but provides, in addition, the tools necessary to account for the hybrid dynamics of such systems. Preparatory for its use later in robust control, we will briefly review in this section the main idea of MLF analysis. To this end, consider the switched process of Eq.7.1, with $u_i = \theta_i \equiv 0,\ i = 1, \cdots, N$, and suppose that we can find a family of Lyapunov functions $\{V_i : i \in \mathcal{I}\}$ such that the value of V_i decreases on each interval when the i-th subsystem is active, i.e.,

$$V_i(x(t_{i'_k})) \ < \ V_i(x(t_{i_k})) \tag{7.3}$$

for all $i \in \mathcal{I}$, $k \in Z_+$. The key idea here is that, even if there exists such a Lyapunov function for each subsystem, f_i, individually (i.e., each mode is stable), restrictions must be placed on the switching logic to guarantee stability of the overall switched system. The reason is that during the time periods when a particular mode is inactive, its energy might be adversely affected by the evolution of the active mode such that

at the next time that the inactive mode is activated, its energy already exceeds the level it had attained during its last period of activity. When this happens, the overall energy of the system may keep increasing indefinitely, as the process keeps switching in and out between the various modes, thus leading to instability. In fact, it is easy to construct examples of globally asymptotically stable systems and a switching rule that sends all trajectories to infinity (see [44] for some classical examples). There are multiple ways of guarding against such instability due to switching. One possibility is to require, in addition to Eq.7.3, that for every $i \in \mathcal{I}$, the value of V_i at the beginning of each interval on which the i-th mode is active exceed (or, at least, be equal to) the value at the beginning of the next such interval (see Figure 7.2); more precisely:

$$V_{\sigma(t_{i_{k+1}})}(x(t_{i_{k+1}})) \leq V_{\sigma(t_{i_k})}(x(t_{i_k})) \tag{7.4}$$

where $\sigma(t_{i_{k+1}}) = \sigma(t_{i_k}) = i$. This guarantees that the switched system is Lyapunov stable (see [81] and the references therein for alternative switching rules). In Theorem 7.1 below, a stronger switching condition than the one given in Eq.7.4 will be invoked to enforce asymptotic stability in the overall switched closed-loop system (i.e., to enforce both Lyapunov stability and asymptotic convergence to the origin).

7.2.3 Illustrative example

In this section, we introduce an example of a hybrid nonlinear chemical process with model uncertainty and actuator constraints that will be used throughout the chapter to illustrate the implementation of the hybrid control strategy. To this end, consider a continuous stirred tank reactor where an irreversible first-order exothermic reaction of the form $A \xrightarrow{k} B$ takes place. As shown in Figure 7.3, the reactor has two inlet streams; the first continuously feeds pure A at flow rate F, concentration C_{A0} and temperature T_{A0}, while the second has a control valve that can be turned on or off

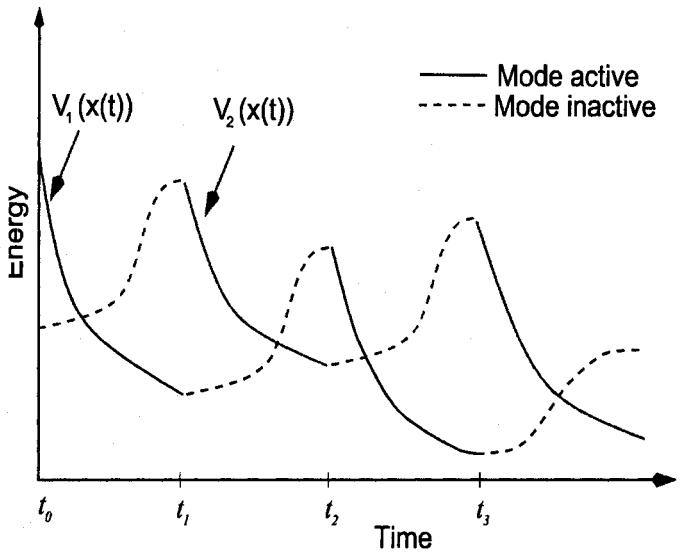

Figure 7.2: Temporal evolution of Multiple Lyapunov Functions for an asymptotically stable switched system consisting of twomodes.

depending on operational requirements. When the control valve is open, the second stream feeds pure A at flow rate F^*, concentration C^*_{A0} and temperature T^*_{A0}. Under standard modeling assumptions, the mathematical model for the process takes the form:

$$\begin{aligned} V\frac{dC_A}{dt} &= F(C_{A0} - C_A) + \sigma(t)F^*(C^*_{A0} - C_A) - k_0 \exp\left(\frac{-E}{RT}\right) C_A V \\ V\frac{dT}{dt} &= F(T_{A0} - T) + \sigma(t)F^*(T^*_{A0} - T) + \frac{(-\Delta H_r)}{\rho c_p} k_0 \exp\left(\frac{-E}{RT}\right) C_A V + \frac{Q}{\rho c_p} \end{aligned} \tag{7.5}$$

where C_A denotes the concentration of A, T denotes the reactor temperature, Q denotes the rate of heat input/removal from the reactor, V denotes the reactor volume, k_0, E, ΔH denote the pre-exponential constant, the activation energy, and the enthalpy of the reaction, c_p and ρ, denote the heat capacity and density of the fluid in the reactor. The process parameters and steady-state values are given in Table 7.1. $\sigma(t)$ is a discrete control variable that takes a value of zero when the control valve, on the second inlet stream, is closed and a value of one when the valve is open. Initially,

we assume that the valve is closed (i.e., $\sigma(0) = 0$). During reactor operation, however, it is desired to open this valve and feed through additional reactant material through the second inlet stream (i.e., $\sigma = 1$) in order to enhance the product concentration leaving the reactor.

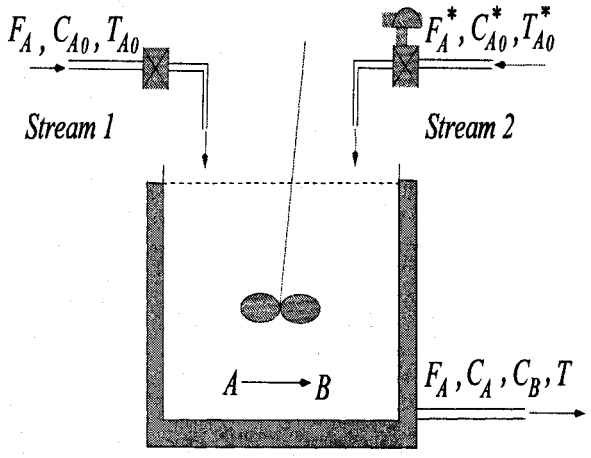

Figure 7.3: A switched non-isothermal continuous stirred tank reactor.

The above requirement gives rise to two distinct modes of reactor operation, between which switching is desired. These modes correspond to the off($\sigma = 0$)/on($\sigma = 1$) conditions of the control valve on the second inlet stream. Since the initial operating mode ($\sigma = 0$) has an open-loop unstable steady-state that corresponds to $T_s = 395.3$ K, our control objective will be to stabilize the reactor temperature at this point by manipulating the rate of heat input. However, since switching to the second mode ($\sigma = 1$) at some later point in time can potentially destabilize the process, our switching objective will be to carry out the transition between the two modes at the earliest time which does not jeopardize process stability. The control and switching objectives are to be accomplished in the presence of: (1) hard constraints on the manipulated input, $|Q| \leq 80$ KJ/hr, (2) time-varying external disturbances in the feed temperature of both inlet streams, and (3) time-varying parametric uncertainty

Table 7.1: Process parameters and steady-state values for the reactor of Eq.7.5.

V	=	0.1	m^3
R	=	8.314	$kJ/kmol.K$
C_{A0}	=	1.0	$kmol/m^3$
T_{A0s}	=	310.0	K
ΔH_{nom}	=	-400	$kJ/kmol$
k_0	=	2.0×10^7	s^{-1}
E	=	8.314×10^4	$kJ/kmol$
c_p	=	0.002	$kJ/kg.K$
ρ	=	1000.0	kg/m^3
F	=	2.77×10^{-5}	m^3/s
$C_{As}(\sigma = 0)$	=	0.577	$kmol/m^3$
$T_s(\sigma = 0)$	=	395.3	K
F^*	=	5.56×10^{-5}	m^3/s
C^*_{A0}	=	2.0	$kmol/m^3$
T^*_{A0s}	=	350.0	K

in the enthalpy of reaction. Note that the disturbances in the feed temperature of the second inlet stream take effect only after switching and, therefore, impact only the second mode, while the disturbances in the first stream's temperature and the parametric uncertainty in the enthalpy influence both modes.

7.3 Coordinating feedback and switching for robust hybrid control

7.3.1 Problem formulation and solution overview

Consider the switched nonlinear process of Eq.7.1 where, for each $i \in \mathcal{I}$, a robust control Lyapunov function, V_i, is available, the vector of manipulated inputs, u_i, is constrained by $\|u_i\| \leq u_i^{max}$, and the vector of uncertain variables is bounded by $\|\theta_i\| \leq \theta_{bi}$, where the notation $\|\cdot\|$ denotes the Euclidean norm of a vector. The bounds that capture the size of the uncertainty can be arbitrarily large. Two control

problems will be considered. In the first problem, the uncertain variables are assumed to be vanishing, in the sense that $W_i(0)\theta_i = 0$ for any $\theta_i \in \Theta$ (note that this does not require the variable, θ_i, itself to vanish in time). Under this assumption, the origin – which is an equilibrium point for the nominal modes of the hybrid process – is an equilibrium point for the uncertain modes as well. For this case, and given that switching is controlled by a higher-level supervisor, the problem is how to coordinate switching between the constituent modes, and their respective controllers, in a way that respects the constraints and guarantees asymptotic stability of the overall closed-loop system in the presence of uncertainty. To address the problem, we formulate the following objectives. The first is to synthesize, using a family of Lyapunov functions, a family of N bounded robust nonlinear continuous feedback control laws of the general form:

$$u_i \;=\; -k_i(V_i, u_i^{max}, \theta_{bi})(L_{G_i}V_i)^T, \;\; i = 1, \cdots, N \tag{7.6}$$

that: (1) enforce robust asymptotic stability for their respective closed-loop subsystems, and (2) provide, for each mode, an explicit characterization of the set of admissible initial conditions starting from where a given mode is guaranteed to be stable in the presence of model uncertainty and input constraints. The scalar gain, $k_i(\cdot)$, of the L_GV controller in Eq.7.6 is to be designed so that $\|u_i\| \leq u_i^{max}$ and the energy of the i-th mode – as captured by V_i – is monotonically decreasing whenever that mode is active. The second objective is to construct a set of robust switching laws that supply the supervisor with the set of switching times that guarantee stability of the constrained uncertain switched closed-loop system, which in turn determines the time-course of the discrete state, $\sigma(t)$.

In the second control problem, the uncertain variables are assumed to be non-vanishing, in the sense that $W_i(0)\theta_i \neq 0$ for all $i \in \mathcal{I}$. In this case, the origin is no

longer an equilibrium point of the uncertain modes or the overall hybrid process and, therefore, the objective is to coordinate feedback controller synthesis and switching in a way that guarantees boundedness of the states of the hybrid process, with an arbitrary degree of attenuation of the effect of uncertainty.

Having formulated the above robust hybrid control problems, we proceed in Sections 7.3.2-7.3.3 to present their solutions. The first result, given in Theorem 7.1 below, addresses the problem of vanishing uncertainty, while the second result, given in Theorem 7.2, deals with the problem of non-vanishing uncertainty.

7.3.2 Hybrid control strategy under vanishing uncertainty

Theorem 7.1 below summarizes the proposed robust hybrid control strategy for the case when the uncertainty does not affect the nominal equilibrium point of the hybrid process. Provided in this theorem are the formulae of the family of bounded robust feedback continuous controllers, together with the appropriate switching rules used by the supervisor to govern the transitions between the various closed-loop modes in a way that guarantees the desired properties in the constrained uncertain hybrid closed-loop system. The proof of this theorem is given in Appendix F.

Theorem 7.1 *Consider the switched uncertain nonlinear process of Eq.7.1, where* $W_i(0)\theta_i = 0$ *for all* $i \in \mathcal{I}$, *under the following family of bounded nonlinear feedback controllers:*

$$u_i = -k_i(V_i, u_i^{max}, \theta_{bi}, \chi_i, \phi_i)(L_{G_i}V_i)^T,\ i = 1, \cdots, N \tag{7.7}$$

where

$$k_i(\cdot) = \left\{ \begin{array}{ll} \dfrac{L_{f_i}^* V_i + \sqrt{(L_{f_i}^{**}V_i)^2 + (u_i^{max}\|(L_{G_i}V_i)^T\|)^4}}{(\|(L_{G_i}V_i)^T\|)^2[1+\sqrt{1+(u_i^{max}\|(L_{G_i}V_i)^T\|)^2}]} & , \|(L_{G_i}V_i)^T\| \neq 0 \\ 0 & , \|(L_{G_i}V_i)^T\| = 0 \end{array} \right\} \tag{7.8}$$

$$
\begin{aligned}
L^{*}_{f_i} V_i &= L_{f_i} V_i + \left(\rho_i \|x\| + \chi_i \|(L_{W_i} V_i)^T\| \theta_{bi} \right) \left(\frac{\|x\|}{\|x\| + \phi_i} \right) \\
L^{**}_{f_i} V_i &= L_{f_i} V_i + \rho_i \|x\| + \chi_i \|(L_{W_i} V_i)^T\| \theta_{bi}
\end{aligned}
\tag{7.9}
$$

V_i is a robust control Lyapunov function for the i-th subsystem and ρ_i, χ_i, ϕ_i are tunable parameters that satisfy $\rho_i > 0$, $\chi_i > 1$ and $\phi_i > 0$. Let $\Omega^*_i(u_i^{max}, \theta_{bi})$ be the largest invariant set embedded within the region described by the inequality:

$$
L_{f_i} V_i + \rho_i \|x\| + \chi_i \|(L_{W_i} V_i)^T\| \theta_{bi} \leq u_i^{max} \|(L_{G_i} V_i)^T\| \tag{7.10}
$$

and assume, without loss of generality, that $x(0) := x_0 \in \Omega^*_i(u_i^{max}, \theta_{bi})$ for some $i \in \mathcal{I}$. If, at any given time T such that:

$$
x(T) \in \Omega^*_j(u_j^{max}, \theta_{bj}) \tag{7.11}
$$

$$
V_j(x(T)) < V_j(x(t_{j'})) \tag{7.12}
$$

for some $j \in \mathcal{I}$, $j \neq i$, where $t_{j'}$ is the time when the j-th subsystem was last switched out, i.e. $\sigma(t_{j'}^+) \neq \sigma(t_{j'}^-) = j$, we set $\sigma(T^+) = j$, then there exists a positive real number ϕ_j^* such that for any $\phi_j \leq \phi_j^*$, the origin of the switched closed-loop system is asymptotically stable.

Remark 7.1 The bounded robust feedback controllers given in Eqs.7.7-7.9 are synthesized, using multiple Lyapunov functions, by reshaping the scalar nonlinear gain of the $L_G V$ controller proposed originally in [204] (see also [93]), in order to account for the effect of the uncertain variables. As a result, the control action now depends explicitly on both the magnitude of the input constraints, u_i^{max}, and the size of the uncertainty, θ_{bi}. Note that only information about the size of the uncertainty (and not the uncertainty itself) is needed for controller design and that this size can be arbitrarily large. Each controller in Eqs.7.7-7.9 is a smooth function of the state away from the origin. It is also continuous at the origin whenever the corresponding control Lyapunov function satisfies the small control property (see [204, 112] for details on this issue).

Remark 7.2 Each controller in Eqs.7.7-7.9 possesses two tuning parameters, ϕ_i and χ_i, responsible for enforcing robust stability and achieving the desired degree of attenuation of the effect of uncertainty on each of the constituent modes of the hybrid process. A significant degree of attenuation can be achieved by selecting the parameter ϕ_i to be sufficiently small and/or choosing the parameter χ_i to be sufficiently large (see Step 1 in the Proof of Theorem 7.1). Another important feature of the uncertainty compensator (i.e., the term $\chi_i \|(L_{W_i} V_i)^T\| \theta_{bi}$) used in designing the controller gain of Eqs.7.8-7.9 is the presence of a scaling function of the form $\frac{\|x\|}{\|x\| + \phi_i}$ that multiplies the compensator. Since ϕ_i is a small positive number, the scaling function approaches a value of 1 when $\|x\|$ is large (far from the equilibrium point) and a value of zero when $\|x\|$ is small (close to the equilibrium point). This allows us, as we get closer and closer to the equilibrium point, to use smaller and smaller control effort to cancel the uncertainties. The full weight of the uncertainty compensator is used only when the state is far from the equilibrium point.

Remark 7.3 The use of bounded nonlinear controllers of the form of Eqs.7.7-7.9 to robustly stabilize the constituent modes is motivated by the fact that this class of controllers provides an explicit characterization of the limitations imposed by uncertainty and constraints on the region of closed-loop stability. Specifically, each controller in Eqs.7.7-7.9 provides an explicit characterization of the set of admissible initial conditions starting from where robust closed-loop stability of the corresponding subsystem is guaranteed with the available control action. This characterization can be obtained from the set of inequalities given in Eq.7.10. For each mode, the corresponding inequality describes a closed region in the state-space (henceforth denoted by $\Phi_i(u_i^{max}, \theta_{bi})$) where the corresponding control law satisfies the constraints and the associated Lyapunov function, V_i, decreases monotonically (see Step 1 in the Proof of Theorem 7.1). Owing to the presence of uncertainty, the size of Φ_i now depends on the size of the uncertainty, in addition to the magnitude of input constraints. The larger the uncertainty and/or the tighter the constraints, the smaller Φ_i is in size. It is important to note that even though a trajectory starting in Φ_i will move from one

Lyapunov surface to an inner Lyapunov surface with lower energy (because $\dot{V}_i < 0$), there is no guarantee that the trajectory will remain forever in Φ_i since it is not necessarily a region of invariance. Once the trajectory leaves Φ_i, however, there is no guarantee that $\dot{V}_i < 0$. To guarantee that $\dot{V}_i$ remains negative for all times during which the i-th mode is active, we compute the largest invariant set, $\Omega_i^*(u_i^{max}, \theta_{bi})$, within $\Phi_i(u_i^{max}, \theta_{bi})$ (see [170] for details on how to construct these sets). This set, which is also parameterized by the constraints and the uncertainty bounds, represents an estimate of the stability region associated with each mode. Finally, note that in the absence of any plant-model mismatch (i.e., when $\theta_{bi} \equiv 0$), the controllers of Eqs.7.7-7.9, together with the expressions for the stability regions, Ω_i^*, reduce to those developed in [93] under nominal conditions.

Remark 7.4 Each of the inequalities in Eq.7.10 captures the classical tradeoff between stability and performance. To see this, note that the size of the region of guaranteed closed-loop stability, obtained from Eq.7.10, can be enlarged by using small values for the controller tuning parameters χ_i and ρ_i. This enlargement of the stability region, however, comes at the expense of the controller's robust performance, since large values for χ_i and ρ_i are typically required to achieve a significant degree of attenuation of the effect of disturbances and plant-model mismatch on the closed-loop system. Therefore, in selecting the controller tuning parameters, one must strike a balance between the need to stabilize the process from a given initial condition and the requirement of achieving a satisfactory robust performance.

Remark 7.5 The two switching laws of Eqs.7.11-7.12 determine, implicitly, the times when switching from mode i to mode j is permissible. The first rule tracks the temporal evolution of the continuous state, x, and requires that, at the desired time for switching, the continuous state be within the stability region of the target mode, $\Omega_j^*(u_j^{max}, \theta_{bj})$. A pictorial representation of this idea is shown in Figure 7.4. This requirement ensures that, once the target mode and its corresponding controller are engaged, the corresponding Lyapunov function continues to decay for as long as the

mode remains active. Note that this condition must be enforced at every time that the supervisor considers switching between modes. In contrast, the second switching rule of Eq.7.12 is checked only if the target mode has been activated (at least once) in the past. In this case, Eq.7.12 allows reactivation of mode j provided that its energy at the current "switch in" is less than its energy at the last "switch out". This condition guarantees that, whenever a given mode is activated, the closed-loop state is closer to the origin than it was when the same mode was last activated. Note that if each of the N modes is activated only once during the course of operation (i.e., we never switch back to a mode previously activated), the second condition is automatically satisfied. Furthermore, for the case when only a finite number of switches (over the infinite time-interval) is considered, this condition can be relaxed by allowing switching to take place even when the value of V_j, at the desired switching time, is larger than that when mode j was last switched in, as long as the increase is finite. The reason owes to the fact that these finite increases in V_j (resulting from switching back to mode j) will be overcome when the process eventually settles in the "final" mode whose controller, in turn, forces its Lyapunov function to continue to decay as time tends to infinity, thus asymptotically stabilizing the overall hybrid process.

Remark 7.6 Even though the switching conditions of Eqs.7.11-7.12 require knowledge of the temporal evolution of the closed-loop state, $x(t)$, the a priori knowledge of the solution of the constrained closed-loop nonlinear system (which is difficult to obtain in general) is not needed for the practical implementation of the proposed approach. Instead, the supervisor can monitor (on-line) how x evolves in time to determine if and when the switching conditions are satisfied. If the conditions are satisfied, then we conclude that it is "safe" to switch from the current mode/controller combination to the one for which the conditions hold. Otherwise, the current mode is kept active. Note that, absent any failures in the control system, maintaining closed-loop stability does not require switching since the closed-loop system is always initialized within the stability region of at least one of the constituent modes

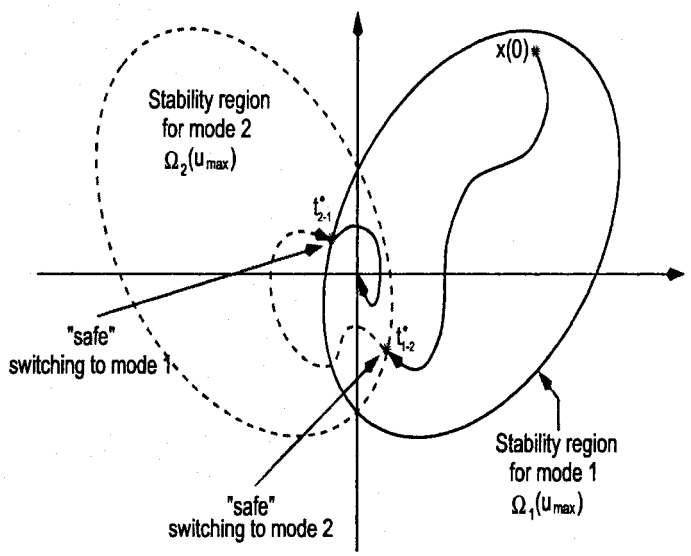

Figure 7.4: Implementation of the switching law based on monitoring the evolution of the closed-loop trajectory with respect to stability regions.

and, therefore, absent switching, the closed-loop trajectory will simply remain in this invariant set and stabilize at the desired equilibrium point. In many practical situations, however, changes in operational conditions and requirements typically motivate switching between various process modes. Under these conditions, the result of Theorem 7.1 provides a strategy for carrying out mode transitions without jeopardizing the stability of the overall process (see the simulation example in Section 7.4).

Remark 7.7 In many practical situations, the ability of the control system to deal with failure situations requires consideration of multiple control configurations and switching between them to preserve closed-loop stability in the event that the active control configuration fails. For such cases, the switching rules proposed in Theorem 7.1 (based on the stability regions) can be used to explicitly identify the appropriate fall-back control actuator configuration that should be activated to preserve closed-loop stability (see Chapter 8 for how this notion can be applied for the design of fault-tolerant control systems). Clearly, if failure occurs when the state is outside the stability regions of all the available configurations, then closed-loop stability cannot be preserved because of the fundamental limitations imposed by the constraints on

the stability regions as well as how many backup configurations are available. However, our approach in this case provides a useful way for analyzing when the control system can or cannot tolerate failures. For example, by analyzing the overlap of the stability regions of the given configurations, one can decide the time periods during which the control system (under a given configuration) cannot tolerate failure (which are the times that the trajectory spends outside the stability region of the other configurations). By relaxing the constraints (i.e., enlarging the stability regions) and/or increasing the available control configurations (this is ultimately limited by system design considerations) one can reduce the possibility of failures taking place outside of the stability regions of all configurations.

Remark 7.8 Note that it is possible for more than one subsystem, j, to satisfy the switching rules given in Eqs.7.11-7.12. This occurs when the process state lies within the intersection of several stability regions. In this case, Theorem 7.1 guarantees only that a transition from the current mode to any of these modes is safe, but does not suggest which one to choose since they all guarantee stability. The decision to choose a particular mode to activate is typically made by the supervisor based on the particular operational requirements of the process.

Remark 7.9 Referring to the practical applications of Theorem 7.1, one must initially identify the constituent modes of the hybrid process. A Lyapunov function is then constructed for each mode to synthesize, via Eqs.7.7-7.9, a bounded robust controller and construct, with the aid of Eq.7.10, the region of closed-loop stability associated with each mode. Implementation of the control strategy then proceeds by initializing the process within the stability region of the desired initial mode of operation and implementing the corresponding robust controller. Then, the switching laws of Eqs.7.11-7.12 are checked on-line, by the supervisor, to determine if it is possible to switch operation to a particular mode at some time. If the conditions are satisfied, then a transition to that mode (and its controller) is executed. If the conditions are not satisfied, then the current operating modes is kept active. A summary of the

proposed robust hybrid control methodology is shown schematically in Figure 7.5.

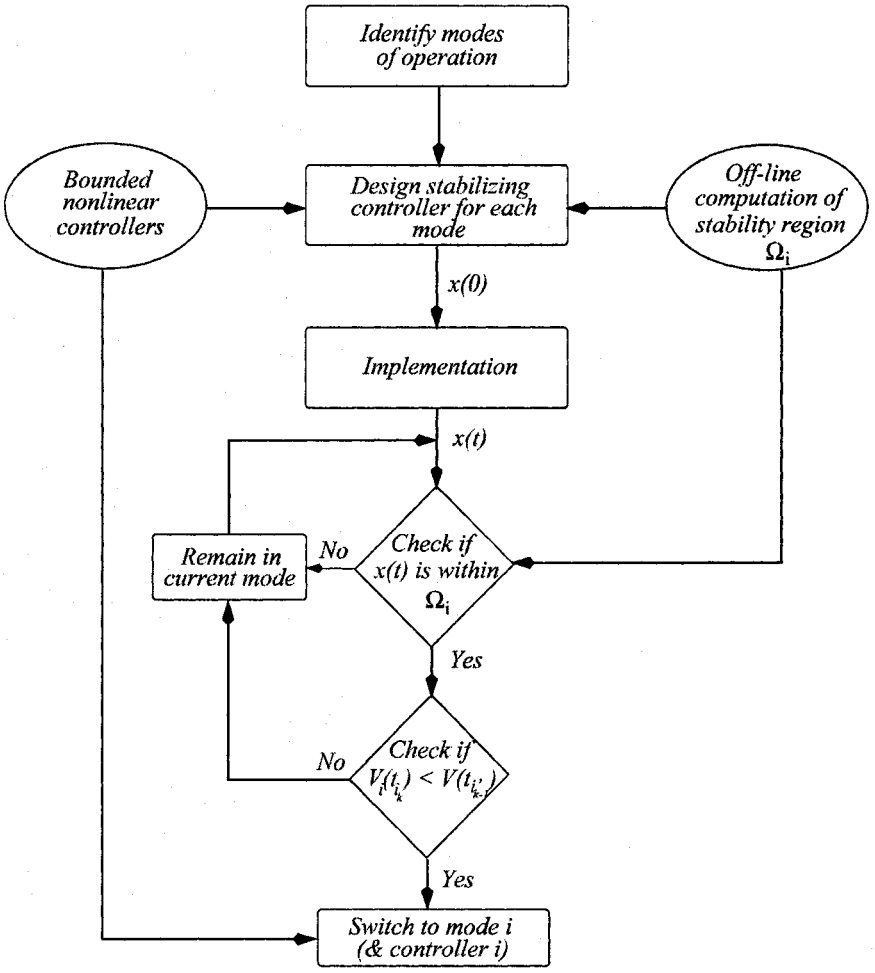

Figure 7.5: Summary of the proposed hybrid control strategy based on coordinating feedback and switching.

7.3.3 Hybrid control strategy under non-vanishing uncertainty

In this section, we address the problem of non-vanishing uncertainty, where the uncertainty changes the nominal equilibrium point of the hybrid process. Theorem 7.2 below summarizes the proposed hybrid control strategy for this case and states precisely the resulting closed-loop properties. The proof of this theorem is given in

Appendix F.

Theorem 7.2 *Consider the switched uncertain nonlinear process of Eq.7.1, where* $W_i(0)\theta_i \neq 0$ *for all* $i \in \mathcal{I}$*, under the family of controllers given in Eq.7.7-7.9. Assume, without loss of generality, that* $x(0) \in \Omega_i^*(u_i^{max}, \theta_{bi})$ *for some* $i \in \mathcal{I}$ *and that, for any given* $T > 0$, $\sigma(T^+) = j$ *only if the conditions of Eqs.7.11-7.12 hold for some* $j \in \mathcal{I}$, $j \neq i$*. Then, given any arbitrarily small real number,* $d > 0$*, there exist a set of positive real numbers* $\{\epsilon_1^*, \cdots, \epsilon_N^*\}$ *such that if* $\epsilon_i \leq \epsilon_i^*$, $i \in \mathcal{I}$*, the trajectories of the switched closed-loop system are bounded and satisfy* $\limsup_{t\to\infty} \|x(t)\| \leq d$*, where* $\epsilon_i = \phi_i/(\chi_i - 1)$.

Remark 7.10 Owing to the non-vanishing nature of the uncertainty influencing each mode, asymptotic convergence to the origin is not possible via continuous feedback for any of the constituent modes of the hybrid process. However, in lieu of asymptotic stability, one can show (see the Proof of Theorem 7.2 in Appendix F) that, for every mode i by itself (without switching), the corresponding controller guarantees convergence of the closed-loop trajectory, in finite time, to a small neighborhood of the origin (called a residual or terminal set) such that the trajectory, once inside this set, cannot escape (see Chapter 3 for further details). The size of this set can be made arbitrarily small by choosing the controller tuning parameter, ϕ_i, to be sufficiently small and/or selecting the tuning parameter, χ_i, to be sufficiently large. In this manner, one can achieve an arbitrary degree of robust attenuation of the effect of uncertainty on each mode of the closed-loop system.

Remark 7.11 Boundedness of the state of the constituent modes does not in and of itself imply boundedness of the state of the overall hybrid process. Boundedness of the switched closed-loop trajectory can be ensured using the switching rules given in Eqs.7.11-7.12, which automatically impose constraints on which mode can be engaged at any given time. These constraints, similar to the case of the vanishing uncertainty, guarantee that whenever a mode is activated (or reactivated), not only is its energy

less than what it was before (Eq.7.12) but also that this energy continues to decay for as long as the mode remains active (Eq.7.11). The only difference in the case of non-vanishing uncertainty is that these rules need only be implemented, by the supervisor, when the state lies outside the residual set. To understand the rationale for this observation, we first observe that since the size of the residual set of each mode can be tuned (by appropriately adjusting ϕ_i and χ_i), a small common residual set can be chosen (for all the modes) that is completely contained within the intersection of the various stability regions. Then, starting from any admissible initial condition, implementation of the switching logic outside this residual set ensures that, for every mode, the closed-loop trajectory moves closer and closer to that set, as we switch in and out of that mode. Since the number of process modes is finite, and only a finite number of switches is allowed over any finite time-interval, then at least one of constituent modes will converge, in finite time, to the residual set. From that time onward, the closed-loop trajectory stays within the common residual set for all times, regardless of any further mode switchings (see Step 2 in the Proof of Theorem 7.2 for the mathematical details).

Remark 7.12 Theorems 7.1 and 7.2 consider, respectively, the cases when the uncertainties affecting the various modes are either all vanishing or all non-vanishing. For the general case when the uncertainty is vanishing for some modes and non-vanishing for others, one can establish only boundedness of the closed-loop trajectory. If, however, only a finite number of switches is allowed over the infinite time-interval, then one can establish asymptotic stability if the uncertainty influencing the final mode – where the hybrid process eventually settles – is vanishing. If such uncertainty, on the other hand, is non-vanishing, then the closed-loop trajectory will instead reach and enter, in finite time, the residual set of the final mode without ever leaving again.

7.3.4 Application to input/output linearizable processes

An important class of nonlinear processes that has been studied extensively within process control is that of input/output feedback linearizable processes. This class arises frequently in practical problems where the objective is to force the controlled output to follow some reference-input trajectory (rather than stabilize the full state at some nominal equilibrium point). In this section, we illustrate how the coordinated robust feedback and switching methodology proposed in this chapter can be applied when the individual modes of the hybrid process are input/output linearizable. For simplicity, we limit our attention to the single-input single-output case with vanishing uncertainty. Consider the hybrid process:

$$\begin{aligned} \dot{x}(t) &= f_{\sigma(t)}(x(t)) + g_{\sigma(t)}(x(t))u_{\sigma(t)} + w_{\sigma(t)}(x(t))\theta_{\sigma(t)} \\ y &= h(x) \\ \sigma(t) &\in \mathcal{I} = \{1, \cdots, N\} \end{aligned} \tag{7.13}$$

where $y \in \mathbb{R}$ is the controlled output and $h(x)$ is a sufficiently smooth scalar function. Suppose that, for all $i \in \mathcal{I}$, there exists an integer r (this assumption is made only to simplify notation and can be readily relaxed to allow a different relative degree, r_i, for each mode) and a set of coordinates:

$$\begin{bmatrix} \zeta \\ \eta \end{bmatrix} = \begin{bmatrix} \zeta_1 \\ \zeta_2 \\ \vdots \\ \zeta_r \\ \eta_1 \\ \vdots \\ \eta_{n-r} \end{bmatrix} = \mathcal{X}(x) = \begin{bmatrix} h(x) \\ L_{f_i}h(x) \\ \vdots \\ L_{f_i}^{r-1}h(x) \\ T_{1,i}(x) \\ \vdots \\ T_{n-r,i}(x) \end{bmatrix} \tag{7.14}$$

where $T_1(x), \cdots, T_{n-r}(x)$ are nonlinear scalar functions of x, such that the system of Eq.7.13 takes the form:

$$\begin{aligned}
\dot{\zeta}_1 &= \zeta_2 \\
&\vdots \\
\dot{\zeta}_{r-1} &= \zeta_r \\
\dot{\zeta}_r &= L_{f_i}^r h(\mathcal{X}^{-1}(\zeta,\eta)) + L_{g_i} L_{f_i}^{r-1} h(\mathcal{X}^{-1}(\zeta,\eta)) u_i + L_{w_i} L_{f_i}^{r-1} h(\mathcal{X}^{-1}(\zeta,\eta))\theta_i \\
\dot{\eta}_1 &= \Psi_{1,i}(\zeta,\eta) \\
&\vdots \\
\dot{\eta}_{n-r} &= \Psi_{n-r,i}(\zeta,\eta) \\
y &= \zeta_1
\end{aligned} \tag{7.15}$$

where $L_{g_i} L_{f_i}^{r-1} h(x) \neq 0$ for all $x \in \mathbb{R}^n$, $i \in \mathcal{I}$. Under the assumption that the η-subsystem is input-to-state stable (ISS) with respect to ζ for each $i \in \mathcal{I}$, the controller synthesis task for each mode can be addressed on the basis of the partially linear ζ-subsystem. To this end, upon introducing the notation $e_k = \zeta_k - v^{(k-1)}$, $e = [e_1\ e_2\ \cdots\ e_r]^T$, $\bar{v} = [v\ v^{(1)}\ \cdots\ v^{(r-1)}]^T$, where $v^{(k)}$ is the k-th time derivative of the reference input, v, which is assumed to be a smooth function of time, the ζ-subsystem of Eq.7.15 can be further transformed into the following more compact form:

$$\dot{e} = \bar{f}_i(e,\eta,\bar{v}) + \bar{g}_i(e,\eta,\bar{v}) u_i + \bar{w}_i(e,\eta,\bar{v})\theta_i,\ i = 1, \cdots, N \tag{7.16}$$

where $\bar{f}_i(e,\eta,\bar{v}) = Ae + bL_{f_i}^r h(\mathcal{X}^{-1}(e,\eta,\bar{v}))$ and $\bar{g}_i(e,\eta,\bar{v}) = bL_{g_i} L_{f_i}^{r-1} h(\mathcal{X}^{-1}(e,\eta,\bar{v}))$, $\bar{w}_i(e,\eta,\bar{v}) = bL_{w_i} L_{f_i}^{r-1} h(\mathcal{X}^{-1}(e,\eta,\bar{v}))$ are $r \times 1$ vector functions, and:

$$A = \begin{bmatrix} 0 & 1 & 0 & \cdots & 0 \\ 0 & 0 & 1 & \cdots & 0 \\ \vdots & & & & \vdots \\ 0 & 0 & 0 & \cdots & 1 \\ 0 & 0 & 0 & \cdots & 0 \end{bmatrix}, \quad b = \begin{bmatrix} 0 \\ 0 \\ \vdots \\ \\ 1 \end{bmatrix} \tag{7.17}$$

are an $r \times r$ matrix and $r \times 1$ vector, respectively. For systems of the form of Eqs.7.16-7.17, a simple choice for a robust control Lyapunov function is a quadratic function of the form $\bar{V}_i = e^T P_i e$ where the positive-definite matrix P_i is chosen to satisfy the

following Riccati inequality:

$$A^T P_i + P_i A - P_i b b^T P_i \ < \ 0 \tag{7.18}$$

Using these quadratic functions, a bounded robust controller can be designed for each mode using Eqs.7.7-7.9 applied to the system of Eq.7.16. Using a standard Lyapunov argument, it can then be shown that each controller robustly asymptotically stabilizes the e states in each mode. This result together with the ISS assumption on the η states can then be used to show, via a small gain argument, that the origin of the full closed-loop e-η interconnection, for each individual mode, is asymptotically stable.

Remark 7.13 Note that, since the objective here is output tracking, rather than full state stabilization, the Lyapunov functions used in designing the controllers, $\bar{V}_i$'s, are in general different from the Lyapunov functions, V_i's, used in implementing the switching rules. Owing to the ISS property of the η-subsystem of each mode, only a Lyapunov function for the e-subsystem, namely $\bar{V}_i$, is needed and used to design a controller that robustly stabilizes the full e-η interconnection for each mode. However, when implementing the switching rules (constructing the Ω_i^*'s and verifying Eq.7.12), we need to track the evolution of x (and hence the evolution of both e and η). Therefore, the Lyapunov functions used in verifying the switching conditions at any given time, V_i, are based on x. From the asymptotic stability of each mode, the existence of these Lyapunov functions is guaranteed by converse Lyapunov theorems (see chapter 3 in [170] for further details). For systems with relative degree $r = n$, the choice $\bar{V}_i = V_i$ is sufficient.

7.4 Application to a switched chemical reactor

In this section, we revisit the switched chemical reactor example, introduced earlier in Eq.7.5, to illustrate, through computer simulations, the application of the proposed hybrid control strategy. Recall that the control objective is to stabilize the reactor

temperature at the open-loop unstable steady-state, by manipulating the rate of heat input, while the switching objective is to carry out the transition between the two modes at the earliest time possible without jeopardizing process stability. The control and switching objectives are to be accomplished in the presence of hard constraints on the manipulated input ($|Q| \leq 80$ KJ/hr), time-varying external disturbances in the feed temperature of both inlet streams, and time-varying parametric uncertainty in the enthalpy of reaction. For the purpose of simulating the effect of uncertainty on the process output, we consider time-varying functions of the form $\theta(t) = \theta_b sin(4t)$, where the upper bounds on the feed temperature disturbances are taken to be 10 K for both streams, and the upper bound on the uncertainty in the enthalpy is taken to be 15% of the nominal value. We note that any other bounded and time-varying function can be used to simulate the effect of uncertainty. This choice does not affect the results since it is only the bounds on these functions that are needed for controller and switching law design.

To accommodate both the control and operational objectives, and since the uncertain variables considered are non-vanishing, we follow the strategy proposed in Theorem 7.2. Using two quadratic Lyapunov functions of the form $V_i = \frac{1}{2}c_i(T - T_s)^2$, where $c_i > 0$, we initially use Eqs.7.7-7.9 to synthesize two bounded robust controllers (one for each mode) that enforce robust closed-loop stability for their respective modes, and also achieve an arbitrary degree of attenuation of the effect of uncertainty on the reactor temperature. Then, with the aid of Eq.7.10, we compute the region of guaranteed closed-loop stability associated with each mode, which will be used in implementing the necessary switching laws. The following tuning parameters were used for each controller: $c_1 = c_2 = 1$, $\phi_1 = \phi_2 = 0.01$, $\chi_1 = 2$, $\chi_2 = 1.1$, $\rho_1 = \rho_2 = 0.001$, to guarantee that the reactor temperature satisfies a relation of the

form $\limsup_{t\to\infty}|T(t) - T_s| \leq 0.01$.

Several closed-loop simulations were performed to evaluate the proposed control strategy. In the first set of simulation runs, the reactor is operated in the first mode (control valve closed, $\sigma = 0$) for all time, with no switching. The feedback controller designed for this mode is consequently implemented to robustly stabilize the reactor temperature, starting from an admissible initial condition. Figure 7.6 (solid lines) depicts the resulting reactor temperature (controlled output) and rate of heat input (manipulated input) profiles. Included in the figure also are the corresponding open-loop profiles with no control (dashed lines). We observe that the controller successfully stabilizes the reactor temperature at the desired steady-state and simultaneously attenuates the effect of disturbances and model uncertainty on the reactor temperature.

In the second set of simulation runs, we seek to accommodate the operational requirement of increasing the product concentration by switching to the second mode (control valve open, $\sigma = 1$) at some point. Note that switching to the second mode (i.e., opening the valve) is accompanied by a switch to the second controller responsible for stabilizing this mode. In the absence of any explicit switching guidelines, suppose that the switching time is randomly set to be as early as $t = 12\ min.$ The resulting temperature and heat input profiles in this case are shown in Figure 7.7. It is clear from the figure that by switching at this arbitrarily chosen time, the controller for the $\sigma = 1$ mode is unable to stabilize the reactor temperature at the desired steady-state nor attenuate the effect of uncertainty on the reactor temperature. The reason – which is reflected in the input profile – is that at this time, the process state lies outside the stability region of the $\sigma = 1$ mode and therefore, the available control action is insufficient to stabilize the temperature.

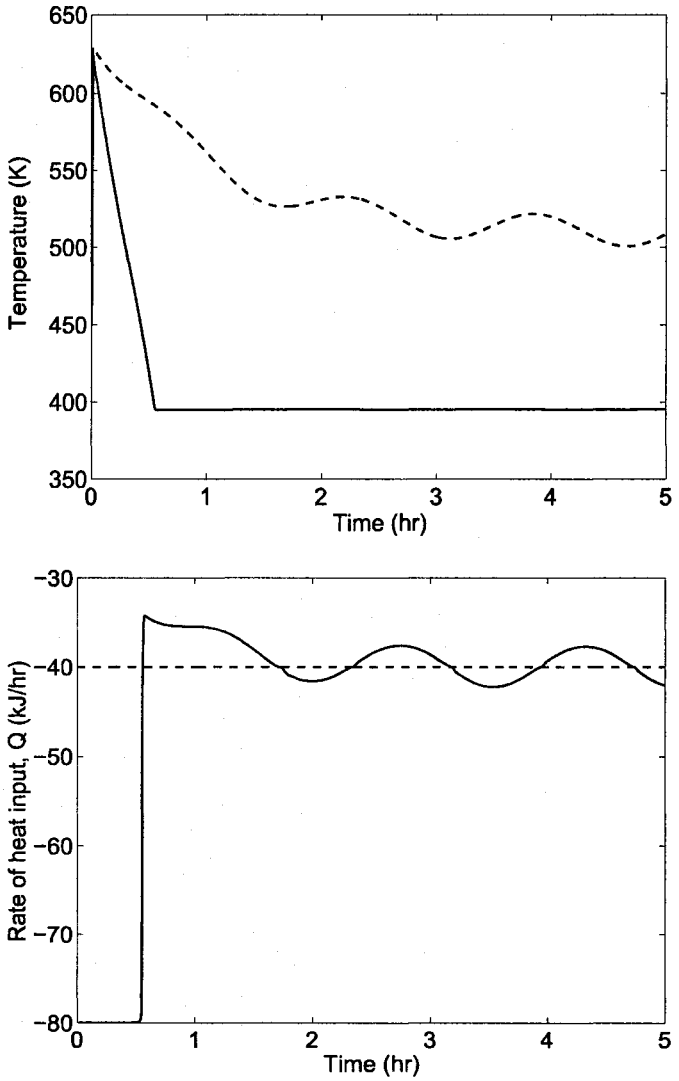

Figure 7.6: Reactor temperature and rate of heat input profiles under the bounded robust controller of the first mode, i.e., control valve closed and $\sigma = 0$ (solid lines) and under open-loop conditions (dashed lines).

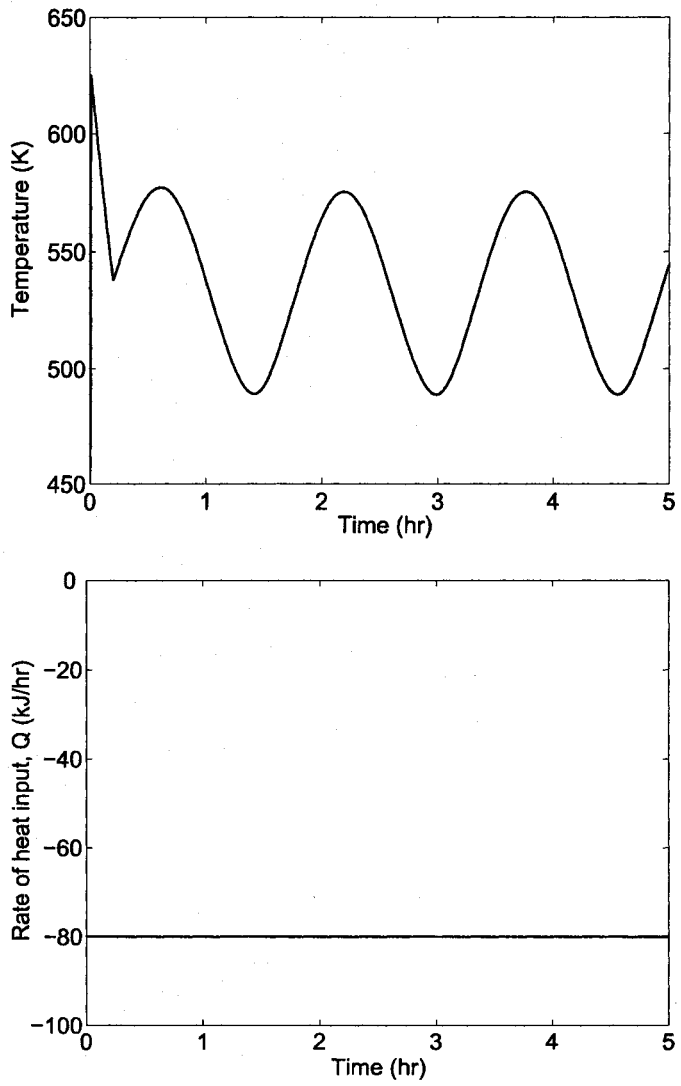

Figure 7.7: Reactor temperature and rate of heat input profiles when the reactor is initially operated in the first mode (control valve closed, $\sigma = 0$) using the corresponding robust controller, then the control valve is opened ($\sigma = 1$) at $t = 12$ min and the robust controller for the second mode is activated in place of the first controller.

Now, instead of choosing the switching time arbitrarily, suppose that the nominal switching laws proposed in [90] are used. These laws were used to address a similar switched reactor control problem under nominal conditions (without uncertainty). This scenario is considered here to study the effect of uncertainty on switching. To this end, consider first the case where no uncertainty is present (i.e., $\theta_i \equiv 0$) and initialize the closed-loop system within the first mode (control valve closed, $\sigma = 0$) at the same admissible initial condition, considered previously, using the first controller with $\rho_1 = \chi_1 = 0$. By tracking the closed-loop trajectory in time, it is found that the process state enters the stability region of the second mode at $t = 24\ min$. Consequently, the mode transition (including a switch to the second controller with $\rho_2 = \chi_2 = 0$) is carried out at this time. The resulting controlled output and manipulated input profiles are depicted by the solid lines in Figure 7.8 which show that the reactor temperature stabilizes at the desired steady-state in the absence of uncertainty.

Suppose now that the "nominally-safe" switching time, $t = 24\ min$, is used when model uncertainty is present. The resulting temperature and heat input profiles are shown by the dashed lines in Figure 7.8 and Figure 7.9, which depict, respectively, the case when the controllers do not compensate for the effect of uncertainty ($\rho_i = \chi_i = 0$) and the case when they compensate for the effect of uncertainty. It is clear from the unstable behavior in both profiles that the effect of uncertainty is significant and that, even when a robust controller is used in each mode, the nominal switching rules (or times) cannot guarantee closed-loop stability when uncertainty is present. As indicated by the input profiles, which remain saturated for all times, the state lies outside the stability region of the second mode at $t = 24\ min$. These results underscore the fact that, for hybrid processes, the impact of model uncertainty transcends the well-known adverse effects on the stability and performance of purely continuous processes

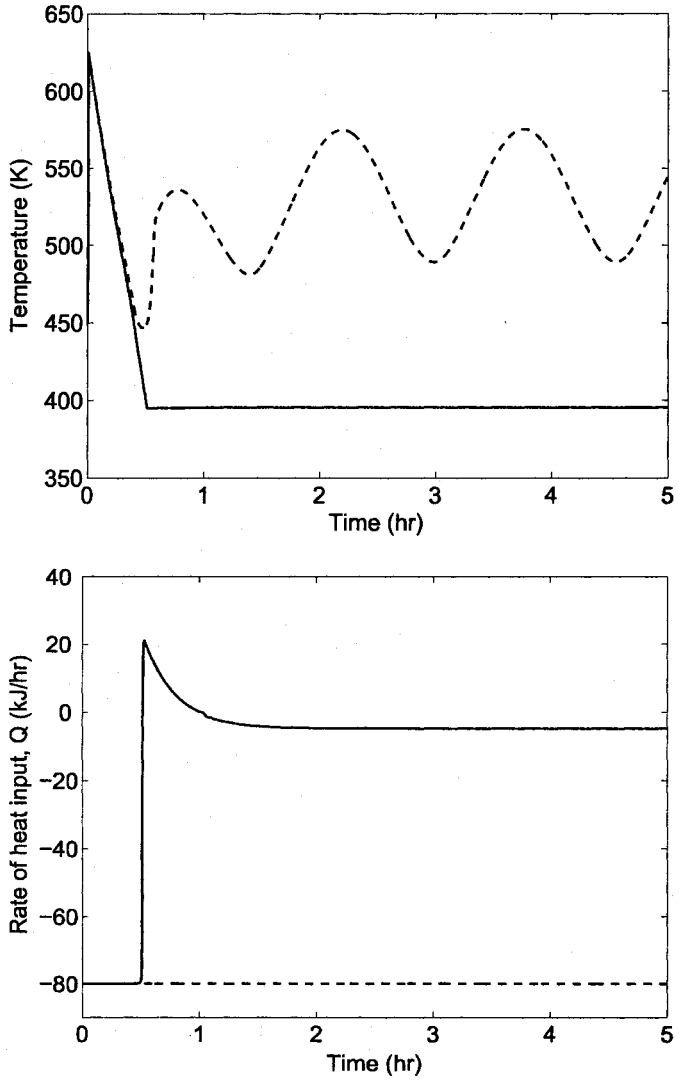

Figure 7.8: Reactor temperature and rate of heat input profiles for the case when mode switching is carried out at $t = 24$ min with no uncertainty present (solid lines) and for the case when uncertainty is present and mode switching (using nominal controllers with $\rho_i = \chi_i = 0$) is carried out at $t = 24$ min (dashed lines).

(which comprise in this case the lower-level modes of the hybrid process) since uncertainty impacts also on the design of the switching logic. Owing to the limitations imposed by actuator constraints on the stability regions of the constituent modes of the hybrid process, the design of a stabilizing switching scheme requires knowledge of these stability regions, in order to decide when (or where, in the state-space,) a particular mode can be activated. However, when plant-model discrepancies are taken into consideration, the actual stability region of each mode can be quite smaller than the one obtained under nominal conditions (compare, for example, the expression in Eq.7.10 with and without the uncertainty term, θ_{bi}). Consequently, nominal characterizations of stability regions can no longer guarantee safe mode switching, and the switching rules need to be modified.

In the final set of simulation runs, the switching scheme proposed in Theorem 7.2, which is based on stability regions that account for the presence of plant-model mismatch, is implemented. In this case, the reactor is initialized in the $\sigma = 0$ mode, using the corresponding robust controller, and then a switch to the $\sigma = 1$ mode (and its robust controller) is carried out only when the condition in Eq.7.11 is satisfied (note that the condition of Eq.7.12 is not needed since the initial mode is not reactivated). The controlled output and manipulated input profiles for this case are depicted by the solid lines in Figure 7.9 which show that the robust hybrid control strategy successfully drives the reactor temperature to the desired steady-state while attenuating the effect of uncertainty. The transition between the two modes becomes safe after about 30 minutes of reactor startup.

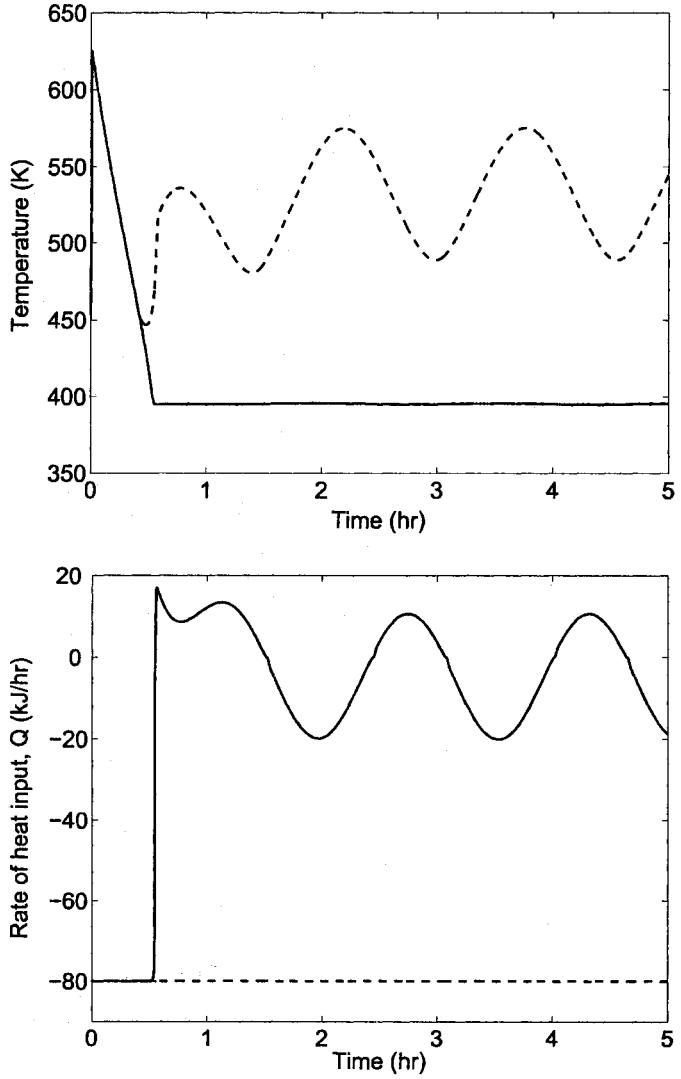

Figure 7.9: Reactor temperature and rate of heat input profiles for the cases when uncertainty is present and mode switching (using the bounded robust controllers) is carried out at $t = 24$ min (dashed lines) and at $t = 30$ min (solid lines).

7.5 Conclusions

In this chapter, a hybrid control strategy, for a broad class of hybrid nonlinear processes with actuator constraints and model uncertainty, was developed. The control strategy coordinated, via multiple Lyapunov functions, the tasks of feedback controller synthesis and logic-based switching between the constituent modes. A family of feedback controllers were designed to enforce robust stability within the constituent modes and provide an explicit characterization of the constrained region of robust stability for each mode. The stability regions were then used to derive stabilizing switching rules that orchestrate the transition between the various modes (and their controllers) in a way that guarantees robust stability for the overall hybrid process. The proposed hybrid control method was applied, through computer simulations, to robustly stabilize an exothermic chemical reactor with switched dynamics, model uncertainty and actuator constraints at an unstable steady-state.

Chapter 8

Fault-Tolerant Control of Process Systems

8.1 Introduction

Safety and reliability are primary goals in the operation of industrial chemical plants. An important national need currently exists for enhancing the safety and reliability of chemical plants in ways that reduce their vulnerability to serious failures. Increasingly faced with the requirements of operational flexibility under tight performance specifications and other economic drivers, plant operation is relying extensively on highly automated process control systems. Automation, however, tends to increase vulnerability of the plant to faults, such as defects/malfunctions in process equipment, sensors and actuators, failures in the controllers or in the control loops, which, if not appropriately handled in the control system design, can potentially cause a host of undesired economic, environmental, and safety problems that seriously degrade the operating efficiency of the plant. These considerations provide a strong motivation for the development of systematic methods and strategies for the design of fault–tolerant control systems and have motivated many research studies in this

area (see, for example, [311, 316, 32] and [236, 41, 209] for references).

Given the complex dynamics of chemical processes (due, for example, to the presence of nonlinearities and constraints) and the geographically distributed, interconnected nature of plant units, as well as the large number of distributed sensors and actuators typically involved, the success of any fault–tolerant control strategy requires an integrated approach that brings together several essential elements, including: (1) the design of advanced feedback control algorithms that handle complex dynamics effectively, (2) the design of supervisory switching schemes that orchestrate the transition from the failed control configuration to available well–functioning fall–back configurations to ensure fault–tolerance, and (3) the efficient exchange of information and communication between the different plant units through a high–level supervisor that coordinates the overall plant response in failure situations and minimizes the effects of failure propagation.

The realization of such an approach is increasingly aided by a confluence of recent, and ongoing, advances in several areas of process control research, including advances in nonlinear controller designs for chemical processes (e.g., [163, 160, 91, 94, 301]) and advances in the analysis and control of hybrid process systems leading to the development of a systematic framework for the integration of feedback and supervisory control [93, 95]. A hybrid systems framework provides a natural setting for the analysis and design of fault–tolerant control systems since the occurrence of failure and subsequent switching to fall–back control configurations induce discrete transitions superimposed on the underlying continuous dynamics. Hybrid control techniques have been useful in dealing with a wide range of problems that cannot be addressed using classical control approaches, including fault–tolerant control of spatially–distributed systems (e.g., [98]), control of processes with switched dynamics (e.g., [95, 37]), and the design

of hybrid predictive control structures that overcome some of the limitations of classical predictive control algorithms (e.g., [101]). In addition to control studies, research work on hybrid systems spans a diverse set of problems ranging from the modeling (e.g., [315, 33]) and simulation (e.g., [33, 118]) to the optimization (e.g., [128, 126]) and stability analysis (e..g, [138, 81]) of several classes of hybrid systems.

In addition to the above fundamental advances, recent innovations in actuator/sensor and communication technologies are increasingly enabling the integration of communication and control domains [319]. For example, the use of communication networks as media to interconnect the different components in an industrial control system is rapidly increasing and expected to replace the more costly point–to–point connection schemes currently employed in distributed control systems. Figure 8.1 shows the basic networked control architecture for (a) a single–unit plant with few actuators and sensors (centralized structure) and (b) a larger plant with several interconnected processing units and larger number of actuators and sensors (distributed hierarchical structure). Currently, networked control systems is an active area of research within control engineering (e.g., see [306, 224, 297, 235, 314] for some recent results and references in this area). In addition to the advantages of reduced system wiring (reduced installation, maintenance time and costs) in this architecture, the increased flexibility and ease of maintenance of a system using a network to transfer information is an appealing goal. In the context of fault–tolerant control in particular, systems designed in this manner allow for easy modification of the control strategy by rerouting signals, having redundant systems that can be activated automatically when component failure occurs, and in general they allow having a high–level supervisor control over the entire plant. The appealing features of communication networks motivate investigating ways for integrating them in the design of fault–tolerant con-

trol systems to ensure a timely and coordinated response of the plant in ways that minimize the effects of failure propagation between plant units. This entails devising strategies to deal with some of the fundamental issues introduced by the network, including issues of bandwidth limitations, quantization effects, network scheduling, and communication delays, which continue to be topics of active research.

Motivated by the above considerations, we develop in this chapter a fault–tolerant control system design methodology, for plants with multiple (distributed) interconnected processing units, that accounts explicitly for the inherent complexities in supervisory control and communication tasks resulting from the distributed interconnected nature of plant units. The approach brings together tools from Lyapunov–based control and hybrid systems theory and is based on a hierarchical distributed architecture that integrates lower–level feedback control of the individual units with upper–level logic–based supervisory control over communication networks. The local control systems consist each of a family of feedback control configurations together with a local supervisor that communicates with actuators and sensors, via a local communication network, to orchestrate the transition between control configurations, on the basis of their fault–recovery regions, in the event of failures. The local supervisors communicate, through a plant–wide communication network, with a plant supervisor responsible for monitoring the different units and coordinating their responses in a way that minimizes the propagation of failure effects. The communication logic is designed to ensure efficient transmission of information between units while also respecting the inherent limitations in network resources by minimizing unnecessary network usage and accounting explicitly for the effects of possible delays due to fault–detection, control computations, network communication, and actuator activation. The proposed approach provides explicit guidelines for managing the interplays between the cou-

pled tasks of feedback control, fault–tolerance and communication. The efficacy of the proposed approach is demonstrated through chemical process examples.

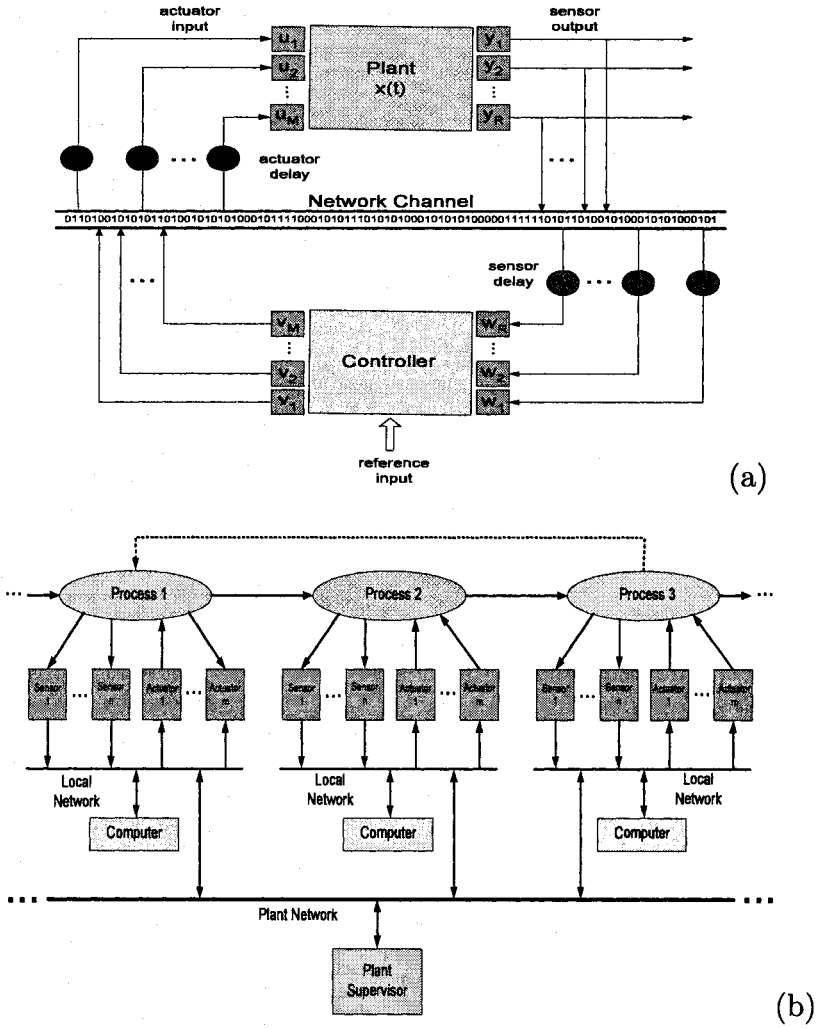

Figure 8.1: Block diagrams of: (a) a centralized networked control system for a single–unit plant, and (b) a hierarchical distributed networked control architecture for a multi–unit plant.

8.2 Preliminaries

8.2.1 System description

We consider a plant composed of l connected processing units, each of which is modeled by a continuous–time multivariable nonlinear system with constraints on the manipulated inputs, and represented by the following state–space description:

$$\begin{aligned}
\dot{x}_1 &= f_1^{k_1}(x_1) + G_1^{k_1}(x_1)u_1^{k_1} \\
\dot{x}_2 &= f_2^{k_2}(x_2) + G_2^{k_2}(x_2)u_2^{k_2} + W_{2,1}^{k_2}(x_2)x_1 \\
&\vdots \\
\dot{x}_l &= f_l^{k_l}(x_l) + G_l^{k_l}(x_l)u_l^{k_l} + \sum_{p=1}^{l-1} W_{l,p}^{k_l}(x_l)x_p \\
\|u_i^{k_i}\| &\leq u_{i,max}^{k_i} \\
k_i(t) &\in \mathcal{K}_i := \{1, \cdots, N_i\}, \quad N_i < \infty, \quad i = 1, \cdots, l
\end{aligned} \tag{8.1}$$

where $x_i := [x_i^{(1)}\ x_i^{(2)}\ \cdots\ x_i^{(n_i)}]^T \in \mathbb{R}^{n_i}$ denotes the vector of process state variables associated with the i–th processing unit, $u_i^{k_i} := [u_{i,1}^{k_i}\ u_{i,2}^{k_i}\ \cdots\ u_{i,m_i}^{k_i}]^T \in \mathbb{R}^{m_i}$ denotes the vector of constrained manipulated inputs associated with the k_i–th control configuration in the i–th processing unit, $u_{i,max}^{k_i}$ is a positive real number that captures the maximum size of the vector of manipulated inputs dictated by the constraints, $\|\cdot\|$ denotes the Euclidean norm of a vector, and N_i is the number of different control configurations that can be used to control the i–th processing unit. The index, $k_i(t)$, which takes values in the finite set $\mathcal{K}_i$, represents a discrete state that indexes the right–hand side of the set of differential equations in Eq.8.1. For each value that k_i assumes in $\mathcal{K}_i$, the i–th processing unit is controlled via a different set of manipulated inputs which define a given control configuration. For each unit, switching between the available N_i control configurations is controlled by a local supervisor that mon-

itors the operation of the unit and orchestrates, accordingly, the transition between the different control configurations in the event of control system failures. This in turn determines the temporal evolution of the discrete state, $k_i(t)$, which takes the form of a piecewise constant function of time. The local supervisor ensures that only one control configuration is active at any given time, and allows only a finite number of switches over any finite interval of time.

Without loss of generality, it is assumed that $x_i = 0$ is an equilibrium point of the uncontrolled i–th processing unit (i.e., with $u_i^{k_i} = 0$) and that the vector functions, $f_i^{k_i}(\cdot)$, and the matrix functions, $G_i^{k_i}(\cdot)$ and $W_{j,p}^{k_j}(\cdot)$, are sufficiently smooth on their domains of definition, for all $k_i \in \mathcal{K}_i$, $i = 1, \cdots, l$, $j = 2, \cdots, l$, $p = 1, \cdots, l-1$. For the j–th processing unit, the term, $W_{j,p}^{k_j}(x_j)x_p$, represents the connection that this unit has with the p–th unit upstream. Note from the summation notation in Eq.8.1 that each processing unit can in general be connected to all the units upstream from it. Our nominal control objective (i.e., in the absence of control system failures) is to design, for each processing unit, a stabilizing feedback controller that enforces asymptotic stability of the origin of the closed–loop system in the presence of control actuator constraints. To simplify the presentation of our results, we will focus only on the state feedback problem where measurements of all process states are available for all times.

8.2.2 Problem statement and solution overview

Consider the plant of Eq.8.1 where, for each processing unit, a stabilizing feedback control system has been designed and implemented. Given some catastrophic fault – that has been detected and isolated – in the actuators of one of the control systems, our objective is to develop a plant–wide fault–tolerant control strategy that: (1)

preserves closed–loop stability of the failing unit, if possible, and (2) minimizes the negative impact of this failure on the closed–loop stability of the remaining processing units downstream. To accomplish both of these objectives, we construct a hierarchical control structure that integrates lower–level feedback control of the individual units with upper–level logic–based supervisory control over communication networks. The local control system for each unit consists of a family of control configurations for each of which a stabilizing feedback controller is designed and the stability region is explicitly characterized. The actuators and sensors of each configuration are connected, via a local communication network, to a local supervisor that orchestrates switching between the constituent configurations, on the basis of the stability regions, in the event of failures. The local supervisors communicate, through a plant–wide communication network, with a plant supervisor responsible for monitoring the different units and coordinating their responses in a way that minimizes the propagation of failure effects. The basic problem under investigation is how to coordinate the tasks of feedback, control system reconfiguration and communication, both at the local (processing unit) and plant–wide levels in a way that ensures timely recovery in the event of failure and preserves closed–loop stability.

Remark 8.1 In the design of any fault–tolerant control system, an important task that precedes the control system reconfiguration is the task of fault–detection and isolation (FDI). There is an extensive body of literature on this topic including, for example, the design of fault–detection and isolation schemes based on fundamental process models (e.g., [110, 80]) and statistical/pattern recognition and fault diagnosis techniques (e.g., [309, 131, 76, 228, 19, 304]). In this work, we focus mainly on the interplay between the communication network and the control system reconfiguration task. To this end, we assume that the FDI tasks take place at a time scale that is very fast compared to the time constant of the overall process dynamics and the time needed for the control system reconfiguration, and thus can be treated separately from

the control system reconfiguration (we note that the time needed for FDI is accounted for in the control system reconfiguration through a time–delay; see the Sections 8.3 and 8.4 for details). In the context of process control applications, this sequential and decoupled treatment of FDI and control system reconfiguration is further justified by the overall slow dynamics of chemical plants.

8.2.3 Motivating example

In this section, we introduce a simple benchmark example that will be revisited later to illustrate the design and implementation aspects of the fault–tolerant control design methodology to be proposed in Section 8.3. While the discussion will center around this example, we note that the proposed framework can be applied to more complex plants involving more complex arrangements of processing units as shown in Eq.8.1. To this end, consider two well–mixed, non–isothermal continuous stirred tank reactors (CSTRs) in series, where three parallel irreversible elementary exothermic reactions of the form $A \xrightarrow{k_1} B$, $A \xrightarrow{k_2} U$ and $A \xrightarrow{k_3} R$ take place, where A is the reactant species, B is the desired product and U, R are undesired byproducts. The feed to CSTR 1 consists of pure A at flow rate F_0, molar concentration C_{A0} and temperature T_0, and the feed to CSTR 2 consists of the output of CSTR 1 and an additional fresh stream feeding pure A at flow rate F_3, molar concentration C_{A03} and temperature T_{03}. Due to the non–isothermal nature of the reactions, a jacket is used to remove/provide heat to both reactors. Under standard modeling assumptions, a mathematical model of the plant can be derived from material and energy balances and takes the following

form:

$$\begin{aligned}
\frac{dT_1}{dt} &= \frac{F_0}{V_1}(T_0 - T_1) + \sum_{i=1}^{3}\frac{(-\Delta H_i)}{\rho c_p}R_i(C_{A1}, T_1) + \frac{Q_1}{\rho c_p V_1} \\
\frac{dC_{A1}}{dt} &= \frac{F_0}{V_1}(C_{A0} - C_{A1}) - \sum_{i=1}^{3}R_i(C_{A1}, T_1) \\
\frac{dT_2}{dt} &= \frac{F_1}{V_2}(T_1 - T_2) + \frac{F_3}{V_2}(T_{03} - T_2) + \sum_{i=1}^{3}\frac{(-\Delta H_i)}{\rho c_p}R_i(C_{A2}, T_2) + \frac{Q_2}{\rho c_p V_2} \\
\frac{dC_{A2}}{dt} &= \frac{F_1}{V_2}(C_{A1} - C_{A2}) + \frac{F_3}{V_2}(C_{A03} - C_{A2}) - \sum_{i=1}^{3}R_i(C_{A2}, T_2)
\end{aligned} \tag{8.2}$$

where $R_i(C_{Aj}, T_j) = k_{i0}\exp\left(\frac{-E_i}{RT_j}\right)C_{Aj}$, for $j = 1, 2$. T, C_A, Q, and V denote the temperature of the reactor, the concentration of species A, the rate of heat input/removal from the reactor, and the volume of reactor, respectively, with subscript 1 denoting CSTR 1 and subscript 2 denoting CSTR 2. ΔH_i, k_i, E_i, $i = 1, 2, 3$, denote the enthalpies, pre–exponential constants and activation energies of the three reactions, respectively, c_p and ρ denote the heat capacity and density of the reactor. Using typical values for the process parameters (see Table 8.1), CSTR 1, with $Q_1 = 0$, has three steady–states: two locally asymptotically stable and one unstable at $(T_1^s, C_{A1}^s) = (388.57\ K, 3.59\ kmol/m^3)$. The unstable steady–state of CSTR 1 corresponds to three steady–states for CSTR 2 (with $Q_2 = 0$), one of which is unstable at $(T_2^s, C_{A2}^s) = (429.24\ K, 2.55\ kmol/m^3)$.

The control objective is to stabilize both reactors at the (open–loop) unstable steady–states. Operation at these points is typically sought to avoid high temperatures, while simultaneously achieving reasonable conversion. To accomplish the control objective under normal conditions (with no failures), we choose as manipulated inputs the rates of heat input, $u_1^1 = Q_1$, subject to the constraint $|Q_1| \leq u_{max}^{Q_1} = 2.7 \times 10^6\ KJ/hr$ and $u_1^2 = Q_2$, subject to the constraint $|Q_2| \leq u_{max}^{Q_2} = 2.8 \times 10^6\ KJ/hr$.

As shown in Figure 8.2, each unit has a local control system with its sensors

Table 8.1: Process parameters and steady–state values for the reactors of Eq.8.2.

F_0	=	4.998	m^3/hr
F_1	=	4.998	m^3/hr
F_3	=	30.0	m^3/hr
V_1	=	1.0	m^3
V_2	=	3.0	m^3
R	=	8.314	$KJ/kmol \cdot K$
T_0	=	300.0	K
T_{03}	=	300.0	K
C_{A0}	=	4.0	$kmol/m^3$
C^s_{A03}	=	2.0	$kmol/m^3$
ΔH_1	=	-5.0×10^4	$KJ/kmol$
ΔH_2	=	-5.2×10^4	$KJ/kmol$
ΔH_3	=	-5.4×10^4	$KJ/kmol$
k_{10}	=	3.0×10^6	hr^{-1}
k_{20}	=	3.0×10^5	hr^{-1}
k_{30}	=	3.0×10^5	hr^{-1}
E_1	=	5.0×10^4	$KJ/kmol$
E_2	=	7.53×10^4	$KJ/kmol$
E_3	=	7.53×10^4	$KJ/kmol$
ρ	=	1000.0	kg/m^3
c_p	=	0.231	$KJ/kg \cdot K$
T^s_1	=	388.57	K
C^s_{A1}	=	3.59	$kmol/m^3$
T^s_2	=	429.24	K
C^s_{A2}	=	2.55	$kmol/m^3$

and actuators connected through a communication network. The local control systems in turn communicate with the plant supervisor (and with each other) through a plant–wide communication network. Note that in designing each control system, only measurements of the local process variables are used (for example, the controller for the second unit uses only measurements of T_2 and C_{A2}). This decentralized architecture is intended to minimize unnecessary communication costs incurred by continuously sending measurement data from the first to the second unit over the network. We note that while this issue may not be a pressing one for the small plant considered here (where a centralized structure can in fact be easily designed), real plants nonetheless involve a far more complex arrangement of units with thousands of actuators and sensors, which makes the complexity of a centralized structure as well as the cost of using the network to share measurements between units quite significant. For this reason, we choose the distributed structure in Figure 8.2 in order to highlight some of the manifestations of the inherent interplays between the control and communication tasks.

The fault–tolerant control problem under consideration involves a total failure in both control systems after some time of startup, with the failure in the first unit being permanent. Our objective will be to preserve closed–loop stability of CSTR 2 by switching to an alternative control configuration involving, as manipulated variables, the rate of heat input, $u_2^1 = Q_2$, subject to the same constraint, and the inlet reactant concentration, $u_2^2 = C_{A03} - C_{A03}^s$, subject to the constraint $|C_{A03} - C_{A03}^s| \leq u_{max}^{C_{A03}} = 0.4\ kmol/m^3$ where $C_{A03}^s = 3.0\ kmol/m^3$. The main question, which we address in the next section, is how to devise the switching and network communication logics in a way that ensures fault–tolerance in the second unit and, simultaneously, accounts for the inherent limitations in network resources and possible delays in fault–detection,

communication and actuator activation.

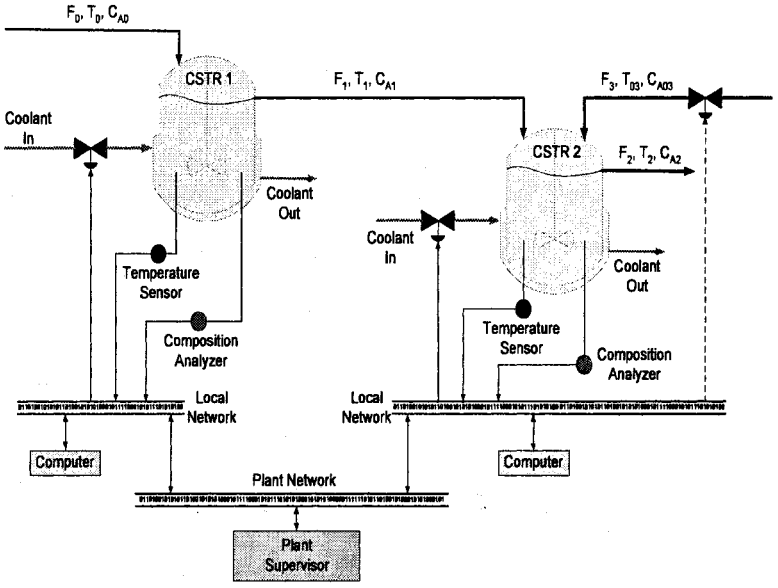

Figure 8.2: Process flow diagram of two CSTR units in series.

8.3 Fault–tolerant control system design methodology

In this section, we outline the main steps involved in the fault–tolerant control system design procedure. These include: (1) the synthesis of a stabilizing feedback controller for each of the available fall–back control configurations, (2) the explicit characterization of the stability region for each configuration which characterize the operating conditions for which fault–recovery can be guaranteed, (3) the design of a switching law that orchestrates the re–configuration of the failing control system in a way that safeguards closed–loop stability in the event of failures, and (4) the design of the network communication logic in a way that minimizes the propagation of failure effects between plant units while also accounting for bandwidth constraints and delays. A major feature of the design methodology is the inherent coupling between the aforementioned tasks whereby each task affects how the rest are carried out. Below is a

more detailed description of each step and a discussion on how the tradeoffs between the different steps are managed.

8.3.1 Constrained feedback controller synthesis

Referring to the system of Eq.8.1, consider first the case when no failures take place anywhere in the plant. Under such conditions, our objective is to design, for each processing unit, a "nominal" feedback controller that enforces asymptotic closed–loop stability and provides an explicit characterization of the stability region under actuator constraints. One way to do this is to use Lyapunov–based control techniques. Specifically, consider the nonlinear system describing the i–th processing unit under the k_i–th control configuration, for which a control Lyapunov function, $V_i^{k_i}$, is available. Using this function, one can construct the following bounded nonlinear control law (see [204, 91]):

$$u_i^{k_i} = -r(x_i, u_{i,max}^{k_i})\beta^T(x_i) \tag{8.3}$$

where

$$r(x_i, u_{i,max}^{k_i}) = \frac{\alpha^*(x_i) + \sqrt{(\alpha^*(x_i))^2 + \left(u_{i,max}^{k_i}\|\beta^T(x_i)\|\right)^4}}{\|\beta^T(x_i)\|^2\left[1+\sqrt{1+(u_{i,max}^{k_i}\|\beta^T(x_i)\|)^2}\right]} \tag{8.4}$$

$\alpha^*(x_i) = \alpha(x_i) + \rho_i^{k_i}\|x_i\|^2$, $\rho_i^{k_i} > 0$ is a real number, $\alpha(x_i) = L_{f_i^{k_i}}V_i^{k_i}(x_i)$, $\beta^T(x_i) = (L_{G_i^{k_i}}V_i^{k_i})^T(x_i)$, the notation $L_{f_i^{k_i}}V_i^{k_i}$ is used to denote the Lie derivative of the scalar function, $V_i^{k_i}$, with respect to the vector field, $f_i^{k_i}$, and $L_{G_i^{k_i}}V_i^{k_i}$ is a row vector whose constituent components are the Lie derivatives of $V_i^{k_i}$ along the column vectors of the matrix $G_i^{k_i}$. Note that the control law of Eqs.8.3–8.4 requires measurements of the local process state variables, x_i, only and not measurements from other plant units upstream. This fully decentralized design is motivated by the desire to minimize unnecessary communication costs which would be incurred when sharing measurement

data between the different units over the communication network. By disregarding the interconnections between the units in the controller design, however, closed–loop stability for a given unit rests on the stability properties of the upstream units. In particular, using a combination of Lyapunov and small–gain theorem type arguments, one can show that, starting from any invariant subset (e.g, a level–set of $V_i^{k_i}$) of the region described by:

$$\Phi_i(u_{i,max}^{k_i}) \;:=\; \{x_i \in \mathbb{R}^{n_i} :\; \alpha(x_i) + \rho_i^{k_i}\|x_i\|^2 \leq u_{i,max}^{k_i}\|\beta^T(x_i)\|\} \qquad (8.5)$$

the control law of Eqs.8.3–8.4 asymptotically stabilizes the i–th unit, under the k_i–th control configuration, at the origin provided that the closed–loop states of the upstream units, $x_1,\; x_2,\; \cdots,\; x_{i-1}$, converge asymptotically to the origin. In this case, and because of the way the various units are connected (see Eq.8.1), the closed–loop states of the upstream units can be viewed as bounded vanishing perturbations that affect the i–th unit and, therefore, a control law that asymptotically stabilizes the unperturbed i–th unit (i.e., disregarding the upstream states) also stabilizes the closed–loop system when the perturbations (connections) are added.

Having designed the nominal feedback control systems, we now proceed to consider the effect of control actuator failure on the feedback controller design for each unit. To this end, let us consider a total failure in the actuators of the k_i–th control configuration in the i–th control system. This failure, if not addressed properly, can lead to closed–loop instabilities both within the i–th processing unit itself (where the failure has occurred) and within all the remaining units downstream. Minimizing the effects of failure propagation throughout the plant can be achieved in one of two ways. The first involves reconfiguring the local control system of the i–th unit – once the failure is detected and isolated – by appropriately switching from the malfunctioning control configuration to some well–functioning fall–back configuration (recall that

each processing unit has a family of control configurations). If this is feasible and can be done sufficiently fast, then the inherent fault–tolerance of the local control system is sufficient to preserve closed–loop stability not only for the i-th unit with the failing control system but also for the other units downstream without having to reconfigure their control systems. However, if local fault–recovery is not possible (this can happen, for example, in cases when the failure occurs at times that the state lies outside the stability regions of all the available fall–back control configurations; see Section 8.3.2 for details), then it becomes necessary to communicate the failure information to the control systems downstream and reconfigure them in order to preserve their closed–loop stability.

The main issue here is how to design the feedback control law for a given fall–back configuration in the units downstream in a way that respects the actuators' constraints and guarantees closed–loop stability despite the failure in the control system of some upstream unit. The choice of the feedback law depends on our choice of the communication policy. To explain this interdependence, we first note that a total failure in the control system of the i–th unit will cause its state, x_i, to move away from the origin (possibly settling at some other steady–state). Therefore, unless the nominal feedback controllers for the downstream units, $i+1,\ i+2,\ \cdots, l$, are re–designed to account for this incoming "disturbance", the evolution of their states, $x_{i+1},\ x_{i+2},\ \cdots, x_l$, will be adversely affected driving them away from the origin. To account for the disturbance caused by the upstream control system failure, one option is to send available measurements of x_i, through the communication network, to the affected units and redesign their controllers accordingly. From a communications cost point of view, however, this option may be costly since it requires continued usage of the network resources after the failure, which can adversely affect the performance of

other units sharing the same communication medium due to bandwidth limitations and overall delays.

To reduce unnecessary network usage, we propose an alternative approach where the failure in the i–th processing unit is viewed as a bounded non–vanishing disturbance affecting units $i+1,\ i+2,\ \cdots, l$, and use the available process models of these units to capture, or estimate, the size of this disturbance (by comparing, for example, the evolution of the process variables for the i–th unit under the failed and well–functioning control configurations through simulations). In this formulation, state measurements from the i–th unit need not be shared with the other units; instead, only bounds on the disturbance size are transmitted to the downstream units. This approach involves using the network only once at the failure time and not continuously thereafter. The disturbance information can then be used to design an appropriate robust controller for each downstream unit to attenuate the effect of the incoming disturbance and enforce robust closed–loop stability. To illustrate how this can be done, let us assume that the failure in the control system of unit i occurs at $t = T_f$ and that the failure is detected immediately (the effect of possible delays in fault–detection and how to account for them are discussed in Section 8.3.4). Consider some unit, j, downstream from the i–th unit, that is described by the following model:

$$\dot{x}_j \ = \ f_j^{k_j}(x_j) + G_j^{k_j}(x_j)u_j^{k_j} + \delta_i \sum_{p=1}^{i-1} W_{j,p}^{k_j}(x_j)x_p + \sum_{p=i}^{j-1} W_{j,p}^{k_j}(x_j)\theta_p \qquad (8.6)$$

for $i = 1, \cdots, l-1$, $j = i+1, \ \cdots, \ l$, where $\delta_i = 0$ for $i = 1$, and $\delta_i = 1$ for $i = 2, \cdots, l-1$. The third term on the right–hand side of Eq.8.6 describes the input from all the units upstream of unit i. The θ_p's are time–varying, but bounded, functions of time that describe the evolution of the states of the i–th unit and all the units downstream from unit i but upstream from unit j (i.e., $\theta_p(t) = x_p(t)$, $p = i, \cdots, j-1$). The choice of using the notation θ_p, instead of x_p, for units $i, \cdots, j-1$

is intended to distinguish the effect of these units (where the failure originates and propagates downstream) as non–vanishing disturbances to the j–th unit, compared with the units upstream from unit i which are unaffected by the failure. Note that for unit $j = i + 1$, which immediately follows the failing unit, the only source of disturbances that should be accounted for in its controller design is that coming from the i–th unit with the failing control system. However, for units that lie further downstream, i.e., for $j = i + 2, \cdots, l$, the controller design needs to account for the additional disturbances resulting from the effect of the failure on the intermediate units separating units i and j.

For a system of the form of Eq.8.6, one possible choice of a stabilizing controller is the following bounded robust Lyapunov–based control law proposed in Chapter 7 (see also Chapter 4 which has the general form:

$$u_j^{k_j} = -r_j(x_j, u_{j,max}^{k_j}, \theta_b)\beta^T(x_j), \tag{8.7}$$

where

$$r_j(x_j, u_{j,max}^{k_j}, \theta_b) = \frac{\alpha_1(x_j) + \sqrt{(\alpha_2(x_j))^2 + \left(u_{j,max}^{k_j}\|\beta^T(x_j)\|\right)^4}}{(\|\beta^T(x_j)\|)^2\left[1 + \sqrt{1 + (u_{j,max}^{k_j}\|\beta^T(x_j)\|)^2}\right]} \tag{8.8}$$

$$\alpha_1(x_j) = \alpha(x_j) + \left(\rho_j^{k_j}\|x_j\| + \sum_{p=i}^{j-1}\chi_j^{k_j}\theta_b^p(T_f)\|\omega_p^T(x_j)\|\right)\left(\frac{\|x_j\|}{\|x_j\| + \phi_j^{k_j}}\right) \tag{8.9}$$

$$\alpha_2(x_j) = \alpha(x_j) + \rho_j^{k_j}\|x_j\| + \sum_{p=i}^{j-1}\chi_j^{k_j}\theta_b^p(T_f)\|\omega_p^T(x_j)\| \tag{8.10}$$

$\theta_b^p(T_f) := \max_{t \geq T_f} \|x_p(t)\|$, $p = i, \cdots, j-1$ are positive real numbers the capture the size of the disturbances, originating from the failure in the control system of the i–th unit and propagating downstream, $\omega_p(x_j) = (L_{W_{j,p}^{k_j}} V_j^{k_j})(x_j)$ is a row vector whose constituent components are the Lie derivatives of $V_j^{k_j}$ along the column vectors of the matrix $W_{j,p}^{k_j}$, $V_j^{k_j}$ is a robust control Lyapunov function for the j–th system under the

k_j–th control configuration, and $\rho_j^{k_j} > 0$, $\chi_j^{k_j} > 1$, $\phi_j^{k_j} > 0$ are tuning parameters. Estimates of the disturbance bounds, θ_b^p, can be obtained by comparing, through simulations for example, the responses of the p–th unit under the pre– and post–failure configurations (see Section 8.4 for an example). It should be noted that since all the incoming disturbances to unit j take effect only after T_f, the controller of Eqs.8.7–8.10 is implemented only for $t \geq T_f$. For $t < T_f$, the nominal controllers of Eqs.8.3–8.4 are used.

Remark 8.2 When compared with the nominal controller of Eqs.8.3–8.4, we observe that the nonlinear gain function for the fall–back controller, $r_j(\cdot)$ in Eqs.8.7–8.10, depends not only on the size of actuator constraints, $u_{j,max}^{k_j}$, and the particular fall–back control configuration being used, k_j, but also on the size of the disturbances caused by the occurrence of failure, θ_b^p. This gain re–shaping procedure is carried out in order to guarantee constraint satisfaction and enforce robust closed–loop stability, with an arbitrary degree of attenuation of the effect of the failure on the j–th unit downstream. Note that, owing to the assumption of a persistent failure in the i–th unit (i.e., a non–vanishing disturbance), asymptotic closed–loop stability cannot be achieved for any of the units downstream. Instead, practical stability can be enforced whereby the states of each unit are driven, in finite–time, to a neighborhood of the origin whose size can be made arbitrarily small by selecting the controller tuning parameters ($\rho_j^{k_j}$, $\chi_j^{k_j}$, $\phi_j^{k_j}$) appropriately (see [94] for a detailed proof). These closed–loop properties are enforced within a well–defined state–space region that is explicitly characterized in Section 8.3.2.

Remark 8.3 Note that since the processing units upstream of unit i are not affected by its failing control system, the nominal controllers designed for these units (see Eqs.8.3–8.4) will asymptotically stabilize their states, x_p, $p = 1, \cdots, i-1$, at the origin regardless of the failure; hence these state can be viewed as bounded vanishing inputs to the j–th unit and thus need not be accounted for in the controller design.

The terms describing the intermediate units, $p = i+1, \cdots, j-1$ cannot however be treated as vanishing inputs. The reason is that even if the control systems of these units are immediately and appropriately re–configured to suppress the effect of the failure, their controllers, as discussed above, will at best be able to drive the states of these units, in finite time, only near the origin without achieving asymptotic convergence.

Remark 8.4 It should be noted that the fault–tolerant control system design methodology proposed in this section is not restricted to the use of the bounded controller designs given in Eqs.8.3–8.4 (for the nominal case) and in Eqs.8.7–8.10 (for the case with failure). Any other stabilizing controller design that accounts for the constraints, enforces the desired robustness properties under failure, and provides an explicit characterization of the stability region can be used.

Remark 8.5 The treatment of the failure in the control system of unit i as a bounded disturbance is rooted in the assumption that x_i, while moving away from the origin after failure, will eventually settle at some other (undesirable) steady–state (recall that this is how the disturbance bound is computed). In the case when the i–th processing unit has only a single steady–state in the post–failure configuration, however, the failure cannot be treated as a bounded disturbance since x_i will simply grow unbounded after the failure and not settle anywhere. In such a case, unless the control system of unit i is fixed in time, a shutdown of the plant will be unavoidable.

8.3.2 Characterization of fault–recovery regions

Consider once again the j–th processing unit described by the model of Eq.8.6. In Section 8.3.1, we outlined how to design, for a given fall–back control configuration, $k_j \in \mathcal{K}_j$, a robust feedback controller that, when implemented, can preserve closed–loop stability for this unit in the event of control system failure in some upstream unit, i. Given that actuator constraints place fundamental limitations on the ability

of the controller to steer the closed–loop dynamics at will, it is important for the control system designer to explicitly characterize these limitations by identifying, or estimating, the set of admissible states starting from where the controller of Eqs.8.7–8.10 is guaranteed to robustly stabilize the closed–loop system for unit j (region of robust closed–loop stability). Since suppression of the upstream failure effects on unit j is formulated as a robust stabilization problem, we shall refer to the robust stability region associated with any of the fall–back configurations also as the fault–recovery region. As discussed in Section 8.3.3, the characterization of this region plays a central role in devising the appropriate switching policy that reconfigures the control system and ensures fault–recovery.

For the class of robust control laws given in Eqs.8.7–8.10, using a Lyapunov argument one can show that the set, $\Pi_j^{k_j}(u_{j,max}^{k_j}, \theta_b(T_f)) :=$

$$\{x_j \in \mathbb{R}^{n_j} : \alpha(x_j) + \rho_j^{k_j}\|x_j\| + \sum_{p=i}^{j-1} \chi_j^{k_j} \theta_b^p(T_f)\|\omega_p^T(x_j)\| \leq u_{j,max}^{k_j}\|\beta^T(x_j)\|\} \qquad (8.11)$$

describes a region in the state–space where the control action satisfies the constraints and the Lyapunov function decays monotonically along the trajectories of the closed–loop system (see [94] for the detailed mathematical analysis). Note that the size of this set depends both on the magnitude of the constraints and the size of the disturbance (which in turn depends on the failure time, T_f). In particular, as the constraints become tighter and/or the disturbances greater, the set gets smaller. For a given control configuration, one can use the above inequality to estimate the fault–recovery region associated with this configuration by constructing, for example, the largest invariant subset of Π_j, which we denote by $\Omega_j^{k_j}(u_{j,max}^{k_j}, \theta_b(T_f))$. For a given fall–back configuration, k_j, implementation of the controller of Eqs.8.7–8.10 at any time that the state is within $\Omega_j^{k_j}$ ensures that the closed–loop trajectory stays within the region defined by Π_j – and hence $V_j^{k_j}$ continues to decay monotonically – for all

the times that the given fall–back control configuration is active.

Remark 8.6 Note that, unlike the nominal stability regions associated with the nominal controllers of Eqs.8.3–8.4 and obtained from Eq.8.5, the fault–recovery region of any downstream unit, j, cannot be computed a priori (i.e., before plant startup) since this region, as can be seen from Eq.8.11, depends on the failure time which is unknown prior to startup. However, once the failure occurs, estimates of the disturbance bounds can be computed by the local supervisors of the upstream units, $i, \cdots, j-1$ (through on–line simulations of each unit's response under the pre– and post–failure configurations) and then transmitted, through the communication network, to unit j which in turn uses these bounds to construct, on–line, both the controller and the fault–recovery region (see Section 8.3.4 for a discussion on how the resulting computational delays can be handled).

8.3.3 Supervisory switching logic design

Having designed the robust feedback control law and characterized the fault–recovery region associated with each fall–back configuration, the third step in our design methodology is to derive the switching policy that the local supervisor of the downstream unit, j, needs to follow in reconfiguring the local control system (i.e., activating/deactivating the appropriate fall–back configurations) in the event of the upstream failure. In the general case, when more than one fall–back control configuration is available for the unit under consideration, the question is how to decide which of these configurations can and should be activated at the time of failure in order to preserve closed–loop stability. The key idea here is that, because of the limitations imposed by constraints on the fault–recovery region of each configuration, the local supervisor can only activate the configuration whose fault–recovery region contains the closed–loop state at the time of the failure. Without loss of generality, let the active control configuration in the j–th unit, priori to the occurrence of failure

in unit i, be $k_j(T_f^-) = \mu$ for some $\mu \in \mathcal{K}_j$, where $k_j(T_f^-) = \lim_{t \to T_f^-} k_j(t)$ and T_f is the time that the control system of unit i fails, then the switching rule given by

$$k_j(T_f^+) \;=\; \nu \;\; if \;\; x_j(T_f) \;\in\; \Omega_j^{\nu}(u_{j,max}^{\nu}, \theta_b(T_f)) \tag{8.12}$$

for some $\nu \in \mathcal{K}_j$, $\nu \neq \mu$, guarantees that the closed–loop system of the j–th unit is stable. The implementation of the above switching law requires monitoring, by the local supervisor, of the evolution of the closed–loop state trajectory with respect to the fault–recovery regions associated with the various control actuator configurations. Another way to look at the above switching logic is that it implicitly determines, for a fixed fall–back configuration, the times that the control system of the j–th unit can tolerate upstream failures by switching to this configuration. If failure occurs at times when x_j lies outside the fault–recovery region of all available configurations, this analysis suggests that either the constraints should be relaxed – to enlarge the fault–recovery region of the given configurations – or additional fall–back control loops must be introduced. The second option, however, is ultimately limited by the maximum allowable number of control loops that can be designed for the given processing unit. If neither option is feasible, a shutdown could be unavoidable. The proposition of constructing the switching logic on the basis of the stability regions was first proposed in [93] for the control of switched nonlinear systems.

8.3.4 Design of the communication logic

Given the distributed interconnected nature of the plant units – and thus the potential for failure effects propagating from one unit to another – an essential element in the design of the fault–tolerant control system is the use of a communication medium that ensures fast and efficient transmission of information during failure events. As discussed in the introduction, communication networks offer such a medium that is

both fast (relative to the typically slow dynamics of chemical processes) and inexpensive (relative to current point–to–point connection schemes which require extensive cabling and higher maintenance time and costs). The ability of the network to fulfill this role, however, requires that we devise the communication policy in a way that respects the inherent limitations in network resources, such as bandwidth constraints and overall delays, by minimizing unnecessary usage of the network.

In Section 8.3.1, we have already discussed how the bandwidth constraint issue can be handled by formulating the problem as a robust control problem, where the failure in the control system of the i–th processing unit and the consequent effects on units $i+1, \cdots, j-1$ are treated as a bounded non–vanishing disturbances that affect unit j downstream. The communication policy requires that the local supervisors of units i, $\cdots, j-1$ perform the following tasks: (1) compute the disturbance bounds using the process model of each unit, and (2) send this information, together with other relevant information such as the failure type, the failure time and operating conditions, to the plant supervisor. The plant supervisor in turn forwards the information to the local supervisor of unit j utilizing the plant–wide communication network (see Figure 8.1b). This policy avoids unnecessary overloading of the network (which could result when measurements from the upstream units are sent continuously to unit j) while also guaranteeing fault–tolerance in the downstream units. The idea of using knowledge of the plant dynamics to balance the tradeoff between bandwidth limitations (which favor reduced communication of measurements) and optimum control performance (which favors increased communication of measurements) is conceptually aligned with the notion of minimum attention control (e.g., see [45, 224]). In our work, however, this idea is utilized in the context of fault–tolerant control.

The second consideration in devising the communication logic is the issue of time–

delays which typically result from the time sharing of the communication medium as well as the computing time required for the physical signal coding and communication processing. The characteristics of these time–delays depend on the network protocols adopted as well as the hardware chosen. For our purposes here, we consider an overall fixed time–delay (which we denote by τ^j_{max}) that combines the contribution of several delays, including: (1) delays in fault–detection, (2) the time that the local supervisors of units $i, \cdots, j-1$ take to compute the effective disturbance bounds (through simulations comparing the pre– and post–failure state evolutions in each unit), (3) the time that the local supervisors of units $i, \cdots, j-1$ take to send the information to the plant supervisor, (4) the time that it takes the plant supervisor to forward the information to the local supervisor of unit j, (5) the time that it takes the local supervisor for unit j to compute the fault–recovery region for the given fall–back configurations using the information arriving from the upstream units and the time that it takes for the supervisor's decision to reach and activate the appropriate fall–back configuration, and (6) the inherent actuator/sensor dead–times.

Failure to take such delays into account can result in activating the wrong control configuration and subsequent instability. For example, even though the upstream failure may take place at $t = T_f$, the fall–back configuration in the control system of unit j will not be switched in before $t = T_f + \tau^j_{max}$. If the delay is significant, then the switching rule in Section 8.3.3 should be modified such that the local supervisor for unit j activates configuration, $k_j = \nu$, for which $x_j(T_f + \tau^j_{max}) \in \Omega^\nu_j(u^\nu_{j,max}, \theta_b)$. This modification is yet another manifestation of the inherent coupling between the switching and communication logics. The implementation of the modified switching rule that accounts for delays requires that the local supervisor of unit j be able to predict where the state trajectory will be at $t = T_f + \tau^j_{max}$ (e.g., through simulations using the

process model) and check whether the state at this time is within the fault–recovery region of a given fall–back configuration. If not, then either an alternative fall–back configuration, for which the fault–recovery region contains the state at the end of the delay, should be activated or a shutdown maybe unavoidable. The availability of several fall–back control loops, however, is limited by process design considerations which dictate, for example, how many variables can be used for control. Figure 8.3 summarizes the overall fault–tolerant control strategy for a two–unit plant.

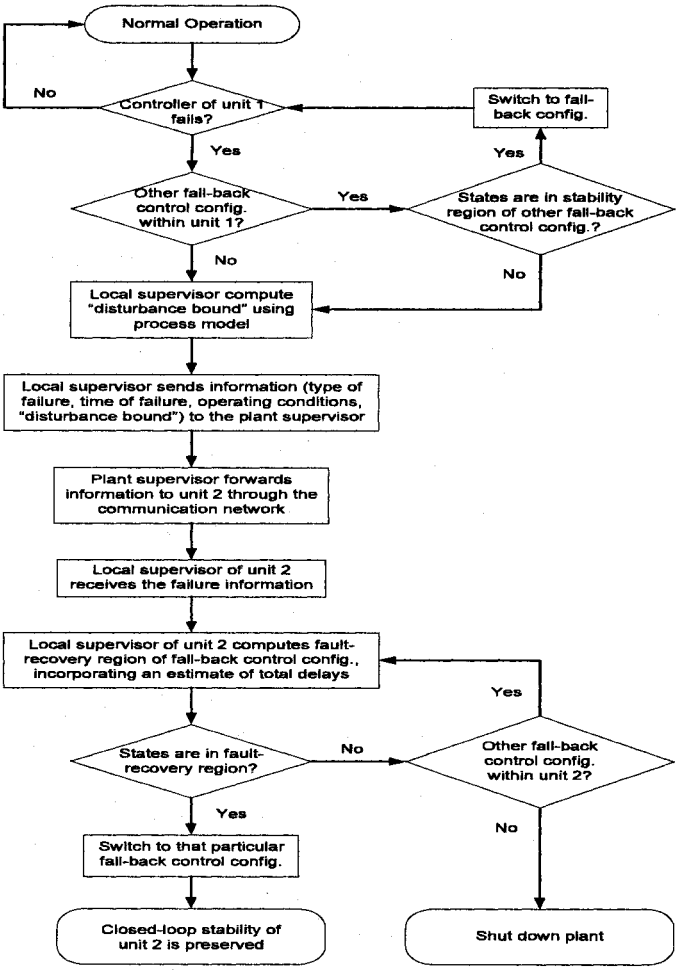

Figure 8.3: Summary of the fault–tolerant control strategy, for a two–unit plant, using communication networks.

8.4 Simulation studies

In this section, we present two simulation studies that demonstrate the application of the proposed fault–tolerant control system design methodology to two chemical processes. In the first application, a single chemical reactor example is considered to demonstrate the idea of re–configuring the local control system in the event of failures on the basis of the stability regions of the constituent control configurations, and how overall communication delays impact the re–configuration logic. In the second application, a cascade of two chemical reactors in series is considered to demonstrate how the issue of failure propagation between a multi–unit plant is handled within the proposed methodology, and how the various interplays between the feedback, supervisory control and communication tasks are handled in the multi–unit setting.

8.4.1 Application to a single chemical reactor

Consider a well–mixed, non–isothermal continuous stirred tank reactor where three parallel irreversible elementary exothermic reactions of the form $A \xrightarrow{k_1} B$, $A \xrightarrow{k_2} U$ and $A \xrightarrow{k_3} R$ take place, where A is the reactant species, B is the desired product and U, R are undesired byproducts. The feed to the reactor consists of pure A at flow rate F, molar concentration C_{A0} and temperature T_{A0}. Due to the non–isothermal nature of the reactions, a jacket is used to remove/provide heat to the reactor. Under standard modeling assumptions, a mathematical model of the process can be derived

from material and energy balances and takes the following form:

$$\begin{aligned}
\frac{dT}{dt} &= \frac{F}{V}(T_{A0} - T) + \sum_{i=1}^{3} \frac{(-\Delta H_i)}{\rho c_p} R_i(C_A, T) + \frac{Q}{\rho c_p V} \\
\frac{dC_A}{dt} &= \frac{F}{V}(C_{A0} - C_A) - \sum_{i=1}^{3} R_i(C_A, T) \\
\frac{dC_B}{dt} &= -\frac{F}{V} C_B + R_1(C_A, T)
\end{aligned} \tag{8.13}$$

where $R_i(C_A, T) = k_{i0} \exp\left(\frac{-E_i}{RT}\right) C_A$, C_A and C_B denote the concentrations of the species A and B, respectively, T denotes the temperature of the reactor, Q denotes the rate of heat input to the reactor, V denotes the volume of the reactor, ΔH_i, k_i, E_i, $i = 1, 2, 3$, denote the enthalpies, pre–exponential constants and activation energies of the three reactions, respectively, c_p and ρ denote the heat capacity and density of the reactor. The values of the process parameters and the corresponding steady–state values are given in Table 8.2. It was verified that under these conditions, the process model of Eq.8.13 has three steady–states: two locally asymptotically stable and one unstable at $(T^s, C_A^s, C_B^s) = (388\ K, 3.59\ kmol/m^3, 0.41\ kmol/m^3)$.

The control objective is to stabilize the reactor at the (open–loop) unstable steady–state. Operation at this point is typically sought to avoid high temperatures while, simultaneously, achieving reasonable reactant conversion. To accomplish this objective in the presence of control system failures, we consider the following manipulated input candidates (see Figure 8.4):

1. Rate of heat input, $u_1 = Q$, subject to the constraint $|Q| \leq u_{max}^1 = 748\ KJ/s$.
2. Inlet stream temperature, $u_2 = T_{A0} - T_{A0}^s$, subject to the constraint $|u_2| \leq u_{max}^2 = 100\ K$.
3. Inlet reactant concentration, $u_3 = C_{A0} - C_{A0}^s$, subject to the constraint $|u_3| \leq u_{max}^3 = 4\ kmol/m^3$.

Table 8.2: Process parameters and steady–state values for the reactor of Eq.8.13.

F	$=$	4.998	m^3/hr
V	$=$	1.0	m^3
R	$=$	8.314	$KJ/kmol \cdot K$
T_{A0}	$=$	300.0	K
C_{A0}	$=$	4.0	$kmol/m^3$
C_{B0}	$=$	0.0	$kmol/m^3$
ΔH_1	$=$	-5.0×10^4	$KJ/kmol$
ΔH_2	$=$	-5.2×10^4	$KJ/kmol$
ΔH_3	$=$	-5.4×10^4	$KJ/kmol$
k_{10}	$=$	3.0×10^6	hr^{-1}
k_{20}	$=$	3.0×10^5	hr^{-1}
k_{30}	$=$	3.0×10^5	hr^{-1}
E_1	$=$	5.0×10^4	$KJ/kmol$
E_2	$=$	7.53×10^4	$KJ/kmol$
E_3	$=$	7.53×10^4	$KJ/kmol$
ρ	$=$	1000.0	kg/m^3
c_p	$=$	0.231	$KJ/kg \cdot K$
T^s	$=$	388.57	K
C_A^s	$=$	3.59	$kmol/m^3$
C_B^s	$=$	0.41	$kmol/m^3$

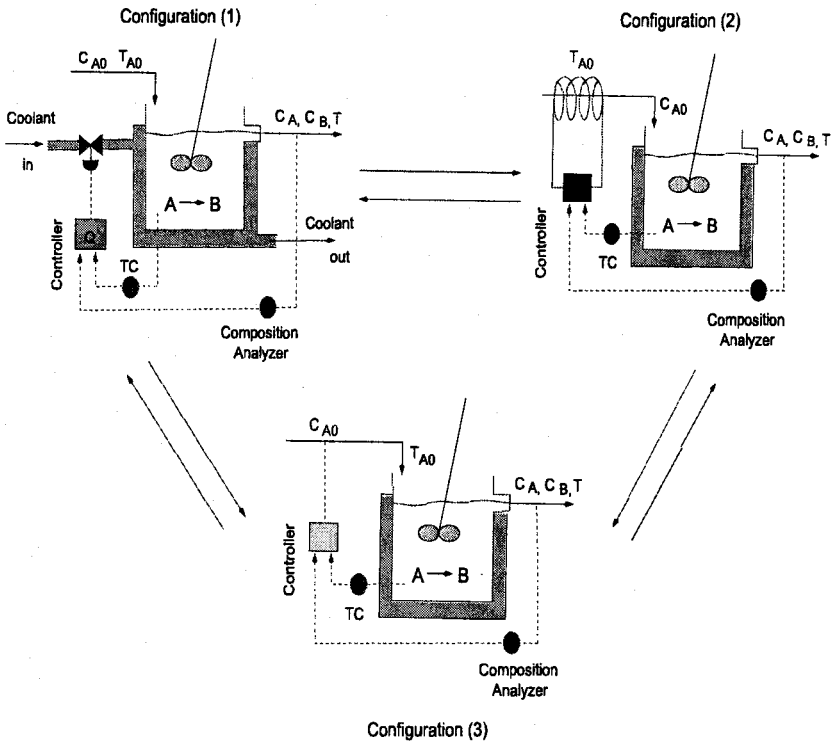

Figure 8.4: Switching between multiple control configurations, each characterized by a different manipulated input, provides a mechanism for fault-tolerant control.

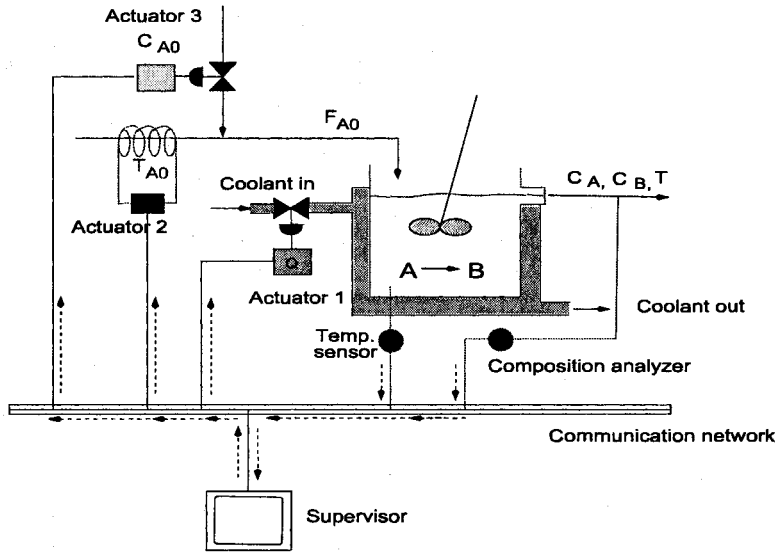

Figure 8.5: Fault–tolerant control structure for a single unit operation, integrating supervisory and feedback control over a communication network.

Each of the above manipulated inputs represents a unique control configuration (or control–loop) that, by itself, can stabilize the reactor using available measurements of the reactor temperature, reactant and product concentrations provided by the sensors. The sensors and control actuators of each configuration are connected to the unit supervisor (e.g., a distant control room) over a communication network (see Figure 8.5). The first loop involving the heat input, Q, as the manipulated variable will be considered as the primary control configuration. In the event of a total failure in this configuration, however, the supervisor will have to activate one of the other two fall–back configurations in order to maintain closed–loop stability. The main question that we address in this simulation study is how can the supervisor determine which control loop to activate once failure is detected in the active configuration and how overall communication delays influence this decision.

Following the proposed methodology, we initially synthesize, for each control configuration, a feedback controller that enforces asymptotic closed–loop stability in the presence of actuator constraints. This task is carried out on the basis of the process input/output dynamics. While our control objective is to achieve full–state stabilization, auxiliary process outputs are introduced here to facilitate transforming the system of Eq.8.13 into a form more suitable for explicit controller synthesis. In the case of the process of Eq.8.13, a further simplification can be obtained by noting that C_B does not affect the evolution of either T or C_A and, therefore, the controller design can be addressed on the basis of the T and C_A equations only. A controller that stabilizes the (T, C_A) subsystem also stabilizes the entire closed–loop system. For the first configuration with $u_1 = Q$, we consider the output $y_1 = C_A - C_A^s$. This choice yields a relative degree of $r_1 = 2$ for the output with respect to the manipulated input. The coordinate transformation (in error variables form) takes the form:

$e_1 = C_A - C_A^s$, $e_2 = \frac{F}{V}(C_{A0} - C_A) - \sum_{i=1}^{3} k_{i0} \exp\left(\frac{-E_i}{RT}\right) C_A$. For the second configuration with $u_2 = T_{A0} - T_{A0}^s$, we choose the output $y_2 = C_A - C_{As}$ which yields the same relative degree as in the first configuration, $r_2 = 2$, and the same coordinate transformation. For the third configuration, with $u_3 = C_{A0} - C_{A0}^s$, we choose the output $y_3 = T - T^s$ which yields a relative degree of $r_3 = 2$ and a coordinate transformation of the form: $e_1 = T - T^s$, $e_2 = \frac{F}{V}(T_{A0} - T) + \frac{Q}{\rho c_p V} + \sum_{i=1}^{3} R_i(C_A, T)$.

Note that since our objective is full–state stabilization, the choice of the output in each case is really arbitrary. However, to facilitate the controller design and subsequent stability analysis, we have chosen in each case an output that produces a system of relative degree 2. For each configuration, the corresponding state transformation yields a system, describing the input/output dynamics, of the following form:

$$\begin{aligned} \dot{e} &= Ae + l_k(e) + b\alpha_k u_k \\ &:= \bar{f}_k(e) + \bar{g}_k(e) u_k, \quad k = 1, 2, 3 \end{aligned} \tag{8.14}$$

where $A = \begin{bmatrix} 0 & 1 \\ 0 & 0 \end{bmatrix}$, $b = \begin{bmatrix} 0 \\ 1 \end{bmatrix}$, $l_k(\cdot) = L_{f_k}^2 h_k(x)$, $\alpha_k(\cdot) = L_{g_k} L_{f_k} h_k(x)$, $h_k(x) = y_k$ is the output associated with the k–th configuration, $x = [x_1 \; x_2]^T$ with $x_1 = T - T_s$, $x_2 = C_A - C_A^s$, and the functions $f_k(\cdot)$ and $g_k(\cdot)$ can be obtained by re–writing the (T, C_A) model equations in Eq.8.13 in the form of Eq.8.1. The explicit forms of these functions are omitted for brevity. Using a quadratic Lyapunov function of the form $V_k = e^T P_k e$, where P_k is a positive–definite symmetric matrix that satisfies the Riccati inequality $A^T P_k + P_k A - P_k b b^T P_k < 0$, we synthesize, for each control–loop, a bounded nonlinear feedback control law of the form of Eqs.8.3–8.4 and characterize the associated stability region with the aid of Eq.8.5. Figure 8.6 depicts the stability region, in the (T, C_A) space, for each configuration. The stability region of configuration 1 includes the entire area of the plot. The stability region of configuration 2 is the entire area to the left of the solid line, while the stability region of configuration

3 covers the area to the right of the dashed vertical line. The desired steady–state is depicted with an asterisk that lies in the intersection of the three stability regions.

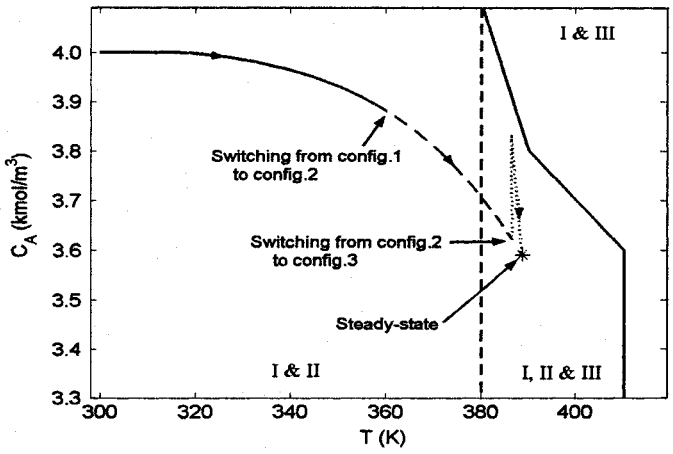

Figure 8.6: Stability regions of the three control configurations (I, II, III) considered for the chemical reactor example of Eq.8.13.

We consider first the case when no time–delays are involved and the supervisor can switch immediately between the different control loops in the event of failures. To this end, the reactor is initialized at $T(0) = 300\ K$, $C_A(0) = 4.0\ kmol/m^3$, $C_B(0) = 0.0\ kmol/m^3$, using the Q—control configuration, and the supervisor proceeds to monitor the evolution of the closed–loop trajectory. As shown by the solid parts of the closed–loop trajectory in Figure 8.6, the state profiles in Figure 8.7 and the rate of heat input profile in Figure 8.8, the controller proceeds to drive the closed–loop trajectory towards the desired steady–state until the control actuators Q–configuration experiences a total failure after 2.0 hrs of startup (simulated by fixing $Q = 0$ for all $t \geq 2.0$ hr).

From the solid part of the trajectory in Figure 8.6, it is clear that the failure of the primary control configuration occurs when the closed–loop trajectory is within the stability region of the second control configuration, and outside the stability region

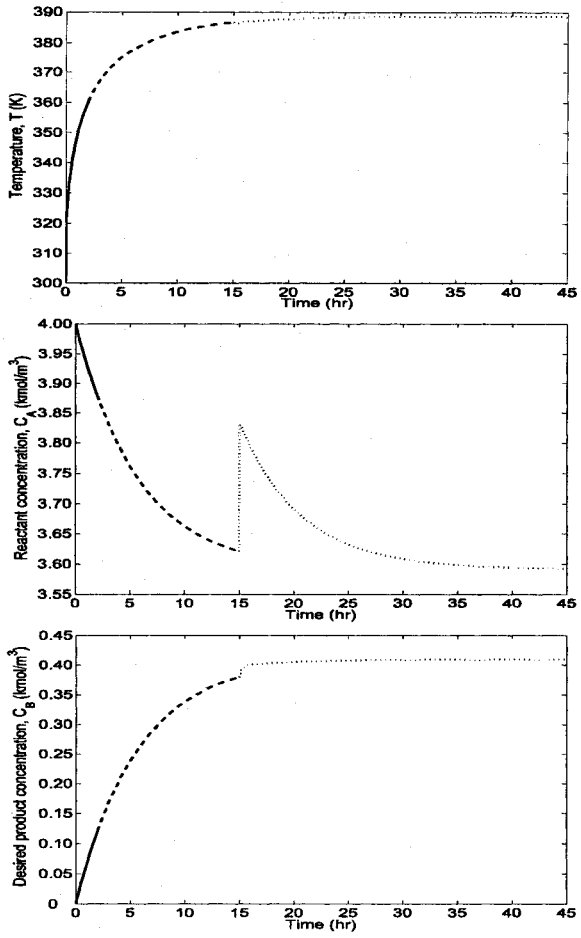

Figure 8.7: Evolution of the closed–loop state profiles under repeated control system failures and subsequent switching by the supervisor from configuration 1 (solid lines) to configuration 2 (dashed lines) to configuration 3 (dotted lines).

of the third control configuration. Therefore, on the basis of the switching logic, the supervisor immediately activates the second configuration, with T_{A0} as the manipulated input. The result is shown by the dashed parts of the closed–loop trajectory in Figure 8.6, the state profiles in Figure 8.7 and the inlet stream temperature profile in Figure 8.8 where it is seen that, upon switching to the T_{A0}–configuration, the corresponding controller continues to drive the closed–loop trajectory closer to the desired steady–state. At $t = 15.0$ hr, we consider another total failure in the control actua-

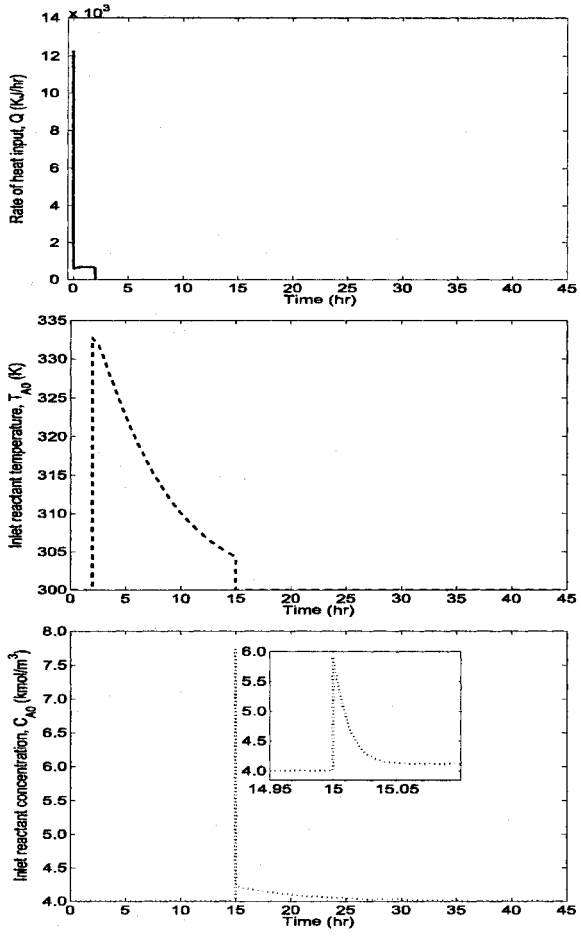

Figure 8.8: Manipulated input profiles for each control configuration as the supervisor switches from configuration 1 to configuration 2 at $t = 2$ hr and from configuration 2 to configuration 3 at $t = 15$ hr.

tors of the T_{A0}–configuration (simulated by fixing T_{A0} for all $t \geq 15.0$ hr). From the dashed part of the trajectory in Figure 8.6, it is clear that this failure occurs when the closed–loop trajectory is within the stability region of the third configuration. Therefore, the supervisor immediately activates the third control configuration, with C_{A0} as the manipulated input, which then successfully stabilizes the reactor at the desired steady–state (see the dotted parts of the closed–loop trajectory in Figure 8.6, the state profiles in Figure 8.7 and the inlet reactant concentration in Figure 8.8).

To demonstrate the effect of delays on the implementation of the switching logic, we consider an overall delay, between the supervisor and the constituent control configurations, of $\tau_{max} = 8.0$ min (accounting for possible delays in fault–detection, control computations, network transmission and actuator activation). In this case, the reactor is initialized at $T(0) = 300\ K$, $C_A(0) = 4.0\ kmol/m^3$, $C_B(0) = 0\ kmol/m^3$ under the first control configuration (with Q as the manipulated input). The actual failure of this configuration occurs at $t = 10$ hr which, as can be seen from Figure 8.9, is a time when the closed–loop state trajectory is within the intersection of all three stability regions.

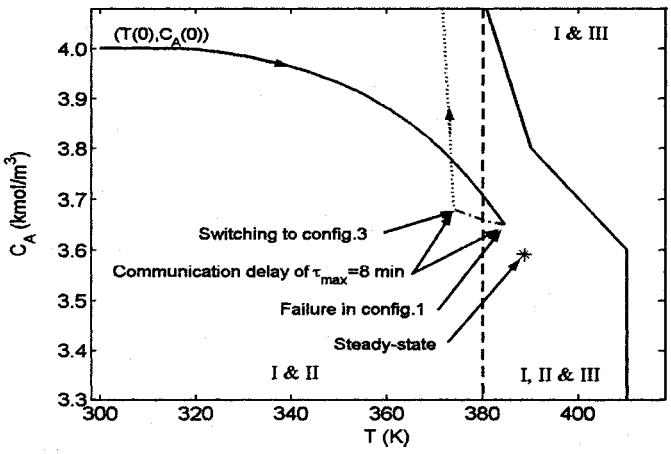

Figure 8.9: A phase plot showing the closed–loop state trajectory leaving the intersection zone (I,II & III) during the delay period (dashed–dotted trajectory) rendering configuration 3 destabilizing (dotted trajectory).

In the absence of delays, this suggests that switching to either configuration 2 or 3 should preserve closed–loop stability. We observe, however, from Figure 8.10 that, when the delay is present, activation of configuration 3 leads to instability (dotted profile) while activation of configuration 2 achieves stabilization at the desired steady–state (dashed profiles). The reason is the fact that, for the time period between the

actual failure ($t = 10$ hr) and the activation of the backup configuration ($t = 10.13$ hr), the process evolves in an open–loop fashion leading the trajectory to move out of the intersection zone such that at $t = 10.13$ hr the state is within the stability region of configuration 2 and outside that of configuration 3. This is shown in Figure 8.9. The corresponding manipulated input profiles are shown in Figure 8.11. To activate the correct configuration in this case, the supervisor needs to predict where the state trajectory will be at the end of the communication delay period.

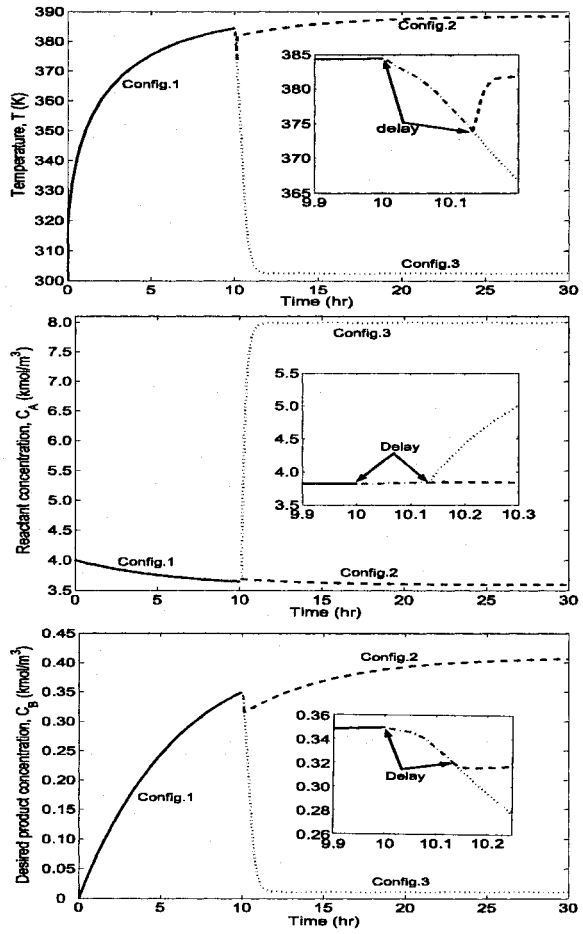

Figure 8.10: Evolution of the closed–loop state profiles when configuration 1 (solid lines) fails at $t = 10$ hr and an overall delay of $\tau_{max} = 8.0$ min elapses before the backup configuration is activated. Activation of configuration 2 preserves closed–loop stability (dashed lines) while activation of configuration 3 leads to instability (dotted lines).

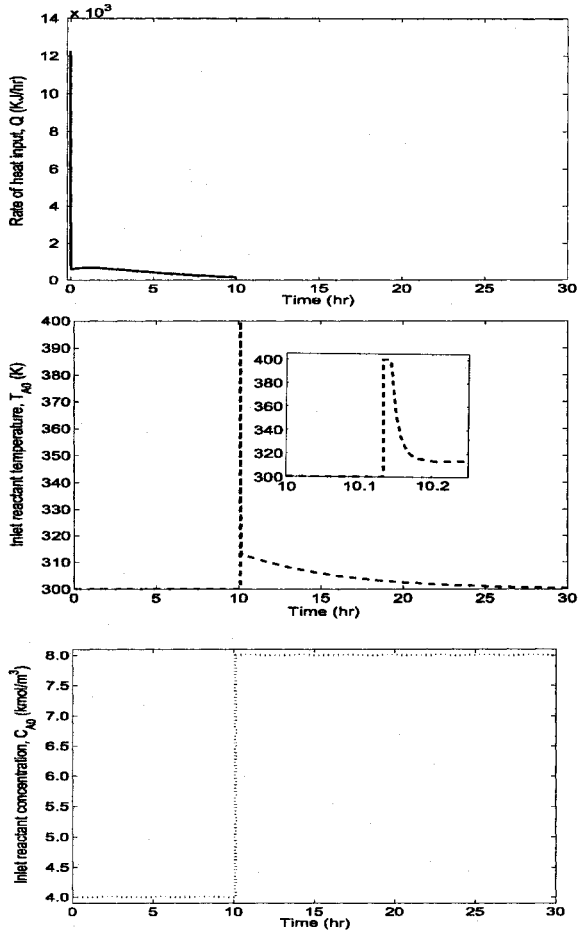

Figure 8.11: Manipulated input profiles when configuration 1 fails at $t = 10$ hr and an overall delay of $\tau_{max} = 8.0$ min elapses before the backup configuration is activated.

8.4.2 Application to two chemical reactors in series

In this section, we revisit the two chemical reactors in series of Eq.8.2, introduced earlier in Section 8.2.3, to illustrate the implementation of the proposed fault–tolerant control methodology. To this end, the reactors are initialized at $(T_1(0), C_{A1}(0)) = (300\ K, 4.0\ kmol/m^3)$, and $(T_2(0), C_{A2}(0)) = (440\ K, 4.0\ kmol/m^3)$. Under normal operating conditions (with no failures), each reactor is controlled by manipulating the rate of heat input, using a bounded nonlinear control law of the form of Eqs.8.3–8.4.

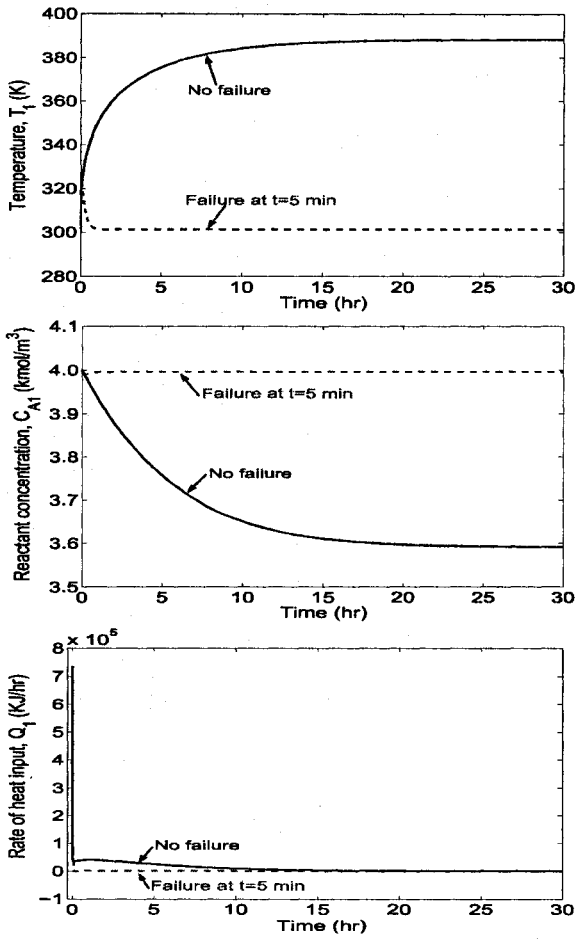

Figure 8.12: Evolution of the closed–loop state and manipulated input profiles for CSTR 1 under a well–functioning control system (solid) and when the control actuator fail at $t = 5$ min (dashed).

To simplify computations, we design each controller on the basis of the temperature equation only. Specifically, a quadratic function of the form $V_i = \frac{1}{2}a_i(x_i^{(2)})^2$, $i = 1, 2$, where $x_i^{(2)} = (T_i - T_i^s)/T_i^s$, is used to design each controller and estimate the resulting stability region using Eq.8.5. The values of the controller tuning parameters are chosen to be $a_i = 0.5$ and $\rho_i = 0.0001$. Figure 8.12 (solid profiles) and Figure 8.13 show the resulting closed–loop state and manipulated input profiles when the controllers are implemented without failure for both reactors. We observe that each

controller successfully stabilizes the corresponding reactor at the desired steady–state.

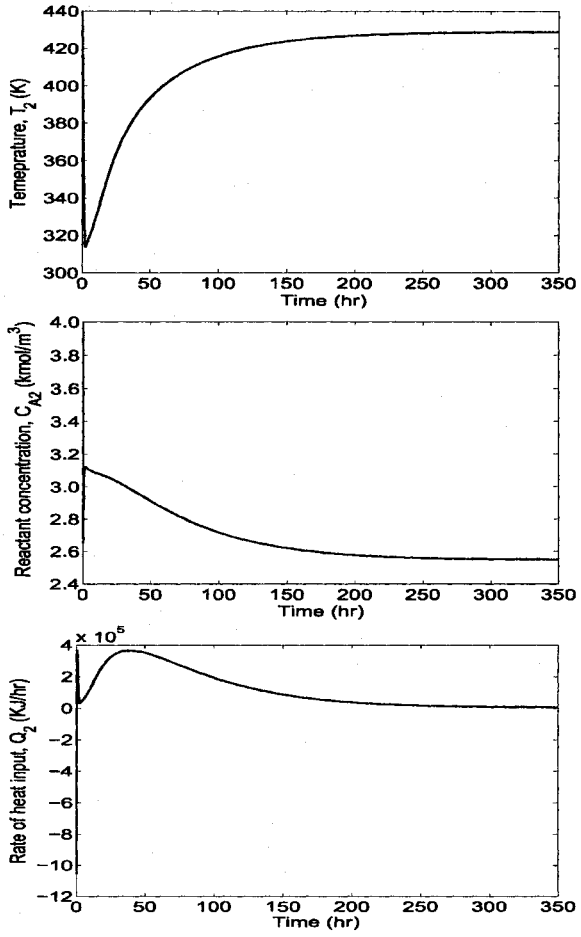

Figure 8.13: Evolution of the closed–loop state and manipulated input profiles for CSTR 2 under a well–functioning control system.

Consider now a total failure in the actuators of both control systems (Q_1 and Q_2) at $T_f = 5$ min. In this case, both reactors revert to their open–loop mode of behavior and, consequently, if no fall–back control configuration is activated, the states move away from the desired steady–state, as shown by the dashed lines in Figure 8.12 for the first reactor, and Figure 8.14 for the second reactor (note that C_{A03} remains fixed for all times since it is not used as a manipulated variable in the pre–failure configuration). As stated in Section 8.2.3, we assume that the controller failure in

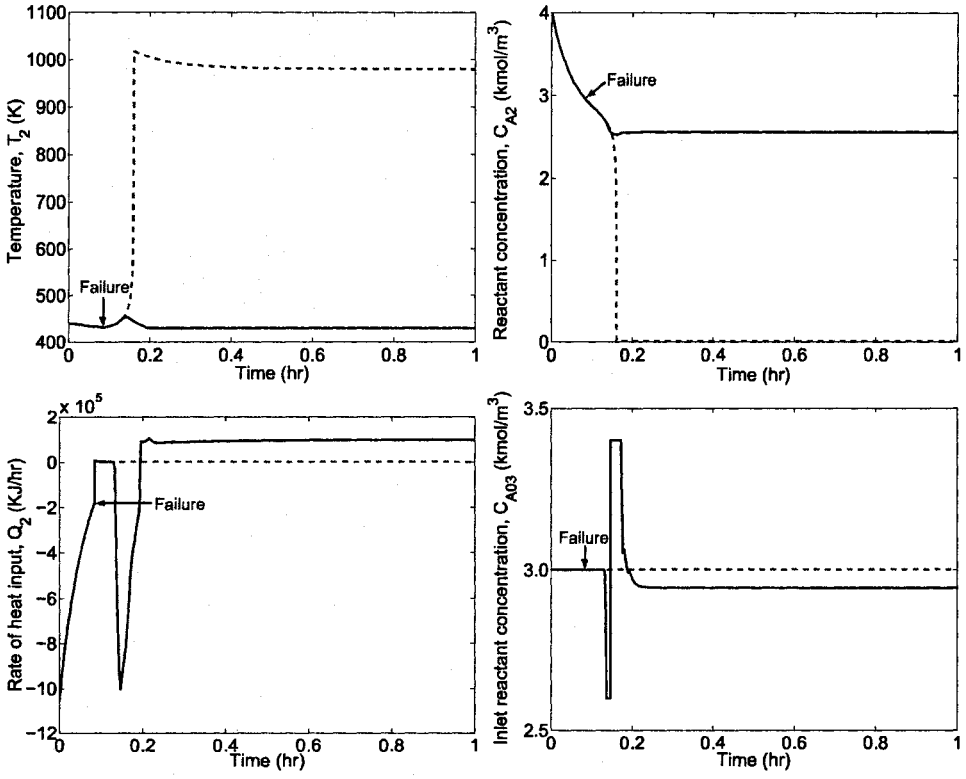

Figure 8.14: Evolution of the closed–loop state and manipulated input profiles for CSTR 2 when the controller of the fall–back configuration (Q_2, C_{A03}) is activated immediately after the failure (solid lines), and the open–loop state and input profiles resulting when the fall–back configuration is not activated after the failure (dashed lines).

the first reactor is permanent; and our objective is to prevent the propagation of this effect to the second reactor. A permanent failure in the first unit could be the result of lack of sufficient fall–back configurations or because failure occurs at a time when the state is outside the stability regions of all the available configurations for this unit.

Using the proposed methodology, the supervisor of CSTR 1, at the failure time, runs both open–loop and closed–loop simulations using the process model of CSTR 1 to estimate the size of the disturbance affecting CSTR 2, and transmits this information to the local supervisor of CSTR 2 through the communication network.

The maximum disturbance size is proportional to the largest discrepancy (after the failure time) between the values of C_{A1}, T_1 in the well–functioning (solid lines in Figure 8.12) and in the failed (dashed lines in Figure 8.12) modes. Using this information, the local supervisor of CSTR 2 designs a robust control law of the form of Eqs.8.7–8.10 to stabilize CSTR 2, using the available fall–back configuration with (Q_2, C_{A03}) as the manipulated inputs, and constructs the associated fault–recovery region for this configuration. The controller design procedure involves re–writing the process model of CSTR 2 in Eq.8.2 in the form of Eq.8.6, using the dimensionless variables, $x_i^{(1)} = (C_{Ai} - C_{Ai}^s)/C_{Ai}^s$, $x_i^{(2)} = (T_i - T_i^s)/T_i^s$, $i = 1, 2$, and with the states of CSTR 1 re–defined as the disturbance variables, $\theta_1(t) = [\theta_1^{(1)}(t)\ \theta_1^{(2)}(t)]^T$, where $\theta_1^{(1)}(t) = (F_1 T_1^s / V_2 T_2^s) x_1^{(1)}(t)$ and $\theta_1^{(2)}(t) = (F_1 C_{A1}^s / V_2 C_{A2}^s) x_1^{(2)}(t)$, for all $t \geq T_f$. Then, using a quadratic function of the form $V_2 = \frac{1}{2} a_2 (x_2^{(1)})^2 + \frac{1}{2} a_2 (x_2^{(2)})^2$, the controller of Eqs.8.7–8.10 is constructed and its fault–recovery region is computed with the aid of Eq.8.11. The disturbance bound is computed as $\theta_b^1 = \sup_{t \geq T_f} \|\theta_1(t)\|$. The values of the controller tuning parameters are selected to be $a_2 = 0.5$, $\rho_2 = 0.0001$, $\chi_2 = 2.0001$ and $\phi_2 = 0.0001$. The fault–recovery region is depicted by the shaded area in Figure 8.15.

From Figure 8.15, we observe that the failure occurs when the states of CSTR 2 are within the fault–recovery region. Therefore, assuming no delays in the fault–detection, computations and communication processing (i.e., instantaneous switching), when the fall–back controllers are activated, closed–loop stability is preserved and the closed–loop states converge close to the desired steady–state as shown by the solid lines in Figure 8.14.

When delay effects are taken into account, we see from Figure 8.15 (top plot) that if an overall delay of 3 min (accounting for delays in fault–detection, controller

computations, information transmission and actuator activation) elapses between the failure and the activation of the (Q_2, C_{A03}) configuration – during this delay, CSTR 2 evolves in an open–loop mode as indicated by the dotted line – the state at the end of the delay still resides within the fault–recovery region and, therefore, closed–loop stability is preserved by switching to the (Q_2, C^s_{A0}) configuration at the end of the delay. The corresponding state and input profiles are shown by the solid lines in Figures 8.15–8.16. By contrast, we see from the bottom plot in Figure 8.15 that when an overall delay of 4.1 min is considered, the state at the end of the delay lies outside the fault–recovery region; hence the fall–back configuration cannot stabilize the system at the desired steady–state, as can be seen from the dashed lines in Figures 8.15–8.16.

Examination of Figure 8.15 provides useful insights into how the tradeoff between the controller design, switching and communication logics can be managed to ensure fault–tolerance. For example, the picture suggests that with a larger fault–recovery region, even large delays maybe tolerated by switching to this particular configuration. A larger region can be obtained by relaxing the constraints. Figure 8.17 shows the resulting fault–recovery region for the (Q_2, C_{A03}) configuration when the constraints are relaxed to $|Q_2| \leq u^{Q_2}_{max} = 1.4 \times 10^7\ KJ/hr$ and $|C_{A03} - C_{A03s}| \leq u^{C_{A03}}_{max} = 2.0\ kmol/m^3$. In this case, the fault–recovery region includes the entire area of the plot. As a result, activation of the fall–back configuration, whether after 3 min or 4.1 min from the failure time, stabilizes the reactor since the state at the end of the delay in both cases is contained within the fault–recovery region. Figure 8.18 shows the corresponding closed–loop state and input profiles of CSTR 2 for both scenarios.

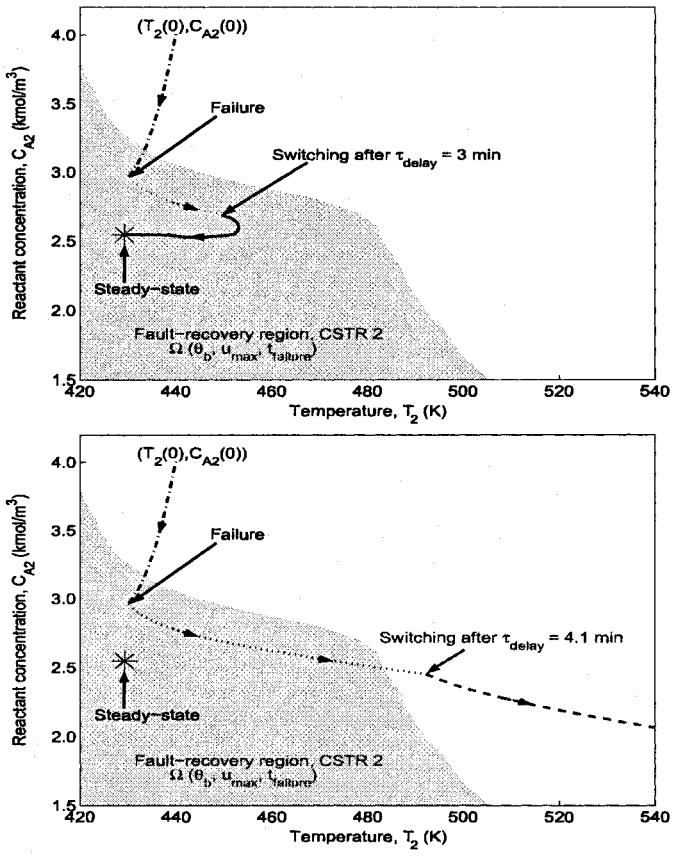

Figure 8.15: Fault–recovery region of the fall–back control configuration (Q_2, C_{A03}) for CSTR 2, with constraints $|Q_2| \leq 2.8 \times 10^6\ KJ/hr$ and $|C_{A03} - C^s_{A03}| \leq 0.4\ kmol/m^3$. when failure occurs at $T_f = 5$ min. Activation of the fall–back configuration after a 3 min delay preserves closed–loop stability (top plot), while activation after 4.1 min delay fails to ensure fault–tolerance (bottom plot).

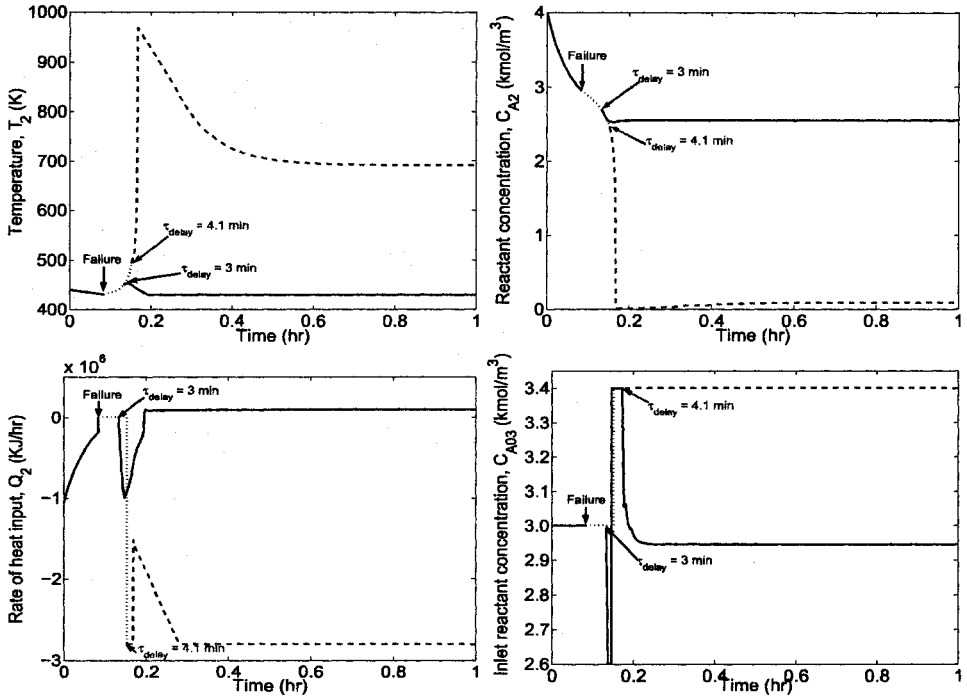

Figure 8.16: Evolution of the closed–loop state and input profiles when the failure occurs at $T_f = 5$ min and the fall–back configuration (Q_2, C_{A03}), with constraints $|Q_2| \leq 2.8 \times 10^6\ KJ/hr$ and $|C_{A03} - C^s_{A03}| \leq 0.4\ kmol/m^3$ is activated after a total delay of 3 min (solid lines) and after a total delay of 4.1 min. (dashed lines).

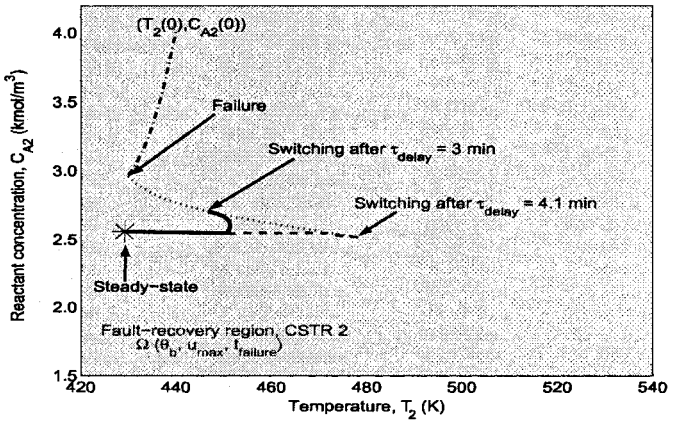

Figure 8.17: Fault–recovery region of the fall–back control configuration (Q_2, C_{A03}) for CSTR 2, with constraints $|Q_2| \leq 1.4 \times 10^7\ KJ/hr$ and $|C_{A03} - C^s_{A03}| \leq 2.0\ kmol/m^3$. when failure occurs at $T_f = 5$ min. Activation of the fall–back configuration after a delay of either 3 min or 4.1 min ensures fault–tolerance.

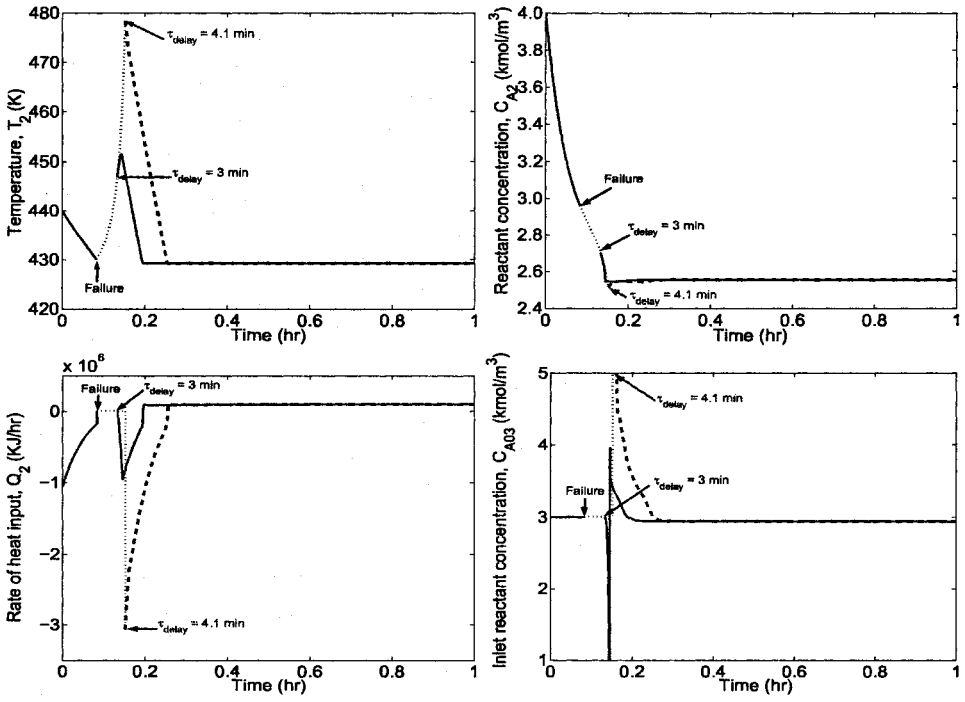

Figure 8.18: Evolution of the closed–loop state and manipulated input profiles when the failure occurs at $T_f = 5$ min and the fall–back configuration (Q_2, C_{A03}), with constraints $|Q_2| \leq 1.4 \times 10^7\ KJ/hr$ and $|C_{A03} - C^s_{A03}| \leq 2.0\ kmol/m^3$ is activated after a total delay of 3 min (solid lines) and after a total delay of 4.1 min. (dashed lines).

8.5 Conclusions

In this chapter, a methodology for the design of fault–tolerant control systems for chemical plants with distributed interconnected processing units was developed. Bringing together tools from Lyapunov–based nonlinear control and hybrid systems theory, the approach is based on a hierarchical architecture that integrates lower–level feedback control of the individual units with upper–level logic–based supervisory control over communication networks. The local control system for each unit consists of a family of control configurations for each of which a stabilizing feedback controller is designed and the stability region is explicitly characterized. The actuators and sensors of each configuration are connected, via a local communication network, to a local supervisor that orchestrates switching between the constituent configurations, on the basis of the stability regions, in the event of failures. The local supervisors communicate, through a plant–wide communication network, with a plant supervisor responsible for monitoring the different units and coordinating their responses in a way that minimizes the propagation of failure effects. The communication logic is designed to ensure efficient transmission of information between units while also respecting the inherent limitations in network resources by minimizing unnecessary network usage and accounting explicitly for the effects of possible delays due to fault–detection, control computations, network communication and actuator activation. Explicit guidelines for managing the various interplays between the coupled tasks of feedback control, fault–tolerance and communication were provided. The efficacy of the proposed approach was demonstrated through chemical process examples.

Chapter 9

Analysis and Control of Biological Networks Using Hybrid Systems Theory

9.1 Introduction

In a biological cell, cellular functions, such as metabolism, DNA synthesis, movement and information processing, are implemented and controlled by vast arrays of complex networks of biochemical interactions. Understanding how these networks are integrated and regulated, and how the regulation may be influenced – possibly for therapeutic purposes – is a major goal of molecular cell biologists and bioengineers. While experimental techniques have been, and will continue to be, an indispensable tool in the quest for such an understanding, it is now clear that the sheer complexity of biological networks is such that informal biochemical intuition alone cannot reliably deduce the underlying logic of these networks. This intuition must be supplemented by precise mathematical and computational tools that can provide both qualitative and quantitative insights into the description, analysis and manipulation

of biological networks underlying basic cellular function. From a practical point of view, such techniques could potentially reduce the degree of trial-and-error experimentation. More importantly, computational and theoretical approaches can lead to testable predictions regarding the current understanding of biological networks, which can serve as the basis for revising existing hypotheses. These realizations, together with recent technological advances that are increasingly enabling experimental validation of theoretical predictions, have been major driving forces behind a large and growing body of research work, in recent years, on the development and application of analytical and computational tools for the modeling and simulation (e.g., [310, 216, 276, 77, 27, 123, 103]), optimization (e.g., [75, 218]), and identification (e.g., [106]). The reader may also refer to the review papers [133, 298, 27, 5] and the references therein for further results on biological networks.

Biological networks are intrinsically dynamical systems, driving the adaptive responses of a cell in space and time. The behavior of these dynamical systems is determined by "biochemical kinetics," or rate equations, in which the variables of interest are the concentrations of individual network components (proteins, metabolites, etc.) within the cell, and the dynamics describe the rates of production and decay of these components. The dynamic models of biological networks typically consist of systems of nonlinear ordinary differential equations, permitting the modeler to apply the analytical techniques of nonlinear dynamics. These techniques have been developed considerably in recent decades, making the rate-equation approach a promising avenue for combining mathematical analysis and computational simulation.

While the resulting models are typically based on purely continuous dynamics, the dynamics of biological networks often involve switching between many qualitatively different modes of behavior. At the molecular level, for example, the fundamental

process of inhibitor proteins turning off the transcription of genes by RNA polymerase reflects a switch between two continuous processes. An example of this is the classic genetic switch observed in the bacteriophage λ (e.g., see [240, 132, 261]), where two distinct behaviors, lysis and lysogeny, each with different mathematical models, are seen. Also, at the cellular level, the cell growth and division in a eukaryotic cell is usually described as a sequence of four processes, each being a continuous process that is triggered by a set of conditions or events (e.g., see [134, 202, 299]). At the inter-cellular level, cell differentiation can also be viewed as a switched system [122]. In addition to naturally occurring switches, switched dynamics can be the result of external intervention that attempts to re-engineer a given network by turning on or off, for example, certain pathways. In all of these examples, the overall behavior of the network is more appropriately viewed as a switched system, i.e. intervals of continuous dynamics interspersed by discrete transitions, and, therefore, a hybrid approach that combines elements of discrete and continuous dynamics is necessary, not only for the modeling, simulation and analysis (e.g., see [10, 9]), but also for controlling and modifying the network behavior.

Hybrid system models are increasingly being used for modeling a diverse array of engineering systems, such as automotive and chemical process control systems. A hybrid system consists of a finite family of continuous dynamical subsystems (or modes), each of which is governed by a different set of differential equations, together with a set of discrete events (or logic-based switching rules) that orchestrate the transition between the constituent modes. Research on hybrid systems, both within control systems theory and computer science, has led to the development of systematic tools for the modeling (e.g., [315, 33]), simulation (e.g., [33]), optimization (e.g., [126]), stability analysis (e..g, [138, 203, 81]), and control (e.g., [37, 178, 95]) of several

classes of hybrid systems. Given the similarity that many biological networks exhibit to switched systems encountered in engineering (e.g., involving feedback mechanisms and switching), it is instructive to investigate how all these tools can be applied to model, analyze and possibly modify the dynamics of biological networks.

Changes in network dynamics can result from alterations in local conditions (e.g., temperature, nutrient and energy source, light, cell density) and/or changes in the molecular environment of individual regulatory components (e.g. intra-cellular concentrations of transcription factors). Often, the network can be switched between different modes by changes in parameter values. These parameter typically include rate constants and total enzyme concentrations that are under genetic control. Changing the expression of certain genes will change the parameter values of the model and move the network across bifurcation boundaries into regions of qualitatively different behavior (e.g., transitions from limit cycles to single and multiple steady-states). Understanding and analyzing the nature of these qualitatively different modes of behavior typically involves bifurcation analysis which determines how the attractors of the vector field depend on parameter values, leading to a characterization of the regions in parameter space where the different behaviors are observed. The boundaries of these regions represent the bifurcation boundaries.

An important question, however, that is not addressed by bifurcation analysis is that of when, or where in state space, is a transition from one mode to another feasible. For example, bifurcations can predict that a change in a certain parameter is required for the network to move from an oscillatory mode (stable limit cycle) to a multi-stable mode (multiple stable steady-states) but cannot tell us when, or which, of the new steady-states will be observed upon switching. This is an important consideration when one tries to manipulate the network behavior to achieve a certain

desirable behavior or steady-state. To address this question, bifurcations must be complemented by a dynamical analysis of the transient behavior of the constituent modes of the overall network. Intuitively, one expects that the newly switched mode will exhibit the desired steady-state if, at the time of switching, the network state is in the vicinity of that steady-state. A precise concept from nonlinear dynamical systems theory that quantifies this closeness is that of the domain of attraction, which is the set of all points in the state space, starting from where the trajectories of the dynamical system converge to a given equilibrium state.

In this chapter, we present a methodology for the dynamic analysis and control of mode transitions in biological networks. The proposed approach is based on the notion of coupling the switching logic to the domains of attraction of the constituent modes introduced in Chapter 7. To this end, we initially model the overall network as a switched nonlinear system that dwells in multiple modes, each governed by a set of continuous-time differential equations. The transition between the continuous modes are triggered by discrete events (changes in model parameters that correspond to alterations in physiological conditions). Then, following the characterization of the steady-state behavior of each mode, Lyapunov techniques are used to characterize the domains of attraction of the steady-states. Finally, by analyzing how the stability regions of the various modes overlap with one other, it is possible to determine when, and if, a given steady-state behavior, for a given mode transition, is feasible or not. The proposed method is demonstrated using models of biological networks that arise in cell cycle regulation and the bacteriophage λ-switch system.

9.2 A Switched system representation of biological networks

We consider biological networks modeled by systems of nonlinear ordinary differential equations of the general form:

$$\begin{aligned} \frac{dx(t)}{dt} &= f_{i(t)}(x(t), p_{i(t)}) \\ i(t) &\in \mathcal{I} = \{1, \cdots, N\} \end{aligned} \tag{9.1}$$

where $x = [x_1 \; x_2 \; \cdots \; x_n]^T \in \mathbb{R}^n$ is the vector of continuous state variables (e.g., concentrations of the various network components such as proteins, genes, metabolites, etc.), $f_i(\cdot)$ is a smooth nonlinear function, p_i is a vector of network parameters (e.g., kinetic constants, total enzyme concentrations) that are typically under genetic control, $i : [0, \infty) \rightarrow \mathcal{I}$ is the switching signal which is assumed to be a piecewise continuous (from the right) function of time, i.e., $i(t_k) = \lim_{t \rightarrow t_k^+} i(t)$ for all k, implying that only a finite number of switches occurs on any finite interval of time. N is the number of modes of the switched system, $i(t)$, which takes different values in the finite index set, $\mathcal{I}$, represents a discrete state that indexes the vector field $f(\cdot)$ which determines $\dot{x}$. For each value that i takes in $\mathcal{I}$, the temporal evolution of the continuous state is governed by a different set of differential equations. The system of Eq.9.1 is therefore a switched (multi-modal) system that consists of a finite family of continuous nonlinear subsystems (modes) and a switching rule that orchestrates the transitions between them. In biological networks, mode transitions can be the result of a fundamental change in the vector field itself (e.g., different modes having different f_i's) or, more commonly, a change in network parameter values due to changes in levels of gene expression and enzyme activities (which can occur spontaneously or be induced externally).

The basic problem that we address in this chapter is that of determining when (or

where in state-space) can a transition from one mode to another produce a certain desired behavior that exists in the target mode (e.g., a desired steady-state). From an analysis point of view, the answer to this question sheds light on why certain naturally-occurring mode transitions seem to always favor a certain steady-state behavior. From a control point of view, on the other hand, the answer provides insight into how and when the designer should enforce the transition in order to bring about a desired steady-state behavior. In the next section, we outline a methodology that addresses these questions.

9.3 Methodology for analysis and control of mode transitions

The methodology proposed here is based on the notion/idea of designing the switching logic on the basis of the stability regions of the constituent modes, which was introduced in [95] in the context of constrained control of switched nonlinear systems. However, unlike the results in [95], where the presence of the stability regions was a consequence of the constraints imposed on the manipulated input of each mode, the stability regions considered here are directly linked to the intrinsic dynamic behavior of the constituent modes, which is dictated by the dependence of the attractors of the vector field on the network parameters. For example, the presence of multiple equilibrium points in a given mode gives rise to multiple stability regions, or domains of attraction, whose union covers the entire state space. Clearly, which equilibrium state is attained depends on which region contains the system state at the switching time. Below is the proposed methodology:

1. Identify the different modes of the network, where each mode is characterized either by a different set of differential equations or by the same set of equations but with different parameters.

2. Compute the steady-state(s) of each mode by solving:

$$0 \;=\; f_i(x_s, p_i) \tag{9.2}$$

where x_s is an admissible steady-state solution. Depending on the values of p, each mode might possess a limit cycle, a single steady-state, or multiple steady-states.

3. Characterize of the domain of attraction (stability region) of each steady-state in each mode. For a given steady-state, x_s, the domain of attraction, $\Omega(x_s)$, consists of the set of all states starting from where the system trajectories converge to that steady-state. Estimates of the domain of attraction can be obtained using Lyapunov techniques [170]. For example, consider the case of isolated equilibrium points and let V_i be a Lyapunov function candidate, i.e. $V_i(x_s) = 0$ and $V_i(x) > 0$ for all $x \neq x_s$. Consider also the set $\Pi(x_s) = \{x \in \mathbb{R}^n : \dot{V}_i(x_s) < 0\}$. Then the level set is $\bar{\Omega}(x_s) = \{x \in \mathbb{R}^n : V_i(x_s) \leq c_i^{max}\}$ where $c_i^{max} > 0$ is the largest constant for which $\bar{\Omega}$ is fully contained in Π, provides an estimate of the domain of attraction of x_s (see [91, 94] for more details on this issue). Due to the possible conservatism of the resulting estimates, Lyapunov techniques are usually coupled with other methods in order to obtain larger estimates (e.g., multiple Lyapunov functions; see chapter 4 in [170] for details).

4. Analyze how the stability regions of a given mode overlap with those of another mode. Suppose, for example, that the network is initialized within mode i and let T be the transition time from mode i to mode j. Also, let x_s be an admissible steady-state (among several others) of the j-th mode. Then, after switching, the x_s steady-state will be observed if and only if

$$x(T) \;\in\; \Omega_j(x_s) \tag{9.3}$$

and no further switches take place. The switching rule of Eq.9.3 requires monitoring the temporal evolution of the state evolution in order to locate where the state is at the switching time, with respect to the stability regions of the mode to be activated.

In the next two sections, we demonstrate, through computer simulations, the application of this methodology to the analysis of mode transitions in two biological networks, one arising in eukaryotic cell cycle regulation and the other in the bacteriophage λ-switch system.

9.4 Application to eukaryotic cell cycle regulation

We consider here an example network of biochemical reactions, based on cyclin-dependent kinases and their associated proteins, which are involved in cell cycle control in frog egg development. A detailed description of this network is given in [229] where the authors use standard principles of biochemical kinetics and rate equations to construct a nonlinear dynamic model of the network that describes the time evolution of the key species including free cyclin, the M-phase promoting factor (MPF), and other regulatory enzymes. The model parameters have either been estimated from kinetic experiments in frog egg extracts or assigned values consistent with experimental observations. For illustration purposes, we will consider below the simplified network model derived by the authors (focusing only on the positive-feedback loops in the network) which captures the basic stages of frog egg development. The model is given by:

$$\begin{aligned} \frac{du}{dt} &= \frac{k_1'}{G} - \left(k_2' + k_2'' u^2 + k_{wee}\right) u + \left(k_{25}' + k_{25}'' u^2\right)\left(\frac{v}{G} - u\right) \\ \frac{dv}{dt} &= k_1' - (k_2' + k_2'' u^2) v \end{aligned} \tag{9.4}$$

where u is a dimensionless concentration of active MPF and v is a dimensionless concentration of total cyclin, k_2' and k_2'' are rate constants for the low-activity and high activity forms, respectively, of cyclin degradation; k_{25}' and k_{25}'' are rate constants for the low-activity and high activity forms, respectively, of tyrosine dephosphorylation of MPF; k_1' is a rate constant for cyclin synthesis, k_{wee} is the rate constant for inhibition of Wee1, an enzyme responsible for the tyrosine phosphorylation of MPF (which inhibits MPF activity) (see [229] for model derivation from the molecular mechanism, and Tables 9.1-9.2 for the parameter and steady-state values). Bifurcation and phase-plane analysis of the above model [229] shows that, by changing the values of k_2', k_2'' and k_{wee}, the following four modes of behavior are predicted:

Table 9.1: Parameter values for the cell cycle model in Eq.9.4.

k_1'	=	0.01
k_{25}'	=	0.04
k_{25}''	=	100
k_{INH}	=	0.1
k_{CAK}	=	1

Table 9.2: Steady-state values (u_s, v_s) for the cell cycle model for different values of k_2', k_2'', k_{wee}.

k_2'	k_2''	k_{wee}	Mode	M-arrest state	$G2$-arrest state	Reference
0.01	10	3.5	G2-arrest	n/a	$(0.016, 0.802)$	
0.01	0.5	2.0	M-arrest	$(0.202, 0.329)$	n/a	
0.015	0.1	3.5	Bi-stable	$(0.276, 0.442)$	$(0.012, 0.666)$	
0.01	10	2.0	Oscillatory	n/a	n/a	Fig.9.2b
0.01	10	2.5	Oscillatory	n/a	n/a	Fig.9.4

- A G2-arrested state (blocked before the G2-M transition) characterized by high cyclin concentration and little MPF activity. This corresponds to a unique, asymptotically stable steady-state ($k_2' = 0.01$, $k_2'' = 10$, $k_{wee} = 3.5$; see Fig.9.1a).

- An M-arrested state (blocked before the meta- to anaphase transition) state with lots of active MPF. This corresponds to a unique, asymptotically stable

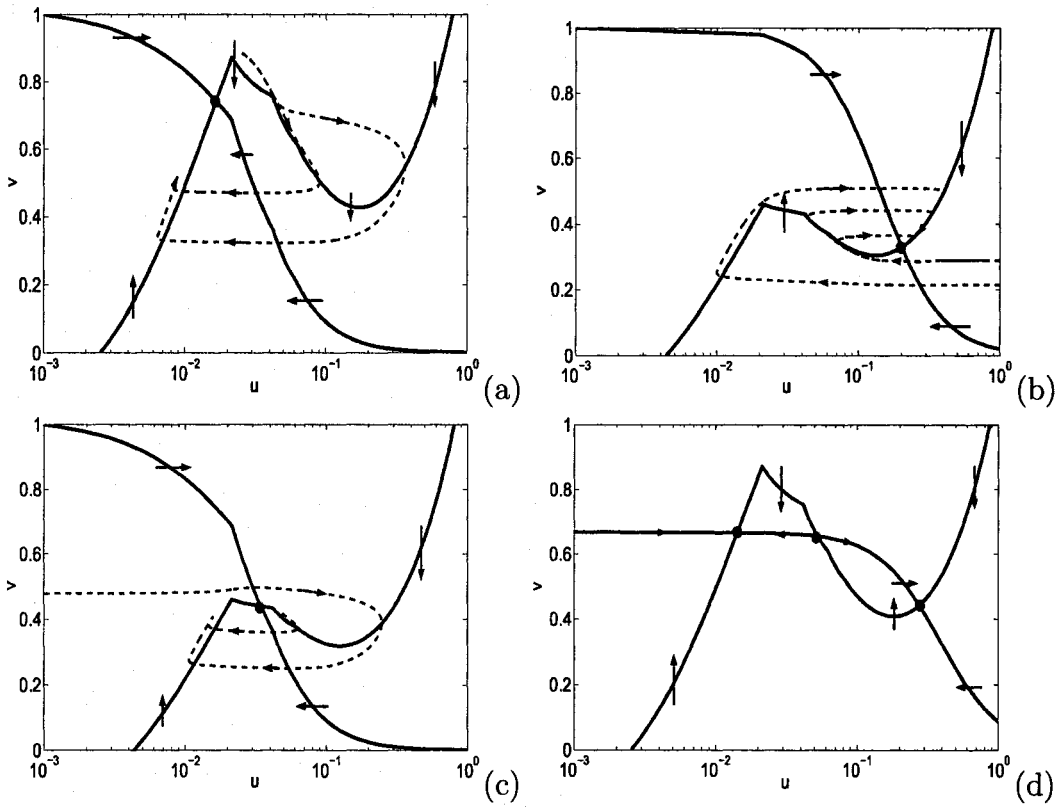

Figure 9.1: Phase-plane portraits of the system of Eq.9.4, for different values of k_2', k_2'', and k_{wee}, showing: (a) Stable steady-state with most MPF inactive, (b) Stable steady-state with most MPF active, (c) Unstable steady-state surrounded by a limit cycle, and (d) Bi-stability: two stable steady-states separated by an unstable saddle point.

steady-state ($k_2' = 0.01$, $k_2'' = 0.5$, $k_{wee} = 2.0$; see Fig.9.1b).

- An oscillatory state (alternating phases of DNA synthesis and mitosis) exhibiting sustained, periodic fluctuation of MPF activity and total cyclin protein. This corresponds to a stable limit cycle surrounding an unstable equilibrium point ($k_2' = 0.01$, $k_2'' = 10$, $k_{wee} = 2.0$; see Fig.9.1c).

- Co-existing stable steady-states of G2 arrest and M arrest. This corresponds to three steady-states; one unstable and two locally asymptotically stable ($k_2' = 0.015$, $k_2'' = 0.1$, $k_{wee} = 3.5$; see Fig.9.1d).

The above analysis predicts that slight increases in k_2', k_{wee}, accompanied by a significant drop in k_2'' (which could be driven, for example, by down-regulation of cyclin degradation) can induce a transition from the oscillatory mode of MPF activity (early embryo stage) to the bi-stable mode. However, it is not clear from this analysis alone whether the cell will end up in a G2- or an M-arrested state upon switching. To address this question, we initially compute the domains of attraction of both steady-states in the bi-stable mode. This is done using a Lyapunov function of the form $V = (u - u_s)^4 + 10(v - v_s)^2$, where u_s and v_s are the steady-state values. The basic idea here is to compute, for each steady-state, the region in the (u, v) space where the time-derivative of V is negative-definite along the trajectories of the dynamical system of Eq.9.4, and then use this region to obtain an estimate of the domain of attraction. While several candidate functions could be used, this particular function was found to yield acceptable estimates of the stability regions. The stability regions for both steady-states are depicted in Fig.9.2a. The entire area above the dashed curve (the separatrix) is the stability region of the M-arrested state while the area below is the stability region of the G2-arrested state. Both steady-states are denoted by asterisks on the plot. By plotting the limit cycle (obtained from the oscillatory

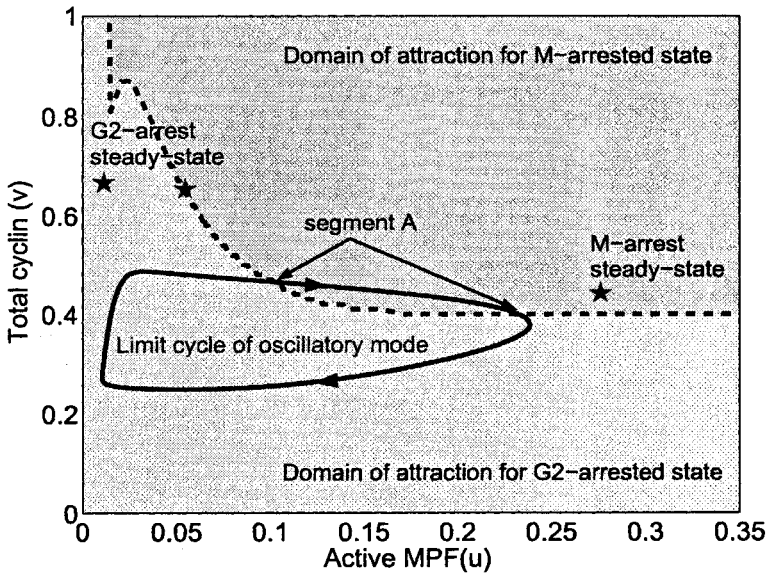

(a)

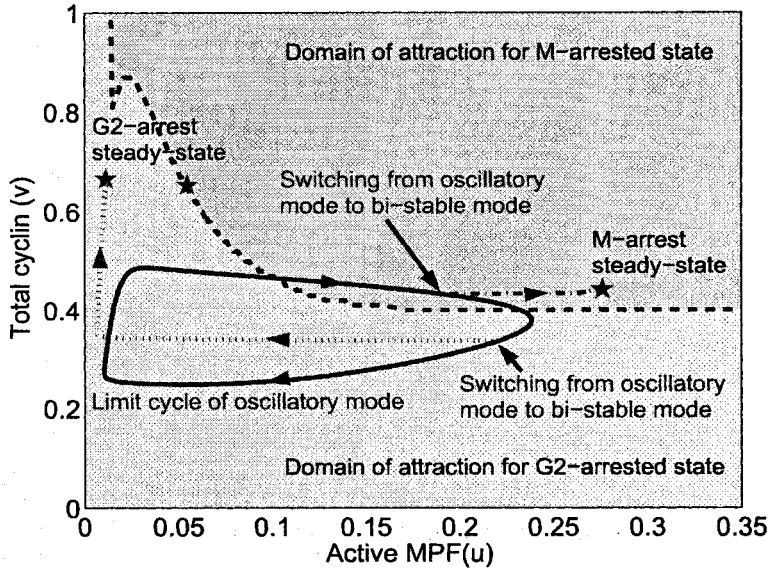

(b)

Figure 9.2: (a) A plot showing the overlap of the limit cycle of the oscillatory mode with the domains of attraction for the M-arrested steady-state (entire area above dashed curve) and for the $G2$-arrested steady-state (entire area below the dashed curve), (b) A plot showing that switching from the oscillatory to the bi-stable mode moves the system to different steady-states depending on where switching takes place. In both cases, the oscillatory mode is fixed at $k_2' = 0.01$, $k_2'' = 10$, $k_{wee} = 2.0$.

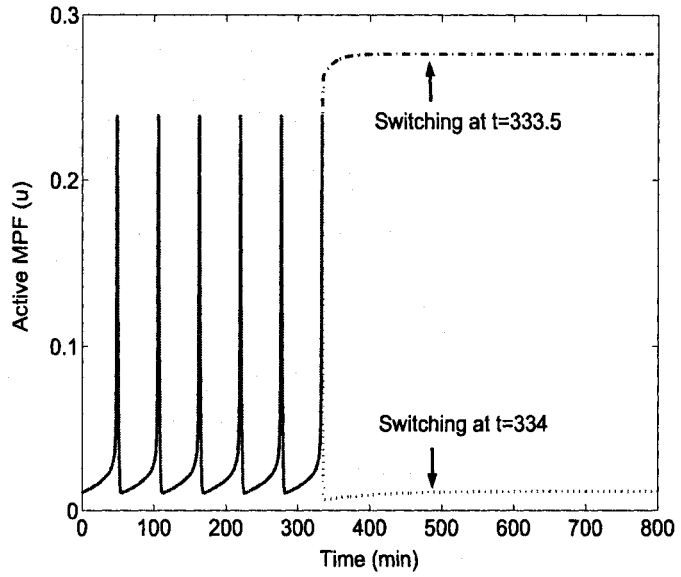

(a)

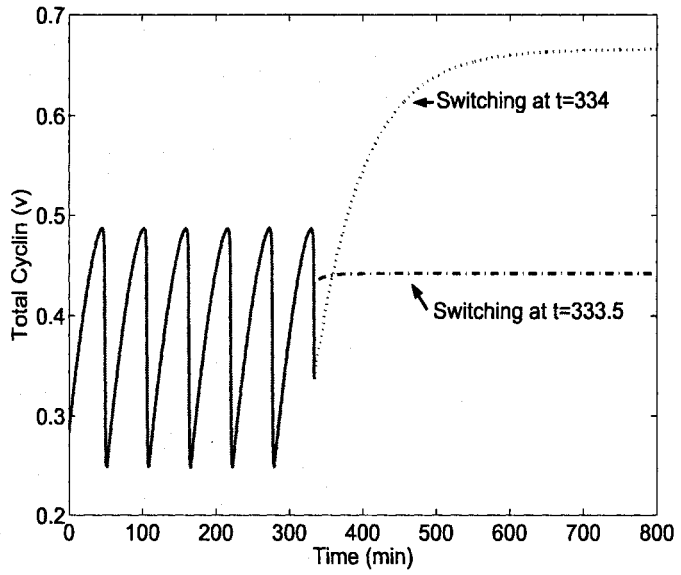

(b)

Figure 9.3: The time evolution plots of (a) active MPF, and (b) total cyclin upon switching from the oscillatory to the bi-stable mode at two representative switching times. At $t =$ 333.5 min, the state trajectory lies on segment A (see Fig.9.2a) and therefore switching lands the state in the M-arrested steady-state (dash-dotted line), while at $t = 334$ min, switching lands the state in the $G2$-arrested steady-state (dotted line). In both cases, the oscillatory mode is fixed at $k_2' = 0.01$, $k_2'' = 10$, $k_{wee} = 2.0$.

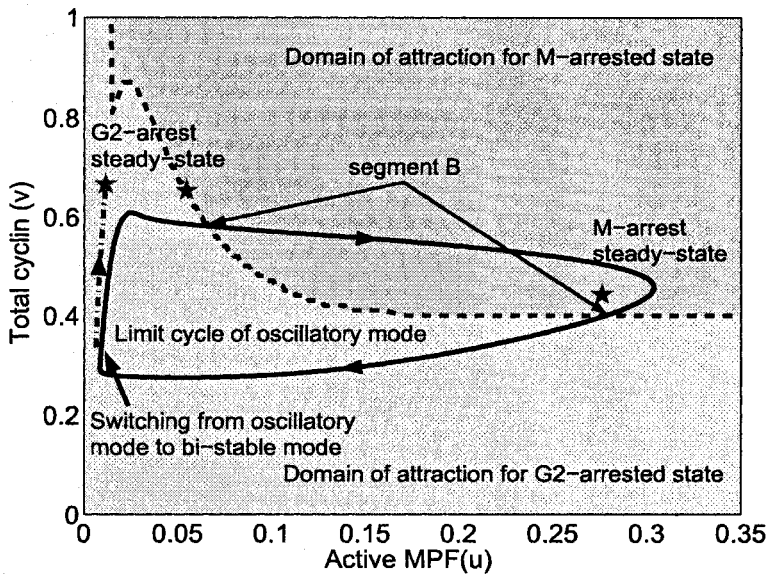

Figure 9.4: A plot showing that switching from the oscillatory mode (of the following parameter values: $k_2' = 0.01$, $k_2'' = 10$, $k_{wee} = 2.5$) to the bi-stable mode at same time as in Fig.9.2b ($t = 333.5$ min) moves the system to $G2$-arrest steady-state (instead of M-arrest steady-state) because switching does not occur on segment B. Note that the portion of the limit cycle overlapping the stability region of the M-arrested steady-state (segment B) is larger than the one in 9.2a (segment A).

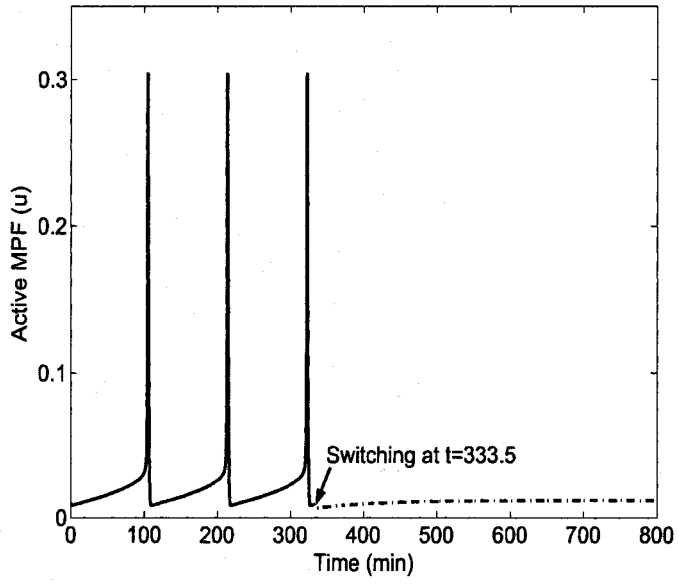

(a)

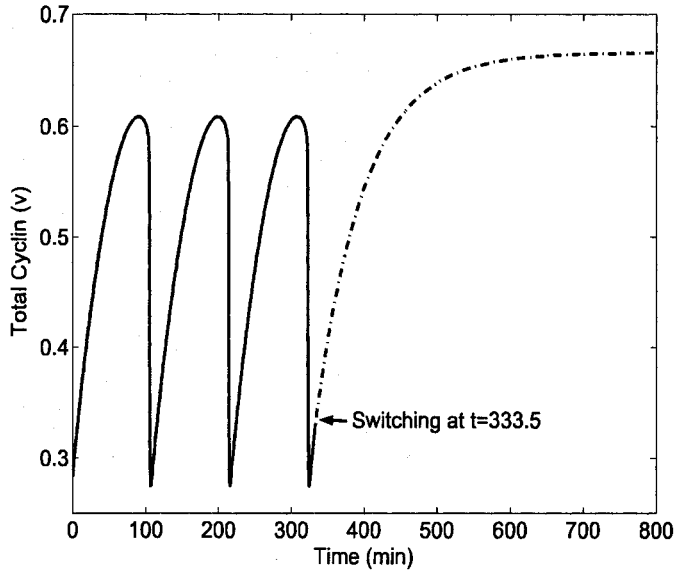

(b)

Figure 9.5: The time evolution plots of (a) active MPF, and (b) total cyclin upon switching from the oscillatory to the bi-stable mode at $t = 333.5$ min. In both cases, the oscillatory mode is fixed at $k_2' = 0.01$, $k_2'' = 10$, $k_{wee} = 2.5$

mode) on the same plot, we see that a portion of the limit cycle lies within the stability region of the M-arrested steady-state (segment A in Fig.9.2a) while the rest is completely within the stability region of the steady-state for the G2-arrested mode. Based on this analysis, we conclude that switching from the oscillatory mode to the bi-stable mode would move the cell to the $G2$-arrested state only if the transition occurs at times when the state is not on segment A, while it would end up in the M-arrested state if switching were to occur on segment A. This conclusion is verified by the dotted and dash-dotted state trajectories, respectively, shown in Fig.9.2b. The corresponding plots of the time-evolution of the states in both switching scenarios are given in Fig.9.3 for two representative switching times. Note that because of the periodic nature of the solution in the oscillatory mode, there are many time-intervals, between $t = 0$ and $t = 333.5$ min, when the limit cycle trajectory is on segment A. These intervals are separated by one period of the limit cycle. Switching during any of these intervals to the bi-stable mode moves the system to the M-arrested state. Similarly, there are many time-intervals when the trajectory is not on segment A. Switching during any of those intervals will land the system at the $G2$-arrested state.

Fig.9.4 shows the limit cycle resulting when the rate of inhibition of Wee1 is increased to $k_{wee} = 2.5$ (with k_2' and k_2'' remaining fixed at 0.01 and 10, respectively). Comparing with Fig.9.2a, we observe that a larger portion of the limit cycle (segment B in Fig.9.4) lies within the stability region of the M-arrested steady-state. Therefore, unlike the case of Fig.9.2a, when switching from the oscillatory mode to the bi-stable mode takes place at $t = 333.5$ min, the state is not within the domain of attraction of the M-arrested steady state. Switching in this case lands the system at the $G2$-arrested steady-state. The corresponding time-evolution plots are given in Fig.9.5.

9.5 Application to the bacteriophage λ-switch system

We consider an example of a biological switch observed in the bacteriophage λ. An excellent review and detailed description of the molecular regulatory mechanisms in the bacteriophage λ-switch can be found in [240]. Bacteriophage λ is a virus capable of infecting *Escherichia coli* bacteria. The virus attaches its tail to the surface of host bacterium cell, drills a hole in the cell wall, and squirts its chromosome into the bacterium, leaving its coat behind. λ is an obligate parasite – it must inject its DNA into the bacterium to multiply. Upon infection, it can follow either one of two different pathways. First, the injected phage chromosome lysogenizes its host: all but one of the phage genes are turned off, and one phage chromosome, called prophage, becomes part of the host chromosome. As the lysogen (the bacterium bearing the prophage) grows and divides, the prophage is passively replicated and quiescently distributed to the progeny bacteria. Second, the phage chromosome enters the lytic mode: various sets of phage genes are turned on and off according to a precisely regulated program, the λ chromosome is extensively replicated, new head and tail proteins are synthesized, new phage particles are formed within bacterium, and some 45 minutes following the infection the bacterium lyses and releases about 100 progeny phage. Once the virus is in the lysogenic state, it can shift to the lysis state under certain conditions, e.g. if the bacterial culture is irradiated with ultraviolet (UV) light.

The molecular regulatory mechanism responsible for the lysogeny/lysis decision is known as the phage λ-switch. The switch to lytic growth is called induction. A schematic representation of the λ-switch performance in the lysogenic and lytic steady-states is shown in Fig.9.6.

To understand how the switch works, we need to consider two regulatory genes

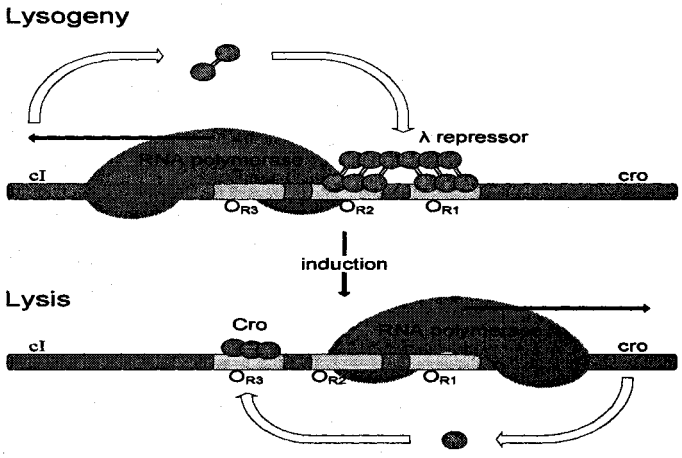

Figure 9.6: A schematic representation of the molecular mechanism responsible for the lysogenic to lytic mode transition in the bacteriophage λ.

(*cI* and *cro*) and the regulatory region called O_R (right operator). In a lysogen, *cI* is on and *cro* is off, and vice versa when lytic growth ensues. The operator comprises three binding sites (O_{R1}, O_{R2}, and O_{R3}) that overlap two opposing promoters. One of these, P_R, directs transcription of lytic genes and the other, P_{RM}, directs transcription of the *cI* gene. In a lysogen, the λ repressor (the product of *cI* gene), at O_R, is bound at the two adjacent sites O_{R1} and O_{R2}. At these positions, it performs two functions: it represses rightward transcription from the promoter P_R, thereby turning off expression of *cro* and other lytic genes; simultaneously it activates transcription of its own gene from the promoter P_{RM}. Upon induction, repressor vacates the operator and transcription from P_R commences spontaneously. The first newly made protein is *Cro*. This protein binds first to O_{R3}, apparently helping to abolish repressor synthesis.

To illustrate the application of our methodology, we consider the following bacte-

riophage λ synthetic network model described in [132]:

$$\begin{aligned} \frac{dx}{dt} &= \frac{m_x(1+x^2+\alpha\sigma_1 x^4)}{Q(x,y)} - \gamma_x x \\ \frac{dy}{dt} &= \frac{m_y\rho_y(1+y^2)}{Q(x,y)} - \gamma_y y \end{aligned} \tag{9.5}$$

where

$$Q(x,y) = 1+x^2+\sigma_1 x^4+\sigma_1\sigma_2 x^6+y^2+(\beta_1+\beta_2)y^4+\beta_1\beta_3 y^6+\sigma_1\beta_4 x^4 y^2+\beta_5 x^2 y^2 \tag{9.6}$$

x and y represent dimensionless concentrations of the *CI* and *Cro* proteins, respectively; t represents dimensionless time; σ_1 and σ_2 are prefactors denoting the relative affinities for dimer binding to O_{R1} versus that of binding to O_{R2} and O_{R3}, respectively; the integers m_x and m_y represent the plasmid copy numbers for the two species; ρ_y represents a constant related to the scaling of y relative to x; γ_x and γ_y are directly proportional to the decay rates of *CI* and *Cro* proteins, respectively. The even polynomials in x occur due to dimerization and subsequent binding to the promoter region. The x^4 term represents the transcription when the two operator sites O_{R1} and O_{R2} are occupied (x^2x^2). The x^6 term represents the occupation of all three operator sites and arises in the denominator because dimer occupation of O_{R3} inhibits polymerase binging and shuts off transcription. The values of the model parameters in Eqs.9.5-9.6 are given in Table 9.3. The steady-state values for different *CI* and *Cro* degradation rate are given in Table 9.4.

Bifurcation and phase-plane analysis of the above model shows that, by changing the values of γ_x and γ_y, the system of Eq.9.5 can exhibit one of the following modes of behavior:

- A mode with a single globally asymptotically stable equilibrium point corresponding to the lysogenic steady-state (low γ_x and high γ_y).

- A mode with a single globally asymptotically stable equilibrium point corresponding to the lytic steady-state (high γ_x and low γ_y).
- A bi-stable mode where the stable lysogenic and lytic steady-states coexist together with a third unstable steady-state.

Table 9.3: Parameter values for the bacteriophage λ model in Eq.9.5.

ρ_y	=	62.92
α	=	11
m_x	=	1
m_y	=	1
σ_1	=	2
σ_2	=	0.08
β_1	=	0.08
β_2	=	0.08
β_3	=	0.08
β_4	=	1
β_5	=	1

Note from Table 9.4 that for a fixed γ_y, as the degradation rate of protein *CI* is increased (larger γ_x value), the lysogenic steady-state keeps shifting to smaller concentrations until the system exhibits only the lytic steady-state (the lysogenic steady-state vanishes). By contrast, for a fixed γ_x, when the degradation rate of protein *Cro* is increased (larger γ_y value), the lytic steady-state keeps shifting to smaller concentrations until the system exhibits only the lysogenic steady-state (the lytic steady-state vanishes).

Focusing on the bi-stable mode, we initially computed the domains of attraction of both steady-states for different values of the *CI* and *Cro* protein degradation rate using the Lyapunov function employed in the previous example (i.e., $V = (x - x_s)^4 + 10(y - y_s)^2$). However, due to the nonlinearity and complexity of the system, such polynomial Lyapunov function did not yield good estimates of the

Table 9.4: Steady-state values (x_s,y_s) for the lysogenic, lytic and unstable states for different values of γ_x and γ_y.

γ_x	γ_y	Lysogenic state	Lytic state	Unstable state
0.004	0.008	(32.39,0)	(0,16.22)	(2.79,15.27)
0.05	0.008	(13.71,0.01)	(0,16.22)	(4.89,6.38)
0.1	0.008	(10.75,0.03)	(0,16.22)	(5.37,4.10)
1	0.008	n/a	(0,16.22)	n/a
0.004	1	(32.39,0)	n/a	n/a
0.05	0.0005	(13.71,0.11)	(0,28.59)	(10.24,3.47)
0.05	0.06	(13.71,0)	(0,10.60)	(2.64,7.65)

domains of attraction. Therefore, computer simulations were used to compute the domains of attraction. Figs.9.7, 9.8a, and 9.8b show the domains of attraction for the lysogenic and lytic steady-states for: (1) a moderate *CI* degradation rate ($\gamma_x = 0.05$, $\gamma_y = 0.008$), (2) a relatively low *CI* degradation rate ($\gamma_x = 0.004$, $\gamma_y = 0.008$), and (3) a relatively high *CI* degradation rate ($\gamma_x = 0.1$, $\gamma_y = 0.008$), respectively, keeping the *Cro* protein degradation rate constant. Figs.9.7, 9.11a, and 9.11b show the domains of attraction for the lysogenic and lytic steady-states for: (1) a moderate *Cro* degradation rate ($\gamma_x = 0.05$, $\gamma_y = 0.008$), (2) a relatively low *Cro* degradation rate ($\gamma_x = 0.05$, $\gamma_y = 0.0005$), and (3) a relatively high *Cro* degradation rate ($\gamma_x = 0.05$, $\gamma_y = 0.06$), respectively, keeping the *CI* protein degradation rate constant. The entire area below (or to the right of) the dotted curve is the domain of attraction for the lysogenic steady-state, while the area above (or to the left of) the dotted curve is the domain of attraction for the lytic steady-state. Both steady-states are denoted by asterisks on each plot.

It is clear from the plots that an increase in the *CI* degradation rate results in a smaller domain of attraction for the lysogenic state (and a larger one for the lytic state) and vice versa. In the limiting case of very high degradation rates, the lysogenic

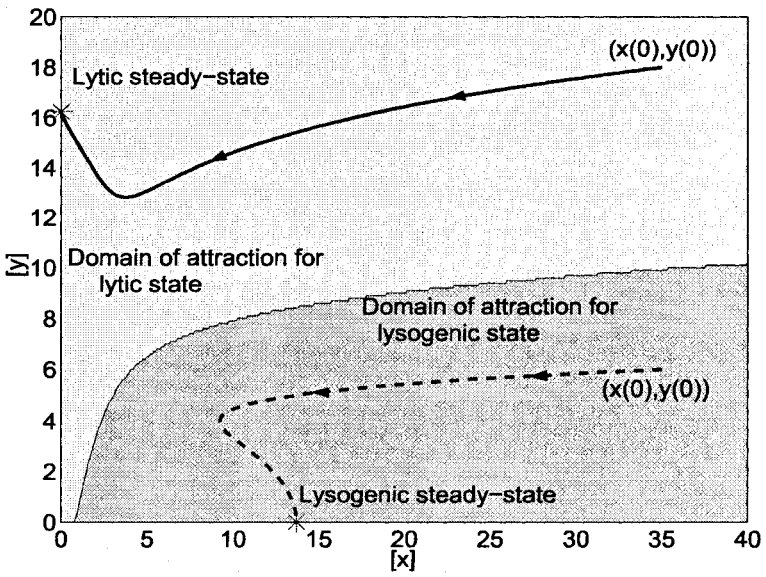

Figure 9.7: A phase plot for the moderate *CI* degradation mode showing that an initial condition within the lysogenic domain of attraction (entire area below the dotted curve) will converge to the lysogenic steady-state (dashed trajectory) and that an initial condition within the lytic domain of attraction (entire area above the dotted curve) will converge to the lytic steady-state (solid trajectory). Here, the *Cro* degradation rate is fixed at $\gamma_y = 0.008$.

state vanishes and the domain of attraction of the lytic state occupies the entire state space (single globally asymptotically stable equilibrium point). The opposite trend is observed when the *Cro* protein degradation rate is increased. In particular, increasing γ_y leads to a smaller domain of attraction for the lytic state and a larger one for the lysogenic state. For very high *Cro* degradation rates, the lytic steady-state vanishes and the domain of attraction for the lysogenic state turns into the entire state-space.

Therefore, in the bi-stable mode, the initial condition plays a critical role in deciding which steady-state the bacteriophage λ will attain. Also, the size of the domain of attraction for each state helps explain why the lysogenic state is more likely to be observed under a given set of conditions (e.g., [261]), while the lytic state is more likely to be seen under a different set of conditions. Fig.9.7 shows that starting from an initial condition of high *CI* and *Cro* concentrations, the phage ends up in the lytic state since the initial condition is within its domain of attraction (solid trajectory). Initializing the system, however, at high *CI* but low *Cro* concentrations drives the phage to the lysogenic state (dashed trajectory).

We now demonstrate the effect of switching in the *CI* protein degradation rate on whether the bacteriophage will exhibit the lytic or lysogenic steady-state. To this end, we initialize the system within the moderate *CI* degradation mode ($\gamma_x = 0.05$, $\gamma_y = 0.008$) at the initial condition $(x(0), y(0)) = (35, 18)$ and allow it to evolve in this mode until, at $t = 20$, a mode transition is enforced (see dashed trajectories in Figs.9.8a-b). The results show that, for a fixed transition time, depending on which mode is being switched in, the phage takes a different path. For example, Fig.9.8a shows that when the system switches to the relatively low *CI* degradation mode ($\gamma_x = 0.004$, $\gamma_y = 0.008$) at $t = 20$, the system state is within the domain of attraction of the lysogenic steady-state and, therefore, the phage ends up with lysogeny. Fig.9.8b,

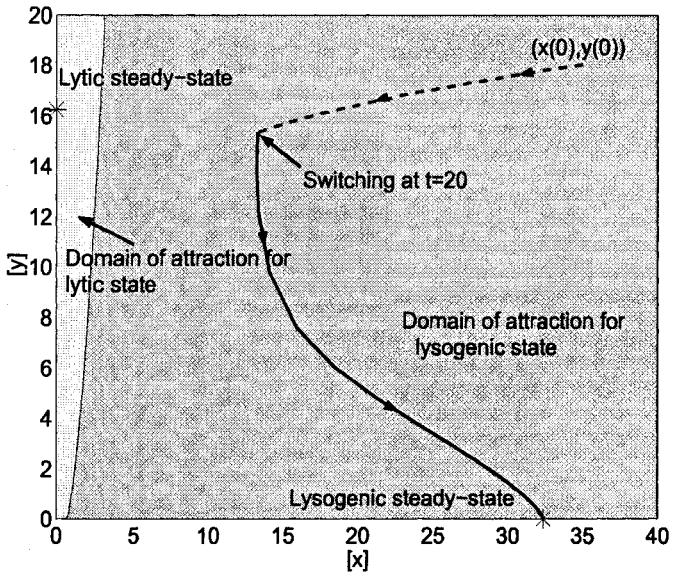

(a)

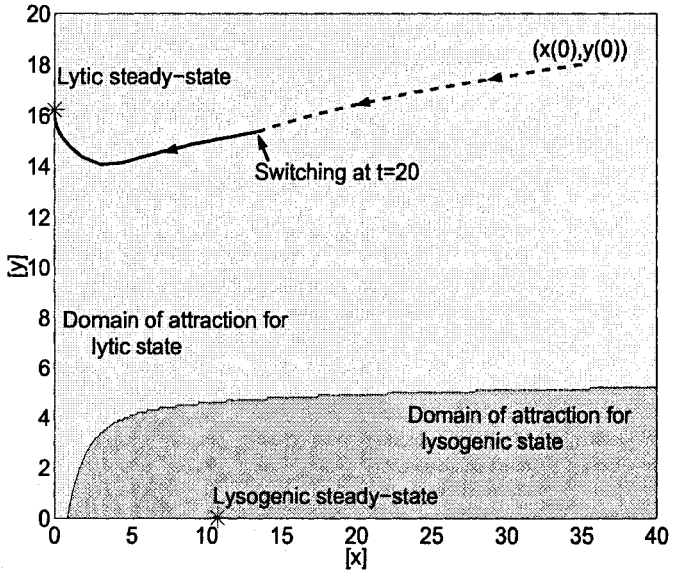

(b)

Figure 9.8: A phase plot showing the system of Eq.9.5 being initialized using $\gamma_x = 0.05$ (dashed trajectory) and undergoing: (a) a decrease in the degradation rate of *CI* protein (to $\gamma_x = 0.004$) at $t = 20$, leading the state to converge to the lysogenic steady-state, and (b) an increase in the degradation rate of *CI* protein (to $\gamma_x = 0.1$) at $t = 20$, leading the state to converge to the lytic steady-state. In both cases, the *Cro* degradation rate is fixed at $\gamma_y = 0.008$.

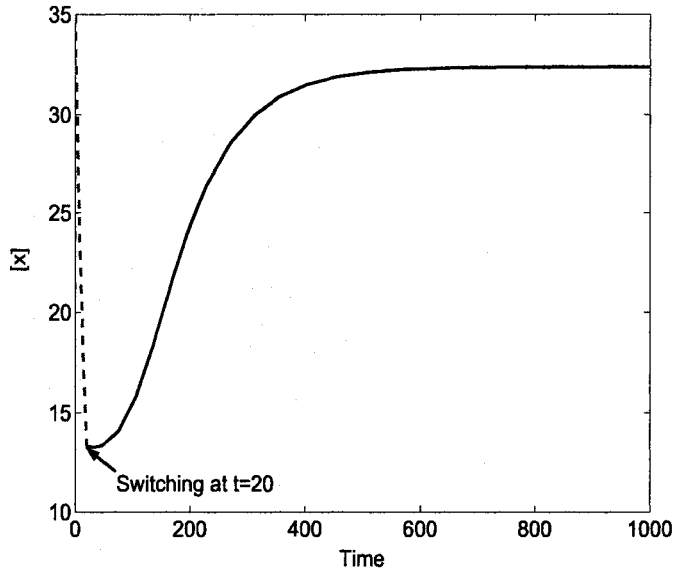

(a)

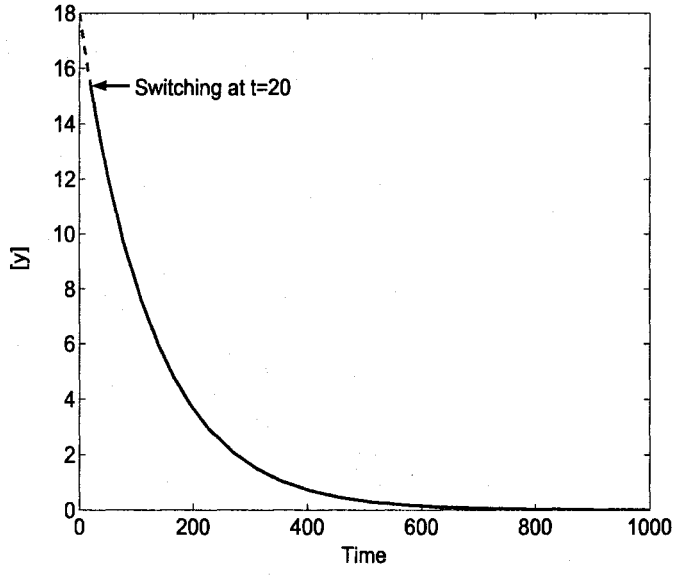

(b)

Figure 9.9: The time evolution plots of the *CI* (left) and *Cro* (right) protein concentrations when the system undergoes a transition from the $\gamma_x = 0.05$ mode (dashed lines) to the $\gamma_x = 0.004$ mode at $t = 20$ and converges (solid lines) to the lysogenic steady-state. The *Cro* degradation rate is fixed at $\gamma_y = 0.008$.

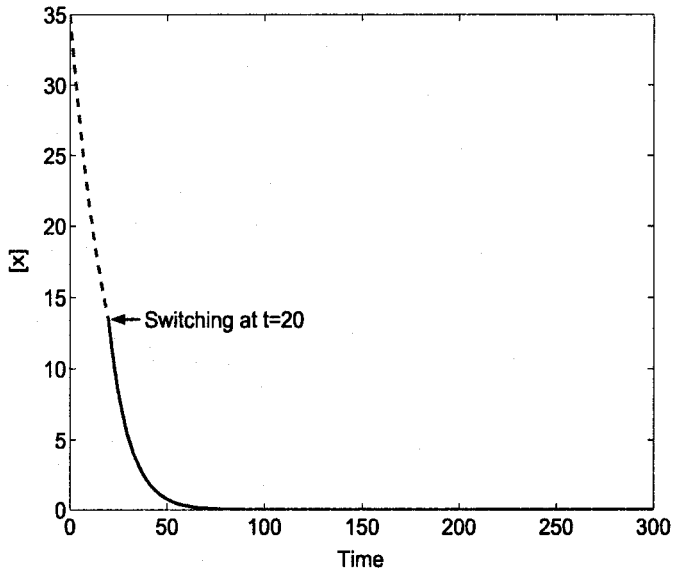

(a)

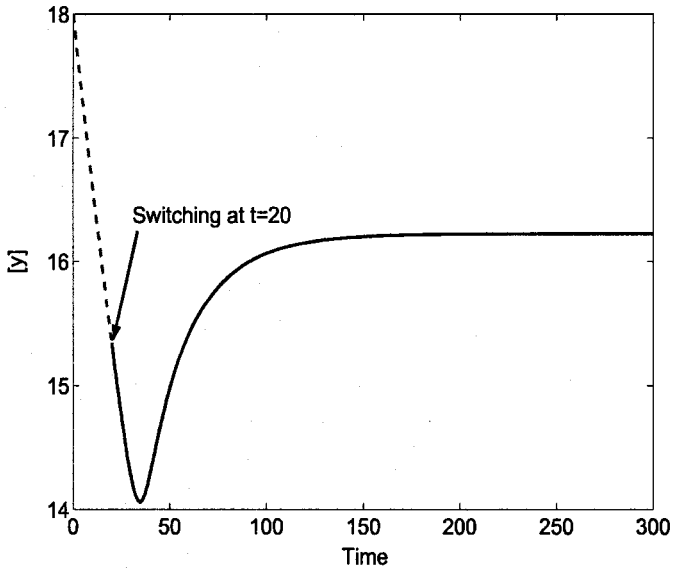

(b)

Figure 9.10: The time evolution plots of the *CI* (left) and *Cro* (right) protein concentrations when the system undergoes a transition from the $\gamma_x = 0.05$ mode (dashed lines) to the $\gamma_x = 0.1$ mode at $t = 20$ and converges (solid lines) to the lytic steady-state. The *Cro* degradation rate is fixed at $\gamma_y = 0.008$.

on the other hand, shows that when the relatively high *CI* degradation mode ($\gamma_x = 0.1,\ \gamma_y = 0.008$) is switched in at $t = 20$, the system state is within the domain of attraction of the lytic steady-state and, therefore, the phage ends up with lysis instead. The time evolution plots for both scenarios are depicted in Figs.9.9-9.10, respectively.

Similarly, we demonstrate the effect of switching in the *Cro* protein degradation rate initialized within the moderate *Cro* degradation mode ($\gamma_x = 0.05,\ \gamma_y = 0.008$) at the same initial condition $(x(0), y(0)) = (35, 18)$ and allow it to evolve in this mode until, at $t = 20$, a mode transition is enforced (see dashed trajectories in Figs.9.11a-b). The results show that, for a fixed transition time, depending on which mode is being switched in, the phage takes a different path. For example, Fig.9.11a shows that when the system switches to the relatively low *Cro* degradation mode ($\gamma_x = 0.05,\ \gamma_y = 0.0005$) at $t = 20$, the system state is within the domain of attraction of the lytic steady-state and, therefore, the phage ends up with lytic. Fig.9.11b, on the other hand, shows that when the relatively high *Cro* degradation mode ($\gamma_x = 0.05,\ \gamma_y = 0.06$) is switched in at $t = 20$, the system state is within the domain of attraction of the lysogenic steady-state and, therefore, the phage ends up with lysogeny instead. The time evolution plots for both scenarios are depicted in Figs.9.12-9.13, respectively.

So far in our analysis, we have fixed the transition time and showed that which mode is activated at that time determines the final state of the phage. Here, we demonstrate the effect of varying the transition time, for a given mode transition, on the steady-state behavior of the phage. To this end, we reconsider the switching scenario presented in Fig.9.8a, where the system switches from the moderate ($\gamma_x = 0.05$) to the relatively low *CI* degradation mode ($\gamma_x = 0.004$) where the *Cro* degradation

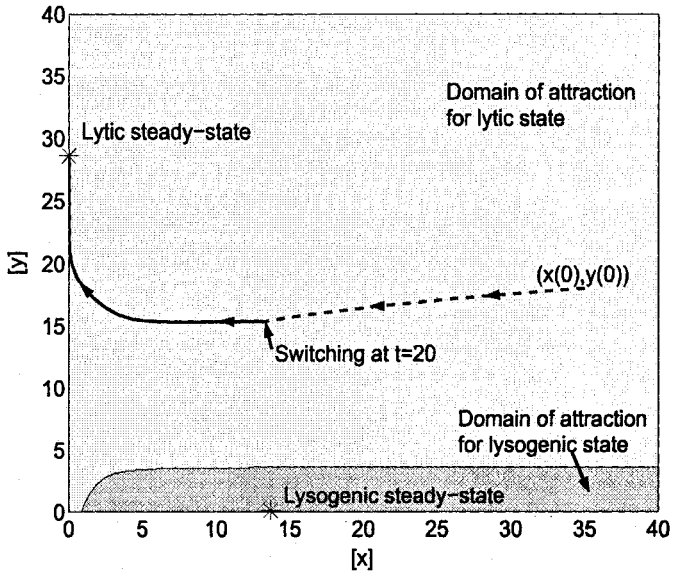

(a)

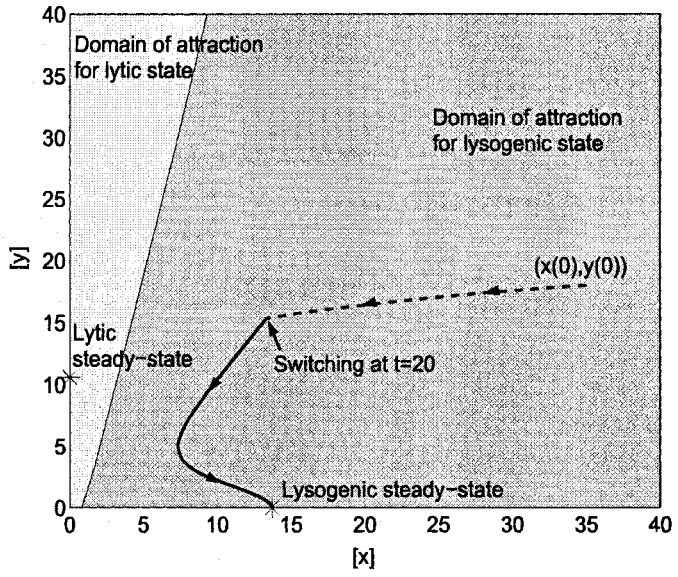

(b)

Figure 9.11: A phase plot showing the system of Eq.9.5 being initialized using $\gamma_y = 0.008$ (dashed trajectory) and undergoing: (a) a decrease in the degradation rate of *Cro* protein (to $\gamma_y = 0.0005$) at $t = 20$, leading the state to converge to the lytic steady-state, and (b) an increase in the degradation rate of *Cro* protein (to $\gamma_y = 0.06$) at $t = 20$, leading the state to converge to the lysogenic steady-state. In both cases, the *CI* degradation rate is fixed at $\gamma_x = 0.05$.

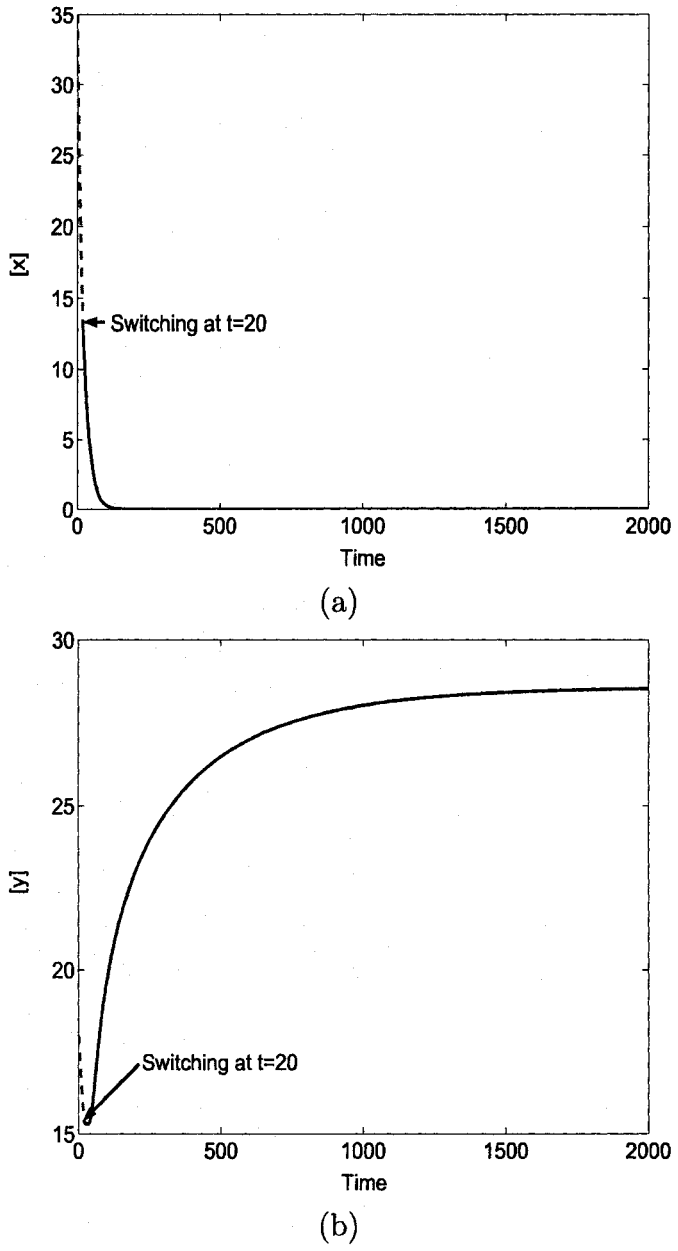

Figure 9.12: The time evolution plots of the *CI* (left) and *Cro* (right) protein concentrations when the system initialized at $(x(0), y(0)) = (35, 18)$ undergoes a transition from the $\gamma_y = 0.008$ mode (dashed lines) to the $\gamma_y = 0.0005$ mode at $t = 20$ and converges (solid lines) to the lytic steady-state. The *CI* degradation rate is fixed at $\gamma_x = 0.05$.

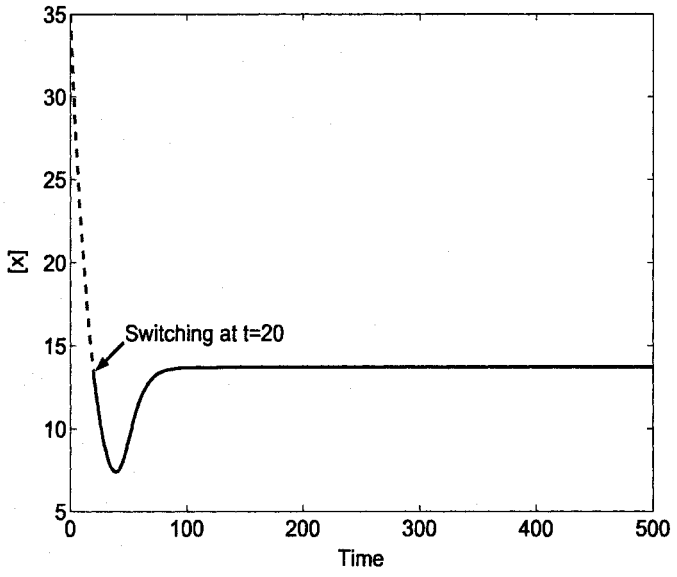

(a)

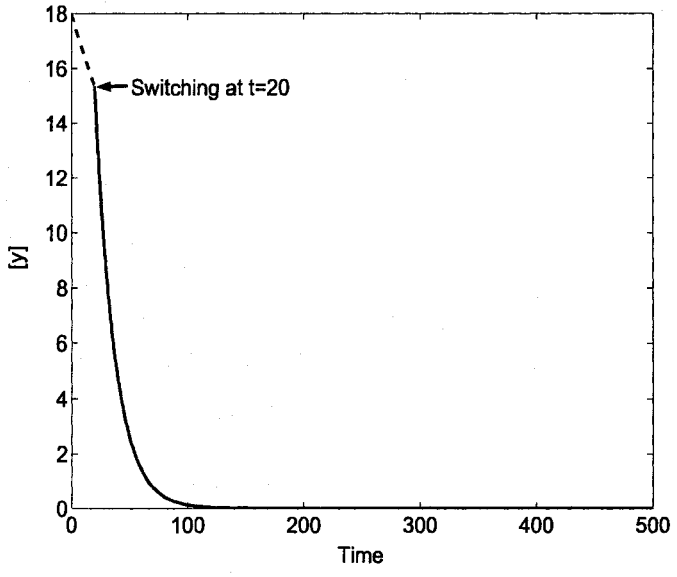

(b)

Figure 9.13: The time evolution plots of the *CI* (left) and *Cro* (right) protein concentrations when the system initialized at $(x(0), y(0)) = (35, 18)$ undergoes a transition from the $\gamma_y = 0.008$ mode (dashed lines) to the $\gamma_y = 0.06$ mode at $t = 20$ and converges (solid lines) to the lysogenic steady-state. The *CI* degradation rate is fixed at $\gamma_x = 0.05$.

rate is fixed at $\gamma_y = 0.008$. However, instead of carrying out the transition at $t = 20$ as in Fig.9.8a, the switch is delayed until $t = 70$. The result is depicted in Fig.9.14 which shows that at $t = 70$, the system state is within the domain of attraction of the lytic steady-state and, therefore, the phage ends up with lysis. The corresponding time evolution plots are given in Fig.9.15. By comparing Fig.9.8a with Fig.9.14, we conclude that an early transition from moderate to relatively low *CI* degradation rate favors lysogeny, while a late transition favors lysis.

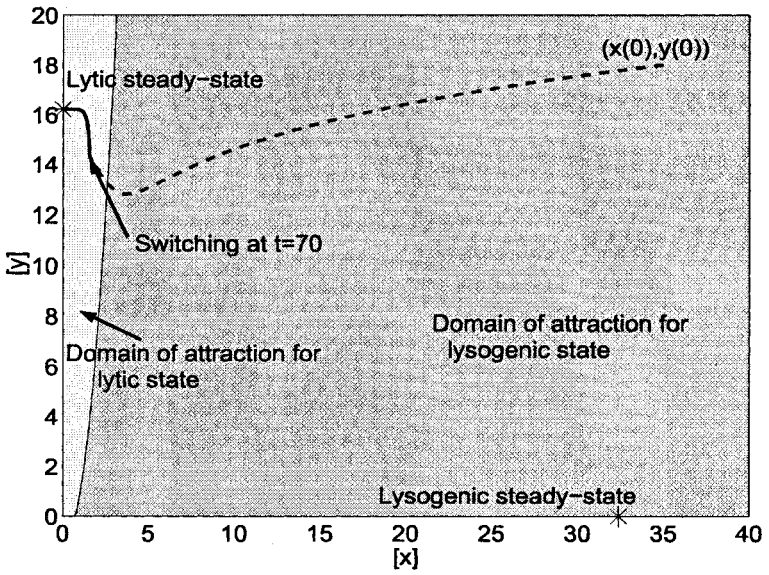

Figure 9.14: A phase plot showing the system undergoing a transition from the $\gamma_x = 0.05$ mode (dashed trajectory) to the $\gamma_x = 0.004$ at $t = 70$ and converging (solid trajectory) to the lytic steady-state. The *Cro* degradation rate is fixed at $\gamma_y = 0.008$.

In the last simulation run, we demonstrate the effect of the initial condition on the outcome of switching for a given transition time. To this end, we initialize the system within the moderate *CI* degradation mode ($\gamma_x = 0.05$, $\gamma_y = 0.008$) at an initial condition different from the one considered in Fig.9.8 and characterized by high concentration of *CI* and low concentration of *Cro* (x(0)=35, y(0)=2). We allow the system to evolve in this mode until, at $t = 40$, a mode transition is enforced (see

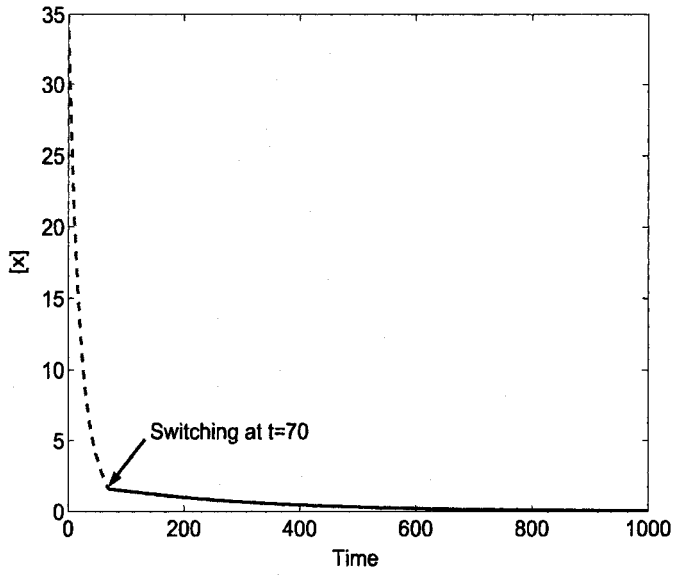

(a)

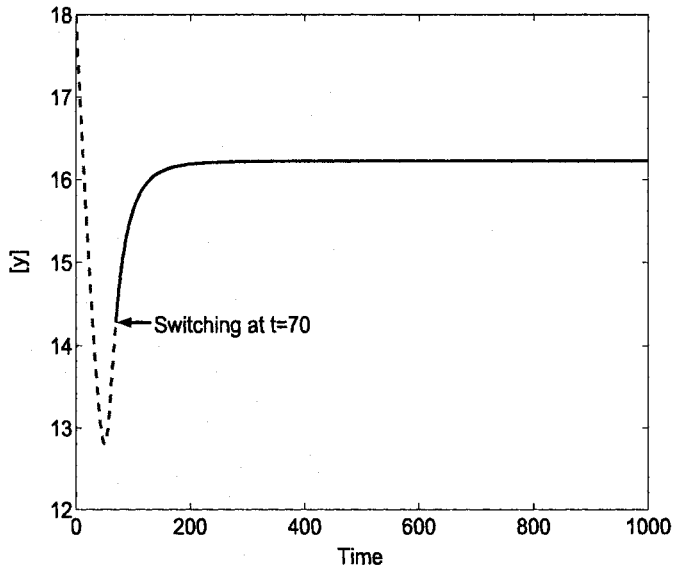

(b)

Figure 9.15: The time evolution plots of the *CI* (left) and *Cro* (right) protein concentrations when the system undergoes a transition from the $\gamma_x = 0.05$ mode (dashed lines) to the $\gamma_x = 0.004$ mode at $t = 70$ and converges (solid lines) to the lytic steady-state. The *Cro* degradation rate is fixed at $\gamma_y = 0.008$.

dashed trajectories in Figs.9.16a-b). The results show that, for a fixed transition time, switching close to a particular steady-state will converge to that particular steady-state, independently of which mode is being switched in. For example, Fig.9.16a shows that when the system switches to the relatively low *CI* degradation mode ($\gamma_x = 0.004,\ \gamma_y = 0.008$) at $t = 40$, the state is within the domain of attraction of the lysogenic steady-state and, therefore, the phage ends up with lysogeny. Similarly, Fig.9.16b shows that when the relatively high *CI* degradation mode ($\gamma_x = 0.1,\ \gamma_y = 0.008$) is switched in at $t = 40$, the state is again within the domain of attraction of the lysogenic steady-state and, therefore, the phage ends up with lysogeny (albeit with a smaller steady-state concentration of *CI* protein). The time evolution plots for both scenarios are depicted in Figs.9.17-9.18, respectively. Note that this result is different from the one obtained in Fig.9.8 where the final steady-state behavior is dependent on which mode is being switched in. The difference lies in the fact that the initial condition considered in Fig.9.16 is contained within the domain of attraction of the lysogenic steady-state for both the low and high *CI* degradation modes, and therefore only the lysogenic steady-state can be observed regardless of whether the low or high *CI* degradation mode is activated.

9.6 Conclusions

In this chapter, a methodology for the analysis and control of mode transitions in biological networks was presented. The proposed approach was predicated upon the notion of orchestrating switching between the domains of attraction of the steady-states of the constituent modes. Initially, the overall network was modeled as a switched nonlinear system that consisted of multiple modes, each governed by a set of continuous-time differential equations. The transitions between the continuous

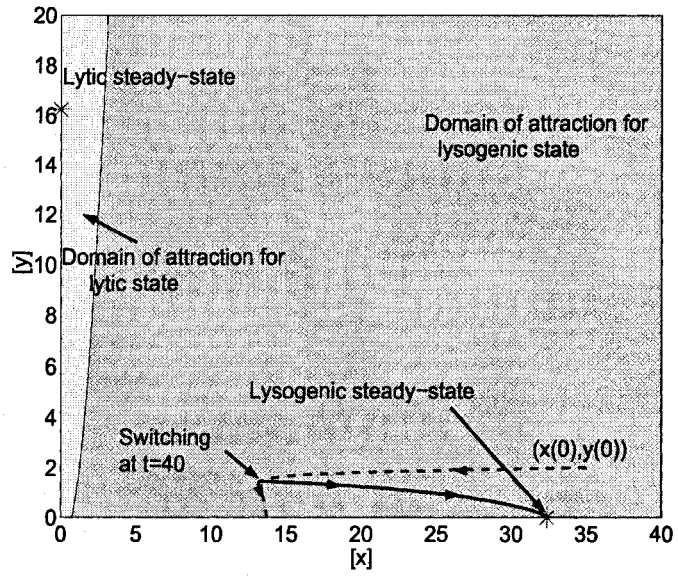

(a)

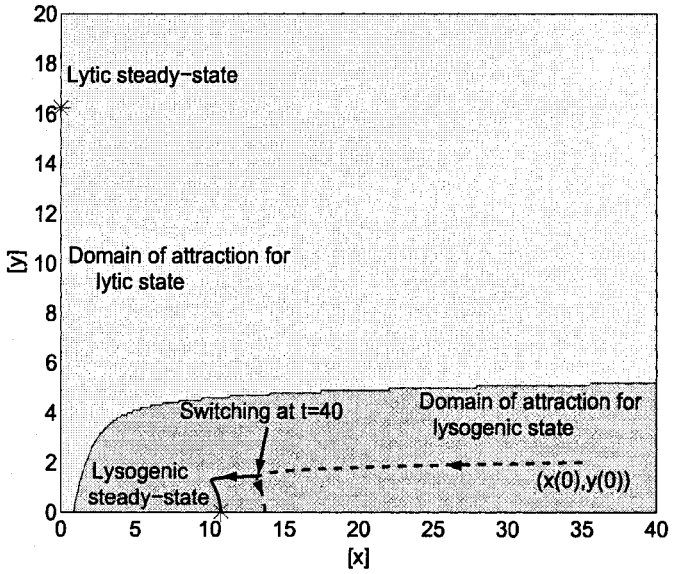

(b)

Figure 9.16: A phase plot showing the system of Eq.9.5 being initialized using $\gamma_x = 0.05$ (dashed trajectory) and undergoing: (a) a decrease in the degradation rate of *CI* protein (to $\gamma_x = 0.004$) at $t = 40$ and (b) an increase in the degradation rate of *CI* protein (to $\gamma_x = 0.1$) at $t = 40$, both leading the state to converge to the lysogenic steady-state. In both cases, the *Cro* degradation rate is fixed at $\gamma_y = 0.008$.

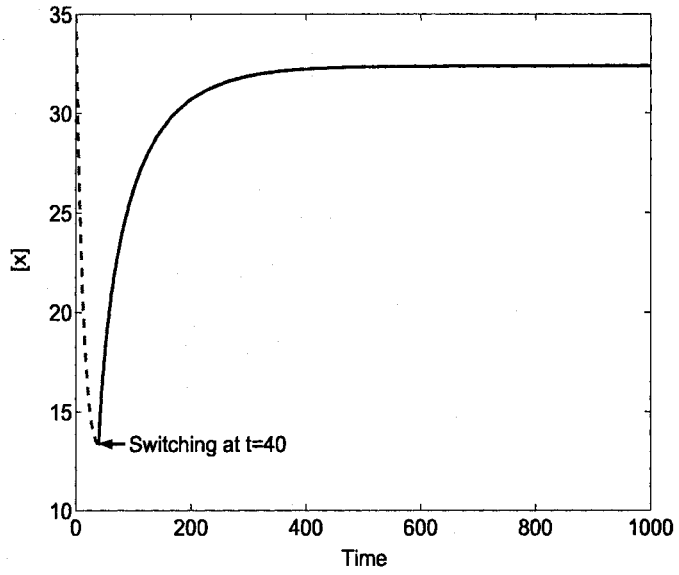

(a)

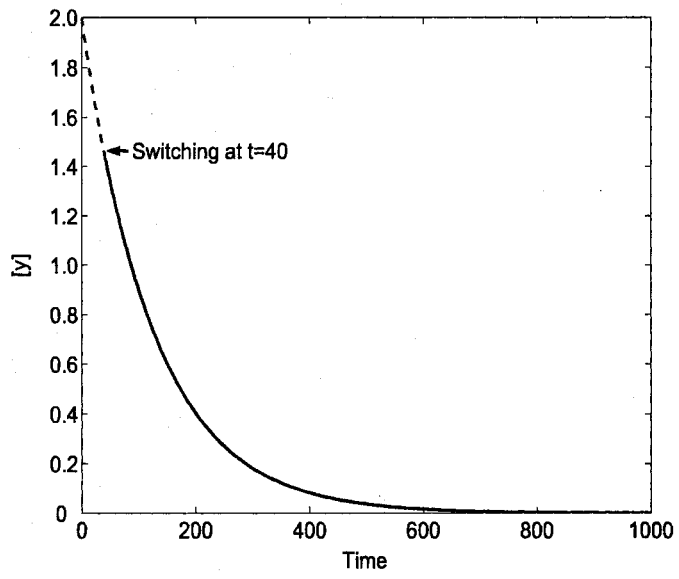

(b)

Figure 9.17: The time evolution plots of the *CI* (left) and *Cro* (right) protein concentrations when the system initialized at $(x(0), y(0)) = (35, 2)$ undergoes a transition from the $\gamma_x = 0.05$ mode (dashed lines) to the $\gamma_x = 0.004$ mode at $t = 40$ and converges (solid lines) to the lytic steady-state. The *Cro* degradation rate is fixed at $\gamma_y = 0.008$.

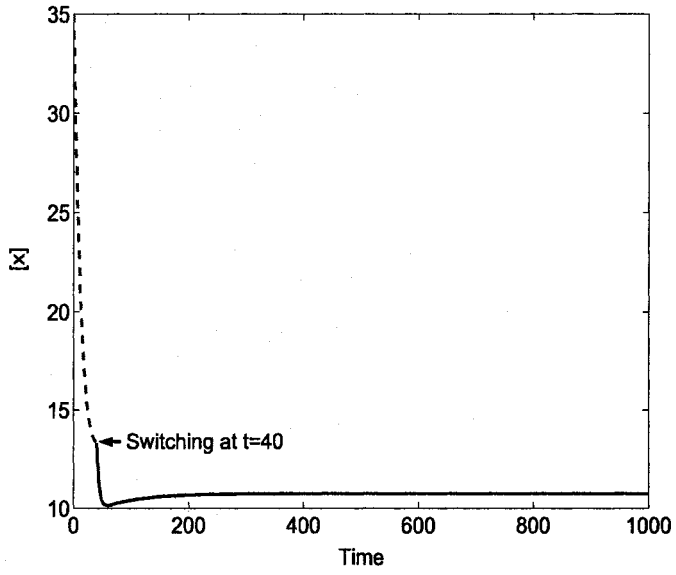

(a)

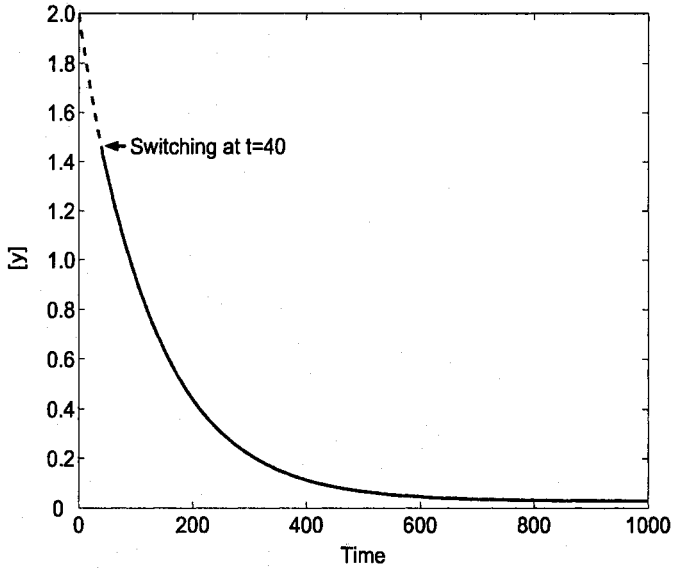

(b)

Figure 9.18: The time evolution plots of the *CI* (left) and *Cro* (right) protein concentrations when the system initialized at $(x(0), y(0)) = (35, 2)$ undergoes a transition from the $\gamma_x = 0.05$ mode (dashed lines) to the $\gamma_x = 0.1$ mode at $t = 40$ and converges (solid lines) to the lytic steady-state. The *Cro* degradation rate is fixed at $\gamma_y = 0.008$.

modes are triggered by discrete events (changes in model parameters that correspond to alterations in physiological conditions). Then, following the characterization of the steady-state behavior of each mode, Lyapunov techniques were used to characterize the domains of attraction of the steady-states. Finally, by analyzing how the domains of attraction of the various modes overlap with one other, a switching rule was derived to determine when, and if, a given mode transition at a given time results in the desired steady-state behavior. The proposed method was demonstrated using models of biological networks that arise in cell cycle regulation and the bacteriophage λ-switch system. The proposed approach has implications both for understanding the outcome of naturally-occurring mode transitions and for the ability to manipulate network behavior by enforcing mode transitions.

Chapter 10

Analysis and Control of Constrained Parabolic PDE Systems

10.1 Introduction

Transport-reaction processes with significant diffusive and convective phenomena are typically characterized by strong nonlinearities and spatial variations, and are naturally described by quasi-linear parabolic partial differential equations (PDEs). Examples include tubular reactors, packed-bed reactors, and chemical vapor deposition reactors. Parabolic PDE systems typically involve spatial differential operators whose eigenspectrum can be partitioned into a finite-dimensional slow one and an infinite-dimensional stable fast complement [116]. This implies that the dynamic behavior of such systems can be approximately described by finite-dimensional systems. Therefore, the standard approach to the control of parabolic PDEs involves the application of Galerkin's method to the PDE system to derive ordinary differential equation (ODE) systems that describe the dynamics of the dominant (slow) modes

of the PDE system, which are subsequently used as the basis for the synthesis of finite-dimensional controllers (e.g., [29, 255]). More recently, research efforts on control of parabolic PDE systems have focused on the problem of synthesizing low-order nonlinear controllers on the basis of ODE models obtained through combination of Galerkin's method with approximate inertial manifolds (see [61] for details and references). In addition to this work, other important contributions include controller design based on the infinite-dimensional system and subsequent use of approximation theory to design and compute low-order finite-dimensional compensators [46] as well as the stabilization of PDE systems using boundary control [47, 205].

Although the above methods lead to the systematic design of nonlinear controllers for transport-reaction processes, these methods do not address the practical problem of input constraints. Virtually all physical and chemical control systems are subject to hard constraints on their manipulated inputs, typically arising from the finite capacity of control actuators. These constraints limit our ability to modify the system dynamics and, if not appropriately accounted for at the stage of controller design, can lead to significant performance deterioration and even cause closed-loop instability. The ill-effects due to actuator constraints have consequently motivated many recent studies on the dynamics and control of systems subject to input constraints. Most of the research in this area, however, has focused on lumped parameter systems modeled by finite-dimensional ODE systems (e.g., see [191, 6, 174, 300, 158, 91]).

Compared with lumped-parameter systems, the problem of constrained control of distributed parameter systems has received less attention. The few results available on this problem have focused primarily on linear distributed parameter systems (e.g., see [52, 43, 83]), with virtually no results on their nonlinear counterparts. A host of issues therefore remain to be resolved, including the synthesis of nonlinear controllers

that account explicitly for input constraints, as well as the explicit characterization of the limitations imposed by input constraints on the set of admissible initial conditions and admissible actuator locations that can be used for stabilization. In contrast to the case of lumped systems, constraints on the manipulated input of distributed parameter systems that exhibit spatial variations impose an additional limitation on *where* the control actuators can be placed to guarantee closed-loop stability.

Motivated by these problems, we develop in this chapter a general framework for the analysis and control of quasi-linear parabolic PDE systems with input constraints. Initially, a finite-dimensional ODE system, that captures the dominant dynamics of the PDE system, is derived using Galerkin's method. This ODE system is then used as the basis for the synthesis, via Lyapunov techniques, of bounded nonlinear feedback controllers that enforce closed-loop stability and provide, simultaneously, an explicit characterization of the limitations imposed by input constraints on both the admissible initial states and admissible control actuator locations that can be used to guarantee closed-loop stability. The proposed analysis and controller synthesis results are used to stabilize an unstable steady-state of a diffusion-reaction process. The results of this chapter were first presented in [88]

10.2 Preliminaries

10.2.1 Parabolic PDE systems with input constraints

We consider quasi-linear parabolic PDE systems of the form:

$$\begin{aligned} \frac{\partial \bar{x}}{\partial t} &= A\frac{\partial \bar{x}}{\partial z} + B\frac{\partial^2 \bar{x}}{\partial z^2} + w\sum_{i=1}^{m} b_i(z)u_i + f(\bar{x}) \\ y_{ci} &= \int_{\alpha}^{\beta} c(z)^i k\bar{x}(z,t)dz \qquad i = 1,\ldots,m \\ y_m^{\kappa} &= \int_{\alpha}^{\beta} s(z)^{\kappa}\omega\bar{x}(z,t)dz \qquad \kappa = 1,\ldots,p \end{aligned} \tag{10.1}$$

subject to the boundary conditions:

$$\begin{aligned} C_1\bar{x}(\alpha,t) + D_1\frac{\partial \bar{x}}{\partial z}(\alpha,t) &= R_1 \\ C_2\bar{x}(\beta,t) + D_2\frac{\partial \bar{x}}{\partial z}(\beta,t) &= R_2 \end{aligned} \tag{10.2}$$

and the initial condition:

$$\bar{x}(z,0) = \bar{x}_0(z) \tag{10.3}$$

where $\bar{x}(z,t) = [\bar{x}_1(z,t) \cdots \bar{x}_n(z,t)]^T \in \mathbb{R}^n$ denotes the vector of state variables, $z \in [\alpha,\beta] \subset \mathbb{R}$ is the spatial coordinate, $t \in [0,\infty)$ is the time, $u_i \in [u_{i,min}, u_{i,max}] \subset \mathbb{R}$ denotes the i-th constrained manipulated input, $y_{ci} \in \mathbb{R}$ denotes the i-th controlled output, and $y_m^\kappa \in \mathbb{R}$ denotes the κ-th measured output. $\frac{\partial \bar{x}}{\partial z}, \frac{\partial^2 \bar{x}}{\partial z^2}$ denote the first- and second-order spatial derivatives of $\bar{x}$, $f(\bar{x})$ is a nonlinear vector function, w, k are constant vectors, A, B, C_1, D_1, C_2, D_2 are constant matrices, R_1, R_2 are column vectors, and $\bar{x}_0(z)$ is the initial condition. $b_i(z)$ is a known smooth function of z which describes how the control action, $u_i(t)$, is distributed in the interval $[\alpha,\beta]$, $c(z)^i$ is a known smooth function of z which is determined by the desired performance specifications in the interval $[\alpha,\beta]$, and $s^\kappa(z)$ is a known smooth function of z which depends on the shape (point or distributing sensing) of the measurement sensors in the interval $[\alpha,\beta]$. Whenever the control action enters the system at a single point z_0, with $z_0 \in [\alpha,\beta]$ (i.e., point actuation), the function $b_i(z)$ is taken to be nonzero in a finite spatial interval of the form $[z_0-\epsilon, z_0+\epsilon]$, where ϵ is a small positive real number, and zero elsewhere in $[\alpha,\beta]$. Throughout the chapter, we will use the order of magnitude notation, $O(\epsilon)$, and the Lie derivative notation. In particular, $\delta(\epsilon) = O(\epsilon)$ if there exist positive real numbers, k_1 and k_2, such that: $|\delta(\epsilon)| \leq k_1|\epsilon|$, $\forall\ |\epsilon| \leq k_2$. $L_f\bar{h}$ denotes the standard Lie derivative of a scalar function, $\bar{h}(\cdot)$, with respect to the vector function $f(\cdot)$, $L_f^k\bar{h}$ denotes the k-th order Lie derivative and $L_gL_f^{k-1}\bar{h}$ denotes the mixed Lie derivative where $g(\cdot)$ is a vector function. Furthermore, the notation,

$|\cdot|$, will be used to denote the standard Euclidean norm, while the notation $|\cdot|_2$ and $\|\cdot\|_2$ will be used to denote the L_2-norms of vectors belonging in a finite-dimensional and an infinite-dimensional Hilbert spaces, respectively.

To precisely characterize the class of parabolic PDE systems considered in this work, we formulate the system of Eq.10.1 as an infinite-dimensional system in the Hilbert space $\mathcal{H}([\alpha,\beta];\mathbb{R}^n)$, with $\mathcal{H}$ being the space of n-dimensional vector functions defined on $[\alpha,\beta]$ that satisfy the boundary condition of Eq.10.2, with inner product and norm:

$$(\omega_1,\omega_2)=\int_\alpha^\beta(\omega_1(z),\omega_2(z))_{\mathbb{R}^n}dz,\quad \|\omega_1\|_2=(\omega_1,\omega_1)^{\frac{1}{2}} \tag{10.4}$$

where ω_1,ω_2 are two elements of $\mathcal{H}([\alpha,\beta];\mathbb{R}^n)$ and the notation $(\cdot,\cdot)_{\mathbb{R}^n}$ denotes the standard inner product in $\mathbb{R}^n$. Defining the state function x on $\mathcal{H}([\alpha,\beta];\mathbb{R}^n)$ as:

$$x(t)=\bar{x}(z,t),\quad t>0,\quad z\in[\alpha,\beta], \tag{10.5}$$

the operator $\mathcal{A}$ in $\mathcal{H}([\alpha,\beta];\mathbb{R}^n)$ as:

$$\begin{aligned}\mathcal{A}x &= A\frac{\partial\bar{x}}{\partial z}+B\frac{\partial^2\bar{x}}{\partial z^2},\\ x\in D(\mathcal{A}) &= \Big\{x\in\mathcal{H}([\alpha,\beta];\mathbb{R}^n): C_1\bar{x}(\alpha,t)+D_1\frac{\partial\bar{x}}{\partial z}(\alpha,t)=R_1,\\ &\qquad C_2\bar{x}(\beta,t)+D_2\frac{\partial\bar{x}}{\partial z}(\beta,t)=R_2\Big\}\end{aligned}$$

and the input, controlled output, and measured output operators as:

$$\mathcal{B}u=w\sum_{i=1}^m b_iu_i,\quad \mathcal{C}x=(c,kx),\qquad \mathcal{S}x=(s,\omega x) \tag{10.6}$$

the system of Eqs.10.1-10.3 takes the form:

$$\begin{aligned}\dot{x} &= \mathcal{A}x+\mathcal{B}u+f(x),\quad x(0)=x_0\\ y_c &= \mathcal{C}x,\quad y_m=\mathcal{S}x\end{aligned} \tag{10.7}$$

where $f(x(t))=f(\bar{x}(z,t))$ and $x_0=\bar{x}_0(z)$. We assume that the nonlinear terms, $f(x)$, are locally Lipschitz with respect to their arguments and satisfy $f(0)=0$. For

$\mathcal{A}$, the eigenvalue problem is defined as:

$$\mathcal{A}\phi_j = \lambda_j \phi_j, \quad j = 1, \ldots, \infty \tag{10.8}$$

where λ_j denotes an eigenvalue and ϕ_j denotes an eigenfunction; the eigenspectrum of $\mathcal{A}$, $\sigma(\mathcal{A})$, is defined as the set of all eigenvalues of $\mathcal{A}$, i.e., $\sigma(\mathcal{A}) = \{\lambda_1, \lambda_2, \ldots\}$. Assumption 10.1 that follows states that the eigenspectrum of $\mathcal{A}$ can be partitioned into a finite part consisting of m slow eigenvalues and a stable infinite complement containing the remaining fast eigenvalues, and that the separation between the slow and fast eigenvalues of $\mathcal{A}$ is large. This assumption is satisfied by the majority of diffusion-convection-reaction processes [61].

Assumption 10.1 *1. $Re\ \{\lambda_1\} \geq Re\ \{\lambda_2\} \geq \cdots \geq Re\ \{\lambda_j\} \geq \cdots$, where $Re\ \{\lambda_j\}$ denotes the real part of λ_j.*

2. $\sigma(\mathcal{A})$ can be partitioned as $\sigma(\mathcal{A}) = \sigma_1(\mathcal{A}) + \sigma_2(\mathcal{A})$, where $\sigma_1(\mathcal{A})$ consists of the first m (with m finite) eigenvalues, i.e. $\sigma_1(\mathcal{A}) = \{\lambda_1, \ldots, \lambda_m\}$, and $\dfrac{|Re\ \{\lambda_1\}|}{|Re\ \{\lambda_m\}|} = O(1)$.

3. $Re\ \lambda_{m+1} < 0$ and $\dfrac{|Re\ \{\lambda_m\}|}{|Re\ \{\lambda_{m+1}\}|} = O(\epsilon)$ where $\epsilon < 1$ is a small positive number.

10.2.2 Galerkin's method

In this section, we apply standard Galerkin's method to the system of Eq.10.7 to derive an approximate finite-dimensional system. Let $\mathcal{H}_s$, $\mathcal{H}_f$ be modal subspaces of $\mathcal{A}$, defined as $\mathcal{H}_s = span\{\phi_1, \phi_2, \ldots, \phi_m\}$ and $\mathcal{H}_f = span\{\phi_{m+1}, \phi_{m+2}, \ldots\}$ (the existence of $\mathcal{H}_s$, $\mathcal{H}_f$ follows from Assumption 10.1). Defining the orthogonal projection operators, P_s and P_f, such that $x_s = P_s x$, $x_f = P_f x$, the state, x, of the system of Eq.10.7 can be decomposed as:

$$x \;=\; x_s + x_f = P_s x + P_f x \tag{10.9}$$

Applying P_s and P_f to the system of Eq.10.7 and using the above decomposition for x, the system of Eq.10.7 can be equivalently written in the following form:

$$\begin{aligned} \frac{dx_s}{dt} &= \mathcal{A}_s x_s + \mathcal{B}_s u + f_s(x_s, x_f) \\ \frac{\partial x_f}{\partial t} &= \mathcal{A}_f x_f + \mathcal{B}_f u + f_f(x_s, x_f) \\ y_c &= \mathcal{C} x_s + \mathcal{C} x_f, \quad y_m = \mathcal{S} x_s + \mathcal{S} x_f, \\ x_s(0) &= P_s x(0) = P_s x_0, \quad x_f(0) = P_f x(0) = P_f x_0 \end{aligned} \tag{10.10}$$

where $\mathcal{A}_s = P_s\mathcal{A}$, $\mathcal{B}_s = P_s\mathcal{B}$, $f_s = P_s f$, $\mathcal{A}_f = P_f\mathcal{A}$, $\mathcal{B}_f = P_f\mathcal{B}$ and $f_f = P_f f$ and the partial derivative notation in $\frac{\partial x_f}{\partial t}$ is used to denote that the state, x_f, belongs to an infinite-dimensional space. In the above system, $\mathcal{A}_s$ is a diagonal matrix of dimension $m \times m$ of the form $\mathcal{A}_s = diag\{\lambda_j\}$, $f_s(x_s, x_f)$ and $f_f(x_s, x_f)$ are Lipschitz vector functions, and $\mathcal{A}_f$ is an unbounded differential operator which is exponentially stable (following from Part 3 of Assumption 10.1 and the selection of $\mathcal{H}_s, \mathcal{H}_f$). Neglecting the fast and stable infinite-dimensional x_f-subsystem in the system of Eq.10.10, the following m-dimensional slow system is obtained:

$$\begin{aligned} \frac{d\bar{x}_s}{dt} &= \mathcal{A}_s \bar{x}_s + \mathcal{B}_s u + f_s(\bar{x}_s, 0) \\ \bar{y}_c &= \mathcal{C}\bar{x}_s, \qquad \bar{y}_m = \mathcal{S}\bar{x}_s \end{aligned} \tag{10.11}$$

where the bar symbol in $\bar{x}_s$, $\bar{y}_c$ and $\bar{y}_m$ denotes that these variables are associated with a finite-dimensional system.

Remark 10.1 We note that the above model reduction procedure which led to the approximate ODE system of Eq.10.11 can also be used, when empirical eigenfunctions of the system of Eq.10.7, computed through Karhunen-Loéve expansion, (see [23] for details) are used as basis functions in $\mathcal{H}_s$ and $\mathcal{H}_f$ instead of the eigenfunctions of $\mathcal{A}$.

Remark 10.2 Although standard Galerkin's method was used to obtain the finite-dimensional system of Eq.10.11, the results of this chapter can be generalized to the

case where the finite-dimensional approximation is obtained through combination of Galerkin's method with approximate inertial manifolds [61]. This approach can be used to further reduce the dimension of the system of Eq.10.11 and ensure that it is of an appropriately low-order, suitable for controller design and analysis.

10.3 Bounded nonlinear control of parabolic PDE systems

10.3.1 State feedback control

In this section, we use the constrained m-dimensional ODE system of Eq.10.11 as the basis for the synthesis of bounded nonlinear state feedback control laws of the general form:

$$u = p(\bar{x}_s, \bar{v}, u_{max}) \tag{10.12}$$

where $p(\cdot)$ is a bounded nonlinear vector function (i.e., $|u| \leq u_{max}$ where u_{max} is the maximum norm of the vector of manipulated inputs allowed by the constraints), and $\bar{v}$ is a vector of the form $\bar{v} = [\bar{v}_1^T \cdots \bar{v}_m^T]^T$ where $\bar{v}_i = [v_i \; v_i^{(1)}, \ldots, v_i^{(r_i)}]$ is a smooth vector function, $v_i^{(k)}$ is the k-th time-derivative of the external reference input, v_i, – which is assumed to be a smooth function of time – and r_i is the relative order of the controlled output y_{ci} with respect to the vector of manipulated inputs (which is assumed to be well-defined). The requested controller design specifications include: (a) enforcing asymptotic stability (and local exponential stability) as well as reference input tracking in the constrained infinite-dimensional closed-loop system, (b) characterizing explicitly the admissible initial states that can be used, for a given actuator location, to guarantee closed-loop stability, and (c) identifying explicitly the set of admissible control actuator locations that can be used, for a given initial condition, to stabilize the constrained closed-loop system.

To proceed with the controller synthesis, we consider the representation of the slow

system of Eq.10.11 in terms of the evolution of the amplitudes of the eigenmodes. The corresponding ODE system is given by:

$$\begin{aligned} \dot{a}_s(t) &= Fa_s(t) + G(z_c)u(t) + d(a_s(t)) \\ \tilde{y}_c(t) &= Ca_s(t) \end{aligned} \tag{10.13}$$

where $a_s(t) = [a_1(t) \cdots a_m(t)]^T \in \mathbb{R}^m$, $a_i(t)$ is the amplitude of the i-th eigenmode, $\bar{x}_s(t) = \sum_{j=1}^{m} a_j(t)\phi_j$, $(\bar{x}_s(t), \phi_j) = a_j(t)(\phi_j, \phi_j)$, F is an $m \times m$ diagonal matrix of the form $F = diag\{\lambda_j\}$, G is an $m \times m$ matrix whose (i,j)-th element is given by $G_{ij} = (b_j(\cdot), \phi_i(\cdot))$, $z_c = [z_{c1}\ z_{c2}\ \cdots\ z_{cm}]^T$ is the vector of actuators' locations, $d(\cdot) = [d_1(\cdot) \cdots d_m(\cdot)]^T$ is a vector function and $(f_s(\cdot), \phi_j) = d_j(\cdot)(\phi_j, \phi_j)$, $\tilde{y}_c(t) = [\tilde{y}_{c,1}(t) \cdots \tilde{y}_{c,m}(t)]^T \in \mathbb{R}^m$, $\tilde{y}_{c,i}$ is the i-th controlled output of the finite-dimensional slow system, C is a constant $m \times m$ matrix. Under the assumption that the relative degree is well-defined, we transform the system of Eq.10.13, by means of an invertible coordinate change of the form $a_s = T^{-1}(\zeta, \eta)$, into the following partially linear form:

$$\begin{aligned} \dot{\zeta}_1^{(i)} &= \zeta_2^{(i)} \\ &\vdots \\ \dot{\zeta}_{r_i-1}^{(i)} &= \zeta_{r_i}^{(i)} \\ \dot{\zeta}_{r_i}^{(i)} &= L_{\tilde{f}}^{r_i}\tilde{h}_i(a_s) + \sum_{j=1}^{m} L_{\tilde{g}_j} L_{\tilde{f}}^{r_i-1}\tilde{h}_i(a_s)u_j \\ \dot{\eta}_1 &= \Psi_1(\zeta, \eta) \\ &\vdots \\ \dot{\eta}_{m-\sum_i r_i} &= \Psi_{m-\sum_i r_i}(\zeta, \eta) \\ \tilde{y}_{ci} &= \zeta_1^{(i)},\ i = 1, \ldots, m,\ k = 1, \cdots, N \end{aligned} \tag{10.14}$$

where $\zeta_j^{(i)} = L_{\tilde{f}}^{j-1}\tilde{h}_i(a_s)$, $\zeta = [\zeta^{(1)^T} \cdots \zeta^{(m)^T}]^T$, $\eta = [\eta_1 \cdots \eta_{m-\sum_i r_i}]^T$. Defining the tracking error variables, $e_k^{(i)} = \zeta_k^{(i)} - v_i^{(k-1)}$, and introducing the vector notation, $e^{(i)} = [e_1^{(i)}\ e_2^{(i)} \cdots e_{r_i}^{(i)}]^T$, $e = [e^{(1)^T}\ e^{(2)^T} \cdots e^{(m)^T}]^T$, where $i = 1, \cdots, m$, $j = 1, \cdots, r_i$, the system of Eq.10.14 can be cast in the following more compact form:

$$\begin{aligned} \dot{e} &= \Lambda e + \Gamma\left[l(e, \eta, \bar{v}) + \bar{C}(e, \eta, \bar{v})u\right] \\ \dot{\eta} &= \Psi(e, \eta, \bar{v}) \end{aligned} \tag{10.15}$$

where $\Lambda = diag\{\Lambda_i\}$ is an $(\sum_{r_i} \times \sum_{r_i})$ block diagonal constant matrix whose constituent blocks are $r_i \times r_i$ matrices of the form:

$$\Lambda_i = \begin{bmatrix} 0 & 1 & 0 & \cdots & 0 \\ 0 & 0 & 1 & \cdots & 0 \\ \vdots & \vdots & \vdots & \ddots & \vdots \\ 0 & 0 & 0 & \cdots & 1 \\ 0 & 0 & 0 & \cdots & 0 \end{bmatrix} \tag{10.16}$$

Γ is an $(\sum_{r_i} \times m)$ constant matrix, $l(\cdot)$ is a $(\sum_{r_i} \times 1)$ smooth vector function. The specific forms of Γ and $l(\cdot)$ are omitted for brevity. Finally, we define $\bar{f}(e, \eta, \bar{v}) = \Lambda e + \Gamma l(e, \eta, \bar{v})$ and denote by $\bar{g}_i$ the i-th column of the matrix $\bar{G} = \Gamma \bar{C}$.

Motivated by the requirement of output tracking and local exponential stability, we impose the following assumption which allows us then to carry out the controller synthesis task on the basis of the input/output dynamics of the system of Eq.10.13.

Assumption 10.2 *The η-subsystem of Eq.10.15 is input-to-state stable with respect to e, uniformly in $\bar{v}$, and locally exponentially stable when $e = 0$.*

Proposition 10.1 below provides an explicit synthesis formula of the desired state feedback control law and states precise conditions that guarantee closed-loop stability and asymptotic reference-input tracking in the closed-loop system of Eq.10.13. The proof is given in Appendix H.

Proposition 10.1 *Consider the system of Eq.10.11, for which Assumption 10.2 holds, under the control law:*

$$u = -\frac{1}{2} R^{-1}(a_s, u_{max}, z_c) \left(L_{\bar{g}} V\right)^T (z_c) \tag{10.17}$$

where

$$\frac{1}{2} R^{-1}(a_s, u^k_{max}, z_c) = \frac{L^*_{\bar{f}} V + \sqrt{(L^*_{\bar{f}} V)^2 + \left(u_{max} |(L_{\bar{g}} V)^T (z_c)|\right)^4}}{|(L_{\bar{g}} V)^T (z_c)|^2 \left[1 + \sqrt{1 + (u_{max} |(L_{\bar{g}} V)^T (z_c)|)^2}\right]} \tag{10.18}$$

$L_{\bar{f}}^{*}V = L_{\bar{f}}V + \rho|e|^2$, $\rho > 0$, $L_{\bar{g}}V = [L_{\bar{g}_1}V \cdots L_{\bar{g}_m}V]$ is a row vector, $V = e^T\Phi e$, Φ is a positive-definite matrix that satisfies the Riccati inequality $\Lambda^T\Phi + \Phi\Lambda - \Phi\Gamma\Gamma^T\Phi < 0$. Let δ_s be a positive real number such that the compact set, $\Omega = \{a_s \in \mathbb{R}^m : a_s^T\Phi a_s \leq \delta_s\}$ is an invariant set embedded within the region described by the following inequality:

$$L_{\bar{f}}^{*}V \leq u_{max}|(L_{\bar{g}}V)^T(z_c)| \tag{10.19}$$

Then, for any $a_s(0) \in \Omega$, the origin of the finite-dimensional closed-loop system of Eq.10.13 and Eqs.10.17-10.18 is asymptotically stable.

Remark 10.3 The inequality of Eq.10.19 characterizes explicitly the region in state space where the control action satisfies the constraints and the time-derivative of the Lyapunov function is negative-definite along the trajectories of the finite-dimensional closed-loop "slow" system of Eq.10.13 and Eqs.10.17-10.18. To guarantee that the trajectories starting within this region do not leave, the initial conditions are confined within the largest invariant set, Ω, embedded within the region, in order to guarantee closed-loop stability. The size of Ω is fixed by δ_s and represents the state feedback estimate of the set of admissible initial "slow" states starting from where stability of the constrained finite-dimensional closed-loop "slow" system is guaranteed (region of guaranteed stability)(see [91] and chapter 4 in [170] for how to compute this estimate).

Remark 10.4 The control law in Eq.10.17-10.18 involves a modification of the controller design proposed in [204] by including the term, $-\rho|e|^2$, where ρ is a strictly positive tuning parameter, which ensures that the control law enforces exponential stability in the closed-loop PDE system. With $\rho = 0$, it can be shown that the control law of Eq.10.17-10.18 enforces only asymptotic stability. We therefore prefer to set $\rho > 0$ and have exponential stability because of its robustness to bounded perturbations, which are always present in most practical applications. Note that in order to use the inequality of Eq.10.19 to compute an estimate of the stability region, as described in Remark 10.3, a value of ρ must be specified.

Utilizing the result of Proposition 10.1, Theorem 10.1 below states precise con-

ditions that guarantee, under the control law of Eqs.10.17-10.18, closed-loop stability and asymptotic reference-input tracking in both the finite-dimensional system of Eq.10.11 and the infinite-dimensional system of Eq.10.7. The proof is given in Appendix H.

Theorem 10.1 *1. Let* $\Theta_s := \{x_s \in \mathcal{H}_s : |x_s|_2 \leq \bar{\delta}_s\}$ *be the set of all* x_s *for which* $a_s^T \Phi a_s^T \leq \delta_s$. *Then, for any* $\bar{x}_s(0) \in \Theta_s$, *the origin of the finite-dimensional closed-loop system of Eq.10.11 and Eqs.10.17-10.18 is asymptotically stable and there exists a function* β *of class* $\mathcal{KL}$ *such that* $|\bar{x}_s(t)|_2 \leq \beta(|\bar{x}_s(0)|_2, t)$, $\forall t \geq 0$.

2. Consider the system of Eq.10.7, for which Assumption 10.1 holds, under the state feedback controller of Eqs.10.17-10.18. Then given any pair of positive real numbers, d *and* $\bar{\delta}_b$, *such that* $\beta(\bar{\delta}_b, 0)+d \leq \bar{\delta}_s$, *and given any positive real number,* δ_f, *there exists* $\epsilon^* > 0$ *such that if* $\epsilon \in (0, \epsilon^*]$, $|x_s(0)|_2 \leq \bar{\delta}_b$, $\|x_f(0)\|_2 \leq \delta_f$, *the origin of the infinite-dimensional closed-loop system is asymptotically (and locally exponentially) stable, and the outputs of the closed-loop system satisfy a relation of the form:*

$$\limsup_{t \to \infty} |y_{ci}(t) - v_i(t)| \;=\; O(\epsilon) \tag{10.20}$$

Remark 10.5 The set, Θ_s, represents an estimate of the stability region for the finite-dimensional system of Eq.10.11 (which corresponds to the set, Ω, for the system of Eq.10.13 describing the modal amplitudes). Owing to the large separation between the slow and fast eigenmodes of the spatial differential operator of the PDE system of Eq.10.1, the estimate of the closed-loop stability region remains preserved for the constrained closed-loop PDE system in the sense that given any initial "slow" state that belongs to any compact subset (size of this subset is fixed by $\bar{\delta}_b$), and given any initial "fast state", there always exists ϵ sufficiently small such that the controller of Eqs.10.17-10.18 continues to enforce stability in the constrained infinite-dimensional closed-loop system. According to Theorem 10.1, selection of the initial slow state within a compact subset of Θ_s with a "radius" of $\bar{\delta}_b$, ensures that, during the evolution

of x, the slow states remain within Θ_s. An estimate of ϵ^* can, in principle, be extracted from the stability proof via singular perturbation analysis. However, this estimate is typically conservative and thus it is useful to check its appropriateness through computer simulations.

Remark 10.6 Owing to the dependence of the operator $\mathcal{B}_s$ in Eq.10.11 on the actuator distribution function, $b_i(z)$, the inequality of Eq.10.19 (and hence the stability region Ω) is parameterized by the actuator locations, and can therefore be used to explicitly identify the admissible locations where the control actuators can be placed to guarantee stability of the constrained closed-loop system. The inequality of Eq.10.19 captures, quantitatively, the interplay between the limitations imposed by input constraints on the admissible initial states and on the admissible control actuator locations. To see this, note that this inequality can be used in two ways. For a given actuator location (i.e., fixed $\mathcal{B}_s$), the inequality provides the set of admissible initial states that guarantee closed-loop stability. Alternatively, for a given initial condition (i.e., fixed δ_s), the inequality provides the admissible actuator locations.

10.3.2 Output feedback control

The nonlinear controller of Eqs.10.17-10.18 was derived under the assumption that measurements of the state variables, $\bar{x}(z,t)$, are available at all positions and times. In this section, we address the problem of synthesizing bounded nonlinear output feedback controllers of the general form:

$$u(t) = \mathcal{F}(y_m, \bar{v}, u_{max}) \tag{10.21}$$

where $\mathcal{F}(y_m, \bar{v}, u_{max})$ is a bounded nonlinear vector function, and y_m is the vector of measured outputs, that: (a) enforce stability and output tracking in the constrained closed-loop PDE system, and (b) recover the state feedback region of guaranteed closed-loop stability. The synthesis of the controller of Eq.10.21 will be achieved

by combining the state feedback controller of Eqs.10.17-10.18 with a procedure proposed in [61] for obtaining estimates for the states of the approximate ODE model of Eq.10.11 from the measurements. To this end, we need to impose the following requirement on the number of measured outputs in order to obtain estimates of the states, x_s, of the finite-dimensional system of Eq.10.11, from the measurements y_m^κ, $\kappa = 1, \ldots, p$.

Assumption 10.3 *$p = m$ (i.e., the number of measurements is equal to the number of slow modes), and the inverse of the operator $\mathcal{S}$ exist, so that $\hat{x}_s = \mathcal{S}^{-1} y_m$.*

We note that the requirement that the inverse of the operator $\mathcal{S}$ exists can be achieved by appropriate choice of the location of the measurement sensors (i.e., the functions $s^\kappa(z)$).

Theorem 10.2 that follows establishes that the proposed output feedback controller enforces stability and reference-input tracking in the constrained infinite-dimensional closed-loop system and practically preserves the region of guaranteed closed-loop stability obtained under state feedback.

Theorem 10.2 *Consider the system of Eq.10.11 for which Assumption 10.3 holds. Consider also the system of Eq.10.7, for which Assumptions 10.1-10.2 hold, under the nonlinear output feedback controller:*

$$u = -\frac{1}{2} R^{-1}(\hat{a}_s, u_{max}, z_c) \left(\widehat{L_{\bar{g}} V}\right)^T (z_c) \tag{10.22}$$

where $\hat{a}_s = [\hat{a}_1 \ \hat{a}_2 \ \cdots, \hat{a}_m]^T$, $(\hat{x}_s, \phi_j) = \hat{a}_j(\phi_j, \phi_j)$, $\hat{x}_s = \mathcal{S}^{-1} y_m$, $R^{-1}(\cdot)$ and V as defined in Theorem 10.1. Then given any pair of positive real numbers, d and $\bar{\delta}_b$, defined in Theorem 10.17, and given any positive real number δ_f, there exists $\epsilon^{**} > 0$ such that if $\epsilon \in (0, \epsilon^{**}]$, $|x_s(0)|_2 \leq \bar{\delta}_b$, $\|x_f(0)\|_2 \leq \delta_f$, the origin of the infinite-dimensional closed-loop system is asymptotically stable (and locally exponentially stable) and its outputs satisfy Eq.10.20.

Remark 10.7 We note that the controller of Eq.10.22 uses static feedback of the measured outputs, y_m^κ, $\kappa = 1, \ldots, p$, and thus it feeds back both x_s and x_f (this is in contrast to the state feedback controller of Eqs.10.17-10.18 which only uses feedback of the slow state, x_s). However, even though the use of x_f feedback could lead to destabilization of the stable fast subsystem, the large separation of the slow and fast modes of the spatial differential operator (i.e., the assumption that ϵ is sufficiently small) and the fact that the controller does not include terms of the form $O(\frac{1}{\epsilon})$ do not allow such a destabilization to occur.

Remark 10.8 Owing to the estimation error, a discrepancy exists between the state and output feedback stability regions. This discrepancy, however, can be made small by increasing the order of the ODE approximation and including more measurements. In the asymptotic limit (as $\epsilon \to 0$), the stability region for both the state and output feedback problems (set of admissible initial "slow" states) approach that for the constrained finite-dimensional system of Eq.10.11. This result is important because it is only the finite-dimensional system that is used to design the controller and carry out any practical computations for the region of closed-loop stability.

10.4 Application to a diffusion-reaction process

Consider a long, thin rod in a reactor. The reactor is fed with pure species A and a zeroth order exothermic catalytic reaction of the form $A \to B$ takes place on the rod. Since the reaction is exothermic, a cooling medium in contact with the rod is used for cooling. Under standard modeling assumptions, the spatiotemporal evolution of the dimensionless rod temperature is described by the following parabolic PDE:

$$\frac{\partial \bar{x}}{\partial t} = \frac{\partial^2 \bar{x}}{\partial z^2} + \beta_T e^{-\frac{\gamma}{1+\bar{x}}} + \beta_U (b(z)u(t) - \bar{x}) - \beta_T e^{-\gamma}$$

subject to the boundary and initial conditions:

$$\bar{x}(0,t) = 0, \quad \bar{x}(\pi,t) = 0, \quad \bar{x}(z,0) = \bar{x}_0(z)$$

where $\bar{x}$ denotes a dimensionless rod temperature, β_T denotes a dimensionless heat of reaction, γ denotes a dimensionless activation energy, β_U denotes a dimensionless heat transfer coefficient, $u(t)$ denotes the vector of manipulated inputs and $b(z)$ the vector of the corresponding actuator distribution functions. The following typical values are given to the process parameters: $\beta_T = 50.0,\ \beta_U = 2.0,\ \gamma = 4.0$. For these values, it was verified that the operating steady-state, $\bar{x}(z,t) = 0$, is an unstable one. The control objective therefore is to stabilize the rod temperature profile at the unstable steady-state, $\bar{x}(z,t) = 0$, by manipulating the temperature of the cooling medium, which is subject to hard constraints. To achieve this objective, the controlled output is defined as:

$$y_c(t) = \int_0^{\pi} \sqrt{\frac{2}{\pi}} sin(z) x(z,t) dz \tag{10.23}$$

and one point control actuator is assumed to be available for stabilization. The eigenvalue problem for the spatial differential operator of the process can be solved analytically and its solution yields:

$$\lambda_j = -j^2, \quad \phi_j(z) = \sqrt{\frac{2}{\pi}} sin(j\ z), \quad j = 1, \ldots, \infty \tag{10.24}$$

For this system, we consider the first eigenvalue as the dominant one and use standard Galerkin's method to derive an ODE which is used for controller synthesis. The controllers are then implemented on a 30-th order Galerkin discretization of the parabolic PDE system (higher order discretizations led to identical results).

Before we proceed with the design and implementation of the controllers, we first use the inequality of Eq.10.17 to explicitly characterize the region of guaranteed closed-loop stability. Figure 10.1 depicts the region of guaranteed closed-loop stability for a value of $u_{max} = 1.4$, $\rho = 0.0001$. This region, which has a dome-like appearance, describes how the set of admissible initial conditions for the amplitude of the first eigenmode, $a_1(t)$, varies as a function of control actuator location, z_c, along the rod

length. It is clear from the figure that the size of this set peaks at the middle of the rod and diminishes, as expected, as we get closer to the edges of the rod owing to the zeros of the first eigenfunction at the boundaries.

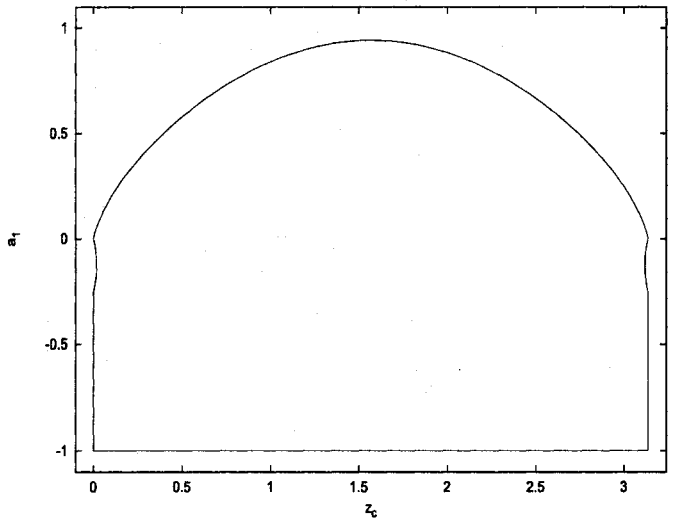

Figure 10.1: Dependence of the set of feasible initial conditions, for a_1, on actuator location for $u_{max} = 1.4$.

Guided by the information contained in Figure 10.1, we now proceed with the implementation of the controllers. The state feedback results are presented first. Figure 10.2 shows the evolution of the closed-loop rod temperature and manipulated input profiles under the controller of Eqs.10.17-10.18 when the actuator is placed in the middle of the rod and $a_1(0) = 0.7$. For this initial condition, it can be easily verified from Figure 10.1 that the location $z_c = 0.5\pi$ is an admissible one when $u_{max} = 1.4$. Clearly, the controller successfully stabilizes the temperature profile at the desired steady-state. In the next simulation run, the actuator location is moved to $z_c = 0.25\pi$ but the initial condition is kept at $a_1(0) = 0.7$. In this case, it is clear from Figure 10.1 that the $(a_1(0), z_c)$ pair falls outside the region of guaranteed closed-loop stability. The simulation results for this case are depicted in Figure 10.3 where we

observe that the controller is unable to stabilize the spatially uniform steady-state and the system moves to the spatially non-uniform steady-state.

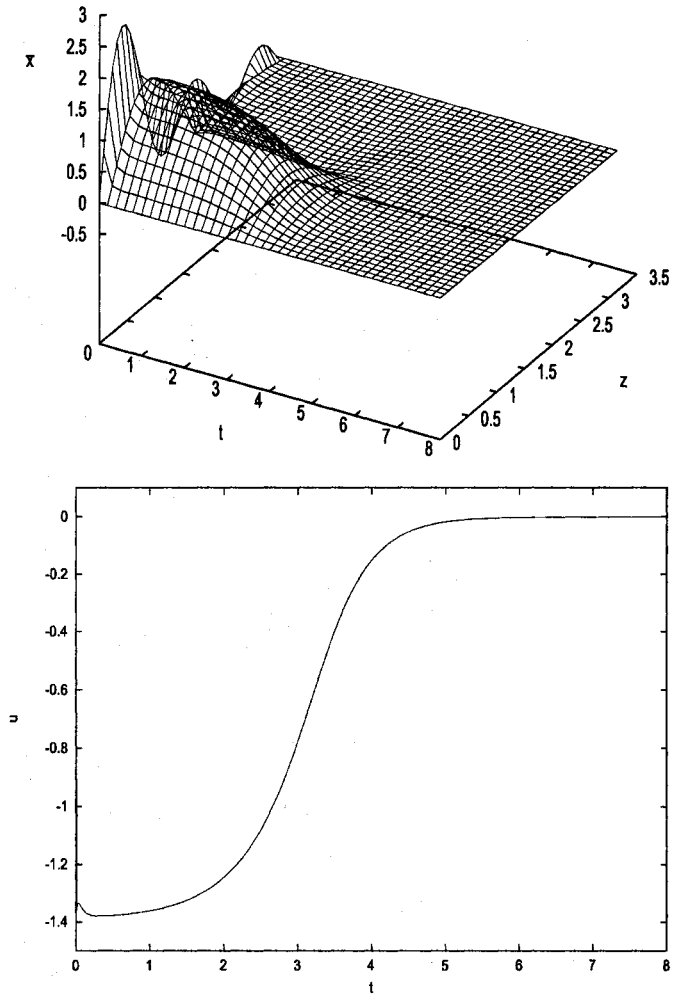

Figure 10.2: Closed-loop temperature (top) and manipulated input (bottom) profiles for $u_{max} = 1.4$, $z_c = 0.5\pi$, $a_1(0) = 0.7$, under state feedback.

For the case of output feedback control, we used a single point sensor located at $z = 0.33\pi$ to obtain estimates of the first eigenmode and then used the synthesis formula of Eq.10.22 to design the output feedback controller. The simulation results for this case are shown in Figures 10.4 and 10.5, for the same combinations of initial

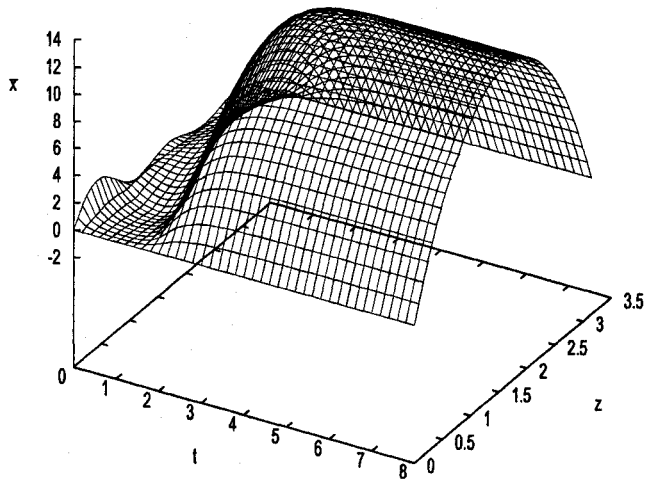

Figure 10.3: Closed-loop temperature profile for $u_{max} = 1.4$, $z_c = 0.25\pi$, $a_1(0) = 0.7$ under state feedback.

conditions and actuator locations considered in the state feedback case. We observe that the output feedback controller successfully stabilizes the constrained closed-loop system when the (initial condition, actuator location) pair lies inside the stability region (Figure 10.4) and fails to do so otherwise (Figure 10.5).

10.5 Conclusions

In this chapter, a general framework for the analysis and control of parabolic PDE systems with input constraints was developed. Initially, Galerkin's method was used for the derivation of a finite-dimensional ODE system that captures the dominant dynamics of the PDE system. This ODE system was then used as the basis for the synthesis, via Lyapunov techniques, of stabilizing bounded nonlinear state and output feedback control laws that provide an explicit characterization of the sets of admissible initial conditions and admissible control actuator locations that can be used to guarantee closed-loop stability in the presence of constraints. Precise conditions that

guarantee stability of the constrained closed-loop parabolic PDE system were provided in terms of the separation between the fast and slow eigenmodes of the spatial differential operator. The results were used to stabilize an unstable steady-state of a diffusion-reaction process using constrained control action.

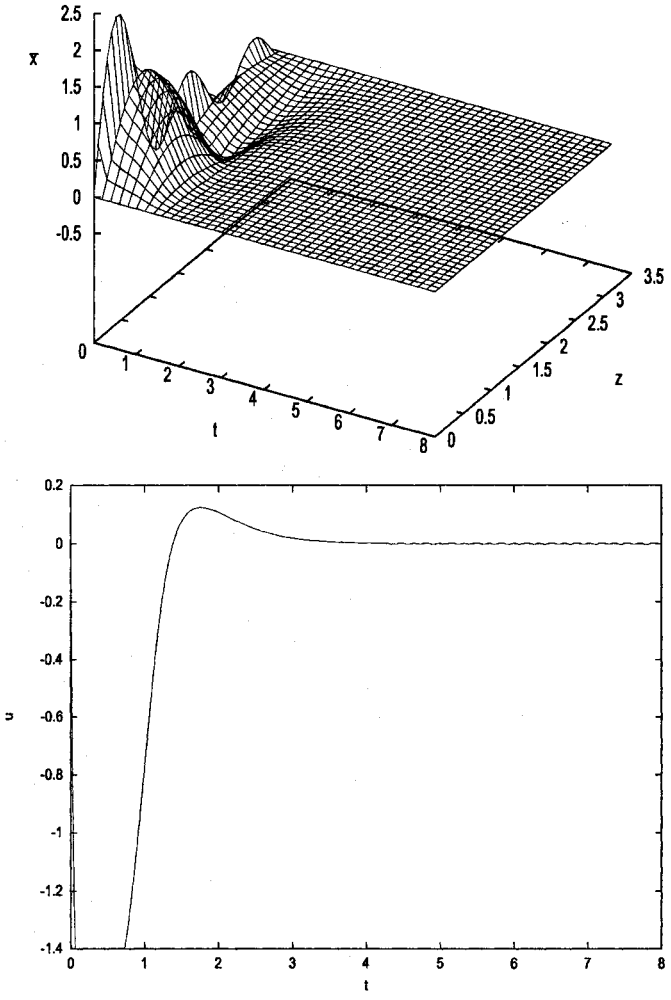

Figure 10.4: Closed-loop temperature (top) and manipulated input (bottom) profiles for $u_{max} = 1.4$, $z_c = 0.5\pi$, $a_1(0) = 0.7$, under output feedback.

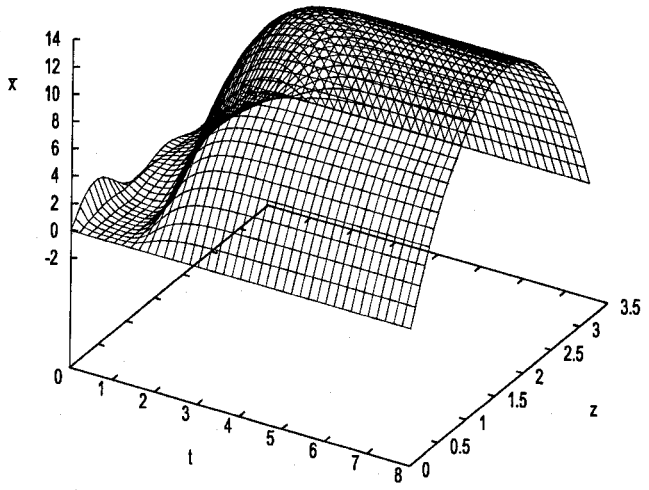

Figure 10.5: Closed-loop temperature profile for $u_{max} = 1.4$, $z_c = 0.25\pi$, $a_1(0) = 0.7$, under output feedback.

Chapter 11

Analysis and Control of Constrained Particulate Processes

11.1 Introduction

Particulate processes are characterized by material domains that comprise of a continuous phase and a dispersed phase and are essential in making many high-value industrial products. Examples include the crystallization of proteins for pharmaceutical applications, the emulsion polymerization reactors for the production of latex and the titania powder aerosol reactors used in the production of white pigments. It is now well-understood that the physico-chemical and mechanical properties of materials made with particulates depend heavily on the characteristics of the corresponding particle size distribution (PSD) (for example, a nearly mono-disperse PSD is required for titania pigments to obtain the maximum hiding powder per unit mass). Therefore, the problem of synthesizing and implementing high-performance model-based feedback control systems on particulate processes to achieve PSDs with desired characteristics has significant industrial value.

Fundamental modeling of particulate processes is usually addressed within the framework of population balances, which allow the derivation of systems of nonlinear partial integro-differential equations that describe the rate of change of the PSD. The population balances are coupled with material and energy balances that describe the rate of change of the state variables of the continuous phase (these are usually systems of nonlinear differential equations which include integrals over the entire particle size spectrum), leading to complete particulate process models. There is a large body of literature on the development of solution methods and the understanding of dynamics of population balance models (see, for example, [115, 119, 244, 139, 153, 253, 187, 188, 227]). On the other hand, research on control of particulate processes has mainly focused on the understanding of fundamental control-theoretic properties (controllability and observability) of population balance models [269] and the application of conventional control schemes (e.g., proportional-integral and proportional-integral-derivative control, self-tuning control) to crystallizers and emulsion polymerization processes (see, for example, [270, 258, 84] and the references therein). Results on population balance model-based control of particulate processes include an optimization-based control method developed in [87] and successfully applied to a batch crystallization process, as well as nonlinear state feedback control of a cell culture in [193]. In [54], a general model reduction procedure, based on combination of the method of weighted residuals and approximate inertial manifolds, was developed that allows deriving ordinary differential equation (ODE) approximations of particulate process models, which were used for the synthesis of finite-dimensional output feedback controllers that can be readily implemented in practice. The method was successfully implemented on a continuous crystallizer. These results were extended to particulate processes with time-varying uncertain variables and unmodeled actuator/sensor dynamics in [55].

Even though the above methods lead to the systematic design of practically implementable nonlinear model-based feedback controllers for particulate processes, they do not deal with the problem of constraints on the capacity of the control actuators. This is an important limitation of these methods, especially in view of the fact that the capacity of control actuators used to regulate particulate processes is almost always limited. Such limitations may arise naturally due to the finite capacity of control actuators (e.g., bounds on magnitude of the opening of valves) or may be imposed on the manipulated input to insure safe process operation, meet environmental regulations, or maintain desired product quality specifications. Input constraints restrict our ability to freely modify the dynamic behavior of particulate processes; and the ill-effects due to actuator constraints manifest themselves, for example, in the form of sluggishness of response and loss of stability. Additional problems that arise in the case of dynamic controllers include undesired oscillations and overshoots, a phenomenon usually referred to as "windup."

Recognition of the detrimental effects of input constraints on the stability and performance of chemical processes in general has motivated many recent studies on the dynamics and control of chemical processes subject to input constraints. Notable contributions in this regard include controller design and stability analysis within the model predictive control framework [248, 263], constrained quadratic-optimal control [57], the design of "anti-windup" schemes in order to prevent excessive performance deterioration of an already designed controller when the input saturates [174, 232, 300], the study of the nonlinear bounded control problem for a class of two and three state chemical reactors [12], and some results on the dynamics of nonlinear systems with input constraints [159].

This chapter focuses on the development and application of a general method-

ology for the analysis and control of constrained spatially-homogeneous particulate processes modeled by population balance equations. Initially, a nonlinear model reduction procedure based on the method of weighted residuals is presented for the construction of finite-dimensional ODE systems that accurately reproduce the dominant dynamics of the particulate process. These ODE systems are then used to analyze the limitations imposed by input constraints on the ability to modify the dynamics of the particulate process, leading to an explicit characterization of the set of admissible set-points that can be achieved in the presence of constraints. This information together with the derived ODE systems are then used as the basis for the synthesis of practically-implementable nonlinear bounded output feedback controllers that enforce exponential stability in the closed-loop system and achieve particle size distributions with desired characteristics in the presence of input constraints. Precise closed-loop stability conditions are given and controller implementation issues are addressed. The proposed methodology is successfully applied to a continuous crystallizer. The results of this chapter were first presented in [89].

11.2 Preliminaries

11.2.1 Particulate process model with input constraints

We focus on spatially homogeneous (well-mixed) particulate processes with simultaneous particle growth, nucleation, agglomeration and breakage and consider the case of a single internal particle coordinate, which is assumed to be the particle size. Applying a population balance to the particle phase as well as material and energy balances to the continuous phase, we obtain the following general nonlinear system

of partial integro-differential equations:

$$\begin{aligned} \frac{\partial n}{\partial t} &= -\frac{\partial (G(x,r)n)}{\partial r} + w(n,x,r), \quad n(0,t) = b(x(t)) \\ \dot{x} &= f(x) + g(x)sat(u(t)) + A\int_0^{r_{max}} a(n,r,x)dr \end{aligned} \tag{11.1}$$

where $n(r,t) \in [L_2[0,r_{max}), \mathbb{R}]$ is the size distribution function which is assumed to be a continuous and sufficiently smooth function of its arguments (we use the symbol $L_2[0,r_{max})$ to denote a Hilbert space of continuous functions defined on the interval $[0,r_{max}))$, $r \in [0,r_{max})$ is the particle size (r_{max} is the maximum particle size, which may be infinity), t is the time, $x \in \mathbb{R}^n$ is the vector of state variables which describe properties of the continuous phase (e.g., solute concentration, temperature and pH in a crystallizer), $u(t) = [u_1(t)\ u_2(t)\ \cdots\ u_m(t)]^T \in \mathbb{R}^m$ is the vector of manipulated inputs, and *sat* refers to the saturation function defined by:

$$sat(u_i) = \left\{ \begin{array}{ccc} u_{i,min} & if & u_i < u_{i,min} \\ u_i & if & u_{i,min} \leq u_i \leq u_{i,max} \\ u_{i,max} & if & u_i > u_{i,max} \end{array} \right\} \tag{11.2}$$

where $u_i \in \mathbb{R}$ and for a vector $u \in \mathbb{R}^m$, $sat(u) = [sat(u_1)\ sat(u_2)\ \cdots\ sat(u_m)]^T$. The presence of the *sat* operator in Eq.11.1 signifies the presence of hard constraints on the manipulated input. Such constraints may arise naturally due to inherent limitations on the capacity of control actuators used to regulate particulate processes or may be imposed for economic or safety reasons.

In Eq.11.1, the n-equation is the population balance where $G(x,r)$ is the growth rate that accounts for particle growth through condensation, and $w(n,x,r)$ is a term that accounts for the net rate of introduction of new particles into the system (it includes all the means by which particles appear or disappear within the system including particle agglomeration, breakage, nucleation, feed and removal). The x-subsystem of Eq.11.1 is derived by applying material and energy balances to the

continuous phase. In this subsystem, $f(x)$, $a(n,r,x)$ are smooth nonlinear vector functions, $g(x)$ is a nonlinear matrix function, and A is a constant matrix. The term $A\int_0^{r_{max}} a(n,r,x)dr$ represents mass and heat transfer from the continuous phase to all the particles in the population.

We define a vector of controlled outputs to express the various control objectives (e.g., regulation of total number of particles, mean particle size, temperature, pH, etc.) as:

$$y_i(t) \;=\; h_i(\int_0^{r_{max}} c_\kappa(r)n(r,t)dr, x), \;\; i=1,\ldots,m, \;\; \kappa=1,\ldots,l \tag{11.3}$$

where $y_i(t)$ is the i-th controlled output, $h_i(\int_0^{r_{max}} c_\kappa(r)n(r,t)dr, x)$ is a nonlinear scalar smooth function of its arguments and $c_\kappa(r)$ is a known smooth function of r which depends on the desired performance specifications. To simplify the notation in our theoretical development, we will not consider measured outputs separately from controlled outputs, which means that we need to assume the availability of on-line measurements of the controlled output, $y_i(t)$.

To state the theoretical results of this chapter, we will need the definition of a class $\mathcal{KL}$ function. In particular, a function $\beta(s,t)$ is said to be of class $\mathcal{KL}$ if, for each fixed t, the function $\beta(s,\cdot)$ is continuous, increasing, and zero at zero and, for each fixed s, the function $\beta(\cdot,t)$ is nonincreasing and tends to zero at infinity.

11.2.2 Motivating example: A continuous crystallizer

Crystallization is a particulate process that is widely used in industry and requires a population balance to be accurately described, analyzed, and controlled. Crystallizers typically exhibit highly oscillatory behavior which suggests the use of feedback control to ensure stable operation and attain a crystal size distribution with desired characteristics. However, one of the biggest problems that hinder the effective imple-

mentation of conventional feedback controller design methods is the presence of hard constraints on the manipulated input. Input constraints restrict our ability to modify the dynamics of the process in the desired manner. In order to motivate our discussion on the problem of input constraints and the approach that we propose for dealing with this problem (detailed in the next section), we highlight first in this section, by means of a continuous crystallizer example, some of the key issues that need to be addressed for the effective control of particulate processes with input constraints. In particular, we demonstrate some of the fundamental limitations imposed by input constraints on our ability to steer particulate process dynamics as well as some of the detrimental effects of input constraints on the performance of conventional feedback controller designs. To this end, we consider the isothermal continuous crystallizer example studied in [54]. The mathematical model for this crystallizer is given by:

$$\begin{aligned} \frac{\partial n}{\partial \bar{t}} &= -k_1(c-c_s)\frac{\partial n}{\partial r} - \frac{n}{\tau} + \delta(r-0)\bar{\epsilon}k_2 \exp\left(-\frac{k_3}{\left(\frac{c}{c_s}-1\right)^2}\right) \\ \frac{dc}{d\bar{t}} &= \frac{(c_0-\rho)}{\bar{\epsilon}\tau} + \frac{(\rho-c)}{\tau} + \frac{(\rho-c)}{\bar{\epsilon}}\frac{d\bar{\epsilon}}{d\bar{t}} \end{aligned} \tag{11.4}$$

where $n(r,\bar{t})$ is the number of crystals of radius $r \in [0,\infty)$ at time $\bar{t}$ per unit volume of suspension, τ is the residence time, c is the solute concentration in the crystallizer, c_0 is the solute concentration in the feed, $\bar{\epsilon} = 1 - \int_0^\infty n(r,\bar{t})\frac{4}{3}\pi r^3 dr$ is the volume of liquid per unit volume of suspension, c_s is the concentration of solute at saturation, k_1, k_2, and k_3 are constants, and $\delta(r-0)$ is the standard Dirac function. The term containing the Dirac function in Eq.11.4 accounts for the production of crystals of infinitesimal (zero) size via nucleation. The parameters used for this crystallizer process model are given in Table 11.1. It was shown in [54] that this crystallizer exhibits highly oscillatory behavior resulting from the interplay between the growth and nucleation terms in the population balance (unstable steady-state surrounded by a stable limit

cycle.)

Table 11.1: Process parameters and dimensionless variables for the crystallizer model of Eq.11.4.

c_0	=	1000.0	$kg\ m^{-3}$
c_s	=	980.2	$kg\ m^{-3}$
ρ	=	1770.0	$kg\ m^{-3}$
τ	=	1.0	hr
k_1	=	5.065×10^{-2}	$mm\ m^3\ kg^{-1}\ hr^{-1}$
k_2	=	7.958	$mm^{-3}\ hr^{-1}$
k_3	=	1.217×10^{-3}	
σ	=	1.0	mm
Da	=	200.0	
F	=	3.0	
α	=	40.0	

The control objective is to stabilize the crystallizer and achieve a crystal-size distribution with desired mass by manipulating the solute feed concentration. The manipulated input is therefore taken to be $u(t) = \frac{c_0 - c_{0s}}{c_0 - c_s}$, where c_{0s} is the steady-state solute feed concentration, and the controlled output is defined as:

$$y(\bar{t}) = 8\pi\sigma^3 \int_0^\infty n(r, \bar{t}) dr = \tilde{x}_0 \tag{11.5}$$

where $\sigma = k_1\tau(c_0 - c_s)$. Note that both variables are in dimensionless form. To achieve the desired control objective, we implement a conventional proportional-integral (PI) control scheme:

$$\begin{aligned} \frac{d\eta}{dt} &= e \\ u &= K_c[e + \frac{1}{\tau_I}\eta] \end{aligned} \tag{11.6}$$

on the crystallizer process model of Eq.11.4, where $e = y_{sp} - y$, y_{sp} is the set-point and u is the controller output. If there are no limits on the maximum solute feed concentration that can be used to achieve the desired control objective, then the controller output and process input are the same. However, suppose that there are

limitations on the maximum solute feed concentration, i.e, $|u| \leq u_{max}$. In this case, if the solute feed concentration calculated by the controller is, for example, higher than u_{max}, then the actual solute concentration fed to the crystallizer will be just u_{max} leading to a mismatch between the controller output and actual crystallizer input.

Initially, closed-loop simulation runs were performed to test the ability of the PI controller to achieve the desired control objective in the absence of limitations (constraints) on the maximum solute feed concentration. Figure 11.1 depicts the dimensionless crystal concentration ($\tilde{x}_0$) and dimensionless solute feed concentration (u) profiles for a 0.4 increase in the set-point in the absence of any constraints on the manipulated input (i.e., $|u| < \infty$.) It is evident from the figure that the PI controller manages eventually to drive the output to its new set-point. By contrast, Figure 11.2 depicts the closed-loop response to the same 0.4 increase in the set-point in the presence of input constraints. The solid line shows the response when $u \in [0, 2]$ and the dashed line shows the response when $u \in [0, 6]$. As can be seen from this figure, the PI controller fails (regardless of the PI tuning parameters) to stabilize the crystallizer when the input is constrained in the interval $[0, 2]$, leading to sustained oscillations, while it successfully drives the crystallizer output (despite the poor transient performance) to the desired set-point when the input is constrained in the interval $[0, 6]$.

The contrast between the two different responses in Figure 11.2 illustrates an example of how input constraints place fundamental limitations on our ability to steer the particulate process to a desired set-point under any control law (linear or nonlinear). To understand these limitations, we refer to the input profiles in Figure 11.2 which show that in order for the process output to reach a set-point of 0.4, the process input must reach a steady-state value of 5.3, i.e., outside $[0, 2]$. Therefore, when the

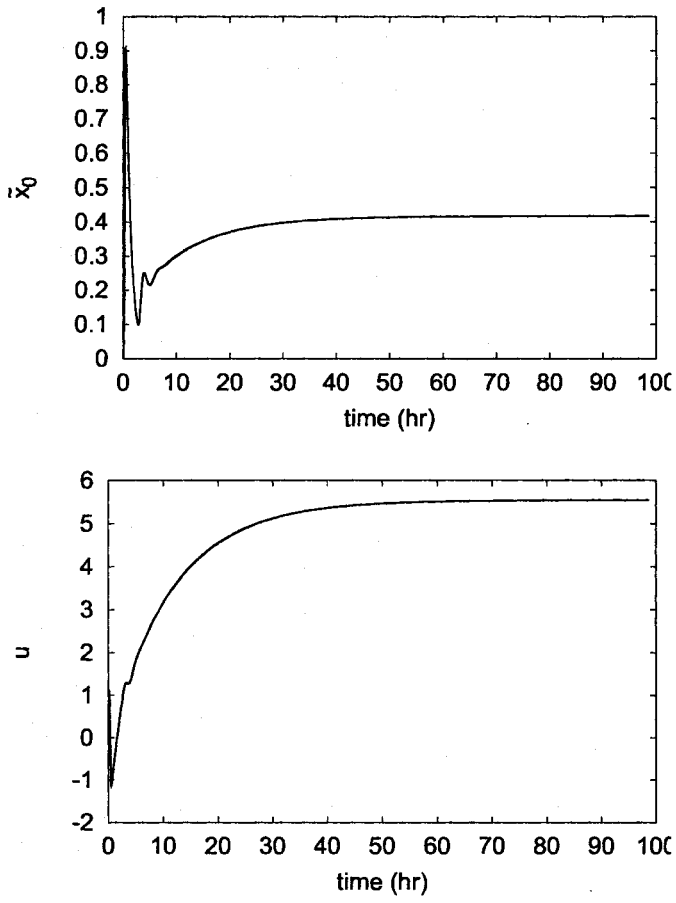

Figure 11.1: Controlled output (crystal concentration) and manipulated input (solute concentration) profiles under PI control in the absence of input constraints.

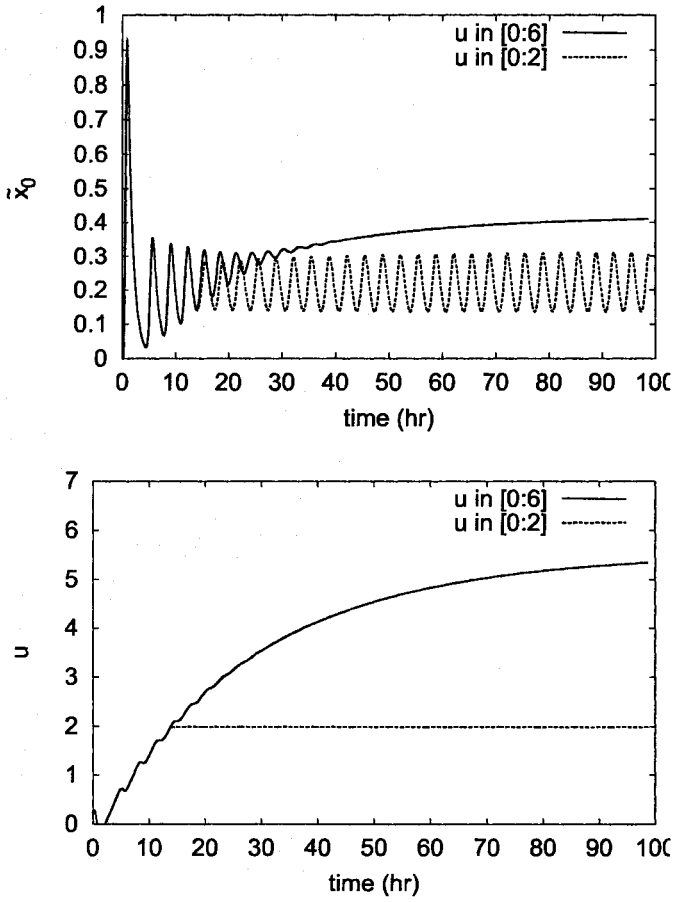

Figure 11.2: Controlled output (crystal concentration) and manipulated input (solute concentration) profiles under PI control when $u \in [0, 2]$ (dashed lines) and when $u \in [0, 6]$ (solid lines).

input is constrained in $[0, 2]$, the process output cannot accommodate the requested set-point change (regardless of the controller used) owing to the fundamental inadmissibility of the desired set-point when $u \in [0, 2]$. Relaxing the constraints to $[0, 6]$ consequently allows the process input to reach a steady-state value of 5.3 and steer the process output to a value of 0.4. It is important to keep in mind therefore that this problem of set-point inadmissibility is independent of the controller used and cannot be remedied simply by choosing another controller in place of the PI controller.

This reasoning immediately raises the following important question: given our knowledge of the constraints on the process input, how can we identify a priori (before controller implementation and without running closed-loop simulations) whether a given set-point is admissible? It is clear from Figure 11.2 that lack of this information can easily lead to a poor (i.e., inadmissible) choice of the set-point and subsequent instability. In the absence of this information, it may not even be clear what the underlying cause of instability is. This, in turn, may prompt the control engineer to suspect the particular controller used and consequently waste time and effort in re-tuning the controller or trying other control schemes without realizing that the problem is one that cannot be solved by any controller and is rather due to the inherent limitations imposed by the constraints. These considerations motivate the need for a systematic approach that explicitly characterizes the limitations imposed by input constraints on our ability to steer the particulate process in a desired direction. Such an approach is needed to provide process operators with the necessary knowledge of which set-point changes are feasible and can be achieved in the presence of known constraints on the manipulated input, *independent of the specific control scheme to be used.* The a priori availability of this kind of feasibility information is a pre-requisite for any effective controller design method that can successfully address the problems

caused by input constraints on the operation of the process.

Another important issue that the above crystallizer example highlights is that of the particular choice of the controller to achieve the desired control objective, once that objective is determined to be admissible. Recall from Figure 11.2 (dashed line) that although the set-point is admissible when $u \in [0, 6]$ and that the PI controller stabilizes the process there, the transient performance is poor (compare with Figure 11.1). This performance deterioration is a direct consequence of input saturation for about two hours in the beginning of crystallizer operation leading to a more sluggish and oscillatory response. While it is possible to reduce the response settling time by further re-tuning of the PI controller, this comes at the expense of unreasonably large overshoot in the process output. It is important to point out here that owing to the complex nonlinear dynamics of the crystallizer, the presence of input constraints, and the large set-point change considered, there are no systematic guidelines for tuning the PI controller. Instead, the PI controller was tuned through extensive trial and error to obtain the best possible performance that yields reasonable overshoot (compared to that of the nonlinear controller shown later in Figure 11.6).

The traditional approaches of designing/tuning the PI controller on the basis of a linearized model of the process are inadequate because they do not account for either the strong nonlinearities present or the input constraints. The performance of any controller designed in this way deteriorates, even in the absence of constraints, as the process moves further away from the steady-state around which the model was linearized. In addition to the performance problem, conventional control schemes (such as the PI controller) which are not designed to explicitly handle input constraints, lack any a priori guarantees regarding stability of the constrained closed-loop system starting from a given initial condition. *It is well known that even if a set-point is*

admissible, not every initial condition can be used to reach it. This initial condition must belong to the region of closed-loop stability. Most conventional control schemes (linear and nonlinear), however, do not provide any systematic way of estimating this region or identifying the initial conditions starting from where closed-loop stability is guaranteed in the presence of input constraints. All these considerations combined clearly motivate the need for an alternative, effective and direct control strategy that can handle input constraints explicitly in the controller design and provide, simultaneously, an explicit characterization of the region of guaranteed closed-loop stability starting from where the requested stability and performance of the particulate process can be guaranteed in the presence of input constraints.

Motivated by the above discussion, the development of a rigorous, yet practical, framework for the analysis and control of constrained particulate processes is the subject of this chapter. In the next section, we outline the proposed framework, which will serve as the road map for our development throughout the chapter.

11.3 Methodological framework for analysis and control

Owing to its distributed parameter nature, the system of Eq.11.1 cannot be used directly as the basis for either the analysis of the limitations imposed by input constraints on particulate process dynamics or the synthesis of practically implementable (low-order) nonlinear controllers that cope effectively with the problem of constraints. This fact, together with the realization that the dominant dynamics of particulate processes are characterized by a small number of degrees of freedom (e.g., see [54]), motivate employing the following methodology for the analysis and control of constrained particulate processes of the form of Eq.11.1:

1. Initially, the method of weighted residuals is used to derive a nonlinear ODE

system that accurately reproduces the solutions and dynamics of the system of Eq.11.1.

2. Next, the low-order ODE approximation of the system of Eq.11.1 is used as the basis for analyzing the fundamental limitations imposed by input constraints on our ability to modify the dynamics of the particulate process. This is done by identifying the set of admissible set-points that can be attained in the presence of the given input constraints.

3. Then, given the set of feasible control objectives, the low-order ODE approximation of the system of Eq.11.1 is used as the basis for the direct synthesis, via Lyapunov techniques, of practically implementable bounded nonlinear output feedback controllers that cope effectively with the problem of input constraints by: (a) enforcing stability and set-point tracking in the constrained closed-loop ODE system , and b) providing an explicit characterization of the set of operating conditions starting from where the desired closed-loop stability and performance are guaranteed in the presence of constraints.

4. Finally, the resulting closed-loop system (particulate process model of Eq.11.1 and controller) is analyzed to derive conditions that guarantee that the desired stability and set-point tracking properties are enforced in the infinite-dimensional closed-loop system.

11.4 Model reduction

We initially use the method of weighted residuals to derive a set of nonlinear ODEs that accurately reproduce the solutions and the dominant dynamics of the distributed parameter system of Eq.11.1. The central idea of the method of weighted residuals is

to approximate the exact solution of $n(r,t)$ by an infinite series of orthogonal basis functions defined on the interval $[0, r_{max})$ with time-varying coefficients, substitute the series expansion into Eq.11.1, and then take the inner product with respect to a complete set of weighted functions, to compute a set of ODEs which describes the rate of change of the time-varying coefficients of the series expansion of the solution. Specifically, we expand the solution of $n(r,t)$ in an infinite series in terms of an orthogonal and complete set of basis functions, $\phi_k(r)$, where $r \in [0, r_{max})$, $k = 1, \ldots, \infty$, as follows:

$$n(r,t) = \sum_{k=1}^{\infty} a_k(t)\phi_k(r) \tag{11.7}$$

where $a_k(t)$ are time-varying coefficients. Substituting the above expansion into the particulate process model of Eq.11.1, we obtain:

$$\begin{aligned} &\sum_{k=1}^{\infty}\phi_k(r)\frac{\partial a_k(t)}{\partial t} = -\sum_{k=1}^{\infty}a_k(t)\frac{\partial(G(x,r)\phi_k(r))}{\partial r} + w(\sum_{k=1}^{\infty}a_k(t)\phi_k(r), x, r) \\ &\dot{x} = f(x) + g(x)sat(u(t)) + A\int_0^{r_{max}} a_2(\sum_{k=1}^{\infty}a_k(t)\phi_k(r), r, x)dr) \end{aligned} \tag{11.8}$$

Multiplying the population balance with the weighting functions, $\psi_\nu(r)$, and integrating over the entire particle size spectrum (i.e., taking inner product in $L_2[0, r_{max})$ with the weighting functions), the following infinite set of nonlinear ODEs is obtained:

$$\begin{aligned} \int_0^{r_{max}}\psi_\nu(r)\sum_{k=1}^{\infty}\phi_k(r)\frac{\partial a_k(t)}{\partial t}dr &= -\sum_{k=1}^{\infty}a_k(t)\int_0^{r_{max}}\psi_\nu(r)\frac{\partial(G(x,r)\phi_k(r))}{\partial r}dr \\ &+\int_0^{r_{max}}\psi_\nu(r)w(\sum_{k=1}^{\infty}a_k(t)\phi_k(r), x, r)dr, \quad \nu = 1, \ldots, \infty \\ \dot{x} &= f(x) + g(x)sat(u(t)) + A\int_0^{r_{max}} a_2(\sum_{k=1}^{\infty}a_k(t)\phi_k(r), r, x)dr) \end{aligned} \tag{11.9}$$

Eq.11.9 is an infinite set of ODEs which describe the rate of change of the time-varying coefficients, $a_k(t)$, where $k = 1, \ldots, \infty$, of the series expansion of the solution. An accurate approximation of Eq.11.9 is obtained by truncating the series expansion of

$n(r,t)$ up to order N and keeping the first N equations (i.e., $\nu = 1,\ldots,N$). The infinite-dimensional system of Eq.11.9 reduces to the following finite set of ODEs:

$$\begin{aligned}
&\int_0^{r_{max}} \psi_\nu(r)\sum_{k=1}^{N}\phi_k(r)\frac{\partial a_{kN}(t)}{\partial t}dr \\
&\qquad = -\sum_{k=1}^{N} a_{kN}(t)\int_0^{r_{max}} \psi_\nu(r)\frac{\partial(G(x_N,r)\phi_k(r))}{\partial r}dr \\
&\qquad +\int_0^{r_{max}} \psi_\nu(r)w(\sum_{k=1}^{N} a_{kN}(t)\phi_k(r), x_N, r)dr, \quad \nu = 1,\ldots,N
\end{aligned} \tag{11.10}$$

$$\dot{x}_N = f(x_N) + g(x_N)sat(u(t)) + A\int_0^{r_{max}} a_2(\sum_{k=1}^{N} a_{kN}(t)\phi_k(r), r, x_N)dr)$$

where x_N and a_{kN} are the approximations of x and a_k obtained by an N-th order truncation. Introducing the vector notation, $a_N = [a_{1N} \cdots a_{NN}]$, and after some rearrangements, Eq.11.10 can be represented in the following general form:

$$\begin{aligned}
\dot{a}_N &= f^*(a_N, x_N) \\
\dot{x}_N &= f(x_N) + g(x_N)sat(u(t)) + A\int_0^{r_{max}} a_2(\sum_{k=1}^{N} a_{kN}(t)\phi_k(r), r, x_N)dr)
\end{aligned} \tag{11.11}$$

where the explicit expression of $f^*(a_N, x_N)$ is omitted for brevity. Setting $\tilde{x} = [a_N^T\ x_N^T]^T$, we obtain the following multi-input multi-output finite-dimensional ODE system:

$$\begin{aligned}
\dot{\tilde{x}} &= \tilde{f}(\tilde{x}) + \sum_{i=1}^{m}\tilde{g}_i(\tilde{x})sat(u_i) \\
y_{si} &= \tilde{h}_i(\tilde{x}), \quad i = 1,\ldots,m
\end{aligned} \tag{11.12}$$

where $\tilde{f}(\tilde{x}), \tilde{g}_i(\tilde{x}), \tilde{w}(\tilde{x})$ are nonlinear vector functions whose explicit form is omitted brevity. Using results from singular perturbation theory, the asymptotic validity of the ODE approximation was established in Proposition 1 in [54].

Remark 11.1 In the series expansion of Eq.11.7, the basis, $\{\phi_k\}$, $j = 1,\ldots,\infty$, of $L_2[0, r_{max})$ can be chosen from standard basis functions sets (for example, when $r_{max} = \infty$, $\{\phi_k\}$ can be chosen to be Laguerre polynomials in which case the method

of weighted residuals reduces to the method of moments when the weighting functions are chosen as $\psi_\nu = r^\nu$), or it can be computed by applying Karhunen-Loève expansion on an appropriately chosen ensemble of solutions of the system of Eq.11.1 (see [140] for details on Karhunen-Loève expansion).

Remark 11.2 When an arbitrary set of basis functions is used in the expansion of Eq.11.7,the ODE system of Eq.11.11 may be of very high order in order to accurately describe the dominant dynamics of the system of Eq.11.1, and thus be suitable for the synthesis of a high-performance nonlinear controller. Unfortunately, high dimensionality of the system of Eq.11.11 leads to complex design and high-order controllers, which cannot be readily implemented in practice. An approach to overcome this problem is to reduce the dimension of the system of Eq.11.11 further by utilizing the concept of approximate inertial manifolds for particulate process models proposed in [54].

11.5 Computation of admissible set-points

Having obtained a low-order approximate ODE system that accurately reproduces the solution and dominant dynamics of the particulate process, we are now in a position to analyze the limitations imposed by constraints on our ability to modify the dynamics of particulate processes, on the basis of the constrained ODE system of Eq.11.12. Particulate processes typically operate at constant set-points corresponding to equilibrium points of the closed-loop system (e.g., a desired total number of particles, mean particle size, temperature). However, it may not be feasible to steer the closed-loop system to the desired operating point, in the presence of constraints, irrespective of the choice of the control strategy. Thus, even before devising a control policy, it is important to investigate the feasibility of controlling the particulate process at a desired set-point in the presence of constraints. Addressing this problem,

in its full generality, entails two main tasks. The first task is that of identifying the set of admissible set-points that the particulate process can be steered to in the presence of constraints. The second task is that of characterizing the set of admissible initial conditions, starting from where, a given admissible set-point can be reached in the presence of constraints. In this section, we will focus on the first task and defer discussion of the second task to the next section.

To accomplish our goal of identifying the set of admissible set-points permitted by input constraints, it is useful to view the constrained ODE system of Eq.11.12 as a dynamical system where the control input u_i is viewed as a parameter that takes values in the set of admissible control inputs, i.e., the interval $U_i = [u_{i,min}, u_{i,max}]$. In other words, we consider the following unforced system:

$$\dot{\tilde{x}} = \tilde{f}(\tilde{x}) + \sum_{i=1}^{m} \tilde{g}_i(\tilde{x}) u_i^0, \quad i = 1, \ldots, m \tag{11.13}$$

obtained from the system of Eq.11.12 for a constant value of u_i denoted by $u_i^0 \in U_i$. An immediate consequence of this view is the realization that the presence of constraints on the values that the parameter u_i^0 can take leads to natural limitations on the steady-states or equilibrium states – and, consequently, the set-points – that the ODE system can attain. Exploiting this fact, the problem of characterizing the limitations imposed by input constraints is equivalent to that of explicitly characterizing the dependence of the equilibrium states of the constrained ODE system of Eq.11.13 on the admissible values of u_i^0 dictated by the given input constraints. For a given value of the control input $u_i^0 \in U_i$, one can obtain the admissible equilibrium states of the system of Eq.11.12 by solving the following set of algebraic equations:

$$0 = \tilde{f}(\tilde{x}_s) + \sum_{i=1}^{m} \tilde{g}_i(\tilde{x}_s) u_i^0, \quad i = 1, \ldots, m \tag{11.14}$$

where $\tilde{x}_s$ represents the admissible steady-state for the above ODE system. As the value of u_i^0 is varied smoothly over the set of admissible control inputs U_i, we obtain

the set of all admissible equilibrium points of the constrained ODE system of Eq.11.12 that can be attained in the presence of constraints. Finally, the admissible set-points can be computed directly from the following relation:

$$v_i \;=\; \tilde{h}_i(\tilde{x}_s), \;\; i = 1, \ldots, m \tag{11.15}$$

Remark 11.3 The above analysis provides a systematic and practical method for computing the approximate admissible set-points of the constrained particulate process of Eq.11.1 on the basis of the ODE system of Eq.11.12. The only task involved in this method is the solution of a small (due to the low-dimensional nature) set of algebraic equations of the form of Eq.11.14 as u_i^0 takes values in the set of admissible control inputs. Note that this analysis is independent of the specific control strategy that one may wish to implement. Note also that this analysis does not provide any information regarding where, in the state-space, a particular admissible set-point can be reached from. In other words, given an admissible equilibrium point, $\tilde{x}_s$, obtained by solving Eq.11.14, the above analysis does not say if this point will actually be achieved under a given controller and starting from a given initial condition. The task of providing such information will be addressed in the controller design step of our methodology. What the above analysis allows us to conclude, however, is whether the given input constraints place any fundamental limitations on our ability to reach a particular set-point, and can therefore be used by process operators to identify a priori (before controller design) admissible control objectives.

Remark 11.4 Recent research on the dynamical analysis of nonlinear control systems with input constraints (see, for example, [69]) has provided a system-theoretic characterization of the regions of controllability under constraints, the so-called control sets, where *any* two points in the state-space can be reached from each other with the available control action. As the range of manipulated input is varied smoothly over a sufficiently small finite range, these control sets emerge and evolve around the equilibrium points of the nominal system of Eq.11.13. Although control sets provide

a more detailed characterization of the limitations imposed by input constraints on the system dynamics, such characterization remains largely theoretical and not very useful from a computational standpoint. The construction of control sets is actually a very cumbersome task even for low-dimensional systems (see, for example, [159].) On the other hand, computation of the set of admissible set-points contained within a control set is a relatively straightforward task that is computationally feasible and provides at the same time a valuable piece of information. It is noteworthy that the concept of using steady-state system analysis to reach certain conclusions about the control of a dynamic system has also been discussed and found useful applications in the context of the integration of process design and control (e.g., see [284, 108]).

Let us now apply our feasibility analysis to the continuous crystallizer example considered in Section 11.2.2. It was shown in [54] that upon application of the method of moments to the continuous crystallizer process of Eq.11.4 and neglecting moments of order four and higher, one can derive the following dimensionless ODE system that accurately reproduces the dynamics of the distributed process model of Eq.11.4:

$$\begin{aligned}
\dot{\tilde{x}}_0 &= -\tilde{x}_0 + (1-\tilde{x}_3) Da \exp\left(\frac{-F}{\tilde{y}^2}\right) \\
\dot{\tilde{x}}_1 &= -\tilde{x}_1 + \tilde{y}\tilde{x}_0 \\
\dot{\tilde{x}}_2 &= -\tilde{x}_2 + \tilde{y}\tilde{x}_1 \\
\dot{\tilde{x}}_3 &= -\tilde{x}_3 + \tilde{y}\tilde{x}_2 \\
\dot{\tilde{y}} &= \frac{1-\tilde{y}-(\alpha-\tilde{y})\tilde{y}\tilde{x}_2}{1-\tilde{x}_3} + \frac{u}{1-\tilde{x}_3}
\end{aligned} \tag{11.16}$$

where

$$\begin{aligned}
&t = \frac{\bar{t}}{\tau},\ \tilde{x}_0 = 8\pi\sigma^3\mu_0,\ \tilde{x}_1 = 8\pi\sigma^2\mu_1,\ \tilde{x}_2 = 4\pi\sigma\mu_2,\ \tilde{x}_3 = \frac{4}{3}\pi\mu_3,\ \ldots, \\
&\sigma = k_1\tau(c_0 - c_s),\ Da = 8\pi\sigma^3 k_2\tau,\ F = \frac{k_3 c_s^2}{(c_0-c_s)^2},\ \alpha = \frac{(\rho - c_s)}{(c_0-c_s)}, \\
&\tilde{y} = \frac{(c-c_s)}{(c_0-c_s)},\ u = \frac{(c_0-c_{0s})}{(c_0-c_s)}
\end{aligned} \tag{11.17}$$

μ_i is the $i-$th moment, $\tilde{x}_0$ is a dimensionless crystal concentration and u is a dimensionless solute feed concentration (for definitions of the remaining variables, the reader is referred to [54]). To compute the admissible set-points for the above system, we take the set of admissible control inputs to be $U = [0, 6]$. Setting the left-hand side of Eq.11.16 equal to zero, we obtain a set of algebraic equations that can be solved for each value of $u \in U$. Figure 11.3 illustrates the admissible set-points for the crystal

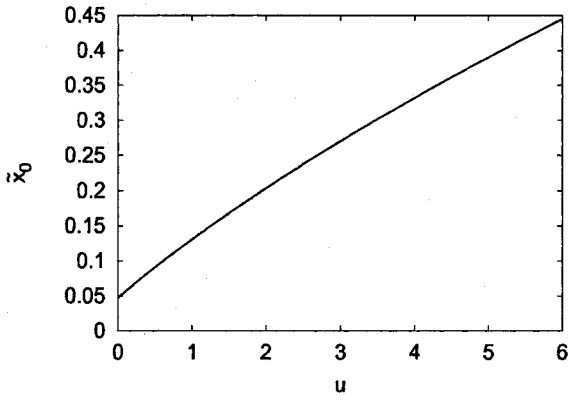

Figure 11.3: Admissible set-points for crystal concentration for $u \in [0, 6]$.

concentration which can be achieved with the available control inputs. From this figure, the reason for the PI controller's failure to stabilize the crystallizer in Section 11.2.2 and achieve the requested 0.4 change in the set point is evident. Allowing the control inputs to vary only in the set $[0, 2]$ renders the requested set-point $\tilde{x}_0 = 0.4$ infeasible.

11.6 Bounded nonlinear control of particulate processes

Having obtained a low-order ODE system that captures the dominant dynamics of the particulate process and identified the set of feasible control objectives that can be achieved in the presence of constraints, we are now motivated to proceed with

the third step of our proposed methodology. In this section, we use the constrained low-order ODE system of Eq.11.12 as the basis for developing an effective control strategy that handles explicitly the problem of constraints. The key components of this strategy involve: (a) the synthesis of a practically implementable bounded nonlinear output feedback controller that enforces stability and set-point tracking in the closed-loop system in the presence of active input constraints and (b) the explicit characterization of the state-space region of guaranteed closed-loop stability associated with the designed controller. The output feedback controller is constructed through a standard combination of a bounded state feedback controller with a state observer. The state feedback controller is synthesized via Lyapunov-based control methods and the state observer is an extended Luenberger-type observer. Before we proceed with the controller design, we begin in the next subsection with some preliminaries that will be used to state the controller synthesis result.

11.6.1 Preliminaries

Referring to the system of Eq.11.12, we define the relative order of the output, y_{si}, with respect to the vector of manipulated inputs, u, as the smallest integer r_i for which:

$$\left[L_{\tilde{g}_1} L_{\tilde{f}}^{r_i-1} \tilde{h}_i(\tilde{x}) \ \cdots \ L_{\tilde{g}_m} L_{\tilde{f}}^{r_i-1} \tilde{h}_i(\tilde{x})\right] \not\equiv [0 \ \cdots \ 0] \tag{11.18}$$

or $r_i = \infty$ if such an integer does not exist. We also define the characteristic matrix:

$$C(\tilde{x}) = \begin{bmatrix} L_{\tilde{g}_1} L_{\tilde{f}}^{r_1-1} \tilde{h}_1(\tilde{x}) & \cdots & L_{\tilde{g}_m} L_{\tilde{f}}^{r_1-1} \tilde{h}_1(\tilde{x}) \\ L_{\tilde{g}_1} L_{\tilde{f}}^{r_2-1} \tilde{h}_2(\tilde{x}) & \cdots & L_{\tilde{g}_m} L_{\tilde{f}}^{r_2-1} \tilde{h}_2(\tilde{x}) \\ \vdots & \cdots & \vdots \\ L_{\tilde{g}_1} L_{\tilde{f}}^{r_m-1} \tilde{h}_m(\tilde{x}) & \cdots & L_{\tilde{g}_m} L_{\tilde{f}}^{r_m-1} \tilde{h}_m(\tilde{x}) \end{bmatrix} \tag{11.19}$$

To proceed with the controller synthesis and under the assumption that the relative degree is well-defined, we transform the system of Eq.11.12 into the following partially

linear form:

$$\begin{aligned}
\dot{\zeta}_1^{(i)} &= \zeta_2^{(i)} \\
&\vdots \\
\dot{\zeta}_{r_i-1}^{(i)} &= \zeta_{r_i}^{(i)} \\
\dot{\zeta}_{r_i}^{(i)} &= L_{\tilde{f}}^{r_i}\tilde{h}_i(\tilde{x}) + \sum_{k=1}^{m} L_{\tilde{g}_k} L_{\tilde{f}}^{r_i-1}\tilde{h}_i(\tilde{x})u_k \\
\dot{\eta}_1 &= \Psi_1(\zeta,\eta) \\
&\vdots \\
\dot{\eta}_{(n+N)-\sum_i r_i} &= \Psi_{(n+N)-\sum_i r_i}(\zeta,\eta) \\
y_{si} &= \zeta_1^{(i)}, \quad i = 1,\ldots,m
\end{aligned} \tag{11.20}$$

where $\tilde{x} = T^{-1}(\zeta,\eta)$, $\zeta = [\zeta^{(1)^T} \cdots \zeta^{(m)^T}]^T$. This transformation is standard in all general nonlinear process control methods whose objective is to force the process output to follow the reference input. Defining the tracking error, $e_k^{(i)} = \zeta_k^{(i)} - v_i^{(k-1)}$, and introducing the vector notation $e^{(i)} = [e_1^{(i)}\ e_2^{(i)} \cdots e_{r_i}^{(i)}]^T$, $e = [e^{(1)^T}\ e^{(2)^T} \cdots e^{(m)^T}]^T$, where $i = 1,\cdots,m$, $k = 1,\cdots,r_i$, the ζ-subsystem of Eq.11.20 can be further transformed into the following more compact form:

$$\dot{e} = Ae + B\left[l_1(e,\eta,\bar{v}) + C(\tilde{x})u\right] \tag{11.21}$$

where A, B, are constant matrices of dimensions $(\sum_{i=1}^m r_i)\times(\sum_{i=1}^m r_i)$ and $(\sum_{i=1}^m r_i)\times m$, respectively, $l_1(e,\eta,\bar{v})$ is a $(\sum_{i=1}^m r_i)\times 1$ continuous nonlinear vector function, and $\bar{v}$ is a vector of the form $\bar{v} = \mathcal{V}(v_i, v_i^{(1)},\ldots,v_i^{(r_i)})$, where $\mathcal{V}(v_i, v_i^{(1)},\ldots,v_i^{(r_i)})$ is a smooth vector function, $v_i^{(k)}$ is the k-th time-derivative of the external reference input v_i (which is assumed to be a smooth function of time.) The specific forms of these functions are omitted for brevity. Finally, we define the function $\bar{f}(e,\eta,\bar{v}) = Ae + Bl_1(\tilde{x})$, and denote by $\bar{g}_i(e,\eta,\bar{v})$ the $i-$th column of the matrix function $BC(\tilde{x})$, $i = 1,\cdots m$.

11.6.2 Controller synthesis

Towards the end goal of synthesizing the necessary bounded nonlinear output feedback controller, we use the nonlinear system of Eq.11.20 first to synthesize, via Lyapunov-based control methods, a bounded nonlinear state feedback controller of the general form:

$$u = p(\tilde{x}, u_{max}, \bar{v}) \tag{11.22}$$

where $p(\cdot)$ is a bounded vector function, i.e., $|u| \leq u_{max}$ where $|\cdot|$ is the Euclidean norm, that: (a) enforces exponential stability and reference input tracking in the closed-loop system in the presence of input constraints and (b) provides an explicit characterization of the region in the state-space where the aforementioned closed-loop properties are guaranteed.

To construct the desired stabilizing state feedback controller for the system of Eq.11.12, we use Lyapunov-based control methods. The basic idea is the selection of an appropriate Lyapunov function whose time-derivative can be rendered negative-definite, via feedback, along the trajectories of the closed-loop system. A natural choice for our system, suggested by the partially linear form of Eq.11.21, is a quadratic Lyapunov function, $V = e^T P e$, where P is a positive-definite matrix chosen to satisfy the following Riccati matrix inequality:

$$A^T P + PA - PBB^T P < 0 \tag{11.23}$$

which consequently guarantees the negative-definiteness of $\dot{V}$. Using this Lyapunov function, we design a bounded nonlinear state feedback controller of the form:

$$u = -\frac{1}{2} R^{-1}(\tilde{x}) \left(L_{\bar{g}} V\right)^T \tag{11.24}$$

where $R^{-1}(\tilde{x})$ is a strictly positive nonlinear scalar function whose specific expression is given in Theorem 11.1 below and $L_{\bar{g}} V$ is a row vector given by $L_{\bar{g}} V =$

$[L_{\tilde{g}_1}V \cdots L_{\tilde{g}_m}V]$. As we will discuss shortly, the bounded nature of the state feedback controller will assist in addressing the problem of constraints by providing an explicit characterization of the set of admissible initial states starting from where the desired closed-loop properties are guaranteed.

Under the hypothesis that the system of Eq.11.12 is locally observable (i.e., its linearization around the desired operating steady-state is observable), the practical implementation of a nonlinear state feedback controller of the form of Eq.11.24 will be achieved by employing the following nonlinear state observer:

$$\frac{d\omega}{dt} = \tilde{f}(\omega) + \tilde{g}(\omega)sat(u) + L(y - \tilde{h}(\omega)) \tag{11.25}$$

where ω denotes the observer state vector (the dimension of the vector ω is equal to the dimension of $\tilde{x}$ in the system of Eq.11.12), $y = [y_1 \ y_2 \ \cdots y_l]^T$ is the measured output vector and L is a matrix chosen so that the eigenvalues of the matrix $C_L = \frac{\partial \tilde{f}}{\partial \omega}_{(\omega=\omega_s)} - L\frac{\partial \tilde{h}}{\partial \omega}_{(\omega=\omega_s)}$, where ω_s is the operating steady-state, lie in the open left-half of the complex plane. The state observer of Eq.11.25 consists of a replica of the system of Eq.11.12 plus a linear gain multiplying the discrepancy between the actual and the estimated value of the output, and therefore it is an extended Luenberger-type observer. Finally, the state feedback control law of Eq.11.24 and the state observer of Eq.11.25 can be combined to yield the desired bounded nonlinear output feedback control law.

We are now in a position to state the main result of this subsection. Theorem 11.1 below provides the explicit synthesis formula for the desired bounded output feedback control law and states precise conditions that guarantee closed-loop stability and asymptotic output tracking in the presence of input constraints in the closed-loop ODE system. The proof can be found in Appendix G.

Theorem 11.1 *Consider the system of Eq.11.12 and assume that: (1) it is locally observable in the sense that there exists a matrix L such that $C_L = \frac{1}{\mu}\bar{A}$ where μ is a small positive parameter and $\bar{A}$ is a Hurwitz matrix, (2) its characteristic matrix, $C(\tilde{x})$, is nonsingular $\forall\ \tilde{x} \in D \subset \mathbb{R}^{n+N}$, and (3) its inverse dynamics are input-to-state stable and exponentially stable when $\zeta = 0$. Consider first the system of Eq.11.12 under the state feedback controller of Eq.11.24 where:*

$$\frac{1}{2}R^{-1}(\tilde{x}) = \frac{L_{\bar{f}}^{*}V + \sqrt{(L_{\bar{f}}^{*}V)^2 + \left(u_{max}^2 (L_{\bar{g}}V)(L_{\bar{g}}V)^T\right)^2}}{(L_{\bar{g}}V)(L_{\bar{g}}V)^T\left[1 + \sqrt{1 + u_{max}^2 (L_{\bar{g}}V)(L_{\bar{g}}V)^T}\right]} \tag{11.26}$$

and $L_{\bar{f}}^{*}V = L_{\bar{f}}V + \rho|e|^2$, $\rho > 0$. Let δ_x be a positive real number such that the compact set $|\tilde{x}| \leq \delta_x$ is an invariant set embedded within the region described by the following inequality:

$$L_{\bar{f}}^{*}V \leq u_{max}|(L_{\bar{g}}V)^T| \tag{11.27}$$

Then, for any initial condition that satisfies $|\tilde{x}(0)| \leq \delta_x$, the origin of the closed-loop system is asymptotically stable in the sense that there exists a function β of class $\mathcal{KL}$ such that $|x(t)| \leq \beta(|x(0)|, t)$, $\forall t \geq 0$. Now consider the system of Eq.11.12 under the output feedback controller:

$$\begin{aligned} \frac{d\omega}{dt} &= \tilde{f}(\omega) - \frac{1}{2}\tilde{g}(\omega)R^{-1}(\omega)\left(L_{\bar{g}}V(\omega)\right)^T + L(y - \tilde{h}(\omega)) \\ u &= -\frac{1}{2}R^{-1}(\omega)\left(L_{\bar{g}}V(\omega)\right)^T \end{aligned} \tag{11.28}$$

Then given any pair of positive real numbers, d and δ_b, such that $\beta(\delta_b, 0) + d \leq \delta_x$, there exists $\mu^* > 0$ such that if $\mu \in (0, \mu^*]$, $|\tilde{x}(0)| \leq \delta_b$, $|\omega(0)| \leq \delta_b$, the following holds in the presence of input constraints: (1) the origin of the closed-loop system is asymptotically (and locally exponentially) stable, (2) the output of the closed-loop ODE system satisfies a relation of the form $\lim_{t\to\infty}|y_{si} - v_i| = 0$, where v_i is the set-point for the i-th controlled output.

Remark 11.5 Theorem 11.1 provides an explicit characterization of a set of admissible initial conditions starting from where the constrained closed-loop ODE system

is guaranteed to be stable with the available control action (region of guaranteed closed-loop stability). This characterization can be obtained from the inequality of Eq.11.27. This inequality describes the largest region in the state-space where $\dot{V}$ is negative-definite under the bounded state feedback controller of Eqs.11.24 and 11.26, and where any closed-loop trajectory evolving is guaranteed to converge to the desired equilibrium point with the available control action. However, since this region is, in general, not an invariant one, it is necessary to guarantee that trajectories starting within the region do not leave, in order to guarantee closed-loop stability. This is done by confining the initial conditions within an invariant set embedded within the region. The size of this set is fixed by δ_x and represents the state feedback estimate of the region of closed-loop stability (see [91] and chapter 4 in [170] for how to compute this estimate). According to Theorem 11.1, this estimate remains practically preserved under output feedback. Specifically, starting from any compact subset (whose size is fixed by δ_b) of the state feedback region, there always exists $\mu > 0$ such that the desired closed-loop properties are guaranteed under the dynamic output feedback controller of Eq.11.28. Note that the size of the output feedback region (δ_b) can be made close to that of the state feedback region (δ_x) by selecting d to be sufficiently small which, in turn, can be done by choosing μ to be sufficiently small. Therefore, although combination of the bounded state feedback controller with an observer results in some loss (represented by d) in the size of the region of guaranteed closed-loop stability, this loss can be made arbitrarily small by selecting μ to be sufficiently small.

Remark 11.6 The inequality of Eq.11.27 captures, in an intuitive way, the dependence of the size of the region of guaranteed closed-loop stability on the magnitude of input constraints. For example, this inequality predicts that the tighter the input constraints are made (i.e., smaller u_{max}), the smaller the resulting closed-loop stability region. This is quite intuitive since, under tighter constraints, fewer initial conditions are admissible and can be used to stabilize the closed-loop system. Finally note that, according to the inequality of Eq.11.27, the largest region of closed-loop stability under the control law of Eq.11.24 is obtained, as expected, in the absence of

constraints (i.e., as $u_{max} \rightarrow \infty$).

Remark 11.7 Although the inequality of Eq.11.27 can be used to compute the region of guaranteed closed-loop stability, the actual construction (e.g., plotting) of this region is not necessary to conclude whether the desired closed-loop properties can be guaranteed for a given initial condition. Instead, all that is required is the verification of some algebraic conditions. In particular, one can directly substitute the desired initial condition into Eq.11.27 and check before implementing the controller whether the inequality is satisfied and $|\tilde{x}(0)| \leq \delta_x$. If so, then both stability and set-point tracking are guaranteed in the presence of input constraints. This aspect of the controller design has important practical implications because it provides process operators with a systematic and easily implementable guide to identify a priori (that is before implementing the controller) feasible initial operating conditions form which to operate and steer the process safely and reliably under input constraints while at the same time satisfying the requested control objectives.

Remark 11.8 Note that the static state feedback component of the proposed output feedback controller of Eq.11.28 (with $\omega = \tilde{x}$) uses directly the available information on input constraints to achieve the requested closed-loop stability and performance properties (note the explicit dependence of the expression in Eq.11.26 on u_{max}.) Note also that, whenever Eq.11.27 holds, the control action is bounded by u_{max} and satisfies the constraints. Both the explicit incorporation of constraints in the controller design and the explicit characterization of the region of guaranteed closed-loop stability follow directly from the inherent boundedness property of the state feedback component in Eq.11.28. It is important to point out here that the design of the state feedback controller of Eqs.11.24 and 11.26 involves a modification of the controller design proposed in [204] by introducing the term, $-\rho|e|^2$, which is necessary to ensure exponential stability in the constrained finite-dimensional closed-loop system.

Remark 11.9 The control law of Eqs.11.24 and 11.26 has two desirable properties not present in other conventional or nonlinear controller designs based on the concept of input/output linearization (see [148] for details.) The first property is the fact that the controller of Eq.11.28 recognizes the beneficial effect of the term $L_f V$ when $L_f V < 0$ and prevents its unnecessary cancellation. In this case, the term $L_f V$ is a beneficial (stabilizing) nonlinearity whose cancellation may generate unnecessarily large control action, and in some cases generate positive feedback and destabilize the process. Under such circumstances, the controller design of Eq.11.28 guards against the wasteful cancellation of such nonlinearities and avoids the expenditure of unnecessarily large control effort. This property is particularly important in the presence of constraints that limit the available control action. The ability of the controller to use reasonably small control action to enforce the desired control objectives makes the controller design proposed in Theorem 11.1 better equipped to handle the problem of constraints. The second property that the controller of Eq.11.28 possesses is the fact that it dominates the term $L_f V$, instead of cancelling it, when $L_f V > 0$. This situation arises, for example, when the process is open-loop unstable. In this case, the term $L_f V$ is a destabilizing one that must be eliminated. The controller of Eq.11.28, however, eliminates the term by domination rather than by cancellation. This property guards against the non-robustness of cancellation designs which increases the risk of instability due to the presence of other uncertainties not taken into account in the controller design. This means that input perturbations (or equivalently, an error in implementing the control law) will be tolerated in the sense that the trajectories will remain bounded.

Remark 11.10 The bounded nonlinear controller of Eqs.11.24 and 11.26 possesses certain optimality properties characteristic of its ability to use small control action to accomplish the desired closed-loop objectives. In fact, one can rigorously prove, through the inverse optimal control approach (see, for example, [112, 271, 91]), that, within a well-defined region of the closed-loop stability region, this controller is optimal with respect to an infinite-time meaningful quadratic cost functional of the

form:

$$J = \int_0^\infty (e^T Q(\tilde{x}) e + u^T R(\tilde{x}) u) dt \tag{11.29}$$

which imposes penalty on both the tracking error and control action. In the above performance index, $Q(\tilde{x})$ is a positive-definite matrix that can be found directly from the steady-state Hamilton-Jacobi-Bellman (HJB) equation (which is the optimality condition for the stabilization problem) associated with the system of Eq.11.12 and cost functional of Eq.11.29:

$$0 \equiv e^T Q(\tilde{x}) e + L_{\tilde{f}} V - \frac{1}{4} (L_{\tilde{g}} V) R^{-1}(\tilde{x}) (L_{\tilde{g}} V)^T \tag{11.30}$$

The inverse optimal approach provides a rigorous framework for associating meaningful optimality (i.e., meaningful performance criteria) with certain stabilizing controllers (such as those of Eqs.11.24 and 11.26) and therefore helps explain the basis for their optimality properties. The key idea of this approach is to first design a stabilizing controller and then show that it minimizes a meaningful performance index of the form of Eq.11.29 by establishing that the resulting weights Q, R are positive-definite, which, in turn, renders the penalties imposed in the cost functional physically sensible. This approach has been used in the literature for the design of nonlinear optimal controllers without recourse to the unwieldy task of solving the HJB equation . For additional details on controller design using this approach as well as some of the history and motivation behind it, the reader is referred to [271, 91]. Finally, one can easily show that the minimum cost achieved by the state feedback controller is $V(e(0))$.

Remark 11.11 The controller-observer combination of Eq.11.28 practically preserves the optimality properties of the state feedback controller explained in Remark 11.10. The output feedback controller design is near-optimal in the sense that the cost incurred by implementing this controller on the system of Eq.11.12 tends to the optimal (minimal) cost achieved by implementing the bounded optimal state feedback controller (i.e., u of Eq.11.28 with $\omega = \tilde{x}$) when μ is selected to be sufficiently small.

Using a standard singular perturbation argument, one can show that cost associated with the output feedback controller is $O(\mu)$ close to the optimal cost associated with the state feedback controller (i.e., $J_{min} = V(e(0)) + O(\mu)$). The basic reason for near-optimality is the fact that by choosing μ to be sufficiently small, the observer states can be made to converge quickly to the process states. This fact can be exploited to make the performance of the output feedback controller arbitrarily close to that of the optimal state feedback controller.

Remark 11.12 The requirement that the observer states start within the region of guaranteed closed-loop stability ($|\omega(0)| \leq \delta_b$) is motivated by the fact that the process states themselves should start inside this region in order to guarantee stability of the constrained closed-loop system; and therefore, one must initiate the observer within the same region to guarantee convergence of the observer states to the process states. Note, however, that no restriction is placed on where, inside the stability region, the observer states can start (i.e., we allow for initialization errors) since they can be made to converge sufficiently fast to the actual states by selecting μ to be sufficiently small.

Remark 11.13 Regarding the practical application of Theorem 11.1, one has to initially use the method of weighted residuals to derive an ODE system of the form of Eq.11.12, and then verify Assumptions 1, 2 and 3 on the basis of this system. Then, given the available input constraints, u_{max}, and the desired initial condition, one should check if the inequality of Eq.11.27 is satisfied and if the initial condition lies within the region of guaranteed closed-loop stability. If this is case, then the desired closed-loop properties are guaranteed and the synthesis formula of Eq.11.28 can be directly used to derive the explicit form of the controller and implement it.

11.6.3 Application to the crystallizer moment model

The objective of this subsection is to illustrate the application of the results of Theorem 11.1 to the fifth-order moment model of Eq.11.16 which describes the domi-

nant dynamics of the continuous crystallizer of Eq.11.4. The control problem here is the same as that considered in the motivating example which involves regulating the crystal concentration by manipulating the solute feed concentration in the presence of constraints on the manipulated input. Utilizing the dimensionless variables of Eq.11.17, the system of Eq.11.16 can be recast in the form of Eq.11.12 with $\tilde{x} = [\tilde{x}_0\ \tilde{x}_1\ \tilde{x}_2\ \tilde{x}_3\ \tilde{y}]^T$ and

$$\tilde{f}(\tilde{x}) = \begin{bmatrix} -\tilde{x}_0 + (1-\tilde{x}_3)Da\exp\left(\dfrac{-F}{\tilde{y}^2}\right) \\ -\tilde{x}_1 + \tilde{y}\tilde{x}_0 \\ -\tilde{x}_2 + \tilde{y}\tilde{x}_1 \\ -\tilde{x}_3 + \tilde{y}\tilde{x}_2 \\ \dfrac{1-\tilde{y}-(\alpha-\tilde{y})\tilde{y}\tilde{x}_2}{1-\tilde{x}_3} \end{bmatrix}, \quad \tilde{g}(\tilde{x}) = \begin{bmatrix} 0 \\ 0 \\ 0 \\ 0 \\ 1 \\ \dfrac{}{1-\tilde{x}_3} \end{bmatrix}$$

On the basis of this system, one can easily verify that Assumptions 1, 2, and 3 of Theorem 11.1 are satisfied. A direct application of the synthesis formula of Eq.11.28 then yields the following bounded nonlinear output feedback controller:

$$\begin{aligned} \dot{\omega}_0 &= -\omega_0 + (1-\omega_3)Da\exp\left(\frac{-F}{\omega_4^2}\right) + L_0[\tilde{x}_0 - \omega_0] \\ \dot{\omega}_1 &= -\omega_1 + \omega_4\omega_0 + L_1[\tilde{x}_0 - \omega_0] \\ \dot{\omega}_2 &= -\omega_2 + \omega_4\omega_1 + L_2[\tilde{x}_0 - \omega_0] \\ \dot{\omega}_3 &= -\omega_3 + \omega_4\omega_2 + L_3[\tilde{x}_0 - \omega_0] \\ \dot{\omega}_4 &= \frac{1-\omega_4-(\alpha-\omega_4)\omega_4\omega_2}{1-\omega_3} - \frac{1}{2}\frac{R^{-1}(\omega)L_{\bar{g}}V(\omega)}{1-\omega_3} + L_4[\tilde{x}_0 - \omega_0] \\ u &= -\frac{1}{2}R^{-1}(\omega)L_{\bar{g}}V(\omega) \end{aligned} \tag{11.31}$$

where

$$V = e^T P e, \quad P = \begin{bmatrix} 1 & c \\ c & 1 \end{bmatrix}, \quad c \in (0,1) \tag{11.32}$$

Guided by the information provided in Figure 11.3, we constrain the admissible values of the manipulated input to vary in the range $0 \leq u \leq 6$ to achieve the requested set-point of $\tilde{x}_0 = 0.4$. Two closed-loop simulation runs were performed to evaluate the set-point tracking capability of the bounded nonlinear output feedback controller

of Eq.11.31 in the presence of constraints. The initial conditions for the states of the moment model, the states of the observer, and the values of the nonlinear controller parameters are all given in Table 11.2 for both runs. Note that in both cases, the initial observer states do not match those of the moment model to study the performance of the controller in the presence of initialization errors.

Table 11.2: Initial conditions and controller parameters for the implementation on the crystallizer moment model.

	First run	Second run
$\tilde{x}(0)$	$[0.059\ 0.035\ 0.022\ 0.014\ 0.60]^T$	$[0.44\ 0.61\ 0.85\ 1.14\ 0.60]^T$
$\omega(0)$	$[0.047\ 0.028\ 0.017\ 0.010\ 0.60]^T$	$[0.42\ 0.59\ 0.80\ 1.07\ 0.60]^T$
L	$[1.0\ 0.0\ 0.0\ 0.0\ 1.0]^T$	$[1.0\ 0.0\ 0.0\ 0.0\ 1.0]^T$
c	0.90	0.90
ρ	0.001	0.001

In the first simulation run, we considered achieving the set-point of $\tilde{x}_0 = 0.4$ starting from an initial condition that lies inside the region of guaranteed closed-loop stability (i.e., satisfies the inequality of Eq.11.27). Figure 11.4 shows the closed-loop output (top plot) and manipulated input (bottom plot) profiles for this case. It is clear from the figure that, starting from this initial condition, the bounded output feedback controller successfully achieves the requested set-point in the presence of input constraints. In the second simulation run, the same set-point was considered starting from an initial condition that lies outside the region of guaranteed stability (note that the initial condition for the second run given in Table 11.2 does not satisfy Eq.11.27). The closed-loop output and manipulated input profiles for this run are depicted in Figure 11.5, which shows that, in this case, the controller is unable to achieve the requested set-point in the presence of constraints although the requested set-point is an admissible one.

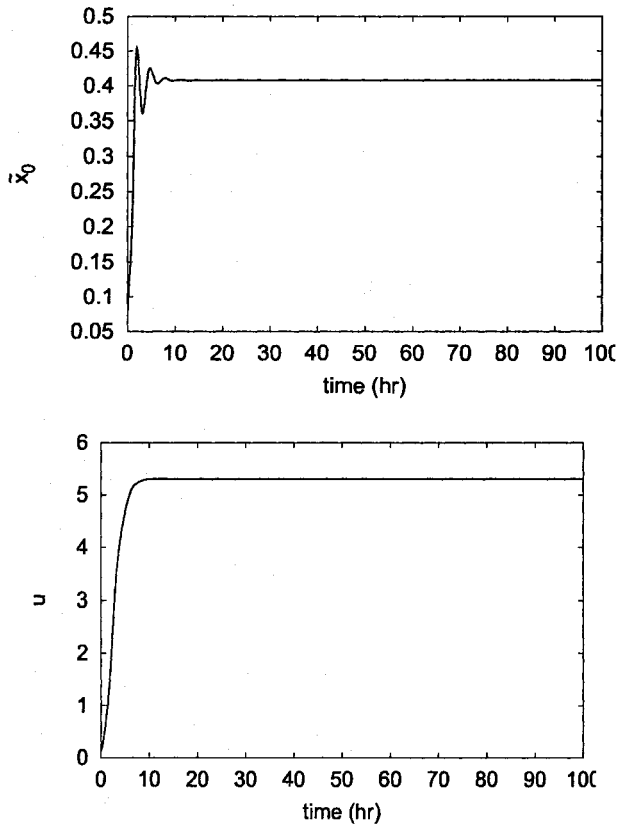

Figure 11.4: Controlled output and manipulated input profiles for the crystallizer moment model under the bounded nonlinear controller, for $u \in [0, 6]$ and an initial condition satisfying Eq.11.27.

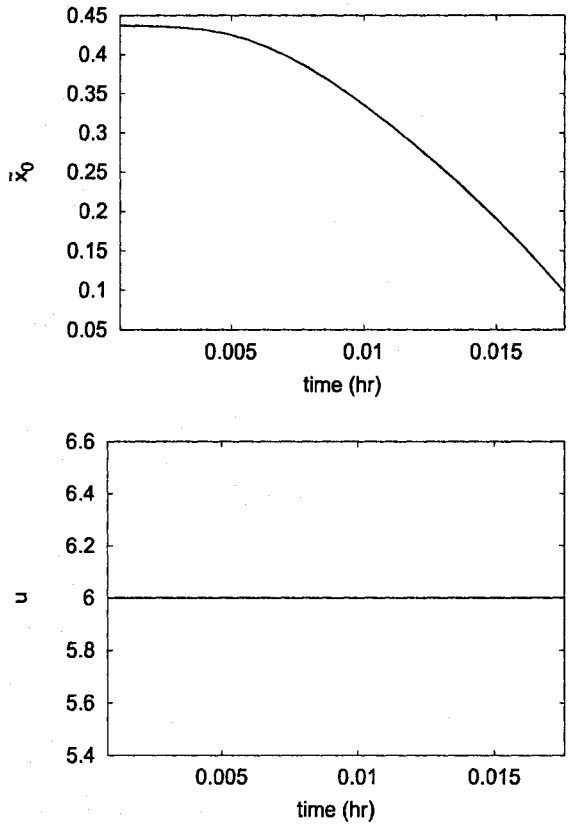

Figure 11.5: Controlled output and manipulated input profiles for the crystallizer moment model under the bounded nonlinear controller, for $u \in [0, 6]$ and an initial condition violating Eq.11.27.

The underlying cause for the instability in Figure 11.5 is the fact that the initial condition lies outside the region of closed-loop stability and therefore the control action required to drive that initial condition to the desired set-point is larger than that available due to the constraints (compare with Figure 11.4). This leads to the process input being saturated for all times as the controller tries unsuccessfully to provide the maximum solute feed concentration to achieve the desired crystal concentration. Note that based on the stability analysis of Theorem 11.1. we can conclude that there is no guarantee that a set-point of $\tilde{x}_0 = 0.4$ can be reached from the given initial condition (which is the only thing of practical concern) but cannot predict how the state x_0, once unstable, will evolve. Therefore, to explain the runaway behavior in Figure 11.5, we may view the closed-loop system under fixed input (see the input profile in Figure 11.5) as an open-loop system and analyze the stability properties of its equilibrium point. Under a fixed input of $u = 6$, this system has an unstable equilibrium point at $x_0 = 0.45$. Therefore, once under a fixed input of $u = 6$, the state $\tilde{x}_0$ does not stabilize at 0.45 and runs away instead. Had this equilibrium point been a stable one, the state x_0 would have settled there. However this is not the desired set-point. So, regardless of this equilibrium point's stability or instability, the controller is unable to achieve the desired set-point of $\tilde{x}_0 = 0.4$. Note that this reasoning, based on open-loop stability analysis, explains only why the state $\tilde{x}_0$ – once under fixed input – runs away instead of settling at another steady-state (i.e., it explains the type of instability that occurs), but does not explain why the process input remains fixed in the first place, which is the underlying cause of instability. The answer to this question is provided by Theorem 11.1 and has to do with the selection of an inadmissible initial condition.

11.6.4 Controller implementation on the infinite-dimensional system

So far, we have designed, on the basis of the ODE system of Eq.11.12, a bounded nonlinear output feedback controller with well-characterized stability properties in the presence of constraints and illustrated its application to the low-dimensional ODE system of Eq.11.12 which captures the dominant dynamics of the particulate process. In this subsection, we proceed with the final step of our methodology and implement the bounded output feedback controller of Eq.11.28 on the infinite-dimensional particulate process model of Eq.11.1. Theorem 11.1 below states precise conditions that guarantee closed-loop stability and asymptotic output tracking in the presence of constraints. The proof of this theorem can be found in Appendix G.

Theorem 11.2 *Consider the system of Eq.11.12, for which Assumptions 1, 2, and 3 of Theorem 11.1 hold. Consider also the particulate process model of Eq.11.1 under the nonlinear output feedback controller of Eq.11.28. Then, for sufficiently large N, there exist positive real numbers $\delta_n, \bar{\delta}_x, \delta_\omega, \bar{\mu}^*$ such that if $\mu \in (0, \bar{\mu}^*]$, $\|n(r,0)\|_2 < \delta_n$, $|x(0)| < \bar{\delta}_x$, $|\omega(0)| < \delta_\omega$:*
(1) The origin of the closed-loop system (particulate process model and controller of Eq.11.28) is exponentially stable.
(2) $\lim_{t\to\infty} |y_i - v_i| = O(\epsilon(N))$, where v_i is the set-point for the i-th controlled output and $\epsilon(N)$ is a small positive real number that depends on N and satisfies $\lim_{N\to\infty} \epsilon(N) = 0$.

Remark 11.14 Theorem 11.2 establishes that a bounded nonlinear output feedback controller which guarantees exponential stability and output tracking in the constrained finite-dimensional closed-loop system (Eqs.11.12 and 11.28), continues to enforce the same properties locally in the constrained infinite-dimensional closed-loop system (Eqs.11.1 and 11.28). This result is intuitively expected because for sufficiently large N: (a) the dynamics of the modes of the particulate process model which are not taken into account in the controller design (i.e., not included in the

ODE model of Eq.11.12) are locally exponentially stable, and (b) the control action, $u(t)$, does not influence the dynamics of the modes which are not taken into account in the controller design.

Remark 11.15 It was pointed out in Remark 11.5 that the inequality of Eq.11.27 provides an estimate of the set of admissible initial conditions starting from where the constrained finite-dimensional closed-loop system (Eqs.11.12 and 11.28) is guaranteed to be stable. Note that owing to the infinite-dimensional nature of the particulate process model of Eq.11.1, this inequality cannot be used directly to check the admissible initial conditions for the infinite-dimensional system (this is because the amplitude of the residual modes not included in the controller design may not, in general, be negligible). Furthermore, the local nature of the result of Theorem 11.2 implies that the initial conditions, for the infinite-dimensional system, must be selected sufficiently small to guarantee exponential stability of the closed-loop system. However, the inequality of Eq.11.27 continues to provide a useful guide for the selection of the admissible initial observer states that guarantee stability of the constrained infinite-dimensional closed-loop system (Eqs.11.1 and 11.28). To see why this is the case, recall from Theorem 11.1 that selection of the initial observer states within an invariant subset of the region described by Eq.11.27 guarantees stability of the constrained finite-dimensional closed-loop system (and consequently local exponential stability of the infinite-dimensional system according to Theorem 11.2). Guided by this result, we conclude that, in order to guarantee stability of the constrained infinite-dimensional closed-loop system, the initial observer states should – at a minimum – not be chosen outside this region. The region of Eq.11.27 therefore provides a reasonable initial guess for where to initialize the observer.

11.7 Application to a continuous crystallizer with constraints

In this section, the proposed nonlinear control method is used to stabilize the continuous crystallizer introduced in Section 11.2.2 in the presence of input constraints. Motivated by the fact that the crystallizer with the crystal size distribution as controlled output and the solute feed concentration as manipulated input is an approximately controllable system (see [269] for a rigorous controllability analysis), we consider the control problem of manipulating the solute feed concentration to achieve a crystal size distribution with desired mass, i.e., the controlled output is defined as:

$$y(\bar{t}) \;=\; 8\pi\sigma^3 \int_0^\infty n(r,\bar{t})dr \;=\; \tilde{x}_0 \tag{11.33}$$

The reader may refer to [198, 245, 87, 251] for the use of other manipulated variables including fines destruction rate and crystallizer temperature for the stabilization of crystallizers (note that the proposed control method can be used for the synthesis of nonlinear controllers when such manipulated inputs are considered).

Following the proposed methodology outlined in Section 11.3, the design of the necessary bounded nonlinear output feedback controller is carried out on the basis of the low-dimensional ODE model (moment model) of Eq.11.16 which captures the dominant dynamics of the crystallizer. The controller design procedure as well as the explicit controller formula are given in Section 11.6 where the controller was implemented first on the constrained ODE moment model. In this section, we implement the same controller on the constrained infinite-dimensional crystallizer model of Eq.11.4. The practical implementation of the nonlinear controller of Eq.11.31 requires on-line measurements of the controlled output, $\tilde{x}_0$; in practice, such measurements can be obtained by using, for example, light scattering techniques (see [42, 251] for details).

Several simulation runs were performed to evaluate the performance, robustness, and constraint-handling properties of the bounded nonlinear controller of Eq.11.31 and compare them with those of a PI controller. The values of the nonlinear controller parameters and the PI controller parameters, K_c and τ_I, which were used in the simulations, are given in Table 11.3 (K_c, τ_I were computed through extensive trial and error).

Table 11.3: Controller parameters for the implementation on the infinite-dimensional crystallizer model.

	Nominal conditions	with parametric uncertainty
K_c	0.5	0.5
τ_I	1.5	1.0
c	0.90	0.90
ρ	0.001	0.001
τ_i'	–	1.0

In all the simulation runs, the initial condition:

$$n(r,0) = 0.0,\ c(0) = 990.0\ kg/m^3$$

was used for the process model of Eq.11.4 and the finite difference method with 1000 discretization points was used for its simulation. The initial conditions for the dynamic system included in the controller of Eq.11.31 were set to be: $\omega_0 = 0.047$, $\omega_1 = 0.028$, $\omega_2 = 0.017$, $\omega_3 = 0.01$ and $\omega_4 = 0.5996$ (note that they do not correspond to the initial conditions used for the distributed parameter model in order to study the performance of the controller in the presence of significant initialization errors).

In the first set of simulation runs, the set-point tracking capability of the nonlinear controller in the presence of input constraints ($0 \leq u \leq 6$) was evaluated under nominal conditions for a 0.4 increase in the value of the set-point ($v = 0.4$). Figure 11.6 shows the closed-loop output (top plot) and manipulated input (middle plot)

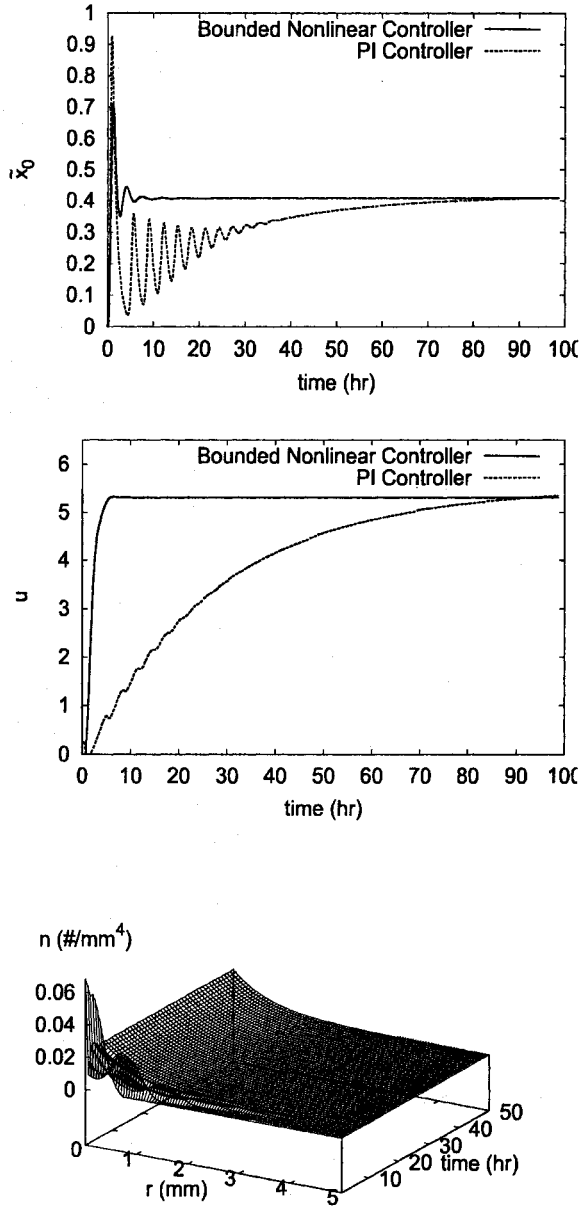

Figure 11.6: Controlled output, manipulated input, and crystal size distribution profiles for the crystallizer process model of Eq.11.4 under the bounded nonlinear controller (solid line) and the PI controller (dashed line) for 0.4 increase in the set-point and $u \in [0, 6]$.

profiles obtained by using the bounded nonlinear controller of Eq.11.31 (solid lines). For the sake of comparison, the corresponding profiles under PI control are also included (dashed lines). Clearly, the bounded nonlinear controller drives the controlled output to its new set-point value in a significantly shorter time than the one required by the PI controller (note that both controlled outputs exhibit the same overshoot). Note also the superior transient behavior of the closed-loop output under the bounded nonlinear controller compared to the oscillatory response obtained under PI control. For the same simulation run, the evolution of the closed-loop profile of the crystal size distribution is shown in Figure 11.6 (bottom plot.) An exponentially-decaying crystal size distribution is obtained at the steady-state.

Next, the robustness properties of the bounded nonlinear controller in the presence of parametric uncertainties were investigated, for a 0.4 increase in the value of the set-point. To ensure offsetless tracking in the presence of constant uncertainty in process parameters, the bounded nonlinear controller of Eq.11.31 was complemented with integral action (i.e., the term $v - \tilde{h}(\omega)$ was substituted by $v - y + \frac{1}{\tau_i'}\xi$, where $\dot{\xi} = v - y$, $\xi(0) = 0$ and τ_i' is the integral time constant). Figure 11.7 shows the closed-loop output (top plot), manipulated input (middle plot), and evolution of the crystal size distribution (bottom plot) profiles under the bounded nonlinear controller (solid lines) in the presence of 5% error in both F and τ. The corresponding output and input profiles under PI control are also included (dashed lines). We observe that the bounded nonlinear controller exhibits very good robustness properties, driving the output quickly to its new set-point.

Finally, we tested the robustness of the bounded nonlinear controller in the presence of unmodeled actuator and sensor dynamics. To account for the actuator and sensor dynamics, the process model of Eq.11.4 was augmented with the dynamical

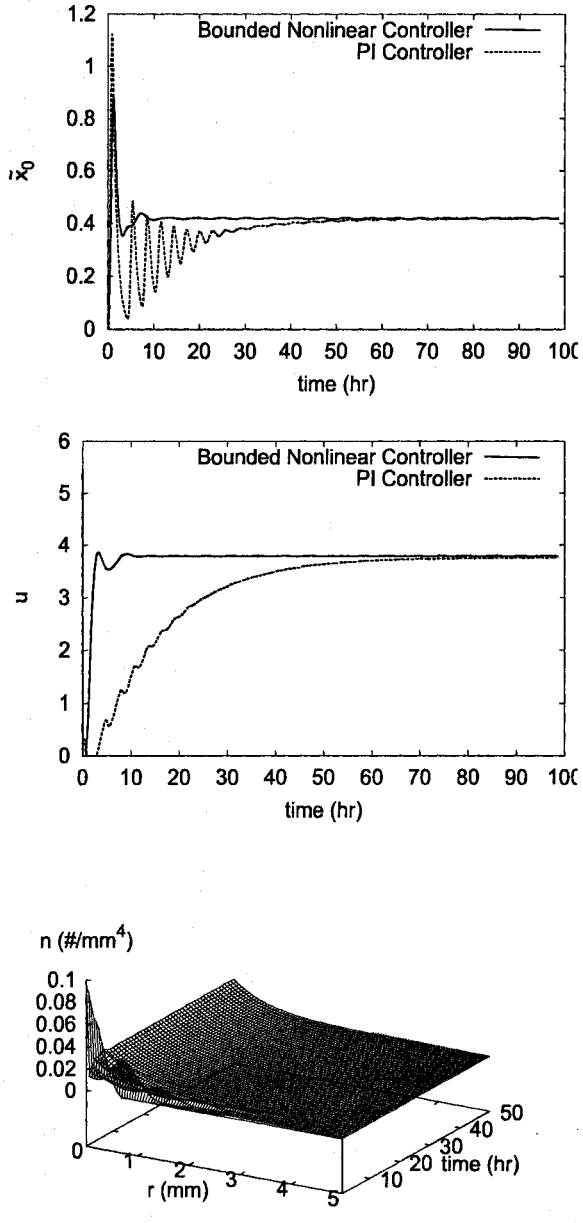

Figure 11.7: Controlled output, manipulated input, and crystal size distribution evolution profiles for the crystallizer process model of Eq.11.4 under the bounded nonlinear controller, for 0.4 increase in the set-point, in the presence of 5% modeling error in both F and τ, and $u \in [0, 6]$.

system $\epsilon_a \dot{z}_1 = -z_1 + z_2$, $\epsilon_a \dot{z}_2 = -z_2 + u$ and the dynamical system $\epsilon_s \dot{z}_3 = -z_3 + z_4$, $\epsilon_s \dot{z}_4 = -z_4 + y$, where $z_1, z_2 \in \mathbb{R}$ are the actuator states, $z_3, z_4 \in \mathbb{R}$ are the sensor states, z_1 is the actuator output, z_3 is the sensor output, and ϵ_a, ϵ_s are small parameters characterizing how fast the actuator and sensor dynamics are, respectively. In this case, the bounded nonlinear controller was also found to be robust with respect to unmodeled dynamics for $\epsilon_a = \epsilon_s = 0.05$. The corresponding closed-loop output (top plot), manipulated input (middle plot), and evolution of crystal size distribution (bottom plot) profiles are depicted in Figure 11.8.

11.8 Conclusions

In this chapter, we considered spatially-homogeneous particulate processes with input constraints and developed a rigorous and general methodology for the analysis and control of such processes. Initially, a model reduction procedure based on the method of weighted residuals was presented for the construction of finite-dimensional ODE systems that accurately reproduce the dynamics of the particulate process. These ODE systems were then used to identify the set of feasible control objectives (set-points) that can be achieved in the presence of constraints. This information, together with the derived ODE systems, was then used as the basis for the synthesis of practically-implementable nonlinear bounded output feedback controllers that enforce exponential stability in the closed-loop system and achieve particle size distributions with desired characteristics, in the presence of input constraints. Precise closed-loop stability conditions were given and controller implementation issues were addressed. The proposed methodology was successfully applied to a continuous crystallizer, which exhibits open-loop unstable (oscillatory) behavior, and shown to cope effectively with the problem of constraints.

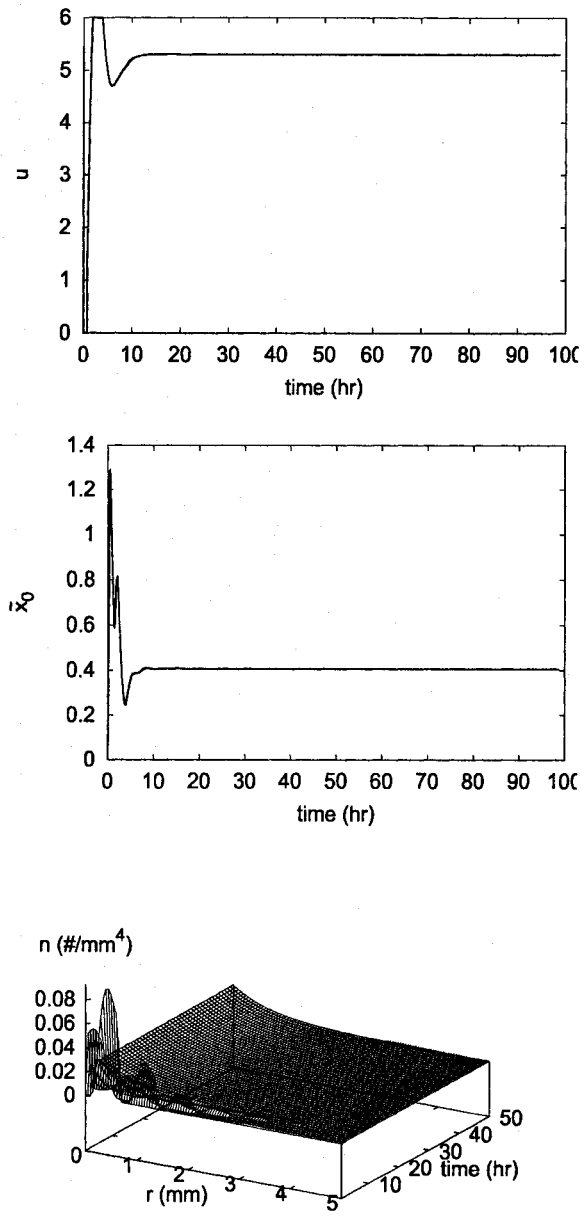

Figure 11.8: Controlled output, manipulated input, and crystal size distribution evolution profiles for the crystallizer process model of Eq.11.4 under the bounded nonlinear controller, for 0.4 increase in the set-point, in the presence of actuator and sensor unmodeled dynamics and $u \in [0, 6]$.

Chapter 12

Hybrid Control of Spatially Distributed Processes

12.1 Introduction

Processes that exhibit significant spatial variations owing to the underlying physical phenomena, such as diffusion, convection, and phase-dispersion, are ubiquitous among modern-day chemical processes essential in making important industrial products. Examples include the catalytic packed-bed reactors used to convert methanol to formaldehyde, the Czochralski crystallization of high-purity crystals and the chemical vapor deposition of thin films for microelectronics manufacturing, as well as the aerosol-based production of nanoparticles used in medical applications. For these processes, the distinguishing attribute of the control problem is that it involves the regulation of distributed variables using spatially-distributed control actuators and measurement sensors. Many of these systems are also naturally modeled by highly dissipative partial differential equation (PDE) systems, such as parabolic PDE systems (transport-reaction processes) whose spatial differential operators are characterized by an eigenspectrum that can be partitioned into a finite slow part and an infinite

stable fast complement [116], which implies that the dominant dynamics of these systems can be captured by finite-dimensional systems. The traditional approach to the control of parabolic PDEs involves the application of Galerkin's method to the PDE system to derive ODE systems that describe the dynamics of the dominant (slow) modes of the PDE system, which are subsequently used as the basis for the synthesis of finite-dimensional controllers (e.g., see [29, 255]). A potential drawback of this approach is that the number of modes that should be retained to derive an ODE system that yields the desired degree of accuracy may be very large, leading to complex controller design and high dimensionality of the resulting controllers.

These considerations have motivated significant recent work on the analysis and control of distributed process systems, bringing together concepts from the dynamics of infinite-dimensional systems, model reduction, and nonlinear control theory, and leading to the development of a general framework for the synthesis of low-order nonlinear controllers for broad classes of nonlinear distributed parameter systems that arise in the modeling of spatially-distributed processes, on the basis of ordinary differential equation (ODE) models obtained through combination of Galerkin's method with approximate inertial manifolds (see the book [61] for details and references). In addition to this work, other advances on control of distributed systems have been made, including, for example, distributed controller design using generalized invariants [233] and concepts from passivity and thermodynamics [8], the development of low-order control-relevant models for distributed systems [142], analysis and control of parabolic PDE systems with actuator saturation [88], reduced spatial order model reference adaptive control of distributed systems [38], and state observation and adaptive control of distributed chemical reactors [85].

While the above efforts have led to the development of a number of systematic

methods for distributed controller design, these methods focus exclusively on the classical control paradigm, where a fixed control structure (single feedback law, fixed actuator/sensor spatial arrangement) is used to achieve ceratin control objectives (see Figure 12.1(a)). There are many practical situations, however, where it is desirable, and sometimes even necessary, to consider a hybrid control paradigm, such as the one depicted in Figure 12.1(b), where the control system consists of a family of controller configurations (e.g., a family of feedback laws and/or a family of actuator/sensor spatial arrangements) together with a higher-level supervisor that uses logic to orchestrate switching between these control configurations. An example, where consideration of hybrid control is necessary, is the problem of coping with control actuator failure. In this case, upon the detection of a fault in the operating actuator configuration, it is often necessary to switch to an alternative, well-functioning actuator configuration, with a different spatial placement of the actuators, in order to preserve closed-loop stability. Switching between spatially-distributed actuators in this case provides a means for fault-tolerant control.

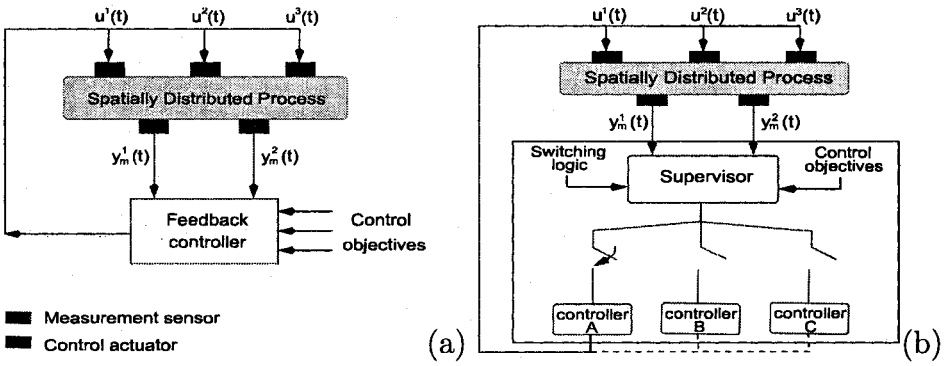

Figure 12.1: Comparison between the control structures arising in (a) the classical control, and (b) the hybrid control paradigms of spatially-distributed systems.

In other instances, switching between actuator configurations can be motivated by some additional performance objectives, such as the desire to optimize a given

performance criterion for the control system, or accommodate inherently competing control objectives that cannot be reconciled using a single configuration. For example, when the performance index associated with the control system penalizes the placement of control actuators at different spatial locations differently, the actuator configuration that minimizes this cost will provide the best performance. However, owing to the presence of actuator constraints, it may not be possible to use this actuator configuration (at least initially) especially if the desired initial condition is infeasible. This conflict can be resolved by considering a number of pre-determined, spatially-distributed actuator configurations and switching between them.

Due to the use of logic-based switching and the variable structure of the control system, the dynamics of the control system in the hybrid control paradigm are an intermix of discrete and continuous components. This is in contrast to the purely continuous dynamics in the classical control paradigm. Furthermore, whereas a fixed control structure can at best achieve a tradeoff between multiple control objectives in classical control, switching in hybrid control allows the accommodation and reconciliation of multiple, possibly conflicting, control objectives.

Motivated by the above considerations, we focus in this chapter on the problem of coupling feedback and switching in the control of spatially-distributed processes described by highly dissipative PDE systems with actuator constraints. The rest of the chapter is organized as follows. In Section 12.2, we present some mathematical preliminaries to characterize the class of spatially-distributed processes considered and formulate precisely the switching problem of interest. Then in Section 12.3, we initially use Galerkin's method to derive an ODE system that captures the dominant dynamics of the PDE system. This ODE system is then used as the basis for the integrated synthesis, via Lyapunov techniques, of stabilizing nonlinear feed-

back controllers together with stabilizing switching laws that orchestrate the switching between the admissible control actuator configurations, in a way that respects the actuator constraints, accommodates inherently conflicting control objectives, and guarantees closed-loop stability at the same time. Precise conditions that guarantee stability of the constrained closed-loop PDE system under switching are provided. Finally, in Section 12.4, we demonstrate, through numerical simulations, applications of the proposed methodology of coordinating feedback and switching to the problem of fault-tolerant, constrained stabilization of unstable steady-states of a typical diffusion-reaction process and a non-isothermal tubular reactor with recycle. The results of this chapter were first presented in [98].

12.2 Preliminaries

12.2.1 Class of spatially-distributed processes

In this chapter, we focus on spatially-distributed processes, described by highly dissipative (in a sense made precise in Assumption 12.1 below) infinite-dimensional systems. This class of systems arises often in the modeling of transport-reaction processes and various classes of fluid dynamic systems. To provide a precise specification of the control problem, we consider an important class of processes that fit this category, namely quasi-linear parabolic PDE systems of the form:

$$\begin{aligned} \frac{\partial \bar{x}}{\partial t} &= A\frac{\partial \bar{x}}{\partial z} + B\frac{\partial^2 \bar{x}}{\partial z^2} + w\sum_{i=1}^{m} b_i(z)u_i + f(\bar{x}) \\ y_{ci} &= \int_{\alpha}^{\beta} c^i(z)k\bar{x}(z,t)dz \qquad i = 1,\ldots,m \end{aligned} \tag{12.1}$$

subject to the boundary conditions:

$$\begin{aligned} C_1\bar{x}(\alpha,t) + D_1\frac{\partial \bar{x}}{\partial z}(\alpha,t) &= R_1 \\ C_2\bar{x}(\beta,t) + D_2\frac{\partial \bar{x}}{\partial z}(\beta,t) &= R_2 \end{aligned} \tag{12.2}$$

and the initial condition:

$$\bar{x}(z,0) = \bar{x}_0(z) \tag{12.3}$$

where $\bar{x}(z,t) = [\bar{x}_1(z,t) \cdots \bar{x}_n(z,t)]^T \in \mathbb{R}^n$ denotes the vector of state variables, $z \in [\alpha,\beta] \subset \mathbb{R}$ is the spatial coordinate, $t \in [0,\infty)$ is the time, $u_i \in [-u_{i,max}, u_{i,max}] \subset \mathbb{R}$ denotes the i-th constrained manipulated input, $y_{ci} \in \mathbb{R}$ denotes the i-th controlled output, $\frac{\partial \bar{x}}{\partial z}, \frac{\partial^2 \bar{x}}{\partial z^2}$ denote the first and second-order spatial derivatives of $\bar{x}$, respectively, $f(\bar{x})$ is a nonlinear vector function, w is a constant column vector, k is a constant row vector, A, B, C_1, D_1, C_2, D_2 are constant matrices, R_1, R_2 are column vectors, and $\bar{x}_0(z)$ is the initial condition. The function $b_i(z)$ is a known smooth function of z that describes how the control action, $u_i(t)$, is distributed in the finite interval $[\alpha,\beta]$ (actuator distribution function), and $c^i(z)$ is a known smooth function of z that is determined by the desired performance specifications in the interval $[\alpha,\beta]$. Whenever the control action enters the system at a single point, z_0, with $z_0 \in [\alpha,\beta]$ (i.e., point actuation), the function $b_i(z)$ is taken to be nonzero in a finite spatial interval of the form $[z_0-\mu, z_0+\mu]$, where μ is a small positive real number, and zero elsewhere in $[\alpha,\beta]$.

Throughout the chapter, the order of magnitude, $O(\epsilon)$, and Lie derivative notations will be used. In particular, $\delta(\epsilon) = O(\epsilon)$ if there exist positive real numbers k_1 and k_2 such that $|\delta(\epsilon)| \leq k_1|\epsilon| \quad \forall\ |\epsilon| \leq k_2$. $L_f\bar{h}$ denotes the standard Lie derivative of a scalar function, $\bar{h}(\cdot)$, with respect to the vector function $f(\cdot)$, $L_f^k\bar{h}$ denotes the k-th order Lie derivative and $L_gL_f^{k-1}\bar{h}$ denotes the mixed Lie derivative where $g(\cdot)$ is a vector function. Furthermore, the notation, $|\cdot|$, will be used to denote the

standard Euclidean norm, while the notation $|\cdot|_2$ and $\|\cdot\|_2$ will be used to denote the L_2-norms of vectors belonging in a finite-dimensional and an infinite-dimensional Hilbert spaces, respectively.

For a precise characterization of the class of PDE systems considered in this chapter, we formulate the system of Eqs.12.1-12.3 as an infinite-dimensional system in the Hilbert space $\mathcal{H}([\alpha,\beta];\mathbb{R}^n)$, with $\mathcal{H}$ being the space of sufficiently smooth n-dimensional vector functions defined on $[\alpha,\beta]$ that satisfy the boundary conditions of Eq.12.2, with inner product and norm:

$$(\omega_1,\omega_2)=\int_\alpha^\beta(\omega_1(z),\omega_2(z))_{\mathbb{R}^n}dz,\quad \|\omega_1\|_2=(\omega_1,\omega_1)^{\frac{1}{2}} \tag{12.4}$$

where ω_1,ω_2 are two elements of $\mathcal{H}([\alpha,\beta];\mathbb{R}^n)$ and the notation $(\cdot,\cdot)_{\mathbb{R}^n}$ denotes the standard inner product in $\mathbb{R}^n$. Defining the state function x on $\mathcal{H}([\alpha,\beta];\mathbb{R}^n)$ as:

$$x(t)=\bar{x}(z,t),\quad t>0,\quad z\in[\alpha,\beta], \tag{12.5}$$

the operator $\mathcal{A}$ in $\mathcal{H}([\alpha,\beta];\mathbb{R}^n)$ as:

$$\begin{aligned}\mathcal{A}x &= A\frac{\partial\bar{x}}{\partial z}+B\frac{\partial^2\bar{x}}{\partial z^2},\\ x\in D(\mathcal{A}) &= \Big\{x\in\mathcal{H}([\alpha,\beta];\mathbb{R}^n): C_1\bar{x}(\alpha,t)+D_1\frac{\partial\bar{x}}{\partial z}(\alpha,t)=R_1,\\ &\qquad C_2\bar{x}(\beta,t)+D_2\frac{\partial\bar{x}}{\partial z}(\beta,t)=R_2\Big\}\end{aligned}$$

and the input and controlled output operators as:

$$\mathcal{B}u=w\sum_{i=1}^m b_iu_i,\quad \mathcal{C}x=(c,kx) \tag{12.6}$$

the system of Eqs.12.1-12.3 takes the form:

$$\begin{aligned}\dot{x} &= \mathcal{A}x+\mathcal{B}u+f(x),\quad x(0)=x_0\\ y_c &= \mathcal{C}x\end{aligned} \tag{12.7}$$

where $f(x(t)) = f(\bar{x}(z,t))$ and $x_0 = \bar{x}_0(z)$. We assume that the nonlinear terms $f(x)$ are locally Lipschitz with respect to their arguments and satisfy $f(0) = 0$. For $\mathcal{A}$, the eigenvalue problem is defined as:

$$\mathcal{A}\phi_j = \lambda_j \phi_j, \quad j = 1, \ldots, \infty \tag{12.8}$$

where λ_j denotes an eigenvalue and ϕ_j denotes an eigenfunction. The eigenspectrum of $\mathcal{A}$, $\sigma(\mathcal{A})$, is defined as the set of all eigenvalues of $\mathcal{A}$, i.e., $\sigma(\mathcal{A}) = \{\lambda_1, \lambda_2, \ldots\}$. Assumption 12.1 that follows states that the eigenspectrum of $\mathcal{A}$ can be partitioned into a finite part consisting of m slow eigenvalues and a stable infinite complement containing the remaining fast eigenvalues, and that the separation between the slow and fast eigenvalues of $\mathcal{A}$ is large.

Assumption 12.1 *1. $Re\ \{\lambda_1\} \geq Re\ \{\lambda_2\} \geq \cdots \geq Re\ \{\lambda_j\} \geq \cdots$, where $Re\ \{\lambda_j\}$ denotes the real part of λ_j.*

2. $\sigma(\mathcal{A})$ can be partitioned as $\sigma(\mathcal{A}) = \sigma_1(\mathcal{A}) + \sigma_2(\mathcal{A})$, where $\sigma_1(\mathcal{A})$ consists of the first m (with m finite) eigenvalues, i.e., $\sigma_1(\mathcal{A}) = \{\lambda_1, \ldots, \lambda_m\}$, and $\dfrac{|Re\ \{\lambda_1\}|}{|Re\ \{\lambda_m\}|} = O(1)$.

3. $Re\ \{\lambda_{m+1}\} < 0$ and $\dfrac{|Re\ \{\lambda_m\}|}{|Re\ \{\lambda_{m+1}\}|} = O(\epsilon)$ where $\epsilon < 1$ is a small positive number.

The assumption of finite number of unstable eigenvalues is always satisfied for parabolic PDE systems [116], while the assumption of discrete eigenspectrum and the assumption of existence of only a few dominant modes that describe the dynamics of the parabolic PDE system are usually satisfied by the majority of diffusion-convection-reaction processes (see the examples in Section 12.4).

12.2.2 Problem formulation and solution overview

Consider the spatially-distributed process of Eqs.12.1-12.3 and assume that N (where N is finite) spatially-distinct control actuator configurations are available (installed)

for feedback control purposes. Each configuration is characterized by: (1) a unique spatial arrangement of the actuators, $\bar{z}^k,\ k = 1, \cdots, N$, where $\bar{z}^k$ is an m-dimensional vector whose components represent the corresponding spatial locations of the actuators associated with the k-th control actuator configuration, and (2) hard actuator constraints, $-u^k_{i,max} \leq u^k_i \leq u^k_{i,max}$. The superscript k in $\bar{z}^k$ is a discrete index that denotes which of the N actuator configurations is active at any given time. Only one configuration can be engaged for control at any time instance and, to ensure controllability of the system, we allow only a finite number of configuration switchings over any finite time-interval. The problem under consideration is how to coordinate switching between the N different control actuator configurations in a way that respects actuator constraints and guarantees closed-loop stability. To address this problem, we formulate the following three objectives:

1. Initially, a model reduction scheme based on Galerkin's method is used to derive a nonlinear finite-dimensional system that accurately reproduces the solutions and dynamics of the system of Eq.12.7

2. Next, the finite-dimensional approximation is used as the basis for the synthesis, via Lyapunov-based control techniques, of bounded nonlinear feedback controllers of the general form:

$$u^k \ = \ p(x_s, \bar{v}, u^k_{max}, \bar{z}^k) \tag{12.9}$$

that enforce asymptotic stability and reference-input tracking in the constrained closed-loop system and provide an explicit characterization of the constrained stability region, associated with each control actuator configuration. Referring to Eq.12.9, $p(\cdot)$ is a bounded nonlinear vector function (i.e.. $|u^k| \leq u^k_{max}$, where $|\cdot|$ is the standard Euclidean norm and u^k_{max} is the maximum norm of the

vector of manipulated inputs allowed by the constraints associated with the k-th actuator configuration), x_s is the vector of slow states, and $\bar{v}$ is a generalized reference input (which is assumed to be a smooth function of time).

3. Finally, a set of switching rules is derived to orchestrate the transition between the available control actuator configurations, and an upper bound on the separation between the slow and fast eigenvalues – which guarantees stability of the switched infinite-dimensional closed-loop system – is computed. The switching laws determine which actuator configuration can be activated at a given moment, i.e., the value of the index k:

$$k(t) \;=\; \phi(x_s(t), t) \tag{12.10}$$

which can be viewed as a piecewise-constant function of time that depends on the slow states.

12.3 Hybrid control of spatially-distributed processes

12.3.1 Galerkin's method

In this section, we apply standard Galerkin's method to the system of Eq.12.7 to derive an approximate finite-dimensional system. Let $\mathcal{H}_s$, $\mathcal{H}_f$ be modal subspaces of $\mathcal{A}$, defined as $\mathcal{H}_s = span\{\phi_1, \phi_2, \ldots, \phi_m\}$ and $\mathcal{H}_f = span\{\phi_{m+1}, \phi_{m+2}, \ldots\}$ (the existence of $\mathcal{H}_s$, $\mathcal{H}_f$ follows from Assumption 12.1). Defining the orthogonal projection operators, P_s and P_f, such that $x_s = P_s x$, $x_f = P_f x$, the state, x, of the system of Eq.12.7 can be decomposed as:

$$x \;=\; x_s + x_f = P_s x + P_f x \tag{12.11}$$

Applying P_s and P_f to the system of Eq.12.7 and using the above decomposition for x, the system of Eq.12.7 can be equivalently written in the following form:

$$\begin{aligned} \frac{dx_s}{dt} &= \mathcal{A}_s x_s + \mathcal{B}_s u + f_s(x_s, x_f) \\ \frac{\partial x_f}{\partial t} &= \mathcal{A}_f x_f + \mathcal{B}_f u + f_f(x_s, x_f) \\ y_c &= \mathcal{C} x_s + \mathcal{C} x_f \\ x_s(0) &= P_s x(0) = P_s x_0, \quad x_f(0) = P_f x(0) = P_f x_0 \end{aligned} \tag{12.12}$$

where $\mathcal{A}_s = P_s\mathcal{A}$, $\mathcal{B}_s = P_s\mathcal{B}$, $f_s = P_s f$, $\mathcal{A}_f = P_f\mathcal{A}$, $\mathcal{B}_f = P_f\mathcal{B}$ and $f_f = P_f f$ and the partial derivative notation in $\frac{\partial x_f}{\partial t}$ is used to denote that the state x_f belongs in an infinite-dimensional space. In the above system, $\mathcal{A}_s$ is a diagonal matrix of dimension $m \times m$ of the form $\mathcal{A}_s = diag\{\lambda_j\}$, $f_s(x_s, x_f)$ and $f_f(x_s, x_f)$ are Lipschitz vector functions, and $\mathcal{A}_f$ is an unbounded differential operator which is exponentially stable (following from Part 3 of Assumption 12.1 and the selection of $\mathcal{H}_s, \mathcal{H}_f$). Neglecting the fast and stable infinite-dimensional x_f-subsystem in the system of Eq.12.12, the following m-dimensional slow system is obtained:

$$\begin{aligned} \frac{d\bar{x}_s}{dt} &= \mathcal{A}_s \bar{x}_s + \mathcal{B}_s u + f_s(\bar{x}_s, 0) \\ \bar{y}_c &= \mathcal{C} \bar{x}_s \end{aligned} \tag{12.13}$$

where the bar symbol in $\bar{x}_s$, $\bar{y}_c$ denotes that these variables are associated with a finite-dimensional system.

Remark 12.1 We note that the above model reduction procedure which led to the approximate ODE system of Eq.12.13 can also be used when empirical eigenfunctions of the system of Eq.12.7, computed through Karhunen-Loeve (KL) expansion, are used as basis functions in $\mathcal{H}_s$ and $\mathcal{H}_f$ instead of the eigenfunctions of $\mathcal{A}$. For approaches on how to compute empirical eigenfunctions through KL expansion, the reader is referred to [23].

Remark 12.2 Although standard Galerkin's method was used to obtain the finite-dimensional system of Eq.12.13, the results of this chapter can be generalized to the case where the finite-dimensional approximation of the system of Eq.12.7 is obtained through combination of Galerkin's method with approximate inertial manifolds [61]. This approach can be used to further reduce the dimension of the system of Eq.12.13 and ensure that it is of an appropriately low order suitable for controller design and analysis.

12.3.2 Coordinating feedback and switching

Having obtained a finite-dimensional model that describes the dominant dynamics of the infinite-dimensional system, we proceed in this section to describe the proposed procedure for designing the hybrid control system. To this end, we consider the equivalent representation of the slow system of Eq.12.13 in terms of the evolution of the amplitudes of the eigenmodes. This ODE system is given by:

$$\begin{aligned} \dot{a}_s(t) &= Fa_s(t) + G(\bar{z}^k)u^k(t) + d(a_s(t)) \\ \tilde{y}_c(t) &= Ca_s(t) \end{aligned} \tag{12.14}$$

where $a_s(t) = [a_1(t) \cdots a_m(t)]^T \in \mathbb{R}^m$, $a_i(t)$ is the amplitude of the i-th eigenmode, $\bar{x}_s(t) = \sum_{j=1}^{m} a_j(t)\phi_j$, $(\bar{x}_s(t), \phi_j) = a_j(t)(\phi_j, \phi_j)$, F is an $m \times m$ diagonal matrix of the form $F = diag\{\lambda_j\}$, G is an $m \times m$ matrix whose (i,j)-th element is given by $G_{ij} = \phi_i(z_j)$, $\bar{z}^k = [z_1^k \; z_2^k \; \cdots \; z_m^k]^T$, $d(\cdot) = [d_1(\cdot) \cdots d_m(\cdot)]^T$ is a vector function and $(f_s(\cdot), \phi_j) = d_j(\cdot)(\phi_j, \phi_j)$, $\tilde{y}_c(t) = [\tilde{y}_{c,1}(t) \cdots \tilde{y}_{c,m}(t)]^T \in \mathbb{R}^m$, $\tilde{y}_{c,i}$ is the i-th controlled output of the finite-dimensional slow system, C is a constant $m \times m$ matrix. Referring to the system of Eq.12.14, we define the relative order of the output $\tilde{y}_{ci}$ with respect to the vector of manipulated inputs, u, as the smallest integer r_i for which:

$$\left[L_{\tilde{g}_1} L_{\tilde{f}}^{r_i - 1} \tilde{h}_i(a_s) \; \cdots \; L_{\tilde{g}_m} L_{\tilde{f}}^{r_i - 1} \tilde{h}_i(a_s)\right] \not\equiv [0 \; \cdots \; 0] \tag{12.15}$$

where $\tilde{g}_i$ is the i-th column of the matrix G, $\tilde{f}(a_s) = Fa_s + d(a_s)$, and $\tilde{y}_{ci} = \tilde{h}_i(a_s)$ is the i-th component of the vector Ca_s, or $r_i = \infty$ if such an integer does not exist. We also define the characteristic matrix:

$$\bar{C}(a_s) = \begin{bmatrix} L_{\tilde{g}_1} L_{\tilde{f}}^{r_1-1} \tilde{h}_1(a_s) & \cdots & L_{\tilde{g}_m} L_{\tilde{f}}^{r_1-1} \tilde{h}_1(a_s) \\ L_{\tilde{g}_1} L_{\tilde{f}}^{r_2-1} \tilde{h}_2(a_s) & \cdots & L_{\tilde{g}_m} L_{\tilde{f}}^{r_2-1} \tilde{h}_2(a_s) \\ \vdots & \cdots & \vdots \\ L_{\tilde{g}_1} L_{\tilde{f}}^{r_m-1} \tilde{h}_m(a_s) & \cdots & L_{\tilde{g}_m} L_{\tilde{f}}^{r_m-1} \tilde{h}_m(a_s) \end{bmatrix} \tag{12.16}$$

which, to simplify our development, is assumed to be nonsingular uniformly in a_s. This assumption can be relaxed if dynamic state feedback is used instead of static state feedback (see [148] for details). To proceed with controller synthesis, and under the assumption that the relative degree is well-defined, we initially transform the system of Eq.12.14, by means of an invertible coordinate change of the form $a_s = T^{-1}(\zeta, \eta)$, into the following partially linear form:

$$\begin{aligned} \dot{\zeta}_1^{(i)} &= \zeta_2^{(i)} \\ &\vdots \\ \dot{\zeta}_{r_i-1}^{(i)} &= \zeta_{r_i}^{(i)} \\ \dot{\zeta}_{r_i}^{(i)} &= L_{\tilde{f}}^{r_i} \tilde{h}_i(a_s) + \sum_{j=1}^{m} L_{\tilde{g}_j} L_{\tilde{f}}^{r_i-1} \tilde{h}_i(a_s) u_j^k \\ \dot{\eta}_1 &= \Psi_1(\zeta, \eta) \\ &\vdots \\ \dot{\eta}_{m-\sum_i r_i} &= \Psi_{m-\sum_i r_i}(\zeta, \eta) \\ \tilde{y}_{ci} &= \zeta_1^{(i)}, \quad i = 1, \ldots, m, \quad k = 1, \cdots, N \end{aligned} \tag{12.17}$$

where $\zeta_j^{(i)} = L_{\tilde{f}}^{j-1} \tilde{h}_i(a_s)$, $\zeta = [\zeta^{(1)^T} \ \cdots \ \zeta^{(m)^T}]^T$, $\eta = [\eta_1 \ \cdots \ \eta_{m-\sum_i r_i}]^T$. Defining the tracking error variables, $e_k^{(i)} = \zeta_k^{(i)} - v_i^{(k-1)}$, and introducing the vector notation $e^{(i)} = [e_1^{(i)} \ e_2^{(i)} \ \cdots \ e_{r_i}^{(i)}]^T$, $e = [e^{(1)^T} \ e^{(2)^T} \ \cdots \ e^{(m)^T}]^T$, where $i = 1, \cdots, m$, $j = 1, \cdots, r_i$, the system of Eq.12.17 can be cast in the following more compact form:

$$\begin{aligned} \dot{e} &= \Lambda e + \Gamma \left[l(e, \eta, \bar{v}) + \bar{C}(e, \eta, \bar{v}) u^k \right] \\ \dot{\eta} &= \Psi(e, \eta, \bar{v}) \end{aligned} \tag{12.18}$$

where $\Lambda = diag\{\Lambda_i\}$ is an $(\sum_{r_i} \times \sum_{r_i})$ block diagonal constant matrix whose constituent blocks are $r_i \times r_i$ matrices of the form:

$$\Lambda_i = \begin{bmatrix} 0 & 1 & 0 & \cdots & 0 \\ 0 & 0 & 1 & \cdots & 0 \\ \vdots & \vdots & \vdots & \ddots & \vdots \\ 0 & 0 & 0 & \cdots & 1 \\ 0 & 0 & 0 & \cdots & 0 \end{bmatrix} \tag{12.19}$$

Γ is an $(\sum_{r_i} \times m)$ constant matrix, $l(\cdot)$ is a $(\sum_{r_i} \times 1)$ smooth vector function. The specific forms of Γ and $l(\cdot)$ are omitted for brevity. Finally, we define $\bar{f}(e, \eta, \bar{v}) = \Lambda e + \Gamma l(e, \eta, \bar{v})$ and denote by $\bar{g}_i$ the i-th column of the matrix $\bar{G} = \Gamma \bar{C}$.

Assumption 12.2 *The η-subsystem of Eq.12.18 is input-to-state stable with respect to e, uniformly in $\bar{v}$, and locally exponentially stable when $e = 0$.*

We are now ready to state the main result of this chapter. Theorem 12.1 below provides both the state feedback control law (see the discussion in Remark 12.11 and the example in Section 12.4 for output feedback controller design and implementation) as well as the necessary switching laws, and states precise conditions that guarantee closed-loop stability and asymptotic reference-input tracking in the switched closed-loop system. The proof is given in Appendix I.

Theorem 12.1

1. *Consider the system of Eq.12.14, in the transformed form of Eq.12.18, for which Assumption 12.2 holds, under the feedback control law:*

$$u^k = -r(a_s, u^k_{max}, \bar{z}^k) \left(L_{\bar{g}} V\right)^T (\bar{z}^k) \tag{12.20}$$

where

$$r(a_s, u^k_{max}, \bar{z}^k) = \frac{L^*_{\bar{f}} V + \sqrt{(L^*_{\bar{f}} V)^2 + (u^k_{max} |(L_{\bar{g}} V)^T (\bar{z}^k)|)^4}}{|(L_{\bar{g}} V)^T (\bar{z}^k)|^2 \left[1 + \sqrt{1 + (u^k_{max} |(L_{\bar{g}} V)^T (\bar{z}^k)|)^2}\right]} \tag{12.21}$$

$\bar{z}^k = [z_1^k \; z_2^k \; \cdots \; z_m^k]^T$, $k = 1, \cdots, N$, $L_{\bar{f}}^* V = L_{\bar{f}} V + \rho|e|^2$, $\rho > 0$, $L_{\bar{g}} V$ *is a row vector of the form* $[L_{\bar{g}_1} V \cdots L_{\bar{g}_m} V]$, $V = e^T \Phi e$, Φ *is a positive definite matrix that satisfies the Riccati inequality* $\Lambda^T \Phi + \Phi \Lambda - \Phi \Gamma \Gamma^T \Phi < 0$. *Let* δ_s^k *be a positive real number such that the compact set* $\Omega(u_{max}^k, \bar{z}^k) = \{a_s \in \mathbb{R}^m : a_s^T \Phi a_s \leq \delta_s^k\}$ *is the largest invariant set embedded within the region described by the following inequality:*

$$L_{\bar{f}}^* V \;\; \leq \;\; u_{max}^k |(L_{\bar{g}} V)^T (\bar{z}^k)| \tag{12.22}$$

Without loss of generality, assume that $\bar{z}^{k(0)} = \bar{z}^1$ *and* $a_s(0) \in \Omega(u_{max}^1, \bar{z}^1)$. *If, at any given time,* T, *the condition:*

$$a_s(T) \;\; \in \;\; \Omega(u_{max}^j, \bar{z}^j) \tag{12.23}$$

holds, for some $j \in \{1, \cdots, N\}$, *then setting* $\bar{z}^{k(t)} = \bar{z}^j$ *for all* $t > T$ *guarantees that the origin of the switched closed-loop system is asymptotically stable.*

2. *Consider the parabolic PDE system of Eq.12.1 under the control law of Eqs.12.20-12.21 and the switching law of Eq.12.23. Let* $\Theta_s^1 := \{x_s(0) \in \mathcal{H}_s : |x_s(0)|_2 \leq \bar{\delta}_s^1\}$ *be the set of all* $x_s(0)$ *for which* $a_s^T(0) \Phi a_s^T(0) \leq \delta_s^1$. *Then given any pair of positive real numbers* $(d, \bar{\delta}_b^1)$ *such that* $\bar{\delta}_b^1 + d \leq \bar{\delta}_s^1$, *and given any positive real number* δ_f, *there exists* $\epsilon^* > 0$ *such that if* $\epsilon \in (0, \epsilon^*]$, $|x_s(0)|_2 \leq \bar{\delta}_b^1$, $\|x_f(0)\|_2 \leq \delta_f$:
   (1) The origin of the infinite-dimensional closed-loop system is asymptotically (and locally exponentially) stable.
   (2) The outputs of the closed-loop system satisfy a relation of the form:

$$\limsup_{t \to \infty} |y_c^i(t) - v_i(t)| \;\; = \;\; O(\epsilon), \;\; i = 1, \cdots, m \tag{12.24}$$

Remark 12.3 Owing to the dependence of the input operator, $\mathcal{B}_s$, in Eq.12.13 on the spatial locations of the control actuators (through the actuator distribution functions $b_i(z)$), the inequality of Eq.12.22 is parameterized by the actuator locations and can therefore be used to explicitly identify the admissible control actuator configurations $(\bar{z}^k)$ for which stability of the constrained closed-loop system is guaranteed under

constraints. For a given actuator configuration (fixed u^k_{max} and $\bar{z}^k$), the inequality of Eq.12.22 describes a region of the state-space where the control action satisfies the constraints and the time-derivative of the Lyapunov function is negative-definite, along the trajectories of the finite-dimensional closed-loop slow system. Therefore, by computing an invariant set, $\Omega(u^k_{max}, \bar{z}^k)$, (preferably the largest) within this region, we obtain an estimate of the stability region associated with each control actuator configuration (see chapter 4 in [170] and [91] for how to compute this estimate). The requirement that the set $\Omega(u^k_{max}, \bar{z}^k)$ be invariant is needed to ensure that the closed-loop trajectories do not leave the region described by Eq.12.22 under a given actuator configuration.

Remark 12.4 Due to the large separation between the slow and fast eigenvalues of the spatial differential operator of the PDE system of Eq.12.1, the characterization (or estimate) of the constrained stability region obtained for the approximate, finite-dimensional closed-loop slow subsystem remains practically preserved for the slow subsystem in the infinite-dimensional closed-loop system, in the sense that given any initial slow state that belongs to any compact subset of $\Omega(u^k_{max}, \bar{z}^k)$, and given any initial fast state, there always exists ϵ sufficiently small such that the controller of Eqs.12.20-12.21 continues to enforce stability and reference-input tracking in the constrained infinite-dimensional closed-loop system. In the asymptotic limit (as $\epsilon \rightarrow 0$), the stability region of the slow subsystem is fully recovered. It should be noted here that this result is fundamentally different from its counter part in the linear case [96] where the stability region of the closed-loop slow subsystem is exactly preserved (i.e. the slow stability region is the same for the finite- and infinite-dimensional closed-loop systems) due to the fact that the evolution of the slow subsystem in the linear case is completely independent of the fast subsystem. As discussed in [96], this decoupling property is a consequence of: (1) the absence of the nonlinear terms, $f_s(x_s, x_f), f_f(x_s, x_f)$ (see Eq.12.12) which introduce an interconnection between the two subsystems, and (2) the fact that the control input is only a function of the slow states.

Remark 12.5 The switching law of Eq.12.23 orchestrates the transition between the N actuator configurations in a way that respects their constraints and guards against any potential instability that may arise due to switching. The basic problem here owes to the limitations imposed by constraints on the set of feasible initial conditions that can be used, for a given actuator configuration, to stabilize the closed-loop system. Different actuator configurations possess different stability regions and, depending on where the state is at a given moment in time, a switch from one configuration to another may land the state outside the stability region of the target configuration, thus leading to instability. To guard against this possibility, the switching law of Eq.12.23 monitors the evolution of the slow state in time (fast states can be neglected since ϵ is sufficiently small) and allows switching to take place only when the state is within the stability region of the desired actuator configuration. This condition determines, implicitly, the earliest time for which switching is safe.

Remark 12.6 The results of Theorem 12.1 can be useful for dealing with a variety of distributed control problems. One example is the problem of actuator failure. In this case, it is often necessary to switch from the failed actuator configuration to an alternative, well-functioning configuration that may already be installed on the process, in order to preserve closed-loop stability. The switching scheme of Theorem 12.1 can be used in this case to determine when the switching can take place and which of the alternative actuator configurations can be used (see Sections 12.4 for simulation examples). Note, however, that in other control problems switching may not be needed to maintain closed-loop stability, but is motivated rather by the desire to achieve some higher objective, such as the desire to optimize a given performance criterion for the control system or to accommodate conflicting control objectives that cannot be reconciled using a single control actuator configuration. For example, when the performance index associated with the control system includes penalty on the actuator location, the actuator configuration (or locations) that minimizes this cost provides the best performance. However, owing to the presence of different constraints for actuators placed at different locations, it may not be possible to use this actuator

configuration if the desired initial condition lies outside its stability region. To resolve this conflict, one may initially use another actuator configuration, for which the initial condition is admissible, and later switch to the desired configuration that provides the better performance when the state of the system enters its stability region.

Remark 12.7 Note that it is possible for more than one control actuator configuration ($\bar{z}^k$) to satisfy the switching rule given in Eq.12.23 at a given time. This can happen when the slow state lies in the intersection of several stability regions. In this case, Theorem 12.1 only guarantees that a switch from the current configuration to any of these configurations is safe, as far as closed-loop stability is concerned. The decision to select a particular configuration should then be made on the basis of some other objective as discussed in Remark 12.6. For example, in the event that the operating actuator fails and it becomes necessary to switch to some backup configuration, then if more than one backup configuration is feasible, one might choose the one that utilizes the smallest control effort or minimizes some other performance criterion (see Section 12.4.2 for an example) in order to minimize any performance losses resulting from the failure of the primary actuator configuration. In Theorem 12.1, however, the selection of the N actuator configurations is assumed to be pre-determined and not necessarily based on any optimality criteria. For some results on the problem of optimal placement of control actuators and measurement sensors for distributed systems, the reader is referred to [82, 16, 18].

Remark 12.8 Owing to the spatially-distributed nature of the control problem, the switching scheme proposed in this chapter is conceptually different from the classical switching schemes studied in the context of hybrid controller design for lumped-parameter systems. For lumped systems, the idea is to achieve the specified control objectives by switching between members of an a priori specified family of feedback functions, whereas the switching scheme presented here seeks to achieve the desired control objectives by switching between members of an a priori specified family of control actuator configurations (or locations), using the same feedback function (pa-

rameterized by $\bar{z}^k$). For each actuator configuration, the temporal evolution of the state is governed by a different set of differential equations which define a particular mode. The closed-loop system can therefore be viewed as multi-modal even though the unforced dynamics themselves are not hybrid in nature. The area of switched and hybrid controller design for lumped-parameter systems is currently an active area of research (see, for example, [37, 203, 95] and the references therein for some results in this area).

Remark 12.9 The control law of Eqs.12.20-12.21 involves a modification of the controller design originally proposed in [204], by including the term $-\rho|e|^2$ which is made to ensure that the control law enforces exponential stability in the closed-loop PDE system (see the proof of Theorem 12.1 in Appendix I). With $\rho = 0$, it can be shown that the control law of Eqs.12.20-12.21 enforces only asymptotic closed-loop stability. It is therefore preferable to set $\rho > 0$ and achieve exponential stability because of its robustness to bounded perturbations, which are always present in most practical applications [30]. We also note that even though a single (common) Lyapunov function is used to design the controller and characterize the stability region for all actuator configurations, it is possible to employ multiple Lyapunov functions (one for each configuration) instead, to achieve greater flexibility in switching (e.g., larger stability regions). In this case, however, additional switching rules, that impose restrictions on the growth of each Lyapunov function at transition times, are needed to ensure closed-loop stability (see [93] for further details on this issue).

Remark 12.10 Referring to the practical applications of the result of Theorem 12.1, one must initially identify the candidate control actuator configurations to be used. A single quadratic Lyapunov function is then used to: (1) synthesize, via Eqs.12.20-12.21, the necessary bounded nonlinear controller, and (2) construct, with the aid of Eq.12.22, the region of guaranteed closed-loop stability, $\Omega(u^k_{max}, \bar{z}^k)$, associated with each actuator configuration, on the basis of the finite-dimensional model that captures the dominant dynamics of the distributed system. Once this is done, one can proceed

with the implementation of the control strategy by initializing the closed-loop system within the stability region of the desired initial actuator configuration and implementing the feedback controller using this configuration. Then, the switching law of Eq.12.23 is checked on-line to determine if it is possible to switch to another actuator configuration at any given time. If the condition is satisfied for some configuration, then this configuration can be safely activated. Otherwise, the current actuator configuration remains active. Note that when switching is necessitated by the failure of the operating actuator, then if none of the backup configurations is feasible at failure time (due to tight constraints), then a process shutdown may be unavoidable. This possibility can be minimized by increasing the number of backup actuators and their capacities.

Remark 12.11 The nonlinear controller of Eqs.12.20-12.21 was derived under the assumption that measurements of the state variables, $\bar{x}(z,t)$, are available at all positions and times. From a practical point of view, measurements of the state variables are available only at a finite number of spatial positions, while in addition, there are many applications where measurements of state variables cannot be obtained on-line. To deal with this problem, an output feedback controller that uses only measurements of the outputs, y_m, can be constructed under the assumption that the number of measurements is equal to the number of slow modes and that the inverse of the measurement operator $\mathcal{S}$ exists, so that $\hat{x}_s = \mathcal{S}^{-1} y_m$ where $\hat{x}_s$ is the estimate of the slow state and y_m is the measured output. The invertibility of the measurement operator can be ensured by appropriate choice of the location of the measurement sensors. The synthesis of the output feedback controller can be carried out by combining the state feedback controller of Eqs.12.20-12.21 with a procedure proposed in [61] for obtaining estimates for the states of the approximate ODE model of Eq.12.13 from the measurements (see Section 10.3.2 in Chapter 10) . While the estimation error leads to some loss in the size of the stability region obtained under state feedback, this loss can be made small by increasing the order of the ODE approximation and including more measurements. This approach allows us to asymptotically (as $\epsilon \rightarrow 0$) recover

the stability region associated with each control actuator configuration.

Remark 12.12 An a priori estimate of the minimum necessary separation between the slow and fast eigenvalues (i.e., a value for ϵ^*) can, in principle, be extracted from the stability proof via singular perturbation techniques. However, as is the case with most singular perturbation techniques, this estimate is typically conservative and therefore it is useful to check its appropriateness through computer simulations. To this end, an initial value for m (the number of slow eigenmodes) is chosen by the user (thus fixing the value of ϵ) and Galerkin's method is applied to derive a finite-dimensional ODE system that describes the dynamics of these m slow modes, which is then used to design the feedback and switching laws of Theorem 12.1 which, in turn, are applied to the parabolic PDE system. Closed-loop stability is then checked through computer simulations and, if not achieved, the initial choice for m is revised, by including more slow eigenvalues and increasing the order of the ODE approximation.

12.4 Simulation studies

12.4.1 Application to a diffusion-reaction process

In this section, we illustrate through computer simulations how the concept of coupling feedback and switching, proposed in Theorem 12.1, can be used to deal with the problem of control actuator failure in control of a diffusion-reaction process. To this end, consider a long, thin rod in a reactor. The reactor is fed with pure species A and a zeroth order exothermic catalytic reaction of the form $A \rightarrow B$ takes place on the rod. Since the reaction is exothermic, a cooling medium in contact with the rod is used for cooling. Under standard assumptions, the spatiotemporal evolution of the

dimensionless rod temperature is described by the following parabolic PDE:

$$\frac{\partial \bar{x}}{\partial t} = \frac{\partial^2 \bar{x}}{\partial z^2} + \beta_T e^{-\frac{\gamma}{1+\bar{x}}} + \beta_U (b(z)u(t) - \bar{x}) - \beta_T e^{-\gamma}$$

subject to the boundary and initial conditions:

$$\bar{x}(0,t) = 0, \quad \bar{x}(\pi,t) = 0, \quad \bar{x}(z,0) = \bar{x}_0(z) \tag{12.25}$$

where $\bar{x}$ denotes the dimensionless temperature in the reactor, β_T denotes a dimensionless heat of reaction, γ denotes a dimensionless activation energy, β_U denotes a dimensionless heat transfer coefficient, $u(t)$ denotes the vector of manipulated inputs and $b(z)$ the vector of the corresponding actuator locations. The following typical values are given to the process parameters: $\beta_T = 50.0$, $\beta_U = 2.0$, $\gamma = 4.0$.

For the above values, it was verified that the operating steady-state, $\bar{x}(z,t) = 0$, is an unstable one. The control objective therefore is to stabilize the rod temperature profile at this unstable steady-state by manipulating the temperature of the cooling medium, subject to hard constraints on the manipulated input. To achieve this objective, the controlled output is defined as:

$$y_c(t) = \int_0^\pi \sqrt{\frac{2}{\pi}} sin(z) x(z,t) dz \tag{12.26}$$

The eigenvalue problem for the spatial differential operator of the process can be solved analytically and its solution is:

$$\lambda_j = -j^2, \quad \phi_j(z) = \sqrt{\frac{2}{\pi}} sin(j\ z), \quad j = 1, \ldots, \infty \tag{12.27}$$

For this system, we consider the first eigenvalue as the dominant one and use standard Galerkin's method to derive an ODE that describes the temporal evolution of the amplitude, $a_1(t)$, of the first eigenmode, where $x_s(t) = a_1(t)\phi_1(z)$. This ODE is used for the synthesis of the controller, using Eqs.12.20-12.21, which is then implemented

on a 30-th order Galerkin discretization of the parabolic PDE system (higher order discretizations led to identical results).

In order to demonstrate the utility of the switching scheme, we consider the following two problems where switching is needed to preserve closed-loop stability. In the first problem, two point control actuators, A and B, placed at two different locations, $z_A = 0.5\pi$ and $z_B = 0.12\pi$, respectively, are assumed to be available for stabilization. Both actuators have the same magnitude constraints of $u_{max} = 1.4$ but only one actuator is to be used for control at any given moment. The question to be addressed in this problem is: when is it possible to switch between the two actuators, to preserve closed-loop stability, in case the operating actuator fails. In the second problem, we assume that three point control actuators, A, B, and C, located at $z_A = 0.5\pi$, $z_B = 0.23\pi$, and $z_C = 0.36\pi$, respectively, are available for stabilization. The three actuators have different constraints of $u^A_{max} = u^B_{max} = 2.5$ and $u^C_{max} = 0.5$. Again, only one actuator is to be active at any given moment. The question in this problem is how to decide which of the two backup actuators can be used to maintain stability once the third actuator fails. The first problem basically deals with the issue of identifying the appropriate switching times that ensure fault-tolerance for a given actuator re-configuration policy, while second problem addresses the issue of how to select the appropriate actuator re-configuration policy among a family of possible choices.

We proceed with the state feedback results first. For the first problem, we initially use Eq.12.22 with $\rho = 0.2$ to compute the stability region as a function of control actuator location. To simplify the presentation of our results, we plot in Figure 12.2(a) the variation of the set of admissible initial conditions for the amplitude, $a_1(0)$, of the first eigenmode, with actuator location (note that $x_s(0) = a_1(0)\phi_1(z)$).

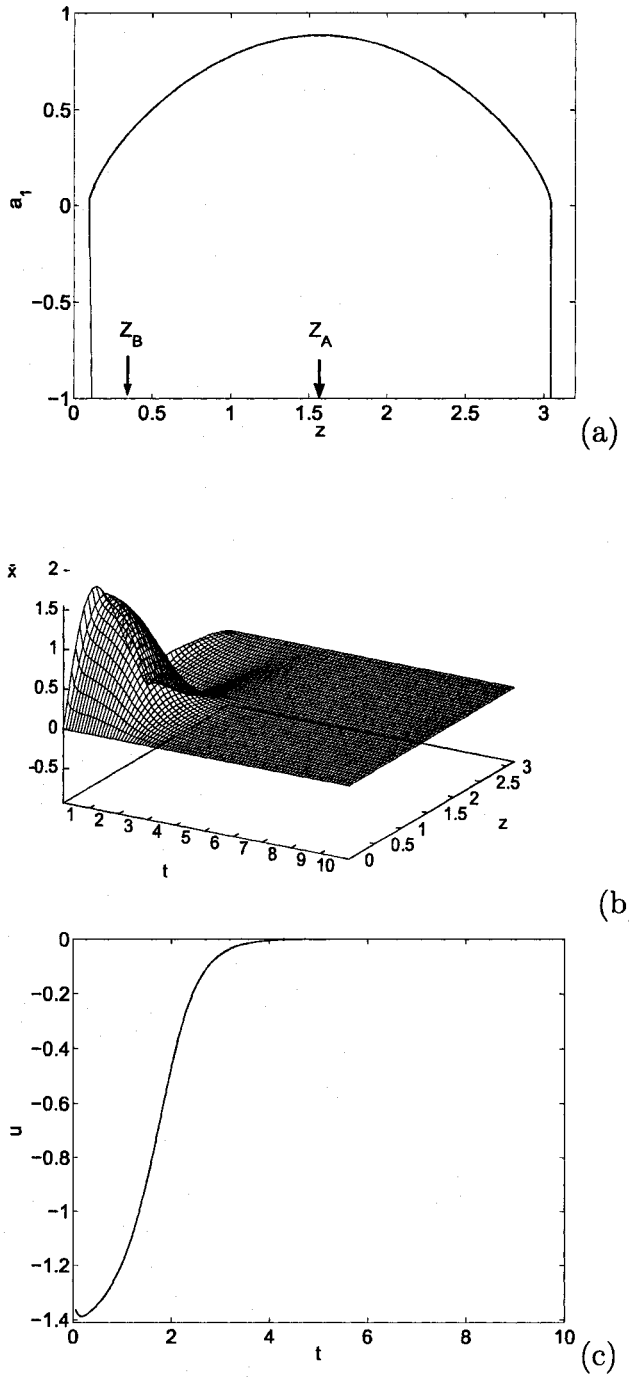

Figure 12.2: (a) Stability region as a function of actuator location for $u_{max} = 1.4$, (b) Closed-loop dimensionless temperature profile (state feedback) for $a_1(0) = 0.78$ when actuator A is used without switching, (c) Corresponding manipulated input profile.

From this figure, it is clear that for the initial condition $a_1(0) = 0.78$, only actuator A can be used initially since the initial condition is outside the stability region of actuator B. Figures 12.2(b)-12.2(c) depict, respectively, the closed-loop temperature and manipulated input profiles corresponding to this initial condition, using actuator A. Clearly, the controller successfully stabilizes the temperature profile at the desired steady-state. Now, suppose that sometime after process startup, a fault is detected in actuator A. From Figure 12.2(a), we conclude that switching to actuator B may or may not solve the problem depending on when the failure of A actually occurs. For example, consider the case when actuator A fails at $t = 1.25$. By tracking the slow state, a_1, in time, we find that $a_1(1.25) = 0.5$ – which is outside the stability region of actuator B – and, therefore, a switch to actuator B is not expected to preserve closed-loop stability. This is confirmed by the closed-loop temperature profile in Figure 12.3(a) and the corresponding manipulated input profile in Figure 12.3(c) (solid profile). Note that the input stays saturated for all times after switching. Suppose now that actuator A fails at $t = 1.75$ instead. By tracking the slow state, we find that $a_1(1.75) = 0.29$ – which is well within the stability region of actuator B – and, therefore, according to the switching scheme of Theorem 12.1, closed-loop stability can be preserved by activating actuator B. This is illustrated in Figures 12.3(b)-12.3(c) (dashed profile) which show that the controller successfully stabilizes the closed-loop temperature when actuator B is activated at the time that actuator A fails. From these results we conclude that a fault in actuator A can be tolerated after $t = 1.75$ by using the proposed switching scheme.

We now turn our attention to the second problem. Using Eq.12.22 with $\rho = 0.02$, the stability regions for $u_{max} = 2.5$ (solid line) and for $u_{max} = 0.5$ (dashed line) are computed and shown in Figure 12.4(a). From this figure, it is easy to see that for the

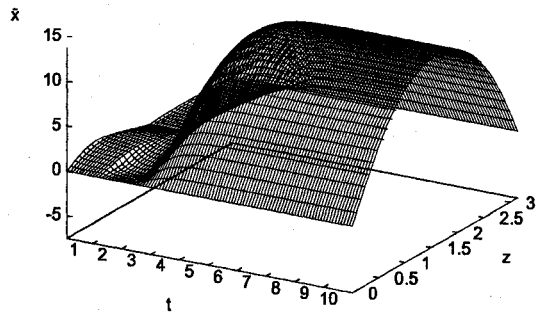

(a)

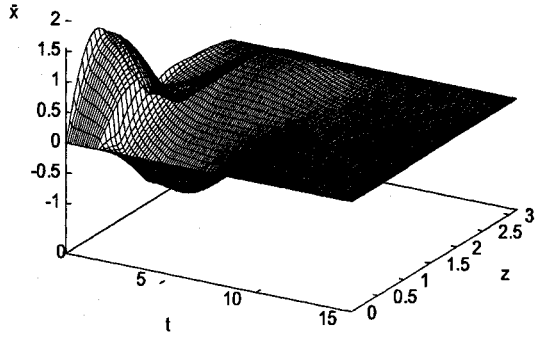

(b)

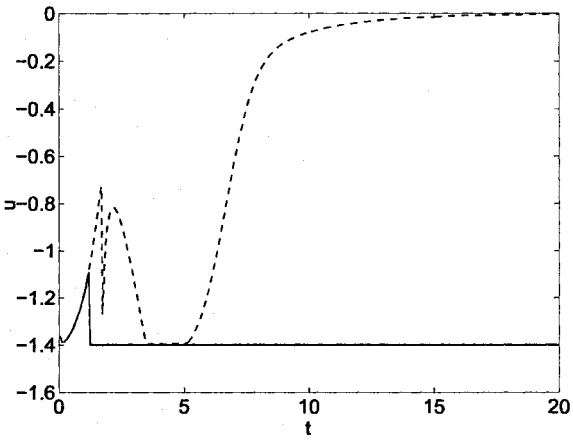

(c)

Figure 12.3: (a) Closed-loop dimensionless temperature profile (state feedback) for $a_1(0) = 0.78$ when actuator A fails at $t = 1.25$ and actuator B is activated, (b) Closed-loop dimensionless temperature profile (state feedback) for $a_s(0) = 0.78$ when actuator A fails at $t = 1.75$ and actuator B is activated, (c) Corresponding manipulated input profiles for case a (solid) and case b (dashed).

initial condition, $a_1(0) = 1.3$, only actuator A ($z_A = 0.5\pi$, $u^A_{max} = 2.5$) can be used initially since the initial condition is outside the stability regions of both actuator B ($z_B = 0.23\pi$, $u^B_{max} = 2.5$) and actuator C ($z_C = 0.36\pi$, $u^C_{max} = 0.5$). Now, suppose that sometime after process startup, say $t = 1.4$, a fault is detected in actuator A and it becomes necessary to switch to another actuator. Without using the switching law of Theorem 12.1, it is not clear whether actuator B or C should be activated at this time. Figures 12.4(b)- and 12.4(d) (solid profile) depict, respectively, the resulting closed-loop temperature and manipulated input profiles when actuator C is chosen. We see in this case that the controller is unable to stabilize the system at the desired steady-state. In contrast, using the proposed switching scheme, we find that the slow state at the time that actuator A fails is $a_1(1.4) = 0.62$, which is inside the stability region of actuator B and outside the stability region of actuator C. So, we choose to activate actuator B. Figures 12.4(c) and 12.4(d) (dashed line) depict the results for this case which show that the controller successfully stabilizes the closed-loop system.

For the case of output feedback, we use a single point sensor, located at $z = 0.33\pi$, to obtain estimates of the first eigenmode, which are then used for implementing the output feedback controller. Owing to the small, $O(\epsilon)$, discrepancy between the stability regions obtained under state and output feedback (due to estimation errors), the switching law of Theorem 12.1 should be used only as an approximate guide for switching between the different actuators in the case of output feedback (see Remark 12.11). The simulation results for this case are consistent with the state feedback results for both problems. For brevity, we present only the results for the second problem. These results are given in Figure 12.5 which shows that the closed-loop system becomes unstable when configuration C is activated at the time that actuator A fails at $t = 1.4$ (Figures 12.5(a) and 12.5(c) (solid line)), whereas closed-loop

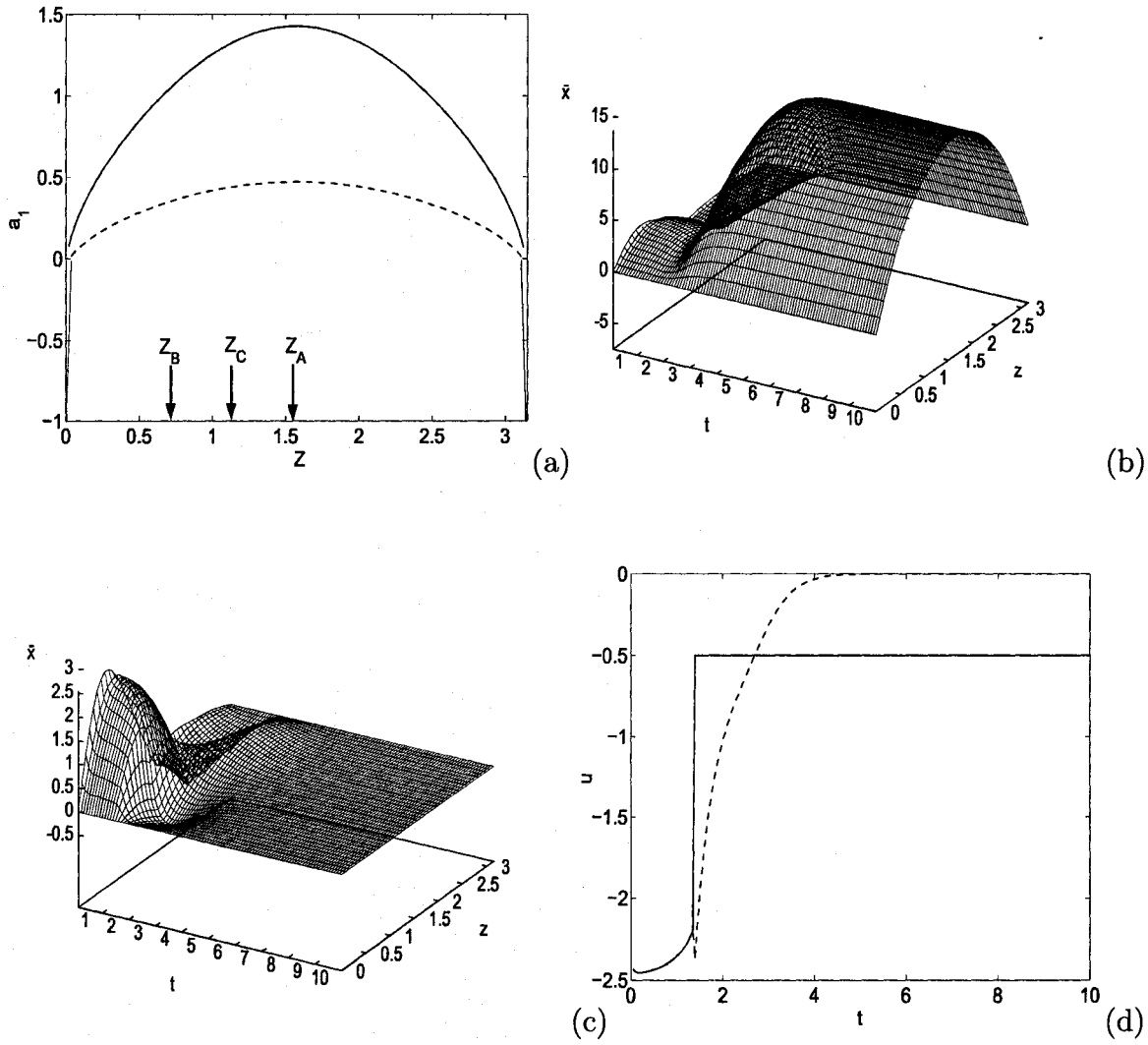

Figure 12.4: (a) Stability region as a function of actuator location for $u_{max} = 2.5$ (solid) and $u_{max} = 0.5$ (dashed),(b) Closed-loop dimensionless temperature profile (state feedback) for $a_1(0) = 1.3$ when actuator A fails at $t = 1.4$ and actuator C is activated, (c) Closed-loop dimensionless temperature profile (state feedback) for $a_1(0) = 1.3$ when actuator A fails at $t = 1.4$ and actuator B is activated, (d) Corresponding manipulated input profiles for case b (solid) and case c (dashed).

stability is maintained by activating configuration B instead (Figures 12.5(b) and 12.5(c) (dashed line)).

12.4.2 Application to a non-isothermal tubular reactor with recycle

We consider the non-isothermal tubular reactor studied in [17], where an irreversible first-order reaction of the form $A \rightarrow B$ takes place. The reaction is exothermic and a cooling jacket is used to remove heat from the reactor. The outlet of the reactor is fed to a separator where the unreacted species A is separated from the product B and then fed back to the reactor through a recycle loop. Under standard modeling assumptions, the dynamic model of the process can be derived from mass and energy balances and takes the following dimensionless form:

$$\begin{aligned}
\frac{\partial \bar{x}_1}{\partial t} &= -\frac{\partial \bar{x}_1}{\partial z} + \frac{1}{Pe_T}\frac{\partial^2 \bar{x}_1}{\partial z^2} + B_T B_C \exp\left(\frac{\gamma \bar{x}_1}{1+\bar{x}_1}\right)(1+\bar{x}_2) + \beta_T(b(z)u(t) - \bar{x}_1) \\
\frac{\partial \bar{x}_2}{\partial t} &= -\frac{\partial \bar{x}_2}{\partial z} + \frac{1}{Pe_C}\frac{\partial^2 \bar{x}_2}{\partial z^2} - B_C \exp\left(\frac{\gamma \bar{x}_1}{1+\bar{x}_1}\right)(1+\bar{x}_2)
\end{aligned} \tag{12.28}$$

subject to the boundary conditions:

$$\begin{aligned}
\frac{\partial \bar{x}_1(0,t)}{\partial z} &= Pe_T(\bar{x}_1(0,t) - (1-r)\bar{x}_{1f}(t) - r\bar{x}_1(1,t)) \\
\frac{\partial \bar{x}_2(0,t)}{\partial z} &= Pe_C(\bar{x}_2(0,t) - (1-r)\bar{x}_{2f}(t) - r\bar{x}_2(1,t)) \\
\frac{\partial \bar{x}_1(1,t)}{\partial z} &= 0\,, \qquad \frac{\partial \bar{x}_2(1,t)}{\partial z} = 0
\end{aligned} \tag{12.29}$$

where $\bar{x}_1$ and $\bar{x}_2$ denote dimensionless temperature and concentration of species A in the reactor, respectively, $\bar{x}_{1f}$ and $\bar{x}_{2f}$ denote dimensionless inlet temperature and inlet concentration of species A in the reactor, respectively, Pe_T and Pe_C are the thermal and mass Peclet numbers, respectively, B_T and B_C denote a dimensionless heat of reaction and a dimensionless pre-exponential factor, respectively, r is the recirculation coefficient (it varies from zero to one, with one corresponding to total

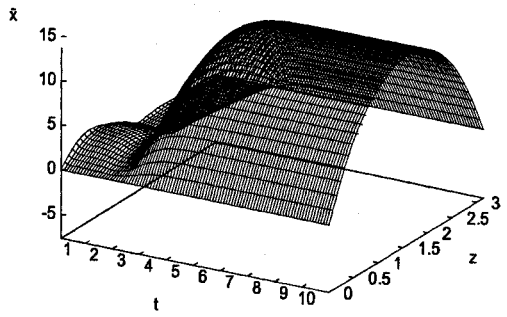

(a)

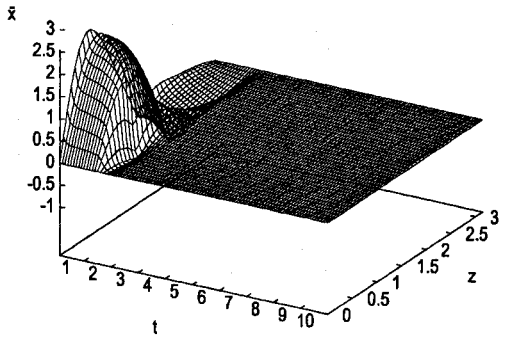

(b)

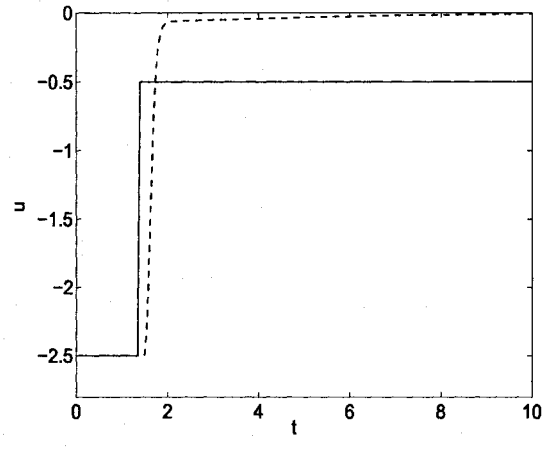

(c)

Figure 12.5: (a) Closed-loop dimensionless temperature profile (output feedback) for $a_1(0) = 1.3$ when actuator A fails at $t = 1.4$ and actuator C is activated, (b) Closed-loop dimensionless temperature profile (output feedback) for $a_1(0) = 1.3$ when actuator A fails at $t = 1.4$ and actuator B is activated, (c) Corresponding manipulated input profiles for case a (solid) and case b (dashed).

recycle with zero fresh feed, and zero corresponding to no recycle), γ is a dimensionless activation energy, β_T is a dimensionless heat transfer coefficient, u is a dimensionless jacket temperature (chosen to be the manipulated input), and $b(z)$ is the actuator distribution function. For the purposes of our analysis here, we will assume that there is no recycle loop dead-time.

In order to transform the boundary condition of Eq.12.29 to a homogeneous one, we insert the non-homogeneous part of the boundary condition into the differential equation and obtain the following PDE representation of the process:

$$\begin{aligned}
\frac{\partial \bar{x}_1}{\partial t} &= -\frac{\partial \bar{x}_1}{\partial z} + \frac{1}{Pe_T}\frac{\partial^2 \bar{x}_1}{\partial z^2} + B_T B_C \exp\left(\frac{\gamma \bar{x}_1}{1+\bar{x}_1}\right)(1+\bar{x}_2) + \beta_T(b(z)u(t) - \bar{x}_1) \\
&\quad +\delta(z-0)((1-r)\bar{x}_{1f} + r\bar{x}_1(1,t)) \\
\frac{\partial \bar{x}_2}{\partial t} &= -\frac{\partial \bar{x}_2}{\partial z} + \frac{1}{Pe_C}\frac{\partial^2 \bar{x}_2}{\partial z^2} - B_C \exp\left(\frac{\gamma \bar{x}_1}{1+\bar{x}_1}\right)(1+\bar{x}_2) \\
&\quad +\delta(z-0)((1-r)\bar{x}_{2f} + r\bar{x}_2(1,t))
\end{aligned} \tag{12.30}$$

where $\delta(\cdot)$ is the standard Dirac function, subject to the homogeneous boundary conditions:

$$\begin{aligned}
\frac{\partial \bar{x}_1(0,t)}{\partial z} &= Pe_T \bar{x}_1(0,t), \quad \frac{\partial \bar{x}_2(0,t)}{\partial z} = Pe_C \bar{x}_2(0,t)\ ; \\
\frac{\partial \bar{x}_1(1,t)}{\partial z} &= 0, \quad \frac{\partial \bar{x}_2(1,t)}{\partial z} = 0
\end{aligned} \tag{12.31}$$

The following values for the process parameters were used in our calculations: $Pe_T = 7.0$, $Pe_C = 7.0$, $B_C = 0.1$, $B_T = 2.5$, $\beta_T = 2.0$, $\gamma = 10.0$, $r = 0.5$, $\bar{x}_{1f} = \bar{x}_{2f} = 0$. For these values, the operating steady-state of the open-loop system is unstable (the linearization around the steady-state possesses one real unstable eigenvalue and infinitely many stable eigenvalues). This instability is shown by the open-loop temperature profile in Figure 12.6 where it is seen that starting close to the unstable steady-state, the temperature profiles moves to an asymptotically stable

periodic (limit cycle) spatially non-uniform steady-state. We note that in the absence of recycle-loop (i.e., $r = 0$), the above process parameters correspond to a unique, globally asymptotically stable spatially non-uniform steady-state for the open-loop system (see [17] for a detailed study of the effect of the recycle ratio on the dynamics of the tubular reactor).

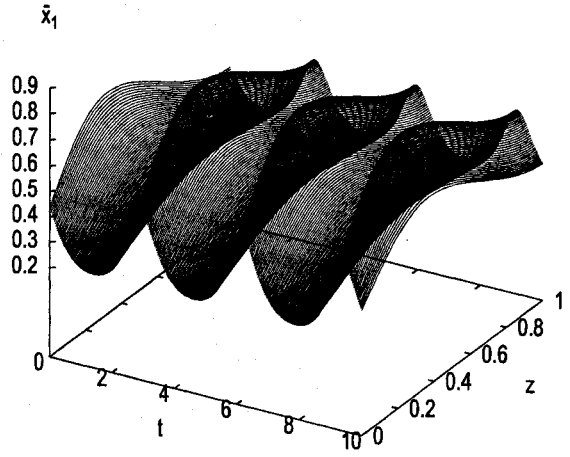

Figure 12.6: Spatiotemporal evolution of the dimensionless tubular reactor temperature profile in the open-loop system.

The control problem is to stabilize the reactor at a spatially non-uniform steady-state where the production of species B is desirable and the 'hot-spot' temperature is acceptable, by manipulating the jacket temperature, $u(t)$, which is subject to hard constraints and possible actuator failures. To achieve this control objective, the controlled output is defined as $y_c(t) = \int_0^1 e^{-Pez}\phi_{11}(z)\bar{x}_1 dz$, and the actuator distribution function is taken to be $b(z) = \delta(z - z_{act})$ (point control actuator placed at $z = z_{act}$). The desired reference input value was set at $v = 0.10$ (this value of y_c corresponds to a steady-state with the desired characteristics of a high production rate with relatively

low 'hot-spot' temperature). Furthermore, we assume that there is available a large number of point measurements of the temperature throughout the reactor so that $y_c(t)$ is known with sufficient accuracy.

The spatial differential operator of the system of Eq.12.30 is of the form:

$$\mathcal{A}\bar{x} = \begin{bmatrix} \mathcal{A}_1\bar{x}_1 & 0 \\ 0 & \mathcal{A}_2\bar{x}_2 \end{bmatrix} = \begin{bmatrix} \frac{1}{Pe_T}\frac{\partial^2\bar{x}_1}{\partial z^2} - \frac{\partial\bar{x}_1}{\partial z} & 0 \\ 0 & \frac{1}{Pe_C}\frac{\partial^2\bar{x}_2}{\partial z^2} - \frac{\partial\bar{x}_2}{\partial z} \end{bmatrix} \tag{12.32}$$

The solution of the eigenvalue problem for $\mathcal{A}_i$ can be obtained by utilizing standard techniques from linear operator theory (see, for example, [255]) and is of the form:

$$\begin{aligned} \lambda_{ij} &= \frac{\bar{a}_{ij}^2}{Pe} + \frac{Pe}{4}, \quad i = 1,2, \quad j = 1,\ldots,\infty \\ \phi_{ij}(z) &= B_{ij} e^{Pe\frac{z}{2}} \left(cos(\bar{a}_{ij}z) + \frac{Pe}{2\bar{a}_{ij}} sin(\bar{a}_{ij}z) \right), \quad i = 1,2, \quad j = 1,\ldots,\infty \\ \bar{\phi}_{ij}(z) &= e^{-Pez}\phi_{ij}(z), \quad i = 1,2, \quad j = 1,\ldots,\infty \end{aligned} \tag{12.33}$$

where $Pe = Pe_T = Pe_C$, and $\lambda_{ij}, \phi_{ij}, \bar{\phi}_{ij}$, denote the eigenvalues, eigenfunctions and adjoint eigenfunctions of $\mathcal{A}_i$, respectively. $\bar{a}_{ij}, B_{ij}$ can be calculated from the following formulas:

$$tan(\bar{a}_{ij}) = \frac{Pe\bar{a}_{ij}}{\bar{a}_{ij}^2 - \left(\frac{Pe}{2}\right)^2}, \quad i = 1,2, \quad j = 1,\ldots,\infty$$

$$B_{ij} = \left\{ \int_0^1 \left(cos(\bar{a}_{ij}z) + \frac{Pe}{2\bar{a}_{ij}} sin(\bar{a}_{ij}z) \right)^2 dz \right\}^{-\frac{1}{2}}, \quad i = 1,2, \quad j = 1,\ldots,\infty \tag{12.34}$$

For this system, we take as the slow modes of the process the first temperature mode and use Galerkin's method to derive an ODE that describes the temporal evolution of the amplitude of the first eigenmode. This ODE is employed for the synthesis of the controller, using Eqs.12.20-12.21, which is then implemented on a 400-th order Galerkin discretization of the system of Eqs.12.30-12.31 (further increases in the order

of the Galerkin truncation were found to give negligible improvement on the accuracy of the results). To deal with possible actuator faults, we consider switching between three point control actuators placed at $z_A = 0$ (constraints magnitude: $u^A_{max} = 0.06$), $z_B = 0.2$ (constraints magnitude: $u^B_{max} = 0.06$), and $z_C = 0.8$ (constraints magnitude: $u^C_{max} = 0.02$).

In the first set of simulation runs, we evaluate the ability of the constrained controller to stabilize the reactor at the desired steady-state in the absence of actuator faults. To this end, we design the bounded nonlinear controller of Eqs.12.20-12.21 with $\rho = 0.001$ and implement it using actuator A placed at the entrance of the reactor. The result is shown by the solid profiles in Figures 12.7(a)-12.7(b) which depict the evolution of the controlled output and manipulated input, respectively. It is seen that the controller successfully stabilizes the output at the desired reference input while satisfying the constraints. The corresponding temperature profile is shown in Figure 12.7(c).

In the second set of simulation runs, we demonstrate how actuator switching can be used to deal with the problem of actuator failure. To this end, the closed-loop system is initialized at the same initial condition, considered earlier, under control actuator A which is assumed to fail at $t = 0.875$. If neither of the two backup actuators, B or C, is activated at this time, we see from the dashed profiles in Figures 12.7(a)-12.7(b) that the system reverts to its open-loop mode where the output moves away from the desired steady-state and exhibits a limit cycle behavior. This instability is also reflected in the temperature profile shown in Figure 12.7(d). When actuator B is activated, however, it is clear from the resulting controlled output (Figure 12.8(a) - solid line) and temperature (Figure 12.8(c)) profiles that the controller successfully preserves closed-loop stability and achieves the desired steady-state despite the failure

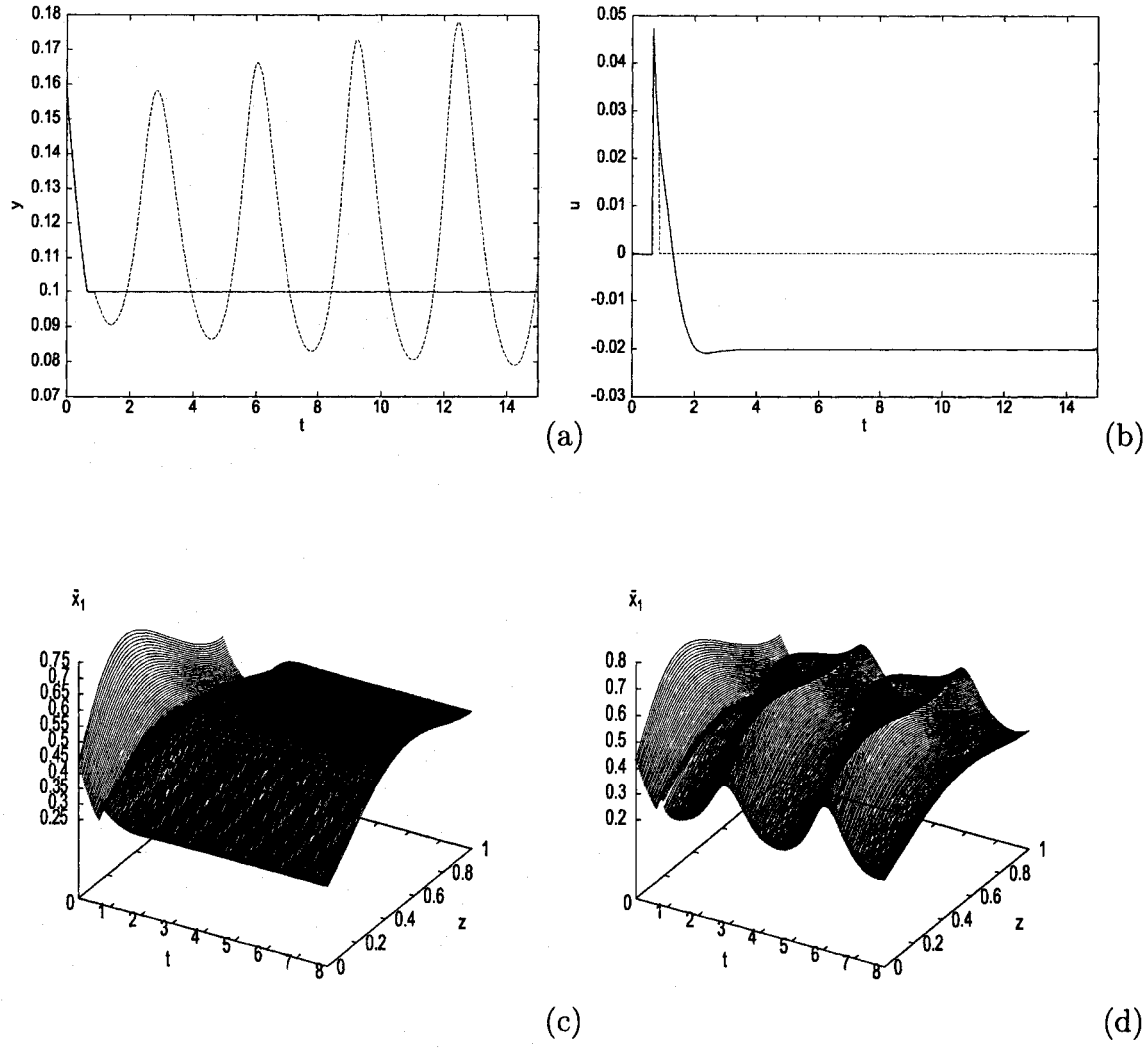

Figure 12.7: (a) Controlled output profiles when actuator A ($u_{max} = 0.06$, $z_A = 0$) operates without failure (solid) and when it fails at $t = 0.875$ without activating any of the backup actuators (dashed), (b) Corresponding manipulated input profiles, (c) Closed-loop dimensionless temperature profile when actuator A operates without failure, (d) Closed-loop dimensionless temperature profile when actuator A fails at $t = 0.875$ without activating any of the backup actuators.

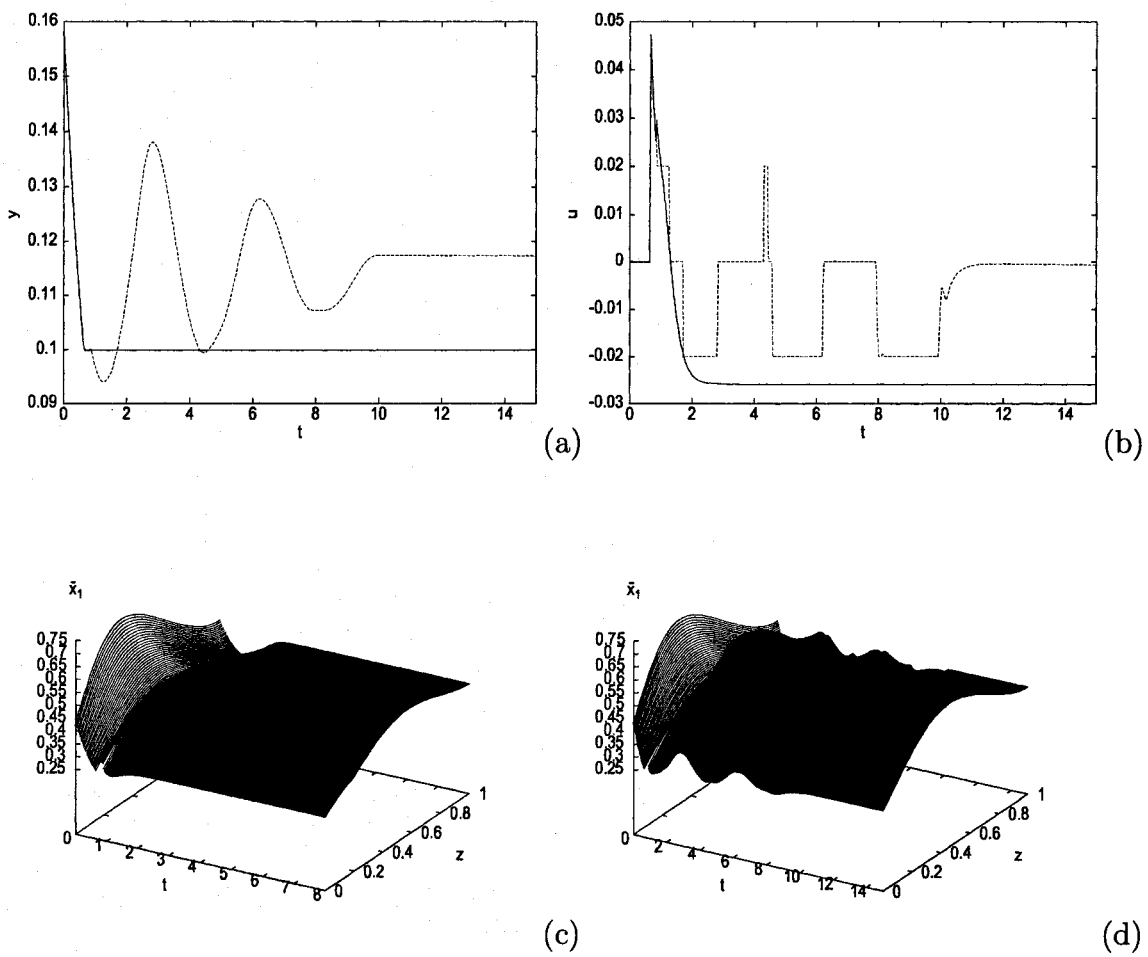

Figure 12.8: (a) Controlled output profiles for the case when actuator A ($u_{max} = 0.06$, $z_A = 0$) fails at $t = 0.875$ and actuator B ($u_{max} = 0.06$, $z_B = 0.2$) is activated (solid) and for the case when actuator C ($u_{max} = 0.02$, $z_C = 0.8$) is activated (dashed) instead of B, (b) Corresponding manipulated input profiles, (c) Closed-loop dimensionless temperature profile when actuator A fails at $t = 0.875$ and actuator B is activated, (d) Closed-loop dimensionless temperature profile when actuator A fails at $t = 0.875$ and actuator C is activated.

of actuator A. In contrast, when actuator C is activated instead of B, we see from the dashed profile in Figure 12.8(a) that the controller is unable to stabilize the output at the desired steady-state, leading to transient oscillatory behavior and offset. The resulting poor performance is also evident in the closed-loop temperature profile depicted in Figure 12.8(d). The difference in outcome between the two switching sequences (activation of B following failure of A vs. activation of C following failure of A) can be explained from the corresponding input profiles shown in Figure 12.8(b). In particular, when actuator C (closer to the reactor exit) is activated, the controller requests large control action to drive the system to the desired steady-state, which is not available due to the tight constraints of this actuator, leading to prolonged periods of actuator saturation that result in poor performance and offset. In the case of actuator B, however, the control action requested is within the allowable range for this actuator, and therefore the desired stability and performance properties are preserved successfully upon switching. These results are consistent with the solution of the optimal actuator placement problem for this tubular reactor obtained in [16], which show that actuators placed closer to the inlet of the reactor utilize smaller control effort than those placed closer to the exit.

12.5 Conclusions

In this chapter, a methodology for coordinating feedback and switching in control of spatially-distributed processes described by highly dissipative, constrained PDE systems was proposed. Under the assumption that the eigenspectrum of the spatial differential operator can be partitioned into a finite slow set and an infinite stable fast complement, Galerkin's method was initially used to derive a finite-dimensional ODE system that captures the dominant dynamics of the PDE system. The ODE system

was then used as the basis for the integrated synthesis, via Lyapunov techniques, of a stabilizing nonlinear feedback controller, together with a switching law that orchestrates the switching between the admissible control actuator configurations, in a way that respects actuator constraints, accommodates conflicting control objectives, and guarantees closed-loop stability at the same time. Precise conditions that guarantee stability of the constrained closed-loop PDE system under switching were provided. Finally, the proposed methodology was successfully applied to stabilize an unstable steady-state of a diffusion-reaction process and a non-isothermal tubular reactor with recycle, under constraints and control actuator failure.

Chapter 13

Fault-Tolerant Control of Fluid Dynamic Systems

13.1 Introduction

The development of general and practical control algorithms for nonlinear partial differential equations (PDEs) that describe fluid flow processes (e.g., Navier-Stokes equations, Kuramoto-Sivashinsky equation (KSE)) is a fundamental problem whose practical significance ranges from feedback control of turbulence for drag reduction, to suppression of fluid mechanical instabilities in coating processes and suppression of waves exhibited by falling liquid films. For example, drag reduction through active feedback control may have a significant impact on the design and operation of underwater vehicles, airplanes and automobiles since, according to some estimates, keeping the flow over the surface of a vehicle laminar could yield up to 30% reduction in fuel consumption. Active control of fluid flow can be achieved by injection of polymers, mass transport through porous walls (e.g., blowing/suction) and application of electro-magnetic forcing.

An example fluid dynamic system, which will be used throughout paper to demonstrate the results, is the KSE. The KSE is a nonlinear dissipative PDE of the form:

$$\frac{\partial U}{\partial t} = -\nu \frac{\partial^4 U}{\partial z^4} - \frac{\partial^2 U}{\partial z^2} - U \frac{\partial U}{\partial z} \tag{13.1}$$

where $\nu > 0$ is the so-called instability parameter, which describes incipient instabilities in a variety of physical and chemical systems, including falling liquid films [51], unstable flame fronts [273], Belouzov-Zabotinskii reaction patterns [189] and interfacial instabilities between two viscous fluids [143]. Both the dynamics and control of the KSE with periodic boundary conditions have been the subject of significant research work. Dynamical studies have led to the discoveries of steady and periodic wave solutions, chaotic behavior for very small values of ν, and the fact that the dominant dynamics of the KSE can be adequately characterized by a small number of degrees of freedom (see, for example, [295, 51, 124, 167]). Control studies of the KSE, on the other hand, have focused on a variety of problems, including the design of finite-dimensional output feedback controllers for stabilization of the zero solution of the KSE based on ODE approximations [21], the global stabilization of the KSE via distributed static output feedback control [63], stabilization enhancement via boundary control [205], adaptive stabilization [172] and robust control [146].

While the above research efforts have led to a number of systematic approaches for control of the KSE and other fluid dynamic systems, a common theme of these approaches is the use of a fixed spatial arrangement (or configuration) of the control actuators/measurement sensors in order to accomplish the desired control objectives. There are many practical situations, however, where it may be desirable, and sometimes even necessary, to consider multiple actuator/sensor configurations and switch between them in a specific manner, in order to achieve the control objectives. One example is the problem of control actuator failure where, upon the detection of a fault

in a control actuator, it may be necessary to switch to an alternative actuator, placed at a different spatial location, in order to preserve stability of the closed-loop system. Spatially-distributed switching between control actuators in this case provides a means for fault-tolerant control. In other cases, switching between actuator configurations may be motivated by some additional performance objective, such as the desire to optimize a given performance criterion or accommodate inherently competing control objectives that cannot be reconciled using a single actuator configuration.

In chapter 12, we considered a class of linear and quasi-linear second-order parabolic PDE systems, and developed a method for handling control actuator failures by integrating feedback and switching among a pre-selected set of spatially-distributed control actuator configurations. The developed method – based on Lyapunov techniques – provides explicit feedback laws and precise switching conditions for guaranteeing closed-loop stability in the presence of actuator failures, and was successfully applied to representative examples of diffusion-reaction processes and a tubular reactor with recycle.

In this chapter, we focus on the problem of coupling feedback and switching between actuator configurations for fault-tolerant control of fluid dynamic systems modeled by highly-dissipative PDEs with constrained control actuators. The results constitute a generalization of the results in Chapter 12 to higher-order (e.g., fourth in the case of the KSE) dissipative PDEs that can model fluid flows. The problem is addressed on the basis of finite-dimensional Galerkin approximations of the PDE system and entails the integrated synthesis, via Lyapunov techniques, of stabilizing nonlinear feedback controllers together with stabilizing switching laws that orchestrate the switching between the admissible control actuator configurations, in a way that respects actuator constraints, accommodates inherently conflicting control objectives,

and guarantees closed-loop stability. Precise conditions that guarantee stability of the constrained closed-loop system under switching are provided. The proposed control methodology is demonstrated through an application to the problem of suppression of wave formation, achieved via the stabilization of the zero solution, $U(z,t) = 0$, of the KSE with periodic boundary conditions, in the presence of control actuator constraints and faults. The results of this chapter were first presented in [99].

13.2 Preliminaries

13.2.1 Mathematical description

To demonstrate the proposed fault-tolerant control methodology, we consider the one-dimensional Kuramoto-Sivashinsky equation with distributed control as our model system:

$$\frac{\partial U}{\partial t} = -\nu\frac{\partial^4 U}{\partial z^4} - \frac{\partial^2 U}{\partial z^2} - U\frac{\partial U}{\partial z} + \sum_{i=1}^{l} b_i u_i(t) \tag{13.2}$$

$$y_m^\kappa = \int_{-\pi}^{\pi} s_\kappa(z) U dz, \ \kappa = 1, \ldots, p \tag{13.3}$$

subject to the periodic boundary conditions:

$$\frac{\partial^j U}{\partial z^j}(-\pi, t) = \frac{\partial^j U}{\partial z^j}(+\pi, t), \quad j = 0, \ldots, 3 \tag{13.4}$$

and the initial condition:

$$U(z,0) = U_0(z) \tag{13.5}$$

where $U(z,t)$ is the state of the system, $z \in [-\pi, \pi]$ is the spatial coordinate, t is the time, ν is the instability parameter, $u_i \in [-u_{max}, u_{max}] \subset \mathbb{R}$ is the i-th constrained manipulated input, l is the total number of manipulated inputs, $b_i(z)$ is the i-th actuator distribution function (i.e., $b_i(z)$ determines how the control action computed

by the i-th control actuator, $u_i(t)$, is distributed (e.g., point or distributed actuation) in the spatial interval $[-\pi, \pi]$), $y_m^\kappa \in \mathbb{R}$ denotes a measured output, and $s_\kappa(z)$ is a known smooth function of z which is determined by the location and type of the measurement sensors (e.g., point or distributed sensing). Whenever the control action enters the system at a single point, z_0, with $z_0 \in [-\pi, \pi]$ (i.e., point actuation), the function $b_i(z)$ is taken to be nonzero in a finite spatial interval of the form $[z_0 - \mu, z_0 + \mu]$, where μ is a small positive real number, and zero elsewhere in $[-\pi, \pi]$.

For a precise presentation of our results, we cast the system of Eq.13.2 as an infinite-dimensional system in the Hilbert space, $\mathcal{H}([-\pi, \pi]; \mathbb{R})$, with $\mathcal{H}$ being the space of sufficiently smooth vector functions defined on $[-\pi, \pi]$ that satisfy the boundary condition of Eq.13.4, with inner product and norm:

$$(\omega_1, \omega_2) = \int_{-\pi}^{\pi} (\omega_1(z), \omega_2(z))_{\mathbb{R}} dz, \quad \|\omega_1\|_2 = (\omega_1, \omega_1)^{\frac{1}{2}} \tag{13.6}$$

where ω_1, ω_2 are two elements of $\mathcal{H}([-\pi, \pi]; \mathbb{R})$ and the notation $(\cdot, \cdot)_{\mathbb{R}}$ denotes the standard inner product in $\mathbb{R}$.

Defining the state function x on $\mathcal{H}([-\pi, \pi]; \mathbb{R})$ as:

$$x(t) = U(z, t), \quad t > 0, \quad z \in [-\pi, \pi], \tag{13.7}$$

the operator $\mathcal{A}$ in $\mathcal{H}([-\pi, \pi]; \mathbb{R})$ as:

$$\begin{aligned} \mathcal{A}x &= -\nu \frac{\partial^4 U}{\partial z^4} - \frac{\partial^2 U}{\partial z^2} \\ x \in D(\mathcal{A}) &= \left\{ x \in \mathcal{H}([-\pi, \pi]; \mathbb{R}) : \frac{\partial^j U}{\partial z^j}(-\pi, t) = \frac{\partial^j U}{\partial z^j}(+\pi, t), \ j = 0, \ldots, 3 \right\} \end{aligned} \tag{13.8}$$

and the input, and measured output operators as:

$$\mathcal{B}u = \sum_{i=1}^{l} b_i u_i, \quad \mathcal{S}x = (s, x) \tag{13.9}$$

the system of Eqs.13.2-13.5 takes the form:

$$\begin{aligned} \dot{x} &= \mathcal{A}x + \mathcal{B}u + f(x), \quad x(0) = x_0 \\ y_m &= \mathcal{S}x \end{aligned} \tag{13.10}$$

where $f(x) = -U\dfrac{\partial U}{\partial z}$ and $x_0 = U_0(z)$.

For $\mathcal{A}$, we can formulate the following eigenvalue problem:

$$\mathcal{A}\phi_n = -\nu\frac{\partial^4\phi_n}{\partial z^4} - \frac{\partial^2\phi_n}{\partial z^2} = \lambda_n\phi_n, \;\; n = 1, \ldots, \infty \tag{13.11}$$

subject to:

$$\frac{\partial^j\phi_n}{\partial z^j}(-\pi) = \frac{\partial^j\phi_n}{\partial z^j}(+\pi), \quad j = 0, \ldots, 3 \tag{13.12}$$

where λ_n denotes an eigenvalue and ϕ_n denotes an eigenfunction. A direct computation of the solution of the above eigenvalue problem yields $\lambda_0 = 0$ with $\psi_0(z) = \dfrac{1}{\sqrt{2\pi}}$, and $\lambda_n = -\nu n^4 + n^2$ (λ_n is an eigenvalue of multiplicity two) with eigenfunctions $\phi_n(z) = \dfrac{1}{\sqrt{\pi}}\sin(nz)$ and $\psi_n(z) = \dfrac{1}{\sqrt{\pi}}\cos(nz)$ for $n = 1, \ldots, \infty$. We also define the eigenspectrum of $\mathcal{A}$, $\sigma(\mathcal{A})$, as the set of all eigenvalues of $\mathcal{A}$, i.e., $\sigma(\mathcal{A}) = \{\lambda_1, \lambda_2, \ldots\}$. We note that the fact that $\mathcal{A}$ has a real pure point spectrum is a result of the fact that the linear part of the spatial differential operator of the KSE with periodic boundary conditions is self-adjoint and the problem is considered in a bounded domain.

From the expression of the eigenvalues, it follows that for a fixed value of $\nu > 0$ the number of unstable eigenvalues of $\mathcal{A}$ is finite and the distance between two consecutive eigenvalues (i.e., λ_n and λ_{n+1}) increases as n increases. Furthermore, for a fixed value of $\nu > 0$, $\sigma(\mathcal{A})$ can be partitioned as $\sigma(\mathcal{A}) = \sigma_1(\mathcal{A}) \bigcup \sigma_2(\mathcal{A})$, where $\sigma_1(\mathcal{A})$ contains the first m (with m finite) "slow" eigenvalues (i.e., $\sigma_1(\mathcal{A}) = \{\lambda_1, \ldots, \lambda_m\}$) and $\sigma_2(\mathcal{A})$ contains the remaining "fast" eigenvalues (i.e., $\sigma_2(\mathcal{A}) = \{\lambda_{m+1}, \ldots\}$ where $\lambda_{m+1} < 0$). To capture the separation between the "slow" and "fast" eigenvalues, we define the parameter $\epsilon = \dfrac{|\lambda_1|}{|\lambda_{m+1}|}$ (note that $\epsilon \to 0$ as $m \to \infty$). The separation between the

"slow" and "fast" eigenvalues suggests that the dominant dynamics of the KSE can be described by a finite-dimensional system and motivates applying Galerkin's method to the system of Eq.13.10 to derive an approximate finite-dimensional system (see Section 13.3.1 below).

Remark 13.1 A physical system that can be described by the KSE is the motion of a liquid film falling down on a vertical wall [51]. In this case, $U(z,t)$ is the film height. Such a system has been found experimentally to exhibit wavy behavior of the type predicted by the KSE for values of ν smaller than 1 (see also Figure 13.1). In many instances, it is desirable to suppress wavy behavior by using control actuators that add/remove fluid mass via blowing/suction. In this case, the control input enters directly into the PDE and does not appear in the boundary conditions. This physical problem is consistent with the formulation of Eq.13.2 since we consider distributed control actuation. Note that problems for which the inputs enters directly into the KSE but nonlinearly can be readily handled within our formulation by simply solving for u through the inversion of an algebraic nonlinear equation.

Remark 13.2 The consideration of approximate point control is motivated by the fact that most experimental point control actuators (including the ones that add/remove fluid mass via blowing/suction) have finite (but small) support and the fact that $b_i(z) = \delta(z - z_0)$ (where $\delta(\cdot)$ is the standard Dirac function) is not an element of $\mathcal{H}([-\pi, \pi]; \mathbb{R})$.

13.2.2 Problem formulation

Consider the system of Eq.13.2, where each manipulated input, u_i, is constrained in the interval $[-u_{max}, u_{max}]$, and assume that available at our disposal is a family of N (with N finite) control actuator configurations, of which only one configuration can be used for control at any given time instance. Each of these N configurations consists of a spatially-distinct arrangement of the control actuators, which we denote

by $\bar{z}^{k(t)}$, $k = 1, \cdots, N$. In this notation, the index $k(t)$ denotes the actuator configuration being active at time t, while $\bar{z}^k := [z_1^k \; z_2^k \; \cdots \; z_l^k]^T$ is a column vector whose components represent the corresponding spatial locations of the actuators associated with the k-th configuration. To ensure controllability of the system, we allow only a finite number of switches between configurations over finite time. The problem is how to coordinate switching between the different control actuator configurations, in the event of actuator failure, in a way that respects actuator constraints and guarantees closed-loop stability. To address this problem, we formulate the following objectives. Initially, Galerkin's method is used to derive a nonlinear finite-dimensional ODE system that captures the dominant dynamics of the KSE. Next, the ODE approximation is used as the basis for the synthesis of bounded nonlinear output feedback controllers of the general form:

$$u \;=\; p(y_m, u_{max}, \bar{z}_k) \tag{13.13}$$

that enforce asymptotic stability and reference-input tracking in the constrained closed-loop system and provide an explicit characterization of the stability region associated with each control actuator configuration. The controller synthesis is carried out via Lyapunov-based control techniques and is inspired by the results on bounded control in [204]. Finally, a set of switching rules is derived to determine which of the N control actuator configurations can be engaged at any given time, and an upper bound on the separation between the slow and fast eigenvalues, which guarantees stability of the infinite-dimensional closed-loop system, is computed.

13.3 Fault-tolerant control system design

13.3.1 Galerkin's method

We apply Galerkin's method to the system of Eq.13.10 to derive an approximate finite-dimensional system. Let $\mathcal{H}_s$, $\mathcal{H}_f$ be modal subspaces of $\mathcal{A}$, defined as $\mathcal{H}_s = span\{\phi_1, \phi_2, \ldots, \phi_m\}$ and $\mathcal{H}_f = span\{\phi_{m+1}, \phi_{m+2}, \ldots\}$ (the existence of $\mathcal{H}_s$, $\mathcal{H}_f$ follows from the properties of $\mathcal{A}$). Defining the orthogonal projection operators, P_s and P_f, such that $x_s = P_s x$, $x_f = P_f x$, the state x of the system of Eq.13.10 can be decomposed as:

$$x = x_s + x_f = P_s x + P_f x \tag{13.14}$$

Applying P_s and P_f to the system of Eq.13.10 and using the above decomposition for x, the system of Eq.13.10 can be equivalently written in the following form:

$$\begin{aligned} \frac{dx_s}{dt} &= \mathcal{A}_s x_s + \mathcal{B}_s u + f_s(x_s, x_f) \\ \frac{\partial x_f}{\partial t} &= \mathcal{A}_f x_f + \mathcal{B}_f u + f_f(x_s, x_f) \\ y_m &= \mathcal{S} x_s + \mathcal{S} x_f, \\ x_s(0) &= P_s x(0) = P_s x_0, \;\; x_f(0) = P_f x(0) = P_f x_0 \end{aligned} \tag{13.15}$$

where $\mathcal{A}_s = P_s\mathcal{A}$, $\mathcal{B}_s = P_s\mathcal{B}$, $f_s = P_s f$, $\mathcal{A}_f = P_f\mathcal{A}$, $\mathcal{B}_f = P_f\mathcal{B}$ and $f_f = P_f f$ and the partial derivative notation in $\frac{\partial x_f}{\partial t}$ is used to denote that the state x_f belongs in an infinite-dimensional space. In the above system, $\mathcal{A}_s$ is a diagonal matrix of dimension $m \times m$ of the form $\mathcal{A}_s = diag\{\lambda_j\}$, $f_s(x_s, x_f)$ and $f_f(x_s, x_f)$ are Lipschitz vector functions, and $\mathcal{A}_f$ is an unbounded differential operator which is exponentially stable (following from the fact that $\lambda_{m+1} < 0$ and the selection of $\mathcal{H}_s, \mathcal{H}_f$). Neglecting the fast and stable infinite-dimensional x_f-subsystem in the system of Eq.13.15, the

following m-dimensional slow system is obtained:

$$\begin{aligned} \frac{d\tilde{x}_s}{dt} &= \mathcal{A}_s\tilde{x}_s + \mathcal{B}_s u + f_s(\tilde{x}_s, 0) \\ \tilde{y}_m &= \mathcal{S}\tilde{x}_s \end{aligned} \tag{13.16}$$

where the tilde symbol in $\tilde{x}_s$ and $\tilde{y}_m$ denotes that these variables are associated with a finite-dimensional system.

13.3.2 Coordinating feedback and switching

Having obtained a finite-dimensional model that describes the dominant dynamics of the KSE, we proceed in this section to describe the proposed procedure for designing the fault-tolerant control system, on the basis of the finite-dimensional approximation in Eq.13.16. To this end, and since our objective is the stabilization of the zero solution of the KSE, we define the controlled outputs as the slow modes of the KSE, and assume (for simplicity) that the number of inputs is equal to the number of slow modes (i.e., $l = m$). Though not discussed explicitly in this chapter, the results can be generalized to address the problem of reference-input tracking (see Chapter 12 for an analogous treatment of the tracking problem). With this in mind, the slow modes of the KSE can be described by the following m-dimensional system:

$$\dot{a}_s(t) = Fa_s(t) + \bar{G}(\bar{z}^k)u(t) + \tilde{f}(a_s(t)) \tag{13.17}$$

where $a_s(t) = [a_1(t) \cdots a_m(t)]^T \in \mathbb{R}^m$, $a_i(t)$ is the amplitude of the i-th eigenmode, $\tilde{x}_s(t) = \sum_{j=1}^{m} a_j(t)\phi_j(z)$, $(x_s(t), \phi_j) = a_j(t)(\phi_j, \phi_j)$, F is an $m \times m$ diagonal matrix of the form $F = diag\{\lambda_j\}$, $\bar{G}$ is an $m \times m$ matrix whose (i,j)-th element is given by $G_{ij} = \phi_i(z_j^k)$, and $\tilde{f}(\cdot)$ is a nonlinear, locally Lipschitz function of its argument. Finally, we define $\bar{f}(a_s) = Fa_s + f(a_s)$ and denote by $\bar{g}_i$ the i-th column of the matrix $\bar{G}$.

The design procedure consists of three basic steps. These include: (1) the synthesis of a stabilizing feedback controller, (2) the characterization of the constrained stability region associated with each control actuator configuration, and (3) the design of a switching law that orchestrates the re-configuration of control actuators in a way that guarantees closed-loop stability in the event of actuator failure. Below is a brief description of each step.

1. *Feedback controller synthesis*

   The first step in designing the fault-tolerant control system is to synthesize a feedback controller that enforces closed-loop stability in the presence of input constraints. This task is carried out on the basis of the finite-dimensional slow system of Eq.13.17 using Lyapunov techniques. In particular, using a quadratic Lyapunov function of the form $V = a_s^T \Phi a_s$, where Φ is a positive-definite symmetric matrix that satisfies the inequality $F^T\Phi + \Phi F - \Phi \bar{G}\bar{G}^T\Phi < 0$, we synthesize the following bounded nonlinear feedback law (see Chapters 3-4 for further details on the controller synthesis and the construction of the stability region):

$$u = -r(a_s, u_{max}^k, \bar{z}_k)\left(L_{\bar{G}}V\right)^T(\bar{z}^k) \tag{13.18}$$

   where:

$$r(a_s, u_{max}^k, \bar{z}^k) = \frac{L_{\bar{f}}^*V + \sqrt{(L_{\bar{f}}^*V)^2 + \left(u_{max}^k|(L_{\bar{G}}V)^T(\bar{z}^k)|\right)^4}}{|(L_{\bar{G}}V)^T(\bar{z}^k)|^2\left[1 + \sqrt{1 + (u_{max}^k|(L_{\bar{G}}V)^T(\bar{z}^k)|)^2}\right]} \tag{13.19}$$

   where $\bar{z}^k = [z_1^k\ z_2^k\ \cdots\ z_m^k]^T$, $k = 1, \cdots, N$, $L_{\bar{f}}^*V = L_{\bar{f}}V + \rho|a_s|^2$, $\rho > 0$, $L_{\bar{G}}V$ is a row vector of the form $[L_{\bar{g}_1}V \cdots L_{\bar{g}_m}V]$. The notation u_{max}^k is used to indicate the magnitude of actuator constraints associated with the k-th configuration. This number is allowed to vary from one configuration to another. The scalar function, $r(\cdot)$, in Eqs.13.18-13.19 can be thought of as a nonlinear controller

gain. This Lyapunov-based gain, which depends on both the magnitude of actuator constraints, u^k_{max}, and the actuator configuration used, $\bar{z}^k$, is shaped in a way that guarantees constraint satisfaction and asymptotic closed-loop stability within a well-characterized region in the state space. The characterization of this region is discussed in the next step.

2. *Characterization of stability regions*

Given that actuator constraints place fundamental limitations on both the initial conditions and actuator locations that can be used for stabilization, it is important for the control system designer to explicitly characterize these limitations by identifying, for each actuator configuration, the set of feasible initial conditions starting from where the constrained closed-loop system is asymptotically stable. As will be discussed in step 3 below, this characterization is necessary for the design of an appropriate switching scheme that ensures fault-tolerance. For the control law designed in step 1, such a characterization can be provided explicitly. Specifically, one can show (see the Proof of Proposition 10.1 in Appendix H for a detailed proof) that the set described by:

$$\Theta(u^k_{max}, \bar{z}_k) \;=\; \{a_s \in \mathbb{R}^m : L^*_{\bar{f}} V \leq u^k_{max} |(L_{\bar{G}} V)^T(\bar{z}_k)|\} \tag{13.20}$$

represents a set where the control action satisfies the constraints and the time-derivative of the Lyapunov function is negative-definite along the trajectories of the closed-loop system of Eq.13.17. Note that the size of this set depends on the magnitude of the constraints. In particular, the set becomes smaller as the constraints become tighter (smaller u^k_{max}). Note also that the set $\Theta(u^k_{max}, \bar{z}_k)$ is parameterized by the actuator locations because the matrix $\bar{G}$ in Eq.13.17 depends on the actuator locations. Therefore, for a given actuator configuration (fixed $\bar{z}_k$), one can use the above inequality to estimate the stability region asso-

ciated with this configuration. This can be done, for example, by constructing an invariant subset of $\Theta(u^k_{max}, \bar{z}_k)$ – preferably the largest – which we denote by $\Omega(u^k_{max}, \bar{z}_k)$. Confining the initial conditions within $\Omega(u^k_{max}, \bar{z}_k)$ ensures that the closed-loop trajectory stays within the region defined by $\Theta(u^k_{max}, \bar{z}_k)$, and thus V continues to decay monotonically, for all times that the k-th actuator configuration is active.

3. *Switching logic for control actuator re-configuration*

   Having designed the feedback control law in step 1, and characterized the stability region associated with each actuator configuration in step 2, the final step in the control system design procedure is to derive a switching rule that orchestrates the re-configuration of the control actuators in the event of actuator failure. This rule determines which of the backup actuator configurations can be activated, in the event of actuator failure, in order to preserve closed-loop stability. The need for a switching rule stems from the fact that, even if the controller enforces closed-loop stability for each actuator configuration individually, closed-loop stability of the switched system is not guaranteed unless restrictions are placed on the switching logic. In particular, owing to the limitations imposed by input constraints on the stability region for each actuator configuration, switching from the current malfunctioning actuator configuration to a well-functioning, but arbitrarily selected, backup configuration will not help preserve closed-loop stability if the state of the system, at the time of actuator failure, lies outside the stability region of the chosen backup configuration. In this case, stabilization using this configuration would require more control action than is allowed by its constraints. This observation underscores the main idea of the proposed switching logic, which is to switch to the actuator con-

figuration for which the closed-loop state resides within the stability region at the time of actuator failure. Without loss of generality, let the initial actuator configuration be $k(0) = 1$ and let T_f be the time when this configuration fails, then the switching rule given by:

$$k(T_f) \;=\; j \;\; if \;\; a_s(T_f) \;\in\; \Omega(u^j_{max}, \bar{z}_j), \;\; j \in \{2, 3, \cdots, N\} \tag{13.21}$$

guarantees asymptotic closed-loop stability. The implementation of the above switching law requires monitoring the closed-loop state trajectory with respect to the stability regions associated with the various actuator configurations.

Remark 13.3 While the fault-tolerant control approach outlined above has been developed on the basis of the finite-dimensional system of Eq.13.17, the large separation between the slow and fast eigenmodes of the spatial differential operator of the KSE allows the application of this approach to the infinite-dimensional system. In particular, one can show (using the singular perturbation formulation of Galerkin's method; see [61]) that the proposed feedback and switching scheme guarantees asymptotic closed-loop stability for the infinite-dimensional system of Eq.13.2, provided that ϵ is sufficiently small. Note that from the definition of ϵ, it follows that $\epsilon \rightarrow 0$ as $m \rightarrow \infty$, which implies that stability of the infinite-dimensional closed-loop system is guaranteed provided that m is sufficiently large. Even though an estimate of how small ϵ needs to be can, in principle, be obtained using singular perturbation methods, such an estimate may be conservative in general and, therefore, the appropriate number of slow modes is usually tested via closed-loop simulations.

Remark 13.4 The stability region associated with each set of actuators is derived on the basis of the approximate ODE model that describes the evolution of the slow modes (with the fast modes neglected). This region describes the set of initial slow states starting from where the reduced-order model can be stabilized for a given set of constrained control actuators. Due to the error introduced by neglecting the fast

modes, this region is not exactly the same as the set of initial slow states starting from where the full system can be stabilized. However, if the separation between the slow and fast modes is large enough, the stability region of the approximate system will approach that of the slow part of the full system. The discrepancy between the two regions can be made small by including additional modes in constructing the reduced-order model. Alternatively, for a given choice of the order of the approximation (that is adequate for stabilization), one can treat the effect of the fast states as a disturbance to the approximate slow system and use this to further constrain the size of the nominal stability region originally derived by neglecting the fast states (e.g., see Chapter 4 for a discussion on the construction of stability regions for constrained nonlinear systems with disturbances).

Remark 13.5 The control objective in this work is to achieve fault-tolerant stabilization of the infinite-dimensional system without using an unnecessarily large number of control actuators. Therefore, from a stability point of view, only a small set (depending on the value of ν) of well-functioning control actuators is needed at any given time to ensure closed-loop stability (which is equal to the number of slow modes being controlled). From a performance standpoint, however, the simultaneous use of multiple sets of actuators at a given time could be useful. On the other hand, this can increase the total cost of control implementation and may not always yield appreciable performance improvement. Furthermore, the simultaneous use of multiple actuator sets to improve performance may not be feasible in some cases due to the fundamental limitations of actuator constraints that restrict the stability region of each actuator set. Therefore, even though a given set of actuators may be non-failing, it may not be possible to use the actuators of that set at a given time if, at this time, the state of the system is outside the corresponding stability region. Using this set in conjunction with the set of operating actuators may in fact lead to instability (see Section 13.4 for simulation examples).

Remark 13.6 Owing to the spatially-distributed nature of the KSE control problem, the switching scheme proposed in this chapter differs from the schemes proposed in hybrid controller design for lumped-parameter systems. For lumped systems, with no spatial variation, the idea is to achieve the control objectives by switching between members of an a priori specified family of feedback functions, whereas in the approach that is followed here, we seek to achieve the control objectives by switching between members of an a priori specified family of spatially-distributed control actuator configurations, using the same feedback function (parameterized by $\bar{z}_k$). The area of switched and hybrid controller design for lumped systems is currently an active area of research (see, for example, [37, 203, 95] and the references therein for some recent results in this area).

Remark 13.7 Under the assumption that the number of measurements is equal to the number of slow modes and that the inverse of the operator $\mathcal{S}$ exists (which can be ensured via appropriate selection of the measurement sensors' locations), an output feedback controller can be designed by combining the state feedback controller of Eqs.13.18-13.19 with an estimator that provides estimates for the states of the approximate ODE model of Eq.13.16 from the measurements. While the estimation error leads to some loss in the size of the stability region obtained under state feedback, this loss can be made small by increasing the order of the ODE approximation and including more measurements. This approach therefore allows us to asymptotically (as $\epsilon \to 0$) recover the state feedback stability region associated with each control actuator configuration.

13.4 Simulation results

In this section, we demonstrate how the integrated feedback and switching scheme outlined in Section 13.3.2 can be used to deal with the problem of actuator failure, in the context of stabilizing the zero solution of the one-dimensional KSE with periodic

boundary conditions and input constraints. For simplicity, we will consider the KSE in the space of odd functions with spatial zero mean. Introducing the Hilbert space $\mathcal{H}$ of sufficiently smooth odd functions that satisfy the boundary conditions of Eq.13.4 and have spatial zero mean (i.e., $\forall\ \omega \in \mathcal{H}$, $\int_{-\pi}^{\pi} \omega(z)dz = 0$) and defining the state function $x \in \mathcal{H}$ as $x(t) = U(z,t), \quad \forall\ z \in [-\pi, \pi]$, the system of Eqs.13.2-13.5 can be written in the form of Eq.13.10, where the domain of definition of the spatial differential operator $\mathcal{A}$ now takes the form:

$$x \in D(\mathcal{A}) = \left\{ x \in \mathcal{H}([-\pi,\pi];\mathbb{R}); \frac{\partial^j U}{\partial z^j}(-\pi,t) = \frac{\partial^j U}{\partial z^j}(\pi,t), \quad j = 0,\ldots,3 \right\} \quad (13.22)$$

and the eigenvalue problem for $\mathcal{A}$ yields $\lambda_j = -\nu j^4 + j^2$, $\phi_j(z) = \sqrt{\frac{1}{\pi}} sin(jz)$, $j = 1,\ldots,\infty$ (note that $\psi_0(z) = \sqrt{\frac{1}{2\pi}}$ and $\psi_j(z) = \sqrt{\frac{1}{\pi}} cos(jz)$, $j = 1,\ldots,\infty$, are not considered here since we focus only on odd functions with spatial zero mean).

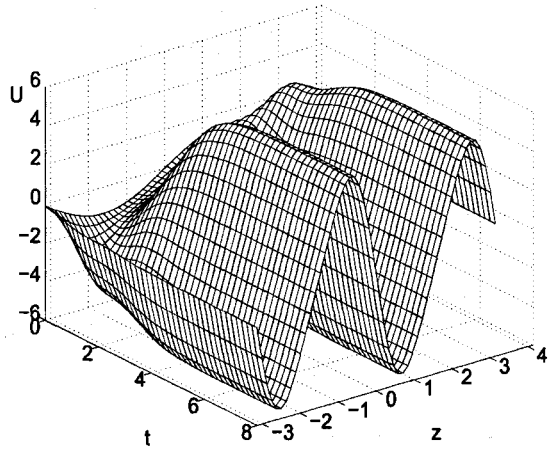

Figure 13.1: Open-loop spatiotemporal profile of $U(z,t)$ for $\nu = 0.2$.

Linearizing the system around the spatially uniform steady-state, we observe that, for $\nu = 0.2$, the system possesses two unstable eigenvalues. Using a 30-th order Galerkin discretization of the KSE, we simulate the open-loop system with $\nu = 0.2$ (higher-order discretizations led to identical results). The resulting spatiotemporal

evolution of $U(z,t)$ is depicted in Figure 13.1 and clearly shows that the spatially uniform steady-state, $U(z,t) = 0$, is unstable for $\nu = 0.2$. The control objective, therefore, is to stabilize the system at this unstable steady-state. To achieve this objective, we consider the first two eigenvalues to be the dominant ones and use standard Galerkin's method to derive the following second-order model (to be used for controller design) that describes the temporal evolution of the amplitudes of the first two eigenmodes:

$$\begin{bmatrix} \dot{a}_1(t) \\ \dot{a}_2(t) \end{bmatrix} = \begin{bmatrix} \lambda_1 & 0 \\ 0 & \lambda_2 \end{bmatrix} \begin{bmatrix} a_1(t) \\ a_2(t) \end{bmatrix} + \begin{bmatrix} \phi_1(z_1) & \phi_1(z_2) \\ \phi_2(z_1) & \phi_2(z_2) \end{bmatrix} \begin{bmatrix} u_1 \\ u_2 \end{bmatrix} + \begin{bmatrix} f_1(a_1, a_2) \\ f_2(a_1, a_2) \end{bmatrix} \tag{13.23}$$

where $(\dot{\tilde{x}}_s, \phi_i) = a_i(t)(\phi_i, \phi_i)$, $i = 1, 2$. z_1 and z_2 are the locations of the two point actuators used for stabilization. The explicit forms of the terms $f_1(a_1, a_2)$ and $f_2(a_1, a_2)$ are omitted for brevity. Before proceeding with controller synthesis on the basis of the above system, we first demonstrate that the first two modes indeed capture the dominant dynamics of the nonlinear KSE. To this end, we simulate the open-loop system, using the high (30-th) order Galerkin discretization, for two values of the instability parameter, $\nu = 1.2$ and $\nu = 0.2$. For each value, we plot the norm of the vector of "fast" modes, $a_f = [a_3 \cdots a_{30}]$, and the amplitude of the first two modes on a three-dimensional plot. The results are shown in Figure 13.2, where the top plot shows the result for $\nu = 1.2$ (where the zero steady-state is globally asymptotically stable), while the bottom plot shows the result for $\nu = 0.2$ (where the zero steady-state is unstable and the system moves to a spatially non-uniform steady-state; see Figure 13.1).

In the bottom plot, for convenience, the results are presented in terms of the deviation from the stable, spatially non-uniform steady-state in order to shift the equilibrium state to the origin, i.e., $a_f^d = [a_3^d \cdots a_{30}^d]$, where $a_i^d = a_i - a_{i,s}$, $i = 3, \cdots, 30$,

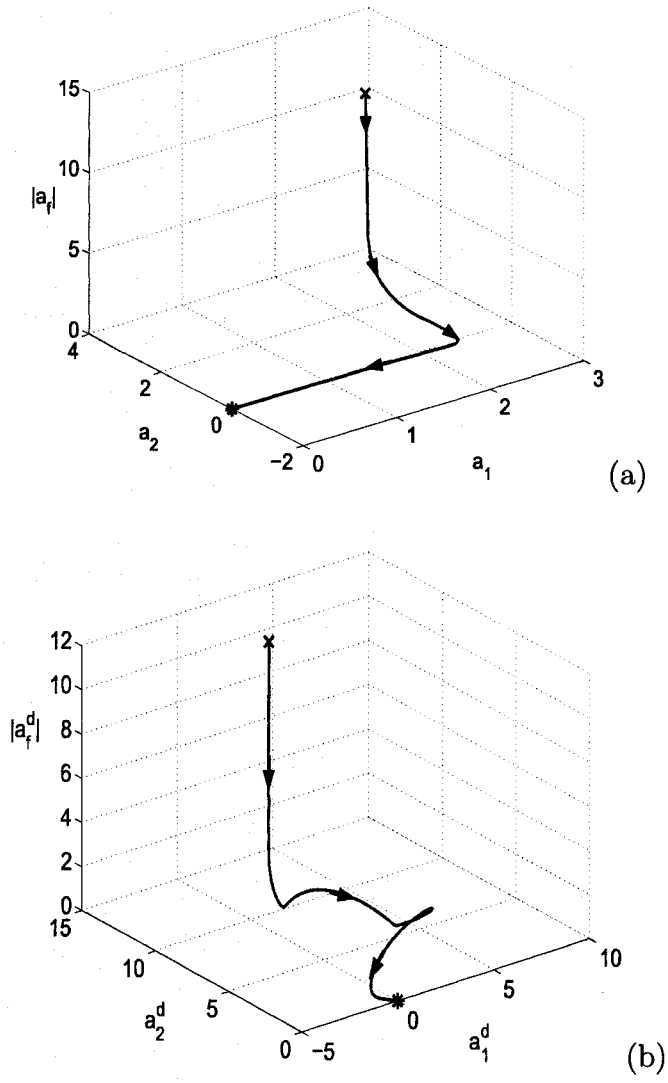

Figure 13.2: (a) Evolution of the norm of the fast modes, $a_f = [a_3, \cdots, a_{30}]$, and of the two dominant modes, a_1 and a_2, for $\nu = 1.2$. (b) Evolution of the norm of the fast modes (in deviation variable form), $a_f^d = [a_3^d, \cdots, a_{30}^d]$, and of the two dominant modes, a_1^d and a_2^d, for $\nu = 0.2$ (all modes are in deviation variable form).

and $a_{i,s}$ is the steady-state value of the i-th mode that corresponds to the spatially non-uniform stable steady-state of the KSE with $\nu = 0.2$. In both plots, it is clear that the dynamics of the high-order system converge quickly to the subspace described by the first two modes, implying that the first two modes are the dominant ones. In particular, note that the norm of the modes $a_f = [a_3 \cdots a_{30}]$ drops quickly to zero and that beyond this point the entire system evolution is basically captured by the evolution of the first two modes. These results motivate the use of the system of Eq.13.23 for the synthesis of the controller, using Eqs.13.18-13.19, and the switching law, using Eqs.13.20-13.21. The controller and switching laws are then implemented on a high-order Galerkin discretization (30-th order) of the nonlinear KSE (further increase in the order of the approximation led to identical results). The closed-loop high-order system is then integrated numerically, forward in time, using explicit Euler method.

To illustrate different aspects of the proposed fault-tolerant control scheme, we consider the following two problems where switching is needed to preserve closed-loop stability. In the first problem, two pairs of point control actuators, placed at $(z_1 = 0.3\pi, z_2 = 0.7\pi)$ (configuration A) and $(z_1 = 0.1\pi, z_2 = 0.9\pi)$ (configuration B) are assumed to be available. Both pairs have the same constraints of $u^A_{max} = u^B_{max} = 2.0$, but only one configuration can be used for control at any given moment. The question to be addressed here is: when is it feasible to switch to configuration B given that a fault is detected in the actuators of configuration A. In the second problem, we assume that a third pair of actuators, located at $(z_1 = 0.2\pi, z_2 = 0.8\pi)$ (Configuration C) with constraints of $u^C_{max} = 0.5$, is also available (in addition to configurations A and B). Again, only one of the three configurations can be active at any given moment. The problem here is to decide which of the two "fall-back" actuator configurations (B

or C) should be activated, once the actuators of configuration A fail. Basically, the first problem deals with the issue of identifying the appropriate switching times for a fixed re-configuration strategy, while second problem addresses the issue of how to select the appropriate actuator re-configuration strategy, among a family of possible choices, in order to provide the necessary fault-tolerance.

The simulation results under state feedback control are presented first. For the first problem, we initially use Eq.13.20 with $\rho = 0.001$ to compute the stability regions for configurations A and B. To simplify the presentation of our results, we show in Figure 13.3a the set of admissible initial conditions for the amplitudes, $a_1(0)$ and $a_2(0)$, of the first two eigenmodes, respectively, for configuration A (solid ellipse) and configuration B (dashed ellipse) (note that $x_s(0) = a_1(0)\phi_1(z) + a_2(0)\phi_2(z)$). From this figure, it is clear that for an initial condition $(a_1(0), a_2(0)) = (0.2, 1.5)$, only configuration A can be used initially since the initial condition is outside the stability region for configuration B. Figures 13.3(b)-13.3(c) depict, respectively, the closed-loop state and manipulated input profiles corresponding to this initial condition and using configuration A. Clearly, the controller successfully stabilizes the KSE at the desired steady-state. Now, suppose that sometime after starting from this initial condition, a fault is detected in configuration A. From Figure 13.3(a), we see that switching to configuration B may or may not solve the problem depending on when the failure of A actually occurs. For example, consider the case when A fails at $t = 3.5$. By monitoring the slow state evolution over time, we find that the state is outside the stability region for B at this time, as shown by point X on the solid trajectory in Figure 13.3(a). Therefore, switching to configuration B will not preserve closed-loop stability (note that the solid trajectory settles at another steady-state after switching at point X). This is also confirmed by the unstable closed-loop state profile in Figure

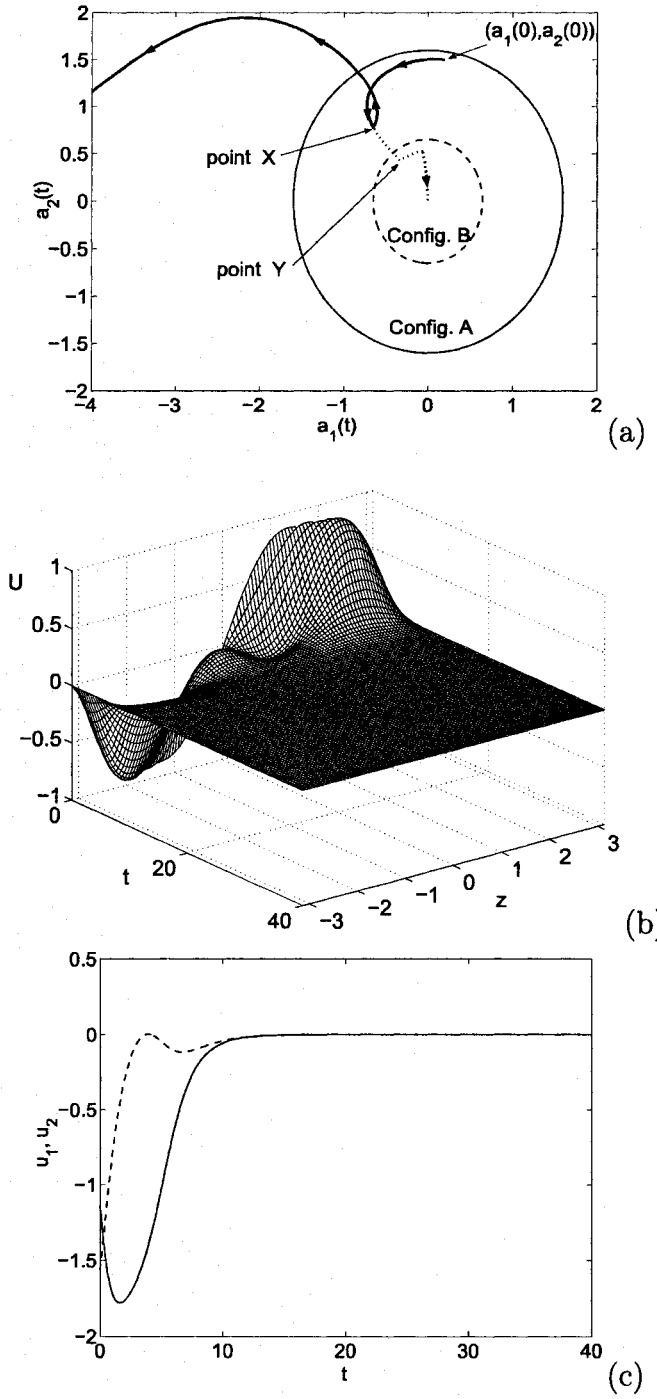

Figure 13.3: (a) Stability regions for configuration A (solid ellipse) and for configuration B (dashed ellipse), (b) Closed-loop state profile (state feedback) for $(a_1(0), a_2(0)) = (0.2, 1.5)$ using configuration A without switching, (c) Corresponding manipulated input profiles for u_1 (solid) and u_2 (dashed).

13.4(a). The corresponding profiles for both manipulated inputs are shown in Figure 13.4(b) which show that the inputs stay saturated. Suppose now that configuration A fails at $t = 5$. In this case, we see from the dashed trajectory in Figure 13.3(a) that the state at this time is within the stability region for configuration B (point Y) and, according to our switching scheme, closed-loop stability can be maintained by switching to configuration B at this time (note that the dashed trajectory in Figure 13.3(a) converges to the origin when configuration B is activated at point Y). This is also demonstrated in Figure 13.5 which shows that the controller successfully stabilizes the KSE when configuration B is activated at $t = 5$.

We now turn our attention to the second problem. The stability regions for configurations A, B, and C are depicted in Figure 13.6(a) by the solid, dashed, and dotted ellipses, respectively. From this figure, it is easy to see that for the initial condition $(a_1(0), a_2(0)) = (0.2, 1.5)$, only configuration A is feasible initially. Suppose that sometime after starting from this initial condition, say $t = 3.5$, a fault is detected in configuration A and it becomes necessary to switch to either configuration B or C. Without using the switching rule of Eq.13.21, it is not clear which of the two configurations should be activated at this time. Figures 13.6(b)-13.6(c) depict, respectively, the resulting closed-loop state and manipulated input profiles when configuration C is chosen. We see in this case that the controller is unable to stabilize the closed-loop system at the desired steady-state. This is expected since the state, at the time of switching, lies outside the stability region for configuration C (see point X on the solid trajectory in Figure 13.6(a)). In contrast, by using the switching logic of the fault-tolerant control scheme proposed in Section 13.3.2, we conclude that it is configuration B – not C – that should be activated because the closed-loop trajectory at this time is inside the stability region of B (see dashed trajectory in Figure 13.6(a)).

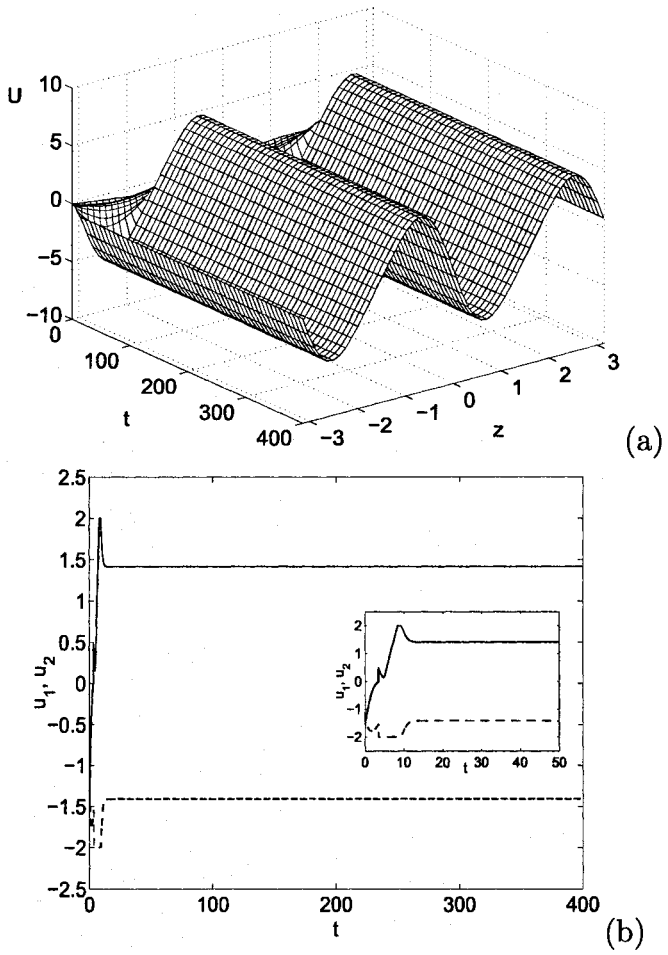

Figure 13.4: (a) Closed-loop state profile (state feedback) for $(a_1(0), a_2(0)) = (0.2, 1.5)$ when configuration A fails at $t = 3.5$ and configuration B is activated, (b) Corresponding manipulated input profiles for u_1 (solid) and u_2 (dashed).

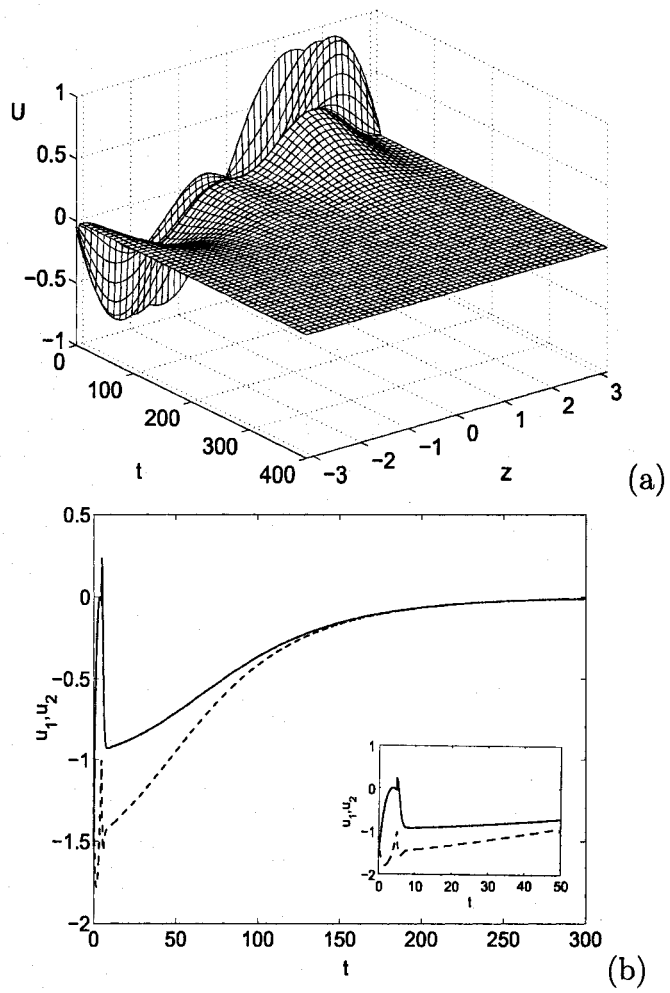

Figure 13.5: (a) Closed-loop state profile (state feedback) for $(a_1(0), a_2(0)) = (0.2, 1.5)$ when configuration A fails at $t = 5$ and configuration B is activated, (b) Corresponding manipulated input profiles for u_1 (solid) and u_2 (dashed).

Figure 13.7 depicts the results for this case which show that the controller successfully stabilizes the closed-loop system when B is activated instead of C. The switching law therefore allows us to choose the appropriate actuator re-configuration scheme.

For the case of output feedback control, measurements from a pair of point sensors, located at $z_1 = 0.35\pi$ and $z_2 = 0.65\pi$, are used to obtain estimates of the first two eigenmodes. The estimates are then used in the implementation of the output feedback controller. Owing to the slight discrepancy between the stability regions obtained under state and output feedback control (see Remark 13.7), the switching law proposed in Eq.13.21 is used only as an approximate guide. The simulation results for this case are consistent with the state feedback results for both problems. We present only the results for the first problem. These are given in Figures 13.8-13.9 which, respectively, show that the closed loop system becomes unstable when configuration A fails at $t = 3.5$ and configuration B is activated, whereas closed-loop stability is maintained by activating configuration B when A fails at $t = 5.0$.

Remark 13.8 The fact that the fast stable modes were neglected in the controller design can result in some degradation in the control performance when the controller is implemented on the full (high-order) system. If these modes die out sufficiently fast, then such degradation would be minimal. However, since the control objective is to achieve stabilization of the PDE system, a second-order model that describes the evolution of the first two modes (which are unstable) was found to be sufficient to design a controller that stabilizes the zero solution of the KSE. Nonetheless, it is possible to enhance the performance further by keeping more modes in the reduced-order model in order to obtain a better approximation of the full system.

Remark 13.9 It should be noted that while the KSE was used in this chapter to demonstrate the design and implementation of the proposed fault-tolerant control scheme, the proposed approach can also be applied to other dissipative PDEs that

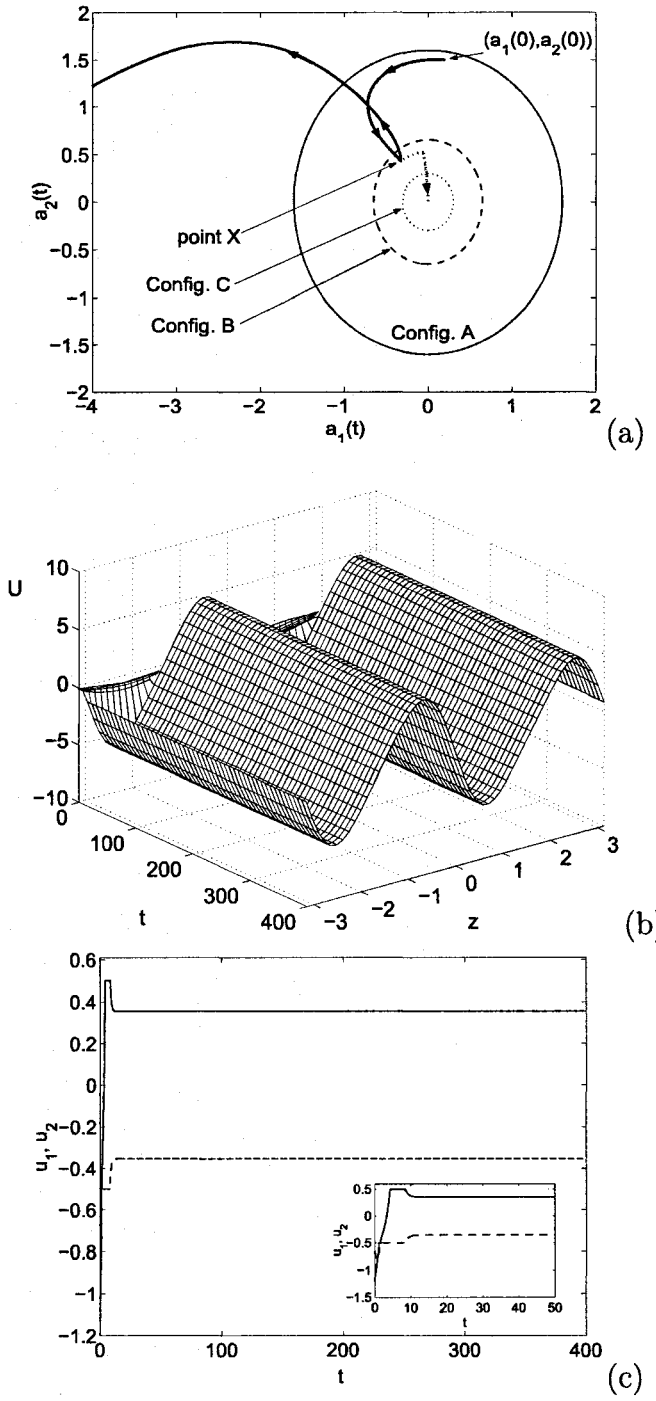

Figure 13.6: (a) Stability regions for configuration A (solid ellipse), configuration B (dashed ellipse), and configuration C, (b) Closed-loop state profile (state feedback) for $(a_1(0), a_2(0)) = (0.2, 1.5)$ when configuration A fails at $t = 3.5$ and configuration C is activated, (b) Corresponding manipulated input profiles for u_1 (solid) and u_2 (dashed).

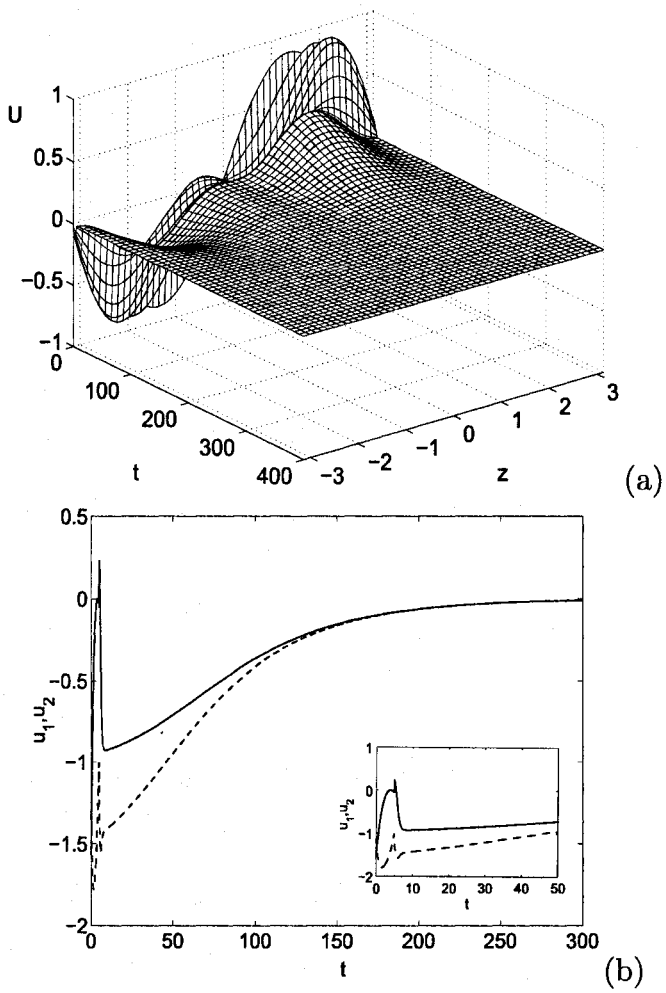

Figure 13.7: (a) Closed-loop state profile (state feedback) for $(a_1(0), a_2(0)) = (0.2, 1.5)$ when configuration A fails at $t = 3.5$ and configuration B is activated, (b) Corresponding manipulated input profiles for u_1 (solid) and u_2 (dashed).

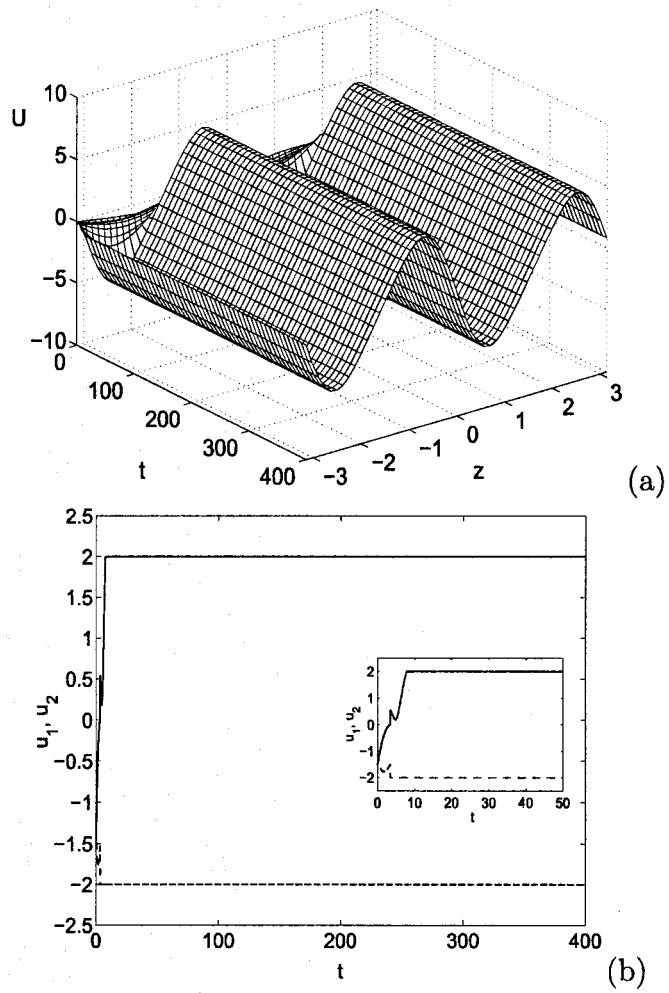

Figure 13.8: (a) Closed-loop state profile (output feedback) for $(a_1(0), a_2(0)) = (0.2, 1.5)$ when configuration A fails at $t = 3.5$ and configuration B is activated, (b) Corresponding manipulated input profiles for u_1 (solid) and u_2 (dashed).

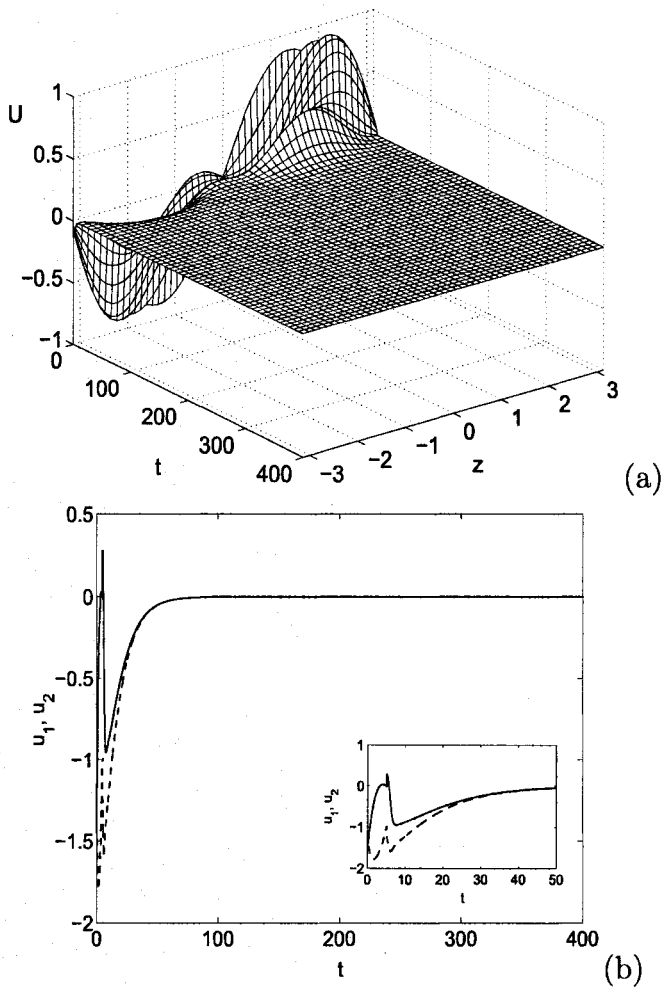

Figure 13.9: (a) Closed-loop state profile (output feedback) for $(a_1(0), a_2(0)) = (0.2, 1.5)$ when configuration A fails at $t = 5$ and configuration B is activated, (b) Corresponding manipulated input profiles for u_1 (solid) and u_2 (dashed).

can model fluid dynamic systems, such as the Burger's equation [28], the Korteweg-de Vries Burgers equation [21] and various forms of the Navier-Stokes equations (such as equations that describe two-dimensional transitional flow in a channel (e.g., see [28])).

13.5 Conclusions

In this chapter, a fault-tolerant control system design methodology was proposed for fluid dynamic systems modeled by highly-dissipative PDEs with constrained control actuators. The central idea of the proposed method is that of coordinating feedback controller synthesis and switching between multiple, spatially-distributed control actuator configurations. Using appropriate finite-dimensional approximations of the PDE system, a stabilizing feedback controller was designed for a given actuator configuration, and an explicit characterization of the constrained stability region was obtained. Switching laws were then derived, on the basis of these stability regions, to orchestrate the transition between the control actuator configurations in a way that guarantees constraint satisfaction and preserves closed-loop stability of the infinite-dimensional system in the event of actuator failures. The results were applied to the problem of suppressing wave formation in falling liquid films via the stabilization of the zero solution of the one-dimensional Kuramoto-Sivashinsky equation with periodic boundary conditions, subject to actuator constraints and failures.

Bibliography

[1] T. Alamo, D. Muoz de la Pea, D. Limon, and E. F. Camacho. Constrained min-max predictive control: a polynomial-time approach. In *Proceedings of 42nd IEEE Conference on Decision and Control*, pages 912–916, Maui, Hawaii, USA, 2003.

[2] F. Allgöwer and H. Chen. Nonlinear model predictive control schemes with guaranteed stability. In R. Berber and C. Kravaris (Eds.), *NATO ASI on Nonlinear Model Based Process Control*, pages 465–494, Kluwer Academic Publishers, Dordrecht, The Netherlands, 1998.

[3] F. Allgöwer and F. J. Doyle. Nonlinear process control - which way to the promised land? In *Proceedings of 5th International Conference on Chemical Process Control*, volume 93, pages 24–45, J. C. Kantor, C. E. Garcia and B. Carnahan Eds., AIChE Symposium Series No. 316, CACHE, AIChE, 1997.

[4] F. Allgöwer, A. Rehm, and E. D. Gilles. An engineering perspective on nonlinear H^∞ control. In *Proceedings of 33rd IEEE Conference on Decision and Control*, pages 2537–2542, Orlando, FL, 1994.

[5] E. Alm and A. P. Arkin. Biological networks. *Current Opinion in Structural Biology*, 13:193–202, 2003.

[6] A. A. Alonso and J. R. Banga. Design of a class of stablizing nonlinear state feedback controllers with bounded inputs. *Ind. & Eng. Chem. Res.*, 37:131–144, 1998.

[7] A. A. Alonso and E. B. Ydstie. Nonlinear control, passivity and the second law of thermodynamics. In *AIChE Annual Meeting, paper 181i, Miami Beach, FL*, 1995.

[8] A. A. Alonso and E. B. Ydstie. Stabilization of distributed systems using irreversible thermodynamics. *Automatica*, 37:1739–1755, 2001.

[9] R. Alur, C. Belta, F. Ivancic, V. Kumar, M. Mintz, G. Pappas, H. Rubin, and J. Schug. Hybrid modeling and simulation of biomolecular networks. In *Lecture Notes in Computer Science Series*, volume 2034, pages 19–32, Di Benedetto, M. D. and A. Sangiovanni-Vincentelli (Eds.), Berlin, Germany: Springer-Verlag, 2001.

[10] R. Alur, C. Belta, V. Kumar, M. Mintz, G. J. Pappas, H. Rubin, and J. Schug. Modeling and analyzing biomolecular networks. *Computing in Science and Engineering*, 4:20–31, 2002.

[11] J. Alvarez, J. J. Alvarez, M. A. Barron, and R. Suarez. The global stabilization of a two-input three-state polymerization reactor with saturated feedback. In *Proceedings of the American Control Conference*, pages 2917–2921, San Francisco, CA, 1993.

[12] J. Alvarez, J. J. Alvarez, and R. Suarez. Nonlinear bounded control for a class of continuous agitated tank reactors. *Chem. Eng. Sci.*, 46:3235–3249, 1991.

[13] C. Antoniades and P. D. Christofides. Feedback control of nonlinear differential difference equation systems. *Chem. Eng. Sci.*, 54:5677–5709, 1999.

[14] C. Antoniades and P. D. Christofides. Robust control of nonlinear time-delay systems. *Appl. Math. & Comp. Sci.*, 9:811–838, 1999.

[15] C. Antoniades and P. D. Christofides. Nonlinear feedback control of parabolic partial differential difference equation systems. *Int. J. Contr.*, 73:1572–1591, 2000.

[16] C. Antoniades and P. D. Christofides. Integrating nonlinear output feedback control and optimal actuator/sensor placement in transport-reaction processes. *Chem. Eng. Sci.*, 56:4517–4535, 2001.

[17] C. Antoniades and P. D. Christofides. Studies on nonlinear dynamics and control of a tubular reactor with recycle. *Nonlinear Analysis: Theory, Methods & Applications*, 47:5933–5944, 2001.

[18] C. Antoniades and P. D. Christofides. Integrated optimal actuator/sensor placement and robust control of uncertain transport-reaction processes. *Comp. & Chem. Eng.*, 26:187–203, 2002.

[19] H. B. Aradhye, J. F. Davis, and B. R. Bakshi. Art-2 and multiscale art-2 for on-line process fault detection - validation via industrial case studies and monte carlo simulation. *Annual Reviews in Control*, 26:113–127, 2002.

[20] Y. Arkun and J. P. Calvet. Robust stabilization of input/output linearizable systems under uncertainty and disturbances. *AIChE J.*, 38:1145–1154, 1992.

[21] A. Armaou and P. D. Christofides. Wave suppression by nonlinear finite-dimensional control. *Chem. Eng. Sci.*, 55:2627–2640, 2000.

[22] Z. Artstein. Stabilization with relaxed control. *Nonlinear Analysis*, 7:1163–1173, 1983.

[23] J. A. Atwell and B. B. King. Proper orthogonal decomposition for reduced basis feedback controllers for parabolic equations. *Mathematical and Computer Modeling*, 33:1–19, 2001.

[24] B. Aufderheide, V. Prasad, and B. W. Bequette. A comparison of fundamental model-based and multiple model predictive control. In *Proceedings of 40th IEEE Conference on Decision and Control*, pages 4863–4868, Orlando, FL, 2001.

[25] T. A. Badgwell. Robust model predictive control of stable linear systems. *Int. J. Contr.*, 68:797–818, 1997.

[26] T. A. Badgwell. Robust stability conditions for SISO model predictive control algorithms. *Automatica*, 33:1357–1361, 1997.

[27] J. E. Bailey. Mathematical modeling and analysis in biochemical engineering: Past accomplishments and future opportunities. *Biotechnology Progress*, 14:8–20, 1998.

[28] J. Baker, A. Armaou, and P. D. Christofides. Nonlinear control of incompressible fluid flows: Application to burgers' equation and 2d channel flow. *J. Math. Anal. Appl.*, 252:230–255, 2000.

[29] M. J. Balas. Feedback control of linear diffusion processes. *Int. J. Contr.*, 29:523–533, 1979.

[30] M. J. Balas. Nonlinear finite-dimensional control of a class of nonlinear distributed parameter systems using residual mode filters: A proof of local exponential stability. *J. Math. Anal. Appl.*, 162:63–70, 1991.

[31] A. Banerjee and Y. Arkun. Model predictive control of plant transitions using a new identification technique for interpolating nonlinear models. *J. Proc. Contr.*, 8:441–457, 1998.

[32] J. Bao, W. Z. Zhang, and P. L. Lee. Passivity-based decentralized failure-tolerant control. *Ind. & Eng. Chem. Res.*, 41:5702–5715, 2002.

[33] P. I. Barton and C. C. Pantelides. Modeling of combined discrete/continuous processes. *AIChE Journal*, 40:966–979, 1994.

[34] G. Bastin and D. Dochain. *On-line Estimation and Adaptive Control of Bioreactors.* Elsevier Science Pub. B. V., Amsterdam, 1990.

[35] A. Batigun, K. R. Harris, and A. Palazoglu. Studies on the analysis of nonlinear processes via functional expansions. I. Solution of nonlinear ODEs. *Chem. Eng. Sci.*, 52:3183–3195, 1997.

[36] A. Bemporad, F. Borreli, and M. Morari. Min-max control of constrained uncertain discrete-time linear systems. *IEEE Trans. Automat. Contr.*, 48:1600–1606, 2003.

[37] A. Bemporad and M. Morari. Control of systems integrating logic, dynamics and constraints. *Automatica*, 35:407–427, 1999.

[38] J. Bentsman and Y. Orlov. Reduced spatial order model reference adaptive control of spatially varying distributed parameter systems of parabolic and hyperbolic types. *Int. J. Adapt. Contr. & Sig. Proc.*, 15:679–696, 2001.

[39] W. B. Bequette. Nonlinear control of chemical processes: A review. *Ind. & Eng. Chem. Res.*, 30:1391–1413, 1991.

[40] R. R. Bitmead, M. Gevers, and V. Wertz. *Adaptive Optimal Control-The Thinking Man's GPC.* Prentice-Hall, Englewood Cliffs, NJ, 1990.

[41] M. Blanke, R. Izadi-Zamanabadi, S. A. Bogh, and C. P. Lunau. Fault-tolerant control systems – a holistic view. *Contr. Eng. Prac.*, 5:693–702, 1997.

[42] C. F. Bohren and D. R. Huffman. *Absorption and Scattering of Light by Small Particles.* Wiley, New York, 1983.

[43] H. Bounit and H. Hammouri. Bounded feedback stabilization and global separation principle of distributed parameter systems. *IEEE Trans. Automat. Contr.*, 42:414–419, 1997.

[44] M. S. Branicky. Multiple Lyapunov functions and other analysis tools for switched and hybrid systems. *IEEE Trans. Automat. Contr.*, 43:475–482, 1998.

[45] R. Brockett. Minimum attention control. In *Proceedings of 36th Conference on Decision and Control*, pages 2628–2632, San Diego, CA, 1997.

[46] J. A. Burns and B. B. King. A reduced basis approach to the design of low-order feedback controllers for nonlinear continuous systems. *Journal of Vibration and Control*, 4:297–323, 1998.

[47] C. A. Byrnes, D. S. Gilliam, and V. I. Shubov. Global Lyapunov stabilization of a nonlinear distributed parameter system. In *Proceedings of 33rd IEEE Conference on Decision and Control*, pages 1769–1774, Orlando, FL, 1994.

[48] J. P. Calvet and Y. Arkun. Feedforward and feedback linearization of nonlinear systems and its implementation using internal model control. *Ind. & Eng. Chem. Res.*, 27:1822, 1991.

[49] P. J. Campo and M. Morari. Robust model predictive control. In *Proceedings of the American Control Conference*, pages 1021–1026, Green Valley, AZ, 1987.

[50] H. Chen and F. Allgöwer. A quasi-infinite horizon nonlinear model predictive control scheme with guaranteed stability. *Automatica*, 34:1205–1217, 1998.

[51] L. H. Chen and H. C. Chang. Nonlinear waves on liquid film surfaces-II. Bifurcation analyses of the long-wave equation. *Chem. Eng. Sci.*, 41:2477–2486, 1986.

[52] F. Chernousko. Bounded controls in distributed parameter systems. *Journal of Applied Mathematics and Mechanics*, 56:707–723, 1992.

[53] L. Chisci, P. Falugi, and G. Zappa. Gain-scheduling MPC of nonlinear systems. *Int. J. Robust & Nonlin. Contr.*, 13:295–308, 2003.

[54] T. Chiu and P. D. Christofides. Nonlinear control of particulate processes. *AIChE J.*, 45:1279–1297, 1999.

[55] T. Chiu and P.D. Christofides. Robust control of particulate processes using uncertain population balances. *AIChE J.*, 46:266–280, 2000.

[56] D. Chmielewski and V. Manousiouthakis. On constrained infinite-time linear quadratic optimal control. *Syst. & Contr. Lett.*, 29:121–129, 1996.

[57] D. Chmielewski and V. Manousiouthakis. Constrained infinite-time nonlinear quadratic-optimal control with application to chemical reactors. In *Proceedings of Conference on Control Applications*, Honolulu, HA, 1998.

[58] J. H. Chow and P. V. Kokotovic. Near-optimal feedback stabilization of a class of nonlinear singularly perturbed systems. *SIAM J. Contr. & Optim.*, 16:756–770, 1978.

[59] P. D. Christofides. Output feedback control of nonlinear two-time-scale processes. *Ind. & Eng. Chem. Res.*, 37:1893–1909, 1998.

[60] P. D. Christofides. Robust output feedback control of nonlinear singularly perturbed systems. *Automatica*, 36:45–52, 2000.

[61] P. D. Christofides. *Nonlinear and Robust Control of PDE Systems: Methods and Applications to Transport-Reaction Processes.* Birkhäuser, Boston, 2001.

[62] P. D. Christofides. *Model-Based Control of Particulate Processes.* Kluwer Academic Publishers, 2002.

[63] P. D. Christofides and A. Armaou. Global stabilization of the Kuramoto-Sivashinsky equation via distributed output feedback control. *Syst. & Contr. Lett.*, 39:283–294, 2000.

[64] P. D. Christofides and P. Daoutidis. Compensation of measurable disturbances in two-time-scale nonlinear systems. *Automatica*, 32:1553–1573, 1996.

[65] P. D. Christofides and P. Daoutidis. Feedback control of two-time-scale nonlinear systems. *Int. J. Contr.*, 63:965–994, 1996.

[66] P. D. Christofides and P. Daoutidis. Robust control of multivariable two-time-scale nonlinear systems. *J. Proc. Contr.*, 7:313–328, 1997.

[67] P. D. Christofides and A. R. Teel. Singular perturbations and input-to-state stability. *IEEE Trans. Automat. Contr.*, 41:1645–1650, 1996.

[68] P. D. Christofides, A. R. Teel, and P. Daoutidis. Robust semi-global output tracking for nonlinear singularly perturbed systems. *Int. J. Contr.*, 65:639–666, 1996.

[69] D. C. Chu and G. E. Karniadakis. A direct numerical simulation of laminar and turbulent flow over riblet-mounted surfaces. *J. Fluid Mech.*, 250:1–42, 1993.

[70] M. Corless. Control of uncertain nonlinear systems. *J. Dyn. Syst. Meas. & Contr.*, 115:362–372, 1993.

[71] E. Coulibaly, S. Maiti, and C. Brosilow. Internal model predictive control. *Automatica*, 31:1471–1479, 1995.

[72] F. A. Cuzzola, J. C. Geromel, and M. Morari. An improved approach for constrained robust model predictive control. *Automatica*, 38:1183–1189, 2002.

[73] P. Daoutidis and P. D. Christofides. Dynamic feedforward/output feedback control of nonlinear processes. *Chem. Eng. Sci.*, 50:1889–2007, 1995.

[74] P. Daoutidis and C. Kravaris. Dynamic output feedback control of multivariable nonlinear processes. *Chem. Eng. Sci.*, 49:433–447, 1994.

[75] M. S. Dasika, A. Gupta, and C. D. Maranas. A mixed integer linear programming (MILP) framework for inferring time delay in gene regulatory networks. In *Proceedings of Pacific Symposium on Biocomputing*, pages 474–485, Hawaii, HI, 2004.

[76] J. F. Davis, M. L. Piovoso, K. Kosanovich, and B. Bakshi. Process data analysis and interpretation. *Advances in Chemical Engineering*, 25:1–103, 1999.

[77] H. De Jong. Modeling and simulation of genetic regulatory systems: A literature review. *Journal of Computational Biology*, 9:67–103, 2002.

[78] G. De Nicolao, L. Magni, and R. Scattolini. On robustness of receding horizon control with terminal constraints. *IEEE Trans. Automat. Contr.*, 41:451–453, 1996.

[79] N. M. C. De oliveira and L. T. Biegler. Constraint handling and stability properties of model-predictive control. *AIChE J.*, 40:1138–1155, 1994.

[80] C. De Persis and A. Isidori. A geometric approach to nonlinear fault detection and isolation. *IEEE Trans. Automat. Contr.*, 46:853–865, 2001.

[81] R. A. DeCarlo, M. S. Branicky, S. Pettersson, and B. Lennartson. Perspectives and results on the stability and stabilizability of hybrid systems. *Proceedings of the IEEE*, 88:1069–1082, 2000.

[82] M.A. Demetriou. Numerical investigation on optimal actuator/sensor location of parabolic PDEs. In *Proceedings of the American Control Conference*, pages 1722–1726, San Diego, CA, 1999.

[83] G. Diblasio. Optimal control with finite horizon for distributed parameter systems with constrained controls. *SIAM J. Contr. & Optim.*, 29:909–925, 1991.

[84] J. Dimitratos, G. Elicabe, and C. Georgakis. Control of emulsion polymerization reactors. *AIChE J.*, 40:1993–2021, 1994.

[85] D. Dochain. State observation and adaptive linearizing control for distributed parameter (bio)chemical reactors. *Int. J. Adapt. Contr. & Sig. Proc.*, 15:633–653, 2001.

[86] D. Dochain and M. Perrier. Control design for nonlinear wastewater treatment processes. *Wat. Sci. Tech.*, 18:283–294, 1993.

[87] J. W. Eaton and J. B. Rawlings. Feedback control of chemical processes using on-line optimization techniques. *Comp. & Chem. Eng.*, 14:469–479, 1990.

[88] N. H. El-Farra, A. Armaou, and P. D. Christofides. Analysis and control of palabolic PDE systems with input constraints. *Automatica*, 39:715–725, 2003.

[89] N. H. El-Farra, T. Chiu, and P. D. Christofides. Analysis and control of particulate processes with input constraints. *AIChE J.*, 47:1849–1865, 2001.

[90] N. H. El-Farra and P. D. Christofides. Feedback control of switched nonlinear systems using multiple Lyapunov functions. In *Proceedings of American Control Conference*, pages 3496–3502, Arlington, VA, 2001.

[91] N. H. El-Farra and P. D. Christofides. Integrating robustness, optimality and constraints in control of nonlinear processes. *Chem. Eng. Sci.*, 56:1841–1868, 2001.

[92] N. H. El-Farra and P. D. Christofides. Robust near-optimal output feedback control of nonlinear systems. *Int. J. Contr.*, 74:133–157, 2001.

[93] N. H. El-Farra and P. D. Christofides. Switching and feedback laws for control of constrained switched nonlinear systems. In *Lecture Notes in Computer Science*, volume 2289, pages 164–178, Tomlin, C. J. and M. R. Greenstreet Eds., Berlin, Germany: Springer-Verlag, 2002.

[94] N. H. El-Farra and P. D. Christofides. Bounded robust control of constrained multivariabe nonlinear processes. *Chem. Eng. Sci.*, 58:3025–3047, 2003.

[95] N. H. El-Farra and P. D. Christofides. Coordinating feedback and switching for control of hybrid nonlinear processes. *AIChE J.*, 49:2079–2098, 2003.

[96] N. H. El-Farra and P. D. Christofides. Hybrid control of parabolic PDEs: Handling faults of constrained control actuators. In *Lecture Notes in Computer Science Series*, volume 2623, pages 172–187, O. Maler and A. Pnueli (Eds.), Springer-Verlag, Berlin, 2003.

[97] N. H. El-Farra and P. D. Christofides. Robust inverse optimal control of nonlinear systems. *Int. J. Robust & Nonlin. Contr.*, 13:1371–1388, 2003.

[98] N. H. El-Farra and P. D. Christofides. Coordinated feedback and switching for control of spatially-distributed processes. *Comp. & Chem. Eng.*, 28:111–128, 2004.

[99] N. H. El-Farra, Y. Lou, and P. D. Christofides. Fault-tolerant control of fluid dynamic systems via coordinated feedback and switching. *Comp. & Chem. Eng.*, 27:1913–1924, 2003.

[100] N. H. El-Farra, P. Mhaskar, and P. D. Christofides. Hybrid control of uncertain process systems. In *Proceedings of 8th International Symposium on Process Systems and Engineering*, pages 814–819, Kumming, P.R. China, 2003.

[101] N. H. El-Farra, P. Mhaskar, and P. D. Christofides. Hybrid predictive control of nonlinear systems: Method and applications to chemical processes. *Int. J. Robust & Nonlin. Contr.*, 14:199–225, 2004.

[102] N. H. El-Farra, P. Mhaskar, and P. D. Christofides. Uniting bounded control and MPC for stabilization of constrained linear systems. *Automatica*, 40:101–110, 2004.

[103] D. Endy and R. Brent. Modelling cellular behavior. *Nature*, 409:391–395, 2001.

[104] S. Engell, S. Kowalewski, C. Schulz, and O. Stursberg. Continuous-discrete interactions in chemical processing plants. *Proceedings of the IEEE*, 88:1050–1068, 2000.

[105] C. A. Farschman, K. P. Viswanath, and E. B. Ydstie. Process systems and inventory control. *AIChE J.*, 44:1841–1857, 1998.

[106] X.-J. Feng and H. Rabitz. Optimal identification of biochemical reaction networks. *Biophysical Journal*, 86:1270–1281, 2004.

[107] A. Fernando, C. Fontes, and L. Magni. Min-max model predictive control of nonlinear systems using discontinuous feedback. *IEEE Trans. Automat. Contr.*, 48:1750–1755, 2003.

[108] W. R. Fisher, M. F. Doherty, and J. M. Douglas. Steady-state control as a prelude to dynamic control. *Chem. Eng. Res. Des.*, 6:353–357, 1985.

[109] B. Foss and S. J. Qin. Interpolating optimizing process control. *J. Proc. Contr.*, 7:129–138, 1997.

[110] P. M. Frank and X. Ding. Survey of robust residual generation and evaluation methods in observer-based fault detection systems. *J. Proc. Contr.*, 7:403–424, 1997.

[111] R. A. Freeman and P. V. Kokotovic. Robust control Lyapunov functions: The measurement feedback case. In *Proceedings of 33rd IEEE Conference on Decision and Control*, pages 3533–3538, Lake Buena Vista, FL, 1994.

[112] R. A. Freeman and P. V. Kokotovic. *Robust Nonlinear Control Design: State-Space and Lyapunov Techniques.* Birkhauser, Boston, 1996.

[113] E. Fridman. Near-optimal H^∞ control of linear sinularly perturbed systems. *IEEE Trans. Automat. Contr.*, 41:236–240, 1996.

[114] E. Fridman. Exact slow-fast decomposition of the hamilton-jacobi equation of singularly perturbed systems. In *Proceedings of American Control Conference*, pages 1503–1507, Philadelphia, PA, 1998.

[115] S. K. Friedlander. *Smoke, Dust, and Haze: Fundamentals of Aerosol Behavior.* Wiley, New York, 1977.

[116] A. Friedman. *Partial Differential Equations.* Holt, Rinehart & Winston, New York, 1976.

[117] C. E. Garcia, D. M. Prett, and M. Morari. Model predictive control: Theory and practice–a survey. *Automatica*, 25:335–348, 1989.

[118] V. Garcia-Onorio and B. E. Ydstie. Distributed, asynchronous and hybrid simulation of process networks using recording controllers. *Int. J. Robust & Nonlin. Contr.*, 14:227–248, 2004.

[119] F. Gelbart and J. H. Seinfeld. Numerical solution of the dynamic equation for particulate processes. *J. Comp. Phys.*, 28:357–375, 1978.

[120] H. Genceli and M. Nikolaou. Robust stability analysis of constrained l(1)–norm model predictive control. *AIChE J.*, 39:1954–1965, 1993.

[121] H. Genceli and M. Nikolaou. Robust stability analysis of constrained l1-norm model predictive control. *AIChE J.*, 39:1954–1965, 1993.

[122] R. Ghosh and C. J. Tomlin. Lateral inhibition through delta-notch signaling: A piecewise affine hybrid model. In *Lecture Notes in Computer Science Series*, volume 2034, pages 232–246, Di Benedetto, M. D. and A. Sangiovanni-Vincentelli (Eds.), Berlin, Germany: Springer-Verlag, 2001.

[123] C. Giersch. Mathematical modelling of metabolism. *Current Opinion in Plant Biology*, 3:249–253, 2000.

[124] J. M. Greene and J. S. Kim. The steady-states of the Kuramoto-Sivashinsky equation. *Physica D.*, 33:99–120, 1988.

[125] G. Grimm, M. Messina, A. Teel, and S. Tuna. Nominally robust model predictive control with state constraints. In *Proceedings of 42nd IEEE Conference on Decision and Control,* to appear, Maui, HI, 2003.

[126] I. E. Grossmann, S. A. van den Heever, and I. Harjukoski. Discrete optimization methods and their role in the integration of planning and scheduling. In *Proceedings of 6th International Conference on Chemical Process Control*, pages 124–152, Tucson, AZ, 2001.

[127] K. M. Hangos, A. A. Alonso, J. D. Perkins, and E. B. Ydstie. Thermodynamic approach to the structural stability of process plants. *AIChE J.*, 45:802–816, 1999.

[128] I. Harjunkoski, V. Jain, and I. E. Grossmann. Hybrid mixed-integer/constrained logic programming strategies for solving scheduling and combinatorial optimization problems. *Comp. & Chem. Eng.*, 24:337–343, 2000.

[129] K. R. Harris and A. Palazoglu. Studies on the analysis of nonlinear processes via functional expansions. II. forced dynamic responses. *Chem. Eng. Sci.*, 52:3197–3207, 1997.

[130] K. R. Harris and A. Palazoglu. Studies on the analysis of nonlinear processes via functional expansions. III. control design. *Chem. Eng. Sci.*, 53:4005–4022, 1998.

[131] T. J. Harris, F. Boudreau, and J. F. MacGregor. Performance assessment of multivariable feedback controllers. *Automatica*, 32:1505–1518, 1996.

[132] J. Hasty, F. Isaacs, M. Dolnik, D. McMillen, and J. J. Collins. Designer gene networks: Towards fundamental cellular control. *Chaos*, 11:207–220, 2001.

[133] J. Hasty, D. McMillen, F. Isaacs, and J. J. Collins. Computational studies of gene regulatory networks: In numero molecular biology. *Nature Reviews Genetics*, 2:268–279, 2001.

[134] V. Hatzimanikatis, K. H. Lee, and J. E. Bailey. A mathematical description of regulation of the G1-S transition of the mammalian cell cycle. *Biotechnology and Bioengineering*, 65:631–637, 1999.

[135] M. A. Henson and D. E. Seborg. Time delay compensation for nonlinear processes. *Ind. & Eng. Chem. Res.*, 33:1493–1500, 1994.

[136] M. A. Henson and D. E. Seborg. *Nonlinear Process Control.* Prentice-Hall, Englewood Cliffs, NJ, 1997.

[137] J. Hespanha, D. Liberzon, A. S. Morse, B. D. O. Anderson, T. S. Brinsmead, and F. De Bruyne. Multiple model adaptive control - Part 2: Switching. *Int. J. Robust & Nonlin. Contr.*, 11:479–496, 2001.

[138] J. P. Hespanha and A. S. Morse. Stability of switched systems with average dwell time. In *Proceedings of 38th IEEE Conference on Decision and Control*, pages 2655–2660, Phoenix, AZ, 1999.

[139] P. J. Hill and K. M. Ng. New discretization procedure for the agglomeration equation. *AIChE J.*, 42:727–741, 1996.

[140] P. Holmes, J. L. Lumley, and G. Berkooz. *Turbulence, Coherent Structures, Dynamical Systems and Symmetry.* Cambridge University Press, New York, 1996.

[141] K. A. Hoo and J. C. Kantor. An exothermic continuous stirred tank reactor is feedback equivalent to a linear system. *Chem. Eng. Comm.*, 37:1–17, 1985.

[142] K. A. Hoo and D. G. Zheng. Low-order control-relevant models for a class of distributed parameter systems. *Chem. Eng. Sci.*, 56:6683–6710, 2001.

[143] A. P. Hooper and R. Grimshaw. Nonlinear instability at the interface between two viscous fluids. *Phys. Fluids*, 28:37–45, 1985.

[144] K. Hrissagis and O. D. Crisalle. Mixed objective optimization for robust predictive controller synthesis. In *Proceedings of 5th International Conference on Chemical Process Control,* in press, Tahoe City, CA, 1997.

[145] B. Hu, X. Xu, P. J. Antsaklis, and A. N. Michel. Robust stabilizing control law for a class of second-order switched systems. *Syst. & Contr. Lett.*, 38:197–207, 1999.

[146] C. B. Hu and R. Temam. Robust control of the Kuramoto-Sivashinsky equation. *Dynamics of Continuous Discrete & Impulsive Systems-Series B-Applications & Algorithms*, 8:315–338, 2001.

[147] T. Hu and Z. Lin. Composite quadratic Lyapunov functions for constrained control systems. In *Proceedings of 41st IEEE Conference on Decision and Control*, pages 3500–3505, Las Vegas, NV, 2002.

[148] A. Isidori. *Nonlinear Control Systems: An Introduction.* Springer-Verlag, Berlin-Heidelberg, second edition, 1989.

[149] A. Isidori. A necessary condition for nonlinear H_∞ control via measurement feedback. *Syst. & Contr. Lett.*, 23:169–177, 1994.

[150] A. Isidori. Stabilization of nonlinear systems using output feedback. In *Dynamical Systems, Control, Coding, Computer Vision: New Trends, Interfaces, and Interplay*, pages 111–133, G. Picci and D. S. Gilliam Eds., Birkhäuser, 1999.

[151] A. Isidori and A. Astolfi. Disturbance attenuation and H_∞ control via measurement feedback in a nonlinear system. *IEEE Trans. Automat. Control*, 37:1283–1293, 1992.

[152] A. Isidori and W. Kang. H_∞ control via measurement feedback for general nonlinear systems. *IEEE Trans. Automat. Control*, 40:466–472, 1995.

[153] G. R. Jerauld, Y. Vasatis, and M. F. Doherty. Simple conditions for the appearance of sustained oscillations in continuous crystallizers. *Chem. Eng. Sci.*, 38:1675–1681, 1983.

[154] Z. P. Jiang, A. R. Teel, and L. Praly. Small-gain theorem for ISS systems and applications. *Math. Control Signals Systems*, 7:95–120, 1995.

[155] R. E. Kalman. When is a control system optimal? *J. Basic Eng.*, 86:51–60, 1964.

[156] I. Kanellakopoulos, P. V. Kokotovic, and R. Marino. An extended direct scheme for robust adaptive nonlinear control. *Automatica*, 27:247–255, 1991.

[157] N. Kapoor and P. Daoutidis. Stabilization of systems with input constraints. *Int. J. Contr.*, 34:653–675, 1998.

[158] N Kapoor and P. Daoutidis. An observer-based anti-windup scheme for nonlinear systems with input constraints. *Int. J. Contr.*, 9:18–29, 1999.

[159] N. Kapoor and P. Daoutidis. On the dynamics of nonlinear systems with input constraints. *Chaos*, 9:88–94, 1999.

[160] N. Kapoor and P. Daoutidis. Stabilization of nonlinear processes with input constraints. *Comp. & Chem. Eng.*, 24:9–21, 2000.

[161] N. Kapoor, A. R. Teel, and P. Daoutidis. An anti-windup design for linear systems with input saturation. *Automatica*, 34:559–574, 1998.

[162] N. Kazantzis and C. Kravaris. A nonlinear Luenberger-type observer with application to catalytic activity estimation. In *Proceedings of American Control Conference*, pages 1756–1760, Seattle, WA, 1995.

[163] N. Kazantzis and C. Kravaris. Energy-predictive control: a new synthesis approach for nonlinear process control. *Chem. Eng. Sci.*, 54:1697–1709, 1999.

[164] N. Kazantzis and C. Kravaris. Nonlinear observer design using Lyapunov's auxiliary theorem. *Syst. & Contr. Lett.*, 34:241–247, 1999.

[165] S. Keerthi and E. Gilbert. Optimal, infinite horizon feedback laws for a general class of constrained discrete time systems. *Journal of Optimization Theory and Applications*, 57:265–293, 1988.

[166] T. A. Kendi and F. J. Doyle. An anti-windup scheme for input-output linearization. In *Proceedings of 3rd European Control Conference*, pages 2653–2658, Rome, Italy, 1995.

[167] I. G. Kevrekidis, B. Nicolaenko, and J. C. Scovel. Back in the saddle again: A computer assisted study of the Kuramoto-Sivashinsky equation. *SIAM J. Appl. Math.*, 50:760–790, 1990.

[168] H. Khalil. Robust servomechanism output feedback controller for feedback linearizable systems. *Automatica*, 30:1587–1599, 1994.

[169] H. K. Khalil. Stability analysis of nonlinear multi-parameter singularly perturbed systems. *IEEE Trans. Automat. Contr.*, 32:260–263, 1987.

[170] H. K. Khalil. *Nonlinear Systems*. Macmillan Publishing Company, New York, second edition, 1996.

[171] H. K. Khalil and F. Esfandiari. Semiglobal stabilization of a class of nonlinear systems using output feedback. *IEEE Trans. Automat. Contr.*, 38:1412–1415, 1993.

[172] T. Kobayashi. Adaptive stabilization of the Kuramoto-Sivashinsky equation. *Int. J. Syst. Sci.*, 33:175–180, 2002.

[173] P. Kokotovic and M. Arcak. Constructive nonlinear control: a historical perspective. *Automatica*, 37:637–662, 2001.

[174] M. V. Kothare, P. J. Campo, M. Morari, and C. N. Nett. A unified framework for the study of anti-windup designs. *Automatica*, 30:1869–1883, 1994.

[175] S. L. D. Kothare and M. Morari. Contractive model predictive control for constrained nonlinear systems. *IEEE Trans. Automat. Contr.*, 45:1053–1071, 2000.

[176] A. Koulouris and G. Stephanopoulos. Stability of NN-based MPC in the presence of unbounded model uncertainty. In *Proceedings of 5th International Conference on Chemical Process Control,* in press, Tahoe City, CA, 1997.

[177] X. D. Koutsoukos, P. J. Antsaklis, J. A. Stiver, and M. D. Lemmon. Supervisory control of hybrid systems. *Proceedings of the IEEE*, 88:1026–1049, 2000.

[178] X. D. Koutsoukos, P. J. Antsaklis, J. A. Stiver, and M. D. Lemmon. Supervisory control of hybrid systems. *Proceedings of the IEEE*, 88:1026–1049, 2000.

[179] C. Kravaris and Y. Arkun. Geometric nonlinear control - an overview. In *Proceedings of 4th International Conference on Chemical Process Control*, pages 477–515, Y. Arkun and W. H. Ray Eds., Padre Island, TX, 1991.

[180] C. Kravaris and C. B. Chung. Nonlinear state feedback synthesis by global input/output linearization. *AIChE J.*, 33:592–604, 1987.

[181] C. Kravaris and J. C. Kantor. Geometric methods for nonlinear process control 1. Background. *Ind. & Eng. Chem. Res.*, 29:2295–2310, 1990.

[182] C. Kravaris and J. C. Kantor. Geometric methods for nonlinear process control 2. Controller synthesis. *Ind. & Eng. Chem. Res.*, 29:2310–2323, 1990.

[183] C. Kravaris and S. Palanki. Robust nonlinear state feedback under structured uncertainty. *AIChE J.*, 34:1119–1127, 1988.

[184] C. Kravaris and R. A. Wright. Deadtime compensation for nonlinear processes. *AIChE J.*, 35:1535–1542, 1989.

[185] M. Krstic and Z-H. Li. Inverse optimal design of input-to-state stabilizing nonlinear controllers. *IEEE Trans. Automat. Contr.*, 43:336–350, 1998.

[186] N. Krstic, I. Kanellakopoulos, and P. Kokotovic. *Nonlinear and Adaptive Control Design.* Wiley, New York, first edition, 1995.

[187] S. Kumar and D. Ramkrishna. On the solution of population balance equations by discretization-I. a fixed pivot technique. *Chem. Eng. Sci.*, 51:1311–1332, 1996.

[188] S. Kumar and D. Ramkrishna. On the solution of population balance equations by discretization-II. a moving pivot technique. *Chem. Eng. Sci.*, 51:1333–1342, 1996.

[189] Y. Kuramoto and T. Tsuzuki. Persistent propagation of concentration waves in dissipative media far from thermal equilibrium. *Prog. Theor. Phys.*, 55:356–369, 1976.

[190] M. J. Kurtz and M. A. Henson. Constrained output feedback control of a multivariable polymerization reactor. In *Proceedings of American Control Conference*, pages 2950–2954, Albuquerque, NM, 1997.

[191] M. J. Kurtz and M. A. Henson. Input output linearizing control of constrained nonlinear processes. *J. Proc. Contr.*, 7:3–17, 1997.

[192] M. J. Kurtz and M. A. Henson. Linear model predictive control of input-output linearized processes with constraints. In *Proceedings of 5th International Conference on Chemical Process Control*, volume 93, pages 335–338, J. C. Kantor, C. E. Garcia and B. Carnahan Eds., AIChE Symposium Series No. 316, CACHE, AIChE, 1997.

[193] M. J. Kurtz, G-Y. Zhu, A. Zamamiri, M. A. Henson, and M. A. Hjortso. Control of oscillating microbial cultures described by population balance models. *Ind. & Eng. Chem. Res.*, 37:4059–4070, 1998.

[194] W. Langson, I. Chryssochoos, S. V. Rakovic, and D. Q. Mayne. Robust model predictive control using tubes. *Automatica*, 40:125–133, 2004.

[195] J. H. Lee and B. Cooley. Recent advances in model predictive control and other related areas. In *Proceedings of 5th International Conference on Chemical Process Control*, volume 93, pages 201–216, J. C. Kantor, C. E. Garcia and B. Carnahan Eds., AIChE Symposium Series No. 316, CACHE, AIChE, 1997.

[196] J. H. Lee and Z. H. Yu. Worst-case formulations of model predictive control for systems with bounded parameters. *Automatica*, 33:763–781, 1997.

[197] Y. I. Lee and B. Kouvaritakis. Superposition in efficient robust constrained predictive control. *Automatica*, 38:875–878, 2002.

[198] S. J. Lei, R. Shinnar, and S. Katz. The stability and dynamic behavior of a continuous crystallizer with a fines trap. *AIChE J.*, 17:1459–1470, 1971.

[199] G. Leitmann. On one approach to the control of uncertain systems. *J. Dyn. Syst. Meas. & Contr.*, 115:373–380, 1993.

[200] A. Leonessa, W. M. Haddad, and V. Chellaboina. Nonlinear system stabilization via hierarchical switching control. *IEEE Trans. Automat. Contr.*, 46:17–28, 2001.

[201] J. Levine and P. Rouchon. Quality control of binary distillation columns via nonlinear aggregated models. *Automatica*, 27:463–480, 1991.

[202] B. Lewin. *Genes VII.* Oxford Univ. Press, Cambridge, UK, 2000.

[203] D. Liberzon and A. S. Morse. Basic problems in stability and design of switched systems. *IEEE Contr. Syst. Mag.*, 19:59–70, 1999.

[204] Y. Lin and E. D. Sontag. A universal formula for stabilization with bounded controls. *Systems & Control Letters*, 16:393–397, 1991.

[205] W. J. Liu and M. Krstic. Stability enhancement by boundary control in the Kuramoto-Sivashinsky equation. *Nonlinear Analysis: Theory, Methods & Applications*, 43:485–507, 2001.

[206] L. Magni, G. Nicolao, R. Scattolini, and F. Allgöwer. Robust model predictive control for nonlinear discrete-time systems. *Int. J. Robust & Nonlin. Contr.*, 13:229–246, 2003.

[207] L. Magni, G. De Nicolao, and R. Scattolini. A stabilizing model-based predictive control algorithm for nonlinear systems. *Automatica*, 37:1351–1362, 2001.

[208] L. Magni and R. Sepulchre. Stability margins of nonlinear receding-horizon control via inverse optimality. *Syst. & Contr. Lett.*, 32:241–245, 1997.

[209] M. Mahmoud, J. Jiang, and Y. Zhang. *Active Fault Tolerant Control Systems: Stochastic Analysis and Synthesis*, volume 287 of *Lecture Notes in Control and Information Sciences.* Springer-Verlag, Heidelberg, 2003.

[210] N. A. Mahmoud and H. K. Khalil. Asymptotic regulation of minimum phase nonlinear systems using output feedback. *IEEE Trans. Automat. Contr.*, 41:1402–1412, 1996.

[211] R. Marino and P. Tomei. Global adaptive output feedback control of nonlinear systems - Part 1: Linear parameterization. *IEEE Trans. Automat. Contr.*, 38:17–32, 1993.

[212] R. Marino and P. Tomei. Global adaptive output feedback control of nonlinear systems - Part 2: nonlinear parameterization. *IEEE Trans. Automat. Contr.*, 38:33–48, 1993.

[213] D. Q. Mayne and H. Michalska. Receeding horizon control of nonlinear systems. *IEEE Trans. Automat. Contr.*, 35:814–824, 1990.

[214] D. Q. Mayne, J. B. Rawlings, C. V. Rao, and P. O. M. Scokaert. Constrained model predictive control: Stability and optimality. *Automatica*, 36:789–814, 2000.

[215] D.Q. Mayne. Nonlinear model predictive control: An assessment. In *Proceedings of 5th International Conference on Chemical Process Control*, volume 93, pages 217–231, J. C. Kantor, C. E. Garcia and B. Carnahan Eds., AIChE Symposium Series No. 316, CACHE, AIChE, 1997.

[216] H. H. McAdams and A. Arkin. Simulation of prokaryotic genetic circuits. *Annual Review of Biophysics and Biomolecular Structure*, 27:199–224, 1998.

[217] M. W. McConley, B. D. Appleby, M. A. Dahleh, and E. Freon. A computationally efficient Lyapunov-based scheduling procedure for control of nonlinear systems with stability guarantees. *IEEE Trans. Automat. Contr.*, 45:33–49, 2000.

[218] P. Mendes and D. Kell. Non-linear optimization of biochemical pathways: Applications to metabolic engineering and parameter estimation. *Bioinformatics*, 14:869–883, 1998.

[219] P. Mhaskar, N. H. El-Farra, and P. D. Christofides. Hybrid predictive control of process systems. *AIChE J.*, 50:1242–1259, 2004.

[220] P. Mhaskar, N. H. El-Farra, and P. D. Christofides. Robust hybrid predictive control of nonlinear systems. *Automatica,* in press, 2004.

[221] H. Michalska and D. Q. Mayne. Receeding horizon control of non-linear systems. *IEEE Trans. Automat. Contr.*, 35:814–824, 1990.

[222] H. Michalska and D. Q. Mayne. Robust receding horizon control of constrained nonlinear systems. *IEEE Trans. Automat. Contr.*, 38:1623–1633, 1993.

[223] H. Michalska and D. Q. Mayne. Moving horizon observers and observer-based control. *IEEE Trans. Automat. Contr.*, 40:995–1006, 1995.

[224] L. A. Montestruque and P. J. Antsaklis. On the model-based control of networked systems. *Automatica*, 39:1837–1843, 2003.

[225] M. Morari and J. H. Lee. Model predictive control: The good, the bad, and the ugly. In *Proceedings of 4th International Conference on Chemical Process Control*, pages 419–444, Y. Arkun and W. H. Ray Eds., Padre Island, TX, 1991.

[226] P. J. Moylan and B. D. O. Anderson. Nonlinear regulator and an inverse optimal control problem. *IEEE Trans. Automat. Contr.*, 18:460–465, 1973.

[227] M. Nicmanis and M. J. Hounslow. Finite-element methods for steady-state population balance equations. *AIChE J.*, 44:2258–2272, 1998.

[228] M. N. Nounou, B. R. Bakshi, P. K. Goel, and X. Shen. Bayesian principal component analysis. *J. Chemometrics*, 16:576–595, 2002.

[229] B. Novak and J. J. Tyson. Modeling the cell division cycle: M-phase trigger, oscillations and size control. *Journal Theoretical Biology*, 165:101–134, 1993.

[230] B. A. Ogunnaike and R. A. Wright. Industrial applications of nonlinear control. In *Proceedings of 5th International Conference on Chemical Process Control*, volume 93, pages 46–59, J. C. Kantor, C. E. Garcia and B. Carnahan Eds., AIChE Symposium Series No. 316, CACHE, AIChE, 1997.

[231] N. M. C. Oliveira and L. T. Biegler. Constraint handling and stability properties of model-predictive control. *AIChE J.*, 40:1138–1150, 1994.

[232] S. L. Oliveira, V. Nevistic, and M. Morari. Control of nonlinear systems subject to input constraints. In *Proceedings of Symposium on Nonlinear Control Systems Design'95*, pages 913–918, Tahoe City, CA, 1995.

[233] A. Palazoglu and A. Karakas. Control of nonlinear distributed parameter systems using generalized invariants. *Automatica*, 36:697–703, 2000.

[234] Z. Pan and T. Basar. Robustness of H^∞ controllers to nonlinear perturbations. In *Proceedings of 32rd IEEE Conference on Decision and Control*, pages 1638–1643, San Antonio, TX, 1993.

[235] R. Patankar. A model for fault-tolerant networked control system using TTP/C communication. In *Proceedings of American Control Conference*, pages 533–537, Denver, CO, 2003.

[236] R. J. Patton. Fault-tolerant control systems: The 1997 situation. In *Proceedings of the IFAC Symposium SAFEPROCESS 1997*, pages 1033–1054, Hull, United Kingdom, 1997.

[237] E. N. Pistikopoulos, V. Dua, N. A. Bozinis, A. Bemporad, and M. Morari. On-line optimization via off-line parametric optimization tools. *Comp. & Chem. Eng.*, 26:175–185, 2002.

[238] E. Polak and T. H. Yang. Moving horizon control of linear systems with input saturation and plant uncertainty - Part 1: Robustness. *Int. J. Contr.*, 58:613–638, 1993.

[239] J. A. Primbs, V. Nevistic, and J. C. Doyle. A receding horizon generalization of pointwise min-norm controllers. *IEEE Trans. Automat. Contr.*, 45:898–909, 2000.

[240] M. Ptashne. *A Genetic Switch: Gene Control and Phage λ*. Cell Press, Cambridge, MA, 1986.

[241] S. J. Qin and T. J. Badgwell. An overview of industrial model predictive control technology. In *Proceedings of 5th International Conference on Chemical Process Control*, volume 93, pages 232–256, J. C. Kantor, C. E. Garcia and B. Carnahan Eds., AIChE Symposium Series No. 316, CACHE, AIChE, 1997.

[242] S. J. Qin and T. J. Badgwell. An overview of nonlinear model predictive control applications. *Presented at Nonlinear MPC Workshop. Ascona, Switzerland*, 1998.

[243] Z. Qu. Robust control of nonlinear uncertain systems under generalized matching conditions. *Automatica*, 29:985–998, 1993.

[244] D. Ramkrishna. The status of population balances. *Rev. Chem. Eng.*, 3:49–95, 1985.

[245] A. D. Randolph, L. Chen, and A. Tavana. Feedback control of CSD in a KCl crystallizer with a fines dissolver. *AIChE J.*, 33:583–591, 1987.

[246] C. V. Rao and J. B. Rawlings. Steady states and constraints in model predictive control. *AIChE J.*, 45:1266–1278, 1999.

[247] C. V. Rao and J. B. Rawlings. Constrained process monitoring: Moving-horizon approach. *AIChE J.*, 48:97–109, 2002.

[248] J. B. Rawlings. Tutotial: Model predictive control technology. In *Proceedings of the American Control Conference*, pages 662–676, San Diego, CA, 1999.

[249] J. B. Rawlings. Tutorial overview of model predictive control. *IEEE Control Systems Magazine*, 20:38–52, 2000.

[250] J. B. Rawlings, E. S. Meadows, and K. R. Muske. Nonlinear model predictive control: A tutorial and survey. In *Proceedings of International Symposium on Advanced Control of Chemical Processes*, pages 203–214, Kyoto, Japan, 1994.

[251] J. B. Rawlings, S. M. Miller, and W. R. Witkowski. Model identification and control of solution crystallization processes. *Ind. & Eng. Chem. Res.*, 32:1275–1296, 1993.

[252] J. B. Rawlings and K. R. Muske. The stability of constrained receding horizon control. *IEEE Trans. Automat. Contr.*, 38:1512–1516, 1993.

[253] J. B. Rawlings and W. H. Ray. Stability of continuous emulsion polymerization reactors: a detailed model analysis. *Chem. Eng. Sci.*, 42:2767–2777, 1987.

[254] V. L. Rawls and R. A. Freeman. Comparison of receding horizon control and an adaptive approach to cost reduction using Lyapunov design in nonlinear systems. In *Proceedings of the American Control Conference*, pages 265–269, Chicago, IL, 2000.

[255] W. H. Ray. *Advanced Process Control.* McGraw-Hill, New York, 1981.

[256] P. Renard, D. Dochain, G. Bastin, H. Naveau, and E. J. Nyns. Adaptive control of anaerobic digestion processes: a pilot-scale application. *Biotech. Bioeng.*, 31:287–294, 1988.

[257] J. Richalet, A. Rault, J. L. Testud, and J. Papon. Model predictive heuristic control: Applications to industrial processes. *Automatica*, 14:413–428, 1978.

[258] S. Rohani and J. R. Bourne. Self-tuning control of crystal size distribution in a cooling batch crystallizer. *Chem. Eng. Sci.*, 12:3457–3466, 1990.

[259] W. J. Rugh and J. S. Shamma. Research on gain scheduling. *Automatica*, 36:1401–1425, 2000.

[260] V. Sakizlis, N. M. P. Kakalis, V. Dua, J. D. Perkins, and E. N. Pistikopoulos. Design of robust model–based controllers via parametric programming. *Automatica*, 40:189–201, 2004.

[261] M. Santillán and M. C. Mackey. Why the lysogenic state of phage λ is so stable: A mathematical modeling approach. *Biophysical Journal*, 86:75–84, 2004.

[262] S. S. Sastry and A. Isidori. Adaptive control of linearizable systems. *IEEE Trans. Automat. Contr.*, 34:1123–1131, 1989.

[263] A. T. Schwarm and M. Nikolaou. Chance-constrained model predictive control. *AIChE J.*, 45:1743–1752, 1999.

[264] P. O. Scokaert, D. Q. Mayne, and J. B. Rawlings. Constrained linear quadratic regulation. *IEEE Trans. Automat. Contr.*, 43:1163–1169, 1998.

[265] P. O. Scokaert, D. Q. Mayne, and J. B. Rawlings. Suboptimal model predictive control (feasibility implies stability). *IEEE Trans. Automat. Contr.*, 44:648–654, 1999.

[266] P. O. M. Scokaert and D. Q. Mayne. Min-max feedback model predictive control for constrained linear systems. *IEEE Trans. Automat. Contr.*, 43:1136–1142, 1998.

[267] P. O. M. Scokaert and J. B. Rawlings. Constrained linear quadratic regulation. *IEEE Trans. Automat. Contr.*, 43:1163–1169, 1998.

[268] P. O. M. Scokaret and J. B. Rawlings. Feasibility issues in linear model predictive control. *AIChE J.*, 45:1649–1259, 1999.

[269] D. Semino and W. H. Ray. Control of systems described by population balance equations-I. controllability analysis. *Chem. Eng. Sci.*, 50:1805–1824, 1995.

[270] D. Semino and W. H. Ray. Control of systems described by population balance equations-II. emulsion polymerization with constrained control action. *Chem. Eng. Sci.*, 50:1825–1839, 1995.

[271] R. Sepulchre, M. Jankovic, and P. Kokotovic. *Constructive Nonlinear Control.* Springer-Verlag, Berlin-Heidelberg, 1997.

[272] P. Singstad, H. Nordhus, K. Strand, M. Lien, L. B. Lyngmo, and O. Moen. Multivariable nonlinear control of industrial LDPE reactors. In *Proceedings of American Control Conference*, pages 615–620, Chicago, Il, 1992.

[273] G. I. Sivashinsky. On flame propagation under conditions of stoichiometry. *SIAM J. Appl. Math*, 39:67–82, 1980.

[274] M. Skliar and W. F. Ramirez. Air-quality monitoring and detection of air contamination in an enclosed environment. *J. Spacecraft & Rockets*, 34:522–532, 1997.

[275] M. Skliar and W. F. Ramirez. Implicit kalman filtering. *Int. J. Contr.*, 66:393–412, 1997.

[276] P. Smolen, D. A. Baxter, and J. H. Byrne. Modeling transcriptional control in gene networks: Methods, recent results, and future directions. *Bulletin of Mathematical Biology*, 62:247–292, 2000.

[277] E. D. Sontag. Smooth stabilization implies coprime factorization. *IEEE Trans. Automat. Contr.*, 34:435–443, 1989.

[278] E. D. Sontag. A 'universal' construction of Artstein's theorem on nonlinear stabilization. *Syst. & Contr. Lett.*, 13:117–123, 1989.

[279] M. Soroush. Nonlinear output feedback control of a polymerization reactor. In *Proceedings of American Control Conference*, pages 2672–2676, Seattle, WA, 1995.

[280] M. Soroush. Nonlinear state observer design with application to reactors. *Chem. Eng. Sci.*, 52:387–404, 1997.

[281] M. Soroush and C. Kravaris. Nonlinear control of a batch polymerization reactor: an experimental study. *AIChE J.*, 38:1429–1443, 1992.

[282] M. Soroush and C. Kravaris. Nonlinear control of a polymerization CSTR with singular characteristic matrix. *AIChE J.*, 40:980–990, 1994.

[283] M. Soroush and S. Valluri. Optimal directionality compensation in processes with input saturation non-linearities. *Int. J. Contr.*, 72:1555–1564, 1999.

[284] G. Stephanopoulos. Synthesis of control systems for chemical plants-a challenge for creativity. *Comp. & Chem. Eng.*, 7:331–365, 1983.

[285] D. Sun and K. A. Hoo. Dynamic transition control structure for a class of SISO nonlinear systems. *IEEE Trans. Contr. Syst. Tech.*, 7:622–629, 1999.

[286] D. Sun and K. A. Hoo. A robust transition control structure for time-delay systems. *Int. J. Contr.*, 72:150–163, 1999.

[287] H. J. Sussmann and P. V. Kokotovic. The peaking phenomenon and the global stabilization of nonlinear systems. *IEEE Trans. Automat. Contr.*, 36:424–440, 1991.

[288] M. Sznaier, J. Cloutier, R. Hull, D. Jacques, and C. Mracek. Receding horizon control Lyapunov function approach to suboptimal regulation of nonlinear systems. *Journal of Guidance Control & Dynamics*, 23:399–405, 2000.

[289] M. Sznaier and M. J. Damborg. Suboptimal control of linear systems with state and control inequality constraints. In *Proceedings of 26th IEEE Conference on Decision and Control*, pages 761–762, Los Angeles, CA, 1987.

[290] M. Sznaier, R. Suarez, and J. Cloutier. Suboptimal control of constrained nonlinear systems via receding horizon constrained control Lyapunov functions. *Int. J. Robust & Nonlin. Contr.*, 13:247–259, 2003.

[291] A. Teel. Global stabilization and restricted tracking for multiple integrators with bounded controls. *Syst. & Contr. Lett.*, 18:165–171, 1992.

[292] A. Teel, R. Kadiyala, P. V. Kokotovic, and S. Sastry. Indirect techniques for adaptive input-output linearization of nonlinear systems. *Int. J. Contr.*, 53:193–222, 1991.

[293] A. Teel and L. Praly. Global stabilizability and observability imply semi-global stabilizability by output feedback. *Syst. & Contr. Lett.*, 22:313–325, 1994.

[294] A. Teel and L. Praly. Tools for semi-global stabilization by partial state and output feedback. *SIAM J. Contr. & Optim.*, 33:1443–1488, 1995.

[295] R. Temam. *Infinite-Dimensional Dynamical Systems in Mechanics and Physics.* Springer-Verlag, New York, 1988.

[296] F. E. Thau. On the inverse optimal control problem for a class of nonlinear autonomous systems. *IEEE Trans. Automat. Contr.*, 12:674–681, 1967.

[297] Y. Tipsuwan and M.-Y. Chow. Control methodologies in networked control systems. *Contr. Eng. Prac.*, 11:1099–1111, 2003.

[298] J. J. Tyson, K. Chen, and B. Novak. Network dynamics and cell physiology. *Nature Reviews Molecular Cell Biology*, 2:908–916, 2001.

[299] J. J. Tyson, A. Csikasz-Nagy, and B. Novak. The dynamics of cell cycle regulation. *BioEssays*, 24:1095–1109, 2002.

[300] S. Valluri and M. Soroush. Analytical control of SISO nonlinear processes with input constraints. *AIChE J.*, 44:116–130, 1998.

[301] S. Valluri and M. Soroush. A non-linear controller design method for processes with saturating actuators. *Int. J. Contr.*, 76:698–716, 2003.

[302] S. Valluri, M. Soroush, and M. Nikravesh. Shortest-prediction-horizon nonlinear model-predictive control. *Chem. Eng. Sci.*, 53:273–292, 1998.

[303] A. J. van der Schaft. L_2-gain analysis of nonlinear systems and nonlinear state feedback H_∞ control. *IEEE Trans. Automat. Contr.*, 37:770–783, 1992.

[304] V. Venkatasubramanian, R. Rengaswamy, K. Yin, and S. N. Kavuri. Review of process fault diagnosis - Parts I, II, III. *Comp. & Chem. Eng.*, 27:293–346, 2003.

[305] P. Vuthandam, H. Genceli, and M. Nikolaou. Performance bounds for robust quadratic dynamic control with end condition. *AIChE J.*, 41:2083–2097, 1995.

[306] G. C. Walsh, H. Ye, and L. G. Bushnell. Stability analysis of networked control systems. *IEEE Trans. Contr. Syst. Tech.*, 10:438–446, 2002.

[307] Z. Wan and M. V. Kothare. Efficient scheduled stabilizing model predictive control for constrained nonlinear systems. *Int. J. Robust & Nonlin. Contr.*, 13:331–346, 2003.

[308] Y. J. Wang and J. B. Rawlings. A new robust model predictive control method I: theory and computation. *J. Proc. Contr.*, 14:231–247, 2004.

[309] J. R. Whiteley and J. F. Davis. Qualitative interpretation of sensor patterns. *IEEE Expert*, 8:54–63, 1992.

[310] H. S. Wiley, S. Y. Shvartsman, and D. A. Lauffenburger. Computational modeling of the EGF-receptor system: A paradigm for systems biology. *Trends in Cell Biology*, 13:43–50, 2003.

[311] A. S. Willsky. A survey of design methods for failure detection in dynamic systems. *Automatica*, 12:601–611, 1998.

[312] R. A. Wright and C. Kravaris. Nonlinear control of pH processes using the strong acid equivalent. *Ind. & Eng. Chem. Res.*, 30:1561–1572, 1991.

[313] R. A. Wright, M. Soroush, and C. Kravaris. Strong acid equivalent control of pH processes: An experimental study. *Ind. & Eng. Chem. Res.*, 30:2439–2448, 1991.

[314] Y. Xu and J. Hespanha. Communication logics for networked control systems. In *Proceedings of American Control Conference*, pages 572–577, Boston, MA, 2004.

[315] E. C. Yamalidou and J. Kantor. Modeling and optimal control of discrete-event chemical processes using petri nets. *Comp. & Chem. Eng.*, 15:503–519, 1990.

[316] G. H. Yang, S. Y. Zhang, J. Lam, and J. Wang. Reliable control using redundant controllers. *IEEE Trans. Automat. Contr.*, 43:1588–1593, 1998.

[317] T. H. Yang and E. Polak. Moving horizon control of nonlinear systems with input saturation, disturbances, and plant uncertainty. *Int. J. Contr.*, 58:875–903, 1993.

[318] E. B. Ydstie. Certainty equivalence adaptive control: Paradigms puzzles and switching. In *Proceedings of 5th International Conference on Chemical Process Control*, volume 93, pages 9–23, J. C. Kantor, C. E. Garcia and B. Carnahan Eds., AIChE Symposium Series No. 316, CACHE, AIChE, 1997.

[319] E. B. Ydstie. New vistas for process control: Integrating physics and communication networks. *AIChE J.*, 48:422–426, 2002.

[320] E. B. Ydstie and A. A. Alonso. Process systems and passivity via the Clausius-Planck inequality. *Syst. & Contr. Lett.*, 30:253–264, 1997.

[321] E. B. Ydstie and P. V. Krishnan. From thermodynamics to a macroscopic theory for process control. In *AIChE Annual Meeting, paper 228a, San Francisco, CA*, 1994.

[322] E. Zafiriou. Robust model predictive control of processes with hard constraints. *Comp. & Chem. Eng.*, 14:359–371, 1990.

[323] A. Zheng. Robust stability analysis of constrained model predictive control. *J. Proc. Contr.*, 9:271–278, 1999.

Appendix A

Proofs of Chapter 2

Proof of Theorem 2.1:

The proof is divided into two parts. In Part 1 we establish that the controller of Eq.2.15 globally asymptotically stabilizes the origin of the closed-loop system and show that the closed-loop output satisfies the relation of Eq.2.18. In Part 2, we prove that the controller of Eq.2.15 is optimal with respect to the cost functional of Eq.2.19. To simplify the development of the proof, we will consider only the case of a single uncertain variable, i.e., $q = 1$ in Eq.2.1. The extension to the case when $q > 1$ is conceptually straightforward.

Part 1: Consider the representation of the closed-loop system in the transformed coordinates of Eq.2.13. We now follow a three-step procedure to establish closed-loop asymptotic stability and output tracking. Initially, we use a Lyapunov argument to show that, starting from any initial condition, the states of the closed-loop e-subsystem converge asymptotically to the origin and derive bounds that capture the evolution of the states of the e and η subsystems. We then invoke a small-gain argument to show that the trajectories of the e-η interconnected system remain bounded for all times starting from any initial condition. Finally, we show that the states of the closed-loop system of Eq.2.13 converge to the origin and that the output satisfies the relation of Eq.2.18.

Step 1: Substituting the control law of Eq.2.15 into Eq.2.13 and computing the time-derivative of V along the trajectories of the closed-loop e-subsystem, we get:

$$\begin{aligned}\dot{V} &= L_{\bar{f}}V + L_{\bar{g}}Vu + L_{\bar{w}}V\theta \\ &= -c_0(L_{\bar{g}}V)^2 - \sqrt{(L_{\bar{f}}V)^2 + (L_{\bar{g}}V)^4} + L_{\bar{w}}V\theta \\ &\quad - \left(\frac{\rho + \chi\theta_b |L_w L_f^{r-1}h(x)|}{(L_g L_f^{r-1}h(x))^2 \left(\frac{|L_{\bar{g}}V|}{|L_g L_f^{r-1}h(x)|} + \phi \right)} \right) (L_{\bar{g}}V)^2 \end{aligned} \tag{A.1}$$

for $L_{\bar{g}}V \neq 0$. Substituting the expressions $L_{\bar{g}}V = 2\left[(L_g L_f^{r-1}h(x)\right] b^T P e$ and $L_{\bar{w}}V = 2\left[L_w L_f^{r-1}h(x)\right] b^T P e$ into the above equation, and using the fact that $c_0 > 0$, we obtain:

$$\begin{aligned}\dot{V} &\leq -c_0(L_{\bar{g}}V)^2 - \sqrt{(L_{\bar{f}}V)^2 + (L_{\bar{g}}V)^4} - \left(\frac{\rho + \chi\theta_b |L_w L_f^{r-1}h(x)|}{(|2b^T Pe| + \phi)} \right) |2b^T Pe|^2 \\ &\quad + |2b^T Pe||L_w L_f^{r-1}h(x)|\theta_b \\ &= -c_0(L_{\bar{g}}V)^2 - \sqrt{(L_{\bar{f}}V)^2 + (L_{\bar{g}}V)^4} - \left(\frac{\rho |2b^T Pe|^2}{|2b^T Pe| + \phi} \right) \\ &\quad - \left(\frac{\theta_b |L_w L_f^{r-1}h(x)||2b^T Pe|((\chi - 1)|2b^T Pe| - \phi)}{|2b^T Pe| + \phi} \right) \end{aligned} \tag{A.2}$$

From the last inequality and the fact that $\rho > 0$ and $\chi > 2$, it is clear that whenever $|2b^T Pe| > \phi(\chi - 1)^{-1}$, the time-derivative of V satisfies:

$$\dot{V} \leq -c_0(L_{\bar{g}}V)^2 - \sqrt{(L_{\bar{f}}V)^2 + (L_{\bar{g}}V)^4} \tag{A.3}$$

which is strictly negative when $L_{\bar{g}}V \neq 0$. For the case when $|2b^T Pe| \leq \phi(\chi - 1)^{-1}$, we have $|2b^T Pe| \leq \phi(\frac{1}{2}\chi - 1)^{-1}$; and, therefore, from the assumption of vanishing uncertainty, we have that the function $L_w L_f^{r-1}h(x)$ satisfies the bound $|L_w L_f^{r-1}h(x)| \leq \delta|2b^T Pe|$ for all $|2b^T Pe| \leq \phi(\frac{1}{2}\chi - 1)^{-1}$, where δ is a positive constant. Substituting this bound, together with the fact that $\phi - (\chi - 1)|2b^T Pe| < \phi$, into the last inequality of Eq.A.2 yields:

$$\dot{V} \leq -\sqrt{(L_{\bar{f}}V)^2 + (L_{\bar{g}}V)^4} + \left(\frac{(\theta_b \delta\phi - \rho)|2b^T Pe|^2}{|2b^T Pe| + \phi} \right) \quad \forall\, |2b^T Pe| < \phi(\chi - 1)^{-1} \tag{A.4}$$

If ϕ is small enough to satisfy the bound $\phi \leq \frac{\rho}{\delta\theta_b} := 2\phi^*$, then it's clear from the above equation that $\dot{V}$ satisfies Eq.A.3, irrespective of the value of $|2b^TPe|$. Consider now the case when $L_{\bar{g}}V = 0$. In this case, we have from Eq.2.15 that $u = 0$ and, hence, computing the time-derivative of $V = e^TPe$, we get:

$$\dot{V} \leq e^T\left(A^TP + PA\right)e + 2b^TPe\left(\bar{f}_r(e,\eta,\bar{v}) + \bar{w}_r(e,\eta,\bar{v})\theta\right) \tag{A.5}$$

where $\bar{f}_r(e,\eta,\bar{v}) = L_f^r h(T^{-1}(e,\eta,\bar{v})) - v^{(r)}$ and $\bar{w}_r(e,\eta,\bar{v}) = L_w L_f^{r-1}(T^{-1}(e,\eta,\bar{v}))$. From the fact that P satisfies $A^TP + PA - Pbb^TP < 0$, we have that there exists a positive-definite matrix, Q, such that $A^TP + PA - Pbb^TP = -Q$. Substituting this relation into Eq.A.5 yields:

$$\dot{V} \leq -e^TQe + (b^TPe)^2 + 2b^TPe\left(\bar{f}_r(e,\eta,\bar{v}) + \bar{w}_r(e,\eta,\bar{v})\theta\right) \tag{A.6}$$

From the assumption that $L_g L_f^{r-1}h(T^{-1}(e,\eta,\bar{v})) \neq 0$ for all $x \in \mathbb{R}^n$ (Assumption 2.1), we have that $L_{\bar{g}}V = 0 \implies b^TPe = 0$; and, consequently, $\dot{V} = -e^TQe < 0 \; \forall \; e \neq 0$.

From the above analysis, it is clear that $\dot{V} < 0 \quad \forall \; e \neq 0$. Consequently, there exists a function β_e of class $\mathcal{KL}$ (see chapter 5 in [170] for details) such that the following ISS inequality holds for the e states of the system of Eq.2.13:

$$|e(t)| \leq \beta_e\left(|e(0)|, t\right) \qquad \forall\, t \geq 0 \tag{A.7}$$

and the origin of the e-subsystem is asymptotically stable. From Assumption 2.2, we have that the η-subsystem of Eq.2.13 possesses an ISS property with respect to e which implies that there exists a function β_η of class $\mathcal{KL}$ and a function γ_η of class $\mathcal{K}$ such that the following ISS inequality holds:

$$|\eta(t)| \leq \beta_\eta(|\eta(0)|, t) + \gamma_\eta(\|e\|) \qquad \forall\, t \geq 0 \tag{A.8}$$

uniformly in θ and $\bar{v}$.

Step 2: We now analyze the behavior of the interconnected dynamical system comprised of the e and η states of the system of Eq.2.13 for which the inequalities of Eq.A.7 and Eq.A.8 hold. In order to proceed with our analysis, we define the following positive real numbers: $\delta_e = D^e + \phi^*$, $\delta_\eta = D^\eta + \gamma_\eta(\delta_e) + \phi^*$, $D^e = \beta_e(\bar{\delta}_e, 0)$,

$D^{\eta} = \beta_{\eta}(\bar{\delta}_{\eta}, 0)$, $\phi^{*} = \dfrac{\rho}{2\delta\theta_b}$ and $\bar{\delta}_e, \bar{\delta}_{\eta}$ are any positive real numbers. Then, using a contradiction argument similar to the one used in [67, 68], one can prove that if $\phi \in (0, \phi^{*}]$, then, starting from any initial state that satisfies $|e(0)| \leq \bar{\delta}_e$, $|\eta(0)| \leq \bar{\delta}_{\eta}$, the evolution of the e and η states satisfies $|e(t)| \leq \delta_e$ and $|\eta(t)| \leq \delta_{\eta}$, respectively, for all times; and that the states are therefore bounded. This argument is omitted for brevity.

Step 3: Having established in the previous two steps that the origin of the closed-loop e-subsystem is globally asymptotically stable and that the η subsystem, with e as input, is ISS, we can apply the results of Lemma 5.6 in [170] directly to conclude that the origin of the interconnected e-η system of Eq.2.13 is globally asymptotically stable. It follows then from Assumption 2.1 that the origin of the closed-loop system of Eq.2.1 is globally asymptotically stable. The asymptotic output tracking result can be obtained by taking the limsup of both sides of Eq.A.7, which yields:

$$\limsup_{t \to \infty} |e(t)| \; = \; 0 \implies \limsup_{t \to \infty} |y(t) - v(t)| \; = \; 0 \tag{A.9}$$

Part 2: In this part, we prove that the control law of Eq.2.15 is optimal with respect to a meaningful cost functional of the form of Eq.2.19. We proceed in two steps. In the first step, we show that the cost functional defined in Eq.2.19 is a meaningful one by proving that the weights, $l(e)$ and $R(x)$, are positive-definite and strictly positive functions, respectively. In the second step, we show that the stabilizing control law of Eq.2.15 minimizes this cost functional.

Step 1: From its definition in Theorem 2.1, $l(e)$ is given by:

$$l(e) \; = \; -L_{\bar{f}}V + \frac{1}{4} L_{\bar{g}}V R^{-1}(x) L_{\bar{g}}V - |L_{\bar{w}}V|\,\theta_b \tag{A.10}$$

Consider first the case when $L_{\bar{g}}V \neq 0$. Direct substitution of the expression for

$R^{-1}(x)$ given in Theorem 2.1 into the above equation yields:

$$\begin{aligned} l(e) &= \frac{1}{2}c_0(L_{\bar{g}}V)^2 + \frac{1}{2}\left[-L_{\bar{f}}V + \sqrt{(L_{\bar{f}}V)^2 + (L_{\bar{g}}V)^4}\right] - |L_{\bar{w}}V|\theta_b \\ &\quad + \frac{1}{2}\frac{\left(\rho + \chi\theta_b|L_w L_f^{r-1}h(x)|\right)|2b^TPe|^2}{|2b^TPe| + \phi} \\ &= \frac{1}{2}c_0(L_{\bar{g}}V)^2 + \frac{1}{2}\left[-L_{\bar{f}}V + \sqrt{(L_{\bar{f}}V)^2 + (L_{\bar{g}}V)^4}\right] + \frac{1}{2}\left(\frac{\rho|2b^TPe|^2}{|2b^TPe| + \phi}\right) \\ &\quad + \frac{\theta_b|2b^TPe||L_w L_f^{r-1}h(x)|\left[(\frac{1}{2}\chi - 1)|2b^TPe| - \phi\right]}{|2b^TPe| + \phi} \end{aligned} \tag{A.11}$$

where we used the expression for $L_{\bar{w}}V$ and the fact that $c_0 > 0$ to derive the above inequality. Note that the second term on the right-hand side of the above equation is strictly positive when $L_{\bar{g}}V \neq 0$. From this and the fact that $\rho > 0$ and $\chi > 2$, it's clear that whenever $|2b^TPe| > \phi(\frac{1}{2}\chi - 1)^{-1}$, we have:

$$l(e) \;\geq\; \frac{1}{2}c_0(L_{\bar{g}}V)^2 \;\geq\; k_1|b^TPe|^2 \tag{A.12}$$

where $k_1 = \frac{1}{2}c_0k_2^2 > 0$, $k_2 = \min_{x\in\mathbb{R}^n}|L_gL_f^{r-1}h(x)|$. To analyze the sign of $l(e)$ when $|2b^TPe| \leq \phi(\frac{1}{2}\chi - 1)^{-1}$, we use the growth bound $|L_wL_f^{r-1}h(x)| \leq \delta|2b^TPe|$ together with the fact that $(\frac{1}{2}\chi - 1)|2b^TPe| - \phi > -\phi$ to write:

$$l(e) \;\geq\; \frac{1}{2}c_0(L_{\bar{g}}V)^2 + \frac{\left(\frac{\rho}{2} - \theta_b\delta\phi\right)|2b^TPe|^2}{|2b^TPe| + \phi} \quad \forall\, |2b^TPe| \leq \phi(\frac{1}{2}\chi - 1)^{-1} \tag{A.13}$$

Clearly, if ϕ is small enough to satisfy $\phi \leq \frac{\rho}{2\theta_b\delta} := \phi^*$, then we have that $l(e)$ satisfies Eq.A.12, irrespective of the value of $|2b^TPe|$. Consider now the case when $L_{\bar{g}}V = 0$. In this case, we have from Eq.A.10, and the fact that $V = e^TPe$ with P satisfying $A^TP + PA - Pbb^TP = -Q$ for some positive-definite matrix, Q, that:

$$\begin{aligned} l(e) &= -L_{\bar{f}}V - |L_{\bar{w}}V|\theta_b \\ &= -e^T\left(A^TP + PA\right)e - 2b^TPe\left(\bar{f}_r(e,\eta,\bar{v})\right) - |2b^TPe||\bar{w}_r(e,\eta,\bar{v})|\theta_b \\ &= e^TQe - (b^TPe)^2 - 2b^TPe\left(\bar{f}_r(e,\eta,\bar{v})\right) - |2b^TPe||\bar{w}_r(e,\eta,\bar{v})|\theta_b \end{aligned} \tag{A.14}$$

where $\bar{f}_r$ and $\bar{w}_r$ were defined following Eq.A.5. Recall that $L_{\bar{g}}V = 0 \implies b^T P e = 0$; and, consequently in this case, $l(e) = e^T Q e > 0 \ \forall \ e \neq 0$. Using the identities: (a) $e^T Q e \geq \lambda_{min}(Q)|e|^2$, where $\lambda_{min}(Q) > 0$ is the minimum eigenvalue of the matrix Q, (b) $|Pe|^2 \leq \lambda_{max}(P^2)|e|^2$, where $\lambda_{max}(P^2) > 0$ is the maximum eigenvalue of the matrix P^2, and (c) $|b^T Pe|^2 \leq |Pe|^2$ (recall from Eq.2.12 that $|b| = 1$), we finally have $l(e) \geq k_3 |b^T Pe|^2$, where $k_3 = \lambda_{min}(Q)\lambda_{max}^{-1}(P^2) > 0$. Combining this result with that obtained in Eq.A.12 for the case when $L_{\bar{g}}V \neq 0$, we conclude that $l(e) > 0 \ \ \forall \ e \neq 0$ and that $l(e) \geq k|b^T Pe|^2$, where $k = \min\{k_1, k_3\}$. Note also that $R(x) > 0$ for all $x \in \mathbb{R}^n$. Therefore, the cost functional of Eq.2.19 is a meaningful one.

Step 2: In this step, we prove that control law of Eq.2.15 minimizes the cost functional of Eq.2.19. Substituting:

$$\alpha \ = \ u + \frac{1}{2} R^{-1}(x) L_{\bar{g}} V \tag{A.15}$$

into Eq.2.19, we get the following chain of equalities:

$$\begin{aligned}
J_v \ &= \ \int_0^\infty (l(e) + uR(x)u) dt \\
&= \ \int_0^\infty \left(-L_{\bar{f}} V + \frac{1}{4} L_{\bar{g}} V R^{-1}(x) L_{\bar{g}} V - |L_{\bar{w}} V| \theta_b + \alpha R \alpha - \alpha (L_{\bar{g}} V) \right) dt \\
&\quad + \int_0^\infty \left(\frac{1}{4} L_{\bar{g}} V R^{-1} \left(L_{\bar{g}} V \right) \right) dt \\
&= \ \int_0^\infty \left(-L_{\bar{f}} V - L_{\bar{g}} V u - |L_{\bar{w}} V| \theta_b \right) dt + \int_0^\infty \alpha R(x) \alpha \ dt \\
&= \ -\int_0^\infty \sup_{\theta \in \mathcal{W}} \left(\dot{V} \right) dt + \int_0^\infty \alpha R(x) \alpha \ dt
\end{aligned}$$

Since $R(x) > 0$ for all $x \in \mathbb{R}^n$, it is clear that the minimum of J_v is achieved when $\alpha(t) \equiv 0$ (which proves that the controller of Eq.2.15 minimizes the cost of Eq.2.19) and is equal to:

$$J_v^* \ = \ -\int_0^\infty \sup_{\theta \in \mathcal{W}} \left(\dot{V} \right) dt \ \leq \ V(e(0)) - \lim_{t \to \infty} V(e(t)) \ = \ V(e(0)) \tag{A.16}$$

where we have used the fact that $\lim_{t \to \infty} V(e(t)) = 0$, which follows from asymptotic stability of the origin, to derive the last equality. To complete the proof of optimality,

we need to show that $J_v^* = V(e(0))$. To this end, consider the uncertain variable $\theta_\Delta \in \mathcal{W}$ where for every $e_\Delta(0) \in \mathbb{R}^r$, every $u \in \mathbb{R}$, and every $\Delta > 0$, we have:

$$\int_0^\infty \dot{V}(e_\Delta, u, \theta_\Delta)\, dt \;\geq\; \int_0^\infty \sup_{\theta \in \mathcal{W}} \dot{V}(e_\Delta, u, \theta)\, dt - \Delta \tag{A.17}$$

(The existence of θ_Δ follows from the properties of $\theta(t)$). From the inequality of Eq.A.17, we obtain:

$$V(e(0)) \;=\; -\int_0^\infty \dot{V} dt \;\leq\; -\int_0^\infty \sup_{\theta \in \mathcal{W}} \dot{V}(e_\Delta, u, \theta)\, dt + \Delta \tag{A.18}$$

Combining the inequalities of Eq.A.18 and Eq.A.16, we get:

$$V(e(0)) - \Delta \leq J_v^* \leq V(e(0)) \tag{A.19}$$

for arbitrarily small Δ. Clearly, if $J_v^* = V(e(0))$, the proof of optimality is complete. Otherwise, there exists $\mu > 0$ such that $J_v^* + \mu = V(e(0))$. Since Δ is arbitrary, we can choose it to be sufficiently small such that $\Delta < \mu$ and the inequality of Eq.A.19 is violated. Thus, the only way to satisfy the inequality of Eq.A.19 for arbitrary Δ is to set $J_v^* = V(e(0))$. This completes the proof of the theorem. Δ

Proof of Theorem 2.2:

The proof of this theorem follows that of Theorem 2.1. We will only highlight the differences.

Part 1: In this part, we establish that the controller of Eq.2.23 enforces global boundedness of the closed-loop trajectories and that the closed-loop output satisfies Eq.2.24.

Step 1: Substituting the control law of Eq.2.23 into Eq.2.13 and computing the time-derivative of V along the trajectories of the closed-loop e-subsystem, it is straightforward to show that $\dot{V}$ satisfies Eq.A.3 whenever $|2b^T Pe| > \phi(\chi - 1)^{-1}$. To analyze the sign of $\dot{V}$ when $|2b^T Pe| \leq \phi(\chi - 1)^{-1}$, we use the bound $|L_w L_f^{r-1} h(x)| \leq \delta |2b^T Pe| + \mu$ and the fact that $\phi - (\chi - 1)|2b^T Pe| < \phi$ to obtain the following estimates:

$$\begin{aligned} \theta_b |L_w L_f^{r-1} h(x)| |2b^T Pe| \left(\phi - (\chi - 1)|2b^T Pe|\right) \;&\leq\; \theta_b |L_w L_f^{r-1} h(x)| |2b^T Pe| \phi \\ &\leq\; \theta_b \delta \phi |2b^T Pe|^2 + \theta_b \mu \phi |2b^T Pe| \end{aligned} \tag{A.20}$$

$\forall\ |2b^TPe| \leq \phi(\chi-1)^{-1}$. Substituting the estimates of Eq.A.20 directly into Eq.A.2 yields:

$$\dot{V} \leq -c_0\left(L_{\bar{g}}V\right)^2 - \sqrt{(L_{\bar{f}}V)^2 + (L_{\bar{g}}V)^4} + \frac{(-\rho+\delta\theta_b\phi)|2b^TPe|^2}{|2b^TPe|+\phi} + \frac{\theta_b\mu\phi|2b^TPe|}{|2b^TPe|+\phi} \tag{A.21}$$

It is clear from the above equation, together with the fact that $\theta_b\mu\phi > 0$ and $\frac{|2b^TPe|}{|2b^TPe|+\phi} \leq 1$, that if $\phi \leq \frac{\rho}{\delta\theta_b} := \phi_1^*$, then $\dot{V}$ satisfies:

$$\dot{V} \leq -c_0\left(L_{\bar{g}}V\right)^2 - \sqrt{(L_{\bar{f}}V)^2 + (L_{\bar{g}}V)^4} + \bar{\phi} \tag{A.22}$$

irrespective of the value of $|2b^TPe|$, where $\bar{\phi} = \theta_b\mu\phi$. Note that the function described by the first two terms on the right-hand side of the above equation is negative-definite, since for all $e \neq 0$, $L_{\bar{g}}V = 0 \implies L_{\bar{f}}V < 0$. Consequently, there exists a function $\alpha_1(\cdot)$ of class $\mathcal{K}$ such that:

$$\dot{V} \leq -\alpha_1(|e|) + \bar{\phi} \tag{A.23}$$

Choosing ϕ small enough such that $\bar{\phi} \leq \frac{1}{2}\alpha_1(|e|)$, we have:

$$\dot{V} \leq -\tfrac{1}{2}\alpha_1(|e|) < 0 \quad \forall\ |e| \geq \alpha_1^{-1}(2\bar{\phi}) \tag{A.24}$$

This inequality shows that $\dot{V}$ is negative outside the set $B_1 := \{e \in \mathbb{R}^r : |e| \leq \alpha_1^{-1}(2\bar{\phi})\}$. A direct application then of the result of Theorem 5.1 and its corollaries in [170] allows us to conclude that starting from any initial condition, the following ISS inequality holds for the e states of the closed-loop system of Eq.2.13 and Eq.2.23:

$$|e(t)| \leq \bar{\beta}_e\left(|e(0)|, t\right) + \bar{\gamma}_e(\phi) \qquad \forall\, t \geq 0 \tag{A.25}$$

where $\bar{\beta}_e$ is a class $\mathcal{KL}$ function and $\bar{\gamma}_e$ is a class $\mathcal{K}_\infty$ function. From Assumption 2.4, we have that the η states of the system of Eq.2.13 possess an ISS property with respect to e and θ:

$$|\eta(t)| \leq \bar{\beta}_\eta\left(|\eta(0)|, t\right) + \bar{\gamma}_\eta\left(\left\|[e^T\ \theta]^T\right\|\right) \leq \bar{\beta}_\eta\left(|\eta(0)|, t\right) + \bar{\gamma}_{\eta_1}\left(\|e\|\right) + \bar{\gamma}_{\eta_2}\left(\|\theta\|\right) \tag{A.26}$$

uniformly in $\bar{v}$, where $\bar{\gamma}_{\eta_1}$, $\bar{\gamma}_{\eta_2}$ are class $\mathcal{K}$ functions defined as $\bar{\gamma}_{\eta_1}(s) = \bar{\gamma}_{\eta_2}(s) = \bar{\gamma}_\eta(2s)$.

Step 2: We now analyze the behavior of the interconnected closed-loop dynamical system of Eq.2.13 and Eq.2.23, comprised of the e and η states for which the inequalities of Eq.A.25 and Eq.A.26 hold. We first define the following positive real numbers: $\delta_e = D^{\bar{e}} + \phi^*$, $\delta_\eta = D^{\bar{\eta}} + \bar{\gamma}_{\eta 1}(\delta_e) + \phi^*$, $D^{\bar{e}} = \bar{\beta}_e(\bar{\delta}_e, 0) + \bar{\gamma}_e(\phi^*)$, $D^{\bar{\eta}} = \bar{\beta}_\eta(\bar{\delta}_\eta, 0) + \bar{\gamma}_{\eta 2}(\theta_b)$, $\phi^* = \min\{\frac{1}{2}\phi_1^*, \bar{\gamma}_e^{-1}(d)\}$ where $d > 0$ is arbitrary and $\bar{\delta}_e, \bar{\delta}_\eta$ are any positive real numbers. Then, using a contradiction argument similar to the one used in [67, 68], one can show that if $\phi \in (0, \phi^*]$, the evolution of the states e and η, starting from any initial states that satisfy $|e(0)| \leq \bar{\delta}_e$, $|\eta(0)| \leq \bar{\delta}_\eta$, satisfies the inequalities $|e(t)| \leq \delta_e$, $|\eta(t)| \leq \delta_\eta$ for all times. Finally, for $\phi \in (0, \phi^*]$ and for any initial states, taking the limsup of both sides of Eq.A.25 as $t \to \infty$, we have:

$$\limsup_{t\to\infty} |y(t) - v(t)| \leq \limsup_{t\to\infty} |e(t)| \leq \limsup_{t\to\infty} \left(\bar{\beta}_e(|e(0)|, t) + \bar{\gamma}_e(\phi)\right) \leq \bar{\gamma}_e(\phi^*) \leq d \tag{A.27}$$

Part 2: In this part, we prove that the control law of Eq.2.23 is optimal with respect to a meaningful cost functional of the form of Eq.2.25. We proceed in two steps. In the first step, we show that the cost functional defined in Eq.2.25 is a meaningful one. In the second step, we show that the stabilizing control law of Eq.2.23 minimizes this cost functional.

Step 1: From its definition in Theorem 2.2, $\bar{l}(e)$ is given by:

$$\bar{l}(e) \;=\; -L_{\bar{f}}V + \frac{1}{4}L_{\bar{g}}V\bar{R}^{-1}(x)L_{\bar{g}}V - |L_{\bar{w}}V|\,\theta_b \tag{A.28}$$

Substitution the expression for $\bar{R}^{-1}(x)$, given in Theorem 2.2, into the above equation, and performing some algebraic manipulations (similar to those in Eq.A.11), it can be shown that, whenever $|2b^T Pe| > \phi(\frac{1}{2}\chi - 1)^{-1}$, $\bar{l}(e)$ satisfies:

$$\bar{l}(e) \;\geq\; \frac{1}{2}\left[-L_{\bar{f}}V + \sqrt{(L_{\bar{f}}V)^2 + (L_{\bar{g}}V)^4}\right] \tag{A.29}$$

which is positive-definite since, away from the origin, $L_{\bar{f}}V$ and $L_{\bar{g}}V$ do not vanish together. To analyze the sign of $\bar{l}(e)$ when $|2b^T Pe| < \phi(\frac{1}{2}\chi - 1)^{-1}$, we use the bound $|L_w L_f^{r-1} h(x)| \leq \delta|2b^T Pe| + \mu$ and the fact that $(\frac{1}{2}\chi - 1)|2b^T Pe| - \phi > -\phi$ to obtain

the following estimates:

$$\begin{aligned}\theta_b|L_wL_f^{r-1}h(x)||2b^TPe|\left(\phi-(\tfrac{1}{2}\chi-1)|2b^TPe|\right) &\geq -\theta_b|L_wL_f^{r-1}h(x)||2b^TPe|\phi \\ &\geq -\theta_b\delta\phi|2b^TPe|^2-\theta_b\mu\phi|2b^TPe|\end{aligned} \tag{A.30}$$

$\forall\ |2b^TPe| \leq \phi(\frac{1}{2}\chi-1)^{-1}$. Substituting the estimates of Eq.A.30 directly into Eq.A.11 yields:

$$\bar{l}(e) \geq \frac{1}{2}\left[-L_{\bar{f}}V+\sqrt{(L_{\bar{f}}V)^2+(L_{\bar{g}}V)^4}\right]+\frac{(\frac{1}{2}\rho-\delta\theta_b\phi)|2b^TPe|^2}{|2b^TPe|+\phi}-\frac{\theta_b\mu\phi|2b^TPe|}{|2b^TPe|+\phi} \tag{A.31}$$

From the above equation, it is clear that if $\phi \leq \dfrac{\rho}{2\delta\theta_b} := \phi_2^*$, $\bar{l}(e)$ satisfies:

$$\bar{l}(e) \geq \frac{1}{2}\left[-L_{\bar{f}}V+\sqrt{(L_{\bar{f}}V)^2+(L_{\bar{g}}V)^4}\right]-\bar{\phi} \tag{A.32}$$

irrespective of the value of $|2b^TPe|$. Therefore, there exists a function $\alpha_2(\cdot)$ of class $\mathcal{K}$ such that:

$$\begin{aligned}\bar{l}(e) &\geq \alpha_2(|e|)-\bar{\phi} \\ &\geq \tfrac{1}{2}\alpha_2(|e|) > 0 \quad \forall\ |e| \geq \alpha_2^{-1}(2\bar{\phi})\end{aligned} \tag{A.33}$$

The last inequality implies that $\bar{l}(e)$ is positive outside the set $B_2 := \{e \in \mathbb{R}^r : |e| \leq \alpha_2^{-1}(2\bar{\phi})\}$. Note that this set is completely contained within the set Γ since $|e| \leq \alpha_2^{-1}(2\bar{\phi}) \leq \alpha_2^{-1}(2\bar{\phi}^*) \leq \epsilon \Longrightarrow e^TPe \leq \lambda_{max}(P)|e|^2 \leq \lambda_{max}(P)\epsilon^2$ where $\epsilon := \max\{\alpha_1^{-1}(2\bar{\phi}^*), \alpha_2^{-1}(2\bar{\phi}^*)\}$ and $\lambda_{max}(P) > 0$ is the maximum eigenvalue of the matrix P. Similarly, the set B_1 – defined right after Eq.A.24 – is also contained within Γ, and therefore $\dot{V} < 0$ on and outside the boundary of Γ. From its definition in Theorem 2.2, T_f is the minimum time for the trajectories of the closed-loop system to reach and enter Γ without ever leaving again (note that Γ is a level set of V). Therefore, we have that $|e(t)| \geq \alpha_2^{-1}(2\bar{\phi})\ \ \forall\ t \in [0, T_f]$. Hence, $\bar{l}(e(t)) > 0\ \ \forall\ t \in [0, T_f]$. Note also that $\bar{R}(x) > 0$ for all x. Therefore the cost functional of Eq.2.25 is a meaningful one.

Step 2: In this step, we prove that control law of Eq.2.23 minimizes the cost functional

of Eq.2.25. Substituting:

$$\alpha \;=\; u + \frac{1}{2}\bar{R}^{-1}(x)L_{\bar{g}}V \tag{A.34}$$

into Eq.2.25, we get the following chain of equalities:

$$\begin{aligned} J_n &= V(e(T_f)) + \int_0^{T_f} \Big(l(e(t)) + u(t)\bar{R}(x(t))u(t)\Big)\, dt \\ &= V(e(T_f)) + \int_0^{T_f} \Big(-L_{\bar{f}}V + \frac{1}{2}L_{\bar{g}}V\bar{R}^{-1}(x)L_{\bar{g}}V - |L_{\bar{w}}V|\theta_b - L_{\bar{g}}V\alpha\Big)\, dt \\ &\quad + \int_0^{T_f} \alpha\bar{R}(x)\alpha\; dt \\ &= V(e(T_f)) - \int_0^{T_f} \sup_{\theta\in\mathcal{W}} \big(\dot{V}\big)\, dt + \int_0^{T_f} \alpha R(x)\alpha\; dt \end{aligned} \tag{A.35}$$

Note that:

$$J_n^* \;=\; V(e(T_f)) - \int_0^{T_f} \sup_{\theta\in\mathcal{W}} \big(\dot{V}\big)\, dt \;\leq\; V(e(T_f)) - \int_0^{T_f} \dot{V} dt \;=\; V(e(0)) \tag{A.36}$$

Since $\bar{R}(x) > 0$ for all $x \in \mathbb{R}^n$, it is clear that the minimum of J_n is J_n^*. This minimum is achieved when $\alpha(t) \equiv 0$ which proves that the controller of Eq.2.23 minimizes the cost of Eq.2.25. Finally, using an argument similar to that used in Eqs.A.17-A.19, we have that $J_n^* = V(e(0))$. This completes the proof of the theorem. $\triangle$

Proof of Theorem 2.3:

The proof of this theorem consists of three parts. In the first part, we use a singular perturbation formulation to represent the closed-loop system of Eq.2.1 and Eq.2.41, and show that the resulting fast subsystem is globally exponentially stable. In the second part, we focus on the closed-loop reduced system and derive ISS bounds for its states. Then, using a technical lemma proved in [60], we establish that these ISS bounds continue to hold up to an arbitrarily small offset, for arbitrarily large initial conditions and uncertainty. The resulting ISS inequalities are then analyzed to establish semi-global boundedness and local exponential stability of the full closed-loop system, which is then used to establish Eq.2.42, provided that ϕ and ϵ are

sufficiently small. Finally, in the third part, we establish the near-optimality of the controller of Eq.2.41 with respect to the cost of Eq.2.19.

Part 1: Defining the auxiliary error variables $\hat{e}_i = L^{r-i}(y^{(i-1)} - \tilde{y}_i)$, $i = 1, \ldots, r$, the vector $e_o = [\hat{e}_1\ \hat{e}_2\ \cdots\ \hat{e}_r]^T$, the parameter $\epsilon = \frac{1}{L}$, the matrix $\tilde{A}$ and the vector $\tilde{b}$:

$$\tilde{A} = \begin{bmatrix} -a_1 & 1 & 0 & \cdots & 0 \\ -a_2 & 0 & 1 & \cdots & 0 \\ \vdots & \vdots & \vdots & \ddots & \vdots \\ -a_{r-1} & 0 & 0 & \cdots & 1 \\ -a_r & 0 & 0 & \cdots & 0 \end{bmatrix}, \quad \tilde{b} = \begin{bmatrix} 0 \\ 0 \\ \vdots \\ 0 \\ 1 \end{bmatrix} \tag{A.37}$$

the system of Eq.2.1 under the controller of Eq.2.41 takes the form:

$$\begin{aligned} \epsilon \dot{e}_o &= \tilde{A} e_o + \epsilon \tilde{b} \Omega(x, \hat{x}, \theta, \phi, \bar{v}) \\ \dot{\omega}_1 &= \Psi_1(sat(\tilde{y}), \omega) \\ &\vdots \\ \dot{\omega}_{n-r} &= \Psi_{n-r}(sat(\tilde{y}), \omega) \\ \dot{x} &= f(x) - g(x)[c_0 + r_s(\hat{x}) + r_d(\hat{x}, \rho, \chi, \phi, \theta_b)]\widehat{L_{\bar{g}} V} + \sum_{k=1}^{q} w_k(x)\theta_k(t) \end{aligned} \tag{A.38}$$

where $\hat{x} = \mathcal{X}^{-1}(sat(y_d - \Delta(\epsilon)e_o), \omega)$ and $y_d = [y^{(0)}\ y^{(1)}\ \cdots\ y^{(r-1)}]^T$, $\Delta(\epsilon)$ is a diagonal matrix whose i-th diagonal element is ϵ^{r-i}, and $\Omega(x, \hat{x}, \theta, \phi, \bar{v})$ is a Lipschitz function of its argument. Owing to the presence of the small parameter ϵ that multiplies the time-derivative $\dot{e}_o$, the system of Eq.A.38 is a two-time-scale one. Defining the fast time-scale $\tau = \frac{t}{\epsilon}$ and setting $\epsilon = 0$, the closed-loop fast subsystem takes the form:

$$\frac{de_o}{d\tau} = \tilde{A} e_o \tag{A.39}$$

Since the constant matrix A is Hurwitz, the origin of the system of Eq.A.39 is globally exponentially stable.

Part 2: In this part of the proof, we initially derive ISS bounds for the states of the system of Eq.A.38, when $\epsilon = 0$, in appropriately transformed coordinates, and then

use the result of Lemma 1 in [60] to show that these bounds hold up to an arbitrarily small offset, for initial conditions and uncertainty in an arbitrarily large compact set, provided that ϵ is sufficiently small. To this end, we first write the closed-loop system in the following form:

$$
\begin{aligned}
\epsilon\dot{e}_o &= \tilde{A}e_o + \epsilon\tilde{b}\Omega(e,\eta,\hat{x},\theta,\phi,\bar{v}) \\
\dot{\omega}_1 &= \Psi_1(sat(\tilde{y}),\omega) \\
&\vdots \\
\dot{\omega}_{n-r} &= \Psi_{n-r}(sat(\tilde{y}),\omega) \\
\dot{e}_1 &= e_2 \\
&\vdots \\
\dot{e}_{r-1} &= e_r \\
\dot{e}_r &= L_f^r h(\mathcal{X}^{-1}(e,\eta,\bar{v})) - v^{(r)} + \sum_{k=1}^{q} L_{wk} L_f^{r-1} h(\mathcal{X}^{-1}(e,\eta,\bar{v}))\theta_k \\
&\quad -L_g L_f^{r-1} h(\mathcal{X}^{-1}(e,\eta,\bar{v}))[c_0 + r_s(\hat{x}) + r_d(\hat{x},\rho,\chi,\phi,\theta_b)]\widehat{L_{\tilde{g}}V} \\
\dot{\eta}_1 &= \Psi_1(e,\eta,\bar{v}) \\
&\vdots \\
\dot{\eta}_{n-r} &= \Psi_{n-r}(e,\eta,\bar{v}) \\
y &= e_1 + v
\end{aligned}
\tag{A.40}
$$

where $e = [e_1\ e_2\ \cdots\ e_r]^T$, $e_i = \zeta_i - v^{(i-1)}$, $i = 1,\cdots,r$, and Ψ_i, $i = 1,\cdots,n$ are Lipschitz functions of their arguments.

Step 1: Consider the system of Eq.A.40 with $\epsilon = 0$. In order to analyze the dynamic behavior of the resulting closed-loop slow (reduced) system, we initially need to show that for the system of Eq.A.40, $\eta(0) = \omega(0) + O(\epsilon)$ implies $\eta(t) = \omega(t) + O(\epsilon)$, $\forall\, t \geq 0$.

To this end, consider the following singularly perturbed system:

$$\begin{aligned}
\epsilon\dot{e}_o &= \tilde{A}e_o + \epsilon\tilde{b}\Omega(e,\eta,\hat{x},\theta,\phi,\bar{v}) \\
\dot{\omega}_1 &= \Psi_1(sat(\tilde{y}),\omega) \\
&\vdots \\
\dot{\omega}_{n-r} &= \Psi_{n-r}(sat(\tilde{y}),\omega) \\
\dot{\eta}_1 &= \Psi_1(e,\eta,\bar{v}) \\
&\vdots \\
\dot{\eta}_{n-r} &= \Psi_{n-r}(e,\eta,\bar{v})
\end{aligned} \tag{A.41}$$

It is straightforward to verify that the above system satisfies the assumptions of Theorem 1 reported in [171]. Applying this theorem, we have that there exists a positive real number ϵ_0, such that for any positive real number δ_ω satisfying:

$$\delta_\omega \geq \max_{|x|\leq\delta_x}\left\{\sum_{\nu=1}^{n-r}|\chi_\nu(x)|\right\} \tag{A.42}$$

where $\chi_\nu(x)$, $\nu = 1,\ldots,n-r$ are the functions defined in Assumption 2.5, the states (η,ω) of this system, starting from any initial condition that satisfies $\eta(0) = \omega(0) + O(\epsilon)$ (with $\max\{\eta(0),\omega(0)\} \leq \delta_\omega$), if $\epsilon \in (0,\epsilon_0]$, satisfy $\eta(t) = \omega(t) + O(\epsilon)$, $\forall\, t \geq 0$.

Since $\eta(t) = \omega(t)\ \forall\, t \geq 0$, when $\epsilon = 0$, the reduced (slow) closed-loop system (i.e., the system of Eq.A.40 with $\epsilon = 0$) reduces to the one studied in the Proof of Theorem 2.1, where it was shown that the evolution of the e-subsystem satisfies:

$$|e(t)| \leq \beta_e\left(|e(0)|,t\right) \quad \forall\ t \geq 0 \tag{A.43}$$

From Assumption 2.6, we have that the η states of the reduced (slow) closed-loop system of Eq.A.40 satisfy the following ISS inequality:

$$|\eta(t)| \leq K_\eta|\eta(0)|e^{-at} + \gamma_\eta(\|e\|) \quad \forall\, t \geq 0 \tag{A.44}$$

uniformly in $\bar{v}$, where $a > 0$, $K_\eta \geq 1$ and $\gamma_\eta(\cdot)$ is a class $\mathcal{K}$ function of its argument. Realizing that the reduced closed-loop slow system is an interconnection of the e

and η subsystems, we show now that the origin of the reduced closed-loop system is asymptotically stable. From Eqs.A.43-A.44, we have that the solutions of the reduced closed-loop system satisfy:

$$|\eta(t)| \leq K_\eta |\eta(s)| e^{-a(t-s)} + \gamma_\eta(\sup_{s\leq\tau\leq t} |e(\tau)|) \tag{A.45}$$

$$|e(t)| \leq \beta_e(|e(s)|, t-s) \tag{A.46}$$

where $t \geq s \geq 0$. Applying Eq.A.45 with $s = \frac{t}{2}$, we obtain:

$$|\eta(t)| \leq K_\eta \left|\eta\left(\tfrac{t}{2}\right)\right| e^{-a\frac{t}{2}} + \gamma_\eta\left(\sup_{\frac{t}{2}\leq\tau\leq t} |e(\tau)|\right) \tag{A.47}$$

To estimate $\eta\left(\frac{t}{2}\right)$, we apply Eq.A.45 with $s = 0$ and t replaced by $\frac{t}{2}$ to obtain:

$$\left|\eta\left(\tfrac{t}{2}\right)\right| \leq K_\eta |\eta(0)| e^{-a\frac{t}{2}} + \gamma_\eta\left(\sup_{0\leq\tau\leq\frac{t}{2}} |e(\tau)|\right) \tag{A.48}$$

From Eq.A.46, we have:

$$\sup_{0\leq\tau\leq\frac{t}{2}} |e(\tau)| \leq \beta_e(|e(0)|, 0) \tag{A.49}$$

$$\sup_{\frac{t}{2}\leq\tau\leq t} |e(\tau)| \leq \beta_e\left(|e(0)|, \tfrac{t}{2}\right) \tag{A.50}$$

Substituting Eqs.A.48-A.50 into Eq.A.47 and using the inequalities $|\eta(0)| \leq |\pi(0)|$, $|e(0)| \leq |\pi(0)|$ and $|\pi(t)| \leq |\eta(t)| + |e(t)|$, where $\pi(0) = [e^T(0) \;\; \eta^T(0)]^T$, we obtain:

$$|\pi(t)| \leq \beta(|\pi(0)|, t) \tag{A.51}$$

where

$$\begin{aligned}\beta(|\pi(0)|, t) = {} & \left[K_\eta |\pi(0)| e^{-a\frac{t}{2}} + \gamma_\eta(\beta_e(|\pi(0)|, 0))\right] e^{-a\frac{t}{2}} + \gamma_\eta\left(\beta_e\left(|\pi(0)|, \tfrac{t}{2}\right)\right) \\ & + \beta_e(|\pi(0)|, t)\end{aligned} \tag{A.52}$$

It can be easily verified that β is a class $\mathcal{KL}$ function. Hence, the origin of the reduced closed-loop system is asymptotically stable (i.e., $\pi(t) \to 0$ as $t \to \infty$). Therefore, there exists a class $\mathcal{KL}$ function, $\bar{\beta}_\eta(\cdot, \cdot)$ such that:

$$|\eta(t)| \leq \bar{\beta}_\eta(|\eta(0)|, t), \quad \forall\, t \geq 0 \tag{A.53}$$

To show exponential stability, we proceed as follows. Repeating the same calculations of Step 1 in Part 1 of the Proof of Theorem 2.1, it is straightforward to show that, when $L_{\bar{g}}V = 0$, there exists a positive real number ϕ^* such that if $\phi \leq \phi^*$, $\dot{V}$ – computed along the trajectories of the reduced closed-loop e-subsystem – satisfies:

$$\begin{aligned} \dot{V} &\leq -\frac{1}{2}c_0(L_{\bar{g}}V)^2 \\ &\leq -2c_0|Pe|^2|L_gL_f^{r-1}h(x)|^2 \\ &\leq -2c_0\lambda_{max}(P^2)|e|^2|L_gL_f^{r-1}h(x)|^2 \end{aligned} \tag{A.54}$$

where we have used the fact that $|L_{\bar{g}}V| \leq 2|Pe||L_gL_f^{r-1}h(x)|$ in deriving the second inequality. From the asymptotic stability of the origin, we have that x is bounded and, consequently, $L_gL_f^{r-1}h(x)$ – which is a smooth function of x – is also bounded. Therefore, given any positive real number, δ_x, there exists positive real numbers, κ_1 and κ_2, such that if $|x(0)| \leq \delta_x$, then $|x(t)| \leq \kappa_1$ and $|L_gL_f^{r-1}h(x(t))|^2 \leq \kappa_2$, for all $t \geq 0$. Hence, $\dot{V} \leq -\kappa_3|e|^2$, where $\kappa_3 = 2c_0\lambda_{max}(P^2)\kappa_2 > 0$. Recall from the analysis of Eq.A.6 in the Proof of Theorem 2.1 that, when $L_{\bar{g}}V = 0$, $\dot{V} \leq -e^TQe \leq -\lambda_{max}(Q)|e|^2$, where Q is a positive-definite matrix. Therefore, we have $\dot{V} \leq -\kappa_4|e|^2$, where $\kappa_4 = \max\{\kappa_3, \lambda_{max}(Q)\}$, and there exist real numbers, $k_1 \geq 1$ and $a_1 > 0$, such that the following inequality holds for the reduced closed-loop e-subsystem:

$$|e(t)| \leq k_1|e(0)|e^{-a_1t} \quad \forall\, t \geq 0 \tag{A.55}$$

From the above inequality and the fact that the η-subsystem, with $e = 0$, is locally exponentially stable (from Assumption 2.6), a direct application of the result of Lemma 5.6 in [170] yields that the e-η interconnected, reduced closed-loop system of Eq.A.40 is locally exponentially stable. Therefore, there exists a positive real number, r, such that:

$$|\pi(t)| \leq k_3|\pi(t_0)|e^{-a_2(t-t_0)} \quad \forall\ |\pi(t_0)| \leq r \tag{A.56}$$

for some $k_3 \geq 1$ and $a_2 > 0$.

Finally, we note that since the static component of the controller of Eq.2.41 with $\hat{x} = x$ enforces global asymptotic stability in the reduced (slow) closed-loop system, the ζ states of this system satisfy a bound of the following form, $\forall\, t \geq 0$:

$$|\zeta(t)| \;\leq\; \beta_\zeta(\delta_\zeta, t) \tag{A.57}$$

where β_ζ is a class $\mathcal{KL}$ function and δ_ζ is the maximum value of the norm of the vector $[h(x)\ L_f h(x)\ \cdots\ L_f^{r-1}h(x)]$, for $|x| \leq \delta_x$. Based on the above bound and following the results of [171, 294], we disregard estimates of $\tilde{y}$, obtained from the high-gain observer, with norm $|\tilde{y}| > \beta_\zeta(\delta_\zeta, 0)$. Hence, we set $sat(\cdot) = \min\{1, \frac{\zeta_{max}}{|\cdot|}\}(\cdot)$ where ζ_{max} is the maximum value of the vector $[\zeta_1\ \zeta_2\ \cdots\ \zeta_r]$, for $|\zeta| \leq \beta_\zeta(\delta_\zeta, 0)$.

Step 2: In order to apply the result of Lemma 1 in [60], we need to define a set of positive real numbers $\{\bar{\delta}_e, \bar{\delta}_\eta, \delta_\theta, \delta_{\bar{v}}, \delta_\eta, \delta_e, d, d_e, d_\eta\}$ where δ_θ and $\delta_{\bar{v}}$ were specified in the statement of the theorem, d, d_e, and d_η are arbitrary positive real numbers,

$$\begin{aligned}
\bar{\delta}_e &\geq \max_{|x|\leq\delta_x, |\bar{v}|\leq\delta_{\bar{v}}} \left\{ \left| \sum_{k=1}^{r} (v^{(k-1)} - L_{\tilde{f}}^{k-1} h(x)) \right| \right\} \\
\bar{\delta}_\eta &\geq \max_{|x|\leq\delta_x, |\bar{v}|\leq\delta_{\bar{v}}} \left\{ \sum_{k=1}^{r} |(v^{(k-1)} - L_{\tilde{f}}^{k-1} h(x))| + \sum_{\nu=1}^{n-r} |\chi_\nu(x)| \right\}
\end{aligned} \tag{A.58}$$

$\delta_e > \beta_e(\bar{\delta}_e, 0) + d_e$, $\delta_\eta > \bar{\beta}_\eta(\bar{\delta}_\eta, 0) + d_\eta$. First, consider the singularly perturbed system comprised of the states (ζ, e_o) of the closed-loop system of Eq.A.40. This system is in standard form, possesses a globally exponentially stable fast subsystem, and its corresponding reduced system is globally asymptotically stable. These properties allow a direct application of the result of Lemma 1 given in [60] with $\delta = \max\{\delta_\zeta, \delta_{e_o}, \delta_\theta, \delta_{\bar{v}}, \delta_\eta\}$ to obtain the existence of a positive real number $\epsilon^\zeta(\phi)$ such that if $\epsilon \in (0, \epsilon^\zeta(\phi)]$, and $|\zeta(0)| \leq \delta_\zeta$, $|e_o(0)| \leq \delta_{e_o}$, $\|\theta\| \leq \delta_\theta$, $\|\bar{v}\| \leq \delta_{\bar{v}}$, $\|\eta\| \leq \delta_\eta$, then:

$$\begin{aligned}
|\zeta(t)| &\;\leq\; \beta_\zeta(\delta_\zeta, t) + d \\
|e_o(t)| &\;\leq\; k_4 |e_o(0)| e^{-a_3 \frac{t}{\epsilon}} + d
\end{aligned} \tag{A.59}$$

for some $k_4 \geq 1$ and $a_3 > 0$.

Consider now the singularly perturbed system comprised of the states (e, e_o) of the system of Eq.A.40. This system is in standard form, possesses a globally exponentially stable fast subsystem, and its corresponding reduced system is globally asymptotically stable. These properties allow a direct application of the result of Lemma 1 in [60] with $\delta = \max\{\bar{\delta}_e, \delta_{e_o}, \delta_\theta, \delta_{\bar{v}}, \delta_\eta\}$ to obtain the existence of a positive real number $\epsilon^e(\phi)$ such that if $\epsilon \in (0, \epsilon^e(\phi)]$, and $|e(0)| \leq \bar{\delta}_e$, $|e_o(0)| \leq \delta_{e_o}$, $\|\theta\| \leq \delta_\theta$, $\|\bar{v}\| \leq \delta_{\bar{v}}$, $\|\eta\| \leq \delta_\eta$, then:

$$|e(t)| \leq \beta_e\left(|e(0)|, t\right) + d_e \tag{A.60}$$

Similarly, it can be shown that Lemma 1, with $\delta = \max\{\bar{\delta}_\eta, \delta_{e_o}, \delta_\theta, \delta_{\bar{v}}, \delta_e\}$, can be applied to the system comprised of the states (η, e_o) of the system of Eq.A.40. Thus, we have that there exist positive real numbers $\epsilon^\eta(\phi)$ such that if $\epsilon \in (0, \epsilon^\eta(\phi)]$ and $|\eta(0)| \leq \bar{\delta}_\eta$, $|e_o(0)| \leq \delta_{e_o}$, $\|\theta\| \leq \delta_\theta$, $\|\bar{v}\| \leq \delta_{\bar{v}}$, $\|e\| \leq \delta_e$, then:

$$|\eta(t)| \;\; \leq \;\; \bar{\beta}_\eta\left(|\eta(0)|, t\right) + d_\eta \tag{A.61}$$

Finally, the inequalities of Eqs.A.43-A.44 and Eqs.A.60-A.61 can be manipulated using a small-gain theorem type argument similar to the one used in the Proof of Theorem 1 in [68] to show that given the following set of positive real numbers $\{\bar{\delta}_e, \bar{\delta}_\eta, \delta_{e_o}, \delta_\theta, \delta_{\bar{v}}, d, d_e, d_\eta\}$ and with $\phi \in (0, \phi^*]$, there exists a positive real number, $\tilde{\epsilon}(\phi) \in (0, \min\{\epsilon^\zeta(\phi), \epsilon^e(\phi), \epsilon^\eta(\phi)\}]$ such that if $\epsilon \in (0, \tilde{\epsilon}(\phi)]$, and $|e(0)| \leq \bar{\delta}_e$, $|\eta(0)| \leq \bar{\delta}_\eta$, $|e_o(0)| \leq \delta_{e_o}$, $\|\theta\| \leq \delta_\theta$, $\|\bar{v}\| \leq \delta_{\bar{v}}$, then the states of the closed-loop system are bounded. For brevity, this argument will not be repeated here.

Step 3: So far in the proof, we have established that the states of the singularly perturbed closed-loop system of Eq.A.40 are semi-globally bounded. In this section we show that the origin of the closed-loop system is (semi-globally) asymptotically stable. To this end, we note – from the inequalities of Eqs.A.59-A.61 – that, as t increases, the trajectories will be ultimately bounded with ultimate bounds that depend on d, d_e, and d_η. Since d, d_e, and d_η are arbitrary, we can choose them small enough such that after a sufficiently large time, say $\tilde{t}$, the trajectories of the closed-loop system are confined within a small compact neighborhood of the origin. Obviously, $\tilde{t}$ depends on

both the initial condition and the desired size of the neighborhood, but is independent of ϵ. Let $\tilde{d} := \max\{d, d_e, d_\eta\} \leq r/4$, where r was defined in Eq.A.56, and $\tilde{t}$ be the earliest time such that $\max\{\beta_e\left(|e(0)|, \tilde{t}\right), \bar{\beta}_\eta\left(|\eta(0)|, \tilde{t}\right), \frac{1}{3}k_4|e_o(0)|e^{-a_3\frac{\tilde{t}}{\epsilon}}\} \leq d$. Then it can be easily verified that:

$$|\pi(t)| \leq r, \quad |e_o(t)| \leq r \quad \forall\, t \geq \tilde{t} \tag{A.62}$$

Recall from Eq.A.56 and Eq.A.39 that both the reduced (slow) and fast closed-loop subsystems are exponentially stable within the balls of Eq.A.62. Therefore, a direct application of the result of Theorem 9.3 in [170] yields that there exists $\bar{\epsilon} > 0$ such that if $\epsilon \in (0, \bar{\epsilon}]$, then:

$$|z(t)| \leq \alpha_1|z(\tilde{t})|e^{-\beta_1(t-\tilde{t})} \tag{A.63}$$

for some $\alpha_1 \geq 1$ and $\beta_1 > 0$, where $z(t) = [e^T(t)\ \eta^T(t)\ \omega^T(t)\ e_o^T(t)]^T$ and $\epsilon \in (0, \min\{\bar{\epsilon}, \epsilon^\zeta, \epsilon^e, \epsilon^\eta\}$. Consequently, the states of the closed-loop system of Eq.A.40 converge to the origin as $t \to \infty$, which together with the boundedness of the close-loop states established in Step 2, implies that the origin of the closed-loop system is asymptotically stable. The asymptotic output tracking result can now be obtained by simply noting that from Eq.A.63 that we have:

$$\limsup_{t\to\infty} |e(t)| = 0 \tag{A.64}$$

and therefore

$$\limsup_{t\to\infty} |e_1(t)| = \limsup_{t\to\infty} |y(t) - v(t)| = 0 \tag{A.65}$$

Part 3: In this part, we show that the controller of Eq.2.41 is near-optimal with respect to the cost of Eq.2.19 in the sense that the cost achieved by this controller tends to the minimum cost for the state feedback problem as $\epsilon \to 0$. To this end, we adopt the following three-step procedure. In Step 1, we show that, for the reduced (slow) closed-loop system, the controller of Eq.2.41 with $\epsilon = 0$ (i.e., $\hat{x} = x$) is optimal with respect to a cost functional of the form of Eq.2.19 with a minimum cost of $V(e(0))$. In Step 2, we establish the closeness of solutions of the reduced and full closed-loop systems on the infinite time-interval. Finally, in Step 3, we exploit the

closeness of solutions result to show that the minimum cost achieved by the controller of Eq.2.41 in the full closed-loop system approaches the optimal cost for the reduced system under state feedback, when the observer gain is sufficiently large.

Step 1: In this step we show that the static component of the controller of Eq.2.41 with $\epsilon = 0$ and $\hat{x} = x$ minimizes the cost functional associated with the reduced (slow) closed-loop system which has the form of Eq.2.19. To this end, consider the closed-loop system of Eq.A.40 with $\epsilon = 0$, where u of Eq.2.41 is applied with $\hat{x} = x$. We note that the resulting reduced closed-loop system is identical to the one studied in the Proof of Theorem 2.1 (state feedback problem) and satisfies the assumptions stated therein. Applying the result of this theorem, we have that the static component of the controller of Eq.2.41 minimizes a cost functional of the form

$$J_r = \int_0^\infty (l(\bar{e}) + uR(\bar{x})u)\, dt \tag{A.66}$$

where $\bar{x} = \mathcal{X}^{-1}(\bar{e}, \bar{\eta}, \bar{v})$ refers to the solution of the reduced closed-loop system under state feedback control. Following the same treatment presented in Part 3 of the Proof of Theorem 2.1 in, it can be readily shown that upon substitution of the static component u of Eq.2.41 in the above expression, the minimum cost obtained is:

$$J_r^* = \min_{u=p(\bar{x})} \int_0^\infty (l(\bar{e}) + uR(\bar{x})u)\, dt = V(\bar{e}(0)) \tag{A.67}$$

Step 2: In this step, we show that starting from an arbitrarily large compact set of initial conditions and for arbitrarily large uncertainties, the following estimates hold:

$$\begin{aligned} z(t,\epsilon) - \bar{z}(t) &= O(\epsilon) \quad \forall\ t \geq 0 \\ e_o(t,\epsilon) &= O(\epsilon) \quad \forall\ t \geq t_b \end{aligned} \tag{A.68}$$

for some $t_b > 0$ where $\bar{z}(t) = [\bar{e}^T(t)\ \bar{\eta}^T(t)\ \bar{\omega}^T(t)]^T$ is the solution of the reduced (slow) problem obtained by setting $\epsilon = 0$ in Eq.A.40. The strategy we shall adopt to prove the above estimates involves, first, the application of Tikhonov's theorem to establish the closeness of solutions on a finite time-interval whose size can be made arbitrarily large by selecting ϵ sufficiently small. Then, once the trajectories of the closed-loop

system become confined within an appropriately small ball around the origin, we apply the result of Theorem 9.4 reported in [170] to obtain the estimates of Eq.A.68.

Referring to the system of Eq.A.40, it is straightforward to show that this system satisfies the conditions of Theorem 9.1 in [170]. Applying the result of this theorem to the system of Eq.A.40, we conclude that there exists a finite time, $t_1 > 0$, and positive constants. K, L , and $\bar{\bar{\epsilon}}$ such that if $\epsilon \in (0, \bar{\bar{\epsilon}}]$ and $|e(0)| \leq \bar{\delta}_e$, $|\eta(0)| \leq \bar{\delta}_\eta$, $|e_o(0)| \leq \delta_{e_o}$, $\|\theta\| \leq \delta_\theta$, $\|\bar{v}\| \leq \delta_{\bar{v}}$, then:

$$|z(t,\epsilon) - \bar{z}(t)| \leq \epsilon K[1 + t_1] \exp(Lt_1) \tag{A.69}$$

and the estimate:

$$z(t,\epsilon) - \bar{z}(t) = O(\epsilon) \tag{A.70}$$

holds uniformly for $t \in [0, t_1]$. Furthermore, given any $t_b > 0$, there is $\epsilon_b \leq \bar{\bar{\epsilon}}$ such that the estimate:

$$e_o(t,\epsilon) = O(\epsilon) \tag{A.71}$$

holds uniformly for $t \in [t_b, t_1]$ whenever $\epsilon < \bar{\bar{\epsilon}}$. In order for the above estimates to hold on the infinite time-interval, we require that $t_1 \geq \tilde{t}$ where $\tilde{t}$ was defined in Step 3 of Part 2 of the proof. From Eq.A.69, it is clear that t_1 can be made arbitrarily large while maintaining the estimate of Eq.A.70 by selecting ϵ sufficiently small. Therefore there exists a positive constant ϵ^{**} such that if $\epsilon \in (0, \epsilon^{**}]$, we have $t_1 \geq \tilde{t}$ and the trajectories of the closed-loop system lie within the neighborhood of the origin defined in Eq.A.56. It can be easily verified that, within this neighborhood, the closed-loop system of Eq.A.40 satisfies the assumptions of Theorem 9.4 in [170]. Applying the result of this theorem, we obtain the existence of a positive constant ϵ' such that if $\epsilon \in (0, \epsilon']$, the estimates of Eq.A.68 hold $\forall$ $|z(t)| \leq r$ and $|e_o(t)| \leq r$. Finally, we now have that if $\epsilon \in (0, \epsilon^*]$ where $\epsilon^* = \min\{\epsilon', \epsilon^{**}, \bar{\bar{\epsilon}}, \bar{\epsilon}, \epsilon^\zeta, \epsilon^e, \epsilon^\eta, \epsilon_0\}$, then Eq.A.68 is satisfied for $|e(0)| \leq \bar{\delta}_e$, $|\eta(0)| \leq \bar{\delta}_\eta$, $|e_o(0)| \leq \delta_{e_o}$, $\|\theta\| \leq \delta_\theta$, $\|\bar{v}\| \leq \delta_{\bar{v}}$.

Step 3: In the last step of this part of the proof, we exploit the closeness of solutions result obtained in Step 2 and combine it with the optimality result established in Step 1 to prove that the output feedback controller of Eq.2.41 is near-optimal in the sense

that it achieves a cost for the full closed-loop system that approaches the minimum cost for the reduced (state feedback) problem provided that the gain of the observer is sufficiently large. To this end, consider re-writing the cost functional of Eq.2.19 as follows:

$$J_v(u) = \int_0^{t_b} (l(e) + uR(x)u)\, dt + \int_{t_b}^{\infty} (l(e) + uR(x)u)\, dt \tag{A.72}$$

From Step 2, we have that the following estimates hold for $t \geq t_b$:

$$\begin{aligned} e(t) &= \bar{e}(t) + O(\epsilon) \\ x(t) &= \bar{x}(t) + O(\epsilon) \\ \hat{x}(t) &= \bar{x}(t) + O(\epsilon) \end{aligned} \tag{A.73}$$

It follows then from the continuity properties of the functions $l(\cdot)$, $u(\cdot)$, $R(\cdot)$ that, for $t \geq t_b$ and as $\epsilon \longrightarrow 0$, $l(e(t)) \longrightarrow l(\bar{e}(t))$, $p(\hat{x}(t)) \longrightarrow p(\bar{x}(t))$, $R(x(t)) \longrightarrow R(\bar{x}(t))$, and therefore:

$$\int_{t_b}^{\infty} (l(e) + p(\hat{x})R(x)p(\hat{x}))\, dt \longrightarrow \int_{t_b}^{\infty} (l(\bar{e}) + p(\bar{x})R(\bar{x})p(\bar{x}))\, dt \tag{A.74}$$

From the stability of the full closed-loop system established in Part 2 of the proof, together with the continuity properties of the functions $l(\cdot)$, $u(\cdot)$, $R(\cdot)$, we have that there exists a positive real number, M, that bounds the integrand, $l(e)+p(\hat{x})R(x)p(\hat{x})$. Using the fact that $t_b = O(\epsilon)$, we get:

$$\begin{aligned} \int_0^{t_b} (l(e) + p(\hat{x})R(x)p(\hat{x}))\, dt &\leq \int_0^{t_b} M dt \\ &\leq M\epsilon \\ &= O(\epsilon) \end{aligned} \tag{A.75}$$

Similarly, from the stability of the reduced closed-loop system (state feedback problem) established in Part 1 and the fact that $t_b = O(\epsilon)$, there exists a positive real number M' such that:

$$\begin{aligned} \int_0^{t_b} (l(\bar{e}) + p(\bar{x})R(\bar{x})p(\bar{x}))\, dt &\leq \int_0^{t_b} M' dt \\ &\leq M'\epsilon \\ &= O(\epsilon) \end{aligned} \tag{A.76}$$

Combining Eqs.A.74-A.76, we have that as $\epsilon \longrightarrow 0$:

$$J_v(u = p(\hat{x})) = \int_0^\infty (l(e) + p(\hat{x})R(x)p(\hat{x}))\, dt \longrightarrow \int_0^\infty (l(\bar{e}) + p(\bar{x})R(\bar{x})p(\bar{x}))\, dt \tag{A.77}$$

and, therefore, from Eq.A.67, we finally have:

$$J_v(u = p(\hat{x})) \longrightarrow V(\bar{e}(0)) \quad as \;\; \epsilon \longrightarrow 0 \tag{A.78}$$

This completes the proof of the theorem. $\triangle$

Proof of Theorem 2.4:

The proof of this theorem follows closely the proof of Theorem 2.3. We will only point out the differences. In Part 1, we establish the global exponential stability of the fast closed-loop subsystem and derive ISS bounds for the states of the reduced closed-loop system. Then using the Lemma 1 in [60], we show that the derived ISS bounds continue to hold up to an arbitrarily small offset, for arbitrarily large initial conditions and uncertainty. In Part 2, the resulting ISS inequalities are studied, using techniques similar to those used in [154, 68]to show boundedness of the closed-loop trajectories and establish the inequality of Eq.2.46. In Part 3, we apply Tikhonov's theorem to obtain closeness of solutions on the finite time-interval and then use this result to prove the finite-horizon near-optimality of the output feedback controller of Eq.2.45.

Part 1: The global exponential stability of the closed-loop fast subsystem was established in Step 1 of Part 1 of the Proof of Theorem 2.1 and will not be repeated here. Instead, we focus on the reduced system and derive ISS bounds that capture the evolution of its states. To this end, we consider again the system of Eq.A.40 with $\epsilon = 0$. Using the same argument presented in Step 2 of Part 1 in the Proof of Theorem 2.1, one can again show that for the system of Eq.A.40, $\omega(0) = \eta(0) + O(\epsilon)$ implies $\eta(t) = \omega(t) + O(\epsilon)\ \forall\ t \geq 0$, which yields that $\omega(t) = \eta(t)$ when $\epsilon = 0$. Therefore, the reduced (slow) closed-loop system (i.e., the system of Eq.A.40 with $\epsilon = 0$) is identical to the one studied in the Proof of Theorem 2.2, where it was shown that the evolution

of the e-subsystem satisfies:

$$|e(t)| \leq \bar{\beta}_e(|e(0)|, t) + \bar{\gamma}_e(\phi) \qquad \forall\, t \geq 0 \tag{A.79}$$

where $\bar{\beta}_e$ is a class $\mathcal{KL}$ function and $\bar{\gamma}_e$ is a class K_∞ function. From Assumption 2.7, we have that the η states of the reduced closed-loop system possess an ISS property with respect to e:

$$|\eta(t)| \leq K_\eta |\eta(0)| e^{-at} + \bar{\gamma}_\eta(\|e\|) \tag{A.80}$$

uniformly in $\bar{v}$,where $\bar{\gamma}_\eta$ is a class $\mathcal{K}$ function. Realizing that the reduced closed-loop system, for which the inequalities of Eqs.A.79-A.80, is identical to the system studied in the Proof of Theorem 2.2, we note that the static component of the controller of Eq.2.45 with $\hat{x} = x$ (i.e., $p(x, , c_0, \hat{x}, \rho, \chi, \phi, \theta_b)$) enforces global ultimate boundedness in the reduced closed-loop system, and thus, the ζ states of the reduced closed-loop system satisfy the following bound:

$$|\zeta(t)| \leq \beta_\zeta(\delta_\zeta, t) + \tilde{\gamma}(\phi) \quad \forall\, t \geq 0 \tag{A.81}$$

where β_ζ is a class $\mathcal{KL}$ function, $\tilde{\gamma}$ is a class $\mathcal{K}_\infty$ function and δ_ζ is the maximum value of the vector $[h(x)\ L_f h(x)\ \cdots L_f^{r-1} h(x)]$ for $|x| \leq \delta_x$.

Based on the above bound and following the results of [171, 294], we disregard estimates of $\tilde{y}$, obtained from the high-gain observer, with norm $|\tilde{y}| > \beta_\zeta(\delta_\zeta, 0) + d$ where $d > \tilde{\gamma}(\phi)$. Hence, we set $sat(\cdot) = \min\{1, \frac{\zeta_{max}}{|\cdot|}\}(\cdot)$ where ζ_{max} is the maximum value of the vector $[\zeta_1\ \zeta_2\ \cdots\ \zeta_r]$ for $|\zeta| \leq \beta_\zeta(\delta_\zeta, 0) + d$.

We are now in a position to apply the result of Lemma 1 in [60]. To this end, we define the following positive real numbers, $\{\bar{\delta}_e, \bar{\delta}_\eta, \delta_\theta, \delta_{\bar{v}}, \delta_\eta, \delta_e, d, d_e, d_\eta\}$ where δ_θ and $\delta_{\bar{v}}$ were specified in the statement of the theorem, $\bar{\delta}_e$ and $\bar{\delta}_\eta$ were defined in Eq.A.58, d, d_e and d_η are arbitrary, $\delta_e > \bar{\beta}_e(\bar{\delta}_e, 0) + \bar{\gamma}_e(\phi) + d_e$, $\delta_\eta > K_\eta \bar{\delta}_\eta + \bar{\gamma}_\eta(\delta_e) + d_\eta$.

First, consider the singularly perturbed system comprised of the states (ζ, e_o) of the closed-loop system. This system is in standard form, possesses a globally exponentially stable fast subsystem, and its corresponding reduced system is ISS. These properties allow a direct application of the result of Lemma 1 in [60] with

$\delta = \max\{\delta_\zeta, \delta_{e_o}, \delta_\theta, \delta_{\bar{v}}, \delta_\eta, \delta_e\}$ and $d = \phi$, to obtain the existence of a positive real number $\epsilon^\zeta(\phi)$ such that if $\epsilon \in (0, \epsilon^\zeta(\phi)]$, and $|\zeta(0)| \leq \delta_\zeta$, $|e_o(0)| \leq \delta_{e_o}$, $\|\theta\| \leq \delta_\theta$, $\|\bar{v}\| \leq \delta_{\bar{v}}$, $\|e\| \leq \delta_e$, $\|\eta\| \leq \delta_\eta$, then:

$$|\zeta(t)| \leq \beta_\zeta(\delta_\zeta, t) + \tilde{\gamma}(\phi) + \phi \tag{A.82}$$

Let $\bar{\phi}$ be such that $\tilde{\gamma}(\bar{\phi}) + \bar{\phi} \leq d$. Consider now the singularly perturbed system comprised of the states (e, e_o) of the system of Eq.A.40. This system is in standard form, possesses a globally exponentially stable fast subsystem, and its corresponding reduced system is ISS. These properties allow a direct application of the result of Lemma 1 with $\delta = \max\{\bar{\delta}_e, \delta_{e_o}, \delta_\theta, \delta_{\bar{v}}, \delta_\eta\}$ and $d = d_e = \phi$, to obtain the existence of a positive real number $\epsilon^e(\phi)$ such that if $\epsilon \in (0, \epsilon^e(\phi)]$, and $|e(0)| \leq \bar{\delta}_e$, $|e_o(0)| \leq \delta_{e_o}$, $\|\theta\| \leq \delta_\theta$, $\|\bar{v}\| \leq \delta_{\bar{v}}$, $\|\eta\| \leq \delta_\eta$, $\|e\| \leq \delta_e$, then:

$$|e(t)| \leq \bar{\beta}_e\left(|e(0)|, t\right) + \bar{\gamma}_e(\phi) + \phi \tag{A.83}$$

where we define Let $\tilde{\phi}$ be such that $\bar{\gamma}_e(\tilde{\phi}) + \tilde{\phi} \leq d$. Similarly, it can be shown that Lemma 1, with $\delta = \max\{\bar{\delta}_\eta, \delta_{e_o}, \delta_\theta, \delta_{\bar{v}}, \delta_e\}$ and $d = d_{\bar{\eta}}$, can be applied to the system comprised of the states (η, e_o) of the system of Eq.A.40. Thus, we have that there exist positive real numbers $\epsilon^\eta(\phi)$ such that if $\epsilon \in (0, \epsilon^\eta(\phi)]$ and $|\eta(0)| \leq \bar{\delta}_\eta$, $|e_o(0)| \leq \delta_{e_o}$, $\|\theta\| \leq \delta_\theta$, $\|\bar{v}\| \leq \delta_{\bar{v}}$, $\|e\| \leq \delta_e$, then:

$$|\eta(t)| \leq K_\eta |\eta(0)| e^{-at} + \bar{\gamma}_\eta(\|e\|) + d_\eta \tag{A.84}$$

Finally, the inequalities of Eqs.A.79-A.84 can be manipulated using a small-gain theorem type argument similar to the one used in the Proof of Theorem 1 in [68] to show that given the set of positive real numbers $\{\bar{\delta}_e, \bar{\delta}_\eta, \delta_{e_o}, \delta_\theta, \delta_{\bar{v}}, d, d_e, d_\eta\}$ and with $\phi^* := \min\{\bar{\phi}, \tilde{\phi}\}$ and with $\phi \in (0, \phi^*]$, there exists $\epsilon^*(\phi) \in (0, \min\{\epsilon^\zeta(\phi), \epsilon^e(\phi), \epsilon^\eta(\phi)\}]$ such that if $\epsilon \in (0, \epsilon^*(\phi)]$, and $|e(0)| \leq \bar{\delta}_e$, $|\eta(0)| \leq \bar{\delta}_\eta$, $|e_o(0)| \leq \delta_{e_o}$, $\|\theta\| \leq \delta_\theta$, $\|\bar{v}\| \leq \delta_{\bar{v}}$, then $|\zeta(t)| \leq \beta_\zeta(\delta_\zeta, 0) + d$ and the remaining states of the closed-loop system are bounded and its output satisfies the relation of Eq.2.46. For brevity, this argument will not be repeated here.

Part 3: In this part of the proof, we show that the output feedback controller of Eq.2.45 is near-optimal over a finite time-interval for the class of systems considered in Eq.2.1 and produces a finite cost which tends to the optimal cost for the reduced (state feedback) problem as $\epsilon \rightarrow 0$. To this end, we adopt a similar three-step procedure to the one employed in Part 3 of the Proof of Theorem 2.1. In the first step, we use Tikhonov's theorem to establish closeness of the solutions of the reduced and full closed-loop systems on the finite time-interval. In Step 2, we show that, for the reduced system, the controller of Eq.2.45 with $\epsilon = 0$ is optimal with respect to a cost functional $\bar{J}_r$ of the form of Eq.2.25. Finally, in Step 3, we combine the results of Steps 1 and 2 to show that the cost associated with the full closed-loop system tends to the optimal cost for the reduced system as $\epsilon \rightarrow 0$.

Step 1: Referring to the system of Eq.A.40, it is straightforward to show that this system satisfies the conditions of theorem 9.1 given in [170]. Applying this theorem to the system of Eq.A.40, we conclude that there exists a finite time $t_1 > 0$ and positive constants K, L, and $\bar{\bar{\epsilon}}$ such that if $\epsilon \in (0, \bar{\bar{\epsilon}}]$ and $|e(0)| \leq \bar{\delta}_e$, $|\eta(0)| \leq \bar{\delta}_\eta$, $|e_o(0)| \leq \delta_{e_o}$, $\|\theta\| \leq \delta_\theta$, $\|\bar{v}\| \leq \delta_{\bar{v}}$, then

$$|z(t,\epsilon) - \bar{z}(t)| \leq \epsilon K[1 + t_1]exp(Lt_1) \tag{A.85}$$

and the estimate:

$$z(t,\epsilon) - \bar{z}(t) = O(\epsilon) \tag{A.86}$$

holds uniformly for $t \in [0, t_1]$ where $\bar{z}(t) = [\bar{e}(t)\ \bar{\eta}(t)\ \bar{\omega}(t)]^T$ is the solution of the reduced (slow) problem. Furthermore, given any $t_b > 0$, there is $\epsilon_b \leq \bar{\bar{\epsilon}}$ such that the estimate:

$$e_o(t,\epsilon) = O(\epsilon) \tag{A.87}$$

holds uniformly for $t \in [t_b, t_1]$ whenever $\epsilon < \bar{\bar{\epsilon}}$.

Step 2: In this step we show that the controller of Eq.2.45 with $\epsilon = 0$ and $\hat{x} = x$ minimizes the cost functional associated with the reduced system. To this end, consider the closed-loop system of Eq.A.40 with $\epsilon = 0$ where u of Eq.2.45 is applied

with $\hat{x} = x$. We note that the resulting slow system is identical to the one studied in Theorem 2.2 under state feedback and satisfies the assumptions stated therein. Applying the result of this theorem, we obtain that the static component of the controller of Eq.2.45 minimizes the cost functional:

$$\bar{J}_r = \lim_{t \to T_f} V(\bar{e}(t)) + \int_0^{T_f} (l(\bar{e}) + u(\bar{x})R(\bar{x})u(\bar{x}))\, dt \tag{A.88}$$

where, as before, $\bar{x} = \mathcal{X}^{-1}(\bar{e}, \bar{\eta}, \bar{v})$ refers to the solution of the reduced closed-loop system under state feedback and T_f is defined in the Proof of Theorem 2.2. Following the same treatment presented in Part 3 of the Proof of Theorem 2.2, it can be readily shown that upon substitution of the static component u of Eq.2.45 in the above expression, the minimum cost obtained is:

$$\bar{J}_r^* = \min_{u=p(\hat{x})} \left[\lim_{t \to T_f} V(\bar{e}(t)) + \int_0^{T_f} (l(\bar{e}) + uR(\bar{x})u)\, dt \right] = V(\bar{e}(0)) \tag{A.89}$$

Step 3: In this step, we exploit the closeness of solutions result obtained in Step 1 and combine it with the optimality result established in Step 2 to prove that the output feedback controller of Eq.2.45 is near-optimal in the sense that the cost functional of Eq.2.25 associated with the full closed-loop system approaches the optimal cost for the reduced (slow) system under state feedback, provided that the gain of the observer is sufficiently large. Note first that in order to guarantee near-optimality, we must require $t_1 \geq T_f$. This requirement guarantees that the solutions of the reduced and full closed-loop systems remain close during the time interval over which the state feedback controller u of Eq.2.45 (with $\epsilon = 0$ and $\hat{x} = x$) is optimal. From Eq:A.85, it is clear that t_1 can be made arbitrarily large while maintaining the estimate of Eq.A.86 by selecting ϵ sufficiently small (or equivalently the gain of the observer sufficiently large). Therefore there exists a positive constant ϵ^{**} such that if $\epsilon \in (0, \epsilon^{**}]$, we have $t_1 \geq T_f$. Therefore, we set ϵ^* in theorem 2 as $\epsilon^* = min\{\epsilon_0, \epsilon^\zeta, \epsilon^\eta, \epsilon^e, \bar{\bar{\epsilon}}, \epsilon^{**}\}$. To proceed with the proof of near-optimality, consider rewriting the cost functional of Eq.2.25 as follows:

$$J_n(u) = \lim_{t \to T_f} V(e(t)) + \int_0^{t_b} (l(e) + uR(x)u)\, dt + \int_{t_b}^{T_f} (l(e) + uR(x)u)\, dt \tag{A.90}$$

From Step 2, we have that the following estimates hold for $t \in [t_b, t_1]$:

$$\begin{aligned} e(t) &= \bar{e}(t) + O(\epsilon) \\ x(t) &= \bar{x}(t) + O(\epsilon) \\ \hat{x}(t) &= \bar{x}(t) + O(\epsilon) \end{aligned} \tag{A.91}$$

It follows then from the continuity properties of the functions, $V(\cdot), l(\cdot), u(\cdot), R(\cdot)$ that for $t \in [t_b, t_1]$, and as $\epsilon \longrightarrow 0$, $V(e(t)) \longrightarrow V(\bar{e}(t))$, $l(e(t)) \longrightarrow l(\bar{e}(t))$, $p(\hat{x}(t)) \longrightarrow p(\bar{x}(t))$, $R(x(t)) \longrightarrow R(\bar{x}(t))$, and therefore:

$$\begin{aligned} &\lim_{t \to T_f} V(e(t)) + \int_{t_b}^{T_f} (l(e) + p(\hat{x})R(x)p(\hat{x}))\, dt \longrightarrow \\ &\lim_{t \to T_f} V(\bar{e}(t)) + \int_{t_b}^{T_f} (l(\bar{e}) + p(\bar{x})R(\bar{x})p(\bar{x}))\, dt \end{aligned} \tag{A.92}$$

From the boundedness of the trajectories of the closed-loop system established in Part 2, there exists a positive real number M that bounds the integrand of Eq.2.25. Using the fact that $t_b = O(\epsilon)$, we have that:

$$\int_0^{t_b} (l(e) + p(\hat{x})R(x)p(\hat{x}))\, dt \;\leq\; \int_0^{t_b} M dt \leq M\epsilon = O(\epsilon) \tag{A.93}$$

Similarly, from the stability of the reduced closed-loop system under state feedback established in Part 2 and the fact that $t_b = O(\epsilon)$, there exists a positive real number M' such that:

$$\int_0^{t_b} (l(\bar{e}) + p(\bar{x})R(\bar{x})p(\bar{x}))\, dt \;\leq\; \int_0^{t_b} M' dt \leq M'\epsilon = O(\epsilon) \tag{A.94}$$

Combining Eqs.A.92-A.94, we obtain that as $\epsilon \longrightarrow 0$:

$$\begin{aligned} J_n(u = p(\hat{x})) &= \lim_{t \to T_f} V(e(t)) + \int_0^{T_f} (l(e) + p(\hat{x})R(x)p(\hat{x}))\, dt \\ &\longrightarrow \lim_{t \to T_f} V(\bar{e}(t)) + \int_0^{T_f} (l(\bar{e}) + p(\bar{x})R(\bar{x})p(\bar{x}))\, dt \end{aligned} \tag{A.95}$$

and from Eq.A.89, we finally have:

$$J_n(u = p(\hat{x})) \longrightarrow V(\bar{e}(0)) \quad as \;\; \epsilon \longrightarrow 0 \tag{A.96}$$

This completes the proof of the theorem. $\triangle$

Appendix B

Proofs of Chapter 3

Proof of Theorem 3.1:

The proof of this theorem is divided into two parts. In the first part, we establish that starting from any initial condition that satisfies the inequality of Eq.3.11, the state feedback controller of Eq.3.10 asymptotically stabilizes the origin of the closed-loop system and that the closed-loop output satisfies Eq.3.12, provided that the evolution of the closed-loop trajectory satisfies Eq.3.11. In the second part, we prove that the controller of Eq.3.10 is optimal with respect to a meaningful cost functional of the form of Eq.3.14. To simplify the development of the proof, we consider only the case of a single uncertain variable, $q = 1$. Extension to the case when $q > 1$ is conceptually straightforward.

Part 1: We initially consider the representation of the closed-loop system in terms of the ζ, η coordinates and introduce the variables $e_i = \zeta_i - v^{(i-1)}, i = 1, \cdots, r$ and the

notation $\bar{v} = [v\ v^{(1)}\ \cdots\ v^{(r)}]^T$, to write the closed-loop system in the following form:

$$\begin{aligned}
\dot{e}_1 &= e_2 \\
&\vdots \\
\dot{e}_{r-1} &= e_r \\
\dot{e}_r &= L_f^r h(T^{-1}(e,\bar{v},\eta)) - v^{(r)} + L_g L_f^{r-1} h(T^{-1}(e,\bar{v},\eta))u \\
&\quad + L_w L_f^{r-1} h(T^{-1}(e,\bar{v},\eta))\theta \qquad \text{(B.1)} \\
\dot{\eta}_1 &= \Psi_1(e,\bar{v},\eta,\theta) \\
&\vdots \\
\dot{\eta}_{n-r} &= \Psi_{n-r}(e,\bar{v},\eta,\theta) \\
y &= e_1 + v
\end{aligned}$$

We now follow a three-step procedure to establish the asymptotic stability of the origin of the closed-loop system of Eq.B.1. Initially, we use a Lyapunov argument to show that, if the evolution of the closed-loop trajectory satisfies Eq.3.11, the states of the closed-loop e-subsystem converge asymptotically to the origin and derive bounds that capture the evolution of the states of the e and η subsystems. We then invoke a small gain argument to show that the trajectories of the e-η interconnected system remain bounded for all times starting from any initial state satisfying Eq.3.11. Finally, we show that the states of the full closed-loop system of Eq.B.1 converge to the origin and that the output satisfies the relation of Eq.3.12.

Step 1: Consider the smooth, positive-definite function, $V : \mathbb{R}^r \rightarrow R_{\geq 0}$, $V = e^T P e$ as a Lyapunov function candidate for the e-subsystem of Eq.B.1. Computing the

time-derivative of V along the trajectories of the closed-loop e-subsystem, we get:

$$\begin{aligned}
\dot{V} &= L_{\bar{f}}V + L_{\bar{g}}Vu + L_{\bar{w}}V\theta \\
&= L_{\bar{f}}V - \left(\frac{L_{\bar{f}}V + \left(\rho|2b^TPe| + \chi\theta_b\,|L_{\bar{w}}V|\right)\left(\dfrac{|2b^TPe|}{|2b^TPe|+\phi}\right)}{\left[1+\sqrt{1+(u_{max}L_{\bar{g}}V)^2}\right]} \right. \\
&\quad \left. + \frac{\sqrt{\left(L^*_{\bar{f}}V + \chi\theta_b\,|L_{\bar{w}}V|\right)^2 + (u_{max}L_{\bar{g}}V)^4}}{\left[1+\sqrt{1+(u_{max}L_{\bar{g}}V)^2}\right]} \right) + L_{\bar{w}}V\theta
\end{aligned} \tag{B.2}$$

Using the fact that $L_{\bar{w}}V\theta \leq |L_{\bar{w}}V|\,\theta_b$, we have – after some algebraic manipulations – that:

$$\begin{aligned}
\dot{V} \leq & \left(\frac{\left(L_{\bar{f}}V + \chi\theta_b\,|L_{\bar{w}}V|\right)\sqrt{1+(u_{max}L_{\bar{g}}V)^2}}{\left[1+\sqrt{1+(u_{max}L_{\bar{g}}V)^2}\right]} \right. \\
& - \frac{\sqrt{\left(L^*_{\bar{f}}V + \chi\theta_b\,|L_{\bar{w}}V|\right)^2 + (u_{max}L_{\bar{g}}V)^4}}{\left[1+\sqrt{1+(u_{max}L_{\bar{g}}V)^2}\right]} \\
& \left. + \frac{\theta_b\,|L_{\bar{w}}V|\left(\dfrac{\phi-(\chi-1)|2b^TPe|}{|2b^TPe|+\phi}\right) - \rho\left(\dfrac{|2b^TPe|^2}{|2b^TPe|+\phi}\right)}{\left[1+\sqrt{1+(u_{max}L_{\bar{g}}V)^2}\right]} \right)
\end{aligned} \tag{B.3}$$

Since $\chi > 2$ and $\rho > 0$, it is clear from the above inequality that, whenever $|2b^TPe| > \dfrac{\phi}{\chi-1}$, the last two terms on the right-hand side are strictly negative, and therefore $\dot{V}$ satisfies:

$$\begin{aligned}
\dot{V} \leq & \left(\frac{\left(L_{\bar{f}}V + \chi\theta_b\,|L_{\bar{w}}V|\right)\sqrt{1+(u_{max}L_{\bar{g}}V)^2}}{\left[1+\sqrt{1+(u_{max}L_{\bar{g}}V)^2}\right]} \right. \\
& \left. - \frac{\sqrt{\left(L^*_{\bar{f}}V + \chi\theta_b\,|L_{\bar{w}}V|\right)^2 + (u_{max}L_{\bar{g}}V)^4}}{\left[1+\sqrt{1+(u_{max}L_{\bar{g}}V)^2}\right]} \right) := K(e,\eta,\bar{v})
\end{aligned} \tag{B.4}$$

$\forall \ |2b^TPe| > \frac{\phi}{(\chi-1)}$. To study the behavior of $\dot{V}$ when $|2b^TPe| \leq \frac{\phi}{(\chi-1)}$, we exploit the fact that the uncertain variables considered in Theorem 3.1 are vanishing in the sense that the function, $\bar{w}(e,\eta,\bar{v}) = L_w L_f^{r-1}h(x)$, satisfies a linear growth bound of the form $|L_w L_f^{r-1}h(x)| \leq \delta|2b^TPe|$, where δ is a positive constant, whenever $|2b^TPe| \leq \frac{\phi}{(\frac{1}{2}\chi-1)}$ (and hence whenever $|2b^TPe| \leq \frac{\phi}{(\chi-1)}$). Using this bound together with the explicit expression for the function $L_{\bar{w}}V$ given by:

$$L_{\bar{w}}V = \frac{\partial V}{\partial e}\bar{w} = 2\left[b^TPe\right] L_w L_f^{r-1}h(x) \tag{B.5}$$

we obtain the following estimates:

$$\begin{aligned} \theta_b \left|L_{\bar{w}}V\right| \left(\phi - (\chi-1)|2b^TPe|\right) &\leq \theta_b \left|L_{\bar{w}}V\right| \phi \\ &= \theta_b |L_w L_f^{r-1}h(x)||2b^TPe|\phi \\ &\leq \theta_b \delta |2b^TPe|^2 \phi \qquad \forall \ |2b^TPe| \leq \frac{\phi}{\chi-1} \end{aligned} \tag{B.6}$$

Substituting the estimate of Eq.B.6 directly into Eq.B.3, we get:

$$\dot{V} \leq K(e,\eta,\bar{v}) + \left(\frac{(\theta_b\delta\phi - \rho)\,|2b^TPe|^2}{\left(|2b^TPe| + \phi\right)\left[1+\sqrt{1+(u_{max}L_{\bar{g}}V)^2}\right]} \right) \tag{B.7}$$

$\forall \ |2b^TPe| \leq \frac{\phi}{\chi-1}$. If ϕ is sufficiently small to satisfy the bound $\phi \leq \frac{\rho}{\delta\theta_b} := 2\phi^*$, then it's clear from Eqs.B.4-B.7 that the inequality of Eq.B.4 is satisfied, irrespective of the value of $|2b^TPe|$. From this equation, it is evident that analyzing the sign of $\dot{V}$ further depends on the sign of the term $L_{\bar{f}}V + \chi\theta_b \left|L_{\bar{w}}V\right|$. To this end, we have the following two cases:

Case 1: $L^*_{\bar{f}}V + \chi\theta_b \left|L_{\bar{w}}V\right| \leq 0$

Since $L^*_{\bar{f}}V = L_{\bar{f}}V + \rho|2b^TPe|$ and ρ is a positive real number, the fact that $L^*_{\bar{f}}V + \chi\theta_b \left|L_{\bar{w}}V\right| \leq 0$ then implies that $L_{\bar{f}}V + \chi\theta_b \left|L_{\bar{w}}V\right| \leq 0$. As a result, the first term on the right-hand side of the inequality of Eq.B.4 is either zero or negative. Therefore,

the time-derivative of V in this case satisfies the following bounds:

$$\begin{aligned}\dot{V} &\leq \frac{-\sqrt{\left(L_{\bar{f}}^{*}V + \chi\theta_b \left|L_{\bar{w}}V\right|\right)^2 + (u_{max}L_{\bar{g}}V)^4}}{\left[1+\sqrt{1+(u_{max}L_{\bar{g}}V)^2}\right]} \\ &\leq \frac{-(u_{max}L_{\bar{g}}V)^2}{\left[1+\sqrt{1+(u_{max}L_{\bar{g}}V)^2}\right]}\end{aligned} \tag{B.8}$$

Substituting the expression for the function $L_{\bar{g}}V$ given by:

$$L_{\bar{g}}V = \frac{\partial V}{\partial e}\bar{g} = 2\left[b^T P e\right] L_g L_f^{r-1}h(x) \tag{B.9}$$

into the last inequality of Eq.B.8, we get:

$$\dot{V} \leq \frac{-4\left(u_{max}L_g L_f^{r-1}h(x)\right)^2 |b^T P e|^2}{\left[1+\sqrt{1+(u_{max}L_{\bar{g}}V)^2}\right]} \tag{B.10}$$

Since $L_g L_f^{r-1}h(x) \neq 0 \ \forall \ x \in \mathbb{R}^n$ from Assumption 2.1, we have that there exists a positive constant k_1 such that $4\left(u_{max}L_g L_f^{r-1}h(x)\right)^2 = L(x) \geq k_1$ (e.g., set $k_1 = \inf_{x\in\mathbb{R}^n} L(x)$). The above inequality therefore reduces to:

$$\dot{V} \leq -\frac{k_1|b^T P e|^2}{\left[1+\sqrt{1+(u_{max}L_{\bar{g}}V)^2}\right]} \tag{B.11}$$

Case 2: $0 < L_{\bar{f}}^{*}V + \chi\theta_b \left|L_{\bar{w}}V\right| \leq u_{max}\left|L_{\bar{g}}V\right|$

In this case, we have:

$$\left(L_{\bar{f}}^{*}V + \chi\theta_b \left|L_{\bar{w}}V\right|\right)^2 \leq (u_{max}L_{\bar{g}}V)^2 \tag{B.12}$$

and therefore:

$$\begin{aligned}&-\sqrt{\left(L_{\bar{f}}^{*}V + \chi\theta_b \left|L_{\bar{w}}V\right|\right)^2 + (u_{max}L_{\bar{g}}V)^4} \\ &= -\sqrt{\left(L_{\bar{f}}^{*}V + \chi\theta_b \left|L_{\bar{w}}V\right|\right)^2 + (u_{max}L_{\bar{g}}V)^2(u_{max}L_{\bar{g}}V)^2} \\ &\leq -\left(L_{\bar{f}}^{*}V + \chi\theta_b \left|L_{\bar{w}}V\right|\right)\sqrt{1+(u_{max}L_{\bar{g}}V)^2}\end{aligned} \tag{B.13}$$

Substituting the estimate of Eq.B.13 in the expression for $\dot{V}$ in Eq.B.4 yields:

$$\begin{aligned}
\dot{V} &\leq \frac{(L_{\bar{f}}V - L^*_{\bar{f}}V)\sqrt{1+(u_{max}L_{\bar{g}}V)^2}}{\left[1+\sqrt{1+(u_{max}L_{\bar{g}}V)^2}\right]} \\
&= \frac{-\rho|2b^TPe|\sqrt{1+(u_{max}L_{\bar{g}}V)^2}}{\left[1+\sqrt{1+(u_{max}L_{\bar{g}}V)^2}\right]} \\
&\leq \frac{-\rho u_{max}|2b^TPe|\,|L_{\bar{g}}V|}{\left[1+\sqrt{1+(u_{max}L_{\bar{g}}V)^2}\right]}
\end{aligned} \tag{B.14}$$

Using the expression for $L_{\bar{g}}V$ in Eq.B.9, the last inequality can be written as:

$$\begin{aligned}
\dot{V} &\leq \frac{-\rho u_{max}|L_gL_f^{r-1}h(x)||2b^TPe|^2}{\left[1+\sqrt{1+(u_{max}L_{\bar{g}}V)^2}\right]} \\
&\leq \frac{-k_2|b^TPe|^2}{\left[1+\sqrt{1+(u_{max}L_{\bar{g}}V)^2}\right]}
\end{aligned} \tag{B.15}$$

where $k_2 = 2\rho\sqrt{k_1} > 0$. Summarizing, we have that if $\phi \leq \phi^*$ and $L^*_{\bar{f}}V + \chi\theta_b\,|L_{\bar{w}}V| \leq u_{max}\,|L_{\bar{g}}V|$, $\dot{V}$ satisfies:

$$\dot{V} \leq \frac{-k_3|b^TPe|^2}{\left[1+\sqrt{1+(u_{max}L_{\bar{g}}V)^2}\right]} \tag{B.16}$$

where $k_3 = \max\{k_1, k_2\} > 0$. Note that since the right-hand side of Eq.B.16 vanishes when $b^TPe = 0$ (and not just when $e = 0$), Eq.B.16 by itself allows us to conclude only that $\dot{V}$ is negative-semidefinite. In what follows, however, we exploit the specific properties of the function V to show that $\dot{V}$ cannot vanish except when $e = 0$ and is, therefore, negative-definite. To this end, consider the representation of the e-subsystem of Eq.B.1 in the following compact form:

$$\dot{e} = Ae + b\,[m_0(e,\eta,\bar{v}) + m_1(e,\eta,\bar{v})u + m_2(e,\eta,\bar{v})\theta] \tag{B.17}$$

where A and b are the $r\times r$ matrix and $r\times 1$ vector, respectively, defined in Eq.2.12, and the functions $m_0(e,\eta,\bar{v}) = L_f^r h(T^{-1}(e,\eta,\bar{v})) - v^r$, $m_1(e,\eta,\bar{v}) = L_gL_f^{r-1}h(T^{-1}(e,\eta,\bar{v}))$,

and $m_2(e,\eta,\bar{v}) = L_w L_f^{r-1} h(T^{-1}(e,\eta,\bar{v}))$ are continuous with $m_1(e,\eta,\bar{v})$ nonsingular for all e and η. Direct computation of the time-derivative of the function $V = e^T P e$ along the trajectories of the system of Eq.B.17 yields:

$$\dot{V} = e^T \left[A^T P + PA\right] e + 2b^T Pe \left[m_0(e,\eta,\bar{v}) + m_1(e,\eta,\bar{v})u + m_2(e,\eta,\bar{v})\theta\right] \tag{B.18}$$

Now we use the fact that the matrix P satisfies the Riccati inequality $A^T P + PA - Pbb^T P < 0$ and choose P, without loss of generality, to be the symmetric positive-definite solution to the Riccati equation:

$$A^T P + PA - Pbb^T P + I = 0 \tag{B.19}$$

The time-derivative of V then satisfies:

$$\begin{aligned} \dot{V} &= -e^T e + b^T Pe \left[b^T Pe + 2m_0(e,\eta,\bar{v}) + 2m_1(e,\eta,\bar{v})u + 2m_2(e,\eta,\bar{v})\theta\right] \\ &\leq -e^T e + b^T Pe \left[b^T Pe + 2m_0(e,\eta,\bar{v}) + 2m_1(e,\eta,\bar{v})u\right] + 2|b^T Pe||m_2(e,\eta,\bar{v})|\theta_b \end{aligned} \tag{B.20}$$

It is clear from the above equation then that whenever $b^T Pe = 0$ and $e \neq 0$, we have $\dot{V} \leq -|e|^2 < 0$; and since $\dot{V} < 0$ whenever $b^T Pe \neq 0$ (from Eq.B.16), we deduce that $\dot{V} < 0 \;\; \forall\, e \neq 0$. Consequently, there exists a function β_e of class $\mathcal{KL}$ (see [170] for details) such that the following ISS inequality holds for the e states of the system of Eq.B.1:

$$|e(t)| \leq \beta_e\left(|e(0)|, t\right) \qquad \forall\, t \geq 0 \tag{B.21}$$

and the origin of the e-subsystem is asymptotically stable. From Assumption 2.2, we have that the η subsystem of Eq.B.1 possesses an ISS property with respect to e which implies that there exists a function β_η of class $\mathcal{KL}$ and a function γ_η of class $\mathcal{K}$ such that the following ISS inequality holds:

$$|\eta(t)| \leq \beta_\eta(|\eta(0)|, t) + \gamma_\eta(\|e\|) \qquad \forall\, t \geq 0 \tag{B.22}$$

uniformly in θ, $\bar{v}$.

Step 2: We now analyze the behavior of the interconnected dynamical system comprised of the e, η states of the system of Eq.B.1 for which the inequalities of Eq.B.21

and Eq.B.22 hold. In order to proceed with our analysis, we need to define the following positive real numbers: $\delta_e = D^e + \phi^*$, $\delta_\eta = D^\eta + \gamma_\eta(\delta_e) + \phi^*$, $D^e = \beta_e(\bar{\delta}_e, 0)$, $D^\eta = \beta_\eta(\bar{\delta}_\eta, 0)$, $\phi^* = \frac{\rho}{\delta\theta_b}$ and $\bar{\delta}_e, \bar{\delta}_\eta$ are any positive real numbers that satisfy Eq.3.11. Using a contradiction argument similar to that used in [67, 68], we show that if $\phi \in (0, \phi^*]$, then, starting from any initial state that satisfies $|e(0)| \leq \bar{\delta}_e$, $|\eta(0)| \leq \bar{\delta}_\eta$, the evolution of the states e, η satisfies the following inequalities:

$$|e(t)| \leq \delta_e, \quad |\eta(t)| \leq \delta_\eta \tag{B.23}$$

for all times and that the states are therefore bounded. Let T be the smallest time such that there is a δ^* so that $t \in (T, T + \delta^*)$ implies either $|e(t)| > \delta_e$ or $|\eta(t)| > \delta_\eta$. Then, for each $t \in [0, T]$ the conditions of Eq.B.23 hold. Consider the functions $e^T(t)$, $\eta^T(t)$ defined as follows:

$$e^T(t) = \left\{ \begin{array}{ll} e(t) & t \in [0, T] \\ 0 & t \in (T, \infty) \end{array} \right\}, \quad \eta^T(t) = \left\{ \begin{array}{ll} \eta(t) & t \in [0, T] \\ 0 & t \in (T, \infty) \end{array} \right\} \tag{B.24}$$

From the fact that $|e(0)| \leq \bar{\delta}_e$, $|\eta(0)| \leq \bar{\delta}_\eta$, we have that:

$$\begin{array}{rcl} \sup\limits_{0 \leq t \leq T} (\beta_\eta(|\eta(0)|, t)) & \leq & \beta_\eta(\bar{\delta}_\eta, 0) =: D^\eta \\ \sup\limits_{0 \leq t \leq T} (\beta_e(|e(0)|, t)) & \leq & \beta_e(\bar{\delta}_e, 0) =: D^e \end{array} \tag{B.25}$$

Combining the above inequalities with Eqs.B.21-B.22, we have that for each $\phi \in (0, \phi^*]$ and for all $t \geq 0$:

$$\begin{array}{rcl} ||e^T|| & \leq & D^e < \delta_e \\ ||\eta^T|| & \leq & D^\eta + \gamma_\eta(||e||) \leq D^\eta + \gamma_\eta(\delta_e) < \delta_\eta \end{array} \tag{B.26}$$

By continuity, we have that there exists some positive real number $\bar{k}$ such that $||e^{T+\bar{k}}(t)|| \leq \delta_e$ and $||\eta^{T+\bar{k}}(t)|| \leq \delta_\eta$, $\forall\ t \in [0, T + \bar{k}]$. This contradicts the definition of T. Hence, Eq.B.23 holds $\forall\ t \geq 0$ and the states are bounded.

Step 3: In this step, we show that if the η subsystem of Eq.B.1, with e as input, is ISS and the origin of the e subsystem of Eq.B.1 is asymptotically stable for initial

conditions satisfying Eq.3.11, then the origin of the interconnected system of Eq.B.1 is asymptotically stable for all initial conditions satisfying Eq.3.11. We proceed by performing calculations similar to those done in [170]. From Eqs.B.21-B.22, we have that the solutions of the system of Eq.B.1 satisfy:

$$|\eta(t)| \leq \beta_\eta(|\eta(s)|, t-s) + \gamma_\eta(\sup_{s\leq\tau\leq t}|e(\tau)|) \tag{B.27}$$

$$|e(t)| \leq \beta_e(|e(s)|, t-s) \tag{B.28}$$

for initial conditions satisfying Eq.3.11, where $t \geq s \geq 0$. Applying Eq.B.27 with $s = \frac{t}{2}$, we obtain:

$$|\eta(t)| \leq \beta_\eta\left(\left|\eta\left(\frac{t}{2}\right)\right|, \frac{t}{2}\right) + \gamma_\eta\left(\sup_{\frac{t}{2}\leq\tau\leq t}|e(\tau)|\right) \tag{B.29}$$

To estimate $\eta\left(\frac{t}{2}\right)$, we apply Eq.B.27 with $s = 0$ and t replaced by $\frac{t}{2}$ to obtain:

$$\left|\eta\left(\frac{t}{2}\right)\right| \leq \beta_\eta\left(|\eta(0)|, \frac{t}{2}\right) + \gamma_\eta\left(\sup_{0\leq\tau\leq\frac{t}{2}}|e(\tau)|\right) \tag{B.30}$$

From Eq.B.28, we have:

$$\sup_{0\leq\tau\leq\frac{t}{2}}|e(\tau)| \leq \beta_e(|e(0)|, 0) \tag{B.31}$$

$$\sup_{\frac{t}{2}\leq\tau\leq 0}|e(\tau)| \leq \beta_e\left(|e(0)|, \frac{t}{2}\right) \tag{B.32}$$

Substituting Eqs.B.30-B.32 into Eq.B.29 and using the following inequalities: $|\eta(0)| \leq \left|[e^T(0)\ \eta^T(0)]^T\right|$, $|e(0)| \leq \left|[e^T(0)\ \eta^T(0)]^T\right|$ and $\left|[e^T(t)\ \eta^T(t)]^T\right| \leq |\eta(0)| + |e(0)|$, we obtain:

$$\left|[e^T(t)\ \eta^T(t)]^T\right| \leq \beta\left(\left|[e^T(0)\ \eta^T(0)]^T\right|, t\right) \tag{B.33}$$

where

$$\beta(r,s) = \beta_\eta\left(\beta_\eta\left(r,\frac{s}{2}\right)+\gamma_\eta\left(\beta_e\left(r,0\right)\right),\frac{s}{2}\right)+\gamma_\eta\left(\beta_e\left(r,\frac{s}{2}\right)\right)+\beta_e\left(r,s\right) \quad \text{(B.34)}$$

It can be easily verified that β is a class $\mathcal{KL}$ function for all $r \geq 0$. Hence the origin of Eq.B.1 is asymptotically stable. It follows then from Assumption 2.1 that the origin of the closed-loop system is asymptotically stable. The asymptotic output tracking result can be obtained by simply taking the limsup of both sides of Eq.B.21 which yields:

$$\limsup_{t\to\infty}\left|e\left(t\right)\right| = 0 \quad \text{(B.35)}$$

It follows then that:

$$\limsup_{t\to\infty}\left|e_1\left(t\right)\right| = \limsup_{t\to\infty}\left|y\left(t\right)-v\left(t\right)\right| = 0 \quad \text{(B.36)}$$

Part 2: In this part, we prove that the control law of Eq.3.10 is optimal with respect to a meaningful cost functional defined in Eq.3.14. We proceed in two steps. In the first step, we show that the cost functional of Eq.3.14 is a meaningful one according to the formulation of the optimal control problem for nonlinear systems. In the second step, we show that the stabilizing control law of Eq.3.10 minimizes this cost functional.

Step 1: In this step, we show that the cost functional defined in Eq.3.14 is meaningful by proving directly that $l(e)$ defined in Theorem 3.1 is a positive-definite function, independently of the designed control. From its definition in Theorem 3.1, $l(e)$ is given by:

$$l(e) = -L_{\bar{f}}V+\frac{1}{4}L_{\bar{g}}VR^{-1}(x)L_{\bar{g}}V-\left|L_{\bar{w}}V\right|\theta_b \quad \text{(B.37)}$$

Direct substitution of the expression for $R^{-1}(x)$ given in Theorem 3.1 in the above

equation yields:

$$l(e) = \left(\frac{-\frac{1}{2}L_{\bar{f}}V - \left(L_{\bar{f}}V + \theta_b \left|L_{\bar{w}}V\right|\right)\sqrt{1+(u_{max}L_{\bar{g}}V)^2}}{\left[1+\sqrt{1+(u_{max}L_{\bar{g}}V)^2}\right]} \right.$$

$$+\frac{\frac{1}{2}\sqrt{(L^*_{\bar{f}}V + \chi\theta_b \left|L_{\bar{w}}V\right|)^2 + (u_{max}L_{\bar{g}}V)^4}}{\left[1+\sqrt{1+(u_{max}L_{\bar{g}}V)^2}\right]} \tag{B.38}$$

$$\left. +\frac{\frac{1}{2}\rho|2b^TPe|^2 + \theta_b \left|L_{\bar{w}}V\right|\left(\left(\frac{1}{2}\chi - 1\right)|2b^TPe| - \phi\right)}{(|2b^TPe| + \phi)\left[1+\sqrt{1+(u_{max}L_{\bar{g}}V)^2}\right]} \right)$$

Using the fact that $L_{\bar{f}}V \leq L^*_{\bar{f}}V + \chi\theta_b \left|L_{\bar{w}}V\right| := L^{**}_{\bar{f}}V$, we have the estimate:

$$l(e) \geq \left(\frac{-L^{**}_{\bar{f}}V\left(\frac{1}{2}+\sqrt{1+(u_{max}L_{\bar{g}}V)^2}\right) + \frac{1}{2}\sqrt{(L^{**}_{\bar{f}}V)^2 + (u_{max}L_{\bar{g}}V)^4}}{1+\left[\sqrt{1+(u_{max}L_{\bar{g}}V)^2}\right]} \right.$$

$$\left. +\frac{\frac{1}{2}\rho|2b^TPe|^2 + \theta_b \left|L_{\bar{w}}V\right|\left(\left(\frac{1}{2}\chi - 1\right)|2b^TPe| - \phi\right)}{(|2b^TPe| + \phi)\left[1+\sqrt{1+(u_{max}L_{\bar{g}}V)^2}\right]} \right) \tag{B.39}$$

which, with the aid of Eq.3.13, reduces to:

$$l(e) \geq \left(\frac{\frac{1}{4}\sqrt{(L^{**}_{\bar{f}}V)^2 + (u_{max}L_{\bar{g}}V)^4}}{1+\left[\sqrt{1+(u_{max}L_{\bar{g}}V)^2}\right]} \right.$$

$$\left. +\frac{\frac{1}{2}\rho|2b^TPe|^2 + \theta_b \left|L_{\bar{w}}V\right|\left(\left(\frac{1}{2}\chi - 1\right)|2b^TPe| - \phi\right)}{(|2b^TPe| + \phi)\left[1+\sqrt{1+(u_{max}L_{\bar{g}}V)^2}\right]} \right) \tag{B.40}$$

Note that Eq.3.13 implies that $L^{**}_{\bar{f}}V \leq u_{max}|L_{\bar{g}}V|$ and therefore the trajectories of the closed-loop system evolve within the stability region described by Eq.3.11. From the last inequality and the fact that $\chi > 2$, it is clear that whenever $|2b^TPe| > \frac{\phi}{\frac{1}{2}\chi - 1}$,

$l(e)$ satisfies:

$$l(e) \;\geq\; \left(\frac{\frac{1}{4}\sqrt{(L_{\bar{f}}^{**}V)^2 + (u_{max}L_{\bar{g}}V)^4}}{1 + \left[\sqrt{1 + (u_{max}L_{\bar{g}}V)^2}\right]} \right) \;\geq\; \alpha_1(|e|) \tag{B.41}$$

where $\alpha_1(\cdot)$ is a class $\mathcal{K}$ function of its argument. The second inequality in Eq.B.41 follows directly from the fact that the left-hand side of this inequality is positive-definite and vanishes only when $e = 0$ (this is because the terms $L_{\bar{g}}V$ and $L_{\bar{f}}^{*}V$ do not vanish together away from $e = 0$). For the case when $|2b^TPe| \leq \frac{\phi}{\frac{1}{2}\chi - 1}$, we substitute the bounds $|L_w L_f^{r-1}h(x)| \leq \delta|2b^TPe|$ and $\left(\frac{1}{2}\chi - 1\right)|2b^TPe| - \phi \geq -\phi$ together with the definition of $L_{\bar{w}}V$ into Eq.B.40 to obtain:

$$l(e) \;\geq\; \alpha_1(|e|) + \left(\frac{\left(\frac{1}{2}\rho - \theta_b\delta\phi\right)|2b^TPe|^2}{(|2b^TPe| + \phi)\left[1 + \sqrt{1 + (u_{max}L_{\bar{g}}V)^2}\right]} \right) \tag{B.42}$$

$\forall\ |2b^TPe| \;\leq\; \frac{\phi}{\frac{1}{2}\chi - 1}$. If ϕ is small enough to satisfy $\phi \leq \frac{\rho}{2\delta\theta_b} := \phi^*$, then the inequality of Eq.B.41 is satisfied irrespective of the value of $|2b^TPe|$ and we have $l(e) \geq \alpha_1(|e|) > 0 \;\; \forall \;\; e \neq 0$. Hence, $l(e)$ is positive-definite. In addition, $R(x) > 0$ for all x satisfying Eq.3.11. The cost functional defined in Eq.3.14 is therefore a meaningful one.

Step 2: In this step, we prove that the control law of Eq.3.10 minimizes the cost functional of Eq.3.14. Substituting:

$$k \;=\; u + \frac{1}{2}R^{-1}(x)L_{\bar{g}}V \tag{B.43}$$

into Eq.3.14 and using the expression for $l(e)$ given in Theorem 3.1, we get the

following chain of equalities:

$$\begin{aligned} J &= \int_0^\infty (l(e) + uR(x)u)dt \\ &= \int_0^\infty \left(-L_{\bar{f}}V + \frac{1}{2}L_{\bar{g}}VR^{-1}(x)L_{\bar{g}}V - |L_{\bar{w}}V|\theta_b - L_{\bar{g}}Vk\right)dt + \int_0^\infty kR(x)k \ dt \\ &= \int_0^\infty \left(-L_{\bar{f}}V - L_{\bar{g}}Vu - |L_{\bar{w}}V|\theta_b\right)dt + \int_0^\infty kR(x)k \ dt \\ &= -\int_0^\infty \sup_{\theta\in\mathcal{W}\subset\mathbb{R}} \left(\frac{\partial V}{\partial e}\left(\bar{f} + \bar{g}u + \bar{w}\theta\right)\right)dt + \int_0^\infty kR(x)k \ dt \\ &= -\int_0^\infty \sup_{\theta\in\mathcal{W}\subset\mathbb{R}} \left(\dot{V}\right)dt + \int_0^\infty kR(x)k \ dt \end{aligned}$$

Note that the first term on the right hand side of the last equality is bounded from above since:

$$-\int_0^\infty \sup_{\theta\in\mathcal{W}\subset\mathbb{R}} \left(\dot{V}\right)dt \ \leq \ -\int_0^\infty \dot{V}dt = V(e(0)) - \lim_{t\to\infty} V(e(t)) \tag{B.44}$$

It was shown in Part 1 of the proof that the control law of Eq.3.10 achieves asymptotic stability of the origin of the closed-loop system, provided the evolution of the closed-loop states satisfies Eq.3.11. Hence, $\lim_{t\to\infty} V(e(t)) = 0$ and:

$$J^* = -\int_0^\infty \sup_{\theta\in\mathcal{W}\subset\mathbb{R}} \left(\dot{V}\right)dt \leq V(e(0)) \tag{B.45}$$

Since $R(x) > 0$, it is clear that the minimum of J is J^*. This minimum is achieved when $k(x) \equiv 0$ which proves that the controller of Eq.3.10 minimizes the cost defined in Eq.3.14. To complete the proof of optimality, we need to show that $J^* = V(e(0))$. To this end, consider the uncertain variable $\theta_\Delta \in \mathcal{W} \subset \mathbb{R}$ where for every $e_\Delta(0) \in \mathbb{R}^r$, every $u \in \mathbb{R}$, and every $\Delta > 0$, we have:

$$\int_0^\infty \dot{V}\left(e_\Delta, u, \theta_\Delta\right)dt \ \geq \ \int_0^\infty \sup_{\theta\in\mathcal{W}\subset\mathbb{R}} \dot{V}\left(e_\Delta, u, \theta\right)dt - \Delta \tag{B.46}$$

(The existence of θ_Δ follows from the properties of $\theta(t)$). From the inequality of Eq.B.46, we obtain:

$$\begin{aligned} V(e(0)) &= -\int_0^\infty \dot{V}dt \\ &\leq -\int_0^\infty \sup_{\theta\in\mathcal{W}\subset\mathbb{R}} \dot{V}\left(e_\Delta, u, \theta\right)dt + \Delta \end{aligned} \tag{B.47}$$

Combining the inequalities of Eq.B.47 and Eq.B.45, we get:

$$V(e(0)) - \Delta \leq J^* \leq V(e(0)) \tag{B.48}$$

for arbitrarily small Δ. Clearly, if $J^* = V(e(0))$, the proof of optimality is complete. Otherwise, there exists $\mu > 0$ such that $J^* + \mu = V(e(0))$. Since Δ is arbitrary, we can choose it to be sufficiently small such that $\Delta < \mu$ and the inequality of Eq.B.48 is violated. Thus, the only way to satisfy the inequality of Eq.B.48 for arbitrary Δ is to set $J^* = V(e(0))$. This completes the proof of the theorem. Δ

Proof of Theorem 3.2:

Similar to the Proof of Theorem 3.1, we initially show that, starting from any initial state satisfying the inequality of Eq.3.15, the trajectories of the closed-loop system remain bounded for all times and that the closed-loop output satisfies the inequality of Eq.3.16, provided that the evolution of the closed-loop trajectory satisfies Eq.3.15. Finally, we show that the control law of Eq.3.10 with $\rho = 0$ is optimal with respect to a meaningful cost functional of the form of Eq.3.18 defined over a finite time-interval.

Part 1: We first consider the representation of the closed-loop system in terms of the e, η coordinates given in Eq.B.1. We show boundedness of the trajectories by first deriving ISS inequalities that capture the evolution of the states e and η, and then, by using a small gain argument.

Step 1: Consider the Lyapunov function candidate $V = e^T P e$. Setting $\rho = 0$ in the controller of Eq.3.10 and evaluating the time-derivative of V along the trajectories of the closed-loop e subsystem of Eq.B.1, we perform similar calculations to those in

Step 1 of Part 1 of the Proof of Theorem 3.1, to conclude that $\dot{V}$ satisfies:

$$\begin{aligned}\dot{V} \leq & \left(\frac{\left(L_{\bar{f}}V + \theta_b \left|L_{\bar{w}}V\right|\right)\sqrt{1+(u_{max}L_{\bar{g}}V)^2}}{\left[1+\sqrt{1+(u_{max}L_{\bar{g}}V)^2}\right]} \right. \\ & - \frac{-\sqrt{\left(L_{\bar{f}}V + \chi\theta_b \left|L_{\bar{w}}V\right|\right)^2 + (u_{max}L_{\bar{g}}V)^4}}{\left[1+\sqrt{1+(u_{max}L_{\bar{g}}V)^2}\right]} \\ & \left. + \frac{\theta_b |L_w L_f^{r-1}h(x)||2b^TPe|\left(\phi - (\chi-1)|2b^TPe|\right)}{(|2b^TPe|+\phi)\left[1+\sqrt{1+(u_{max}L_{\bar{g}}V)^2}\right]} \right)\end{aligned} \tag{B.49}$$

From the above inequality and the fact that $\chi > 2$, we have that whenever $|2b^TPe| > \frac{\phi}{\chi-1}$, the last term on the right-hand side of the above equation is negative and, therefore, $\dot{V}$ is bounded from above by the first two terms. For the case when $|2b^TPe| \leq \frac{\phi}{\chi-1}$, we use the fact that the uncertain variables considered in Theorem 3.2 are non-vanishing in the sense that the function $L_wL_f^{r-1}h(x)$ satisfies a growth bound of the form $|L_wL_f^{r-1}h(x)| \leq \bar{\delta}|2b^TPe| + \mu$, where $\bar{\delta} > 0$ and $\mu > 0$, whenever $|2b^TPe| \leq \frac{\phi}{\frac{1}{2}\chi-1}$, to obtain the following estimates:

$$\begin{aligned}\frac{\theta_b |L_w L_f^{r-1}h(x)||2b^TPe|\left(\phi-(\chi-1)|2b^TPe|\right)}{(|2b^TPe|+\phi)\left[1+\sqrt{1+(u_{max}L_{\bar{g}}V)^2}\right]} &\leq \theta_b |L_wL_f^{r-1}h(x)||2b^TPe| \\ &\leq \theta_b\bar{\delta}|2b^TPe|^2 + \theta_b\mu|2b^TPe| \\ &\leq \frac{\theta_b\bar{\delta}\phi^2 + \theta_b\mu\phi(\chi-1)}{(\chi-1)^2} \\ &\equiv \epsilon(\phi) \quad \forall \ |2b^TPe| \leq \frac{\phi}{\chi-1}\end{aligned} \tag{B.50}$$

where we have used the fact that $(|2b^TPe|+\phi)[1+\sqrt{1+(u_{max}L_{\bar{g}}V)^2}] \geq \phi$ to derive the first inequality. Substituting the estimates of Eq.B.50 directly into Eq.B.49 yields

that $\dot{V}$ satisfies:

$$\begin{aligned}\dot{V} \leq & \left(\frac{\left(L_{\bar{f}}V + \theta_b |L_{\bar{w}}V|\right)\sqrt{1+(u_{max}L_{\bar{g}}V)^2}}{\left[1+\sqrt{1+(u_{max}L_{\bar{g}}V)^2}\right]} \right. \\ & \left. - \frac{\sqrt{\left(L_{\bar{f}}V + \chi\theta_b |L_{\bar{w}}V|\right)^2 + (u_{max}L_{\bar{g}}V)^4}}{\left[1+\sqrt{1+(u_{max}L_{\bar{g}}V)^2}\right]} \right) + \epsilon(\phi)\end{aligned} \tag{B.51}$$

irrepective of the value of $|2b^T Pe|$, where $\epsilon(\phi) > 0$. To analyze the sign of $\dot{V}$ further, we consider the following two cases:

Case 1: $L_{\bar{f}}V + \chi\theta_b |L_{\bar{w}}V| \leq 0$

Since $\chi > 0$, then $L_{\bar{f}}V + \chi\theta_b |L_{\bar{w}}V| \leq 0$ implies $L_{\bar{f}}V + \theta_b |L_{\bar{w}}V| \leq 0$. Analyzing the right-hand side of Eq.B.51 in this case yields:

$$\dot{V} \leq - \left(\frac{\sqrt{\left(L_{\bar{f}}V + \chi\theta_b |L_{\bar{w}}V|\right)^2 + (u_{max}L_{\bar{g}}V)^4}}{\left[1+\sqrt{1+(u_{max}L_{\bar{g}}V)^2}\right]} \right) + \epsilon(\phi) \tag{B.52}$$

Note that the first term on the right-hand side of the above equation is negative-definite and vanishes only when $e = 0$.

Case 2: $0 < L_{\bar{f}}V + \chi\theta_b |L_{\bar{w}}V| \leq u_{max}|L_{\bar{g}}V|$

In this case, we have that the estimate of Eq.B.13 holds with $\rho = 0$. Substituting this estimate into Eq.B.51 yields:

$$\dot{V} \leq \left(\frac{(1-\chi)\,\theta_b |L_{\bar{w}}V| \sqrt{1+(u_{max}L_{\bar{g}}V)^2}}{\left[1+\sqrt{1+(u_{max}L_{\bar{g}}V)^2}\right]} \right) + \epsilon(\phi) \tag{B.53}$$

Note that since $\chi > 2$, the first term on the right-hand side of the above equation is strictly negative when $b^T Pe \neq 0$. For the case when $b^T Pe = 0$ and $e \neq 0$, it can also be shown from Eq.B.20 that $\dot{V}$ is bounded by a negative-definite function. To summarize, we deduce from Eqs.B.52-B.53 that whenever $L_{\bar{f}}V + \chi\theta_b |L_{\bar{w}}V| \leq u_{max}|L_{\bar{g}}V|$, there exists a function $\alpha_2(\cdot)$ of class $\mathcal{K}$ such that:

$$\dot{V} \leq -\alpha_2(|e|) + \epsilon(\phi) \tag{B.54}$$

Choosing ϕ small enough such that $\epsilon(\phi) \leq \frac{1}{2}\alpha_2(|e|)$, we have:

$$\dot{V} \leq -\tfrac{1}{2}\alpha_2(|e|) < 0 \quad \forall\ |e| \geq \alpha_2^{-1}(2\epsilon(\phi)) := \gamma(\epsilon(\phi)) \tag{B.55}$$

This inequality shows that $\dot{V}$ is negative outside a ball of radius $\gamma(\epsilon(\phi))$, $B_1 := \{e \in \mathbb{R}^r : |e| \leq \gamma(\epsilon(\phi))\}$. A direct application then of the result of Theorem 5.1 and its corollaries in in [170] allows us to conclude that starting from any initial state within any invariant subset of the region described by Eq.3.15, the following ISS inequality holds for the e states of the system of Eq.B.1:

$$|e(t)| \leq \bar{\beta}_e\left(|e(0)|, t\right) + \bar{\gamma}_e(\phi) \qquad \forall\, t \geq 0 \tag{B.56}$$

where $\bar{\beta}_e$ is a class $\mathcal{KL}$ function and $\bar{\gamma}_e$ is a class $\mathcal{K}_\infty$ function. From Assumption 2.4, we have that the η states of Eq.B.1 possess an ISS property with respect to e and θ:

$$\begin{aligned} |\eta(t)| &\leq \bar{\beta}_\eta\left(|\eta(0)|, t\right) + \bar{\gamma}_\eta\left(\|[e^T\ \theta]^T\|\right) \\ &\leq \bar{\beta}_\eta\left(|\eta(0)|, t\right) + \bar{\gamma}_{\eta_1}\left(\|e\|\right) + \bar{\gamma}_{\eta_2}\left(\|\theta\|\right) \end{aligned} \tag{B.57}$$

where $\bar{\gamma}_{\eta_1}$, $\bar{\gamma}_{\eta_2}$ are class $\mathcal{K}$ functions defined as $\bar{\gamma}_{\eta_1}(s) = \bar{\gamma}_{\eta_2}(s) = \bar{\gamma}_\eta(2s)$.

Step 2: We now analyze the behavior of the interconnected dynamical system comprised of the states e, η of the system of Eq.B.1 for which the inequalities of Eq.B.56 and Eq.B.57 hold. We first define the following positive real numbers: $\delta_e = D^{\bar{e}} + \phi^*$, $\delta_\eta = D^{\bar{\eta}} + \bar{\gamma}_{\eta 1}(\delta_e) + \phi^*$, $D^{\bar{e}} = \bar{\beta}_e(\bar{\delta}_e, 0) + \bar{\gamma}_e(\phi^*)$, $D^{\bar{\eta}} = \bar{\beta}_\eta(\bar{\delta}_\eta, 0) + \bar{\gamma}_{\eta 2}(\theta_b)$, and $\bar{\delta}_e, \bar{\delta}_\eta$ are any positive real numbers that satisfy Eq.3.15. We proceed by contradiction to show that if $\phi \in (0, \phi^*]$ where $\phi^* \leq \bar{\gamma}_e^{-1}(d)$, the evolution of the states e,η, starting from any initial states that satisfy $|e(0)| \leq \bar{\delta}_e$, $|\eta(0)| \leq \bar{\delta}_\eta$, where $\bar{\delta}_e$ and $\bar{\delta}_\eta$ are any nonnegative real numbers that satisfy Eq.3.15, satisfies the following inequalities:

$$|e(t)| \leq \delta_e, \quad |\eta(t)| \leq \delta_\eta \tag{B.58}$$

for all times. Let T be the smallest time such that there is a δ^* so that $t \in (T, T + \delta^*)$ implies either $|e(t)| > \delta_e$ or $|\bar{\eta}(t)| > \delta_\eta$. Then, for each $t \in [0, T]$ the conditions of Eq.(B.58) hold. Consider the functions $e^T(t)$, $\eta^T(t)$ defined in Eq.B.24. From the

fact that $|e(0)| \leq \bar{\delta}_e$, $|\eta(0)| \leq \bar{\delta}_\eta$, $\|\theta(t)\| \leq \theta_b$, we have that:

$$\begin{aligned} \sup_{0\leq t\leq T}\left(\bar{\beta}_\eta(|\eta(0)|,t)+\bar{\gamma}_{\eta_2}(\|\theta\|)\right) &\leq \bar{\beta}_\eta(\bar{\delta}_\eta,0)+\bar{\gamma}_{\eta_2}(\theta_b) =: D^{\bar{\eta}} \\ \sup_{0\leq t\leq T}\left(\bar{\beta}_e(|e(0)|,t)+\bar{\gamma}_e(\phi)\right) &\leq \bar{\beta}_e(\bar{\delta}_e,0)+\bar{\gamma}_e(\phi^*) =: D^{\bar{e}} \end{aligned} \tag{B.59}$$

Combining the above inequalities with Eq.B.57, we have that for each $\phi \in (0, \phi^*]$ and for all $t \geq 0$:

$$\begin{aligned} \|e^T\| &\leq D^{\bar{e}} < \delta_e \\ \|\eta^T\| &\leq D^{\bar{\eta}} + \bar{\gamma}_{\eta_1}(\|e\|) \leq D^{\bar{\eta}} + \bar{\gamma}_{\eta_1}(\delta_e) < \delta_\eta \end{aligned} \tag{B.60}$$

By continuity, we have that there exist some positive real number $\bar{k}$ such that $\|e^{T+\bar{k}}(t)\| \leq \delta_e$ and $\|\eta^{T+\bar{k}}(t)\| \leq \delta_\eta$, $\forall\ t \in [0, T+\bar{k}]$. This contradicts the definition of T. Hence, Eq.B.58 holds $\forall\ t \geq 0$. Finally, for $\phi \in (0, \phi^*]$ and for any initial state satisfying Eq.3.15, taking the limsup of both sides of Eq.B.56 as $t \to \infty$, we have:

$$\limsup_{t\to\infty}|e(t)| \leq \limsup_{t\to\infty}\left(\bar{\beta}_e(|e(0)|,t)+\bar{\gamma}_e(\phi)\right) = \bar{\gamma}_e(\phi) \leq d \tag{B.61}$$

Part 2: In this part, we prove that the controller of Eq.3.10 is optimal with respect to a meaningful finite-time cost functional defined in Eq.3.18. We first prove that this cost functional is meaningful by showing that $l(e)$ is positive-definite for all times in the interval $[0, T_f]$. Repeating the same calculations performed in Step 1 of Part 2 of the Proof of Theorem 3.1 with $\rho = 0$, it can easily verified that if the trajectories of the closed-loop system evolve such that, $\forall\ \ t \in [0, T_f]$, Eq.3.17 holds, then there exists a function $\alpha_3(\cdot)$ of class $\mathcal{K}$ such that:

$$\begin{aligned} l(e) &\geq \alpha_3(|e|) \quad \forall\ |2b^TPe| > \frac{\phi}{\frac{1}{2}\chi - 1} \\ l(e) &\geq \alpha_3(|e|) - \theta_b|L_wL_f^{r-1}h(x)||2b^TPe|\phi \quad \forall\ |2b^TPe| \leq \frac{\phi}{\frac{1}{2}\chi - 1} \end{aligned} \tag{B.62}$$

The first inequality in Eq.B.62 implies that $l(e) > 0$ outside the set D. Using the fact that $|L_wL_f^{r-1}h(x)| \leq \bar{\delta}|2b^TPe| + \mu$ and $|2b^TPe| \leq \frac{\phi}{\frac{1}{2}\chi - 1}$ inside the set D, the

second inequality in Eq.B.62 can be re-written as:

$$\begin{aligned} l(e) &\geq \alpha_3(|e|) - \frac{\theta_b \bar{\delta} \phi^2 + \theta_b \mu \phi (\frac{1}{2}\chi - 1)}{\left(\frac{1}{2}\chi - 1\right)^2} \\ &= \alpha_3(|e|) - \epsilon'(\phi) \\ &\geq \tfrac{1}{2}\alpha_3(|e|) > 0 \quad \forall \ |e| \geq \alpha_3^{-1}(2\epsilon'(\phi)) \geq \alpha_3^{-1}(2\epsilon(\phi)) := \gamma'(\epsilon(\phi)) \end{aligned} \tag{B.63}$$

where $\epsilon'(\phi) > \epsilon(\phi) > 0$. The last inequality implies that $l(e)$ is positive outside the set $B_2 := \{e \in \mathbb{R}^r : |e| \leq \alpha_3^{-1}(2\epsilon(\phi))\}$. Note that this set is completely contained within the set Γ since $|e| \leq \alpha_3^{-1}(2\epsilon(\phi)) \leq \alpha_3^{-1}(2\epsilon(\phi^*)) \leq \bar{\epsilon} \Longrightarrow e^T P e \leq \lambda_{max}(P)|e|^2 \leq \lambda_{max}(P)\bar{\epsilon}^2$ where $\bar{\epsilon} := \max\{\alpha_2^{-1}(2\epsilon(\phi^*)), \alpha_3^{-1}(2\epsilon(\phi^*))\}$ and $\lambda_{max}(P) > 0$ is the maximum eigenvalue of the matrix P. Similarly, the set B_1 – defined right after Eq.B.55 – is also contained within Γ, and therefore $\dot{V} < 0$ on and outside the boundary of Γ. From its definition in Theorem 3.2, T_f is the minimum time for the trajectories of the closed-loop system to reach and enter Γ without ever leaving again (note that Γ is a level set of V). Therefore, we have that $|e(t)| \geq \gamma'(\epsilon'(\phi)) \ \ \forall \ t \in [0, T_f]$ and, hence, $l(e) > 0 \ \ \forall \ t \in [0, T_f]$. Note also that $R(x) > 0$. Therefore, the cost functional of Eq.3.18 is a meaningful one. To prove that the control law of Eq.3.10 with $\rho = 0$ minimizes the cost functional of Eq.3.18, we substitute:

$$k = u + \frac{1}{2} R^{-1}(x) L_{\bar{g}} V \tag{B.64}$$

into Eq.3.18 and use the expression given in Theorem 3.1 for $l(e)$, to get the following

chain of equalities:

$$\begin{aligned} J &= \lim_{t\to T_f} V(e(t)) + \int_0^{T_f} (l(e) + uR(x)u)\, dt \\ &= \lim_{t\to T_f} V(e(t)) + \int_0^{T_f} \left(-L_{\bar{f}}V + \frac{1}{2}L_{\bar{g}}VR^{-1}(x)L_{\bar{g}}V - |L_{\bar{w}}V|\theta_b - L_{\bar{g}}Vk\right) dt \\ &\quad + \int_0^{T_f} kR(x)k \\ &= \lim_{t\to T_f} V(e(t)) - \int_0^{T_f} \sup_{\theta\in\mathcal{W}\subset\mathbb{R}} \left(\frac{\partial V}{\partial e}\left(\bar{f} + \bar{g}u + \bar{w}\theta\right)\right) dt + \int_0^{T_f} kR(x)k\ dt \\ &= \lim_{t\to T_f} V(e(t)) - \int_0^{T_f} \sup_{\theta\in\mathcal{W}\subset\mathbb{R}} \left(\dot{V}\right) dt + \int_0^{T_f} kR(x)k\ dt \end{aligned}$$

Note that the term $\bar{J}^* = \lim_{t\to T_f} V(e(t)) - \int_0^{T_f} \sup_{\theta\in\mathcal{W}\subset\mathbb{R}} \left(\dot{V}\right) dt$ is bounded from above since:

$$\lim_{t\to T_f} V(e(t)) - \int_0^{T_f} \sup_{\theta\in\mathcal{W}\subset\mathbb{R}} \left(\dot{V}\right) dt \ \leq\ \lim_{t\to T_f} V(e(t)) - \int_0^{T_f} \dot{V} dt = V(e(0)) \qquad \text{(B.65)}$$

Since $R(x) > 0$, it is clear that the minimum of J is $\bar{J}^*$. This minimum is achieved when $k(x) \equiv 0$ which proves that the controller of Eq.3.10 (with $\rho = 0$) minimizes the cost defined in Eq.3.18. To complete the proof of optimality, we need to show that $\bar{J}^* = V(e(0))$. To this end, consider the uncertain variable $\theta_\Delta \in \mathcal{W} \subset \mathbb{R}$ where for every $e_\Delta(0) \in \mathbb{R}^r$, every $u \in \mathbb{R}$, and every $\Delta > 0$, we have:

$$\int_0^{T_f} \dot{V}\left(e_\Delta, u, \theta_\Delta\right) dt \ \geq\ \int_0^{T_f} \sup_{\theta\in\mathcal{W}\subset\mathbb{R}} \dot{V}\left(e_\Delta, u, \theta\right) dt - \Delta \qquad \text{(B.66)}$$

(The existence of θ_Δ follows from the properties of $\theta(t)$). Using a similar argument to that in Part 2 of the proof of Theorem 2.1, we obtain:

$$V(e(0)) - \Delta \leq \bar{J}^* \leq V(e(0)) \qquad \text{(B.67)}$$

for arbitrarily small Δ, and then we have $\bar{J}^* = V(e(0))$. This completes the proof of the theorem. Δ

Appendix C

Proofs of Chapter 4

Proof of Theorem 4.1:

Consider the representation of the closed-loop system in terms of the transformed coordinates (e, η) introduced in Eqs.4.5-4.6:

$$\begin{aligned} \dot{e} &= \bar{f}(e,\eta,\bar{v}) - \frac{1}{2}\sum_{i=1}^{m}\bar{g}_i(e,\eta,\bar{v})R^{-1}(x)L_{\bar{g}_i}V + \sum_{k=1}^{q}\bar{w}_k(e,\eta,\bar{v})\theta_k \\ \dot{\eta} &= \Psi(e,\eta,\bar{v},\theta) \\ y_i &= e_1^{(i)} + v_i, \quad i = 1,\cdots,m \end{aligned} \tag{C.1}$$

where $\Psi(\cdot) = [\Psi_1(\cdot) \ \cdots \ \Psi_{n-\sum_{r_i}}(\cdot)]^T$. We now follow a four-step procedure to establish both asymptotic stability and reference-input tracking in the closed-loop system of Eq.C.1. Initially, we show that the controller of Eqs.4.8-4.10 satisfies the constraints within the region described by the set $\Pi(\theta_b, u_{max})$ in Eq.4.11. Then, using a Lyapunov argument we show that, starting from any initial condition that belongs to any invariant subset of Π, Ω, the state feedback controller of Eqs.4.8-4.10 asymptotically stabilizes the closed-loop e-subsystem and derive bounds that capture the evolution of the states of the e and η subsystems. Next, a small gain argument is invoked to show that the trajectories of the e-η interconnected closed-loop system remain bounded for all times. Finally, we show that the states of the full closed-loop system of Eq.C.1 converge to the origin and that the outputs satisfy the relation of

Eq.4.12.

Step 1: To prove that the control law of Eqs.4.8-4.10 satisfies the constraints within the region described by the set $\Pi(\theta_b, u_{max})$, we have from Eqs.4.8-4.10 that:

$$\begin{aligned} |u(x)| &\leq \left|\frac{1}{2}R^{-1}(x)\right|\left|(L_{\bar{g}}V)^T\right| \\ &\leq \frac{\left|L_{\bar{f}}^{*}V + \sqrt{\left(L_{\bar{f}}^{**}V\right)^2 + \left(u_{max}\left|(L_{\bar{g}}V)^T\right|\right)^4}\right|}{\left|(L_{\bar{g}}V)^T\right|\left[1+\sqrt{1+\left(u_{max}\left|(L_{\bar{g}}V)^T\right|\right)^2}\right]} \end{aligned} \tag{C.2}$$

From the definitions of $L_{\bar{f}}^{*}V$ and $L_{\bar{f}}^{**}V$ in Eq.4.10 and the fact that $\rho > 0$, it is clear that if $L_{\bar{f}}^{**}V \leq u_{max}\left|(L_{\bar{g}}V)^T\right|$, then we also have $L_{\bar{f}}^{*}V \leq u_{max}\left|(L_{\bar{g}}V)^T\right|$. Therefore, for any $x \in \Pi$, the following estimates hold:

$$\begin{aligned} \left(L_{\bar{f}}^{**}V\right)^2 &\leq \left(u_{max}\left|(L_{\bar{g}}V)^T\right|\right)^2 \\ L_{\bar{f}}^{*}V &\leq u_{max}\left|(L_{\bar{g}}V)^T\right| \end{aligned} \tag{C.3}$$

Substituting the above estimates into Eq.C.2 yields:

$$|u(x)| \leq \frac{u_{max}\left|(L_{\bar{g}}V)^T\right|\left[1+\sqrt{1+\left(u_{max}\left|(L_{\bar{g}}V)^T\right|\right)^2}\right]}{\left|(L_{\bar{g}}V)^T\right|\left[1+\sqrt{1+\left(u_{max}\left|(L_{\bar{g}}V)^T\right|\right)^2}\right]} = u_{max} \tag{C.4}$$

Step 2: Consider the smooth, positive-definite function, $V : \mathbb{R}^{\sum_i r_i} \rightarrow R_{\geq 0}$, $V = e^T P e$ as a Lyapunov function candidate for the e-subsystem of Eq.C.1. Computing the time-derivative of V along the trajectories of the closed-loop e-subsystem, we get:

$$\begin{aligned} \dot{V} &= L_{\bar{f}}V + L_{\bar{g}}Vu + \sum_{k=1}^{q} L_{\bar{w}_k}V\theta_k \\ &= L_{\bar{f}}V - \left(\frac{L_{\bar{f}}^{*}V + \sqrt{\left(L_{\bar{f}}^{**}V\right)^2 + \left(u_{max}|(L_{\bar{g}}V)^T|\right)^4}}{\left[1+\sqrt{1+\left(u_{max}|(L_{\bar{g}}V)^T|\right)^2}\right]}\right) + \sum_{k=1}^{q} L_{\bar{w}_k}V\theta_k \\ &\leq \left(L_{\bar{f}}V + \chi\sum_{k=1}^{q}|L_{\bar{w}_k}V|\theta_{bk}\right) - \left(\frac{L_{\bar{f}}^{*}V + \sqrt{\left(L_{\bar{f}}^{**}V\right)^2 + \left(u_{max}|(L_{\bar{g}}V)^T|\right)^4}}{\left[1+\sqrt{1+\left(u_{max}|(L_{\bar{g}}V)^T|\right)^2}\right]}\right) \end{aligned} \tag{C.5}$$

After performing some algebraic manipulations, the above inequality can be re-written as:

$$\dot{V} \leq \alpha(e,\eta,\bar{v}) + \left(\frac{\sum_{k=1}^{q} \theta_{bk} \left| L_{\bar{w}_k} V \right| \left(\frac{\phi - (\chi - 1)\left|2Pe\right|}{\left|2Pe\right| + \phi} \right) - \rho \left(\frac{\left|2Pe\right|^2}{\left|2Pe\right| + \phi} \right)}{\left[1 + \sqrt{1 + (u_{max} |(L_{\bar{g}} V)^T|)^2} \right]} \right) \tag{C.6}$$

where

$$\begin{aligned} \alpha(e,\eta,\bar{v}) &= \frac{\left(L_{\bar{f}} V + \chi \sum_{k=1}^{q} \theta_{kb} \left| L_{\bar{w}_k} V \right| \right) \sqrt{1 + (u_{max} |(L_{\bar{g}} V)^T|)^2}}{\left[1 + \sqrt{1 + (u_{max} |(L_{\bar{g}} V)^T|)^2} \right]} \\ &- \frac{\sqrt{\left(L_{\bar{f}}^{**} V \right)^2 + (u_{max} |(L_{\bar{g}} V)^T|)^4}}{\left[1 + \sqrt{1 + (u_{max} |(L_{\bar{g}} V)^T|)^2} \right]} \end{aligned} \tag{C.7}$$

To analyze the sign of $\dot{V}$ in Eq.C.6, we will initially study the sign of the term, $\alpha(e,\eta,\bar{v})$, on the right-hand side. It is clear that the sign of this term depends on the sign of the term $L_{\bar{f}} V + \chi \sum_{k=1}^{q} \theta_{kb} \left| L_{\bar{w}_k} V \right|$. To this end, we consider the following two cases:

Case 1: $L_{\bar{f}}^{**} V \leq 0$

Since $L_{\bar{f}}^{**} V = L_{\bar{f}} V + \rho \left|2Pe\right| + \chi \sum_{k=1}^{q} |L_{\bar{w}_k} V| \theta_{bk}$ and ρ is a positive real number, the fact that $L_{\bar{f}}^{**} V \leq 0$ implies that $L_{\bar{f}} V + \chi \sum_{k=1}^{q} \left| L_{\bar{w}_k} V \right| \theta_{bk} \leq 0$. As a result, we have that $\alpha(e,\eta,\bar{v}) \leq 0$ and the time-derivative of V in this case satisfies the following bound:

$$\dot{V} \leq \left(\frac{\sum_{k=1}^{q} \theta_{bk} \left| L_{\bar{w}_k} V \right| \left(\frac{\phi - (\chi - 1)\left|2Pe\right|}{\left|2Pe\right| + \phi} \right) - \rho \left(\frac{\left|2Pe\right|^2}{\left|2Pe\right| + \phi} \right)}{\left[1 + \sqrt{1 + (u_{max} |(L_{\bar{g}} V)^T|)^2} \right]} \right) := \beta(e,\eta,\bar{v}) \tag{C.8}$$

Case 2: $0 < L_{\bar{f}}^{**} V \leq u_{max} \left| (L_{\bar{g}} V)^T \right|$

In this case, we have:

$$\left(L_{\bar{f}}^{**}V\right)^2 \leq \left(u_{max}|(L_{\bar{g}}V)^T|\right)^2 \tag{C.9}$$

and therefore:

$$\begin{aligned} -\sqrt{\left(L_{\bar{f}}^{**}V\right)^2 + (u_{max}|(L_{\bar{g}}V)^T|)^4} &= -\sqrt{\left(L_{\bar{f}}^{**}V\right)^2 + (u_{max}|(L_{\bar{g}}V)^T|)^2(u_{max}|(L_{\bar{g}}V)^T|)^2} \\ &\leq -\left(L_{\bar{f}}^{**}V\right)\sqrt{1+(u_{max}|(L_{\bar{g}}V)^T|)^2} \end{aligned} \tag{C.10}$$

Substituting the estimate of Eq.C.10 into the expression for $\dot{V}$ in Eqs.C.6-C.7 yields:

$$\begin{aligned} \dot{V} &= \frac{-\rho|2Pe|\sqrt{1+(u_{max}|(L_{\bar{g}}V)^T|)^2}}{\left[1+\sqrt{1+(u_{max}|(L_{\bar{g}}V)^T|)^2}\right]} + \beta(e,\eta,\bar{v}) \\ &\leq \beta(e,\eta,\bar{v}) \end{aligned} \tag{C.11}$$

From the above analysis, it is clear that whenever $L_{\bar{f}}^{**}V \leq u_{max}|(L_{\bar{g}}V)^T|$, the inequality of Eq.C.8 holds. To guarantee that the state of the closed-loop system satisfies $L_{\bar{f}}^{**}V \leq u_{max}|(L_{\bar{g}}V)^T|$ for all time, we confine the initial conditions within an invariant subset, Ω, embedded within the region described by Eq.4.11. Therefore, starting from any $x(0) \in \Omega$, the inequality of Eq.C.8 holds. Referring to this inequality, note that since $\chi > 1$ and $\rho > 0$, it is clear that, whenever $|2Pe| > \dfrac{\phi}{\chi - 1}$, the first term on the right-hand side is strictly negative, and therefore $\dot{V}$ satisfies:

$$\begin{aligned} \dot{V} &\leq -\frac{\rho\,|2Pe|^2}{(|2Pe|+\phi)\left[1+\sqrt{1+(u_{max}|(L_{\bar{g}}V)^T|)^2}\right]} \\ &\leq -\frac{k_1\,|e|^2}{(|2Pe|+\phi)\left[1+\sqrt{1+(u_{max}|(L_{\bar{g}}V)^T|)^2}\right]} \end{aligned} \tag{C.12}$$

where $k_1 = 2\rho\lambda_{min}(P^2) > 0$. To study the behavior of $\dot{V}$ when $|2Pe| \leq \phi/(\chi-1)$, we first note that since the functions $\bar{w}_k(e,\eta,\bar{v})$ are smooth and vanish when $e = 0$, then there exists positive real constants ϕ_1^*, δ_k, $k = 1, \cdots, q$, such that if $\phi \leq \phi_1^*$, the

bound $|\bar{w}_k(e,\eta,\bar{v})| \leq \delta_k|e|$, holds for $|2Pe| \leq \phi/(\chi-1)$. Using this bound, we obtain the following estimates:

$$\begin{aligned}\sum_{k=1}^{q}\theta_{bk}\left|L_{\bar{w}_k}V\right|\left(\phi-(\chi-1)\left|2Pe\right|\right) &\leq \sum_{k=1}^{q}\theta_{bk}\left|L_{\bar{w}_k}V\right|\phi \\ &= \sum_{k=1}^{q}\theta_{bk}\left|\bar{w}_k\right|\left|2Pe\right|\phi \\ &\leq k_2\phi\sum_{k=1}^{q}\theta_{bk}\delta_k|e|^2 \qquad \forall\ \ |2Pe| \leq \frac{\phi}{\chi-1}\end{aligned} \tag{C.13}$$

where $k_2 = 2\sqrt{\lambda_{max}(P^2)} > 0$. Substituting the estimate of Eq.C.13 directly into Eq.C.8, we get:

$$\dot{V} \leq \left(\frac{\left(k_2\phi\sum_{k=1}^{q}\theta_{bk}\delta_k - 2k_1\right)|e|^2}{(|2Pe|+\phi)\left[1+\sqrt{1+(u_{max}|(L_{\bar{g}}V)^T|)^2}\right]}\right) \qquad \forall\ \ |2Pe| \leq \frac{\phi}{\chi-1} \tag{C.14}$$

If ϕ is sufficiently small to satisfy the bound $\phi \leq \dfrac{k_1}{k_2\sum_{k=1}^{q}\delta_k\theta_{bk}} := \phi_2^*$, then it is clear from Eqs.C.12-C.14 that the last inequality in Eq.C.12 is satisfied, irrespective of the value of $|2Pe|$. In summary, we have that for any initial condition in the invariant set Ω (where Eq.4.11 holds $\forall\ t \geq 0$), there exists $\phi^* := \min\{\phi_1^*, \phi_2^*\}$ such that if $\phi \leq \phi^*$, $\dot{V}$ satisfies:

$$\dot{V} \leq \frac{-k_1|e|^2}{(|2Pe|+\phi)\left[1+\sqrt{1+(u_{max}L_{\bar{g}}V)^2}\right]} < 0 \quad \forall\, e \neq 0 \tag{C.15}$$

Consequently, there exists a function β_e of class $\mathcal{KL}$ (see [170] for details) such that the following ISS inequality holds for the e states of the system of Eq.C.1:

$$|e(t)| \leq \beta_e\left(|e(0)|, t\right) \qquad \forall\, t \geq 0 \tag{C.16}$$

and the origin of the e-subsystem is asymptotically stable. From Assumption 4.2, we have that the η-subsystem of Eq.C.1 possesses an ISS property with respect to e which implies that there exists a function, β_η, of class $\mathcal{KL}$ and a function, γ_η, of class

$\mathcal{K}$ such that the following ISS inequality holds:

$$|\eta(t)| \leq \beta_\eta(|\eta(0)|, t) + \gamma_\eta(\|e\|) \qquad \forall\, t \geq 0 \tag{C.17}$$

uniformly in θ, $\bar{v}$. Using the inequalities of Eqs.C.16-C.17, it can be shown by means of a small gain argument, similar to that used in [67, 68], that the origin of the full closed-loop system is asymptotically stable for all initial conditions inside the invariant set Ω. The asymptotic output tracking result can finally be obtained by simply taking the limsup of both sides of Eq.C.16 which yields:

$$\limsup_{t\to\infty} |e(t)| = 0 \tag{C.18}$$

and, hence:

$$\limsup_{t\to\infty} |e_1^{(i)}(t)| = \limsup_{t\to\infty} |y_i(t) - v_i(t)| = 0, \quad i = 1, \cdots, m \tag{C.19}$$

This completes the proof of the theorem. $\triangle$

Proof of Theorem 4.2:

The proof of this theorem consists of three parts. In the first part, we use a singular perturbation formulation to represent the closed-loop system and show that the resulting fast subsystem is globally exponentially stable. In the second part, we focus on the closed-loop reduced (slow) system and derive bounds for its states. Then, in the third part, we use a technical lemma proved in [60], to establish that these bounds continue to hold up to an arbitrarily small offset, for arbitrarily large compact subsets of the stability region obtained under state feedback. The resulting bounds are then analyzed to establish asymptotic and local exponential stability of the full closed-loop system, which is then used to establish Eq.4.21, provided that ϕ and $\bar{\epsilon}$ are sufficiently small.

Part 1: Defining the auxiliary error variables $\hat{e}_j^{(i)} = L_i^{r_i - j}(y_i^{(j-1)} - \tilde{y}_j^{(i)})$, $j = 1, \ldots, r_i$, the vectors $e_o^{(i)} = [\hat{e}_1^{(i)}\ \hat{e}_2^{(i)}\ \cdots\ \hat{e}_{r_i}^{(i)}]^T$, $e_o = [e_o^{(1)^T}\ e_o^{(2)^T}\ \cdots\ e_o^{(m)^T}]^T$, the parameters $\epsilon_i = \dfrac{1}{L_i}$, the matrices $\tilde{A}_i$ and the vector $\tilde{b}$:

$$\tilde{A}_i = \begin{bmatrix} -a_1^{(i)} & 1 & 0 & \cdots & 0 \\ -a_2^{(i)} & 0 & 1 & \cdots & 0 \\ \vdots & \vdots & \vdots & \ddots & \vdots \\ -a_{r_i-1}^{(i)} & 0 & 0 & \cdots & 1 \\ -a_{r_i}^{(i)} & 0 & 0 & \cdots & 0 \end{bmatrix}, \quad \tilde{b} = \begin{bmatrix} 0 \\ 0 \\ \vdots \\ 0 \\ 1 \end{bmatrix} \tag{C.20}$$

where $i = 1, \cdots, m$, the system of Eq.4.1 under the controller of Eq.4.20 takes the following form:

$$\begin{aligned} \epsilon_i \dot{e}_o^{(i)} &= \tilde{A}_i e_o^{(i)} + \epsilon_i \tilde{b} \psi_i(x, \hat{x}, \theta, \phi, \bar{v}), \quad i = 1, \cdots, m \\ \dot{\omega} &= \Psi(sat(\tilde{y}), \omega) \\ \dot{x} &= f(x) - \frac{1}{2} \sum_{i=1}^{m} g_i(x) R^{-1}(\hat{x}) (\widehat{L_{\bar{g}_i} V})^T + \sum_{k=1}^{q} w_k(x) \theta_k(t) \end{aligned} \tag{C.21}$$

where $\psi_i(x, \hat{x}, \theta, \phi, \bar{v})$ is a Lipschitz function of its argument. Owing to the presence of the small parameters ϵ_i that multiply the time-derivatives, $\dot{e}_o^{(i)}$, the system of Eq.C.21 can be, in general, a multiple-time-scale system. Therefore, the results proved in [169] will be used to establish exponential stability of the fast dynamics. Defining $\bar{\epsilon} = \max\{\epsilon_i\}$, $i = 1, \cdots, m$, multiplying each $e_o^{(i)}$-subsystem by $\bar{\epsilon}/\epsilon$, introducing the fast time-scale $\bar{\tau} = \dfrac{t}{\bar{\epsilon}}$ and setting $\bar{\epsilon} = 0$, the closed-loop fast subsystem takes the form:

$$\frac{de_o}{d\bar{\tau}} = \frac{\bar{\epsilon}}{\epsilon} \tilde{A}_i e_o, \; i = 1, \cdots, m \tag{C.22}$$

The above system possesses a triangular (cascaded) structure, with the constant matrices $\tilde{A}_i$ being Hurwitz. Therefore, it satisfies Assumption 3 in [169] and, since $\bar{\epsilon}/\epsilon \geq 1$, the same approach, as in [169], can be used to deduce that the origin of this system is globally exponentially stable, i.e., there exists real numbers, $k_3 \geq 1$, $a_3 > 0$ such that:

$$|e_o(\bar{\tau})| \leq k_3|e_o(0)|e^{-a_3\bar{\tau}} \ \forall\, \bar{\tau} \geq 0 \tag{C.23}$$

Part 2: Using the coordinate change of Eq.4.5 and Eq.4.19, together with the notation introduced thereafter, we can re-write the closed-loop system of Eq.C.21 in the following form:

$$\begin{aligned}
\epsilon_i \dot{e}_o &= \tilde{A}_i e_o + \epsilon_i \tilde{b} \psi_i(e, \eta, \hat{x}, \theta, \phi, \bar{v}) \\
\dot{\omega} &= \Psi(sat(\tilde{y}), \omega) \\
\dot{e} &= \bar{f}(e, \eta, \bar{v}) - \frac{1}{2}\sum_{i=1}^{m} \bar{g}_i(e, \eta, \bar{v}) R^{-1}(\hat{x})(\widehat{L_{\bar{g}_i} V})^T + \sum_{k=1}^{q} \bar{w}_k(e, \eta, \bar{v})\theta_k \\
\dot{\eta} &= \Psi(e, \bar{v}, \eta) \\
y_i &= e_1^{(i)} + v_i, \quad i = 1, \cdots, m
\end{aligned} \tag{C.24}$$

Consider the above system with $\bar{\epsilon} = \max\{\epsilon_i\} = 0$. Using the result of Theorem 1 in [171], it can be shown that $\eta(0) = \omega(0) + O(\bar{\epsilon})$ implies $\eta(t) = \omega(t) + O(\bar{\epsilon})$, $\forall\, t \geq 0$ and therefore $\eta(t) = \omega(t)\ \forall\, t \geq 0$, when $\bar{\epsilon} = 0$. The closed-loop reduced (slow) system of Eq.C.24 therefore reduces to the one studied in the Proof of Theorem 4.1 (see Eq.C.1) under state feedback, where we have already shown that given any initial condition such that $|x(0)| \leq \delta_s$, there exists $\phi^* > 0$ such that if $\phi \leq \phi^*$ and $|x(0)| \leq \delta_s$, the origin of the closed-loop system is asymptotically stable. Consequently, the denominator expression in Eq.C.15 is bounded and there exist real numbers, $k_e > 0$, $k_1 \geq 1$, $a_1 > 0$ such that if $|e(0)| \leq \delta_e$, $|\eta(0)| \leq \delta_\eta$, $\|\bar{v}\| \leq \delta_{\bar{v}}$, where $\delta_s = T^{-1}(\delta_e, \delta_\eta, \delta_{\bar{v}})$, we have that $\dot{V}$ satisfies $\dot{V} \leq -k_e|e|^2$ and the e states of the closed-loop system satisfy:

$$|e(t)| \leq k_1|e(0)|e^{-a_1 t} \ \forall\, t \geq 0 \tag{C.25}$$

which shows that the origin of the e-subsystem is exponentially stable. From this result and the fact that the η-subsystem (with $e = 0$) is locally exponentially stable, we have that the e, η interconnected closed-loop reduced (slow) system is also locally exponentially stable (see [170] for details). Therefore, given the set of positive real

numbers, $\{\delta_e, \delta_\eta, \delta_{\bar{v}}\}$, there exists $b > 0$ such that if $|e(0)| \leq \delta_e$, $|\eta(0)| \leq \delta_\eta$, $\|\bar{v}\| \leq \delta_{\bar{v}}$, the following bound holds:

$$|\pi(t)| \;\leq\; k_2|\pi(t_0)|e^{-a_2(t-t_0)} \;\forall\; t \geq t_0 \tag{C.26}$$

for all $|\pi(t_0)| \leq b$, where $\pi(t) = [e^T(t) \;\; \eta^T(t)]^T$, for some $k_2 \geq 1$, $a_2 > 0$. Note that since the static component of the controller of Eq.4.20 with $\hat{x} = x$ enforces asymptotic stability in the closed-loop slow system, the state, ζ, of the closed-loop slow system satisfies a bound of the following form $\forall\, t \geq 0$:

$$|\zeta(t)| \;\leq\; \beta_\zeta(\delta_\zeta, t) \tag{C.27}$$

where β_ζ is a class $\mathcal{KL}$ function and δ_ζ is the maximum value of the norm of the vector $[l_1^T(x) \; l_2^T(x) \; \cdots \; l_m^T(x)]^T$ for $|x| \leq \delta_b$, where $l_i(x) = [h_i(x) \; L_f h_i(x) \; \cdots L_f^{r_i-1} h_i(x)]^T$. Based on the above bound and following the results of [171, 294], we disregard estimates of $\tilde{y}$, obtained from the high-gain observer, with norm $|\tilde{y}| > \beta_\zeta(\delta_\zeta, 0)$. Hence, we set $sat(\cdot) = \min\{1, \frac{\zeta_{max}}{|\cdot|}\}(\cdot)$ where ζ_{max} is the maximum value of the vector $[\zeta_1 \; \zeta_2 \; \cdots \; \zeta_r]$ for $|\zeta| \leq \beta_\zeta(\delta_\zeta, 0)$.

Part 3: Having analyzed the stability properties of both the fast and slow closed-loop systems in Parts 1 and 2, respectively, it can be shown, with the aid of calculations similar to those performed in [67, 92], that the inequalities of Eq.C.23 (derived for the fast system), and Eqs.C.17-C.25 (derived for the slow system) continue to hold, for the states of the full closed-loop system, up to an arbitrarily small offset, d, for initial conditions in large compact subsets ($\Omega_b \subset \Omega$) where $\Omega_b := \{x \in \mathbb{R}^m : \; |x| \leq \delta_b\}$ and $\beta(\delta_b, 0) + d \leq \delta_s$, provided that the singular perturbation parameter, $\bar{\epsilon}$, is sufficiently small. The requirement that $\beta(\delta_b, 0) + d \leq \delta_s$ guarantees that during the initial boundary layer (when the fast states have not decayed yet), the slow states of the closed-loop system remain within the invariant region Ω. Therefore, given the pair (δ_b, d), the set $(\delta_\theta, \delta_{\bar{v}}, \delta_\zeta)$, and with $\phi \in (0, \phi^*]$, there exists $\bar{\epsilon}^{(1)} > 0$ such that if $\bar{\epsilon} \in (0, \bar{\epsilon}^{(1)}]$, $|x(0)| \leq \delta_b$, $|\tilde{y}| \leq \delta_\zeta$, $\|\theta_k\| \leq \delta_\theta$, $\|\bar{v}\| \leq \delta_{\bar{v}}$, then, for all $t \geq 0$, the states

of the closed-loop singularly perturbed system satisfy:

$$\begin{aligned} |\pi(t)| &\leq k_2|\pi(0)|e^{-a_2 t} + d \\ |e_o(t)| &\leq k_3|e_o(0)|e^{-a_3\frac{t}{\bar{\epsilon}}} + d \end{aligned} \tag{C.28}$$

The above inequalities imply that the trajectories of the closed-loop singularly perturbed system will be bounded. Furthermore, as t increases, they will be ultimately bounded with an ultimate bound that depends on d. Since d is arbitrary, we can choose it small enough such that after a sufficiently large time, say $\tilde{t}$, the trajectories of the closed-loop system are confined within a small compact neighborhood of the origin of the closed-loop system. Obviously, $\tilde{t}$ depends on both the initial conditions and the desired size of the neighborhood, but is independent of $\bar{\epsilon}$. For reasons that will become obvious shortly, we choose $d = b/2$ and let $\tilde{t}$ be the smallest time such that $\max\{k_2|\pi(0)|e^{-a_2\tilde{t}}, k_3|e_o(0)|e^{-a_3\tilde{t}/\epsilon}\} \leq d$. Then it can be easily verified that:

$$|\pi(t)| \leq b, \;\; |e_o(t)| \leq b \;\; \forall\, t \geq \tilde{t} \tag{C.29}$$

Recall from Eq.C.23 and Eq.C.26 that both the fast and slow subsystems are exponentially stable within the ball of Eq.C.29. Then, a direct application of the result of Theorem 9.3 in [170] can be performed to show that there exists $\bar{\epsilon}^{(2)}$ such that if $\bar{\epsilon} \leq \bar{\epsilon}^{(2)}$, the singularly perturbed closed-loop system is locally exponentially stable and, therefore, once inside the ball of Eq.C.29, the closed-loop trajectories converge to the origin as $t \to \infty$.

To summarize, we have that given the pair of positive real numbers (δ_b, d) such that $\beta(\delta_b, 0)+d \leq \delta_s$, given the set of positive real numbers $(\delta_\theta, \delta_{\bar{v}}, \delta_\zeta)$, and with $\phi \in (0.\phi^*]$, there exists $\bar{\epsilon}^* := \min\{\bar{\epsilon}^{(1)}, \bar{\epsilon}^{(2)}\}$ such that if $|x(0)| \leq \delta_b$, $|\tilde{y}(0)| \leq \delta_\zeta$, $\|\theta_k\| \leq \delta_\theta$, $\|\bar{v}\| \leq \delta_{\bar{v}}$, and $\bar{\epsilon} \in (0, \bar{\epsilon}^*]$, the closed-loop trajectories are bounded and converge to the origin as time tends to infinity, i.e., the closed-loop system is asymptotically stable. The asymptotic output tracking result can then be established by noting that from Eq.C.26 we have:

$$\limsup_{t\to\infty} |e(t)| = 0 \tag{C.30}$$

and therefore:

$$\limsup_{t\to\infty} |e_1^{(i)}(t)| = \limsup_{t\to\infty} |y_i(t) - v_i(t)| = 0, \quad i = 1, \cdots, m \tag{C.31}$$

This completes the proof of the theorem. $\triangle$

Appendix D

Proofs of Chapter 5

Proof of Theorem 5.1:

To prove this theorem, we proceed in two steps. In the first step we show that, starting from any initial condition within the set $\Omega(u_{max})$, the bounded control law of Eqs.5.7-5.8 asymptotically stabilizes the constrained closed-loop. Then, in the second step, we show that switching between the model predictive controller of Eqs.5.3-5.5 and the bounded controller, according to the rule of Eqs.5.13-5.14, guarantees asymptotic stability in the switched closed-loop system, starting from any initial condition that belongs to $\Omega(u_{max})$.

Step 1: Consider first the system of Eq.5.1, under the control law of Eq.5.7-5.8. Evaluating the time-derivative of the Lyapunov function along the closed-loop trajectories, we have:

$$\begin{aligned}
\dot{V} &= L_f V + L_g V u \\
&= L_f V - L_g V \frac{L_f^* V + \sqrt{(L_f^* V)^2 + (u_{max}\|(L_g V)^T\|)^4}}{\|(L_g V)^T\|^2 \left[1 + \sqrt{1 + (u_{max}\|(L_g V)^T\|)^2}\right]} (L_{\bar{g}} V)^T \\
&= \frac{-\rho x' P x + L_f V \sqrt{1 + (u_{max}\|(L_g V)^T\|)^2} - \sqrt{(L_{\bar{f}}^* V)^2 + (u_{max}\|(L_g V)^T\|)^4}}{\left[1 + \sqrt{1 + (u_{max}\|(L_g V)^T\|)^2}\right]}
\end{aligned} \tag{D.1}$$

From the above equation, and the fact that $L_f^* V < 0 \Longrightarrow L_f V < 0$ (since $\rho > 0$), we have that V satisfies:

$$\dot{V} \leq \frac{-\rho x' P x}{\left[1 + \sqrt{1 + (u_{max}\|(L_g V)^T\|)^2}\right]} < 0 \quad \forall\, x \neq 0 \tag{D.2}$$

Furthermore, whenever $0 < L_f^* V \leq u_{max}\|(L_g V)^T\|$, we have:

$$\sqrt{(L_f^* V)^2 + (u_{max}\|(L_g V)^T\|)^4} \geq L_f V \sqrt{1 + (u_{max}\|(L_g V)^T\|)^2}$$

Substituting the above estimate into Eq.D.1, we have that $\dot{V}$ satisfies Eq.D.2. To summarize, we see that whenever $L_f^* V \leq u_{max}\|(L_g V)^T\|$, we have $\dot{V} < 0$. Since $\Omega(u_{max})$ is taken to be the largest invariant set where this inequality holds for all $x \neq 0$, then starting from any initial state $x(0) \in \Omega(u_{max})$, the inequality of Eq.5.9 holds for all times and consequently:

$$\dot{V} < 0 \quad \forall\, x \in \Omega(u_{max}) \backslash \{0\} \tag{D.3}$$

which implies that the origin of the closed-loop system, under the control law of Eqs.5.7-5.8 is asymptotically stable.

Step 2: Consider the switched system of Eq.5.11, subject to the switching rule of Eqs.5.13-5.14, with any initial state $x(0) \in \Omega(u_{max})$. From the definition of T_s given in Theorem 5.1, it is clear that if T_s is a finite number, then $\dot{V}(x^M(t)) < 0 \quad \forall\, 0 \leq t < T$, where the notation $x^M(t)$ denotes the closed-loop state under MPC at time t, which implies that $x(t) \in \Omega(u_{max}) \quad \forall\, 0 \leq t < T_s$ (or that $x(T^-) \in \Omega(u_{max})$). This fact, together with the continuity of the solution of the switched system, $x(t)$, (which follows from the fact that the right hand side of Eq.5.11 is continuous in x and piecewise continuous in time (only finite number of switches is allowed over any finite time interval)) implies that, upon switching (instantaneously) to the bounded controller at $t = T_s$, we have $x(T_s) \in \Omega(u_{max})$ and $u(t) = b(x(t))$ for all $t \geq T_s$. Therefore, from our analysis in Step 1 we conclude that $\dot{V}(x^b(t)) < 0 \quad \forall\, t \geq T_s$. In summary, the switching rule of Eqs.5.13-5.14 guarantees that, starting from any $x(0) \in \Omega(u_{max})$, $\dot{V}(x(t)) < 0 \quad \forall\ 0 \neq x \in \Omega(u_{max}), \quad \forall\ t \geq 0$. which implies that the origin of the

switched closed-loop system is asymptotically stable. Note that if no such T_s exists, then we simply have $\dot{V}(x^M(t)) < 0 \quad \forall \; t \geq 0$ and the origin of the closed-loop system is, again, asymptotically stable. This completes the proof of the theorem. $\triangle$

Proof of Theorem 5.2:

To prove this theorem, we first note that if neither T_b nor T_N exists, then no switching takes place and we simply have $\dot{V}(x^M(t)) < 0 \quad \forall \; t \geq 0$ implying that the origin of the closed-loop system is asymptotically stable under the model predictive controller of Eqs.5.3-5.5. Therefore, in what follows we consider only the case when at least one of these numbers exists. From the definition of T_N given in Theorem 5.2, it is clear that (if this number exists) the Lyapunov function under the model predictive controller, $V(x^M(t))$, changes sign no more than N times over the time interval $[0, T_N)$. Since the set $\Omega(u_{max})$ is not necessarily invariant under the control law of Eqs.5.3-5.5, the trajectory of the closed-loop system can possibly leave $\Omega(u_{max})$ at some time during the interval $[0, T_N)$ which implies that in this case there exists (at least one) finite time $t_1 \in [0, T_N)$ such that $V(x^M(t_1)) = c_{max}$. From the definition of T_b given in Theorem 5.2, it is clear that the smallest such t_1 is equal to T_b, and that $T_b \in [0, T_N)$, i.e. $\min\{T_b, T_N\} = T_b$. If, on the other hand, the closed-loop trajectory under the model predictive controller remains within $\Omega(u_{max})$ for all times in $[0, T_N)$, then we have $V(x^M(t)) \leq c_{max} \quad \forall \; t \in [0, T_N)$ and we set $\min\{T_b, T_N\} = T_N$.

From the above analysis we can deduce that, starting from any initial state $x(0) \in \Omega(u_{max})$, the closed-loop trajectory satisfies $x^M(t) \in \Omega(u_{max}) \quad \forall \; 0 \leq t < \min\{T_b, T_N\}$. This fact, together with continuity of the solution of the switched closed-loop system implies that, upon switching (instantaneously) to the bounded controller at $t = \min\{T_b, T_N\} := T_p$, we have $x(T_p) \in \Omega(u_{max})$ and $u(t) = b(x(t))$ for all $t \geq T_p$. Then, by repeating the arguments of Step 1 in the Proof of Theorem 5.1, we can show that $\dot{V}(x^b(t)) < 0 \quad \forall \; t \geq T_p$ and that the origin of the switched closed-loop system is therefore asymptotically stable for any $x(0) \in \Omega(u_{max})$. This completes the proof of the theorem. $\triangle$

Proof of Proposition 5.1:

The proof consists of two parts. In the first part, we establish that the bounded state feedback control law of Eqs.5.7–5.8 enforces asymptotic stability for all initial conditions within Ω. In the second part, we compute an estimate of the tolerable measurement error, e_m, which guarantees that a state trajectory starting within Ω remains within it for all $\|e\| \leq e_m$, for all $t \geq 0$.

Part 1: We have already shown in Step 1 of Part 1 of the Proof of Theorem 5.1 that the time–derivative of the V, along the trajectories of the closed–loop system of Eq.5.22 and Eqs.5.7–5.8, satisfies:

$$\begin{aligned} \dot{V}(x) &= L_f V(x) + L_g V(x) u(x) \\ &\leq \frac{-\rho x' P x}{\left[1 + \sqrt{1 + (2u_{max}\|B'Px\|)^2}\right]} \end{aligned} \tag{D.4}$$

for all $x \in \Phi$, and hence for all $x \in \Omega$, where Φ and Ω were defined in Eqs.5.9–5.10, respectively. Since the denominator term in Eq.D.4 is bounded on Ω, there exists a positive real number, ρ^*, such that:

$$\dot{V} \leq -\rho^* x' P x \tag{D.5}$$

for all $x \in \Omega$, which implies that the origin of the closed–loop system, under the control law of Eqs.5.7–5.8, is asymptotically stable, with Ω as an estimate of the domain of attraction.

Part 2: In this part, we analyze the behavior of $\dot{V}$ on the boundary of Ω (i.e., the level surface described by $V(x) = c_{max}$) under bounded measurement errors, $\|e\| \leq e_m$. To

this end, we have:

$$\begin{aligned}\dot{V}(x) &= L_f V(x) + L_g V(x) u(x-e) \\ &= L_f V(x) + L_g V(x) u(x) + L_g V(x)\left[u(x-e) - u(x)\right] \\ &\leq -\rho^* c_{max} + \|L_g V\| \|u(x-e) - u(x)\| \\ &\leq -\rho^* c_{max} + M\|u(x-e) - u(x)\|\end{aligned} \tag{D.6}$$

for all $x = V^{-1}(c_{max})$, where $M = \max_{V(x)=c_{max}} (\|L_g V(x)\|)$ (note that M exists since $\|L_g V(\cdot)\|$ is continuous and the maximization is considered on a closed set). Since $u(\cdot)$ is continuous, then given any positive real number r such that $\mu = \dfrac{\rho^* c_{max} - r}{M} > 0$, there exists $e_m > 0$ such that if $\|(x-e)-x\| = \|e\| \leq e_m$, then $\|u(x-e)-u(x)\| \leq \mu$ and, consequently:

$$\dot{V}(x) \leq -\rho^* c_{max} + M\mu = -r < 0 \tag{D.7}$$

for all $x = V^{-1}(c_{max})$. This implies that for all measurement errors such that $\|e\| \leq e_m$, we have $\dot{V} < 0$ on the boundary of Ω. Therefore, under the bounded controller, any closed–loop state trajectory, starting within Ω, cannot escape this region, i.e., $x(t) \in \Omega \; \forall t \geq 0$. This completes the proof of the proposition. $\triangle$

Proof of Proposition 5.2:

The proof is divided into two parts. In the first part, we show that given $\delta_b > 0$ (the size of the output feedback stability region) such that $\Omega_b \subset \Omega$, there exists a choice of β such that the closed–loop trajectories are bounded for all $x(0)$ and $\hat{x}(0)$ belonging in Ω_b. In the second part, we use a Lyapunov argument, together with boundedness of the states of the closed–loop system and of the estimation error, to show that the state is ultimately bounded with a bound that depends on the norm of the estimation error; and, therefore, converges to zero as the error tends to zero.

Part 1: From Eq.5.26, we have that the error dynamics are given by $\dot{e} = (A - LC)e$, where $A - LC$ is Hurwitz, and all the eigenvalues of the matrix $A - LC$ satisfy

$\lambda \leq -\beta$. It then follows that an estimate of the form $\|e(t)\| \leq \kappa(\beta)\|e(0)\|\exp(-\beta t)$ holds for some $\kappa(\beta) > 0$, for all $t \geq 0$. Given any positive real number, δ_b, such that $\Omega_b = \{x \in \mathbb{R}^n : \|x\|_P^2 \leq \delta_b\} \subset \Omega$, let $T_{min} = \min\{t \geq 0 : V(x(0)) = \delta_b, V(x(t)) = c_{max}, u(t) \in \mathcal{U}\}$ (i.e., T_{min} is the shortest time during which the closed–loop state trajectory can reach the boundary of Ω starting from the boundary of Ω_b using *any* admissible control action). Furthermore, let $e_{max}(0) = \max_{x,\hat{x} \in \Omega_b} \|x(0) - \hat{x}(0)\|$ ($e_{max}(0)$ therefore is the largest possible initial error given that both the states and state estimates are initialized within Ω_b). Choose T_d such that $0 < T_d < T_{min}$ and let β^* be such that $e_m \leq \kappa(\beta^*)e_{max}(0)\exp(-\beta^* T_d)$ (the existence of such a β^* follows from the fact that $\kappa(\beta)$ is polynomial in β). For any choice of $\beta \geq \beta^*$, therefore, it follows that $\|e(T_{min})\| \leq e_m$ (since $\|e(T_d)\| \leq e_m$, $T_{min} \geq T_d$ and the bound on the norm of the estimation error decreases monotonically with time for all $t \geq 0$). This implies that the norm of the estimation error decays to a value less than e_m before the closed–loop state trajectory, starting within Ω_b, could reach the boundary of Ω. It then follows from Proposition 5.1 that the closed–loop state trajectory cannot escape Ω for all $t \geq 0$, i.e., the trajectories are bounded and $\|x(t)\|_p^2 \leq c_{max}\ \forall\, t \geq 0$.

Part 2: To prove asymptotic stability, we note that for all $x \in \Omega$:

$$\begin{aligned} \dot{V}(x) &= L_f V(x) + L_g V(x) u(x - e) \\ &= L_f V(x) + L_g V(x) u(x) + \|L_g V(x)\| \|u(x - e) - u(x)\| \\ &\leq -\rho^* \|x\|_p^2 + M \|u(x - e) - u(x)\| \end{aligned} \tag{D.8}$$

The term $\|u(x - e) - u(x)\|$ is continuous and vanishes when $e = 0$. Therefore, since both x and e are bounded, there exists a positive real number φ such that $\|u(x - e) - u(x)\| \leq \varphi\|e\|$ for all $\|x\|_p^2 \leq c_{max}$, $\|e\| \leq e_m$. Substituting this estimate into Eq.D.8 yields:

$$\begin{aligned} \dot{V}(x) &\leq -\rho^* \|x\|_p^2 + M\varphi\|e\| \\ &\leq -\frac{\rho^*}{2}\|x\|_p^2 \ \forall\ \|x\|_p \geq \sqrt{\frac{2M\varphi\|e\|}{\rho^*}} := \gamma_1(\|e\|) \end{aligned} \tag{D.9}$$

where $\gamma_1(\cdot)$ is a class $\mathcal{K}$ function (a continuous function $\alpha(\cdot)$ is said to belong to class

$\mathcal{K}$ if it is strictly increasing and $\alpha(0) = 0$; see also [170]). The above inequality implies that $\dot{V}$ is negative outside some residual set whose size depends on $\|e\|$. Using the result of Theorem 5.1-Corollary 5.2 in [170], this implies that, for any $x(0) \in \Omega_b$, there exists a class $\mathcal{KL}$ function $\bar{\beta}(\cdot,\cdot)$ and a class $\mathcal{K}$ function $\gamma_2(\cdot)$, such that:

$$\|x(t)\| \leq \bar{\beta}(\|x(0)\|, t) + \gamma_2(\sup_{\tau \geq 0} \|e(\tau)\|) \; \forall \, t \geq 0 \tag{D.10}$$

implying that the x subsystem of Eq.5.29, with e as input, is input-to-state stable (recall, from Proposition 5.1, that $x(t) \in \Omega_b \; \forall t \geq 0$). Noting also that the origin of the e-subsystem of Eq.5.29 is asymptotically stable ($\lim_{t \to \infty} \|e(t)\| = 0$), and using Lemma 5.6 in [170], we get that the origin of the interconnected system of Eq.5.29 is asymptotically stable. This completes the proof of the proposition. $\triangle$

Proof of Proposition 5.3:

Since the error dynamics obey a bound of the form $\|e(t)\| \leq \kappa(\beta) e_{max}(0) \exp(-\beta t)$, substituting T_d^* into this expression yields $\|e(T_d^*)\| := e^* \leq \epsilon \sqrt{c_{max}/\lambda_{max}(P)}$. Then, for all $t \geq T_d^*$, if $\hat{x}'(t) P \hat{x}(t) \leq \delta_s$ for some $\delta_s > 0$, we can write:

$$\begin{aligned} x'(t)Px(t) &= (\hat{x}(t) + e(t))' P (\hat{x}(t) + e(t)) \\ &= \hat{x}'(t)P\hat{x}(t) + 2\hat{x}'(t)Pe(t) + e'(t)Pe(t) \\ &\leq \delta_s + 2\|P\hat{x}(t)\|\|e(t)\| + \|e(t)\|_P^2 \\ &\leq \delta_s + 2\sqrt{\frac{\lambda_{max}(P^2)\delta_s}{\lambda_{min}(P)}}\, e^* + \lambda_{max}(P) e^{*2} \\ &:= f(\delta_s) \end{aligned} \tag{D.11}$$

Note that $f(\cdot)$ is a continuous, monotonically increasing function of $\delta_s \geq 0$, with $f(0) = \epsilon^2 c_{max} < c_{max}$ and $f(c_{max}) > c_{max}$. This implies that there exists $0 < \delta_s^* < c_{max}$ such that, for all $\delta_s \leq \delta_s^*$, the relation $f(\delta_s) \leq c_{max}$ holds, i.e., $x'(t)Px(t) \leq c_{max}$. This completes the proof of the proposition. $\triangle$

Proof of Theorem 5.3:

Given $x(0) \in \Omega_b$, $\hat{x}(0) \in \Omega_b$, $\beta \geq \beta^*$ (see Proposition 5.2), and $\delta_s \leq \delta_s^*$ (see Proposition 5.3), we consider the following cases:

Case 1: Consider first the case when $T_m = \infty$ (i.e., MPC is never feasible). Then, we have from Eq.5.32 that $i(t) = 1$ and $u(\hat{x}(t)) = b(\hat{x}(t))$ for all $t \geq 0$. It then follows from Proposition 5.2 that the origin of the closed–loop system is asymptotically stable.

Case 2: Now, consider the case when $T_m < \infty$ and $T_f = \infty$. Since $T_m \geq T_d$ and $\|e(T_d)\| \leq e_m$ (see Part 1 of the Proof of Proposition 5.2), we have that $\|e(T_m)\| \leq e_m$. Since only the bounded controller is implemented, i.e. $i(t) = 1$, for $0 \leq t < T_m$, it follows from Proposition 5.1 that $x(t) \in \Omega$ for all $0 \leq t < T_m$ (or that $x(T_m^-) \in \Omega$). This fact, together with the continuity of the solution of the switched closed–loop system – which follows from the fact that the right hand side of Eq.5.30 is continuous in x and piecewise continuous in time since only a finite number of switches is allowed over any finite time interval – implies that, upon switching (instantaneously) to the model predictive controller at $t = T_m$, we have $x(T_m) \in \Omega$. Since $T_f = \infty$, then from the definition of T_f in Theorem 5.3 it follows that $u(\hat{x}(t)) = M_s(\hat{x}(t))$ and $\dot{V}(\hat{x}(t)) < 0$ for all $t \geq T_m$. This implies that $\hat{x}(t) \in \Omega_s$ for all $t \geq T_m$ and, consequently from the definition of T_m (note that $T_m \geq T_d^*$ where T_d^* was defined in Proposition 5.3), that $x(t) \in \Omega$ for all $t \geq T_m$ (i.e., the closed–loop state trajectory is bounded). Furthermore, since $\hat{x}(t) = x(t) - e(t)$ and $\lim_{t\to\infty} \|e(t)\| = 0$, it follows that $\lim_{t\to\infty} \hat{x}'(t)P\hat{x}(t) = 0$; and, hence, $\lim_{t\to\infty} x'(t)Px(t) = 0$. The origin of the switched closed–loop system is therefore asymptotically stable.

Case 3: Finally, consider the case when $T_m < \infty$ and $T_f < \infty$. From the analysis in case 2 above, we have that $x(t) \in \Omega \quad \forall\ 0 \leq t < T_f$ (or that $x(T_f^-) \in \Omega$). This fact, together with the continuity of the solution of the switched closed–loop system, implies that, upon switching (instantaneously) to the bounded controller at $t = T_f$, we have $x(T_f) \in \Omega$ and $u(t) = b(\hat{x}(t))$ for all $t \geq T_f$. We also have $\|e(t)\| \leq e_m$ for all $t \geq T_f$ since $T_f > T_d$. Therefore, from Proposition 5.1 it is guaranteed that $x(t) \in \Omega$ for all $t \geq T_f$. Finally, following the same arguments presented in Part 2 of the Proof

of Proposition 5.2, it can be shown that $\|x(t)\| \to 0$ as $t \to \infty$, which together with boundedness of the state trajectory, establishes asymptotic stability of the origin of the closed–loop system. This completes the proof of the theorem. $\triangle$

Appendix E

Proofs of Chapter 6

Proof of Theorem 6.1:

Step 1: Substituting the control law of Eqs.6.3-6.4 into the system of Eq.6.1 and evaluating the time-derivative of the Lyapunov function along the trajectories of the closed–loop system, it can be shown that $\dot{V}_k < 0$ for all $x \in \Phi_k(u_{max})$ (where $\Phi_k(u_{max})$ was defined in Eq.6.5). Since $\Omega_k(u_{max})$ (defined in Eq.6.6) is an invariant subset of $\Phi_k(u_{max}) \bigcup \{0\}$, it follows that for any $x(0) \in \Omega_k(u_{max})$, the origin of the closed–loop system, under the control law of Eqs.6.3-6.4, is asymptotically stable.

Step 2: Consider the switched closed–loop system of Eq.6.12, subject to the switching rule of Eqs.6.13-6.14, with any initial state $x(0) \in \Omega_k(u_{max})$. From the definition of $\bar{T}$ given in Theorem 6.1, it is clear that if $\bar{T}$ is a finite number, then $\dot{V}_k(x^M(t)) < 0 \quad \forall\ 0 \leq t < \bar{T}$, where the notation $x^M(t)$ denotes the closed–loop state under MPC at time t, which implies that $x(t) \in \Omega_k(u_{max}) \quad \forall\ 0 \leq t < \bar{T}$ (or that $x(\bar{T}^-) \in p\Omega_k(u_{max})$). This fact, together with the continuity of the solution of the switched system, $x(t)$, (following from the fact that the right hand side of Eq.6.12 is continuous in x and piecewise continuous in time) implies that, upon switching (instantaneously) to the bounded controller at $t = \bar{T}$, we have $x(\bar{T}) \in \Omega_k(u_{max})$ and $u(t) = b_k(x(t))$ for all $t \geq \bar{T}$. Therefore, from our analysis in Step 1, we conclude that $\dot{V}_k(x^{b_k}(t)) < 0 \quad \forall\ t \geq \bar{T}$. In summary, the

switching rule of Eqs.6.13-6.14 guarantees that, starting from any $x(0) \in \Omega_k(u_{max})$, $\dot{V}_k(x(t)) < 0 \ \forall \ x \neq 0, \ x \in \Omega_k(u_{max}), \ \forall \ t \geq 0$, which implies that the origin of the switched closed–loop system is asymptotically stable. Note that if no such $\bar{T}$ exists, then we simply have from Eqs.6.13-6.14 that $\dot{V}_k(x^M(t)) < 0 \ \forall \ t \geq 0$, and the origin of the closed–loop system is also asymptotically stable. This completes the proof of the theorem. Δ

Proof of Theorem 6.2:

The proof of this theorem, for the case when only one bounded controller is used as the fall–back controller (i.e., $p = 1$), is same as that of Theorem 6.1. To simplify the proof, we prove the result only for the case when the family of fall–back controllers consists of 2 controllers (i.e., $p = 2$). Generalization of the proof to the case of a family of p controllers, where $2 < p < \infty$, is conceptually straightforward. Also, without loss of generality, we consider the case when the optimization problem in MPC is feasible for all times (i.e., $T^i = \infty$), since if it is not (i.e., $T^i < \infty$), then the switching time is simply taken to be the minimum of $\{T^i, T^f\}$, as stated in Theorem 6.2.

Without loss of generality, let the closed–loop system be initialized within the stability region of the first bounded controller, $\Omega_1(u_{max})$, under MPC. Then one of the following scenarios will take place:

Case 1: $\dot{V}_1(x^M(t)) < 0$ for all $t \geq 0$. The switching law of Eqs.6.15-6.17 dictates in this case that MPC be implemented for all times. Since $x(0) \in \Omega_1(u_{max})$, where Ω_1 is a level set of V_1, and $\dot{V}_1 < 0$, then the state of the closed–loop system is bounded and converges to the origin as $t \rightarrow \infty$.

Case 2: $\dot{V}_1(x^M(T_1)) \geq 0$ and $x^M(T_1) \in \Omega_1(u_{max})$, for some finite $T_1 > 0$. In this case, one of the following scenarios will occur:

(a) If $x(T_1)$ is outside of $\Omega_2(u_{max})$, then it follows from Eqs.6.15-6.17 that the supervisor will set $T^* = T_f = T_1$ and switch to the first bounded controller at $t = T_1$,

using V_1 as the CLF, which enforces asymptotic stability as discussed in step 2 of the proof of Theorem 6.1.

(b) If $x(T_1) \in \Omega_2(u_{max})$ and $\dot{V}_2(x(T_1)) < 0$ (i.e., $0 < T_1 < T_2$), then the supervisor will keep MPC in the closed–loop system at T_1. If T_2 is a finite number, then the supervisor will set $T^* = T_f = T_2$ (since $T_1^* = 0$ for all $t > T_1$ from Eq.6.16) at which time it will switch to the second bounded controller, using V_2 as the CLF. Since $\dot{V}_2(x^M(t)) < 0$ for all $T_1 \leq t < T_2$, and $x(T_1) \in \Omega_2(u_{max})$, then $x(T^{*^-}) \in \Omega_2(u_{max})$. By continuity of the solution of the closed–loop system, it follows that $x(T^*) \in \Omega_2(u_{max})$; and since $\Omega_2(u_{max})$ is the stability region corresponding to V_2, then implies that upon implementation of the corresponding bounded controller for all future times, asymptotic stability is achieved. Note that if T_2 does not exist (or $T_2 = \infty$), then we simply have $x(T_1) \in \Omega_2(u_{max})$ and $\dot{V}_2(x(T_1)) < 0$ for all $t \geq T_1$, which implies that the origin of the closed–loop system is again asymptotically stable.

(c) If $0 < T_2 < T_1$ (i.e., $x(T_2) \in \Omega_2(u_{max})$, $V_1(x(T_2)) < 0$ and $V_2(x(T_2)) \geq 0$), then it follows from Eqs.6.15-6.17 that the supervisor will set $T^* = T_f = T_1$ (since $T_2^* = 0$ for all $t > T_2$ from Eq.6.16) and switch to the first bounded controller, using V_1 as the CLF. Since $\dot{V}_1(x^M(t)) < 0$ for all $t < T_1$, and $x(0) \in \Omega_1(u_{max})$, then $x(T^{*^-}) \in \Omega_1(u_{max})$. By continuity of the solution of the closed–loop system, we have $x(T^*) \in \Omega_1(u_{max})$, and since $\Omega_1(u_{max})$ is the stability region corresponding to V_1, this implies that upon implementation of the first bounded controller for the remaining time, asymptotic closed–loop stability is achieved. This completes the proof of the theorem. $\triangle$

Proof of Theorem 6.3: The proof draws upon the fact that if the state of the closed–loop system resides in Ω at the time that the bounded controller is switched in, i.e., $x(T_{switch}) \in \Omega$, then boundedness of closed–loop state, and convergence to the set $\mathbb{D}$ under the bounded robust controller are guaranteed (for a proof, see [94, 95]). Therefore, we need only show that, under the switching scheme of Eqs.6.34–6.36, the closed–loop state is always within Ω at the time the bounded controller is switched

in. For this purpose, we enumerate the four possible values that T_{switch} could take, and show that $x(T_{switch}) \in \Omega$ in all cases.

- Case 1: If $T_{switch} = T_s$, then from the definition of T_s in Eq.6.34, $x(T_s^-) \in \Omega$. By continuity of the solution of the system of Eq.6.24 (which follows from the fact that the right hand side of Eq.6.33 is continuous in x and piecewise continuous in time, since only a finite number of switches is allowed), we have $x(T_s) \in \Omega$, i.e., $x(T_{switch}) \in \Omega$.

- Case 2: If $T_{switch} = T_D$, then from the definition of T_D in Eq.6.35, $x(T_D) \in \mathbb{ID} \subset \Omega$; hence $x(T_{switch}) \in \mathbb{ID} \subset \Omega$.

- Case 3: If $T_{switch} = T_{design}$, then from the definition of T_{switch}, $T_{design} \leq T_s$. To prove that $x(T_{design}) \in \Omega$, we proceed by contradiction. Assume $x(T_{design}) \notin \Omega$. Then $V(x(T_{design})) > c^{max}$ (from the definition of Ω). By continuity of the solution, continuity of $V(\cdot)$ and the fact that $V(x_0) \leq c^{max}$, there exists a time $0 \leq T_s' \leq T_{design}$ for which $V(x(T_s'^-)) = c^{max}$. Since T_s is the *earliest* time for which Eq.6.34 holds, then it must be that $T_s \leq T_s' \leq T_{design}$, which leads to a contradiction ($T_{design} \leq T_s$). Therefore, once again, $x(T_{switch}) \in \Omega$.

- Case 4: If $T_{switch} = T_{inf}$, the same argument as in Case 3 can be used (replacing T_{design} by T_{inf}) to show that $x(T_{switch}) \in \Omega$.

This completes the proof of the theorem, $\triangle$

Proof of Theorem 6.4: Similar to the proof of Theorem 6.3, the proof of this theorem also draws upon the fact that if the state of the closed–loop system resides in Ω_L^0 at the time that the f^{th} bounded controller, for which $x(T_{switch}) \in \Omega_f^0$, is switched in (and kept in the closed–loop for all future times), then under the bounded robust controller f, the region Ω_f^0 is invariant (for a proof, see [94, 95]), and since $\Omega_f^0 \subset \Omega_L^0$, the closed–loop state evolves in Ω_L^0 for all future times.

We now show that for $t \leq T_{switch}$ (i.e., up until the time that the switching between the controllers is governed by Eqs.6.39-6.40), the closed–loop state, initialized within Ω_L^0, stays within Ω_L^0. We only need to show that the switching logic ensures that the bounded controller is switched in before the states have escaped Ω_L^0 under MPC. To this end, we first note that $c_{k,j}^{max} < c_{k,0}^{max}$, for all $k = 1, \cdots, l$. Therefore $\Omega_L^j \subset \Omega_L^0$. This implies that if $x \in \Omega_L^j$ then $x \in \Omega_L^0$.

Consider any time, t, when $T_j \leq t < T_{j+1} < T_{switch}$, for some $j \geq 1$. Between T_j and T_{j+1}, we have from Eq.6.40 that MPC is switched in (and the bounded controller is switched out) only when $x(t) \in \Omega_L^j$. Now consider the time T_{j+1} at which time the bounded controller is switched back in, either due to Eq.6.39 or because MPC is infeasible. In the first case, $x(T_{j+1}) \in \Omega_L^j \subset \Omega_L^0$. In the second case, since the right hand side of the equation 6.37 is a piecewise continuous function of time and a continuous function of its states, and the closed–loop system is initialized within Ω_L^j under MPC, any time the MPC optimization problem is infeasible, $x(t) \in \Omega_L^j \subset \Omega_L^0$.

At the time $t = T_{switch}$, the state of the closed–loop system can be shown to be within Ω_L^0 following the same line of reasoning used in the proof of Theorem 6.3, with the additional possibility of $T_{switch} = T_N$. As shown above, $x(t) \in \Omega_L^0$ for all $T_{j-1} \leq t \leq T_j$, and therefore $x \in \Omega_L^0$ for $T_{N-1} \leq t \leq T_N$ and therefore $x(T_N) \in \Omega_L^0$ implying once again that $x(T_{switch}) \in \Omega_L^0$.

For all $t \geq T_{switch}$, the closed–loop state evolves under some bounded controller $u(x) = b_k(x)$, for which $x(T_{switch}) \in \Omega_k^0$. Therefore, $\limsup_{t \to \infty} \|x(t)\| \leq d_k$ (see [94, 95] for the proof). Note that since d^{max} is chosen to be the largest of d_k, $k = 1, \cdots, l$, $\|x(t)\| \leq d_k$ implies $\|x(t)\| \leq d^{max}$; hence $\limsup_{t \to \infty} \|x(t)\| \leq d^{max}$. This completes the proof of Theorem 6.4. $\triangle$

Appendix F

Proofs of Chapter 7

Proof of Theorem 7.1:

To prove this theorem, we proceed in two steps. In the first step we show that, for each individual mode (without switching), the control law of Eqs.7.7-7.8 satisfies the constraints within the region described by Eq.7.10 and that, starting from any initial condition within the set, Ω_i^*, the corresponding feedback control law robustly asymptotically stabilizes the origin of the i-th closed-loop subsystem. In the second step, we use this fact together with MLF stability analysis to show that the switching laws of Eqs.7.11-7.12 enforce asymptotic stability in the switched uncertain closed-loop system, starting from any initial condition that belongs to any of the sets, Ω_i^*, $i \in \mathcal{I}$.

Step 1: To prove that the control law of Eqs.7.7-7.8 satisfies the constraints within the region described by the inequality of Eq.7.10, we need consider only the case when $\|(L_{G_i}V_i)^T\| \neq 0$ (since when $\|(L_{G_i}V_i)^T\| = 0$, $u_i = 0$ and the constraints are trivially satisfied). For this case, we have from Eqs.7.7-7.8:

$$\begin{aligned} \|u_i(x)\| &\leq \|k_i(V_i, u_i^{max}, \theta_{bi}, \chi_i, \phi_i)\| \left\|(L_{G_i}V_i)^T\right\| \\ &\leq \frac{\left\|L_{f_i}^* V_i + \sqrt{\left(L_{f_i}^{**}V_i\right)^2 + \left(u_i^{max}\|(L_{G_i}V)^T\|\right)^4}\right\|}{\left\|(L_{G_i}V_i)^T\right\|\left[1+\sqrt{1+\left(u_i^{max}\|(L_{G_i}V_i)^T\|\right)^2}\right]} \end{aligned} \tag{F.1}$$

From the definitions of $L_{f_i}^{*}V_i$ and $L_{f_i}^{**}V_i$ in Eq.7.9 and the fact that $\rho > 0$, it is clear that if $L_{f_i}^{**}V_i \leq u_i^{max}\left\|(L_{G_i}V_i)^T\right\|$, then we also have $L_{f_i}^{*}V_i \leq u_i^{max}\left\|(L_{G_i}V_i)^T\right\|$. Therefore, for any x satisfying Eq.7.10, the following estimates hold:

$$\begin{aligned}\left(L_{f_i}^{**}V_i\right)^2 &\leq \left(u_i^{max}\left\|(L_{G_i}V_i)^T\right\|\right)^2 \\ L_{f_i}^{*}V_i &\leq u_i^{max}\left\|(L_{G_i}V_i)^T\right\|\end{aligned} \tag{F.2}$$

Substituting the above estimates into Eq.F.1 yields:

$$\|u_i(x)\| \leq \frac{u_i^{max}\left\|(L_{G_i}V_i)^T\right\|\left[1+\sqrt{1+(u_i^{max}\|(L_{G_i}V_i)^T\|)^2}\right]}{\left\|(L_{G_i}V_i)^T\right\|\left[1+\sqrt{1+(u_i^{max}\|(L_{G_i}V_i)^T\|)^2}\right]} = u_i^{max} \tag{F.3}$$

which shows that the constraints are satisfied. Consider now the i-th subsystem of the switched nonlinear system of Eq.7.1. Substituting the control law of Eqs.7.7-7.9, evaluating the time-derivative of the Lyapunov function along the closed-loop trajectories, and using the fact that $\|(L_{G_i}V_i)^T\|^2 = (L_{G_i}V_i)(L_{G_i}V_i)^T$, we obtain:

$$\begin{aligned}\dot{V}_i &= L_{f_i}V_i + L_{G_i}V_i u_i + L_{W_i}V_i\theta_i \\ &\leq L_{f_i}V_i + \chi_i\|\left(L_{W_i}V_i\right)^T\|\theta_{bi} - \left(\frac{L_{f_i}^{*}V_i + \sqrt{(L_{f_i}^{**}V_i)^2 + (u_i^{max}\|(L_{G_i}V_i)^T\|)^4}}{\|(L_{G_i}V_i)^T\|^2\left[1+\sqrt{1+(u_i^{max}\|(L_{G_i}V_i)^T\|)^2}\right]}\right)\end{aligned} \tag{F.4}$$

After performing some algebraic manipulations, the above inequality can be re-written as:

$$\dot{V}_i \leq \alpha_i(x) + \left(\frac{\theta_{bi}\left\|(L_{W_i}V_i)^T\right\|\left(\frac{\phi_i - (\chi-1)\|x\|}{\|x\|+\phi_i}\right) - \rho_i\left(\frac{\|x\|^2}{\|x\|+\phi_i}\right)}{\left[1+\sqrt{1+(u_i^{max}\|(L_{G_i}V_i)^T\|)^2}\right]}\right) \tag{F.5}$$

where

$$\begin{aligned}\alpha_i(x) &= \left(\frac{\left(L_{f_i}V_i + \chi_i\theta_{bi}\left\|(L_{W_i}V_i)^T\right\|\right)\sqrt{1+(u_i^{max}\|(L_{G_i}V_i)^T\|)^2}}{\left[1+\sqrt{1+(u_i^{max}\|(L_{G_i}V_i)^T\|)^2}\right]}\right) \\ &\quad - \left(\frac{-\sqrt{\left(L_{f_i}^{**}V_i\right)^2 + (u_i^{max}\|(L_{G_i}V_i)^T\|)^4}}{\left[1+\sqrt{1+(u_i^{max}\|(L_{G_i}V_i)^T\|)^2}\right]}\right)\end{aligned} \tag{F.6}$$

To analyze the sign of $\dot{V}_i$ in Eq.F.5, we initially study the sign of the term, $\alpha_i(x)$, on the right-hand side. It is clear that the sign of this term depends on the sign of the term $L_{f_i}V_i + \chi_i \left\|(L_{W_i}V_i)^T\right\| \theta_{bi}$. To this end, we consider the following two cases:

Case 1: $L_{f_i}^{**}V_i \leq 0$

Since $L_{f_i}^{**}V_i = L_{f_i}V_i + \rho_i \|x\| + \chi_i\| (L_{W_i}V_i)^T \|\theta_{bi}$ and ρ_i is a positive real number, the fact that $L_{f_i}^{**}V_i \leq 0$ implies that $L_{f_i}V_i + \chi_i \|L_{W_i}V_i\| \theta_{bi} \leq 0$. As a result, we have that $\alpha_i(x) \leq 0$ and the time-derivative of V_i in this case satisfies the following bound:

$$\dot{V}_i \leq \left(\frac{\left\|(L_{W_i}V_i)^T\right\| \theta_{bi} \left(\frac{\phi_i - (\chi_i - 1)\|x\|}{\|x\| + \phi_i} \right) - \rho_i \left(\frac{\|x\|^2}{\|x\| + \phi_i} \right)}{\left[1 + \sqrt{1 + (u_i^{max}\|(L_{G_i}V_i)^T\|)^2}\right]} \right) := \beta_i(x) \qquad \text{(F.7)}$$

Case 2: $0 < L_{f_i}^{**}V_i \leq u_i^{max} \left\|(L_{G_i}V_i)^T\right\|$

In this case, we have:

$$\left(L_{f_i}^{**}V_i\right)^2 \leq \left(u_i^{max}\|(L_{G_i}V_i)^T\|\right)^2 \qquad \text{(F.8)}$$

and therefore:

$$\begin{aligned} & - \sqrt{\left(L_{f_i}^{**}V_i\right)^2 + (u_i^{max}\|(L_{G_i}V_i)^T\|)^4} \\ = & -\sqrt{\left(L_{f_i}^{**}V_i\right)^2 + (u_i^{max}\|(L_{G_i}V_i)^T\|)^2 (u_i^{max}\|(L_{G_i}V_i)^T\|)^2} \qquad \text{(F.9)} \\ \leq & -\left(L_{f_i}^{**}V_i\right) \sqrt{1 + (u_i^{max}\|(L_{G_i}V_i)^T\|)^2} \end{aligned}$$

Substituting the estimate of Eq.F.9 in the expression for $\dot{V}_i$ in Eqs.F.5-F.6 yields:

$$\begin{aligned} \dot{V}_i &= \frac{-\rho_i\|x\|\sqrt{1 + (u_i^{max}\|(L_{G_i}V_i)^T\|)^2}}{\left[1 + \sqrt{1 + (u_i^{max}\|(L_{G_i}V_i)^T\|)^2}\right]} + \beta_i(x) \qquad \text{(F.10)} \\ &\leq \beta_i(x) \end{aligned}$$

From the above analysis, it is clear that whenever $L_{f_i}^{**}V_i \leq u_i^{max}\|(L_{G_i}V_i)^T\|$, the inequality of Eq.F.7 holds. Since $\Omega_i^*(u_i^{max}, \theta_{bi})$ is taken to be the largest invariant set

embedded within the region described by Eq.7.10, we have that starting from any $x(0) \in \Omega_i^*$, the inequality of Eq.F.7 holds. Referring to this inequality, note that since $\chi_i > 1$ and $\rho_i > 0$, it is clear that, whenever $\|x\| > \dfrac{\phi_i}{\chi_i - 1}$, the first term on the right-hand side is strictly negative, and therefore $\dot{V}_i$ satisfies:

$$\dot{V}_i \leq -\frac{\rho_i \|x\|^2}{(\|x\| + \phi_i)\left[1 + \sqrt{1 + (u_i^{max}\|(L_{G_i}V_i)^T\|)^2}\right]} \tag{F.11}$$

To study the behavior of $\dot{V}_i$ when $\|x\| <\leq \phi_i/(\chi_i - 1)$, we first note that since the entries of the matrix function, $W_i(x)$, and the entries of the row vector, $\nabla_x V_i$, are smooth and vanish when $x = 0$, then there exists positive real constants, ϕ_i^1, δ_i and δ_i', such that if $\phi_i \leq \phi_i^1$, the bounds $\|W_i(x)\| \leq \delta_i\|x\|$, $\|\nabla_x^T V_i\| \leq \delta_i'\|x\|$ hold for $\|x\| \leq \phi_i/(\chi_i - 1)$. Using this bound, we obtain the following estimates:

$$\begin{aligned}
\left\|(L_{W_i}V_i)^T\right\| \theta_{bi}\left(\phi_i - (\chi_i - 1)\|x\|\right) &\leq \left\|(L_{W_i}V_i)^T\right\| \theta_{bi}\phi_i \\
&= \|W_i(x)\| \left\|\nabla_x^T V_i\right\| \theta_{bi}\phi_i \\
&\leq \phi_i\theta_{bi}\delta_i\delta_i'\|x\|^2 \qquad \forall \ \|x\| \leq \frac{\phi_i}{\chi_i - 1}
\end{aligned} \tag{F.12}$$

Substituting the estimate of Eq.F.12 directly into Eq.F.7, we get:

$$\dot{V}_i \leq \left(\frac{(\phi_i\theta_{bi}\delta_i\delta_i' - \rho_i)\|x\|^2}{(\|x\| + \phi_i)\left[1 + \sqrt{1 + (u_i^{max}\|(L_{G_i}V_i)^T\|)^2}\right]}\right) \qquad \forall \ \|x\| \leq \frac{\phi_i}{\chi_i - 1} \tag{F.13}$$

If ϕ_i is sufficiently small to satisfy the bound $\phi_i \leq \dfrac{\rho_i}{\theta_{bi}\delta_i\delta_i'} := \phi_i^2$, then it is clear from Eqs.F.11-F.13 that the inequality in Eq.F.11 is satisfied, irrespective of the value of $\|x\|$. In summary, we have that for any initial condition in the invariant set, Ω_i^*, there exists $\phi_i^* := \min\{\phi_i^1, \phi_i^2\}$ such that if $\phi_i \leq \phi_i^*$, $\dot{V}_i$ satisfies:

$$\dot{V} \leq \frac{-\rho_i \|x\|^2}{(\|x\| + \phi_i)\left[1 + \sqrt{1 + (u_i^{max}\|(L_{G_i}V_i)^T\|)^2}\right]} < 0 \quad \forall\, x \neq 0, \ \ i = 1, \cdots, N \tag{F.14}$$

which implies that the origin of the individual closed-loop subsystems are asymptotically stable.

Step 2: Consider now the switched closed-loop system and, without loss of generality, suppose that $x(0) \in \Omega_i^*$ for some $i \in \mathcal{I}$. Then it follows from Eq.F.14 above and the invariance of Ω_i^* that the Lyapunov function for this mode, V_i, decays monotonically, along the trajectories of the closed-loop system, for as long as mode i is to remain active, i.e., for all times such that $\sigma(t) = i$. If at any time T, such that $x(T) \in \Omega_j^*$ for some $j \in \mathcal{I}$, $j \neq i$, we set $\sigma(T^+) = j$ (i.e., activate mode j and its respective controller), then using the same argument, it is clear that the corresponding Lyapunov function for this mode, V_j, will also decay monotonically for as long as we keep $\sigma(t) = j$. Note that T, which is the time that mode i is switched out, is not known a priori but is rather determined by the evolution of the closed-loop continuous state. By tracking the closed-loop trajectory in this manner, we conclude that, starting from any $x(0) \in \Omega_i^*$ for any $i \in \mathcal{I}$ and as long as the i-th mode (and its controller) is activated only at a time when $x(t) \in \Omega_i^*$, we have that for all $i \in \mathcal{I}$, $k \in Z_+$:

$$\dot{V}_{\sigma(t_{i_k})} < 0 \quad \forall\ t \in [t_{i_k}, t_{i'_k}) \tag{F.15}$$

where t_{i_k} and $t_{i'_k}$ refer, respectively, to the times that the i-th mode is switched in and out for the k-th time, by the supervisor. Furthermore, from Eq.7.12, we have that for any admissible switching time, t_{i_k}:

$$V_i(x(t_{i_k})) < V_i(x(t_{i'_{k-1}})) \tag{F.16}$$

which consequently implies that:

$$V_i(x(t_{i_k})) < V_i(x(t_{i_{k-1}})) \tag{F.17}$$

since $V_i(x(t_{i'_{k-1}})) < V_i(x(t_{i_{k-1}}))$ from Eq.F.15. Using Eqs.F.15-F.17, a direct application of the MLF result of Theorem 2.3 in [44] can be performed to conclude that the switched closed-loop system, under the switching laws of Theorem 7.1, is Lyapunov

stable. To prove asymptotic stability, we note that Eq.F.16 also implies:

$$V_i(x(t_{i'_k})) \;<\; V_i(x(t_{i'_{k-1}})) \tag{F.18}$$

since $V_i(x(t_{i'_k})) < V_i(x(t_{i_k}))$ from Eq.F.15. From the strict inequality in Eq.F.18, it follows that for every (infinite) sequence of switching times, $t_{i'_1}, t_{i'_2}, \cdots$, such that $\sigma(t^+_{i_k}) = \sigma(t^-_{i'_k}) = i$, the sequence $V_{\sigma(t^-_{i'_1})}, V_{\sigma(t^-_{i'_2})}, \cdots$ is decreasing and positive, and therefore has a limit $L \geq 0$. We have:

$$\begin{aligned} 0 \;&=\; L - L = \lim_{k\to\infty} V_{\sigma(t^-_{i'_{k+1}})}(x(t_{i'_{k+1}})) - \lim_{k\to\infty} V_{\sigma(t^-_{i'_k})}(x(t_{i'_k})) \\ &=\; \lim_{k\to\infty} \left[V_i(x(t_{i'_{k+1}})) - V_i(x(t_{i'_k}))\right] \end{aligned} \tag{F.19}$$

Note that the term in brackets in the above equation is strictly negative for all nonzero x and zero only when $x = 0$ (from Eq.F.18) . Therefore, there exists a function α of class $\mathcal{K}$ (i.e., continuous, increasing, and zero at zero) such that:

$$\left[V_i(x(t_{i'_{k+1}})) - V_i(x(t_{i'_k}))\right] \;\leq\; -\alpha(\|x(t_{i'_k})\|) \tag{F.20}$$

Substituting the above estimate into Eq.F.19, we have:

$$\begin{aligned} 0 \;&=\; \lim_{k\to\infty} \left[V_i(x(t_{i'_{k+1}})) - V_i(x(t_{i'_k}))\right] \\ &\leq\; \lim_{k\to\infty} \left[-\alpha(\|x(t_{i'_k})\|)\right] \leq 0 \end{aligned} \tag{F.21}$$

which implies that $x(t)$ converges to the origin. This fact, together with Lyapunov stability, implies that the origin of the switched closed-loop system is asymptotically stable. This concludes the proof of the theorem. △

Proof of Theorem 7.2:

The proof of this theorem shares several steps with the Proof of Theorem 7.1. We will highlight only the differences.

Step 1: We have already shown in Step 1 of the Proof of Theorem 7.1 that, for each mode considered separately, the evolution of the corresponding Lyapunov function,

starting from any $x(0) \in \Omega_i^*$, obeys the growth bound of Eq.F.11 whenever $\|x\| \geq \frac{\phi_i}{\chi_i - 1}$. Since the uncertain variables are non-vanishing, the bounds used in Eq.F.12 to establish asymptotic convergence to the origin cannot be invoked here and no further conclusion can be made regarding the sign of $\dot{V}_i$ when $\|x\| < \frac{\phi_i}{\chi_i - 1}$. However, from Eq.F.11, we conclude that $\dot{V}_i$ is negative-definite outside a ball of radius $\epsilon_i = \phi_i/(\chi_i - 1)$, which implies (see Theorem 5.1 and its corollaries in [170]) that, for any $x(0) \in \Omega_i^*$, there exists a finite time t_1 such that the solution to the i-th closed-loop system satisfies:

$$\begin{aligned} \|x(t)\| &\leq \beta_i(\|x_0\|, t), \quad \forall\, 0 \leq t < t_1 \\ \|x(t)\| &\leq b_i(\epsilon_i), \quad \forall\, t \geq t_1 \end{aligned} \tag{F.22}$$

where $\beta_i(\cdot,\cdot)$ is a class $\mathcal{KL}$ function and $b_i(\cdot)$ is of class $\mathcal{K}_\infty$. This implies that the state is ultimately bounded and that the ultimate bound can be made arbitrarily small by choosing ϵ_i to be sufficiently small.

Step 2: Having established boundedness of the trajectory of the individual closed-loop modes of the hybrid system, we proceed in this step to show boundedness of the overall switched closed-loop trajectory. To this end, given any positive real number, d, it follows from the properties of class $\mathcal{K}_\infty$ functions that there exist a set of positive real numbers, $\{\epsilon_1^*, \epsilon_2^*, \cdots, \epsilon_N^*\}$, such that:

$$b_1(\epsilon_1^*) = b_2(\epsilon_2^*) = \cdots = b_N(\epsilon_N^*) \leq d \tag{F.23}$$

where $\epsilon_i^* \geq \epsilon_i$, $\forall\, i \in \mathcal{I}$, which ensures that all modes share a common residual set. Since switching occurs only in regions where the various stability regions intersect (as required by Eq.7.11), we need consider only the case when the intersection, $\bigcap_i \Omega_i^*$, is nonempty and choose d such that the set $D = \{x \in \mathbb{R}^n : \|x\| \leq d\} \subset \bigcap_i \Omega_i^*$, $i = 1, \cdots, N$.

Without loss of generality, assume that $x(0) \in \Omega_i^*$ for some $i \in \mathcal{I}$. If this mode remains active for all times, then boundedness follows directly from the analysis in Step 1 above. If switching takes place, however, then it follows from the switching rules

of Eqs.7.11-7.12 that for every admissible sequence of switching times, $t_{i_1}, t_{i_2}, \cdots$, such that $\sigma(t_{i_k}^+) = i$ and $\|x(t_{i_k})\| > d$, the positive sequence $V_{\sigma(t_{i_1})}, V_{\sigma(t_{i_2})}, \cdots$ is monotonically decreasing. This, together with the fact that the set D is non-empty and completely contained within Ω_i^*, implies the existence of a finite k^* such that $\|x(t_{i_k})\| \leq d$ for some $k \geq k^*$, $k \in Z_+$. Since N is finite, and only a finite number of switches are allowed over any finite time-interval, the preceding analysis implies that, if $\epsilon_i \leq \epsilon_i^*$, $\forall\, i \in \mathcal{I}$, there exists finite time, $t' > 0$, during which (at least) one of the modes will converge to D. Since D was chosen to be a common residual set for all the modes (Eq.F.23), it follows that $\|x(t)\| \leq d$ for all $t \geq t'$, regardless of which mode is switched in or out for $t \geq t'$. Therefore, the switched closed-loop trajectory is bounded for all times. This concludes the proof of the theorem. $\triangle$

Appendix G

Proofs of Chapter 11

Proof of Theorem 11.1 :

Consider the representation of the system of Eq.11.12 in the form of Eqs.11.20-11.21. Under the controller of Eq.11.28, the closed-loop system takes the following form

$$\begin{aligned}
\frac{d\omega}{dt} &= \tilde{f}(\omega) - \frac{1}{2}\tilde{g}(\omega)R^{-1}(\omega)I\left(L_{\bar{g}}V(\omega)\right)^T + L(y - \tilde{h}(\omega)) \\
\dot{e} &= Ae + B\left[l_1(e,\eta,\bar{v}) - \frac{1}{2}C(\tilde{x})R^{-1}(\omega)I\left(L_{\bar{g}}V(\omega)\right)^T\right] \\
\dot{\eta}_1 &= \Psi_1(\zeta,\eta) \\
&\vdots \\
\dot{\eta}_{(n+N)-\sum_i r_i} &= \Psi_{(n+N)-\sum_i r_i}(\zeta,\eta) \\
y_{si} &= \zeta_1^{(i)}, \quad i = 1,\ldots,m
\end{aligned} \tag{G.1}$$

Defining the observer error vector, $e_o = \omega - \tilde{x}$, using the assumption $C_L = \frac{1}{\mu}\bar{A}$ where $\bar{A}$ is a Hurwitz matrix, and multiplying the $\dot{e}_o$-subsystem by μ, the system of Eq.G.1

can be written as:

$$\begin{aligned}
\mu\frac{de_o}{dt} &= \bar{A}e_o + \mu\hat{f}(\omega,\tilde{x},v) \\
\dot{e} &= Ae + B\left[l_1(e,\eta,\bar{v}) - \frac{1}{2}C(\tilde{x})R^{-1}(\omega)I\left(L_{\bar{g}}V(\omega)\right)^T\right] \\
\dot{\eta}_1 &= \Psi_1(\zeta,\eta) \\
&\vdots \\
\dot{\eta}_{(n+N)-\sum_i r_i} &= \Psi_{(n+N)-\sum_i r_i}(\zeta,\eta) \\
y_{si} &= \zeta_1^{(i)},\ \ i=1,\ldots,m
\end{aligned} \tag{G.2}$$

where $\hat{f}(\omega,\tilde{x},v)$ is a nonlinear vector function. The above system is in singularly perturbed form (see [170] for details) and possesses an exponentially stable fast subsystem: $\frac{de_o}{d\tau} = \bar{A}e_o$, where $\tau = t/\mu$, and a slow subsystem that has the form:

$$\begin{aligned}
\dot{e} &= Ae + B\left[l_1(e,\eta,\bar{v}) - \frac{1}{2}C(\tilde{x})R^{-1}(\tilde{x})I\left(L_{\bar{g}}V(\tilde{x})\right)^T\right] \\
\dot{\eta}_1 &= \Psi_1(\zeta,\eta) \\
&\vdots \\
\dot{\eta}_{(n+N)-\sum_i r_i} &= \Psi_{(n+N)-\sum_i r_i}(\zeta,\eta) \\
y_{si} &= \zeta_1^{(i)},\ \ i=1,\ldots,m
\end{aligned} \tag{G.3}$$

Consider now the Lyapunov function candidate, $V = e^TPe$, introduced in Theorem 11.1. Evaluating the time-derivative of this function along the trajectories of the closed-loop slow e-subsystem in Eq.G.3, we obtain:

$$\begin{aligned}
\dot{V} &= L_{\bar{f}}V + L_{\bar{g}}Vu \\
&= L_{\bar{f}}V - L_{\bar{g}}V\frac{L_{\bar{f}}^*V + \sqrt{(L_{\bar{f}}^*V)^2 + \left(u_{max}^2(L_{\bar{g}}V)(L_{\bar{g}}V)^T\right)^2}}{(L_{\bar{g}}V)(L_{\bar{g}}V)^T\left[1+\sqrt{1+u_{max}^2(L_{\bar{g}}V)(L_{\bar{g}}V)^T}\right]}(L_{\bar{g}}V)^T \\
&= \frac{-\rho|e|^2 + L_{\bar{f}}V\sqrt{1+u_{max}^2(L_{\bar{g}}V)(L_{\bar{g}}V)^T} - \sqrt{(L_{\bar{f}}^*V)^2 + \left(u_{max}^2(L_{\bar{g}}V)(L_{\bar{g}}V)^T\right)^2}}{\left[1+\sqrt{1+u_{max}^2(L_{\bar{g}}V)(L_{\bar{g}}V)^T}\right]}
\end{aligned} \tag{G.4}$$

It is clear from the above equation and the fact that $\rho > 0$ that whenever $L_{\bar{f}}^{*}V \leq 0$, we have $L_{\bar{f}}V \leq 0$ and the time-derivative of V satisfies:

$$\dot{V} \leq \frac{-\rho|e|^2}{\left[1+\sqrt{1+u_{max}^2(L_{\bar{g}}V)(L_{\bar{g}}V)^T}\right]} < 0 \quad \forall \ e \neq 0 \tag{G.5}$$

Furthermore, whenever $0 < L_{\bar{f}}^{*}V \leq u_{max}|(L_{\bar{g}}V)^T|$, we have:

$$\sqrt{(L_{\bar{f}}^{*}V)^2 + \left(u_{max}^2(L_{\bar{g}}V)(L_{\bar{g}}V)^T\right)^2} \geq L_{\bar{f}}V\sqrt{1+u_{max}^2(L_{\bar{g}}V)(L_{\bar{g}}V)^T}$$

and $\dot{V}$ satisfies Eq.G.5. Summarizing, we have that whenever $L_{\bar{f}}^{*}V \leq u_{max}|(L_{\bar{g}}V)^T|$, the origin of the closed-loop slow e-subsystem is asymptotically stable. Therefore, given any positive real number, δ_x, such that $|\tilde{x}(0)| \leq \delta_x$ (and Eq.11.27 holds for all $|\tilde{x}| \leq \delta_x$), there exists a positive real number, M, such that $|\tilde{x}(t)| \leq M \ \forall \ t \geq 0$ (i.e., the closed-loop trajectories are bounded) and, consequently, the denominator expression in Eq.G.5 is bounded. It follows then that there exists a positive real number, k_1, such that $\dot{V} \leq -k_1|e|^2$ and the origin of the closed-loop slow e-subsystem is exponentially stable. Therefore, the following inequality holds for the e-states of the closed-loop slow system:

$$|e(t)| \leq K_e|e(0)|e^{-a_1 t} \ \forall \ t \geq 0 \tag{G.6}$$

for some $K_e \geq 1$, $a_1 > 0$. From Assumption 2, we have that the η states of the closed-loop slow system satisfy the following inequality:

$$|\eta(t)| \leq K_\eta|\eta(0)|e^{-at} + \gamma_\eta(\|e\|) \ \forall \ t \geq 0 \tag{G.7}$$

for some $K_\eta \geq 1$, $a > 0$, where γ_η is a class $\mathcal{K}$ function . At this point, one can show, using the results in [67], that the inequalities of Eqs.G.6-G.7 continue to hold, for the states of the closed-loop singularly perturbed system of Eq.G.2, up to an arbitrarily small offset, d, for initial conditions in arbitrarily large compact subsets of the region described by Eq.11.27, provided that the singular perturbation parameter, μ, is sufficiently small. This offset can be selected to be sufficiently small such that, after a sufficiently large time (when the exponential terms in Eqs.G.6-G.7 die out),

the states of the closed-loop system are confined within a small ball centered around the origin. Direct application then of the result of Theorem 9.3 in [170] yields that there exists a $\mu^* > 0$ such that if $\mu \leq \mu^*$, the origin of the closed-loop system of Eq.G.2 is exponentially stable (a somewhat similar argument was used in the Proof of Theorem 2.3 in Appendix A; see this proof for mathematical details.) It follows then that:

$$|e(t)| \leq \alpha |e(0)| e^{-\beta t} \quad \forall\, t \geq 0 \tag{G.8}$$

for some $\alpha \geq 1$ and $\beta > 0$. The asymptotic output tracking result can be easily obtained by taking the limit of both sides of Eq.G.8 as $t \rightarrow \infty$:

$$\lim_{t \rightarrow \infty} |e_i(t)| = \lim_{t \rightarrow \infty} |y_{si}(t) - v_i(t)| = 0, \quad i = 1, \cdots, m$$

This completes the proof of the theorem. Δ

Proof of Theorem 11.2 :

Under the controller of Eq.11.28, the infinite-dimensional closed-loop system takes the form:

$$\begin{aligned}
\frac{d\omega}{dt} &= \tilde{f}(\omega) - \frac{1}{2}\tilde{g}(\omega) R^{-1}(\omega) (L_{\bar{g}} V(\omega))^T + L(y - \tilde{h}(\omega)) \\
\frac{\partial n}{\partial t} &= -\frac{\partial (G(x,r)n)}{\partial r} + w(n,x,r) \\
\dot{x} &= f(x) - \frac{1}{2} g(x) R^{-1}(\omega) (L_{\bar{g}} V(\omega))^T + A \int_0^{r_{max}} a(n,r,x) dr
\end{aligned} \tag{G.9}$$

Applying the method of weighted residuals to the above system, we obtain the fol-

lowing approximate ODE system:

$$\frac{d\omega}{dt} = \tilde{f}(\omega) - \frac{1}{2}\tilde{g}(\omega)R^{-1}(\omega)(L_{\bar{g}}V(\omega))^T + L(y - \tilde{h}(\omega))$$

$$\int_0^{r_{max}} \psi_\nu(r)\sum_{k=1}^{N}\phi_k(r)\frac{\partial a_{kN}(t)}{\partial t}dr = -\sum_{k=1}^{N}a_{kN}(t)\int_0^{r_{max}} \psi_\nu(r)\frac{\partial(G(x_N,r)\phi_k(r))}{\partial r}dr$$

$$+\int_0^{r_{max}} \psi_\nu(r)w(\sum_{k=1}^{N}a_{kN}(t)\phi_k(r), x_N, r)dr, \quad \nu = 1,\ldots,N$$

$$\dot{x}_N = f(x_N) - \frac{1}{2}g(x_N)R^{-1}(\omega)(L_{\bar{g}}V(\omega))^T + A\int_0^{r_{max}} a(\sum_{k=1}^{N}a_{kN}(t)\phi_k(r), r, x_N)dr \tag{G.10}$$

Using the vector notation, $a_N = [a_{1N} \cdots a_{NN}]$, and after some rearrangements, the above system can be written as:

$$\begin{aligned}
\frac{d\omega}{dt} &= \tilde{f}(\omega) - \frac{1}{2}\tilde{g}(\omega)R^{-1}(\omega)(L_{\bar{g}}V(\omega))^T + L(y - \tilde{h}(\omega)) \\
\dot{a}_N &= f^*(a_N, x_N) \\
\dot{x}_N &= f(x_N) - \frac{1}{2}g(x_N)R^{-1}(\omega)I(L_{\bar{g}}V(\omega))^T \\
&\quad +A\int_0^{r_{max}} a_2(\sum_{k=1}^{N}a_{kN}(t)\phi_k(r), r, x_N)dr)
\end{aligned} \tag{G.11}$$

where the explicit expression of the nonlinear function, $f^*(a_N, x_N)$, is omitted for brevity. Setting $\tilde{x} = [a_N^T\ x_N^T]^T$, we finally obtain the following closed-loop system:

$$\begin{aligned}
\frac{d\omega}{dt} &= \tilde{f}(\omega) - \frac{1}{2}\tilde{g}(\omega)R^{-1}(\omega)(L_{\bar{g}}V(\omega))^T + L(y - \tilde{h}(\omega)) \\
\dot{\tilde{x}} &= \tilde{f}(\tilde{x}) - \frac{1}{2}\sum_{i=1}^{m}\tilde{g}_i(\tilde{x})R^{-1}(\omega)L_{\bar{g}_i}V(\omega), \quad i = 1,\ldots,m
\end{aligned} \tag{G.12}$$

Under Assumptions 1, 2, and 3 stated in Theorem 11.1, we have already shown in the Proof of Theorem 11.1 above that there exists $\mu^* > 0$ such that if $\mu \in (0, \mu^*]$, the origin of the above system is locally exponentially stable and $\lim_{t\to\infty}|y_{si} - v_i| = 0$. Using the results of Proposition 1 in [54], we have that, for sufficiently large N, the

following estimates hold:

$$\begin{aligned} n(r,t) &= n_N(r,t) + O(\epsilon(N)) \\ x(t) &= x_N(t) + O(\epsilon(N)) \end{aligned} \tag{G.13}$$

where $\epsilon(N)$ is a small positive real number that depends on N and satisfies $\lim_{N\to\infty} \epsilon(N) = 0$, and $n_N(r,t) = \sum_{k=1}^{N} a_{kN}(t)\phi_k(r)$ is the approximation of $n(r,t)$. It follows then that, for sufficiently large N, there exist positive real numbers $\delta_n, \bar{\delta}_x, \delta_\omega, \bar{\mu}^*$ such that if $\mu \in (0, \bar{\mu}^*]$, $\|n(r,0)\|_2 < \delta_n$, $|x(0)| < \bar{\delta}_x$, $|\omega(0)| < \delta_\omega$, the origin of the closed-loop system of Eq.G.9 is exponentially stable and $\lim_{t\to\infty} |y_i - v_i| = O(\epsilon(N))$. This completes the proof of the theorem. $\triangle$

Appendix H

Proofs of Chapter 10

Proof of Proposition 10.1:

Consider the representation of the system of Eq.10.13 in the e, η transformed coordinates introduced in Eqs.10.14-10.15. Evaluating the time-derivative of the Lyapunov function candidate, $V = e^T \Phi e$, defined in Theorem 10.1, along the trajectories of the e-subsystem in Eq.10.15, we obtain:

$$\dot{V} = L_{\bar{f}} V + L_{\bar{g}} V u \tag{H.1}$$

Substituting the controller of Eqs.10.17-10.18 into the above equation yields, after some algebraic manipulations:

$$\dot{V} = \frac{-\rho|e|^2 + L_{\bar{f}} V \sqrt{1 + (u_{max}|(L_{\bar{g}} V)^T|)^2} - \sqrt{(L_{\bar{f}}^* V)^2 + (u_{max}|(L_{\bar{g}} V)^T|)^4}}{\left[1 + \sqrt{1 + (u_{max}|(L_{\bar{g}} V)^T|)^2}\right]} \tag{H.2}$$

Using the fact that $L_{\bar{f}}^* V = L_{\bar{f}} V + \rho|e|^2$, where $\rho > 0$, it's clear that whenever $L_{\bar{f}}^* V \leq 0$, we have $L_{\bar{f}} V \leq 0$ and therefore:

$$\dot{V} \leq \frac{-\rho|e|^2}{\left[1 + \sqrt{1 + (u_{max}|(L_{\bar{g}} V)^T|)^2}\right]} < 0 \quad \forall \; e \neq 0 \tag{H.3}$$

For the case when $0 < L_{\bar{f}}^* V \leq u_{max}|(L_{\bar{g}} V)^T|$, we have $(L_{\bar{f}}^* V)^2 \leq u_{max}^2 |(L_{\bar{g}} V)^T|^2$ and

consequently:

$$\begin{aligned} -\sqrt{(L_{\bar{f}}^{*}V)^2 + (u_{max}|(L_{\bar{g}}V)^T|)^4} &\leq -L_{\bar{f}}^{*}V\sqrt{1 + (u_{max}|(L_{\bar{g}}V)^T|)^2} \\ &\leq -L_{\bar{f}}V\sqrt{1 + (u_{max}|(L_{\bar{g}}V)^T|)^2} \end{aligned} \tag{H.4}$$

Substituting the last estimate, obtained above, into Eq.H.2, we conclude that $\dot{V}$ satisfies Eq.H.3. Summarizing, if the inequality of Eq.10.19 holds, we have that $\dot{V}$ satisfies Eq.H.3. Since Ω is an invariant set embedded within the region described by the inequality of Eq.10.19, it is clear then that starting from any $a_s(0) \in \Omega$, the evolution of the closed-loop trajectory obeys Eq.10.19 and $\dot{V}$ satisfies Eq.H.3, which implies that the origin of the closed-loop e-subsystem is asymptotically stable, i.e., there exists a function β_e of class $\mathcal{KL}$ such that the e states of the closed-loop system satisfy:

$$|e(t)| \leq \beta_e(|e(0)|, t) \quad \forall\ t \geq 0 \tag{H.5}$$

Since the η subsystem, with e as input, is ISS, uniformly in $\bar{v}$, (from Assumption 10.2), the η states of the closed-loop system satisfy the following inequality:

$$|\eta(t)| \leq K_\eta|\eta(0)|e^{-at} + \gamma_\eta(\|e\|) \quad \forall\ t \geq 0 \tag{H.6}$$

for some $K_\eta \geq 1$, $a > 0$, where γ_η is a class $\mathcal{K}$ function. Using the inequalities of Eqs.H.5-H.6, it can be shown by means of a small gain argument that, given any initial condition such that $|a_s(0)| \leq \delta_s$, the origin of the closed-loop e-η interconnection – and hence the closed-loop system of Eq.10.13 and Eqs.10.17-10.18 – is asymptotically stable.

Proof of Theorem 10.1:

Part 1: From the asymptotic stability result of Proposition 10.1, there exists a function $\bar{\beta}$ of class $\mathcal{KL}$ such that $|a_s(t)| \leq \bar{\beta}(|a_s(0)|, t)\ \ \forall\ t \geq 0$ (a function $\bar{\beta}(s,t)$ is said to be of class $\mathcal{KL}$ if, for each fixed t, the function $\bar{\beta}(s,\cdot)$ is continuous, increasing, and zero at zero and, for each fixed s, the function $\bar{\beta}(\cdot,t)$ is nonincreasing and tends to zero at infinity.) Using the fact that $\bar{x}_s = \sum_{j=1}^{m} a_j(t)\phi_j(z)$, and the definition of the

L_2-norm associated with the finite-dimensional Hilbert space, $\mathcal{H}_s$, we have:

$$|\bar{x}_s|_2 \;=\; \sqrt{\int_\alpha^\beta \left(a_1^2(t)\phi_1^2(z) + \cdots + a_m^2(t)\phi_m^2(z)\right)dz} \tag{H.7}$$

Since the functions $\phi_j(\cdot)$ are continuous on the closed interval, $[\alpha, \beta]$, then there exist real numbers $\varphi_j \geq 0$, $j = 1, \cdots, m$ such that $\phi_j^2(z) \leq \varphi_j \;\forall\; z \in [\alpha, \beta]$, and consequently:

$$\begin{aligned} |\bar{x}_s|_2 \;&\leq\; \sqrt{\int_\alpha^\beta \varphi^* \left(a_1^2(t) + \cdots + a_m^2(t)\right)dz} \\ &=\; \sqrt{\int_\alpha^\beta \left(\varphi^* \, |a_s(t)|^2\right)dz} \\ &\leq\; \sqrt{\varphi^*(\beta - \alpha)}\; \bar{\beta}(|a_s(0)|, t) \end{aligned} \tag{H.8}$$

where $\varphi^* = \max\limits_{j=1,\cdots,m} \{\varphi_j\}$, which implies that the state $\bar{x}_s$ is bounded and $|\bar{x}_s|_2 \to 0$ as $t \to \infty$. Therefore, the origin of the closed-loop slow subsystem of Eq.10.11 and Eqs.10.17-10.18 is asymptotically stable, i.e., there exists a class $\mathcal{KL}$ function, β, such that:

$$|\bar{x}_s|_2 \;\leq\; \beta_s(|\bar{x}_s(0)|_2, t) \quad \forall\, t \geq 0 \tag{H.9}$$

Part 2: From the stability result obtained in Proposition 10.1, it is clear that the state a_s is bounded and therefore the denominator term (henceforth denoted by $D(a_s)$) in Eq.H.3, which is a continuous function of a_s, is also bounded by some positive real number, k_s, where $k_s = \max\limits_{|a_s| \leq \delta_s} D(\bar{x}_s)$, and there exist real numbers $k_e = \rho/k_s > 0$, $k_1 \geq 1$, $a_1 = k_e/2\lambda_{min}(\Phi) > 0$, where $\lambda_{min}(\Phi)$ is the minimum eigenvalue of the matrix Φ, such that if $|a_s(0)| \leq \delta_s$, $\dot{V}$ satisfies $\dot{V} \;\leq\; -k_e|e|^2$ and the e states of the closed-loop system satisfy:

$$|e(t)| \;\leq\; k_1|e(0)|e^{-a_1 t} \quad \forall\; t \geq 0 \tag{H.10}$$

which shows that the origin of the e-subsystem is exponentially stable. From this result and the fact that the η-subsystem (with $e = 0$) is locally exponentially stable, we have that the closed-loop e-η interconnection, and hence the closed-loop system of Eq.10.13 and Eqs.10.17-10.18, is locally exponentially stable (see [170] for details).

Using calculations similar to those in Part 1 above, we also have that the origin of the closed-loop system of Eq.10.11 and Eqs.10.17-10.18, is locally exponentially stable. Therefore, given the positive real number δ_s, there exists $b > 0$ such that if $|\bar{x}_s(0)|_2 \leq \delta_s$, the following bound holds:

$$|\bar{x}_s(t)| \leq \ k_2|\bar{x}_s(t_0)|e^{-a_2(t-t_0)} \quad \forall \ t \geq t_0 \tag{H.11}$$

for all $|\bar{x}_s(t_0)|_2 \leq b$, for some $k_2 \geq 1$, $a_2 > 0$.

Substituting the controller of Eqs.10.17-10.18 into Eq.10.10 and using the fact that $\epsilon = \dfrac{|Re\ \lambda_1|}{|Re\ \lambda_{m+1}|}$, the closed-loop PDE system can be written in the following form:

$$\begin{aligned} \frac{dx_s}{dt} &= \mathcal{A}_s x_s - \tfrac{1}{2}\mathcal{B}_s R^{-1}(x_s)(L_{\bar{g}}V)^T + f_s(x_s,0) + [f_s(x_s,x_f) - f_s(x_s,0)] \\ \epsilon\frac{\partial x_f}{\partial t} &= \mathcal{A}_{f\epsilon}x_f + \epsilon\bar{f}_f(x_s,x_f) \end{aligned} \tag{H.12}$$

where $\mathcal{A}_{f\epsilon}$ is an unbounded differential operator defined as $\mathcal{A}_{f\epsilon} = \epsilon\mathcal{A}_f$, and $\bar{f}_f(x_s,x_f) = -\frac{1}{2}\mathcal{B}_s R^{-1}(x_s)(L_{\bar{g}}V)^T + f_f(x_s,x_f)$. Note that $f_f(x_s,x_f)$ is independent of ϵ. Since ϵ is a small positive number less than unity (Assumption 10.1, Part 3), the system of Eq.H.12 is in the standard singularly perturbed form, with x_s being the slow states and x_f being the fast states. Introducing the fast time-scale, $\tau = \dfrac{t}{\epsilon}$, and setting $\epsilon = 0$, we obtain the following infinite-dimensional fast subsystem from the system of Eq.H.12:

$$\frac{\partial \bar{x}_f}{\partial \tau} = \mathcal{A}_{f\epsilon}\bar{x}_f \tag{H.13}$$

where the bar symbol in $\bar{x}_f$, denotes that the state $\bar{x}_f$ is associated with the approximation of the fast x_f-subsystem. From the fact that $Re\ \lambda_{m+1} < 0$ and the definition of ϵ, we have that the origin of the above system is globally exponentially stable. Therefore there exists real numbers, $k_3 \geq 1$, $a_3 > 0$, such that:

$$\|\bar{x}_f(\tau)\|_2 \ \leq \ k_3\|\bar{x}_f(0)\|_2 e^{-a_3\tau} \quad \forall\, t \geq 0 \tag{H.14}$$

Setting $\epsilon = 0$ in the system of Eq.H.12 and using the fact that the operator $\mathcal{A}_{f\epsilon}$ is invertible, we have that $\bar{x}_f = 0$. The finite-dimensional closed-loop slow system therefore reduces to the one analyzed in Part 1 of the proof where we have already shown

that its origin is asymptotically (and locally exponentially) stable for all $x_s(0) \in \Theta_s$ (equivalently $a_s(0) \in \Omega$) and that its states are bounded. By exploiting the stability properties of the fast and slow systems, it can be shown, with the aid of calculations similar to those performed in [67], that the inequalities of Eq.H.14, Eq.H.6, and Eq.H.10 continue to hold, for the states of the infinite-dimensional closed-loop system, up to an arbitrarily small offset, d, for initial conditions in large compact subsets ($\Theta_b \subset \Theta_s$) where $\Theta_b = \{x_s \in \mathcal{H}_s : \ |x_s|_2 \leq \bar{\delta}_b\}$ and $\beta(\bar{\delta}_b, 0) + d \leq \bar{\delta}_s$, provided that the singular perturbation parameter ϵ is sufficiently small. The requirement that $\beta(\bar{\delta}_b, 0) + d \leq \bar{\delta}_s$ guarantees that the slow states of the closed-loop system remain within the invariant region Θ_s. Therefore, given the pair $\left\{\bar{\delta}_b, d\right\}$, and given any $\delta_f > 0$, there exists $\epsilon^{(1)} > 0$ such that if $\epsilon \in (0, \epsilon^{(1)}]$, $|x_s(0)|_2 \leq \bar{\delta}_b$, $\|x_f(0)\|_2 \leq \delta_f$, then, for all $t \geq 0$, the states of the closed-loop singularly perturbed system satisfy:

$$\begin{aligned} |x_s(t)|_2 &\leq k_2|x_s(0)|_2 e^{-a_2 t} + d \\ \|x_f(t)\|_2 &\leq k_3\|x_f(0)\|_2 e^{-a_3 \frac{t}{\epsilon}} + d \end{aligned} \tag{H.15}$$

The above inequalities imply that the trajectories of the closed-loop singularly perturbed system will be bounded. Furthermore, as t increases, they will be ultimately bounded with an ultimate bound that depends on d. Since d is arbitrary, we can choose it small enough such that after a sufficiently large time, say $\tilde{t}$, the trajectories of the closed-loop system are confined within a small compact neighborhood of the origin of the closed-loop system. Obviously, $\tilde{t}$ depends on both the initial condition and the desired size of the neighborhood, but is independent of ϵ. Choose $d = b/2$ and let $\tilde{t}$ be the smallest time such that $\max\{k_2|x_s(0)|_2 e^{-a_2\tilde{t}}, k_3\|x_f(0)\|_2 e^{-a_3\frac{\tilde{t}}{\epsilon}}\} \leq d$. Then it can be easily verified that:

$$|x_s(t)|_2 \leq b, \quad \|x_f(t)\|_2 \leq b \ \forall\, t \geq \tilde{t} \tag{H.16}$$

Recall from Eq.H.14 and Eq.H.11 that both the fast and slow subsystems are exponentially stable within the ball of Eq.H.16. It follows then from Proposition 4.1 in [61] that there exists $\epsilon^{(2)}$ such that if $\epsilon \leq \epsilon^{(2)}$, the singularly perturbed

closed-loop system of Eq.H.12 is locally exponentially stable and, therefore, once inside the ball of Eq.H.16, the closed-loop trajectories converge to the origin as $t \rightarrow \infty$. To summarize, we have that given the pair of positive real numbers $\bar{\delta_b}$ and d, such that $\beta(\bar{\delta_b}, 0) + d \leq \bar{\delta_s}$, and given any positive real number, δ_f, there exists $\epsilon^* := \min\{\epsilon^{(1)}, \epsilon^{(2)}\}$ such that if $|x_s(0)|_2 \leq \bar{\delta_b}$, $\|x_f(0)\|_2 \leq \delta_f$, and $\epsilon \in (0, \epsilon^*]$, the closed-loop trajectories are bounded and converge to the origin as time tends to infinity, i.e., the origin of the closed-loop system is asymptotically stable. Taking the limsup of both sides of Eq.H.10 as $t \rightarrow \infty$, we have that:

$$\limsup_{t\rightarrow\infty} |e_1^i(t)| \;=\; \limsup_{t\rightarrow\infty} |\bar{y}_{ci}(t) - v_i(t)| \;=\; 0 \tag{H.17}$$

for $i = 1, \cdots, m$, where $\bar{y}_{ci}$ is the i-th output of the closed-loop slow system (with $\epsilon = 0$). From the exponential stability of the closed-loop system, it follows that there exists $t_b > 0$ such that, for all $t \geq t_b$, the following estimates hold:

$$\begin{aligned} x_s(t) &= \bar{x}_s(t) + O(\epsilon) \\ x_f(t) &= O(\epsilon) \end{aligned} \tag{H.18}$$

Using the above estimates together with the notation $y_c = y_s + y_f$, $y_s = \mathcal{C}x_s$, $y_f = \mathcal{C}x_f$, it is clear that:

$$\begin{aligned} \limsup_{t\rightarrow\infty} |y_{ci}(t) - v_i(t)| &= \limsup_{t\rightarrow\infty} |y_{si}(t) + y_{fi}(t) - v_i(t)| \\ &= \limsup_{t\rightarrow\infty} |\bar{y}_{ci}(t) - v_i(t)| + O(\epsilon) \\ &= O(\epsilon),\ i = 1, \cdots, m \end{aligned} \tag{H.19}$$

This completes the proof of the theorem. $\triangle$

Proof of Theorem 10.2:

The proof of this theorem is similar to the Proof of Theorem 10.1. We will only highlight the differences. Under the output feedback controller of Eq.10.22, the closed-

loop system takes the form:

$$\begin{aligned} \frac{dx_s}{dt} &= \mathcal{A}_s x_s - \tfrac{1}{2}\mathcal{B}_s R^{-1}(\hat{x}_s)(L_{\bar{g}}V)^T + f_s(x_s,0) + [f_s(x_s,x_f) - f_s(x_s,0)] \\ \epsilon\frac{\partial x_f}{\partial t} &= \mathcal{A}_{f\epsilon} x_f + \epsilon \bar{f}_f^*(x_s,x_f) \end{aligned} \tag{H.20}$$

where $\hat{x}_s = \mathcal{S}^{-1}y_m = x_s + x_f$, $\mathcal{A}_{f\epsilon}$ is an unbounded differential operator defined as $\mathcal{A}_{f\epsilon} = \epsilon\mathcal{A}_f$, and $\bar{f}_f^*(x_s,x_f) = -\frac{1}{2}\mathcal{B}_s R(\hat{x}_s)(L_{\bar{g}}V)^T + f_f(x_s,x_f)$. Since ϵ is a small positive number less than unity (Assumption 10.1, Part 3), the system of Eq.H.20 is in the standard singularly perturbed form, with x_s being the slow states and x_f being the fast states. Note that the term $\bar{f}_f^*(x_s,x_f)$ does not contain any terms of the form $O(\frac{1}{\epsilon})$. Therefore, by performing two-time scale decomposition, we obtain the same fast and slow systems obtained under state feedback (analyzed in the Proof of Theorem 10.1). It follows then from the result of this theorem that given the positive real numbers, $\bar{\delta}_b$ and d, as defined in Theorem 10.1, and given any positive real number, δ_f, there exists $\epsilon^{**} > 0$ such that if $\epsilon \in (0,\epsilon^{**}]$, $|x_s(0)|_2 \leq \bar{\delta}_b$, $\|x_f(0)\|_2 \leq \delta_f$, then the origin of the infinite-dimensional closed-loop system is asymptotically stable (and locally exponentially stable) and its output satisfies Eq.10.20. This completes the proof of the theorem. $\triangle$

Appendix I

Proofs of Chapter 12

Proof of Theorem 12.1:

The proof of this theorem is divided into three parts. In the first part, we show that, for each fixed actuator configuration (without switching), the origin of the finite-dimensional closed-loop system is asymptotically (and locally exponentially) stable for any initial condition $a_s(0) \in \Omega(u^k_{max}, \bar{z}^k)$. In the second part, we show that switching among the N actuator configurations, using the switching rule of Eq.12.23, guarantees that the origin of the switched finite-dimensional closed-loop system remains also asymptotically (and locally exponentially) stable. Finally, in the third part, we use the stability results obtained for the finite-dimensional closed-loop system to prove closed-loop stability and reference-input tracking for the infinite-dimensional closed-loop system.

Part 1: Consider first the finite-dimensional system of Eq.12.14 in the transformed coordinates introduced in Eqs.12.17-12.18, subject to the control law of Eqs.12.20-12.21. Using a standard Lyapunov argument, it can be shown that whenever Eq.12.22 is satisfied, for a given actuator configuration, $\bar{z}^k$, the time-derivative of the Lyapunov function, along the trajectories of the closed-loop e-subsystem, satisfies:

$$\dot{V} \leq \frac{-\rho|e|^2}{\left[1+\sqrt{1+(u^k_{max}|(L_{\bar{g}}V(\bar{z}^k))^T|)^2}\right]} < 0 \quad \forall\ e \neq 0,\ k=1,\cdots,N \tag{I.1}$$

Since the function $D(a_s, u^k_{max}, \bar{z}^k) := \left[1+\sqrt{1+(u^k_{max}|(L_{\bar{g}}V(\bar{z}^k))^T|)^2}\right]$ is continuous everywhere, then given any compact set $\Omega(u^k_{max}, \bar{z}^k)$, there exists a positive real number $\nu(u^k_{max}, \bar{z}^k) > 0$ such that $D(u^k_{max}, \bar{z}^k) \leq \nu(u^k_{max}, \bar{z}^k)$ for all $a_s \in \Omega(u^k_{max}, \bar{z}^k)$, which implies that $\dot{V} \leq -\alpha(u^k_{max}, \bar{z}^k)|e|^2 < 0$ for all $e \neq 0$, $k = 1,\cdots,N$, where $\alpha(u^k_{max}, \bar{z}^k) = \rho/\nu(u^k_{max}, \bar{z}^k) > 0$. Consider now any initial condition such that $a_s(0) \in \Omega(u^k_{max}, \bar{z}^k)$. Since the set $\Omega(u^k_{max}, \bar{z}^k)$ is an invariant set within the region described by Eq.12.22, then starting from $a_s(0)$, the closed-loop state satisfies Eq.12.22 for all time and, consequently from Eq.I.1 above, we have that V decreases monotonically according to the dissipation inequality $\dot{V} \leq -\alpha(u^k_{max}, \bar{z}^k)|e|^2 < 0$, which implies that the origin of the closed-loop e-subsystem is exponentially stable under the k-th actuator configuration. Therefore, there exists positive real numbers $\sigma^k_1 \geq 1$, $\phi^k_1 > 0$ such that the e states of the finite-dimensional closed-loop system satisfy:

$$|e(t)| \leq \sigma^k_1|e(0)|e^{-\phi^k_1 t} \quad \forall\ t \geq 0 \tag{I.2}$$

Since the η-subsystem, with e as input, is ISS (from Assumption 12.2), uniformly in $\bar{v}$, the η states of the closed-loop system satisfy the following inequality:

$$|\eta(t)| \leq \sigma_2|\eta(0)|e^{-\phi_2 t} + \gamma_\eta(\|e\|) \quad \forall\ t \geq 0 \tag{I.3}$$

for some $\sigma_2 \geq 1, \phi_2 > 0$, where γ_η is a class $\mathcal{K}$ function of its argument and $\|e\| :=$ ess.sup $|e(t)|$, $\forall t \geq 0$. Using the inequalities of Eqs.I.2-I.3, it can be shown by means of a small gain argument that the origin of the closed-loop (e, η) interconnected system, and hence that of Eqs.12.14,12.20-12.21, is asymptotically stable. Furthermore, from this result and the fact that the η-subsystem (with $e = 0$) is locally exponentially stable, we have that the closed-loop system of Eq.12.14,12.20-12.21 is locally exponentially stable (see [170] for details).

Part 2: Without loss of generality, assume that $a_s(0) \in \Omega(u^1_{max}, \bar{z}^1)$. Since the set $\Omega(u^1_{max}, \bar{z}^1)$ is invariant, then for all times that the configuration $\bar{z}^k = \bar{z}^1$ is active, the closed-loop state satisfies Eq.12.22 with $\bar{z}^k = \bar{z}^1$ and V decreases monotonically according to the dissipation inequality $\dot{V} \leq -\alpha(u^1_{max}, \bar{z}^1)|e|^2 < 0$. Now, if at any time T, such that $a_s(T) \in \Omega(u^j_{max}, \bar{z}^j)$ (Eq.12.23) for some $j \in \{2, \cdots, N\}$, configuration $\bar{z}^j$ is activated (and $\bar{z}^1$ switched out), then it is clear from the invariance of $\Omega(u^j_{max}, \bar{z}^j)$ that, for all times that the configuration $\bar{z}^k = \bar{z}^j$ remains active, the closed-loop state will satisfy Eq.12.22 with $\bar{z}^k = \bar{z}^j$ and, consequently from Eq.I.1 above, we have that V continues to decrease monotonically, but with a different dissipation rate $\dot{V} \leq -\alpha(u^j_{max}, \bar{z}^j)|e|^2 < 0$. Therefore, we conclude that, as long as the k-th configuration is switched in at time T when $a_s(T) \in \Omega(u^k_{max}, \bar{z}^k)$, the time-derivative of the Lyapunov function (for the switched e-subsystem) will always satisfy the following worst-case dissipation inequality for all $t \geq 0$:

$$\dot{V} \leq \max_{k=1,\cdots,N}\{-\alpha(u^k_{max}, \bar{z}^k)\}|e|^2 < 0 \tag{I.4}$$

which implies that the origin of the switched closed-loop e-subsystem is exponentially stable and that the switched closed-loop system of Eqs.12.14,12.20-12.23 is asymptotically stable (by invoking the ISS property of the η-subsystem similar to Part 1 of the proof). Therefore, there exists a function $\bar{\beta}$ of class $\mathcal{KL}$ such that $|a_s(t)| \leq \bar{\beta}(|a_s(0)|, t) \ \forall\, t \geq 0$ (a function $\bar{\beta}(s,t)$ is said to be of class $\mathcal{KL}$ if, for each fixed t, the function $\bar{\beta}(s, \cdot)$ is continuous, increasing, and zero at zero and, for each fixed s, the function $\bar{\beta}(\cdot, t)$ is nonincreasing and tends to zero at infinity.) Using the fact that $\bar{x}_s = \sum_{j=1}^{m} a_j(t)\phi_j(z)$, and the definition of the L_2-norm associated with the finite-dimensional Hilbert space, $\mathcal{H}_s$, we have:

$$|\bar{x}_s|_2 = \sqrt{\int_\alpha^\beta \left(a_1^2(t)\phi_1^2(z) + \cdots + a_m^2(t)\phi_m^2(z)\right)dz} \tag{I.5}$$

Since the functions $\phi_j(\cdot)$ are continuous on the closed interval $[\alpha, \beta]$, then there exist real numbers $\varphi_j \geq 0$, $j = 1, \cdots, m$ such that $\phi_j^2(z) \leq \varphi_j \ \forall\ z \in [\alpha, \beta]$, and conse-

quently:

$$\begin{aligned} |\bar{x}_s|_2 &\leq \sqrt{\int_\alpha^\beta \varphi^* \left(a_1^2(t) + \cdots + a_m^2(t)\right) dz} \\ &= \sqrt{\int_\alpha^\beta \left(\varphi^* \, |a_s(t)|^2\right) dz} \\ &\leq \sqrt{\varphi^*(\beta - \alpha)} \, \bar{\beta}(|a_s(0)|, t) \end{aligned} \tag{I.6}$$

where $\varphi^* = \max_{j=1,\cdots,m} \{\varphi_j\}$, which implies that the state $\bar{x}_s$ is bounded and $|\bar{x}_s|_2 \rightarrow 0$ as $t \rightarrow \infty$. Therefore the origin of the switched closed-loop slow subsystem of Eq.12.13,12.20-12.23 is asymptotically stable, i.e., there exists a class $\mathcal{KL}$ function, β_s, such that:

$$|\bar{x}_s|_2 \leq \beta_s(|\bar{x}_s(0)|_2, t) \quad \forall \, t \geq 0 \tag{I.7}$$

Furthermore, from the exponential stability of the switched closed-loop e-subsystem (see Eq.I.4) and the local exponential stability of the η-subsystem (Assumption 12.2), we have that the switched closed-loop system of Eq.12.14,12.20-12.23 (hence that of Eq.12.13,12.20-12.23) is locally exponentially stable. Therefore, given the positive real number δ_s^1 (or $\bar{\delta}_s^1$), there exists $b > 0$ such that if $|a_s(0)| \leq \delta_s^1$ (or $|\bar{x}_s(0)| \leq \bar{\delta}_s^1$), the following bound holds:

$$|\bar{x}_s(t)|_2 \leq \sigma_3 |x_s(t_0)|_2 e^{-\phi_3(t-t_0)} \quad \forall \; t \geq t_0 \tag{I.8}$$

for all $|\bar{x}_s(t_0)|_2 \leq b$, for some $\sigma_3 \geq 1$, $\phi_3 > 0$.

Part 3: Substituting the controller of Eq.12.20-12.21 into Eq.12.12 and using the fact that $\epsilon = \dfrac{|Re\{\lambda_1\}|}{|Re\{\lambda_{m+1}\}|} < 1$, the closed-loop system can be written in the following form:

$$\begin{aligned} \frac{dx_s}{dt} &= \mathcal{A}_s x_s - \mathcal{B}_s r(x_s, u_{max}^k, \bar{z}^k)(L_{\bar{g}} V)^T + f_s(x_s, 0) + [f_s(x_s, x_f) - f_s(x_s, 0)] \\ \epsilon \frac{\partial x_f}{\partial t} &= \mathcal{A}_{f\epsilon} x_f + \epsilon \bar{f}_f(x_s, x_f) \end{aligned} \tag{I.9}$$

where $\mathcal{A}_{f\epsilon}$ is an unbounded differential operator defined as $\mathcal{A}_{f\epsilon} = \epsilon \mathcal{A}_f$, and the function $\bar{f}_f$ defined as $\bar{f}_f(x_s, x_f) = -\mathcal{B}_s r(x_s, u_{max}^k, \bar{z}^k)(L_{\bar{g}} V)^T + f_f(x_s, x_f)$. The system of Eq.I.9 is in the standard singularly perturbed form, with x_s being the slow states

and x_f being the fast states. Introducing the fast time-scale $\tau = \frac{t}{\epsilon}$ and setting $\epsilon = 0$, we obtain the following infinite-dimensional fast subsystem from the system of Eq.I.9:

$$\frac{\partial \bar{x}_f}{\partial \tau} = \mathcal{A}_{f\epsilon} \bar{x}_f \tag{I.10}$$

where the bar symbol in $\bar{x}_f$ denotes that the state $\bar{x}_f$ is associated with the approximation of the fast x_f-subsystem. From the fact that $Re\{\lambda_{m+1}\} < 0$ and the definition of ϵ, we have that the origin of the above system is globally exponentially stable. Therefore there exists real numbers $\sigma_4 \geq 1$, $\phi_4 > 0$ such that:

$$\|\bar{x}_f(\tau)\|_2 \leq \sigma_4 \|\bar{x}_f(0)\|_2 e^{-\phi_4 \tau} \quad \forall\, t \geq 0 \tag{I.11}$$

Setting $\epsilon = 0$ in the system of Eq.I.9 and using that the operator $\mathcal{A}_{f\epsilon}$ is invertible, we have that $\bar{x}_f = 0$ and thus the finite-dimensional closed-loop slow system takes the form of Eq.12.13,12.20-12.23. We have already shown in Part 2 of the proof that the origin of this slow system is asymptotically (and locally exponentially) stable starting from any initial condition $\bar{x}_s(0) \in \Theta_s(u^1_{max}, \bar{z}^1)$ (equivalently, from any initial condition $a_s(0) \in \Omega(u^1_{max}, \bar{z}^1)$) and under the switching rule of Eq.12.23 and that its states are bounded. Therefore, exploiting the stability properties of the fast and slow systems, it can be shown, using techniques similar to those performed in [67] for the analysis of singularly perturbed systems, that the inequalities of Eq.I.7 and Eq.I.11 continue to hold, for the states of the infinite-dimensional singularly perturbed closed-loop system, up to an arbitrarily small offset, d, for initial conditions in large compact subsets, $\Theta_b(u^1_{max}, \bar{z}^1) \subset \Theta_s(u^1_{max}, \bar{z}^1)$, (equivalently, $\Omega_b(u^1_{max}, \bar{z}^1) \subset \Omega(u^1_{max}, \bar{z}^1)$) where $\Theta_b(u^1_{max}, \bar{z}^1) = \{x_s(0) \in \mathcal{H}_s : \ |x_s(0)|_2 \leq \bar{\delta}^1_b\}$. Therefore, given any pair of positive real numbers $(\bar{\delta}^1_b, d)$, such that $\bar{\delta}^1_b + d \leq \bar{\delta}^1_s$, and given any δ_f, there exists $\epsilon^{(1)} > 0$ such that if $\epsilon \in (0, \epsilon^{(1)}]$, $|x_s(0)|_2 \leq \bar{\delta}^1_b$, $\|x_f(0)\|_2 \leq \delta_f$, then, for all $t \geq 0$, the states of the closed-loop singularly perturbed system satisfy:

$$
\begin{aligned}
|x_s(t)|_2 &\leq \beta_s(|x_s(0)|_2, t) + d \\
\|x_f(t)\|_2 &\leq \sigma_4 \|x_f(0)\|_2 e^{-\phi_4 \frac{t}{\epsilon}} + d
\end{aligned}
\tag{I.12}
$$

The above inequalities imply that the trajectories of the switched closed-loop singularly perturbed system will be bounded. Furthermore, as t increases, they will be ultimately be bounded with an ultimate bound that depends on d. Since d is arbitrary, we can choose it small enough such that after a sufficiently large time, say $\tilde{t}$, the trajectories of the closed-loop system are confined within a small compact neighborhood of the origin of the closed-loop system. Obviously, $\tilde{t}$ depends on both the initial condition and the desired size of the neighborhood, but is independent of ϵ. Let $d = b/2$ and $\tilde{t}$ be the smallest time such that $\max\{\beta_s(|\bar{x}_s(0)|_2, \tilde{t}), \sigma_4 \|x_f(0)\|_2 e^{-\phi_4 \frac{\tilde{t}}{\epsilon}}\} \leq d$. Then it can be easily verified that:

$$
|x_s(t)|_2 \leq b, \quad \|x_f(t)\|_2 \leq b \quad \forall\, t \geq \tilde{t} \tag{I.13}
$$

Recall from Eq.I.8 and Eq.I.11 that both the fast and slow subsystems are exponentially stable within the ball of Eq.I.13. Therefore there exists $\epsilon^{(2)} > 0$ such that if $\epsilon \leq \epsilon^{(2)}$, the singularly perturbed closed-loop system of Eq.I.9 is locally exponentially stable and, therefore, once inside the ball of Eq.I.13, the closed-loop trajectories converge to the origin as $t \to \infty$. The details of this argument can be found in the Proof of Proposition 4.1 in [61] and will not be repeated here. To summarize, we have that given any pair of positive real numbers $(\bar{\delta}_b^1, d)$ such that $\bar{\delta}_b^1 + d \leq \bar{\delta}_s^1$, and given any positive real number δ_f, there exists $\epsilon^* := \min\{\epsilon^{(1)}, \epsilon^{(2)}\}$ such that if $|x_s(0)|_2 \leq \bar{\delta}_b^1$, $\|x_f(0)\|_2 \leq \delta_f$, and $\epsilon \in (0, \epsilon^*]$, the closed-loop trajectories are bounded and converge to the origin as time tends to infinity, i.e., the origin of the closed-loop system is asymptotically stable. By taking the limsup of both sides of Eq.I.2 as $t \to \infty$, we have that $\limsup_{t\to\infty} |e_1^i(t)| = 0$ and, therefore, $\limsup_{t\to\infty} |\bar{y}_c^i(t) - v_i(t)| = 0$, $i = 1, \cdots, m$. Owing to the exponential stability of the infinite-dimensional closed-loop system, standard results from singular perturbation theory on closeness of solutions can be

used (see [61]) to show that there exists $t_b > 0$ such that, for all $t \geq t_b$, the following estimates hold:

$$\begin{aligned} x_s(t) &= \bar{x}_s(t) + O(\epsilon) \\ x_f(t) &= O(\epsilon) \end{aligned} \tag{I.14}$$

Using the above estimates together with the definition of y_c, given in Eq.12.12, we get:

$$y_c = \mathcal{C}x_s + \mathcal{C}x_f = \mathcal{C}\bar{x}_s + O(\epsilon) = \bar{y}_c + O(\epsilon) \tag{I.15}$$

where we have used the fact that $\bar{y}_c = \mathcal{C}\bar{x}_s$ to derive the last equality. From Eq.I.15, we can write:

$$y_c^i = \bar{y}_c^i + O(\epsilon),\ i = 1, \cdots, m \tag{I.16}$$

and therefore:

$$\limsup_{t\to\infty} |y_c^i(t) - v_i(t)| = \limsup_{t\to\infty} |\bar{y}_c^i(t) - v_i(t)| + O(\epsilon), \quad i = 1, \cdots, m \tag{I.17}$$

Since the limit on the right hand side of Eq.I.17 is zero, we finally have:

$$\limsup_{t\to\infty} |y_c^i(t) - v_i(t)| = O(\epsilon), \quad i = 1, \cdots, m \tag{I.18}$$

This completes the proof of the theorem. $\triangle$